Czech University of Life Sciences Prague

Faculty of Engineering

TAE 2022

Proceeding of the 8th International Conference on Trends in Agricultural Engineering 2022

20th – 23rd September 2022

Prague, Czech Republic

CZECH UNIVERSITY OF LIFE SCIENCES PRAGUE

8th International Conference on Trends in Agricultural Engineering 2022

Proceeding of the 8th International Conference on Trends in Agricultural Engineering 2022

September 20th 2022 – September 23rd 2022

Prague

Czech Republic

Editor in chief: David Herák

An online version is available at http://proceedings.tae-conference.cz/

ISBN 978-80-213-3207-2

8th International Conference on Trends in Agricultural Engineering 2022

September 20th 2022 – September 23rd 2022

The 8th International Conference on Trends In Agricultural Engineering is organized on the occasion of the 70th anniversary of the Faculty of Engineering, Czech University of Life Sciences Prague.

The conference's objective is focused on the research in engineering and physical sciences that represent advances in understanding or modelling the performance of biological and physical systems, bioproduction processes and the food chain, logistics systems in agriculture, manufacturing, and material systems in the design of agriculture engineering.

Conference venue:

Faculty of Engineering**,** Czech University of Life Sciences Prague**,** Kamýcká 129, Praha 6, Prague, 16521**,** Czech Republic

The 8th TAE conference is organized under the auspices of the dean of the Faculty of Engineering **doc. Ing. Jiří Mašek, Ph.D.**

Chairman of the conference: David Herák, Czech Republic

Scientific committee:

Vigen Arakelyan – France
Feto Berisso - Ethiopia
Jiří Blahovec - Czech Republic
Roberto D'Amato - Spain
Luis Caicedo - Ecuador
Richard Godwin - UK
Gurkan Gurdil - Turkey
Rostislav Chotěborský - Czech Republic
Jaime Janairo - Philipine
Vytenis Jankauskas - Lithuania
Algirdas Jasinskas - Lithuania
Marián Kučera - Slovakia
František Kumhála - Czech Republic
Martin Libra - Czech Republic
José Machado - Portugal
Alessandro Ruggiero – Italy
Naufal B M Saad – Malaysia
John Schueller - USA
Riswanti Sigalingging - Indonesia
Willi Toisuta - Australia
Sotos Voskarides - Cyprus
Stavros Yanniotis - Greece
Vladislav Zubko - Ukraine

All manuscripts in conference proceedings have been reviewed by the peer review process.

Reviewers:

Z. Aleš, V. Arakelyen, C. Demirel, O. Dajbych, G. Gurdil, D. Herák, A. Horas, P. Hrabě, R. Chotěborský, V. Jurča, A. Kabutey, A. Kešner, M. Kroulík, F. Kumhála, J. Kumhalová, M. Libra, M. Linda, J. Mašek, Č. Mizera, M. Müller, R. Napitupulu, P. Neuberger, S. Pandiangan, M. Petrů, K. Selvi, R. Sigalingging, M. Simanjuntak.

Warm Welcome to Trends in Agriculture Engineering 2022

The progressive prestige that the Trends in Agriculture Engineering International Conference has reached during the last three decades has made it as a world-wide reference about fast development of agriculture from its engineering point of view, and the meeting point for professionals with responsibilities in the improvement of this essential area of whole nations. 69 scientific papers have been selected for TAE 2022 through the Scientific Committee of the conference to be presented in a wide thematic spectrum, to promote and to share the newest and the most relevant aspects of agricultural engineering area. Trends in Agriculture Engineering conference become the scientific hub of the global agricultural engineering research and a forum for the future of agri-food production.

This year conference TAE is organized also on the occasion of the seventieth anniversary of the Faculty of Engineering. Since its establishment in 1952, the faculty has continuously been evolving and responding to technical progress and the needs of practice in its curricula. Throughout its history, the faculty has contributed to technical development in agriculture engineering and, more recently, in other areas in line with accredited study programmes.

The Faculty of Engineering, Czech University of Life Sciences Prague, organizer of this 8th TAE conference, welcomes you to this event. Prague, the capital and the largest city of the Czech Republic, welcomes you with its cordiality for making your stay with us the most pleasant possible.

Sincerely

assoc. prof. Ing. Jiří Mašek, Ph.D.
Dean of Faculty of Engineering
Czech University of Life Sciences Prague

CONTENTS

USING SIMULATION TO OPTIMIZE PREVENTIVE MAINTENANCE INTERVAL

Zdeněk ALEŠ[1], Jan NOVÁK[2], Marián KUČERA[3], Jindřich PAVLŮ[1]

[1]*Department for Quality and Dependability of Machines, Faculty of Engineering, Czech University of Life Sciences Prague, Czech Republic*
[2]*Kleentek, spol. s r.o., Sazečská 560, 108 00 Prague 10, Czech Republic*
[3]*Technical University in Zvolen, Faculty of Technology, Department of Mechanics, Mechanical Engineering and Design, Slovak Republic*

Abstract
Today's modern agricultural and processing companies use complex machines and equipment that use automated or robotic systems. These machines are usually key objects for the company, and it is therefore necessary to ensure proper maintenance, as the failure of these machines is very costly for companies. The mentioned technologies enable the collection of a large amount of not only data from operation, but also operational data concerning technical condition and faults. This data must be processed using algorithms to obtain feedback for decisions on preventive maintenance. Information technology allows you to create simulations that can be used retrospectively to plan maintenance activities. The paper describes the possibilities of using information technology to optimize preventive maintenance.

Key words: *preventive maintenance, failure, average unit costs, renewal.*

INTRODUCTION

The current maintenance status within industrial companies has improved significantly over previous years in favour of preventive maintenance. At the same time industrial companies began to increasingly implement predictive maintenance tools using a variety of diagnostic methods for determining the operational or structural parameters of a particular manufacturing machinery. The trend of the current development of technical progress in connection with the current challenge Industry 4.0 is characterized, among other things, by an enormous increase in data collection. Industrial companies have a large amount of data; however, they are mostly not able to analyse them and gain valuable information that can be used as feedback for decision making.

Preventive maintenance can be understood as a set of activities aimed at preventing the occurrence of failures and accidents (*Pacaiova & Izarikova, 2019*). Preventive maintenance is performed to maintain and increase the reliability of machines and equipment by restoring worn-out machinery objects before they fail. Preventive maintenance activities include inspections of machinery and equipment, partial or complete changes at predetermined intervals, oil changes, lubrication, and more. In addition, maintenance workers can collect data on the gradual deterioration of the technical condition of machines and equipment. The obtained data help in deciding on the replacement or maintenance of worn-out machinery before the failure. Current technological advances make it possible to monitor many diagnostic signals with relatively high accuracy (*Legat, Mosna, Ales & Jurca, 2017*).

The field of processing and evaluation of reliability data is closely related to the operation of machines and equipment in agriculture. This fact is supported by the application of precision agriculture tools, which are characterized by using navigation systems, sensors, electronics, and information technology in general.

Preventive maintenance in the production industry is one of the most essential measures to eliminate accidental machinery failures by replacing/repairing worn out machines or parts. The decision of when and where to perform preventive maintenance is non-trivial due to the complex and stochastic nature of the industry where preventive maintenance is implemented. Some authors use theoretical and practical implementation of preventive maintenance based on a unique modification of the total productive maintenance methodology. The innovative approach of preventive maintenance management was already implemented in the real production. Within preventive maintenance, the new concept may bring in an innovative method of managing the maintenance process, from abstract methodical conception to practical usage. A challenging task while implementing Industry 4.0 technologies is the issue of how to

fully gather and analyse operational data from various items of equipment and users under various conditions, which would result in innovative services of equipment maintenance to increase production and maintenance efficiency *(Hardt, Kotyrba, Volna & Jarusek, 2021)*.
Industry 4.0 has become more popular due to recent developments in cyber-physical systems, big data, cloud computing, and industrial wireless networks. Intelligent manufacturing has produced a revolutionary change, and evolving applications, such as product lifecycle management, are becoming a reality. Other authors proposed and implemented a manufacturing big data solution for active preventive maintenance in manufacturing environments. The manufacturing big data method used for active preventive maintenance has the potential to accelerate implementation of Industry 4.0 (*Wan, Tang, Li, Wang, Liu, Abbas & Vasilakos, 2017*).
Conventional preventive maintenance models often assume that equipment is always available for maintenance activities. However, in many mission-critical industries, equipment may not be available for scheduled maintenance due to busy operational schedules. Forced shutdown of the equipment may incur extra costs that cannot be offset by the benefits from preventively maintaining the equipment. Other paper proposes innovative preventive maintenance policies to address the challenges caused by equipment unavailability. Maintenance models with possible rescheduling are developed for both time-based and condition-based maintenance policies, and the objective is to minimize the long-run cost rate of all maintenance activities (*Zhu, Xiang, Li, Zhu & Schneider, 2019*).
Preventive maintenance is an important component of the Industry 4.0. Modern industry requires intelligent, autonomous, and reliable manufacturing systems. Furthermore, other authors propose methodology for the acquisition of maintenance knowledge, using the computer simulation method to predict possible failures and prepare scenarios for the behaviour of a system *(Klos, 2018).*
The use of system analysis and preventive maintenance in today's industry becomes a necessity as it increases equipment availability. One of the new proposed methods combine three tools: SADT modelling, the FMECA analysis and the Pareto diagram to achieve an optimal maintenance approach that will be a decision support tool to minimize the repair costs and the downtime of the system (*Karoui & Lakhoua, 2021*).
The paper describes how to use computational algorithms to determine the optimal interval for performing preventive maintenance. Knowledge of the characteristics of reliability is a necessity for the application of the theory of renewal, to determine the most appropriate maintenance strategy. Created computational algorithms are validated on model examples. The results can be used as a decision-making tool for maintenance management to determine the optimal interval of preventive maintenance of specific machinery components, and the entire manufacturing machinery. At the same time utilizing the results of the paper may help to simplify the planning of plant downtime, optimizing of maintenance personnel capacity and a quantity of spare parts, which ultimately help to increase the availability of production facilities while reducing costs spent on maintenance.

MATERIALS AND METHODS

According to the standard EN 13306:2010 Maintenance – Maintenance terminology, the maintenance strategy is defined as a management method used to achieve maintenance objectives.
The general objectives of maintenance include:

- carry out the correct renewal, modernization and reconstruction of the property and take care of its optimal use,
- to maintain tangible assets in a serviceable and fit condition and at the required level of availability, efficiency, use and its optimal recovery as a whole,
- prevent the occurrence of faults and the following fault conditions,
- operatively eliminate the failures,
- reduce the environmental impact of the operation and maintenance of production facilities,
- ensure the safety of operation and maintenance of production equipment,
- spend optimal maintenance costs in relation to the availability and efficiency of the production equipment and
- manage asset management and maintenance to excellence using the methods of world best practice – asset management.

Maintenance activities are based on technical and economic decision-making, and it is costs that are essential and need to be paid close attention to. It is always necessary to compare two types of costs, namely the unit cost of corrective maintenance and the unit cost of preventive periodic maintenance. If a diagnostic method can be applied during maintenance, it is necessary to add the unit cost of the diagnostics. The general relations for calculation are described further in the text. Presented calculations were used in algorithms to obtain optimal values.
The calculation model is also based on the calculation of unit costs for operation and maintenance, including induced losses associated with the application of individual maintenance policies (systems). The most suitable is the maintenance system for the given object, which will show the lowest unit costs (3). According to this criterion, the optimal maintenance policy (system) for the given object is selected (*Pavlu, Ales & Jurca 2013*).
The unit costs of corrective maintenance $u_{up}(MOTTF)$ are given by the ratio of the cost of corrective maintenance and the mean operational time to failure and is calculated according to the relation (1)

$$u_{up}(MOTTF) = \frac{N_{up}}{MOTTF} \tag{1}$$

where: N_{up} is the cost of corrective maintenance (costs of primary and secondary (dependent) failures (CZK), spare parts and material inventory holding, production losses, environmental impacts, safety, maintenance personnel availability), *MOTTF* is mean operational time to failure during corrective maintenance (hrs).

If Weibull distribution is considered for the calculation of the mean operational time to failure *MOTTF*, it is calculated according to relation (2)

$$MOTTF = \beta \cdot \Gamma\left(1 + \frac{1}{\alpha}\right) \tag{2}$$

where: *MOTTF* is mean operational time to failure during corrective maintenance (hrs), α is shape parameter of Weibull distribution, β is scale parameter of Weibull distribution, Γ is Gamma function.

The average unit costs of preventive periodic maintenance $u_{pu}(t_{pu})$ are again given by the ratio, where the numerator is the sum of the costs of preventive maintenance N_{pu} multiplied by the reliability $R(t_{pu})$ for the selected interval of periodic maintenance (technical condition without failures) and the costs of corrective maintenance N_{up} multiplied by the probability of failure $F(t_{pu})$ for the selected interval of periodic maintenance (it is a state with the occurrence of failure) and where the denominator is the mean operational time until preventive periodic maintenance is carried out and are calculated according to relation (3)

$$u_{pu}(t_{pu}) = \frac{N_{pu} \cdot R(t_{pu}) + N_{up} \cdot F(t_{pu})}{t_s(t_{pu})} = min \Rightarrow t_{pu} = t_{puo} \tag{3}$$

where: $R(t_{pu})$ is reliability function, $F(t_{pu})$ is the probability of failure, $t_s(t_{pu})$ is the mean time of operation until preventive periodic maintenance is performed with an interval and t_{puo} is the optimal periodical maintenance interval (unit costs reach the minimum value).

If Weibull distribution is considered, it is possible to adjust the calculation relation to the form (4)

$$u_{pu}(t_{pu}) = \frac{N_{pu} \cdot exp\left[-\left(\frac{t_{pu}}{\beta}\right)^{\alpha}\right] + N_{up} \cdot \left\{1 - exp\left[-\left(\frac{t_{pu}}{\beta}\right)^{\alpha}\right]\right\}}{\int_{t_p=0}^{t_{pu}} exp\left[-\left(\frac{t}{\beta}\right)^{\alpha}\right] dt} \tag{4}$$

where: t is operational time (hrs).
In order to model the optimal interval for renewal t_{puo}, different values of Weibull distribution, respectively the shape parameter α, and ratios of the costs of preventive maintenance N_{pu} and corrective

maintenance N_{up} were chosen. The selected values are shown in Tab. 1. More than 7,000 complex calculations were performed using the object-oriented language Visual Basic for Applications.

Tab. 1 Input values for the renewal optimization computational model

Indicator	Minimum value	Maximum value	Increment
Shape parameter α	1.05	10	0.05
Scale parameter β	1000	1000	constant
Ratio of corrective maintenance costs to preventive maintenance costs (N_{up}/N_{pu})	1	10	0.5

Probability density function of failure *f(t)* from table 1 is for better visualization shown for the whole range of shape parameter α are shown in Fig. 1. The result of the model is two 3D graphs for two variable inputs and one calculated output. A description of the axes of the first 3D graph is shown in Fig. 2. The value of the shape parameter α of Weibull distribution is plotted on the x-axis. On the y-axis, the optimal average unit costs of preventive periodic maintenance are calculated. On the z-axis is the ratio of corrective maintenance costs to preventive maintenance costs. At Fig. 3 on the y-axis, the optimal interval of mean operation time for renewal is calculated.

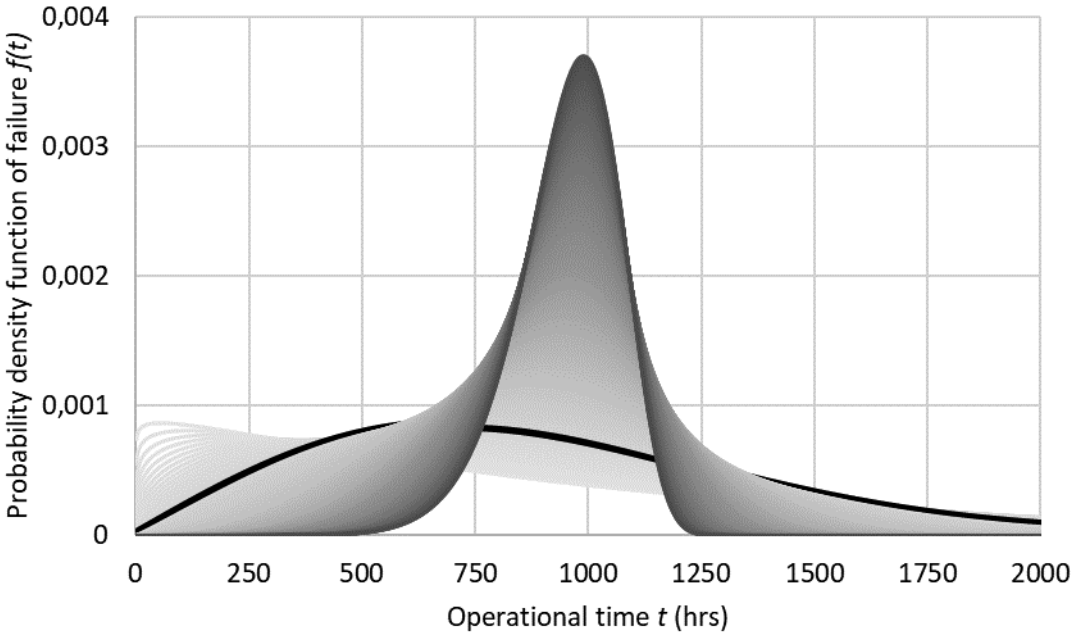

Fig. 1 Probability density function of failure *f(t)* for different shape parameter α of Weibull distribution (α = 1.05 light grey curves, α = 10 dark grey curves, increment 0.05, α = 2 black curve)

RESULTS AND DISCUSSION

The presented Fig.2 and Fig. 3 clearly show the influence of the economic point of view, that when the ratio of N_{up}/N_{pu} increases, then average unit costs for preventive maintenance decrease. The shape parameter α of Weibull distribution can be considered a technical condition of object, and its increase has the greatest effect on the intensity of failures, which has a progressive course if $\alpha > 2$. This fact can be demonstrated by black curve of failure probability density curve *f(t)* in Fig. 1. Simply put, as the shape parameter α of the Weibull distribution increases, the optimal interval for periodic preventive maintenance increases, which contributes to the reduction of maintenance interventions in the long term.

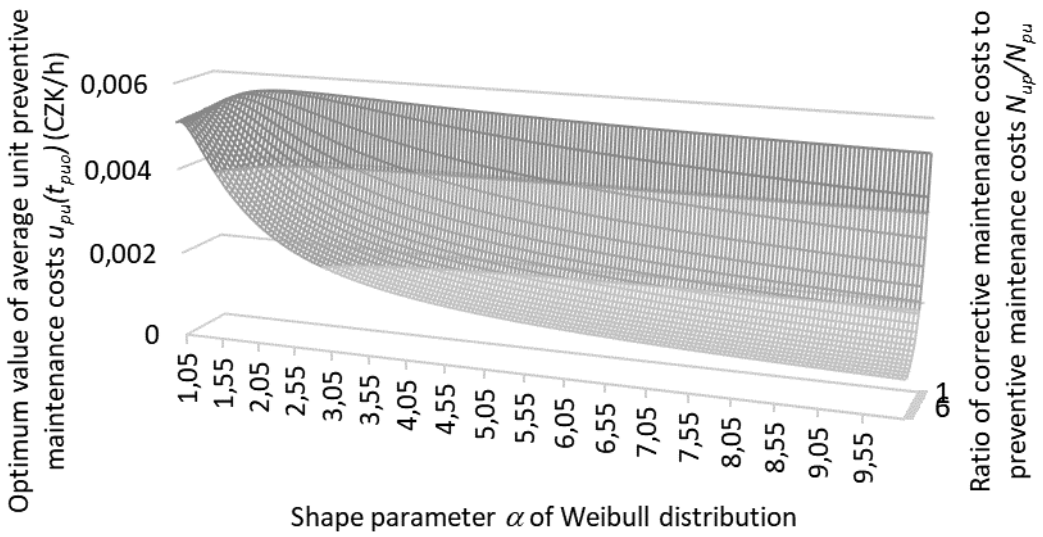

Fig. 2 Dependence of the values of the optimal average unit costs $u_{pu}(t_{puo})$ depending on value of shape parameter α of Weibull distribution and the ratio of corrective maintenance costs N_{up} to preventive maintenance costs N_{pu}

Performed simulation is very important, because it considers both aspects, both economic in the sense of the cost ratio, and technical, how the technical object behaves in terms of reliability characteristics (*Legat, Mosna, Ales & Jurca, 2017*). As mentioned earlier, apart from the solution proposed by the authors, it is advisable to combine with other analysis related to equipment availability (*Karoui & Lakhoua, 2021*) and at the same time implement technologies of Industry 4.0 approach (*Klos, 2018; Hardt, Kotyrba, Volna & Jarusek, 2021*). Results of the paper contribute to preventive maintenance optimization, which is important from the point of view of ensuring machine operability.

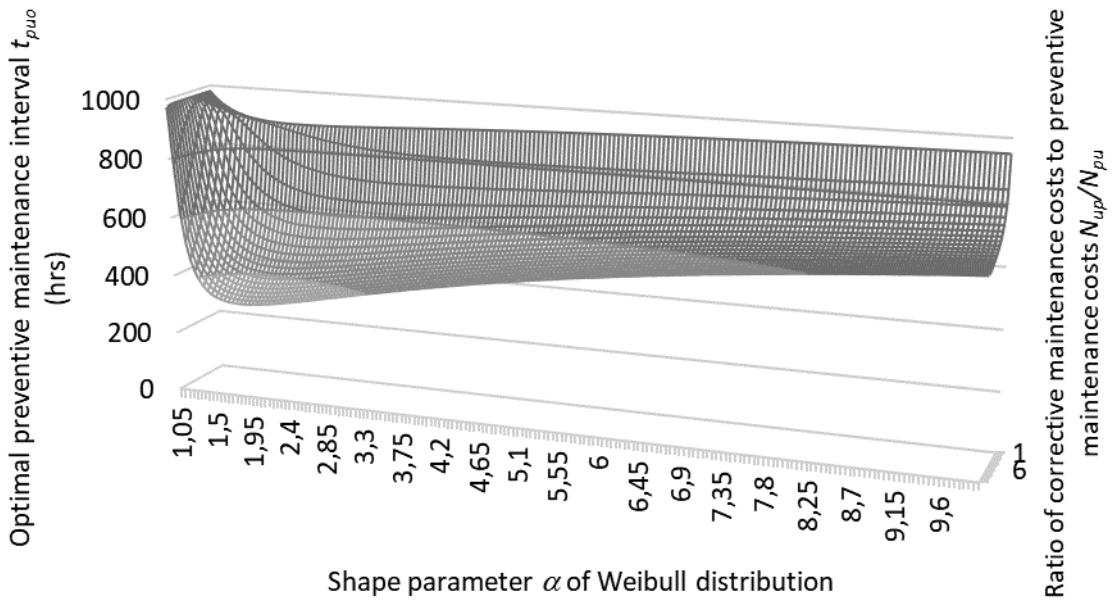

Fig. 3 Dependence of the optimal preventive maintenance operation time interval t_{puo} depending on the size shape parameter α of Weibull distribution and the ratio of corrective maintenance costs N_{up} to preventive maintenance costs N_{pu}

CONCLUSIONS

The use of algorithms in conjunction with computer technology offers several possibilities for specifying the optimal interval for performing preventive maintenance in real time. The proposed algorithms can be used not only as a decision-making tool in maintenance management with the aim of determining the optimal preventive maintenance interval of specific machine elements and thus of the entire production equipment. At the same time, the use of the results of the algorithms will contribute to simpler planning of production equipment shutdowns, the capacity of maintenance personnel and the number of spare parts, which will ultimately help to increase the availability of the production equipment while simultaneously reducing the maintenance costs.

ACKNOWLEDGMENT

This study was supported by Ministry of Industry and Trade – CZU: 31190/1484/314802; MPO: FV20286 - Maintenance management information system with benchmarking module respecting Industry 4.0.

REFERENCES

1. Hardt, F., Kotyrba, M., Volna, E., & Jarusek, R. (2021) Innovative Approach to Preventive Maintenance of Production Equipment Based on a Modified TPM Methodology for Industry 4.0, *APPLIED SCIENCES-BASEL*. Volume: 11. Issue: 15. Article Number: 6953. DOI: 10.3390/app11156953
2. Klos, S. (2018) Knowledge Acquisition Using Computer Simulation of a Manufacturing System for Preventive Maintenance. *INFORMATION AND SOFTWARE TECHNOLOGIES*, ICIST 2018. Book Series: Communications in Computer and Information Science. Volume: 920. Pages: 29-40 DOI: 10.1007/978-3-319-99972-2_3
3. Legat, V., Mosna, F., Ales, Z., & Jurca, V. (2017). Preventive maintenance models – higher operational reliability. *Eksploatacja i Niezawodnosc – Maintenance and Reliability*, 19 (1):134141.
4. Pacaiova, H., & Izarikova, G. (2019) Base Principles and Practices for Implementation of Total Productive Maintenance in Automotive Industry. *Quality Innovation Prosperity*, 23(1), 45-59.DOI: 10.12776/qip.v23i1.1203. ISSN 1338-984X.
5. Pavlu, J., Ales, Z & Jurca, V. (2013) Utilization of satellite monitoring for determination of optimal maintenance interval of agricultural machines. *Trends in Agricultural Engineering 2013*, 5th International Conference on Trends in Agricultural Engineering (pp. 512-517). CULS Prague.
6. Wan, JF., Tang, SL., Li, D., Wang, SY., Liu, CL., Abbas, H., & Vasilakos, AV. (2017) A Manufacturing Big Data Solution for Active Preventive Maintenance. IEEE TRANSACTIONS ON INDUSTRIAL INFORMATICS. Volume: 13 Issue: 4 Pages: 2039-2047 DOI: 10.1109/TII.2017.2670505
7. Zhu, ZC., Xiang, YS., Li, MY., Zhu, WH., & Schneider, K (2019) Preventive Maintenance Subject to Equipment Unavailability. IEEE *TRANSACTIONS ON RELIABILITY*. Volume: 68. Issue: 3. Pages: 1009-1020. DOI: 10.1109/TR.2019.2913331

Corresponding author:
doc. Ing. Zdeněk Aleš, Ph.D., Department of Quality and Dependability of Machines, Faculty of Engineering, Czech University of Life Sciences Prague, Kamýcká 129, Prague Suchdol, 16521, Czech Republic, e-mail: ales@tf.czu.cz

KNOWLEDGE OF PACKAGING WASTE IN THE CZECH REPUBLIC: A STUDENT'S AWARENESS STUDY

Vlastimil ALTMANN[1], Shuran ZHAO[1]

[1]Department of Machinery Utilization, Faculty of Engineering, Czech University of Life Sciences Prague (CZU), Kamýcká 129, 165 00 Praha – Suchdol, Czech Republic

Abstract
The residential sector generates around 14% of the overall waste production in the Czech Republic. This essential share requires special attention to analyze with particular emphasis on citizen education. Thus, this research is dedicated to citizens' awareness about packaging waste to increase their knowledge. The experiment was conducted in the form of a survey, and the students were asked to estimate the weight of the packaging presented to them. This experiment featured three different groups of students over time. The results did not demonstrate a significant difference between these groups over time. The long-term home study caused by COVID-19 did not appear to have affected students' knowledge of packaging waste. Further, each group was compared to the actual weight value and evaluated. This study showed students' actual knowledge about packaging waste and highlighted the gap and importance of education in waste management.

Key words: *municipal waste; estimation; packaging waste.*

INTRODUCTION

The rapid growth of waste is a constant reminder to European Union to effectively manage with it in order to minimize their environmental impact. Packaging waste is one of the most critical environmental issues due to its big volume, reusability, and recyclability (*Han et al., 2010*). The process of a suitable treatment of every type of waste starts at its generation site, in case of municipal waste, it is the household. There are several factors that might have a direct impact on the amount of waste produced by families, e.i. higher incomes, urbanization dynamics, changing in lifestyles and consumption patterns, smaller households *(Monavari et al., 2012; Tencati et al., 2016*), but social awareness and environmental education level, among others, are two of the factors that can play a role on sorting and recycling rate (*Suthar and Singh, 2015*). Thus, this research is dedicated to one of those indicators - the awareness of citizens about packaging waste. Source separation waste collection systems are essential to increase resource efficiency, achieve European recycling goals, and achieve a circular economy *(Tallentire and Steubing, 2020*).
This aim of this study was to analyse students' awareness and knowledge about packaging waste generated at home over a medium-long period. We consider time as an important factor which can change the view of people on waste generation at source, therefore this study was repeated. COVID-19 causes a wide home office and can also change the awareness of people and their view on waste production at home.

MATERIALS AND METHODS

This experiment focuses on the awareness of citizens about different types of waste. Three different groups of students from a university in Prague, Czech Republic, participated in this study. Nine types of packaging waste were used in this experiment. Approximately 90 students participated in this experiment; they were given the task of guessing the weight of prepared samples stated in Tab. 1. This experiment lasted several years to capture changes in perception about packaging waste over time and to include the impact of COVID-19 on citizens. Estimates from all years and groups were collected and analyzed. The comparison was conducted within groups as well as each group to the real weight value. Due to the fact, that not all data showed a normal distribution, the non-parametric method of statistics was applied for data without normal distribution. Kruskal-Wallis test (*Kruskal and Wallis, 1952*) was applied for assessing the difference among three student groups. The Student's t-test and its non-parametric equivalent Wilcoxon signed-rank test (*Wilcoxon, 1945*) were used for evaluating the difference between each group and the real value.

Tab. 1 List of packaging waste used in the experiment

Packaging waste	PET 2l	Plastic bottle 1.5 l	Plastic bottle 0.5 l	Can 0.5 l	Milk carton 1 l	Juice carton 1 l	Champagne 0.75 l	Wine 0.75 l	Beer PET 1.5 l
Weight (g)	56	37	24	15	30	38	611	420	47

RESULTS AND DISCUSSION

This study had the objective of assessing the awareness of packaging waste among students at university. Also during the same time frame, the COVID-19 has emerged and left certain impact on students. The form of study switched to online environment and students spent more time at home. Therefore, we collected data from a group of students in 2022, about two years after COVID-19 first appeared in the Czech Republic and compared them to groups of students from before the coronavirus spread. Furthermore, we assessed each group separately and compared their estimation to the real value.

The result of comparing among groups has shown, that there is no significant difference between assessed groups in the time period (Fig. 1). P value of comparison of each group was all out of critical region (p value > 0,05), this results in a fact that fails to reject the null hypothesis. So it suggested that there is no significant difference between surveyed groups over time. This is related to the fact that COVID-19 and home studying appear not to have had an impact on the perception and knowledge of students about waste packaging even students have stayed at home for a long time and the waste composition has changed during this season.

Then we compared each group of students separately with the real value of the packaging weight to test how they performed (Fig. 2 and 3). The summary of statistical result can be found in Tab. 2. Most of the data did not have the normal distribution, therefore non-parametric method of Student's t-test was chosen. Data with a normal distribution were tested using the parametric Student's t-test and marked in grey and p values above the threshold of significance are marked in bold (without significance). The most accurate students came from both groups A and C, who succeeded in 6 different types of packaging weight where their estimation was close to the real value. Group B has only one correct estimate less than others, but it still has more than half of the accurate estimates. All three groups had a good estimate when guessing the weight of the 1.5-liter plastic bottle, as well as the milk carton and the wine glass. The most difficult packaging type for students was 2-liter PET, which did not meet success in any of the three groups. Across all groups, the average estimate was higher than the actual level. A similar situation occurred with champagne glasses when the average estimate was higher than the actual weight. On the other hand, students in three groups estimated plastic beer bottles to be lighter than they actually were. The possible reason might be that PET is a special plastic type and has a different weight than other types of plastic bottles, therefore, even students were successful in both sizes of plastic bottles (0.5 l and 1.5 l), but failed in 2-liter PET. Also the reason might be the unusual size of the PET bottle (2 l), which is not used by students very often. The same reason is suitable for cans with 0.5 l of volume; this type of packaging is very rarely used for beverages.

The summary demonstrates that students at university have common knowledge and do not differ through grades. However, the university must continue to encourage via education and awareness on managing the municipal waste including packaging waste. This is important according to (*Hines et al., 1987*) which suggests that a person's knowledge and awareness, and sense of responsibility influence the amount of consistency between attitude and action toward the environment. Not only students at universities, it is necessary to promote awareness and draw attention to the necessity of recycling materials already among the younger generations (*Licy et al., 2013*).

Tab. 2 Summary of p-values of the statistical analysis. Each group was compared to the real value of packaging weight.

Group	PET 2l	Plastic bottle 1.5 l	Plastic bottle 0.5 l	Can 0.5 l	Milk carton 1 l	Juice carton 1 l	Champa-gne 0.75 l	Wine 0.75 l	Beer PET 1.5 l
A	0.0125	0.3764	0.5338	0.0562	0.1310	0.3012	0.0008	0.1030	0.0008
B	0.0285	0.1433	0.0243	0.0188	0.4712	0.3271	0.4864	0.7981	$1.39E^{-07}$
C	0.0055	0.9795	0.7678	$3.57E^{-05}$	0.0791	0.2024	0.0094	0.6344	0.5440

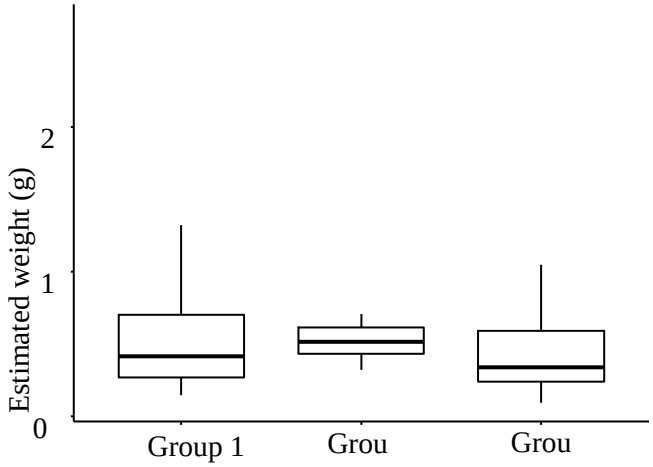

Fig. 1 Comparing means withing groups of students.

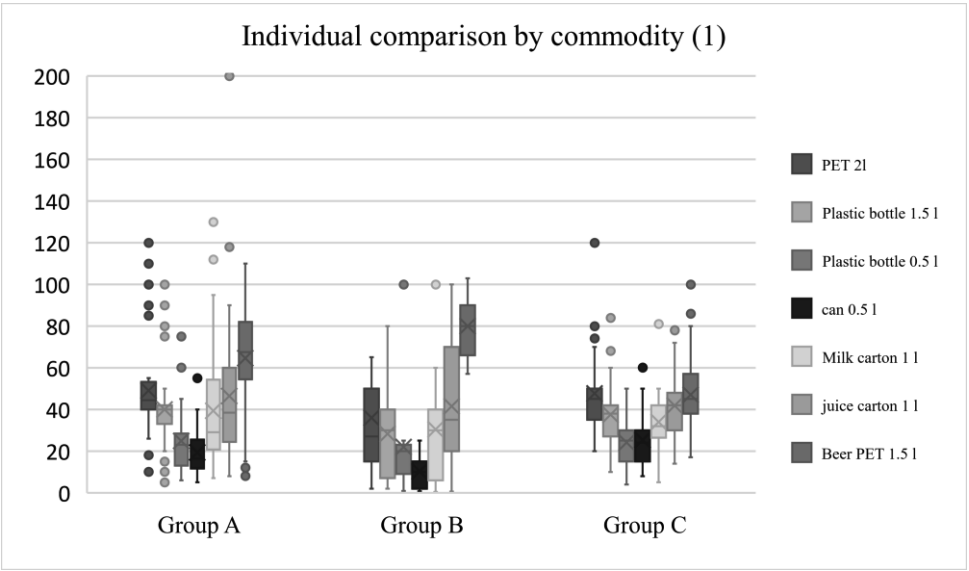

Fig. 2 A more detailed look at the comparison between groups by type of packaging waste type.

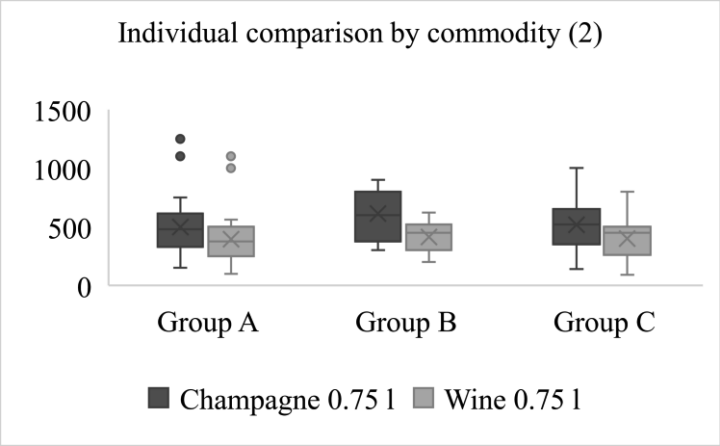

Fig. 3 Comparison between groups separated from the overall data.

CONCLUSIONS

In this study, an application of knowledge testing method is presented. The experiment showed the actual knowledge of students about packaging waste and pointed out the gap and importance of education in waste management. Further, it is suggested to perform this experiment at other educational levels in order to obtain a more thorough and comprehensive evaluation of all age groups.

ACKNOWLEDGMENT

This study was supported by Intern grant agency of Faculty of Engineering, Czech University of Life Sciences Prague with no. 2021:31180/1312/3104.

REFERENCES

1. Han, G.S.A., Bektaş, N., Öncel, M.S., (2010). Separate collection practice of packaging waste as an example of Küçükçekmece, Istanbul, Turkey. Resources, *Conservation and Recycling 54*, 1317–1321.
2. Hines, J.M., Hungerford, H., Tomera, A.N., 1987. Analysis and synthesis of research on responsible environmental behavior: A meta-analysis.
3. Kruskal, W.H., Wallis, W.A., 1952. Use of Ranks in One-Criterion Variance Analysis. *Journal of the American Statistical Association 47*, 583–621.
4. Licy, C., Raghavan, V., Saritha, K., Anies, T., Josphina, C., 2013. Awareness, Attitude and Practice of School Students towards Household Waste Management. *Jouranal of Environmment 02*, 147–150.
5. Monavari, S.M., Omrani, G.A., Karbassi, A., Raof, F.F., 2012. The effects of socioeconomic parameters on household solid-waste generation and composition in developing countries (a case study: Ahvaz, Iran). *Environ Monit Assess 184*, 1841–1846.
6. Suthar, S., Singh, P., 2015. Household solid waste generation and composition in different family size and socio-economic groups: A case study. *Sustainable Cities and Society 14*, 56–63.
7. Tallentire, C.W., Steubing, B., 2020. The environmental benefits of improving packaging waste collection in Europe. *Waste Management 103*, 426–436.
8. Tencati, A., Pogutz, S., Moda, B., Brambilla, M., Cacia, C., 2016. Prevention policies addressing packaging and packaging waste: Some emerging trends. *Waste Management 56*, 35–45.
9. Wilcoxon, F., 1945. Individual Comparisons by Ranking Methods. *Biometrics Bulletin 1*, 80–83.

Corresponding author:
doc. Ing. Vlastimil Altmann, Ph.D., Department of Machinery Utilisation, Faculty of Engineering, Czech University of Life Sciences Prague, Kamýcká 129, Praha 6, Prague, 16521, Czech Republic, phone: +420 22438 3144, e-mail: altv@tf.czu.cz

A REVIEW ON ORGANIC FARMING IN SUSTAINABLE ENVIRONMENT

Elnaz AMIRAHMADI[1], Jan MOUDRÝ[1]

[1]Department of Agroecosystems, Faculty of Agriculture, University of South Bohemia in Ceske Budejovice, 370 05 Ceske Budejovice, Czech Republic.

Abstract
Population growth and increasing demand for food lead to excessive use of pesticides and chemical fertilizers, which has led to nitrate leaching, groundwater pollution, soil degradation, greenhouse gas emissions and climate change. Climate change for our planet is very real and dangerous; many efforts are being made to reduce greenhouse gas emissions into the atmosphere. One of the agricultural method that uses organic origin fertilizers and emphasis on techniques such as crop rotation and co- planting is organic farming. Organic farming can be described as a system of management and agricultural production that is a combination of a high level of biodiversity with environmental practices that help to conserve natural resources. The main goal of this article was reviewed the effect of organic farming system on greenhouse gases emissions, soil property, nutrient contents and human health.

Key words: *conventional agriculture, climate change, soil properties, greenhouse gases emission, human health.*

INTRODUCTION

With growing population, the need to increase agricultural production is unavoidable. In fact, agricultural production has grown significantly in recent decades. one of the agricultural methods that used all over the world is conventional system of farming. In this system, agricultural yields have increased (*Philip Robertson et al., 2014*), because this system based on improved crop varieties, the use of synthetic and mineral fertilizers and pesticides. The result leads to nitrate leaching and groundwater pollution, soil degradation, greenhouse gas emissions, in addition excessive land use has also led to the loss of soil organic matter and soil biodiversity (*Schrama et al., 2018*). The use of inappropriate agricultural techniques leads to soil degradation. On the other hand, deforestation to find new agricultural land is one of the most important factors in greenhouses emission and global warming (*Matuštík et al., 2020*). Agriculture contributes a large share of the greenhouse gases (GHGs) emissions that are causing 17% of climate change directly through agricultural activities and an additional 7-14% through changes in land use (*FAO, 2020*). Overall, conventional farming system has a negative impact on the ecosystem (*Stubenrauch et al., 2021*).

One suggested solution to reduce negative effect of agriculture on the environment, is organic farming (*Seufert et al., 2012*). organic farming systems based on less or no use of pesticides and synthetic fertilizers, less nitrate leaching and other pollutants into underground water, recycling of animal or farm waste, and reduced soil erosion and degradation (*Schweizer et al., 2018; Neri et al., 2019; González-Cencerrado et al., 2020*). The use of this method of farming leads to maintain and increase soil fertility, preserve the genetic diversity, minimize environmental pollution and obtain high quality food by applying sustainable productions (*Orpet., 2020; Santarelli et al., 2020; Sainju et al., 2021., Stubenrauch et al., 2021*). Some of the main effect of organic farming are shown in Fig. 1.

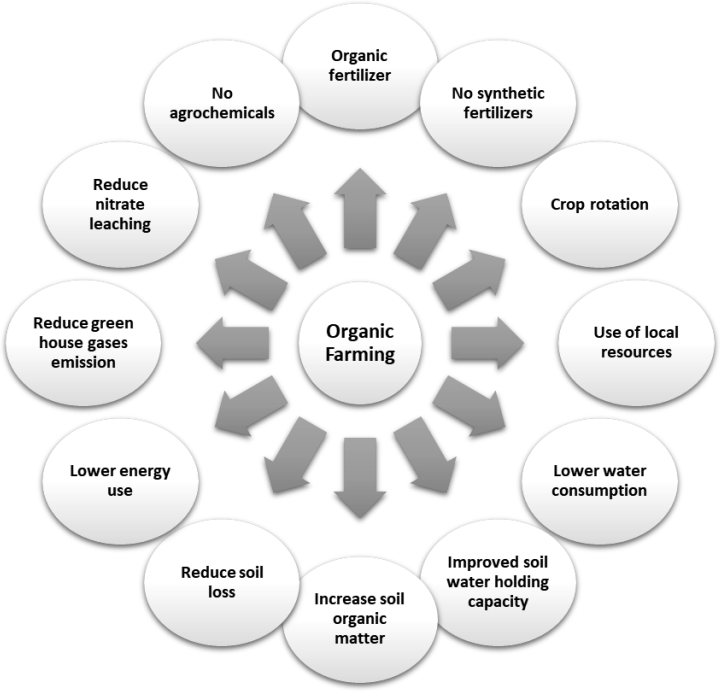

Fig. 1 The main effects and principals of organic farming (*Furtak, & Gałązka., 2019*)

Organic farming has been adopted in about 186 countries (*Ramakrishnan et al., 2021*), With covering a total area of 72.3 million hectares around the world (*Willer et al., 2021*). As shown in Fig. 2, Oceania (35.9 million hectares, 50 percent) and Europe (16.5 million hectares, 23 percent) are the Continents with the largest organic agricultural land in the world. After them, South America has (8.3 million hectares, 11 percent), Asia (5.9 million hectares, 8 percent), North America (3.6 million hectares, 5 percent) and Africa (2 million hectares, 3 percent) (*Willer et al., 2021*).
The main aim of this article was reviewed the effect of organic farming system on GHGs emissions, soil property, nutrient contents and human health.

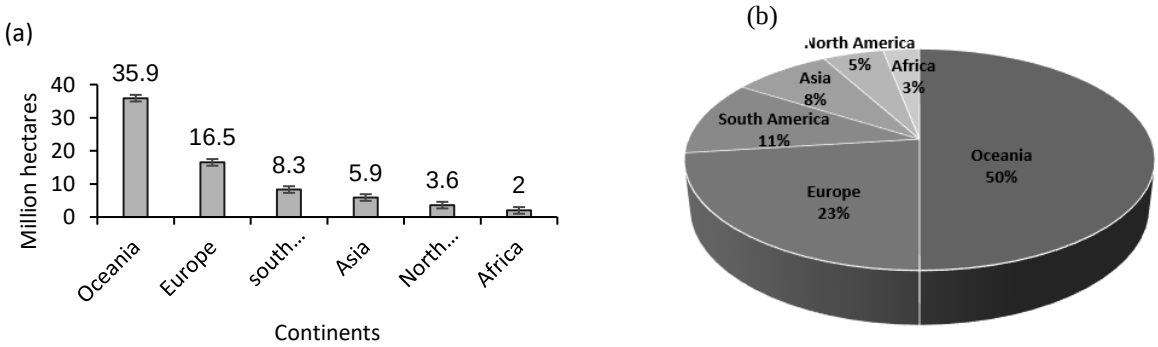

Fig. 2 Organic agricultural land areas around the world depending on (a) the Million hectares and (b) percent in 2019 (*Willer et al., 2021*)

MATERIALS AND METHODS

This review was carried out by identifying original English papers; reviews of recent case studies; national reports that focused on the effect of farming systems (organic and conventional) on GHGs emission, global warming, soil properties, nutrient contents of productions and human health. Microsoft PowerPoint and Microsoft Excel version 2016 were used to draw the figures.

RESULTS AND DISCUSSION

The effect of organic farming system on greenhouse gases emissions: Climate change and global warming become a much-debated issue in recent years (*Moudrý et al., 2013*). *Engler & Krarti. (2021)* stated that currently agriculture is responsible for about one-third of GHGs emissions which is the cause of climate change. Climate change is very real and dangerous for our planet, many efforts are being made to reduce greenhouse gas emissions into the atmosphere (*Sujatha et al., 2021*). In addition to using methods to reduce anthropogenic GHGs emissions, it is essential to look for rapidly methods to absorb carbon dioxide from the atmosphere.

Since management of organic farming systems, based on using less gasoline, diesel, natural gas and using no synthetic fertilizers or pesticides**,** thereupon directly and indirectly, emitting less carbon from combusted fossil fuels. All of this would strongly suggest that a switch to organic farming would lead to a reduction in net GHGs emissions (*Makaju et al., 2021*). *Kitamura et al. (2012)* has been reported that lower emissions of GHGs emissions (CO_2, CH_4 and N_2O) from organic fertilizers compared to chemical fertilizers. For the future farmers should focus on organic agriculture, because conventional system based on the use of synthetic and mineral fertilizers and pesticides, and leads to groundwater pollution and greenhouse gas emissions.

The effect of organic farming system on soil property: Soil productivity and quality are key factors in plants performance. Organic farming method allows to sustainable soil management, conserve the biodiversity of the environment and to maintain the closed circle of elements (*Furtak, & Gałązka, 2019*). Accumulation of organic matter in the soil improves soil quality. *Lori et al. (2017)* demonstrated that the positive effect of organic farming on soil quality including the characteristics of the microbial community (*Lori et al., 2017*). Microbial biomass is affected by agricultural methods, systems of farming and soil management. Many studies showed that organic farming has a positive effect on soil's microbial biomass compared to other farming systems (*Lagomarsino et al., 2009; Wolińska et al., 2015; Kabiri et al., 2016*).
One of the soil quality indicators is the amount of soil organic matter. in organic farming systems amount of soil organic matter are significantly higher than conventional systems (*Crystal-Ornelas et al., 2021*). Soil organic matter plays a very important role in soil fertility and affects a wide range of physical, chemical and biological of soil properties, including nutrient cycling, aggregate formation, water retention and maintain soil moisture, suppression of the disease, pH buffering and cation exchange capacity (*Celestina et al., 2019; Murphy, 2015*).
To achieve environmental sustainability, farmers should use organic amendments instead of chemical fertilizers. Biochar is known as an amendment that has a very good effect on soil properties. addition of biochar to soil cause to increases carbon sequestration and improvement of soil properties, reduction of GHGs emission, reduction of heavy metals bioavailability and decrease amount the leaching of nutrients and pollutants from soil (*Asadi et al., 2021; Ghorbani et al., 2019*).

The effect of organic farming on nutrient contents and human health: Since chemical fertilizers and pesticides have a negative effect on ecosystem and health of humans and other living organisms, special attention should be paid to reducing the use of chemical fertilizers. organic farming is based on using natural materials in agricultural products and cause to produce safe food products with preserving ecological balance and sustainability. Many studies and researches have shown that fruits and vegetables grown from organic production have a higher nutritional value (*Hallmann & Rembiałkowska, 2012; Yu et al., 2018*). *Armesto et al. (2020),* has been reported that the ratio of compounds was higher in organic squashes than in conventional ones.

Essential issues in organic farming: Green waste (consisting of garden refuse, domestic or industrial kitchen waste) due to its nutritional value (because of high nitrogen content), and potentials to mitigate the greenhouse gas emissions (*Diacono et al., 2019*) is widely used in organic farming. If green wastes contain persistent herbicides, they pose health risks to organic farming (*CalRecycle, 2020*).
Another thing that is widely used as an organic amendment in organic farming is municipal sewage sludge and due to good source of nitrogen, phosphorous, and organic matter, helps improve plant growth

and soil properties (*Ramakrishnan et al., 2021*). The presence of high amount of organic matter in the sludge cause to absorbs heavy metals from sewage during the treatment process. Therefore, the use of municipal sewage sludge in organic farming in the presence of heavy metals, is a hidden danger because heavy metals can readily enter the plant tissues and if it is higher than the allowable level, it is considered a threat to human health. (*Weldegebriel et al., 2012*). The future research and policy regulations need to ensure the unintentional entry of pollutants into organic products and protect the health of humans and ecosystems.

Disadvantage of organic farming: Despite the positive effects of organic farming, we have to accept that nothing is not complete perfect. some studies have reported lower performance of the organic farming than conventional farming system in relation to the amount of yield, indeed, the lower yields of organic farming systems are considered as their main disadvantage (*de Ponti et al., 2012; Seufert et al., 2012*). it means that, for produce the same amount of food more land is usually needed in organic farming systems than conventional farming.

CONCLUSIONS

There are many future challenges in the agricultural sector. Efforts to reduce greenhouse gas emissions and Protecting climate and biodiversity, protecting water pollution with reduce nitrate leaching and pollutions, closing nutrient cycles with organic amendments and achieving healthy yields in resilient agricultural systems require further developing organic farming. Due to the positive effects of organic farming on the environment, we need to look for solutions for the lower yields of this system of farming. The use of organic amendments in organic farming systems can increase crop yields, but different organic amendments have different effects and requires careful consideration.

REFERENCES

1. Asadi, H., Ghorbani, M., Rezaei-Rashti, M., Abrishamkesh, S., Amirahmadi, E., Chengrong, C. H. E. N., & Gorji, M. (2021). Application of Rice Husk Biochar for Achieving Sustainable Agriculture and Environment. *Rice Science*, *28*(4), 325-343.
2. Toscano, S., Branca, F., Ferrante, A., & Romano, D. (2021). Zucchini squash production in conventional and organic cultivation systems. *Advances in Horticultural Science*, *35*(2).
3. Ramakrishnan, B., Maddela, N. R., Venkateswarlu, K., & Megharaj, M. (2021). Organic farming: Does it contribute to contaminant-free produce and ensure food safety?. *Science of The Total Environment*, 145079.
4. Celestina, C., Hunt, J. R., Sale, P. W., & Franks, A. E. (2019). Attribution of crop yield responses to application of organic amendments: A critical review. *Soil and Tillage Research*, *186*, 135-145.
5. Crystal-Ornelas, R., Thapa, R., & Tully, K. L. (2021). Soil organic carbon is affected by organic amendments, conservation tillage, and cover cropping in organic farming systems: A meta-analysis. *Agriculture, Ecosystems & Environment*, *312*, 107356.
6. De Ponti, T., Rijk, B., & Van Ittersum, M. K. (2012). The crop yield gap between organic and conventional agriculture. *Agricultural systems*, *108*, 1-9.
7. Diacono, M., Persiani, A., Testani, E., Montemurro, F., & Ciaccia, C. (2019). Recycling agricultural wastes and by-products in organic farming: Biofertilizer production, yield performance and carbon footprint analysis. *Sustainability*, *11*(14), 3824.
8. Engler, N., & Krarti, M. (2021). Review of energy efficiency in controlled environment agriculture. *Renewable and Sustainable Energy Reviews*, *141*, 110786.
9. FAO, (2020). Emissions Due to agriculture. Global, Regional and Country Trends 20 0 0–2018. FAOSTAT Analytical Brief 18. FAO, Rome, Italy.
10. Furtak, K., & Gałązka, A. (2019). Effect of organic farming on soil microbiological parameters. *Polish Journal of Soil Science*, *52*(2), 259.
11. Ghorbani, M., Asadi, H., & Abrishamkesh, S. (2019). Effects of rice husk biochar on selected soil properties and nitrate leaching in loamy sand and clay soil. *International soil and water conservation research*, *7*(3), 258-265.

12. González-Cencerrado, A., Ranz, J. P., Jiménez, M. T. L. F., & Gajardo, B. R. (2020). Assessing the environmental benefit of a new fertilizer based on activated biochar applied to cereal crops. *Science of The Total Environment*, *711*, 134668.
13. Hallmann, E., & Rembiałkowska, E. (2012). Characterisation of antioxidant compounds in sweet bell pepper (Capsicum annuum L.) under organic and conventional growing systems. *Journal of the Science of Food and Agriculture*, *92*(12), 2409-2415.
14. Kabiri, V., Raiesi, F., & Ghazavi, M. A. (2016). Tillage effects on soil microbial biomass, SOM mineralization and enzyme activity in a semi-arid Calcixerepts. *Agriculture, Ecosystems & Environment*, *232*, 73-84.
15. Kitamura, R., Sugiyama, C., Yasuda, K., Nagatake, A., Yuan, Y., Du, J., ... & Hatano, R. (2021). Effects of Three Types of Organic Fertilizers on Greenhouse Gas Emissions in a Grassland on Andosol in Southern Hokkaido, Japan. *Frontiers in Sustainable Food Systems*, *5*, 100.
16. Lagomarsino, A., Moscatelli, M. C., Di Tizio, A., Mancinelli, R., Grego, S., & Marinari, S. (2009). Soil biochemical indicators as a tool to assess the short-term impact of agricultural management on changes in organic C in a Mediterranean environment. *Ecological Indicators*, *9*(3), 518-527.
17. Lori, M., Symnaczik, S., Mäder, P., De Deyn, G., & Gattinger, A. (2017). Organic farming enhances soil microbial abundance and activity—A meta-analysis and meta-regression. *PLoS One*, *12*(7), e0180442.
18. Makaju, S., & Kurunju, K. (2021). A review on use of agrochemical in agriculture and need of organic farming in Nepal. *Archives of Agriculture and Environmental Science*, *6*(3), 367-372.
19. Matuštík, J., Hnátková, T., & Kočí, V. (2020). Life cycle assessment of biochar-to-soil systems: A review. *Journal of Cleaner Production*, *259*, 120998.
20. Moudrý Jr, J., Jelínková, Z., Jarešová, M., Plch, R., Moudrý, J., & Konvalina, P. (2013). Assessing greenhouse gas emissions from potato production and processing in the Czech Republic. *Outlook on AGRICULTURE*, *42*(3), 179-183.
21. Murphy, B. W. (2015). Impact of soil organic matter on soil properties—a review with emphasis on Australian soils. *Soil Research*, *53*(6), 605-635.
22. Neri, L., Santarelli, V., Di Mattia, C. D., Sacchetti, G., Faieta, M., Mastrocola, D., & Pittia, P. (2019). Effect of dipping and vacuum impregnation pretreatments on the quality of frozen apples: A comparative study on organic and conventional fruits. *Journal of food science*, *84*(4), 798-806.
23. Orpet, R. J., Jones, V. P., Beers, E. H., Reganold, J. P., Goldberger, J. R., & Crowder, D. W. (2020). Perceptions and outcomes of conventional vs. organic apple orchard management. *Agriculture, Ecosystems & Environment*, *289*, 106723.
24. Philip Robertson, G., Gross, K. L., Hamilton, S. K., Landis, D. A., Schmidt, T. M., Snapp, S. S., & Swinton, S. M. (2014). Farming for ecosystem services: An ecological approach to production agriculture. *BioScience*, *64*(5), 404-415.
25. Ramakrishnan, B., Maddela, N. R., Venkateswarlu, K., & Megharaj, M. (2021). Organic farming: Does it contribute to contaminant-free produce and ensure food safety?. *Science of The Total Environment*, 145079.
26. Sainju, U. M., Hatfield, P. G., & Ragen, D. L. (2021). Greenhouse gas emissions under winter wheat-based organic and conventional crop productions. *Soil Science Society of America Journal*.
27. Santarelli, V., Neri, L., Sacchetti, G., Di Mattia, C. D., Mastrocola, D., & Pittia, P. (2020). Response of organic and conventional apples to freezing and freezing pre-treatments: Focus on polyphenols content and antioxidant activity. *Food chemistry*, *308*, 125570.
28. Schrama, M., De Haan, J. J., Kroonen, M., Verstegen, H., & Van der Putten, W. H. (2018). Crop yield gap and stability in organic and conventional farming systems. *Agriculture, ecosystems & environment*, *256*, 123-130.
29. Schweizer, S. A., Seitz, B., Van Der Heijden, M. G., Schulin, R., & Tandy, S. (2018). Impact of organic and conventional farming systems on wheat grain uptake and soil bioavailability of zinc and cadmium. *Science of the Total Environment*, *639*, 608-616.
30. Seufert, V., Ramankutty, N., & Foley, J. A. (2012). The yield performance of organic ag-

riculture. In Proceedings of the 8th International Conference on Life Cycle Assessment in the Agri-Food Sector (pp. 1-4) (LCA Food 2012).
31. Stubenrauch, J., Ekardt, F., Heyl, K., Garske, B., Schott, V. L., & Ober, S. (2021). How to legally overcome the distinction between organic and conventional farming Governance approaches for sustainable farming on 100% of the land. *Sustainable Production and Consumption*.
32. Sujatha, M. P., Lathika, C., & Smitha, J. K. (2021). Sustainable and efficient utilization of weed biomass for carbon farming and productivity enhancement: A simple, rapid and ecofriendly approach in the context of climate change scenario. *Environmental Challenges*, *4*, 100150.
33. Weldegebriel, Y., Chandravanshi, B. S., & Wondimu, T. (2012). Concentration levels of metals in vegetables grown in soils irrigated with river water in Addis Ababa, Ethiopia. *Ecotoxicology and Environmental Safety*, *77*, 57-63.
34. Willer, H., Trávníček, J., Meier, C., Schlatter. B. (2021). The world of organic agriculture. Statistics and emerging trends 2021(pp. 1-340). Research Institute of Organic Agriculture FiBL and IFOAM Organics International.
35. Wolińska, A., Szafranek-Nakonieczna, A., Banach, A., Błaszczyk, M., & Stępniewska, Z. (2016). The impact of agricultural soil usage on activity and abundance of ammonifying bacteria in selected soils from Poland. *SpringerPlus*, *5*(1), 1-13.
36. Yu, X., Guo, L., Jiang, G., Song, Y., & Muminov, M. A. (2018). Advances of organic products over conventional productions with respect to nutritional quality and food security. *Acta Ecologica Sinica*, *38*(1), 53-60.

Corresponding author:
Elnaz Amirahmadi, Ph.D., Department of Agroecosystems, Faculty of Agriculture, University of South Bohemia in Ceske Budejovice, 370 05 Ceske Budejovice, Czech Republic, phone: +420 776824426, e-mail: amirae00@zf.jcu.cz

A COBOTIC AND FLEXIBLE SOLUTION FOR HANDLING OF HEAVY LOADS

Vigen ARAKELIAN[1, 2]

[1]*INSA-Rennes / Mecaproce, 20 av. des Buttes de Coësmes, CS 70839, F-35708 Rennes, France*
[2]*LS2N / ECN UMR 6004, 1 rue de la Noë, BP 92101, F-44321 Nantes, France*

Abstract
The aim of the work is to describe the Cobot++ project solution to develop a modular system that combines a cobot and a balancer. Such a system to be able to co-manipulate heavy loads by increasing the capacity of a classic cobot, often limited to loads of less than 10 kg. In the paper, the advantages of the coupled cobot and balancer are disclosed, as well as the optimal design of the cooperative workspace is discussed. The behavior of the coupled system in the static mode under the limitation of the speeds of the cobot does not present any special problems. In this case, the inertial forces are much less than the gravitational ones. The payload is fully compensated by the balancer and the cobot assumes the prescribed displacements. However, in dynamic mode, massive links of the balancer creates additional loads on the cobot, which can be significant. This study considers a method for determining the inertial impact of the balancer on the cobot. Numerical simulations show a significant increase in input torques due to inertia forces of the balancer. It should be noted that the study carried out in the framework of the Cobot++ project took into account safety and ergonomics issues to arrive at a solution compatible with industrial constraints.

Key words: *handling of heavy payloads; balancer; gravity compensation; cobot; dynamic behaviour.*

INTRODUCTION

Workers in industries such as manufacturing and assembly often handle heavy objects. However, manual handling is often repetitive and tedious, reduces efficiency, and leads to back pain and musculoskeletal disorders. It is obvious that industrial robot applications can have a number of advantages over manual control: improved repeatability, increased accuracy and speed. However, industrial robots still have many disadvantages compared to humans. For example, industrial robots currently have a limited ability to perceive their surroundings requiring costly safety measures to avoid serious injury. These safety measures are especially important and expensive when working with large and powerful industrial robots. Obviously, serial robots have a poor payload-to-weight ratio (*Taghirad, 2017*). For example, a manipulator working with a payload of 50 kg must have a weight of at least 400 kg. The purchase, installation and operation of such a robot is quite expensive. In addition, the heaviness of the robot and load leads to rather complex system dynamics, which makes it difficult to move accurately and quickly. This becomes especially noticeable during the assembly process, when heavy parts must be installed on the surface using guide pins. In this case, the manipulator should move smoothly, without significant vibrations, and any sudden movement can damage the mechanical surface of the part. Such a task is not easy to accomplish. Thus, autonomous manipulation does not always provide the expected reliability and flexibility. The aim of the study is to describe the Cobot++ project, which is a new design solution combining a cobot and a balancer.

ADVANTAGES AND FEATURES OF THE COUPLED COBOT AND BALANCER

In all likelihood, balanced robotic systems, such as cobots coupled with balancers, can be effectively used to handle heavy objects. The combination of motion programming for a cobot and the simplicity of a balancer arm can make a system much better than using an industrial robot arm.
Design and application of balancers is a well-known problem. Different approaches and solutions devoted to these systems have been developed and documented (*Matsumoto, 1975; Patarinski, Markov, Konstantinov, 1985; Bittenbinder, 1995; Moor, Akouna, 2003; Arakelian, 2004; Arakelian, Briot, 2015; Arakelian, 2016; Arakelian, 2022*). They have found wide application in several fields of industries, where it is necessary to mechanize heavy manual labor. Now consider the collaboration of a cobot and a balancer for handling of heavy parts. In other words, consider a new-coupled system in which the operator is replaced by the cobot (Fig. 1).

a) Balancer controled by the opertator.

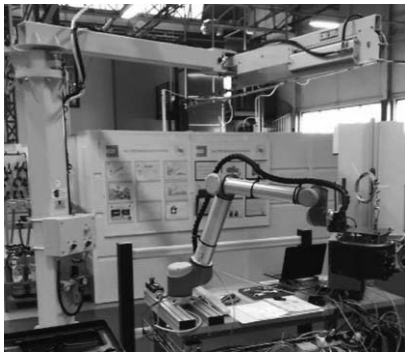

b) Coupled system in which the operator is replaced by the cobot.

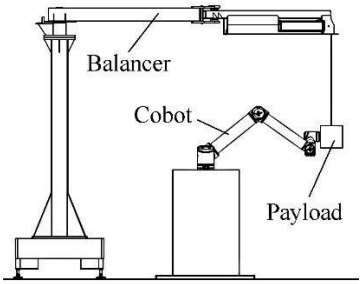

c) Schematic representation of the coupled system.

Fig. 1 Coupled system consisting of a cobot and a balancer.

At present, given the great capabilities of cobots that allow human intervention to control the payload, such a cooperation becomes much more effective, since it does not exclude the possibility of human presence in the cobot's workspace. Note that this is optional purpose. However, in some circumstances this may be the most optimal solution. Thus, it can reduce security measures compared to the use of industrial robots, since the space can be shared.
When designing coupled systems, it is necessary to keep in mind that they consist of two units with different characteristics. However, some of their parameters can be modified during the interaction of these units. One of the first is the consideration of constructive conformity, i.e. the balancer must accompany any payload movement performed by the cobot. If there is a discrepancy between the movements of these two units, the coupled system will be blocked. From this point of view, it is of particular importance to take into account the singular configurations of both the cobot and the balancer.
Figure 2 shows an example when the balancer is in the singular configuration.

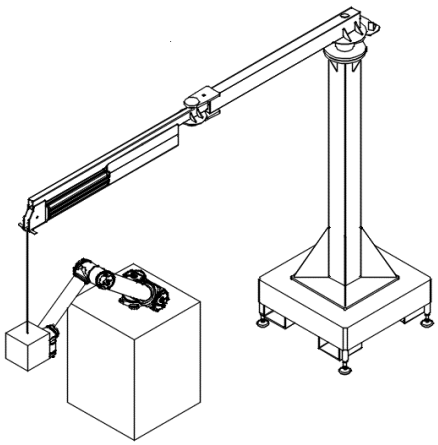

Fig. 2 Coupled system in which the balancer is in the singular configuration.

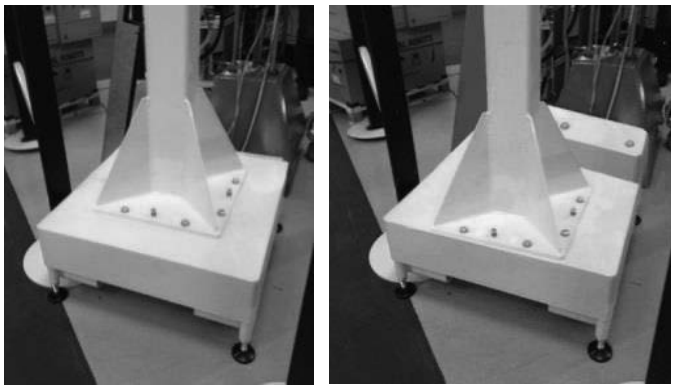

(a) (b)

Fig. 3 Frame of the balancer (a) and its modified version (b) for cobot - balancer cooperation.

In the case of a traditional use of the balancer, this configuration is not inconvenient, since the operator will not move the payload in the radial direction. He will move the payload in such a direction that allows the balancer to come out of the singular position. Then, the operator will perform the necessary movements. However, in a coupled system, it is imperative to consider this when planning the path of the cobot, because one can impose such movements of the cobot, which cannot be carried out by the

balancer. Thus, it is necessary to avoid not only singular configurations of the cobot, but also the balancer. The design of the units can also be changed. In the coupled system with common workspace, the balancer uses only a small part of its accessible space due to the workspace of the cobot, which is generally limits the common volume. Thus, the design of the balancer can be modified to adapt to new conditions. The vertical axis of the balancer can be moved closer to the cobot, and the gravity balancing can be adjusted by a counterweight as shown in figure 3. Such an arrangement is more optimal in terms of cooperative workspace.

STATIC AND DYNAMIC BEHAVIORS OF THE COUPLED COBOT AND BALANCER

The behavior of the coupled system in static mode when the speeds of the links of the balancer are limited does not present any particular problems. In this mode, the inertial forces are much lower than the gravitational forces. The payload is completely compensated by the balancer and the cobot supports low loads. However, when the accelerations increase, the inertial forces also increase and, respectively, the efficiency of gravitational balancing decreases. Therefore, the balancer with massive links creates additional loads on the cobot. Our observations have shown that the behavior of the coupled system in dynamic mode is completely different for the balancer, assuming gravity compensation of the payload. In this case, dynamic loads on the cobot occur in the form of the balancer's oscillations at the end of the working cycle when the cobot is stopped. These oscillations essentially depend on the friction in the joints of the balancer. Such dependence is shown in figure 4. One of the ways to reduce these unwanted vibrations is to increase the friction on the balancer's joints.

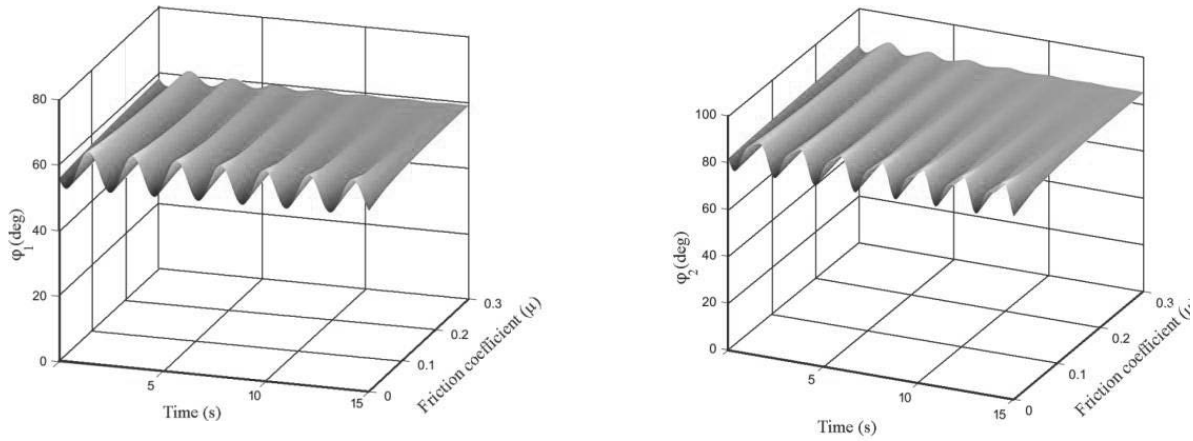

a) Oscillations of the first link of the balancer with cable lift after stopping the cobot.

b) Oscillations of the second link of the balancer with cable lift after stopping the cobot.

Fig. 4 Oscillations of the rotating links of the balancer with cable lift after stopping the cobot.

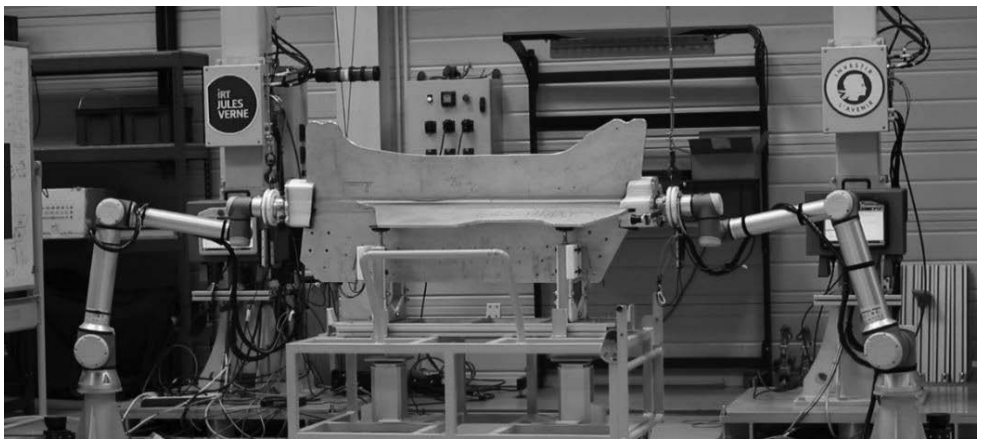

Fig. 5 Two coupled cobot/balancer systems developped for AIRBUS Nantes.

Unfortunately, the increase in friction in the balancer's joints creates a drag force that the cobot has to overcome in any movement. Then two efforts compete: 1) the inertial force due to the oscillations of the balancer, and 2) the drag effort created by the friction. A decrease in the first means an increase in the second. Thus, it is necessary to find the optimal friction so that the drag force will be minimized and the vibration reduction remains effective. Such an optimization highly depends on the application for the coupled system. Indeed, the efforts will mainly depend on the friction, of course, but they will also depend on the accelerations and trajectories imposed by the cobot and the payload. A more detailed discussion of this issue can be found in (*Zhang et al., 2019*).
The application of the described above solution to move a payload of 30 kg was tested on an assembly line at the SAUNIER DUVAL site in Nantes (*https://www.youtube.com/watch?v=vWx53wem_zo*). A demonstrator for heavy and long payloads consisting of two coupled cobot/balancer systems (Fig. 5) for a part turning application during adjustment operations for AIRBUS Nantes has also been developed (*https://www.youtube.com/watch?v=0YiIAFwk3zk*).

CONCLUSIONS

This study deals with the main characteristics of coupled balancers and cobots. It is disclosed the particularities of design of the cooperative workspace, the need to consider singular configurations of the balancer and the cobot. It is revealed that in dynamic mode, the massive-link balancer creates additional loads on the cobot, which can be significant. Observations and tests, as well as numerical simulations have shown the significant increase in input torques of the cobot due to the inertial forces of the balancer. Behavior of the balancer with cable lift and the cobot has been also examined. It is disclosed that there are significant oscillations of the rotating links of the balancer with cable lift after stopping the cobot. It is proposed to eliminate these unwanted oscillations by controlling friction in the joints of the balancer. The author believes that the proposed solution is promising because it is not expensive taking into account the coasts of a balancer and a cobot. It can be easily applied to solve various problems related with the moving of heavy payloads. The coupled balancer/cobot systems can be widely used in various engineering projects.

REFERENCES

1. Taghirad, H., (2017). Parallel robots: mechanics and control. 1st ed. CRC Press, New York.
2. Matsumoto, R. (1975). Load handling equipment. Patent US 3 883 105, May 13.
3. Patarinski, S., Markov, L., Konstantinov, M. (1985). Robot-balancing manipulator cooperation for handling of heavy parts. In the 15th ISIR, Tokyo, Vol. 2 (pp. 649-656).
4. Bittenbinder, W.A. (1995). Lifting device for manual manipulator. Patent DE 4342716, June 22.
5. Moor, B.R., Akouna, H.M. (2003). Vertical counter balanced test head manipulator, Patent CN 1408065T, April 2.
6. Arakelian, V. (2004). The history of the creation and development of hand-operated balanced manipulators. In the International Symposium on History of Machines and Mechanisms (Ed.: M. Ceccarelli), (pp. 347-356). Springer, Netherlands.
7. Arakelian, V., Briot, S. (2015). Balancing of linkages and robot manipulators. Advanced methods with illustrative examples. Springer, Netherlands.
8. Arakelian, V. (2016). Gravity compensation in robotics. Advanced Robotics, 30(2), 79-96.
9. V. Arakelian (ed.) (2022). Gravity compensation in robotics, Mechanisms and Machines Sciences 115, Springer, Switzerland.
10. Zhang, Y., Arakelian, V., Veron, B., Chablat, D. (2019). Key features of the coupled hand-operated balanced manipulator and lightweight robot. In the Advances in Mech. and Mach. Science, vol. 73, (pp. 2289-2298). Springer.

Corresponding author:
Prof. Vigen Arakelian, Department of Mechanical and Control Systems Engineering, INSA Rennes, 20 av. des Buttes de Coësmes, CS 70839, F-35708 Rennes Cedex 7, France, phone: +33223238492, e-mail: vigen.arakelyan@insa-rennes.fr

INFLUENCE OF SOIL COMPACTION ON GROWTH OF SPRING BARLEY

Marek BARÁT[1], Miroslav MACÁK[1], Vladimír RATAJ[1], Jana GALAMBOŠOVÁ[1], Róbert LÁMOŠ[1]

[1]Institute of Agricultural Engineering, Transport and Bioenergetics, Faculty of Engineering, Slovak University of Agriculture in Nitra, Tr. A. Hlinku 2, 949 76 Nitra, Slovak Republic

Abstract
Soil compaction made with traffic by agricultural machinery can be one of the factors limiting crop yields. In any case, some cultivated crops are more sensitive to excessive soil compaction, such as spring barley (Hordeum Vulgare). In this research, the development and growth of spring barley was monitored in a field where a long-term CTF (Controlled Traffic Farming) is established. The RTF (Random Traffic Farming), is simulated using three areas, that are passed once a year by tractor wheels. The results show that soil compaction affected the emergence of barley, while fewer plants were emerged per square meter on compacted soil, however, these plants formed similar number of tillers (on average 2.92 - 3.02 stems in different degrees of soil compaction). The number of ears was lowest in 1x trafficked soil and in multiple-times trafficked soil (501 and 509 ears per m^2), while in non-compacted soil it was higher (572 ears per m^2). Grain yield was highest on non-trafficked soil with CTF system - 5.23 $t.ha^{-1}$.

Key words: *Controlled Traffic Farming; spring barley; soil compaction.*

INTRODUCTION

Modern agricultural production has brought an increase in the power and weight of tractors used in crop production. Since 1966, the weight of agricultural tractors has increased by 300% (*Kumhála, et al., 2013*), while *Keller et al. (2019)* found, that the load on the wheels of harvesting machines increased by up to six-times from year 1960. Some research shows, that first or second pass of a heavy tractor has a negative effect on the growth of cultivated crops (*Pytka & Szymaniak, 2004; Sakai et al., 2008; etc.*), but *Schjonning et al. (2016)* state, that only multiple passes have a negative impact. Increased soil compaction reduces soil porosity, restricts root growth of cultivated crops, thereby reducing water and fertilizer use (*Reintam & Kuht, 2012*) and increasing the risk of water erosion.
It has been found that in conventional tillage system, 88% of the soil surface is trafficked in one year, with minimal tillage the trafficked area is reduced to 65% (*Kumhála, et al., 2013; Rataj, et al., 2014*). *Kroulík et al. (2009)* states similar numbers, and calculated that up to 145,6 % of area can be trafficked repeatedly in conventional tillage. CTF (Controlled Traffic Farming) is a technology that organizes the movement and tracks of machines into permanent lines, thus reducing the trafficked area to a minimum. CTF technology has a positive effect on the reduction of soil compaction, while it is suitable in combination with No-Till and Min-Till technologies, as it is not possible to use a plough when using CTF (*Antille, et al., 2019*).
Some plants tolerate compacted soil conditions better, some worse (*Orzech, et al, 2021; Arvidsson & Håkansson, 2014*). Barley is more sensitive crop for soil compaction, as it prefer porous soil, it restrics the growth of roots in compacted soil (*Bingham, et al., 2009; Mulholland, et al., 1996; Willatt, 1986*). For this reason, the effect of negative soil compaction will be more significant.
The aim of this article is to monitor the impact of soil compaction and CTF traffic management on growth and yield of spring barley sown with zero tillage technology.

MATERIALS AND METHODS

Spring barley (Hordeum Vulgare, variety IS Maltigo) was seeded by direct drilling technology on an 16 hectares experimental field with a long-term experiment with CTF (Control Traffic Farming), which was established in 2009. The crop rotation on this field includes cereals, peas, corn and oilseed rape. The field is located in the University farm in Kolíňany, which belongs to Slovak University of Agriculture in Nitra.
The OutTrack CTF system with a 6 m module is implemented to organize the traffic of machines without additional modifications to the machinery. For the simulation of RTF (Random Traffic Farming), three

areas are set in the field, which are trafficked by tractor wheel once a year, while they are placed perpendicular to the standard CTF tillage direction. There are 18 monitoring points on the experimental field, and it is possible to obtain data from different degrees of soil compaction:

- A – non-compacted soil (non-trafficked soil since the beginning of the experiment - since 2009)
- B – 1x annually compacted soil
- C – multiple-times compacted soil (permanent lines for machinery traffic)

For the purposes of this experiment, a spring barley crop was established in 2021 by direct drilling after the corn harvest. The soil surface was covered with a large amount of corn crop residues left after the harvest, which caused lower crop emergence.

Barley growth was monitored in two growth stages at different degrees of soil compaction, as follows:

- End of tillering (BBCH 29-30) – Plants were taken up, and all tillers and stems on individual plants were counted. Subsequently, the number of plants per meter squared, the current number of stems per meter squared (main stem with tillers), and the average number of stems per plant were determined.
- Before harvesting – The plants were cut above the ground. The number of ears per meter squared, thousand kernel weight, grain moisture and yield (converted to tons per hectare) were determined.

RESULTS AND DISCUSSION

The crop developed differently on all intensities of soil compaction through the whole season. The crop was established by direct drilling into corn stubble, which caused lower emergence. The number of plants also depended on the degree of soil compaction, with an average of 270 plants per m^2 emerged in the non-trafficked soil. In compacted soil, the number of emerged plants was even smaller, 204 plants per m^2 in 1x trafficked soil and 222 plants per m^2 in multiple-times trafficked soil.

During the first measurement, the number of stems per m^2 on the non-trafficked soil in experimental field was 788 stems per m^2. Once a year trafficked soil and multiple-times trafficked soil had similar number of tillers as non-compacted soil (average 2.92 - 3.02 stems per plant), but due to the smaller number of emerged plants in those areas there was a lower number of stems per m^2, resulting in lower current stand density.

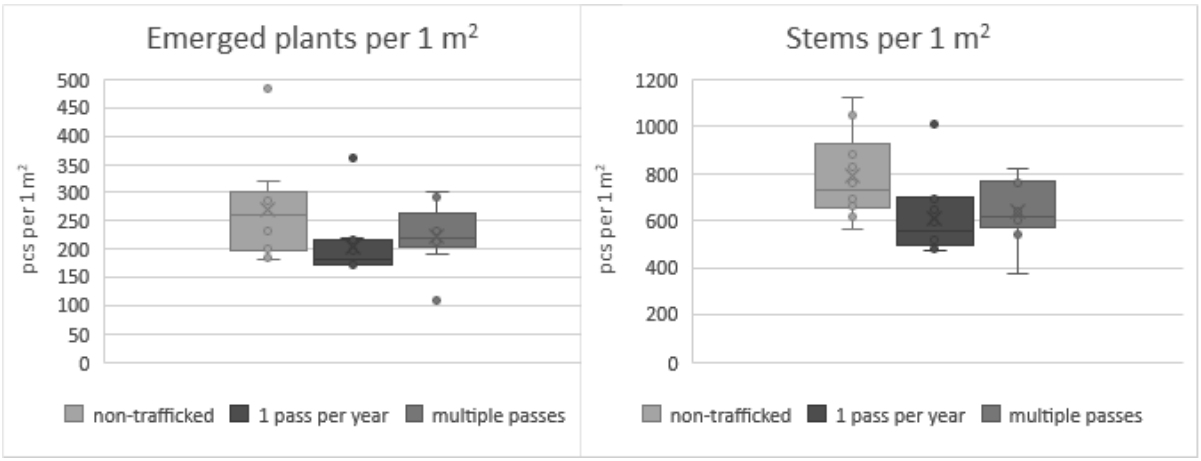

Fig. 1 Average number of emerged plants per 1 m^2 (Left) and average number of stems per 1 m^2 (right)

The second measurement of the stand took place just before the crop was harvested. It was found that the final number of productive ears in the area was lower than the number of stems found in the first measurement. The stand density relatively to the intensity of soil compaction was unchanged, where the highest density was on average 572 ears per m^2 in non-trafficked soil. 1x trafficked soil and multiple-times trafficked soil had approximately the same number of ears (on average 501 and 509 ears per m^2).

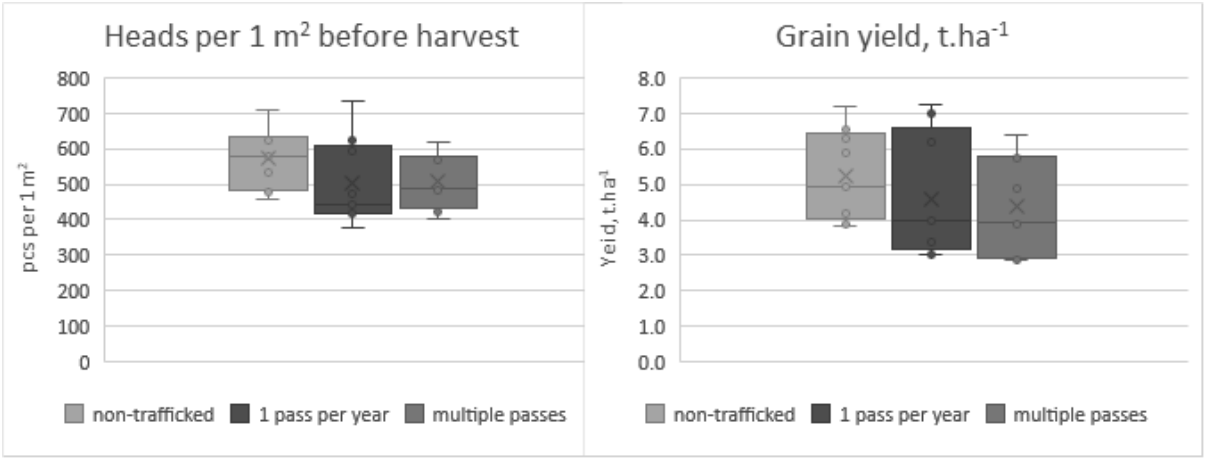

Fig. 2 Average number of heads per 1 m^2 before harvest (Left) and average barley grain yield (right)

The final grain yield was affected by TKW (Thousand Kernel Weight) only slightly. It was found that the TKW was similar in different degrees of soil compaction (54.3 g for non-trafficked soil, up to 53.7 g for multiple-times trafficked soil). Relatively similar TKW on compacted soil may be the result of lower stand density.

These parameters had a significant effect on the grain yield at harvest. The highest yield was on non-trafficked soil with an average 5.23 $t.ha^{-1}$. The average yield in 1x trafficked soil was 4.58 $t.ha^{-1}$ and in multiple-times trafficked soil 4.37 $t.ha^{-1}$. All of the above parameters in the experimental field with different soil compaction intensity are shown in Tab. 1.

Based on those results it can be concluded, that even the first pass of agricultural machinery has a negative effect on barley growth and yield. Similar results were reported by *Pytka & Szymaniak (2004); Sakai et al. (2008)*; etc. It was also proved that barley is a sensitive crop on soil compaction, as reported by *Bingham et al. (2009)*, etc.

Tab. 1 Crop stand parameters and yield parameters of spring barley in experimental field

	MEASUREMENT 1			MEASUREMENT 2		
Traffic intensity (relates to soil compaction)	Number of plants per m^2	Number of stems (main stem + tillers) per m^2	Number of stems (main stem + tillers) per plant	Number of ears per m^2 before harvest	Thousand kernel weight, g	Grain yield, $t.ha^{-1}$
Non-trafficked	270	788	3.00	572	54.3	5.23
1x trafficked per year	204	613	3.02	501	54.1	4.58
Permanent track line	222	637	2.92	509	53.7	4.37

CONCLUSIONS

Soil compaction has a negative effect on the growth and yield of cultivated crops. Spring barley sown by direct drilling after the corn harvest had low number of emerged plants per m^2, while it was even less on the compacted soil. CTF system minimizes soil compaction by organizing the movement of machines on permanent track lines, thus creating areas with non-trafficked and non-compacted soil. It was found that the spring barley crop was better in this non-compacted soil, which was also reflected in the yield, where the average grain yield in non-trafficked soil was 5.23 $t.ha^{-1}$. That was more than 4.58 $t.ha^{-1}$ and 4.37 $t.ha^{-1}$ on average in area with one annual machinery pass and multiple passes of agricultural machinery wheels.

This experiment shows that the CTF system can also be used in soil-conservation tillage technologies with a system of direct drilling and that one yearly pass of tractor has a significant effect on grain yield of spring barley.

ACKNOWLEDGMENT

This publication is the result of the project implementation: „Scientific support of climate change adaptation in agriculture and mitigation of soil degradation" (ITMS2014+ 313011W580) supported by the Integrated Infrastructure Operational Programme funded by the ERDF.

The authors are grateful to the staff at the University Farm in Kolinany, Slovakia, for technical and operational support to conduct this research.

REFERENCES

1. Antille, D.L., Peets, S., Galambošová, J., Botta, G.F., Rataj, V., Macák, M., Tullberg, J.N., Chamen, W.C.T., White, D.R., Misiewicz, P.A., Hargreaves, P.R., Bienvenido, J.F., & Godwin, R.J. (2019). Review: Soil compaction and controlled traffic farming in arable and grass cropping systems. In Agronomy Research, 17(3), 653–682. https://doi.org/10.15159/AR.19.133
2. Arvidsson, J., & Håkansson, I. (2014). Response of different crops to soil compaction – Short-term effects in Swedish field experiments. In *Soil & Tillage Research, 138*, 56-63. https://doi.org/10.1016/j.still.2013.12.006
3. Bingham, I.J., Rees, R.M., & Bengough, A.G. (2009). Influence of Soil Compaction on the Dynamics of Root Growth and Mortality in Spring Barley. *Internal Symposium "Root Research and Applications" RootRAP*. 2.
4. Keller, T., Sandin, M., Colombi, T., Horn, R., & Or, D. (2019). Historical increase in agricultural machinery weights enhanced soil stress levels and adversely affected soil functioning. In *Soil and Tillage Research, 194*. 104293. https://doi.org/10.1016/j.still.2019.104293
5. Kroulík, M., Kumhála, F., Hůla, J., & Honzík, I. (2009) The evaluation of agricultural machines field trafficking intensity for different soil tillage technologies. In *Soil and Tillage Research*, Vol. 105, Issue 1. 171-175. https://doi.org/10.1016/j.still.2009.07.004
6. Kumhála, F., Gutu, D., Hůla, J., Chyba, J., Kovaříček, P., Kroulík, M., Kvíz, Z., Mašek, J. & Vlášková, M. (2013). Technology of Controlled Traffic Farming on fields. *Certificated methodology*. 40. ISBN 978-80-213-2425-1. (in Czech).
7. Mulholland, B.J., Black, C.R., Taylor, I.B., Roberts, J.A., & Lenton, J.R. (1996). Effect of soil compaction on barley (Hordeum vulgare L.) growth – I. Possible role for ABA as a root-sourced chemical signal. In *Journal of Experimental Botany*. 297. Vol 47. 539-549.
8. Orzech, K., Wanic, M., Załuski, D. (2021). The Effects of Soil Compaction and Different Tillage Systems on the Bulk Density and Moisture Content of Soil and the Yields of Winter Oilseed Rape and Cereals. In *Agriculture*. 11(7). 666. https://doi.org/10.3390/agriculture11070666
9. Pytka, J., & Szymaniak, G. (2004). Investigations of stress state in soil under tractor tyres. In *Teka Komisji Morotyzacji I Energetyki Rolnictwa*. 04. 172-176.
10. Rataj, V., Galambošová, J., Macák, M. & Nozdrovický, L. (2014). Precision Agriculture: System – machines – experiences. 160 p. ISBN 978-80-86726-64-9. (in Slovak)
11. Reintam, E. & Kuht, J. (2012). Weed Responses to Soil Compaction and Crop Management. In *Weed Control*. 243-263. ISBN 978-953-51-0159-8.
12. Sakai, H., Nordfjell, T., Suadicani, K., Tabot, B., Ebbe, B. (2008). Soil Compaction on Forest Soils from Different Kinds of Tires and tracks and Possibility of Accurate Estimate. In *Croatian Journal of Forest Engineering*. 29(1). 15-27.
13. Schjonning, P., Lamandé, M., Munkholm, L. J., Lyngvig, H. S. & Nielsen, J. A. (2016). Soil precompression stress, penetration resistance and crop yields in relation to differently-trafficked, temperare-region sandy loam soils. In *Soil & Tillage Research*. 163. 298–308.
14. Willat, S.T. (1986). Root growth of winter barley in a soil compacted by the passage of tractors. In *Soil & Tillage Research*. Vol. 7, Issues 1-2. 41-50. https://doi.org/10.1016/0167-1987(86)90006-1

Corresponding author:

Ing. Marek Barát, PhD., Institute of Agricultural Engineering, Transport and Bioenergetics, Faculty of Engineering, Slovak University of Agriculture in Nitra, Tr. A. Hlinku 2, 949 76 Nitra, Slovak Republic, phone: +421 37 641 4355, e-mail: marek.barat@uniag.sk

TENSILE TESTING AND FEA SIMULATION OF A 3D PRINTED ONYX SPECIMEN

Martin BARÁTH[1], Martin KOTUS[1], Patrik KÓSA[1], Danica ČERVINKOVÁ[2]

[1]Institute of Design and Engineering Technologies, Slovak University of Agriculture in Nitra, Tr. A. Hlinku 2, 94976 Nitra, Slovak Republic
[2]VÚSAPL, a.s., Novozámocká 179, 949 05 Nitra, Slovak Republic

Abstract
Additive manufacturing is a relatively new process, so it needs many studies to be able to produce parts with the required properties. This is the reason why this domain has had a sustained development in recent decades. This paper is focused on the comparison between the mechanical properties of ONYX material determined by tensile testing and the results from a Finite Element Analysis (FEA). The use of simulation will allow a significant shortening of the design time of new structures. The application of FEA for the tensile testing of 3D printed specimens led to the results close to results obtained by the real tensile tests. Difference between the values obtained by real tensile tests and values obtained by simulation are up to 6.19%. The simulation was applied for the printed specimens from a single material. The results of applied FEA are close to results obtained by real testing.

Key words: *additive manufacturing, finite element analysis, tensile strength, nylon, simulation.*

INTRODUCTION

Nowadays additive manufacturing (AM) is used in many areas of production and development. The ASTM society defined AM as "the process of joining materials to produce objects from 3D model data, mostly layer by layer (*Kumar & Prasad, 2021*). AM originated in the 1980s. Initially, the use of AM was limited to the production of prototypes, due to the small choice of materials, mostly polymers. But today we can use AM for a wide range of materials from thermoplastics to metals, ceramics, composites and biocompatible materials. Recently mentioned materials include a composite material reinforced with a continuous fiber. With proper fiber distribution, objects can achieve the strength of aluminum castings (*Morgan, 2005; Kuncius, et al., 2021*). One of the main advantages of AM is the unlimited freedom of geometric shapes and the complexity of the created objects, which allows AM to match or even surpass conventional production technologies.

Fused deposition modeling (FDM) is the most commonly used AM technology (*Kuncius, et al., 2021*). FDM creates objects by extruding molten plastic layers. The material in the form of a thin fiber is fed to an extruder, where the material is melted and extruded through a nozzle onto the surface of the object (*Madaj & Kohár, 2020*). The mechanical properties of composites produced by FDM are worse than the mechanical properties produced by injection molding. The main reason is the insufficient bonding between individual layers and also; there is high porosity and residual stress (*Jain, et al., 2022*).

A large variation in the mechanical properties of 3D printed polymers has promoted designers to develop simulation strategies for the prediction of mechanical properties of 3D printed objects. Several testing techniques are generally used to determine the mechanical properties of a material. The most common mechanical tests include a uniaxial compression test, a plane-strain compression test, and a uniaxial tensile test. The uniaxial tensile test is the most commonly used mechanical test, providing accurate values of key mechanical parameters such as Young's modulus, yield strength, ultimate tensile strength, elongation at break and Poisson's ratio (*Kalova, et al., 2021; Majko, et al., 2019*). *Provaggi et al. (2019)* recently employed finite element analysis (FEA) to predict mechanical properties of 3D printed polymers under compression and concluded that inputs provided by FEA could be potentially useful for reducing product design and development time. The aim of the study was verification of material parameters by comparing simulation results and real experiment results.

MATERIALS AND METHODS

For our research we have used a Markforged Mark Two 3D printer. This 3D printer offers continuous fiber fabrication (CFF) process. Printer has two nozzles, first for plastic material called Onyx and second for continuous fiber. The printer builds the matrix from Onyx and irons down continuous strands of fibers into the part. The fibers are impregnated with nylon and are fused to the Onyx layer. Printing parameters are shown in Tab. 1.

Tab. **1** Printing parameters

Parameter	Value
Print temperature (°C)	275
Layer height (mm)	0.125
Nozzle size (mm)	0.4
Infill	solid
Number of perimeters	2

Markforged Onyx was used for manufacturing of specimens. Onyx is a micro carbon fiber filled nylon. It is 1.4 times stronger and stiffer than ABS and can be reinforced with any continuous fiber from Markforged. Mechanical properties of the Onyx material are shown in Tab. 2.

Tab. 2 Mechanical properties of Markforged Onyx

Property	Testing method (ASTM)	Typical value
Tensile Modulus (GPa)	D638	2.4
Tensile stress at Yield (MPa)	D638	40
Tensile stress at Break (MPa)	D638	37
Tensile strain at Break (%)	D638	25
Flexural Strength (MPa)	D790	71
Flexural Modulus (GPa)	D790	3.0
Heat Deflection Temp (°C)	D648 B	145
Izod Impact - notched ($J.m^{-2}$)	D256-10 A	330
Density ($g.cm^{-3}$)		1.2

Tensile tests were performed in accredited laboratory VÚSAPL, a.s., Nitra. For tensile tests we used a MTS Exceed E43.104 universal tensile testing machine with maximal force 10 kN. Tests were performed according to ISO 527-1 and ISO 527-2 standards. Total number of specimens was 5. Speed rate was set to $1mm.min^{-1}$. Shape and dimensions of test specimens are shown in the Fig. 1.
For finite element analysis (FEA) we used Solidworks 2020 software. Despite on the fact infill value was 100%, in the FEA it was considered that the specimen was working like a single block and has the same properties in the entire volume. We have used an ONYX plasticity model for the simulation where a curvature-based mesh was applied. Mesh type was Solid Mesh and we used triangles (tetrahedrons) type of elements. The mesh consists of 13195 nodes with mesh size of 1.03714614 mm with a 1.4 ratio of a/b.

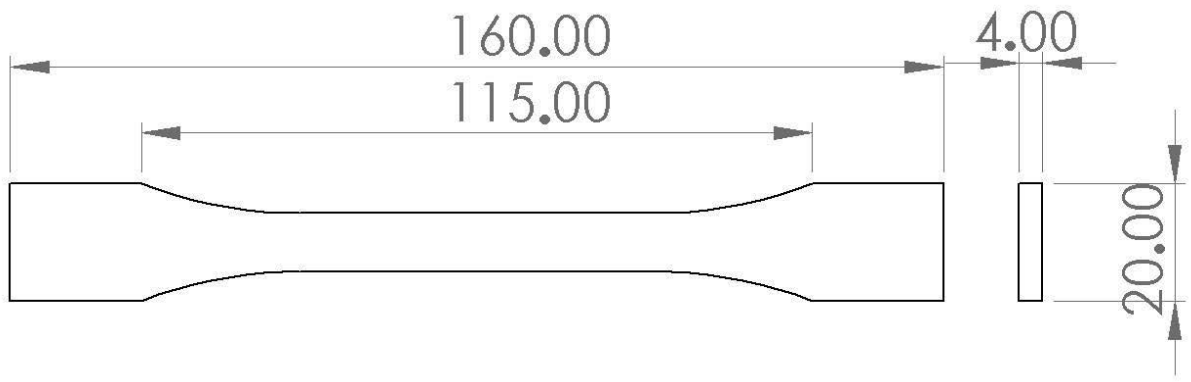

Fig. 1 Specimen shape and dimensions

RESULTS AND DISCUSSION

All specimens were printed at the same time, so ambient conditions were the same. Nylon is hygroscopic and it can absorb moisture from air. Humidity absorbed in nylon can influence mechanical properties of material (*Zhou, et al., 2001*). Due to this fact tensile tests were performed in short time after specimens were printed. Tensile tests allowed us to obtain values of tensile strength and values of maximal force. In the next step, the FEA analysis was performed. Specimens were loaded by forces from 1000 N to 2000 N with 100 N steps. From results obtained from FEA analysis we created a dependence of von Mises stress on force (see Fig. 2.). As we can see this dependence is linear. Based on this fact equation (1) was used to calculate von Mises stress of specimen loaded by maximal force reached during the test.

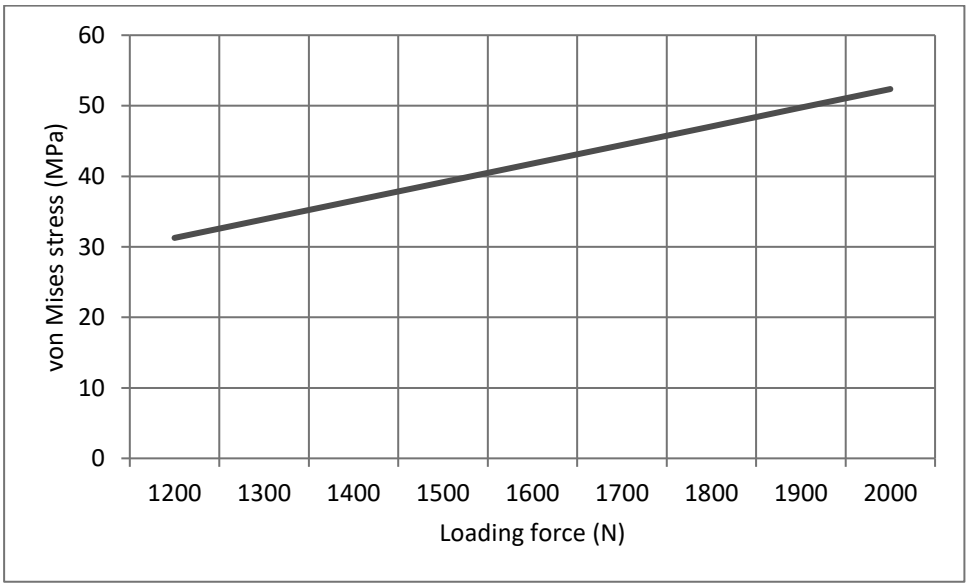

Fig. 2 Dependence of von Mises stress on force

$$VM_{F_M} = \frac{F_L}{VM} . F_M \qquad (1)$$

where F_M is the maximal force reached during test (N), F_L is the loading force during the FEA analysis (N), VM is the von Mises stress in specimen loaded by F_L (MPa), VM_{F_M} is the von Misses stress in specimen loaded by F_M (N).

In the Tab. 3 are shown the results of the tensile tests, but also the results obtained by the simulation. The results consist of the maximal force reached during tensile test for each specimen, of the tensile strength for each specimen and of the von Mises stress under load with maximal force. We can clearly see that the difference between experiment result and simulation is low. Results of the simulation are up to 6.19% higher than results of tests. This fact indicates that model is designed in the right way and material parameters are right too.

Tab. 3 Results of tensile tests and FEA analysis

Speci-men number	Maxi-mum force N	Tensile strength MPa	von Mises stress MPa
1	1377.03	34.50	35.92
2	1427.60	35.07	37.24
3	1390.57	34.72	36.27
4	1454.76	36.16	37.94
5	1429.52	35.56	37.29

In the Fig. 3 is shown the result of the simulation under 1400 N load. Specimens after tensile tests are shown in the Fig. 4. If we look closer to both figures, it can be clearly seen that area with maximal von Mises stress and area of real break corresponds. Even every specimen was broken at the same area. This indicates that we can use 3D printing for manufacturing series of parts with the almost the same properties.

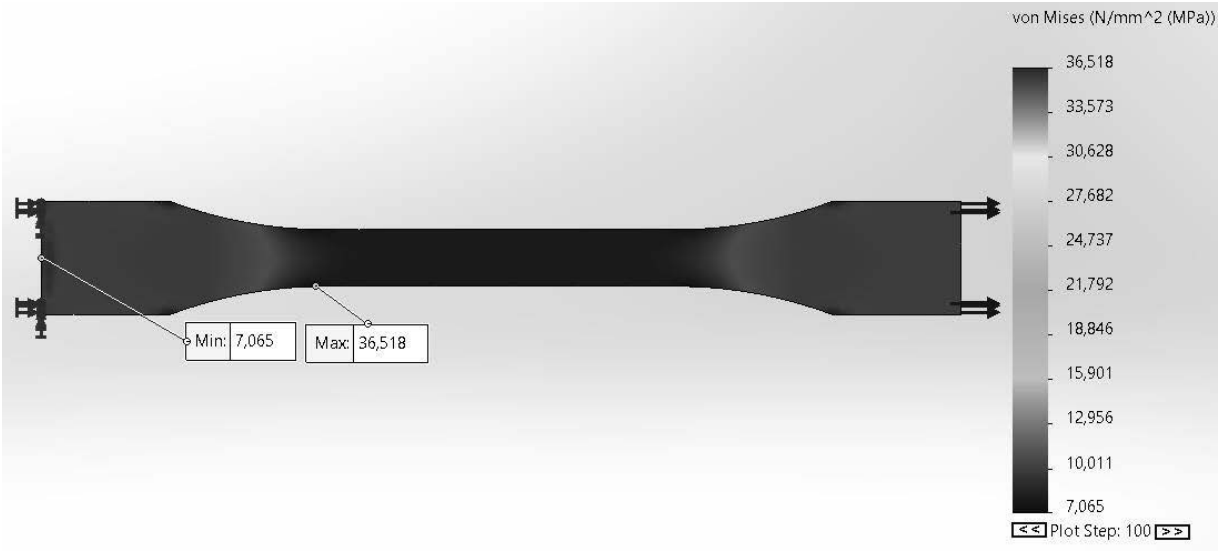

Fig. 3 Result of the simulation with load force 1400 N

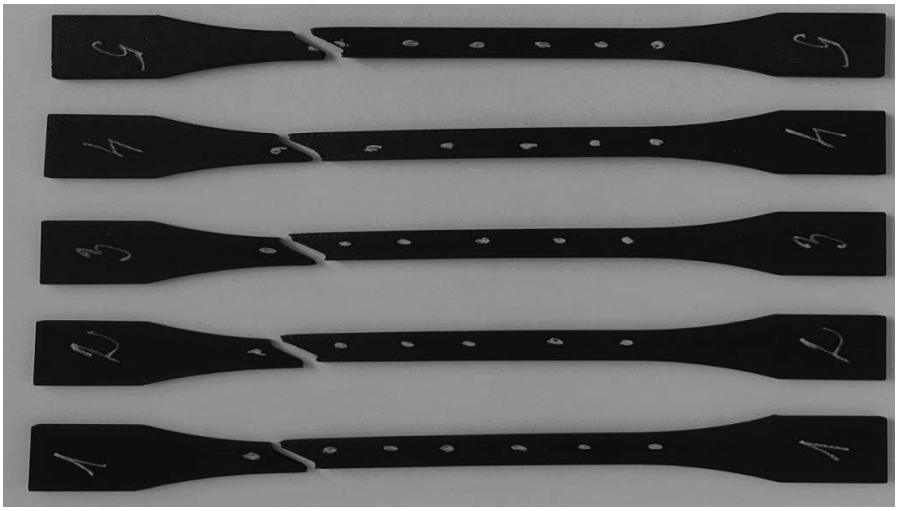

Fig. 4 Specimens after tensile tests

Some authors have done similar researches but they used other material, mostly PLA. We focused on Markforged Onyx material. For example (*Catana & Mihai, 2020*) were comparing results of experiment with results obtained by simulation. They had similar results and the deviation was between 4.7% and 7.2%. *Catana et al. (2021)* also studied the differences between simulation and experimental result but in this case they did bending tests. Despite this fact, differences between simulation and experiment were also up to 10 %. *Alhabri et al. (2020)* studied tensile strength of PLA. They used specimens with different dimensions, but they used the same software Solidworks as we used. They also had similar results, where the deviation of tensile strength was up to 6.7%. Also authors like *Mouti et al. (2011)* or *López et al. (2017)*, who used different testing methods in their researches, had similar differences between experiment and simulation results. All these authors used material properties for simulation obtained from experimental tests of 3D prints. Material properties we used for simulation were from the datasheet of Onyx material. Nevertheless our results almost correspond to results from authors mentioned above. This can be caused by fact that Markforged has closed system. Also, in a Markforged printer you can use material only from Markforged and the printer does not have option to change key printing parameter like printing temperature. Marforged has printing parameters set exactly to their materials, so quality of 3D prints is on high level and properties of 3D prints almost reach properties of filament.

CONCLUSIONS

We can conclude that the simulation process can be applied to 3D printed objects with good results. The results obtained from the simulation are in a line with the results obtained from real tensile tests, but it should be emphasized that their accuracy depends on the model used in the simulation process and how accurately it describes the 3D-printed structure. In this research were used specimens with 100% infill. They had the same properties in whole volume and they work like single block. Tensile tests results were consistent and the standard deviation was 0.67. This corresponds with fact that the technology of 3D printing has potential to repeatedly manufacture parts with the same mechanical properties. Results obtained by the FEA analysis in comparison to the real tests have only small deviation from 4.12% to 6.19% from results obtained by experiment.

ACKNOWLEDGMENT

This study was supported by project KEGA no. 003SPU-4/2021 “An Innovation of Study Programs using New Education Methods and Advanced Manufacturing Technologies.”

REFERENCES

1. Alhabri, M., Kong, I., & Patel, V. I. (2020). Simulation of uniaxial stress - strain response of 3D-printed polylactic acid by nonlinear finite element analysis. *Applied Adhesion Science*, 8, 5.
2. Catana, D., & Pop, M. A. (2020). Studies regarding simulation process to static loading of the structures obtained from polylactic acid, 3D printed. *Appliead polymer science, 138*(6), 50036.
3. Catana, D., Pop, M. A., & Brus, D. I. (2021). Comparison between the Test and Simulation Results for PLA Structures 3D Printed, Bending Stressed. *Molecules, 26*, 3325.
4. Jain, P. K., Sattar, S., Mulqueen, D., Pedrazzoli, D., Kravchenko, S. G., & Kravchenko, O.G. (2022). Role of annealing and isostatic compaction on mechanical properties of 3D printed short glass fiber nylon composites. *Additive Manufacturing, 51*, 102599.
5. 14. Kalova, M., Rusnakova, S., Krzikalla, D., Mesicek, J., Tomasek, R., Podeprelova, A., Rosicky, J., & Pagac, M. (2021). 3D Printed Hollow Off-Axis Profiles Based on Carbon Fiber-Reinforced Polymers: Mechanical Testing and Finite Element Method Analysis. *Polymers 13*, 2949.
6. Kumar, S. A., & Prasad, R. V. (2021). Basic principles of additive manufacturing: different additive manufacturing technologies. *Additive Manufacturing: A Tool for Industrial Revolution 4.0*, 17-35.
7. Kuncius, T., Rimašauskas, M., & Rimašauskiene, R. (2021). Interlayer Adhesion Analysis of 3D-Printed Continuous Carbon Fibre-Reinforced Composites. *Polymers, 10*, 1653.
8. López, I. G., Chiné, B., & León, J. (2017). FEM Modeling of a 3D Printed Carbon Fiber Pylon. *Proceedings of the COMSOL Conference, 18-19.*
9. Madaj, R., & Kohár, R. (2020). Additive technologies (in Slovak). Žilinská univerzita, Žilina.
10. Majko, J., Saga, M., Vasko, M., Handrik, M., Barnik, F., & Dorčiak, F. (2019). FEM analysis of long-fibre composite structures created by 3D printing. *Transportation Research Procedia, 40*, 792-799.
11. Marforged, "Mark two (Gen 2)", product specification, July 2022a.
12. Markforged, "Composites", material datasheet, January 2022b.
13. Morgan, P 2005, Carbon fibers and their composites, Boca Raton, Florida, CRC Press.
14. Provaggi E., Capelli C., Rahmani B., Burriesci G., Kalaskar D. M. (2019). 3D printing assisted finite element analysis for optimising the manufacturing parameters of a lumbar fusion cage. *Materials & Design*, 163,107540.
15. Mouti, Z., Westwood, K., Long, D., & Njuguna, J. (2017). Finite element analysis of localised impact loading on short glass fibrereinforced polyamide engine oil pan subjected to low velocity impact from flying projectiles. *Steel Research International, 83, 957-963.*
16. Zhou, S. M., Tashiro, K., & Tadaoki, I. (2001). Moisture Effect on Structure and Mechanical Property of Nylon 6 as Studied by the Time-Resolved and Simultaneous Measurements of FT-IR and Dynamic Viscoelasticity under the Controlled Humidity at Constant Scanning Rate. *Polymer Journal, 33*(4) 344-355.

Corresponding author:
Ing. Patrik Kósa, PhD. Institute of Design and Engineering Technologies, Slovak University of Agriculture in Nitra, Tr. A. Hlinku 2, 94976 Nitra, Slovak Republic, phone: +421 37 641 4104, e-mail: patrik.kosa@uniag.sk

QUANTIFYING THE TRAFFIC FOOTPRINT OF ZERO-TILLAGE SYSTEMS

Guido F. BOTTA[1], Gustavo F. NARDON[2], David RIVERO[3], Mauro E. REMERSARO[4], Enrique E. CONTESSOTTO[1], Fernando BIENVENIDO[5], Diego G. GHELFI[1], Diogenes L. ANTILLE[6,*]

[1]*Universidad Nacional de Luján, Departamento de Tecnologia, Lujan, Buenos Aires, Argentina.*
[2] *Universidad Nacional de Rosario, Facultad de Ciencias Exactas, Ingeniería y Agrimensura, Rosario, Santa Fe, Argentina.*
[3]*Universidad Nacional de La Pampa, Facultad de Agronomía, Santa Rosa, La Pampa, Argentina.*
[4]*Campos de Keen S.A., Lujan, Buenos Aires, Argentina.*
[5]*Universidad de Almería, CIMEDES, Facultad de Ciencias Económicas y Empresariales, Almería, Spain.*
[6]*CSIRO Agriculture and Food, Canberra, Australian Capital Territory, Australia.*

Abstract
This work was conducted to determine the area of a field trafficked by farm machinery over a cropping season. The case-study field had been established to wheat and managed under zero-tillage for over 10 years, and the soil type was a Typic Argiudoll. Measurements showed that the total wheeled area was 12-ha, representing 68% of the 19-ha field used for the study. Given that operating and track gauge widths of different the machinery did not match, and field traffic was random, the total area of the field affected by traffic over the rotation cycle could be greater than the area reported in this study (single-season). Adoption of controlled traffic farming, with fully matched machinery, could reduce the area affected by traffic from current 68% to less than 20% depending upon the design of the system, which will help optimize field efficiency and logistics, reduce fuel-use and labour, and lift productivity.

Key words: *controlled traffic farming; no-tillage; random traffic; soil compaction; wheeled soil.*

INTRODUCTION

The arable land area established to wheat in Argentina is estimated to be approximately 7 M ha per year, and more than 90% of this area is managed under permanent zero-tillage (ZT). The soils in the main wheat-growing region of Argentina are susceptible to compaction, and the risk of compaction occurring is exacerbated by the timing of field operations, and the combined effects of vehicle mass and wheel configuration, with most mechanization systems managed without controlled traffic. Previous studies in Argentina (e.g., *Botta et al., 2007*) have shown that traffic intensities in ZT cropping systems can be as high as 40 Mg km^{-1} ha^{-1} and given typical rotation cycles (e.g., wheat/soybean, 12 months), the opportunities for alleviation of such compaction through natural processes are therefore limited. The adverse effects of compaction on the soil physical and hydraulic properties are well documented, and affect crop yield and therefore the profitability and sustainability of farming (*Soane et al., 1982*). In rainfed agriculture, the effect of compaction on yield is can be more significant in dry years (*Hussein et al., 2021a-b*). Whilst adoption of zero- and reduced tillage systems has enabled field traffic to be significantly reduced compared with conventional tillage systems that require primary and secondary tillage operations for crop establishment, the overall traffic footprint measured as a percentage of field-cropped area can be still large (e.g., 40-60%), as shown by several studies outside Argentina (e.g., *Chamen, 2015*). Such traffic footprints mean that the benefits of ZT may not be fully realized (*Antille et al., 2015*). The objective of this work was to estimate the total area of a field wheeled over a single cropping season. The work was conducted on a commercial field that had been managed under ZT and without controlled traffic for more than 10 years. Results derived from this work may be used to increase awareness of the extent and potential impact of field traffic on soil and encourage farmers in Argentina to consider options for converting to controlled traffic farming.

MATERIALS AND METHODS

The study was conducted on a commercial farm located near Lujan (Buenos Aires, Argentina) during the 2021 winter season (Figure 1). The soil at the site is a Typic Argiudoll with 22% clay, 73% silt and 5% sand in the top 0-200 mm depth interval. The 19 ha field had been managed under continuous zero-

tillage for more than ten years. The crops typically grown at the site are wheat (Triticum aestivum L.), established in late June to early July and harvested in December, followed by soybean (Glycine max L.), established immediately after wheat and harvested mid-May. The specifications of the equipment used in the study are presented in Table 1.

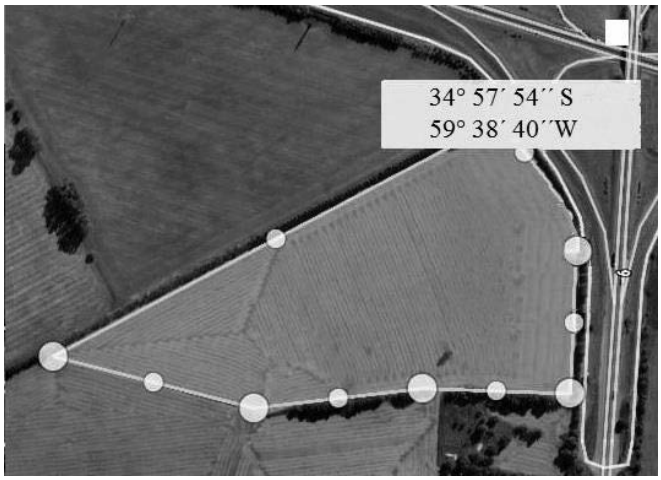

Fig. 1 Aerial view and GPS coordinates of the commercial field used for the study

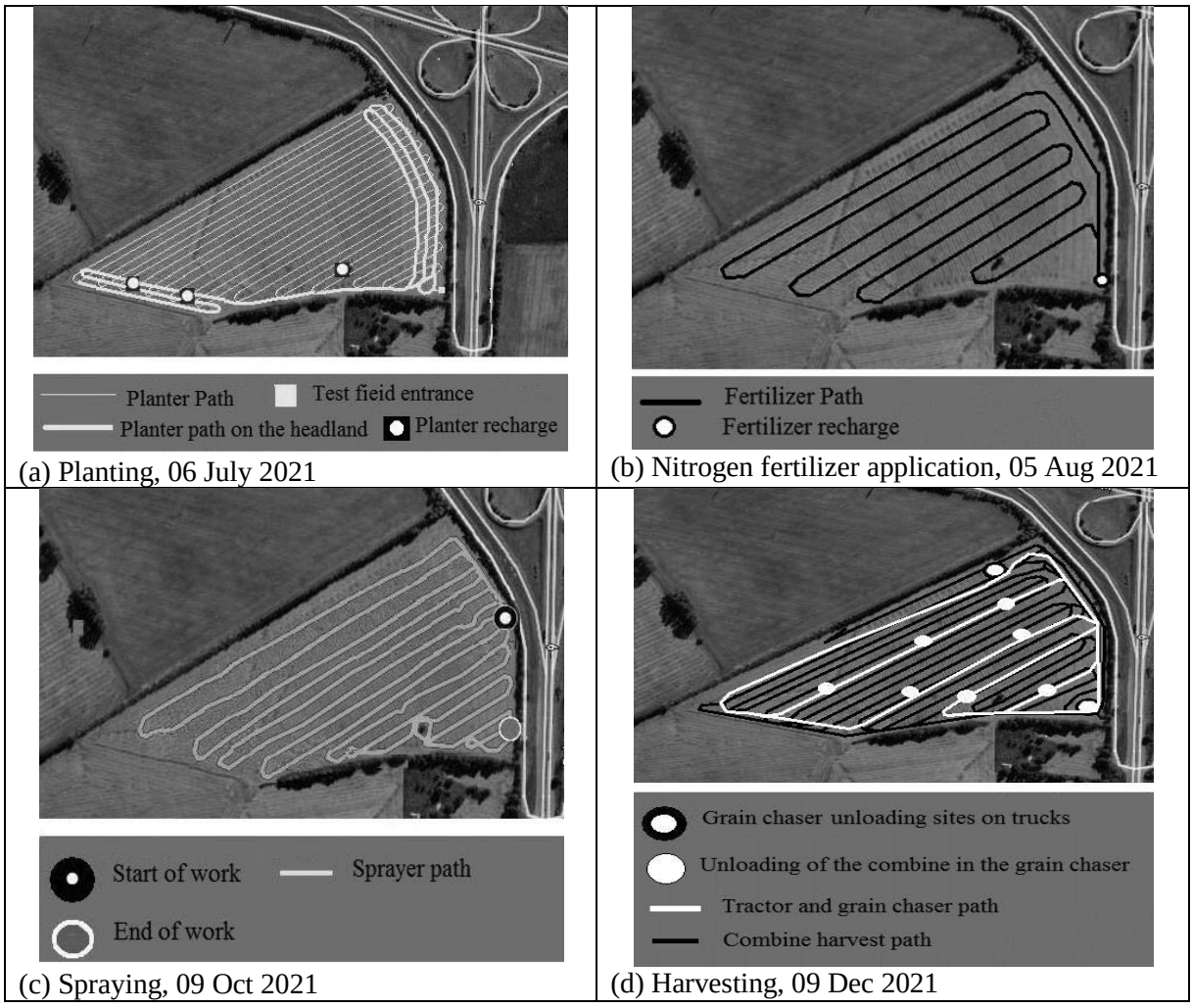

(a) Planting, 06 July 2021

(b) Nitrogen fertilizer application, 05 Aug 2021

(c) Spraying, 09 Oct 2021

(d) Harvesting, 09 Dec 2021

Fig. 2 Vehicle's trajectories

Tab. 1 Specifications of the farm equipment used in the study

Equipment	Brand/Model	Rear tires	Front tires	Width, m	Load, kN
FWA Tractor	CASE 200	710/70 R38	600/45 R28	-	74.67
FWA Tractor	JD6600	23.1-30	16.9/14-24	-	45.57
Combine harvester	CASE 2388	19.5-24	800/65 R32	9	93.10
Sprayer	Metalfor 7030	320/85 R36 (all tires)		28	90.16
Fertiliser applicator	Fertec	12.4-36 (all tires)		28	68.60
Planter	Crucianelli 3520	400/60-18 (all tires)		7	111.23
Chaser bin	AGROMEC	21L30 (single axle)		-	137.20

All vehicles used in the field from planting to harvest were equipped with a DGPS signal receiver, which enabled trajectories within the field to be mapped. Wheeled areas were subsequently estimated by multiplying the total distance travelled by each vehicle by two times the section width of the tires fitted to corresponding vehicle. For the two tractors, the section width was given by the wider (rear) tires; this was possible because the tires fitted on the front and rear axles are aligned. Field trajectories were drawn for each operation conducted in the field and super-imposed to the aerial image of the field. The area affected by traffic was estimated for each operation as percentage of the field cropped area; the sum of which returned the traffic footprint across all operations performed during the season.

RESULTS DISCUSSION

Vehicle's trajectories are shown in Figures 2a-d for each operation performed between, and including, planting and harvesting. Table 2 shows the calculated wheeled areas for each operation.

Tab. 2 Wheel tracked areas for all field operations (ha), and expressed as a percentage of the field-cropped area

Field operation	Area, ha	% of field-cropped area
Planting	6.69	35.20
Fertilizer application	0.36	1.89
Spraying	0.54	2.85
Harvesting	5.36	28.20
Total	12.95	68.14

The total area affected by traffic was greater than that reported in other studies in Europe (e.g., *Galambošová et al., 2017*), Australia (e.g., *Tullberg et al., 2007; Antille et al., 2019*) and Argentina (e.g., *Botta et al., 2007, 2022*) for ZT systems, which was attributed to the configuration of the equipment used in this study. The total wheeled area estimated by this study could be reduced to less than 20% through the adoption of controlled traffic farming (CTF). This would require modification of the farm equipment to fit a common track gauge width that matches that of the combine harvester (3-m wheel spacing, single tire configuration), and by enabling all equipment to operate in modules that have; for example, a 3:1 ratio (that is, sprayer/fertilizer applicator-to-planter/combine harvester). For the equipment listed in Table 1, this means that the planter should be 9-m wide to match the cutter front of the combine harvester. The operating width of the sprayer and fertilizer applicator would need to be reduced from 28 to 27 m. Conversion from the current unmatched mechanization system to a fully matched CTF system should be considered as part of the machinery replacement program over a timeframe that is economical and compatible with the farming enterprise.

CONCLUSIONS

The total wheeled area estimated in this study over a single cropping season represented approximately two-thirds of the field-cropped area. This wheeled area could be reduced to less than 20% with careful planning and modification of the equipment to meet the specifications of a fully matched controlled traffic farming (CTF) system operated at 3-m center and 9-m base module with a 3:1 ratio (planter/combine harvester-to-sprayer rig/fertilizer applicator). Conversion to a fully matched CTF system needs to be considered as part of the machinery replacement program over a timeframe that is economical and

compatible with the farming enterprise. Based on other studies in Argentina, adoption of CTF could lift productivity by a conservative 12%-15%, while reducing inter-annual yield variability and improving fuel-use efficiency and the timelines of field operations.

ACKNOWLEDGMENTS
This study received financial support from Facultad de Agronomia at Universidad Nacional de La Pampa (Santa Rosa, La Pampa, Argentina) through Project ID: I-153/19-FA. Operational support received from Campos de Keen S.A., on whose property this study was conducted, is gratefully acknowledged.

REFERENCES

1. Antille, D.L., Imhoff, S.C., Alesso, C.A., Chamen, W.C.T., & Tullberg, J.N. (2015). Potential to increase productivity and sustainability in Argentinean agriculture with controlled traffic farming: a short discussion. *Acta Technologica Agriculturae* 18(3): 83-87.
2. Antille, D.L., Peets, S., Galambošová, J., Botta, G.F., Rataj, V., Macák, M., Tullberg, J.N., Chamen, W.C.T., White, D.R., Misiewicz, P.A., Hargreaves, P.R., Bienvenido, J.F., & Godwin, R.J. (2019). Review: Soil compaction and controlled traffic farming in arable and grass cropping systems. *Agronomy Research* 17(3): 653-682.
3. Botta, G.F., Antille, D.L., Nardon, G.F., Rivero, D., Bienvenido, F., Contessotto, E.E., Ezquerra-Canalejo, A., & Ressia, J.M. (2022). Zero and controlled traffic improved soil physical conditions and soybean yield under no-tillage. *Soil Tillage Research* 215, Article number: 105235.
4. Botta, G.F., Pozzolo, O., Bomben, M., Rosatto, H., et al. (2007). Traffic alternatives in harvest of soybean (*Glycine max* L.): effect on yields and soil under direct sowing system. *Soil Tillage Research* 96 (1-2): 145-154.
5. Chamen, T. (2015). Controlled traffic farming – from worldwide research to adoption in Europe and its future prospects. *Acta Technologica Agriculturae* 18(3): 64-73.
6. Galambošová, J., Macák, M., Rataj, V., Antille, D.L., Godwin, R.J., Chamen, W.C.T., Žitňák, M., Vitázková, B., Ďuďák, J., & Chlpík, J. (2017). Field evaluation of controlled traffic farming in Central Europe using commercially available machinery. *Transactions of the ASABE* 60(3): 657-669.
7. Hussein, M.A., Antille, D.L., Kodur, S., Chen, G., & Tullberg, J.N. (2021a). Controlled traffic farming delivers improved agronomic performance of wheat as a result of enhanced rainfall and fertilizer nitrogen use efficiency. *Acta Agriculturae Scandinavica Section B: Soil Plant Science* 71(5): 377-398.
8. Hussein, M.A., Antille, D.L., Kodur, S., Chen, G., Tullberg, J.N. (2021b). Controlled traffic farming effects on productivity of grain sorghum, rainfall and fertiliser nitrogen use efficiency. *Journal of Agriculture and Food Research* 3, Article number 100111.
9. Soane, B.D., Dickson, J.W., & Campbell, D.J. (1982). Compaction by agricultural vehicles: a review III. Incidence and control of compaction in crop production. *Soil Tillage Research* 2(1): 3-36.
10. Tullberg, J.N., Yule, D.F., & McGarry, D. (2007). Controlled traffic farming from research to adoption in Australia. *Soil Tillage Research* 97 (2): 272-281.

Corresponding author:
Dr Diogenes L. Antille, CSIRO Agriculture and Food, Canberra, Australian Capital Territory, Australia.
E-mail: Dio.Antille@csiro.au

EXPERIMENTAL DETECTION OF THE PELLETS DRYING CHARACTERISTICS

Monika BOŽIKOVÁ[1], Matúš BILČÍK[1], Ján CSILLAG[1], Tomáš HOLOTA[2], Maroš SZENTESI[2]

[1]*Institute of Electrical Engineering, Automation, Informatics and Physics, Faculty of Engineering, Slovak University of Agriculture in Nitra, Slovakia*
[2]*Institute of Agricultural Engineering, Transport and Bioenergetics, Faculty of Engineering, Slovak University of Agriculture in Nitra, Slovakia*

Abstract
The article is focused on the experimental detection of pellets drying characteristic. Experimentally were examined pellets made on pelletizing line MGL 200. The mass losses during the drying process were measured by Radwag MAC 210. Five pellet samples with different content of wheat straw and poppy capsules in initial material were investigated. The reference sample was pellet with natural moisture content and its characteristics were compared with pellets which have simulated moisture content. The measurements results were graphically processed and the time relations, regression equations for the mass loss were created. The results for mass losses of pellets with different moisture content were calculated and statistically processed. Presented drying curves declare nonlinear decreasing progresses. The biggest difference for drying curve shape was identified for samples with simulated moisture content, this sample has also the highest mass losses and finally, its structure was after drying process noncompact with visible destruction.

Key words: *simulated moisture content, mass losses, wheat straw, poppy capsules.*

INTRODUCTION

Green fuel sources have nowadays big attention (*Kažimírová, Kubik & Mihina, 2020; Nilsson, Bernesson & Hansson, 2010*). Nowadays, material of biological origin is largely processed into pellets, which have better physical properties and, above all, energy recovery in practice (*Pradhan, Arora & Mahajani, 2018*). Pellets are used for two primary sectors: industrial sector (substitute for coal in power plants), and residential sector for domestic heating. Usages of pellets have had significant growth in the past decade (*Pradhan et al., 2019*). Pellets have many advantages from the physical properties point of view, for example high bulk density, low moisture content and the high stability of energetic parameters (*Caroll & Finnan, 2012*). Next advantage is transport costs. Pellets have less volume to handle and facilitate less storage and transportation due to its high energy content than straw, chips etc. than other raw biomass (*Zamorano et al., 2011*). From the practical point of view is very important to know the influence of moisture changes on bio-based materials, especially on energetically usable products made from agricultural and food waste (*Vladut et al., 2010*). The way of processing, storage and pellets energetic characteristics is significantly affected by the moisture content of input material, this fact was presented by *Castellano et al., (2015); Ishii, & Furuichi, (2014)*. The moisture content is in relationship with pellet durability, which was discussed in detail by authors *Whittaker & Shield (2017)*. High moisture content of pellets has negative effect on the pellets performance by reducing the net energy output during combustion and generating high emissions of air pollutants (*Serrano et al., 2011; Unpinit et al., 2015*). The optimum moisture content of input material is important for palletization (*Golinski & Foltynowicz, 2012*). Storage conditions are affected and have effect on the material moisture content changes (*Graham et al., 2017*). Usage of non-adequate storage conditions leads to increase in the moisture content of the pellets and eventually deteriorating the physico-chemical properties of the pellets (*Bennamoun, Simo-Tagne, & Ndukwu, 2020*). For determining the ideal storage conditions, it is important to know the moisture adsorption behaviour of the pellets during storage at different conditions (*Lee et al., 2021*). Based on the presented facts from literature the next important aim of this research is determination of the original wheat and poppy capsules pellet's moisture content influence on its structure and drying characteristics. The originality of the research is declared by using of non-standard material to produce pellets. Pellets made from poppy capsules are one of the possibilities of energy recovery of agricultural waste.

MATERIALS AND METHODS

Measured samples were made from the agricultural waste, especially wheat straw and poppy capsules. The 1st sample was made from 100% wheat straw with moisture content 10.2% and the 5th sample was processed from poppy capsules with moisture content 12.8%. Next three samples (marked as Sample 2 – 4) had different fraction of poppy capsules and wheat straw in the input material (e.g., 25% poppy capsules and 75% wheat straw, 50% poppy capsules and 50% wheat straw, 75% poppy capsules and 25% wheat straw). The agricultural waste was mixed and then it was processed to the pellets by pelleting device MGL 200 (Kovo Novák Znojmo, Czech Republic). The final pellets had the moisture content in range (3.97 – 5.95) %. Before the experimental examination they were stabilized in the laboratory settings with the ambient temperature 21 °C and the relative air humidity 50%. The mass of the pellets was determined using laboratory scales Libra Axis AG100C (Libra Ltd., Podunajské Biskupice, Slovakia) with accuracy 1 mg. The moisture content of samples was identified by gravimetric method. The samples were dried by laboratory dryer at the temperature (103 ± 2) °C and then the relative moisture content was calculated from Eq. (1)

$$MC = \frac{m_\omega - m_0}{m_\omega} \cdot 100 = \frac{m_w}{m_\omega} \cdot 100 \quad (1)$$

where: m_ω – is mass of the wet sample, m_0 – is the mass of dry sample and m_w– is the mass of water. The samples of pellets were before experimental identification of the dried curves exposed to humid environments for 5 days in laboratory settings. The moisturizing of pellets was used for the simulation of increasing ambient humidity. The humid weather can cause the destruction of the pellets compact structure during the storage.

The pellets were moistened by spontaneous evaporation of water in an enclosed space. Distilled water was used as the humidifying liquid. The pellets were not in direct contact with the liquid. (Fig. 1A). The drying curves were experimentally detected by the moisture analyser Radwag MAC 210 (Fig. 1B) (Radwag Ltd., Radom, Poland). The temperature during continuous drying process was 150 °C ± 2 °C. The samples were measured until their mass changed by 1 milligram over 240 seconds. Then the moisture analyser automatically stopped the drying process. The final drying product can be considered as the dry matter of the pellets sample. The accuracy of mass measurement by MAC 200 was 1 mg. Experimentally were obtained parameters as: diameter of pellets, length of pellets, initial mass, final mass and the mass changes during the drying process, time, total time duration of the drying process. Calculated were parameters as: relative moisture content, the standard deviation, the probable error of arithmetic average in %, average mass loss per minute and the difference of relative moisture content of pellets. Experimental data were numerically processed and statistically evaluated by program Statistica® (TIBCO Software Inc., California, USA).

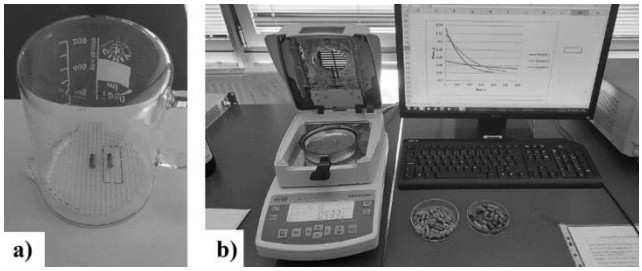

Fig. 1 a) Moistening of pellets samples, b) Detection of drying curves by moisture analyser MAC 210

RESULTS AND DISCUSSION

At the first were measured diameters of pellet samples, the length of pellets was in range (7.88 – 23.04) mm. The initial mass of samples was minimal 0.452 g for straw pellets with natural moisture content 6.4% and the maximal initial mass 0.698 had samples made from the poppy capsules with moisture content 5.014%. From initial and final mass of pellets were calculated total mass losses (Tab. 1). The other experimentally detected characteristics of pellet samples with different fraction of poppy capsules and wheat straw in the input material are summarised in the Tab. 1. From presented numerical values is

clear that minimal experimentally detected mass loss was 0.029 g for wheat pellet and the maximal mass loss was obtained for pellet made from poppy capsules. The drying process for pellet sample made from 100% wheat straw – 1b (sample with natural moisture content and then moistened) taken longer time 398 s than the same process for sample 1a. This sample was completely dried with moisture analyser and then were selected samples laboratory moistened. The drying time depended on the type of sample. For pellets samples with natural moisture was the drying time 583 s (pellets from wheat straw), (627 – 715) s for the mix (wheat straw and poppy capsules) and 743 s for pellets made only from poppy capsules. For simulated moisture content, drying times of 399 s (pellets from 100% wheat straw), (421 - 486) s (mix) and 508 s (pellets from 100% poppy capsules) were achieved.

Tab. 1 Experimental results for pellet samples with the different content ratio of wheat straw and the poppy capsules in the input material

Pellet composition		Initial mass g			Final mass g			Total mass loss g			Initial relative moisture content of sample %		
Wheat straw	Poopy capsules										Natural MC	Simulated MC	
100%	0%	1	1a	1b	1	1a	1b	1	1a	1b	1	1a	1b
		0.452	0.532	0.517	0.423	0,423	0.426	0.029	0.109	0.091	6.416	20.489	17.602
75%	25%	2	2a	2b	2	2a	2b	2	2a	2b	2	2a	2b
		0.552	0.547	0.524	0.519	0.439	0.436	0.033	0.108	0.088	5.978	19.744	16.794
50%	50%	3	3a	3b	3	3a	3b	3	3a	3b	3	3a	3b
		0.601	0.596	0.573	0.567	0.483	0.481	0.034	0.113	0.092	5.657	18.961	16.056
25%	75%	4	4a	4b	4	4a	4b	4	4a	4b	4	4a	4b
		0.654	0.641	0.639	0.619	0.532	0.541	0.035	0.109	0.099	5.352	17.005	15.493
0%	100%	5	5a	5b	5	5a	5b	5	5a	5b	5	5a	5b
		0.698	0.683	0.668	0.663	0.569	0.568	0.035	0.114	0.100	5.014	16.569	14.971

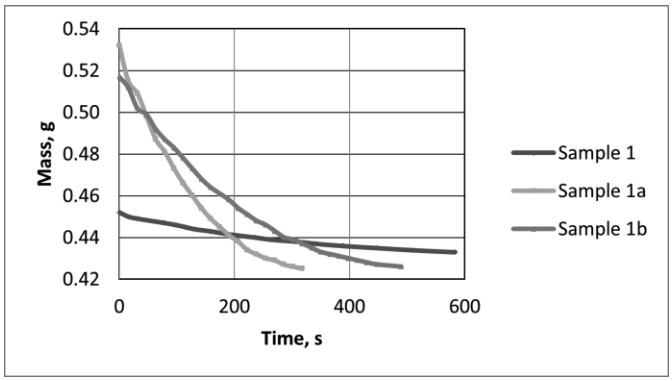

Fig. 2 Pellets drying curves: 1 – sample with natural moisture content, 1a – sample completely dried with moisture analyser before the moistened, 1b – pellet with natural moisture content and then moistened

From Fig.2 is evident, that the mass losses of the straw pellet sample 1b was more moderate during the drying process. The drying curves had nonlinear shape, which can be described by polynomial function of the second degree – Eq. (2), but the regression coefficient of quadratic term is too small. The regression coefficients for all measured pellet samples are presented on Tab. 2. The coefficients of determination for all detected graphical dependencies were in range (0.9662 – 0.9987).

$$m = A\,t^2 - Bt + C \qquad (2)$$

Measurement results for pellets drying curves agree with facts described in drying theory (*Selivanovs et al., 2012; Li et al., 2011*) and experimental results for bio-based materials presented by *Lambert et al.,*

(2018); Gebreegziabher, Oyedun & Hui (2013). In general, second and higher order polynomial functions are presented in the literature (*Azaka, Enibe & Achebe, 2019*) for the description of drying curves. From the mathematical description point of view and the influence of the individual regression coefficients on the shape of the displayed model dependence, the polynomial function of the second degree, which is also presented by the authors *Wang et al., (2012)* in their works, can be considered optimal.

Tab. 2 Coefficients of regression equation for drying curves of pellets

Pellet composition		Sample with natural MC			Sample with simulated MC Type of pellet a			Sample with simulated MC Type of pellet b		
Wheat straw	Poopy capsules	A $g \cdot s^{-2}$	B $g \cdot s^{-1}$	C g	A $g \cdot s^{-2}$	B $g \cdot s^{-1}$	C g	A $g \cdot s^{-2}$	B $g \cdot s^{-1}$	C g
100%	0%	$5 \cdot 10^{-8}$	$6 \cdot 10^{-5}$	0.4511	$1 \cdot 10^{-6}$	0.0006	0.526	$4 \cdot 10^{-7}$	0.0004	0.5155
75%	25%	6.1·10, $^{-8}$	$7.31 \cdot 10^{-5}$	0.5503	$1.02 \cdot 10^{-6}$	0.00061	0.537	$4 \cdot 10^{-7}$	0.0004	0.5206
50%	50%	$6.65 \cdot 10^{-8}$	$7.98 \cdot 10^{-5}$	0.5998	$1.12 \cdot 10^{-6}$	0.000672	0.589	$4.4 \cdot 10^{-7}$	0.00044	0.5722
25%	75%	$7.2 \cdot 10^{-8}$	$8.64 \cdot 10^{-5}$	0.6494	$1.21 \cdot 10^{-6}$	0.00072	0.6312	$4.94 \cdot 10^{-7}$	0.000492	0.6371
0%	100%	$7.7 \cdot 10^{-8}$	$9.24 \cdot 10^{-5}$	0.6931	$1.28 \cdot 10^{-6}$	0.000768	0.673	$5.16 \cdot 10^{-7}$	0.00051	0.666

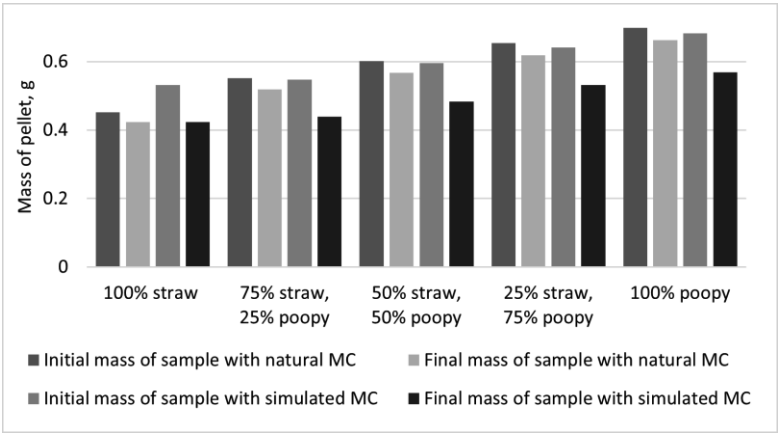

Fig. 3 Comparison of pellet´s initial and final mass for samples with natural and simulated MC

The similar graphical relations of the drying curves were obtained for pellet samples made from combination of initial material (wheat straw and poppy capsules), but the individual values differed. Based on presented facts were calculated the average differences between the mass values detected for points on the experimental curve. The differences were calculated with respect to the values obtained for sample of pellets made from 100% wheat straw.

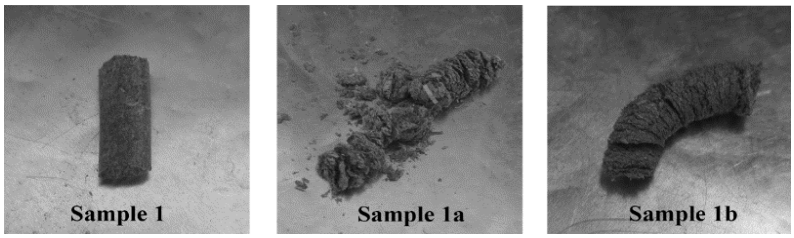

Fig. 4 Pellets samples after the drying process: 1 – sample with natural moisture content, 1a – sample dried with completely moisture analyser before the moistened, 1b – pellet with natural moisture content and then moistened

The graphical comparison of the initial and the final mass for selected pellets with poppy capsules content ratio are shown on the Fig. 3. From Fig. 3 is evident, that the pellets mass increases with increased percentage ratio of poppy capsules content. This fact was confirmed by repeating a series of 10 measurements for each pellet sample. The results were statistically processed by program Statistica®. The standard deviations were from ±0,00055 g to ±0,0034 g and the probable errors of arithmetic average were in range (0.693 – 2.184)%.
Furthermore, the constancy of the pellet samples compactness was monitored after processes that simulated the change in the moisture. As shown in Figure 4, sample 1a (dried to dryness and then moistened) disintegrated. Sample 1b, which originally had natural moisture content and was subsequently subjected to a simulated increase in moisture, did not disintegrate. Despite the relative preservation of the pellet compactness, changes in its structure are evident from Figure 4 – 1a. It follows from the mentioned facts that due to the repeated application of thermal processes (or changes in temperature), which result in repeated changes in moisture content, a permanent change in the pellet structure may occur. The presented results correspond to the results presented in the literature (*Graham et al., 2017; Cutz et al., 2021*), who also observed changes in the compactness of the pellet structure because of heat-moisture stress.

CONCLUSIONS

The research benefit was the identification of the moisture changes on the mass characteristics of pellets made from a non-standard combination of input raw materials, namely wheat straw and poppy capsules. The results obtained for poppy capsules can be considered original and innovative, as they have not been presented so far. The main result of the work was finding out the drying curves of pellet samples made from combination of wheat straw and poppy capsules. Results pointed to the relevant influence of the input material composition to drying process. Drying process can be described by nonlinear drying curves. Graphical course of curves depends on the ratio of input material. Drying curves can be mathematically described by polynomial function of the second degree. Furthermore, the influence of the method of moistening on the input mass of the pellets and its dry matter was confirmed. In general, it was confirmed that the input mass of the pellets increases with the increasing proportion of poppy capsules in the input raw material. On the contrary, the mass losses decrease with the increasing content of poppy capsules in the pellet. The presented differences are influenced by the chemical and physical properties of poppy capsules, which differ significantly from the composition of wheat straw. Research results confirmed, that both materials are well usable for the production of pellets. However, optimal moisture and temperature conditions must be ensured during the processing, handling and storage of the material. This fact was confirmed by observing visible structural changes after repeated simulation of moisture changes. The results of the research can be used in the optimization of the conditions of storage and handling of the pellets, to ensure its required quality.

ACKNOWLEDGMENT

This study was supported by the Operational Program Integrated Infrastructure within the project: Demand-driven research for the sustainable and innovative food, Drive4SIFood 313011V336, cofinanced by the European Regional Development Fund.

REFERENCES

1. Azaka, O. & Achebe, Ch. (2019). Determination of Moisture Diffusivity during Drying of Rectangular Cassava Pellets: Experimental and Modeling Study. *Journal of Engineering and Applied Sciences*, *15*, 56-63.
2. Bennamoun, L., Simo-Tagne, M., & Ndukwu, M.C. (2020). Simulation of Storage Conditions of Mixed Biomass Pellets for Bioenergy Generation: Study of the Thermodynamic properties. *Energies*, 2020, *13*, 2544.
3. Caroll, J. P. & Finnan, J. (2012). Physical and chemical properties of pellets from energy crops and cereal straws. *Biosystems Engineering*, 112, 151-159.
4. Castellano, J.M., Gomez, M., Fernandez, M., Esteban, L.S. & Carrasco. J.E. (2015). Study on the effects of raw materials composition and pelletization conditions on the quality and properties of pellets obtained from different

woody and non woody biomasses. *Fuel*, *139*, 629-635.
5. Cutz, L., Tiringer, U., Gilvari, H., Schott, D., Mol, J.M.C. & Jong, W. (2021). Microstructural degradation during the storage of biomass pellets. *Communications Materials*, *2*(1), 1-12.
6. Golinski, T. & Foltynowicz, Z. (2012). Pellet – a Key to Biomass Energy; *International Journal of Economic Practices and Theories*, *2*(4), 197-204.
7. Graham, S., Eastwick, C., Snape, C. & Quick W. (2017). Mechanical degradation of biomass wood pellets during long term stockpile storage. *Fuel Processing Technology*, *160*, 143-151.
8. Gebreegziabher, T., Oyedun, A. & Hui, D. (2013). Optimum biomass drying for combustion – A modeling approach. *Energy*, *53*, 67-73.
9. Ishii, K. & Furuichi, T. (2014). Influence of moisture content, particle size and forming temperature on productivity and quality of rice straw pellets. *Waste Management*, *34*, 2621-2626.
10. Kažimírová, V., Kubik, L. & Mihina, S. (2020). Evaluation of Properties of Pellets Made of Swine Manure. *Acta Technologica Agriculturae*, *23*(1), 137-143.
11. Lambert, Ch., Cartailler, J., Rouchouse, S., Almeida, G. & Courtois, F. (2017). Characterization and Modeling of Cooling and Drying of Pellets for Animal Feed. *Drying Technology*, *36*, 255-266.
12. Lee, J.S., Sokhansanj, S., Lau, A., Lim, J. & Bi, X., (2021). Moisture adsorption rate and durability of commercial softwood pellets in a humid environment. *Journal of Biosystems Engineering*, *203*, 1-8.
13. Li, H., Chen, Q., Zhang, X., Finney, K., Sharifi, V. & Swithenbank, J. (2011). Evaluation of a biomass drying process using waste heat from process industries: A case study. *Applied Thermal Engineering*, *35*, 71-80.
14. Nilsson, D., Bernesson, S. & Hansson, P. (2010). Pellet production from agricultural raw materials - a systems study. *Biomass Bioenergy*, *35*, 679-689.
15. Pradhan, P., Arora, A. & Mahajani, S.M. (2018) Pilot scale evaluation of fuel pellets production from garden waste biomass *Energy for Sustainable Development*, *43*, 1-14.
16. Pradhan, P., Gadkari, P., Arora, A. & Mahajani, S. (2019). Economic feasibility of agro waste pelletization as an energy option in rural India. *Energy Procedia*. *158*. 3405-3410.
17. Selivanovs, J., Blumberga, D., Ziemele, J., Blumberga, A. & Barisa, A. (2012). Research of Woody Biomass Drying Process in Pellet Production. *Environmental and Climate Technologies*, *10*, 46-50.
18. Serrano, C., Monedero, E., Lapuerta, M. & Portero, H. (2011). Effect of moisture content, particle size and pine addition on quality parameters of barley straw pellets. *Fuel Process Technology, 92*, 699-706.
19. Unpinit, T., Poblarp, T., Sailoon, N., Wongwicha P. & Thabuot M. (2015). Fuel properties of bio-pellets produced from selected materials under various compacting pressure. *Energy Procedia*, *79*, 657-662.
20. Vladut, V., Chitoiu, M., Danciu, A., Militaru, M. & Lehr, C. (2010). The importance of humidity on agricultural and forestry biomass in the process of pellets and agri-pellets production. *Bulletin USAMV Agriculture*, *67*(1), 292-300.
21. Wang, Z., Xiao, B., Wang, M., Zhang, J., Ding, T., Liu, X.D. & Yang, D. (2012). Drying Kinetics of Extruded Pellets in Fixed Beds. *Drying Technology*, *30*(16), 1881-1889.
22. Whittaker, C., & Shield, I., (2017). Factors affecting wood, energy grass and straw pellet durability–A review. *Renewable and Sustainable Energy Reviews*, *71*, 1-11.
23. Zamorano, M., Popov, V., Rodríguez, M.L. & García-Maraver, A. (2011). A comparative study of quality properties of pelletized agricultural and forestry lopping residues. *Renewable energy*, *36*(11), 3133-3140.

Corresponding author:
Ing. Matúš Bilčík, PhD., Institute of Electrical Engineering, Automation, Informatics and Physics, Faculty of Engineering, Slovak University of Agriculture in Nitra, Tr. A. Hlinku 2, SK - 949 76 Nitra, Slovak Republic, phone: +421 917 048 772,e-mail: matus.bilcik@uniag.sk

SOIL EROSION DURING SECONDARY TILLAGE

Pavel BROŽ[1], Josef HŮLA[1], Petr NOVÁK[1], Jitka EDROVÁ[1], Jaroslav KORBA[2], Václav NOVÁK[2]

[1]*Department. of Agricultural Machines, Faculty of Engineering, Czech University of Life Sciences Prague, Czech Republic*
[2]*Department of Machinery Utilization, Faculty of Engineering, Czech University of Life Sciences Prague, Czech Republic*

Abstract
Today's agriculture faces many challenges, the greatest is providing enough food on an ever decreasing amount of farmland for an ever-increasing population. In addition, other influences such as climate change, changes in cropping practices, and land degradation must be taken into account. Much of the research on soil degradation in the Czech Republic has focused on water and wind erosion. More than 50 % of the soil in the Czech Republic is threatened by water erosion, with wind erosion affecting almost 25 %. The research carried out in this paper focused on the shifting of soil particles due to secondary tillage during contour tillage. The experiment was based on the "tracer" method at different values of the slope of the experimental plot (2°,6°, and 11°). The results show that the shift of soil particles is significantly influenced by the slope on which the agronomic tillage is carried out. Statistical significance of the data was observed for tracers placed at the depth of tillage between 2° and 11° slope. In secondary tillage, working tools hurt soil erosion. It is necessary to observe these undesirable effects and minimize soil erodibility in the context of sustainable management.

Key words: *soil, soil translocation, soil tillage, cultivator, degradation, sustainability, monitoring.*

INTRODUCTION

Soil is one of the most precious resources on Earth. Soil resources are essential for humans and ecosystems (*Turner et al., 2007*). Currently, soil degradation is a major global environmental problem. Globally, about 30 % of the Earth's landmass is degraded. The importance of the problem is evidenced by the fact that 3.2 billion people are affected by land degradation. Soil erosion is usually referred to as the primary cause of land degradation. Soil erosion is recognized as an environmental problem in many regions (*Xin and Xiangzheng, 2020*). In the Czech Republic, much of the research has focused on water and wind erosion. These types of erosion are among the most discussed factors affecting soil degradation, both at the professional level and at the level of the general public. The current state of knowledge of this issue allows monitoring and subsequent analysis of the impacts of erosion. This subsequent evaluation provides a valuable basis for designing sustainable management practices (*Skleničkа et al., 2022*). Although erosion caused by tillage is currently not as well studied as the above-mentioned erosion processes, it also contributes significantly to soil degradation (*Fiener et al., 2018*). *Novara. et al.* (*2022*) state that the effects of soil erosion resulting from tillage are more significant than soil erosion resulting from water erosion. Soil tillage on very sloping land can even involve up to six times more soil particle transport compared to water erosion (*Richter, 1999*). This fact confirms that erosion during tillage is one of the major processes of soil degradation and this issue needs to be investigated. The average rate of soil loss on soils in the Czech Republic was found to be 2.52 $t \cdot ha^{-1} \cdot year^{-1}$ (*Panagos. et al., 2015*). This soil loss can be estimated at approximately 4.3 billion CZK per year (*Podhrázská et al., 2016*). The susceptibility of a plot of land to soil erosion is influenced by, among other things, agricultural mechanization or the size of the soil block. *Žížala et al., (2021)* state that erosion phenomena most often affect land plots of 20-50 ha in size and 500-750 m slope length. Considering the history of soil block formation in the Czech Republic, when smaller plots of land were merged into larger soil blocks, the phenomenon of soil degradation has gained in intensity. Currently, the average size of soil blocks in the Czech Republic is one of the largest in Europe.

Žížala et al., (2021) point out the dangers of simultaneous water erosion and soil erosion due to tillage. It also highlights that the area at risk of erosion from tillage is almost 1.5 times larger than the area at risk from water erosion alone. The average contribution of tillage erosion to total soil erosion is between 20 % and 30 %. In the past, water erosion was considered the dominant soil degradation process in Central Europe, often with extreme impacts that are easily visible. Erosion by tillage is not so visible. The shift of soil particles only becomes apparent after the soil has been worked several times. Due to gravity and the kinetic energy generated by the movement of the working tools, the soil particles do not fall back to their original location but are transported slightly down the slope. This processing causes soil erosion leading to the gradual removal of soil particles from the soil horizon and the accumulation of soil sediments and nutrients at the bottom of the slope (*Wilken et al., 2020*). Convex and concave eroded soil sections are described, for example, by *Govers et al., (1994); Hrabalikova et al., (2016); Lobb et al., (1995); Novák and Hůla (2018).* Tillage erosion is a relevant soil redistribution process in sloping cropland (*Gristina. et al., 2022*). According to the available literature, the effect of agricultural machinery acting in the longitudinal direction has been resolved.

However, there are very few studies dealing with longitudinal and lateral soil translocation with variable slope angle magnitude and focusing on secondary tillage. The lack of research conducted on this issue may bias the overall assessment of soil erosion on sloping farmland. This paper aims to assess the effect of slope angle on the longitudinal and lateral translocation of soil particles during secondary tillage.

MATERIALS AND METHODS

The experiment took place at Nesperská Lhota near Vlašim (GPS 49.690435 N";14.815578 E") on a plot with sandy loam, particles < 0.01 mm: 29 % by weight. The average slope of the plot is 4.2°, and the elevation is 461 meters above sea level. Parcel size of 4.74 ha was measured in LPIS using GIS as the total area. The area of moderate and severe erosion-prone land is 3.64 ha. The experimental plot is classified as standard arable land with conventional management. At the same time as the soil displacement measurements, intact soil samples were collected on the plot for laboratory determination of the soil's physical properties. The sampling was carried out using the Kopecky Physical Roller Kit method to collect 100 cm^3 physical cylinders from depths of 0.1, 0.15, and 0.2 m and calculate selected soil hydro-physical parameters such as reduced bulk density and porosity. Soil samples were collected before and after the measurements. The rolls were evaluated in the laboratories of the Czech University of Agriculture in Prague according to the ISO EN 17989-2 standard. Samples for the determination of physical properties should be taken in at least three repetitions (*Pokorný et al., 2007*). The results of the averages are recorded in Tab. 1 and 2.

Tab. 1 Soil bulk density and porosity before secondary tillage

Depth m	Bulk Density $g.cm^{-3}$	Porosity %
0.1	1.49	43.8
0.15	1.52	43.3
0.2	1.51	43.2

Tab. 2 Soil bulk density and porosity after secondary tillage

Depth m	Bulk Density $g.cm^{-3}$	Porosity %
0.1	1.37	50.2
0.15	1.39	48.2
0.2	1.39	47.2

The soil experiment was started after harvesting winter wheat with an average yield of 5.5 $t \cdot ha^{-1}$. The post-harvest residues were crushed and a subsoiling to a depth of 0.1 m was carried out for the initial incorporation of biomass. The land was plowed at the beginning of September. A Ross plow was used for plowing. The plowing depth was 0.22 m. Immediately after plowing, the land was leveled using a skid and harrow. The land was left at this stage until the end of September. Natural subsidence was therefore taking place. The three most suitable experimental plots for the measurements were then located and marked. The first measurement area was on the relative plane. The slope of the plane was 2°. The second area was selected on a higher slope with a value of 6°. The third area had the highest slope of the plot, 11°, which is the maximum allowed range of slope for a secondary tillage machine. The slope was measured using a digital inclinometer (BMI, Germany).
A Saturn combination cultivator was used for secondary tillage. The cultivator is used to cultivate the soil before sowing and to create the seedbed. The machine used for the measurements was a trailer-mounted machine with a working width of 6 m, divided into 4 sections, so each section has a working width of 1.5 m. The cultivator levels loosen, crumble, and back compact the soil. The Saturn cultivator has been reattached to a Zetor 130 HSX 16V tractor. The power of the tractor is slightly undersized which reduces the possibility of selecting the working speed. The working speed of the machine was 9 $\pm$ 0.2 $km \cdot h^{-1}$.
The,"tracer" method was used to assess soil particle displacement (*Govers et al., 1999*). These methods are based on placing tracers in the soil and noting their initial position (in this case in two axes). Once the tracers have been placed and recorded, the soil is processed by the machine and the position of the tracers is again detected. An M6 metal detector (Whites Devices) was used to determine the position. The numbered aluminum cube method was used in the experiment. The aluminum cubes were numbered from 1 to 20. The numbered "tracers" were divided into two groups. The color was used to divide the tracers. The yellow marked tracers were located on the soil surface. The tracers marked in silver were placed in the soil treatment depth, which was 0.8 m. The cube edge length was 16 mm. As reported by *Kouselou et al., (2018)*, the high recovery rate of the applied tracers is essential for accurate quantification of soil movement. The larger the more accurate and representative the approximation of soil movement. In this research, 120 indicators were applied to measure soil movement and all 120 indicators were found and recorded. The recovery rate is 100 %. Data were processed using MS Excel (Microsoft Corp., Redmond, WA, USA), Statistica 12 (Statsoft Inc., Tulsa, OK, USA), and Oriana (Kovach Computing Services, Pentraeth, UK).

RESULTS AND DISCUSSION

The data were evaluated with respect to the length of the marker offset and the directional angle of the markers. The length of the directional vector represents the length of the translocation of a particular tracer from its original location. The directional vector is the angle of the vector that indicates the difference from the direction of movement of the device. A positive value of this angle represents a translocation in the direction of the gradient line (perpendicular to the direction of device movement). Tukey's HSD test was applied to the measured data. The results of the Tukey HSD test are recorded in Table 3. Table 3 shows the statistical significance of the tracer data located at the depth of tillage. Columns 1 and 2 indicate with asterisks groups containing factor levels that are not significantly different from each other in their means.

Tab. 3 Statistical significance table for tracers located at processing depth (alfa=,0500)

Velikost svahu °	Průměr m	1	2
2	1,03707111	****	
6	1,53578592	****	****
11	2,66079882		****

The results of the measurements are further illustrated in Figure 1. The results show the effect of slope on the displacement of particles in the slope direction. The longest measured marker distance was 10.52 m and was measured in the experimental plot with a slope of 6°. The effect of slope and the magnitude of the directional angle vector were also observed. These results were recorded for both sets of tracers. It was found that the values of the angles in both sets of tracers increased as the slope increased. These results are recorded in Figure 2.

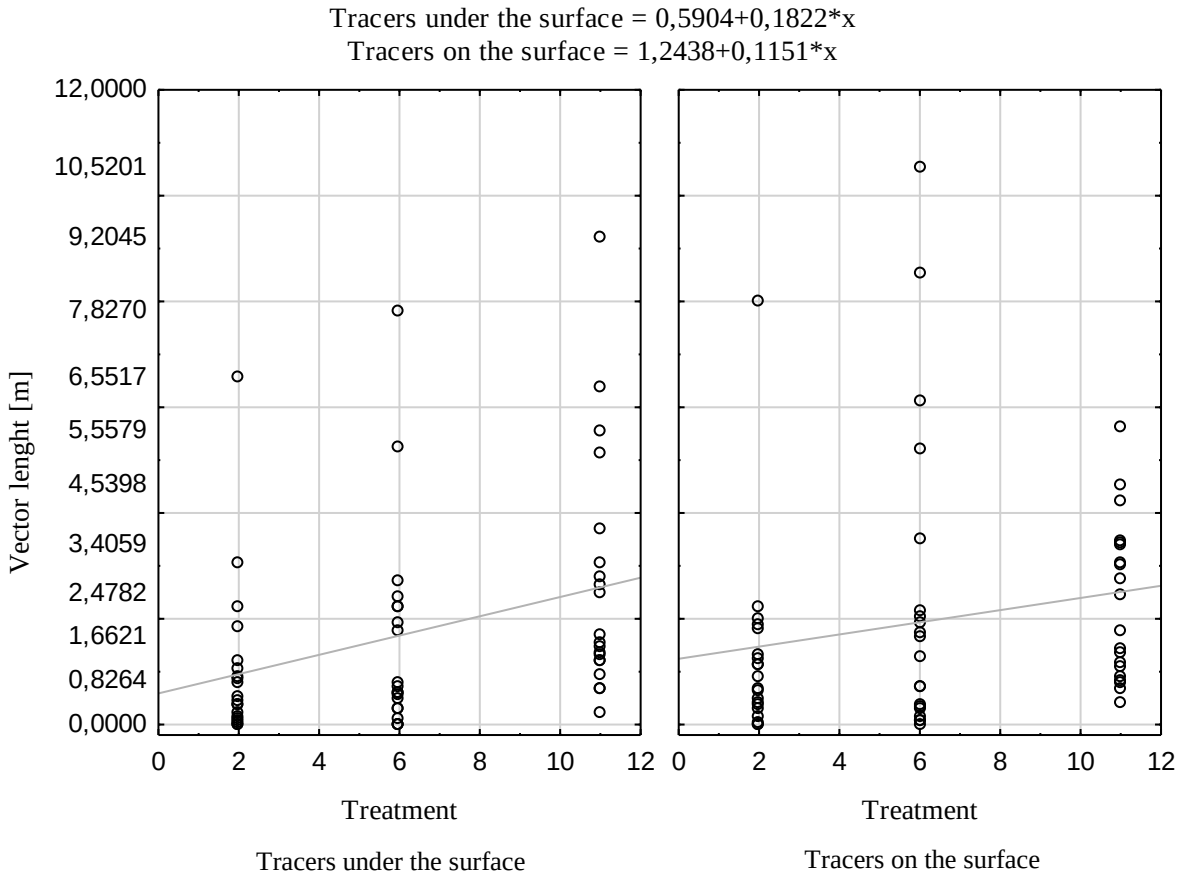

Fig. 1 Length of travel of soil markers

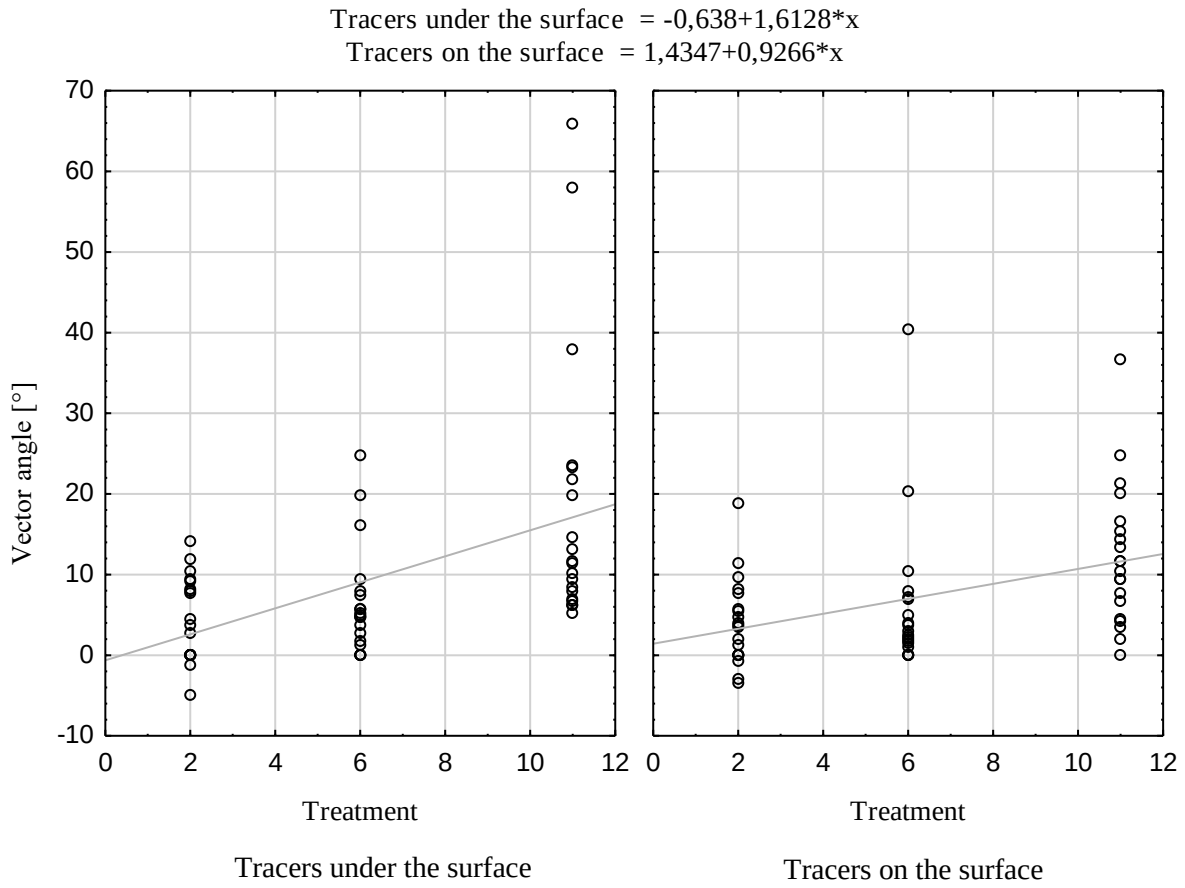

Fig. 2 Shift angle size

In the last two decades, a number of studies have been conducted that report different soil translocation rates for different soils (properties, conditions) and tillage techniques (speed, direction, depth, tool type, etc.) determined from different measurement techniques (*e.g., Loob et al., 1999; Kouselou et al., 2018; Turkelboom et al., 1999; Novara et al., 2019; Novara et al., 2022; Logsdon, 2013*). These aforementioned studies show that there are substantial differences for similar categories of tillage (e.g., secondary tillage), which have mostly been interpreted as differences resulting from differences in soil properties (bulk density) and tillage techniques (in particular, tillage depth, tillage rate, and tillage direction). *Lobb et al., (1999)* looked at soil translocation in Ontario, Canada. He used a field cultivator for secondary tillage with a processing speed of 6.48 km·h^{-1} and values with an average displacement of 0.321 m were measured. *Kouselou et al., (2018)* also used a cultivator with a working speed of 8 km·h^{-1} for measurements and measured a soil displacement of only 0.152 m. The measured values published in this study do not fully confirm these results. Much higher values of displacement occur in the study of *Turkelboom et al., (1999),* who recorded displacement in a plot with a 16 % slope of 2.88 m, and in a plot with a 22 % slope of 3.81 m. The measured values in this paper do not differ significantly from those of *Turkelboom et al., Novara et al., (2019)* observed the translocation of soil particles in the area of Santa Margherita del Belice, Sicily, using a cultivator with a working speed of 4 km·h^{-1} for soil processing. The slope on which the experiment was conducted was 15° and the particle displacement was 1.2 m. *Novara et al., (2022)* further compared the effect of a disc cultivator with a working speed of 2 to 5 km·h^{-1} and a slope of 6°. The results showed that the mean soil translocation distance was up to 1.14 m. These results agree with the measured results for a slope of 6°. The authors *Novák and Hůla (2018),* concluded that at a working speed of 7 km·h^{-1}, the maximum particle displacement occurs up to 10 m. The authors further observe the vector direction of the displacement. They conclude that on a slope of 11°, a vector displacement of up to 60° occurs. This was only partially confirmed. The vector displacement of the markers was observed up to 76° on a slope with a slope of 6°.

CONCLUSIONS

In this experiment, the impact of secondary tillage on the longitudinal and lateral transport effect was evaluated. High variability of values was found, but the expected trend was confirmed, and a direct relationship was found between the lateral displacement of particles downslope when the machine moved along the contour. The transport effect was significantly influenced by the value of the lateral tilt of the machine. Slope values from very low values of 2° to maximum values for safe machine operation of 11° were evaluated in this work. A statistically significant difference in the results of the tracer data was found between the data obtained at slope gradients of 2° and 11°. On the basis of the measured and evaluated results, we conclude that soil degradation occurs by soil processing on sloping land in the conditions of the Czech Republic. The study of soil erosion by tillage should be intensively continued, because it is a phenomenon with significance for the preservation of soil fertility during intensive soil management.

ACKNOWLEDGMENT

Supported by the Faculty of Engineeering (CULS) - IGA no. 2021:31160/1312/3101.

REFERENCES

1. Fiener, P., Wilken, F., Aldana-Jague, E., Deumlich, D., Gómez, J. A., Guzmán, G., & Wexler, R. (2018). Uncertainties in assessing tillage erosion–how appropriate are our measuring techniques?. Geomorphology, 304, 214-225.
2. Govers, G., Lobb, D. A., & Quine, T. A. (1999). Tillage erosion and translocation: emergence of a new paradigm in soil erosion research. Soil & Tillage Research, 51, 167-174.
3. Govers, G., Vandaele, K., Desmet, P., Poesen, J., & Bunte, K. (1994). The role of tillage in soil redistribution on hillslopes. European Journal of Soil Science, 45(4), 469-478.
4. Gristina, L., Novara, A., & Minacapilli, M. (2022). Rethinking vineyard ground management to counter soil tillage erosion. Soil and Tillage Research, 217, 105275.
5. Hrabalíková, M., Huislová, P., Ureš, J., Holubík, O., Žížala, D., & Kumhálová, J. (2016). Assessment of changes in topsoil depth redistribution in relation to different tillage technologies. In Proceedings of the 3rd WASWAC Conference, Belgrade, Serbia, 22-26.
6. Kouselou, M., Hashemi, S., Eskandari, I., McKenzie, B. M., Karimi, E., Rezaei, A., & Rahmati, M. (2018). Quantifying soil displacement and tillage erosion rate by different tillage systems in dryland northwestern Iran. Soil Use and Management, 34(1), 48-59.
7. Lobb, D. A., Kachanoski, R. G., & Miller, M. H. (1995). Tillage translocation and tillage erosion on shoulder slope landscape positions measured using 137Cs as a tracer. Canadian Journal of Soil Science, 75(2), 211-218.
8. Lobb, D. A., Kachanoski, R. G., & Miller, M. H. (1999). Tillage translocation and tillage erosion in the complex upland landscapes of southwestern Ontario, Canada. Soil and Tillage Research, 51(3-4), 189-209
9. Logsdon, S. D. (2013). Depth dependence of chisel plow tillage erosion. Soil and Tillage Research, 128, 119-124.
10. Novara, A., Novara, A., Comparetti, A., Santoro, A., Cerdà, A., Rodrigo-Comino, J., & Gristina, L. (2022). Effect of Standard Disk Plough on Soil Translocation in Sloping Sicilian Vineyards. Land, 11(2), 148.
11. Novara, A., Stallone, G., Cerdà, A., & Gristina, L. (2019). The effect of shallow tillage on soil erosion in a semi-arid vineyard. Agronomy, 9(5), 257.
12. Novák, P., & Hůla, J. (2018). Translocation of soil particles during secondary soil tillage along contour lines. Water, 10(5), 568.
13. Panagos, P., Borrelli, P., Poesen, J., Ballabio, C., Lugato, E., Meusburger, K., Montanarella, L., & Alewellb, CH., (2015). The new assessment of soil loss by water erosion in Europe. Environmental science & policy, 54, 438-447.
14. Podhrazska, J., Kučera, J., Karasek, P., & Konečná, J. (2015). Land degradation by erosion and its economic consequences for the region of South Moravia (Czech Republic). Soil and Water Research, 10(2), 105-113.

15. Pokorný, E., Šarapatka, B., & Hejátková, K. (2007). Soil quality assessment in an organic farm: a methodological aid. ZERA-Zemědělská a ekologická regionální agentura (in czech).
16. Richter, G. (1999). Soil erosion by ploughing operations in vineyards on steep slopes. In Proceedings of the second international symposium on tillage erosion and tillage translocation, (pp. 55), Leuven, Belgium.
17. Sklenicka, P., Efthimiou, N., Zouhar, J., van den Brink, A., Kottova, B., Vopravil, J., ... & Azadi, H. (2022). Impact of sustainable land management practices on controlling water erosion events: The case of hillslopes in the Czech Republic. Journal of Cleaner Production, 130416.
18. Turkelboom, F., Poesen, J., Ohler, I., & Ongprasert, S. (1999). Reassessment of tillage erosion rates by manual tillage on steep slopes in northern Thailand. Soil and Tillage Research, 51(3-4), 245-259.
19. Turner, B. L., Lambin, E. F., & Reenberg, A. (2007). The emergence of land change science for global environmental change and sustainability. Proceedings of the National Academy of Sciences, 104(52), 20666-20671.
20. Xin, W., & Xiangzheng, D. (2020). Current soil erosion assessment in the Loess Plateau of China: A mini-review. Journal of Cleaner Production, 276, 123091.
21. Wilken, F., Ketterer, M., Koszinski, S., Sommer, M., & Fiener, P. (2020). Understanding the role of water and tillage erosion from 239+ 240 Pu tracer measurements using inverse modelling. Soil, 6(2), 549-564.
22. Žížala, D., Juřicová, A., Kapička, J., & Novotný, I. (2021). The potential risk of combined effects of water and tillage erosion on the agricultural landscape in Czechia. Journal of Maps, 17(2), 428-438.

Corresponding author:
Ing. Pavel Brož, Department of Agricultural Machines, Faculty of Engineering, Czech University of Life Sciences Prague, Kamýcká 129, Praha 6, Prague, 16521, Czech Republic, phone: +420 721 402 927, e-mail: brozp@tf.czu.cz

THE EFFECT OF FIELD ROBOT PARAMETERS ON WEED CONTROL EFFICIENCY

Indrė BRUČIENĖ[1], Egidijus ŠARAUSKIS[1]

[1]Vytautas Magnus University, Agriculture Academy, Faculty of Engineering, Department of Agricultural Engineering and Safety, Studentu 15A, LT-53362 Akademija, Kaunas Reg., Lithuania

Abstract
Inter-row and intra-row weed control (WC) by self-propelled robots is a solution to reducing the need for tiring and time-consuming manual weeding. Field tests were performed with a solar-powered field robot in four treatments (RWC1, RWC2, RW3, and RWC4) by changing the performance parameters of the robot. The aim was to determine the efficiency of mechanical WC in sugar beet by controlling weeds at different speeds (740 and 400 m h^{-1}), distances (45 and 60 mm) between the weeding knife and the sugar beet in a row, and the percentage of the knife entering the crop row (85 or 100%). The results showed that the average WC efficiency was the highest (47%) with the robot operating speed of 740 m h^{-1} and a distance of 60 mm. To sum up, high-precision self-propelled field robots can replace manual weeding, but these systems need to be improved and more research is needed to achieve greater efficiency in WC.

Key words: *weeding, intra-row, solar-powered robot, operating speed, sugar beet, organic farming.*

INTRODUCTION

Weeds are considered to be a major problem in crop production and especially in organic farming. Weeds compete with staple crops for space, water, nutrients, and light (*Cioni and Maines, 2010*). In sugar beet, which is particularly susceptible to weed competition, yield losses due to poor weed control can be as high as 26–100% (*Cioni and Maines, 2010; Jalali and Salehi, 2013; Kunz et al., 2018; Bhadra et al., 2020*). Therefore, weed control is one of the most important factors in sugar beet production to ensure crop yield and quality (*Sabanci and Aydin, 2017*). Efficient weed control is particularly relevant in organic crop production, which already yields less compared to conventional farming that uses chemical weed control (*Abouziena and Haggag, 2016*).

Mechanical weed control methods such as harrowing and inter-row cultivation are commonly used in organic farming (*Šarauskis, 2019*). However, mechanical weed control methods require a high degree of precision, i.e. knowing the exact location of weeds and crop plants (*Åstrand and Baerveldt, 2002*). For this reason, precision technologies such as automatic machine control, video cameras, optical sensors, Real-Time Kinematic Global Positioning System (RTK-GPS), and others have been introduced. These advanced technologies not only increase the working speed of technological operations, and the mechanical efficiency of weed control, but also reduce crop damage (*Kunz et al., 2018; Gerhards et al., 2020*). Efficient weed control has become possible not only in the inter-row but also in the intra-row, which can significantly increase crop yield and quality (*Jalali and Salehi, 2013; Sabanci and Aydin, 2017*). Studies conducted by *Melander et al. (2015)* have shown that 50–90% weed control efficiency can be obtained by applying weed control within plant rows. According to other researchers, more than 90% weed control efficiency can be achieved by controlling weeds inter-row and intra-row (*Chandel et al., 2021; Gerhards et al., 2020*).

Robotic weed control systems with high precision enable site-specific weed management. The development and improvement of such systems has been a popular and relevant area of research over the last decade (*Åstrand and Baerveldt, 2002; Bawden et al., 2017; Sabanci and Aydin, 2017; Utstumo et al., 2018).* Autonomous weeding robots such as AVO (Ecorobotix), Dino and Oz (Naïo Technologies), Robotti (Agrointelli), FD20 (FarmDroid), Robot One (Pixelfarming Robotics), etc. are also available on the market. Robotic weed control systems that can improve weeding efficiency, save resources, improve crop yield and quality, replace manual weeding and reduce environmental pollution, have a great potential to replace traditional weeding methods.

Although there is a large body of research in the scientific literature on the development and improvement of robotic weed control systems, there are few research papers evaluating the efficiency of robotic

weed control systems. The aim of this study was to experimentally investigate the efficiency of different robotic weed control methods in organic sugar beet production. It was aimed to determine the optimal robot operating parameters at which the robot performs the best weed control without damaging the sugar beet.

MATERIALS AND METHODS

The experimental trials were carried out in July 2021 in Panevėžys district, central Lithuania (55°49'19.4"N, 23°55'13.0"E), in an organic sugar beet field with sandy loam soil. The average air temperature during the study period was 22.2 °C and the average precipitation was 58 mm.

Sugar beet sowing and weed control were carried out by the same FD20 robot (FarmDroid, Denmark), powered by electricity, and equipped with solar modules and batteries. The sugar beet (variety Marley) was sown on 8 June 2021 with an inter-row spacing of 0.45 m and intra-row spacing of 0.18 m (sowing density 123 000 seeds ha^{-1}). The working width of the robot – 2.7 m. The FD20 uses GPS, so that after sowing, by knowing exactly where the seeds have been placed, the robot is able to carry out weed control inter-row and intra-row before the plants germinate, and later after germination without damaging the sugar beet plants.

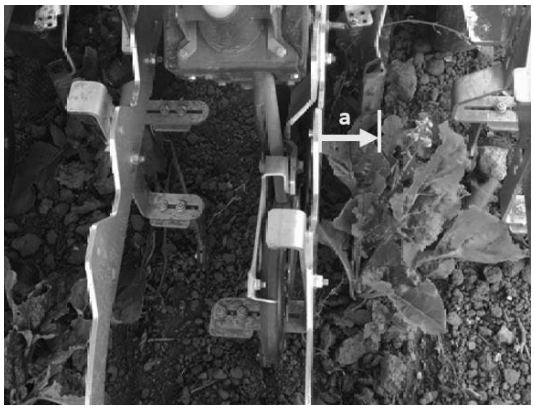

Fig. 1 Workflow of the robotic weeding knife in the crop row: a – entry of the weeding knife into the crop row

For the mechanical weed control of sugar beet, the robot's operating parameters were varied: the robot's working speed, the distance between the weeding knife and the sugar beet in the crop row, and the percentage of the knife entering the crop row (a) (Fig. 1). The different robotic weed control treatments RWC1, RWC2, RWC3, and RWC4 with different robot operational parameters are described in Table 1.

Tab. 1 Robot operational parameters

Treatment	Working speed m h^{-1}	Distance between weeding knife and sugar beet mm	Knife entered the crop row (a) %
RWC1	740	60	85
RWC2	740	60	100
RWC3	400	60	85
RWC4	400	45	85

To assess the efficiency of the robotic weed control methods, the number of weeds in an area of 0.25 m^2 using a 0.5 × 0.5 m frame was counted before the weed control operation (control) and after weeding. The trials were carried out in 8 different randomly selected field sites. The efficiency (E) of the different weed control methods was calculated according to the formula (*Chandel et al., 2021*):

$$E\ (\%) = (Wb - Wa)/\ Wb \times 100 \quad (1)$$

where *Wb* is the number of weeds in the control before the weed control operation, and *Wa* is the number of weeds after the weed control operation.
Statistical analysis of the data was performed using Tukey's *HSD* test (*Tukey, 1979*) to detect significant differences between means. Different letters in the figures indicate significant differences between weed control methods ($p < 0.05$).

RESULTS AND DISCUSSION

The experimental results showed that the weed density before the robotic weed control ranged from 21 to 41 weeds m^{-2} and after the technological operation – from 15 to 30 weeds m^{-2}. The average weed control efficiency of the robotic weed control process in sugar beet rows and inter-rows was 47% in RWC1, 16, 23, and 32% in RWC2, RWC3, and RWC4, respectively (Fig. 2). The best result was achieved in RWC1 when the robot speed was 740 m h^{-1}, the distance between the weeding knife and the sugar beet was 60 mm and the knife entered the crop row at 85%. The worst result was obtained by RWC2 with only 16% weed control efficiency. The higher working speed of the robot and the longer path of the weeding knife resulted in one cut and one damaged sugar beet in this treatment. Thus, the selection and setting of the technological parameters of the robot is a very important element for the efficiency of weed control.

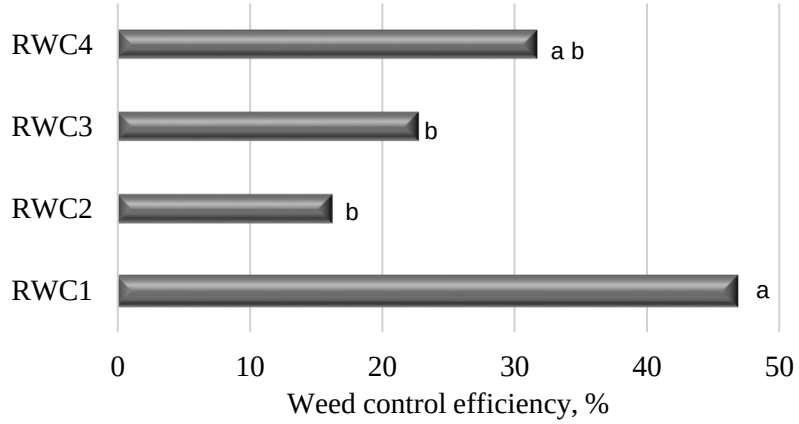

Fig. 2 The efficiency of different robotic weed control methods in sugar beet

It should be noted that the late sowing of sugar beet and the unfavorable weather conditions (rainy period) did not allow the robot to control weeds in time and at the right frequency, and led to weeds that were large and difficult to eradicate. Another possible reason for the low efficiency of weed control is that the weeds were not destroyed at the point of emergence and near the sugar beet, as the weeding knife was working at a distance of 45 to 60 mm around the plants. Abrasion of the weeding knife blades may also have contributed to poor weed control.
Pannacci et al. (2020) reported that 63–92% weed control efficiency could be achieved using combined inter-row and intra-row weed control. *Lati et al. (2016)* in a study with the Robovator found that the robotic intra-row cultivator removed 18–41% more weeds compared to a standard cultivator. *Bleeker et al. (2002)* obtained weed control efficiency of 30–88% in a sugar beet row. Meanwhile, studies with the robotic weed control platform BoniRob, which performs mechanical weed control with a tube-stamp, showed much better results than were obtained in our study. It has been found that the effectiveness of weed control can reach up to 94%. However, due to the special soil conditions required and the slow working process, robotic weed control platform has not been evaluated as a viable method for weed control (*Langsenkamp at al., 2014*).

CONCLUSIONS

In this study, experimental field trials were carried out in organic sugar beet crops comparing four different robotic mechanical weed control methods with each other. Robotic weed control in the plant row

and in the inter-row was evaluated. The results showed that weed control efficiency in sugar beet crops ranged from 16 to 47%. The best result (47%) was achieved in the RWC1 variant, where the robot traveled at 740 m h^{-1}, the weeding knife was set at 60 mm from the sugar beet and the knife entered the crop row at 85%. This study only confirms that different operating parameters, field, and weather conditions need to be taken into account and evaluated when assessing the efficiency of robotic machines. Therefore, further extensive research is needed.

REFERENCES

1. Abouziena, H. F., & Haggag, W. M. (2016). Weed control in clean agriculture: a review. *Planta daninha*, *34*, 377-392.
2. Åstrand, B., & Baerveldt, A. J. (2002). An agricultural mobile robot with vision-based perception for mechanical weed control. *Autonomous robots*, *13*(1), 21-35.
3. Bawden, O., Kulk, J., Russell, R., McCool, C., English, A., Dayoub, F., ... & Perez, T. (2017). Robot for weed species plant-specific management. *Journal of Field Robotics*, *34*(6), 1179-1199.
4. Bhadra, T., Mahapatra, C. K., & Paul, S. K. (2020). Weed management in sugar beet: A review. *Fundamental and Applied Agriculture*, *5*(2), 147-156.
5. Bleeker, P., van der Weide, R., Kurstjens, D., & Cloutier, D. C. (2002, March). Experiences and experiments with new intra-row weeders. In *Proceedings of the 5th EWRS Workshop on Physical and Cultural Weed Control* (pp. 97-100).
6. Chandel, N. S., Chandel, A. K., Roul, A. K., Solanke, K. R., & Mehta, C. R. (2021). An integrated inter-and intra-row weeding system for row crops. *Crop Protection*, *145*, 105642.
7. Cioni, F., & Maines, G. (2010). Weed control in sugarbeet. *Sugar Tech*, *12*(3), 243-255.
8. Gerhards, R., Kollenda, B., Machleb, J., Möller, K., Butz, A., Reiser, D., & Griegentrog, H. W. (2020). Camera-guided weed hoeing in winter cereals with narrow row distance. *Gesunde Pflanzen*, *72*(4), 403-411.
9. Jalali, A. H., & Salehi, F. (2013). Sugar beet yield as affected by seed priming and weed control. *Archives of Agronomy and Soil Science*, *59*(2), 281-288.
10. Kunz, C., Weber, J. F., Peteinatos, G. G., Sökefeld, M., & Gerhards, R. (2018). Camera steered mechanical weed control in sugar beet, maize and soybean. *Precision Agriculture*, *19*(4), 708-720.
11. Langsenkamp, F., Sellmann, F., Kohlbrecher, M., Kielhorn, A., Strothmann, W., Michaels, A., ... & Trautz, D. (2014, September). Tube Stamp for mechanical intra-row individual Plant Weed Control. In *Proceedings of the 18th World Congress of CIGR, Beijing, China* (pp. 16-19).
12. Lati, R. N., Siemens, M. C., Rachuy, J. S., & Fennimore, S. A. (2016). Intrarow weed removal in broccoli and transplanted lettuce with an intelligent cultivator. *Weed technology*, *30*(3), 655-663.
13. Pannacci, E., Farneselli, M., Guiducci, M., & Tei, F. (2020). Mechanical weed control in onion seed production. *Crop protection*, *135*, 105221.
14. Sabanci, K., & Aydin, C. (2017). Smart robotic weed control system for sugar beet. *Journal of Agricultural Science and Technology*, *19*(1), 73-83.
15. Tukey, J. W. (1979). Methodology, and the statistician's responsibility for both accuracy and relevance. *Journal of the American Statistical Association*, *74*(368), 786-793.
16. Utstumo, T., Urdal, F., Brevik, A., Dørum, J., Netland, J., Overskeid, Ø., ... & Gravdahl, J. T. (2018). Robotic in-row weed control in vegetables. *Computers and electronics in agriculture*, *154*, 36-45.

Corresponding author:
Indrė Bručienė, Department of Agricultural Engineering and Safety, Faculty of Engineering, Agriculture Academy, Vytautas Magnus University, Studentu 15A, LT-53362 Akademija, Kaunas Reg., Lithuania, phone: +370 37 752357, e-mail: indre.bruciene@vdu.lt

FIELD INVESTIGATIONS OF THE EXPERIMENTAL CLEANER OF THE ROOT CROP HEADS FROM THE TOP RESIDUES

Volodymyr BULGAKOV[1], Ivan HOLOVACH[1], Valerii ADAMCHUK[2], Yevhen IHNATIEV[3], Aivars ABOLTINS[4], Semjons IVANOVS[4]

[1]*National University of Life and Environmental Sciences of Ukraine, Ukraine*
[2]*Institute of Mechanics and Automation of Agricultural Production of the National Academy of Agrarian Sciences of Ukraine, Ukraine*
[3]*Dmytro Motorny Tavriya State Agrotechnological University, Ukraine*
[4]*Latvia University of Life Sciences and Technologies, Latvia*

Abstract
Despite the presence of a large number of technical solutions, the problem of improving the quality of harvesting root crops is still relevant. A new design of the working body for the top removal without extraction the beets from the soil has been developed and researched, and investigations have been carried out to substantiate the optimal parameters and operating modes. Based on the analysis of the obtained functional and graphical dependencies, rational values of the operating modes of the investigated cleaner have been established in which the most high-quality work is possible when removing the remains of the tops from the surface of the root crops heads. In comparison with the top-removing module of the serial Holmer beet harvester, the experimental equipment reduces the loss of the sugar-bearing mass by 37%.

Key words: *root crops, machine, cleaner, top residues.*

INTRODUCTION

Beet growing is an important branch of agriculture in many European countries (*Ivančan, Sito & Fabijanić, 2002; Bulgakov et al., 2016*). Thus the volume of the sugar beet production in 2017 in France amounted to 34.4 million tons, in Germany – to 34.0 million tons, in Poland – to 15.7 million tons, in Ukraine – to 14.9 million tons. In addition, the yield of the sugar beet in France was more than 80 tons ha^{-1}. In the technology of production of sugar and fodder beets the most labor-intensive and expensive technological process is their harvesting. Harvesting accounts for about 60% of the energy costs of the beet production (*Hoffmann, 2018*). In addition the beet gathering determines the quality of the resulting product, its storage properties over time, as well as the losses of the grown biological mass. Preservation of beet root crops is affected by the presence of the top residues since the tops, unlike the root crops, is a more perishable mass, and it can provoke the crop rotting. But, on the other hand, the tops can be used as livestock feed, for the biogas generation, etc. Obtaining clean root crops with minimal losses of the tops is an important task of the technological process of harvesting. Therefore the task of high-quality separation of the remains of the tops from the root crops is of great relevance. There are many investigations devoted to the problem of cleaning the heads of root crops from the top remnants (*Bulgakov et al., 2017; Hoffmann, 2018*). Initial requirements for the cleaners of the sugar beet heads: tops on the sugar beets must be cut off without additional cleaning by a bush harvester; the cut of the head must be straight, smooth, without chips; the cutting plane must pass not lower than the level of the green cuttings and not higher than 20 mm from the top of the head. Besides, the cropped mass of the root crops from the tops should not exceed 5%; the total losses of the green mass of the tops, including the free mass, on highly cut and uncut root crops in the pile and lost on the soil surface, should not exceed 10% of its yield; the number of the damaged root crops should not be more than 20%, including the severely damaged ones – up to 5%. Since the mass introduction of mechanization, beet harvesting has been over 60 years. During this time several generations of machines for its collection have already been created; however, the tasks of improving the machines for the implementation of this technological process are still of great scientific relevance and practical need. An important contribution to the theory and practice of this issue some time ago was made by the following scientists: Helemendik N., Pogorely L. and other researchers (*Helemendik, 1996; Bulgakov et al., 2015; Alami et al., 2021*). The purpose of

this research is to determine the optimal design and kinematic characteristics of the developed experimental cleaner of the root crops heads to ensure high-quality work.

MATERIALS AND METHODS

When conducting experimental investigations, generally accepted and specially developed methods were used (*Bulgakov et al., 2017*). Assessment of the conditions for conducting the experimental research included determination of the soil and climatic conditions and characteristics of planting the root crops, substantiation for the operating modes of the machine, and determination of the quality indicators (*Helemendik, 1996*). The conditions for conducting the field experimental investigations were as follows: deviation of the root crops from the theoretical axis of the line – ± 22 mm; the average height of the protruding heads above the ground surface – 34 mm; the width of the main row spacing – 44.5 mm; density of root crops – 82.9 thousand pieces ha^{-1}; the biological yield of the tops – 13.3 t ha^{-1}; the biological yield of the beets – 53.4 t ha^{-1}. Conducting experimental research of the new design of the cleaner to determine the quality indicators of its work was carried out by an experimental setup that allows full simulation of the operation of the cleaner in the field. Fig. 1 shows a structural and technological scheme of the experimental setup with an installed experimental twin-shaft cleaner of the sugar beet heads from the top residues.

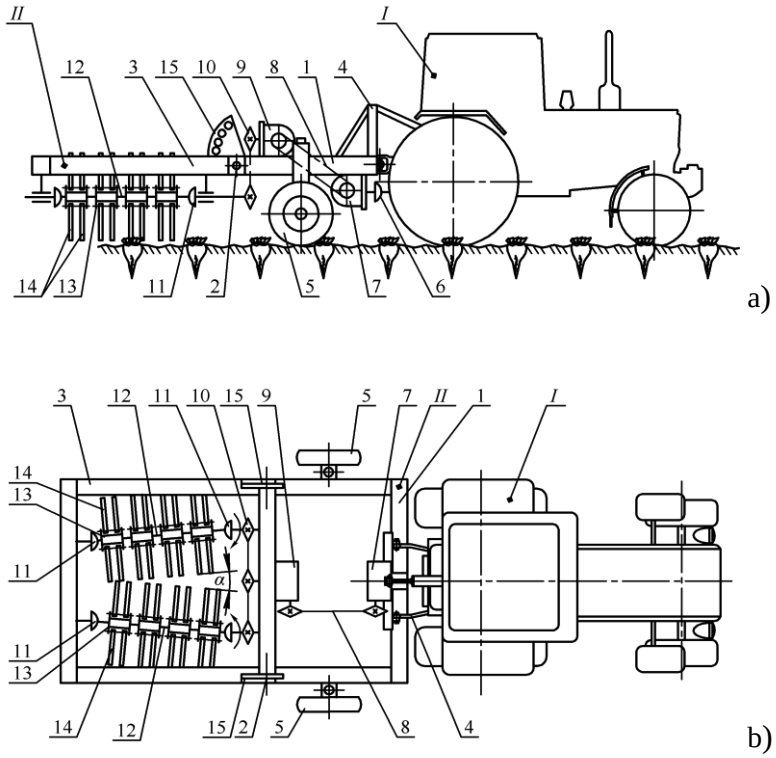

Fig. 1 Structural-technological scheme of the aggregate with an experimental setup, simulating a two-shaft cleaner of the root crop heads from the residues of the tops: a – a general side view; b – a top view: I – the wheeled aggregating tractor; II – the experimental setup: 1 – the main frame; 2 – the transverse beam; 3 – the rotary frame; 4 – the hitch; 5 – the gauge wheels; 6 – the cardan transmission from the tractor power take-off shaft; 7 – the bevel gear on the main frame; 8 – the chain drive; 9 – the gearbox on the transverse beam; 10 – the chain transmission for the drive of cleaning shafts; 11 – the cardan shafts; 12 – the cleaning shafts; 13 – the hinges on which the blades are installed; 14 – the flexible cleaning blades; 15 – the sector for setting the angles of inclination

The experimental setup (*Patent UA115404, 2017*) consists of the main frame 1 connected to the tractor, using hitch 4. On the main frame 1, the rotary frame 3 is installed with the help of a transverse beam 2 (Fig. 1). The rotary frame 3 is necessary for mounting the cleaning blades 14 of the hinges 11 with horizontal drive shafts 12 installed at an angle α to each other. Rotary frame 3 has an ability to be

installed due to main frame 2 at different angles to the surface of the sugar beet field. The installation height of the cleaning working bodies relative to the level of the soil surface is adjusted using gauge wheels 5. Each of the two cleaning shafts 12 is driven by cardan 11 from the power take-off shaft 6 of the aggregating tractor through bevel gear 7. Then, by means of the chain drive 8, gearbox 9 is driven from it, which is mounted on the rotary frame 3, due to which shafts 12 with the blocks of the hinges with working bodies 13 are driven by transmission through chain 10 and cardan drive 11. The horizontal drive shafts 12 have hinges 13 fixed at certain distances along their lengths, on which flexible cleaning blades 14 are pivotally mounted with the help of hinges. In total, each hoop has four cleaning blades 14. Drive shafts 12 with the hinged flexible cleaning blades 14 make counter rotational movement. During operation the cleaner, aggregated with a wheeled tractor, is installed along the axis of the row of the sugar beets, from which the main mass of the tops have already been cut (entire cut at a higher height); however, the remains of tops in the form of short green and strong residues remained on the heads of the beets, as well as dry and dry fallen residues, which are mainly firmly connected with the heads of the root crops and are located in the spaces between the rows or in a row between adjacent root crops. Moving progressively along the row, the drive cleaning shafts cover the row of the root crops from two sides, and their flexible blades 14 strike the heads, effectively knocking down (crushing and combing) the remains of the tops from the entire surface of the root heads.

To study the influence of the operating modes of the cleaner upon the quality of cleaning the heads of root crops from the remnants of the tops, a multifactorial experiment was made (*Montgomery, 2013*). In this experiment the input parameters were: V – the speed of the forward movement of the two-shaft cleaner, m s^{-1}; ω – the angular velocity of the rotational movement of the driven cleaning shafts, rad s^{-1}; h – the installation height of the cleaner blades above the level of the ground surface, cm. The output parameter, that is, a quality indicator of the operation of the cleaner of the root crop heads, was the mass of the top residues per square meter of the experimental area of the sugar beet field, on which a continuous cut of the top mass was already made, and the passage and additional cleaning of the heads of the root crops from the top residues was completed. In experimental studies the speed of the forward movement of the two-shaft cleaner was regulated by switching the gearbox of a wheeled aggregating tractor. The lower limit of the forward speed of the movement was 0.8 m s^{-1}, the upper limit was 2.0 m s^{-1}, the average value was 1.4 m s^{-1}. Adjustment of the angular speed of rotation of the drive shafts of the cleaner was made by changing the gear ratio of the drive. The maximum value of the angular velocity of the rotational movement of the cleaner shafts was 34.8 rad s^{-1}, the maximum value was 78 rad s^{-1}, the average value was 54 rad s^{-1}. The installation height of the cleaning blade above the level of the ground surface was regulated by changing the position of the gauge wheels of the two-shaft cleaner. The minimum value of the installation height of the blades was taken equal to 0 (when the ends of the blades were strictly at the level of the ground surface without gaps), the average value of the installation height was 0.02 m (2 cm), and the maximum value of the installation height of the blades above the level of the soil surface was 0.04 m (4 cm). The field experimental investigations were conducted in five repetitions at the appropriate values of the installation height of the blades relative to the level of the soil surface, various operating speeds of the cleaner and various modes of rotation of the cleaner shafts in accordance with the standard plan matrix. The quality of cleaning of the root crops heads from the residues of the tops at each repetition of the experiment was checked by manually removing the remnants of the tops from the root crop heads in the experimental area and weighing them on electronic scales. Processing of the obtained experimental data was performed on a PC in accordance with the existing program of statistical calculations Statistica 5.0.

RESULTS AND DISCUSSION

The results of the experimental investigations (based on a full three-factor experiment) of the quality of the experimental top cleaner under various operating modes are presented in Table 1.

There are obtained the functional dependencies of the amount of the top residues (Y) upon the forward speed of movement of the cleaner (X_1), the angular speed of the rotational movement of the cleaner drive shafts (X_2) and the height at which the blades of the cleaner are installed relative to the level of the soil surface (X_3). These functional dependencies are described by the following regression equation in the form of a polynomial dependence of the 2nd degree:

$$Y = 209.38 - 6.34X_1 - 6.66X_2 + 61.16X_3 + 0.99X_1^2 + 0.05X_2^2 - \\ -1.13X_3^2 + 0.28X_1 \cdot X_2 - 28.98X_1 \cdot X_3 - 0.7X_2 \cdot X_3 + 0.34X_1 \cdot X_2 \cdot X_3 \ , \quad (1)$$

at the coefficient of multiple determination $D = 0.707$, the coefficient of multiple correlation $R = 0.841$. This analytical dependence shows that its most significant factor is the angular speed of the drive shafts X_2. According to the results of the numerical calculations, performed on a PC, graphs were constructed and presented in the form of response surfaces of the dependences of the mass of the top residues upon the angular velocity ω of the rotational movement of the drive shafts of the cleaner and the installation height h of the blades above the level of the soil surface at a forward speed V of the cleaner, equal to: 0.8 m s^{-1} (Fig. 2), 1.4 m·s^{-1} (Fig. 3), 2.0 m s^{-1} (Fig. 4).

Tab. 1 Results of the experimental investigations of the quality of the experimental top cleaner under various operating modes

Angular speed of rotation of the drive hafts, rad·s^{-1}	Speed of the movement								
	0.8 m·s^{-1}			1.4 m·s^{-1}			2.0 m·s^{-1}		
	Installation height of the cleaning blades above a flat surface of the field, cm								
	0	2	4	0	2	4	0	2	4
	Top residues, g·m^{-2}			Top residues, g·m^{-2}			Top residues, g·m^{-2}		
78.0	5.3	5.8	4	10.3	12.3	2.1	34.9	54.1	67.5
	3.4	6.9	4.2	9.4	16.8	2.5	26.2	49.1	23.4
	8.7	8,8	11	3.9	12.3	12.4	34.2	40.2	23.1
	6.6	12.6	6.2	14.8	24.5	6.3	10.7	34.8	23.1
	4.1	22.1	5.8	8.1	9.8	10.2	8.1	31.7	20.2
54.0	6.7	3.1	22.4	10.1	28.7	54.6	8.4	4.3	94.2
	12.1	22.9	12.1	23.1	14.2	67.2	16.1	10.1	83.1
	14.2	10.6	19.2	7.8	23.1	70.3	7.2	17.1	58.7
	3.7	8.1	10.2	7.4	12.4	103.1	7.8	10.4	32.1
	4.1	3.1	9.7	20.1	10.7	114.1	14.5	16.3	127.3
34.8	74.5	63.1	180.3	40.4	12.4	50.7	2.4	16.4	12.9
	62.9	70.9	164.5	27.2	26.4	79.5	3.9	10.6	8.4
	54.6	90.1	132.1	28.4	28.5	74.8	2.8	11.1	26.7
	36.7	62.8	97.9	28.9	16.2	72.1	3.8	10.8	22.5
	82.5	50.7	117.4	30.5	34.1	97.4	6.2	15.9	10.4

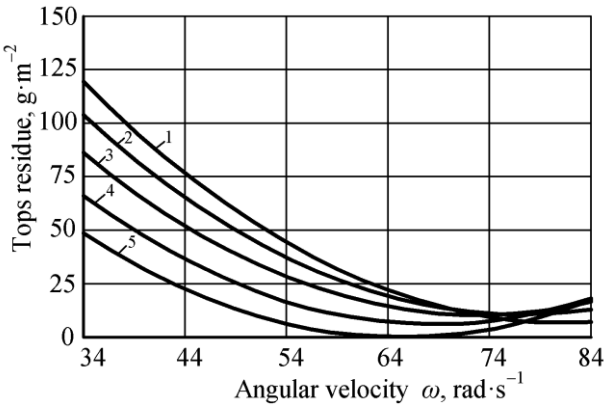

Fig. 2 Response surface of dependence of the top residues on the angular velocity of the rotational movement of the drive shafts of the cleaner and the installation height of the blades at the forward speed of the cleaner 0.8 m s^{-1}: 1 – h = 4 cm; 2 – h = 3 cm; 3 – h = 2 cm; 4 – h = 1 cm; 5 – h = 0 cm

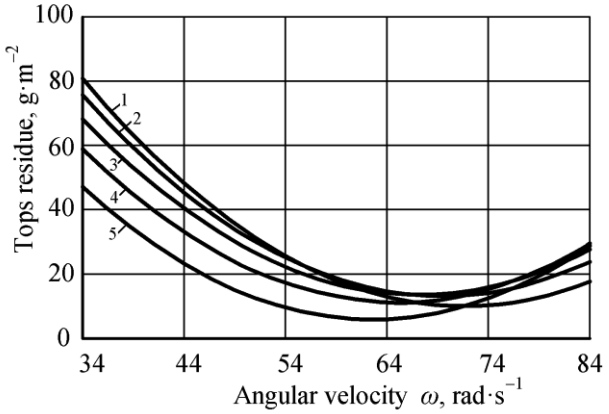

Fig. 3 Response surface of dependence of the top residues on the angular velocity of the rotational movement of the drive shafts of the cleaner and the installation height of the blades at the forward speed of the cleaner 1.4 m s^{-1}: 1 – h = 4 cm; 2 – h = 3 cm; 3 – h = 2 cm; 4 – h = 1 cm; 5 – h = 0 cm

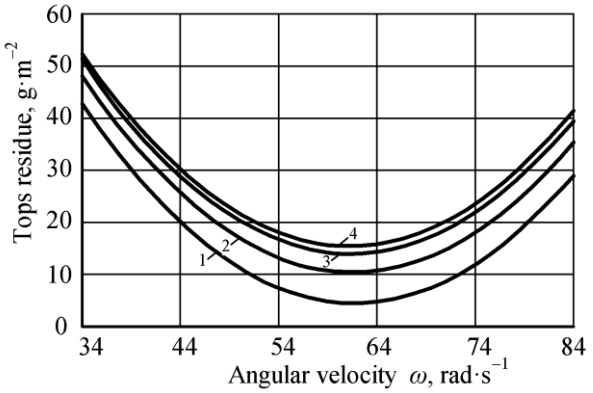

Fig. 4 Response surface of dependence of the top residues on the angular velocity of the rotational movement of the drive shafts of the cleaner and the installation height of the blades at the forward speed of the cleaner 2.0 m s^{-1}: 1 – h = 4 cm; 2 – h = 3 cm; 3 – h = 2 cm; 4 – h = 1 cm

In addition it is evident from the presented graphical dependencies that. with an increase in the angular velocity ω of the rotational movement of the drive shafts of the cleaner and a decrease in the installation height h of the blades above the level of the soil surface, a decrease in the top residue on the surfaces of the root crop heads is mainly observed. However, at the values of the forward speed V of the cleaner movement, equal to 1.4 m s^{-1}, the dependences are more complex, and at the speed of 2.0 m s^{-1}, on the contrary, an increase in height h leads to a decrease in the top residues. It is also evident from these graphical dependencies that within the range of speeds V of the forward movement 0.8...1.4 m s^{-1}, with an increase in the angular speed ω of the rotational movement of the cleaner drive shafts up to 70 rad s^{-1} and 64 rad s^{-1}, first, a gradual decrease in the mass of the top residues on the heads of root crops is observed, and then a slight increase. At a speed of 2.0 m s^{-1}, rapid growth of the top residues starts already at ω = 60 rad s^{-1}. At an angular speed of rotation of the drive shafts of the cleaner, equal to 34.8 rad s^{-1}, the nature of the impact of the forward speed V of movement upon the quality indicators of work is changeable. So, at the "zero" height of the installation of the blades h = 0, with an increase in the forward speed of the cleaner within 0.8…1.4 m s^{-1}, the mass of the top residues decreases. However, within the range of speed 1.4...2.0 m s^{-1}, a certain increase in this indicator is observed. At the blade installation height of 2 cm, the tendencies are similar to the installation height h = 0 and the angular velocity of rotation 54 rad s^{-1} and 78 rad s^{-1}. But at the installation height of the blades of 4 cm, with an increase in the forward speed V of the cleaner, the mass of the top residues decreases intensively. On the whole, raising the quality of the technological process by means of the cleaner of the root crop heads

from the top residues with horizontal drive shafts can be achieved by increasing the angular velocity ω of the drive shafts of the cleaner and reducing the installation height h of the blades above the soil surface at a speed of up to 1.4 m s^{-1}. In the investigations by other authors, it is also indicated that an increase in the speed of more than 1.5 m s^{-1} leads to a decrease in the quality of harvesting the remains of sugar beet tops *(Kukhmazov & Zyabirov, 2008).* According to the results of the field experimental investigations of the two-shaft cleaner, the rational modes of its operation are: speed V of the forward movement of the cleaner is 0.8...1.2 m s^{-1}; the angular speed ω of the rotational movement of the driven cleaning shafts is 63…78 rad s^{-1} and the height h of the cleaner blades above the ground level is 0…2 cm.

To evaluate the efficiency of the experimental machine, research was made of five main indicators of the quality of work in comparison with the serial machines, used to perform this technological process. The loss of the mass of the root crop heads due to the removal of the tops when cut by the top-removing module of a serial Holmer beet harvester is 3.2%, but for the experimental equipment 2.0% (i.e., there is a decrease in the losses by 37%). In other mass-produced machines, common in Ukraine, this indicator of loss of mass is even greater *(Kukhmazov & Zyabirov, 2008).* The set of technical documentation for the experimental equipment of the top removal was transferred to the Ternopil Combine Plant (Ukraine) to be used in industrial production of the beet harvesting equipment.

CONCLUSIONS

1. Improving the quality of the technological process with a cleaner of the root crop heads from the top residues by means of horizontal drive shafts can be achieved by increasing the angular speed of the drive shafts of the cleaner and reducing the installation height of the blades above the soil surface at low forward speeds of the machine.
2. Based on the analysis of the obtained functional and graphical dependencies, it has been established that the rational values of the operating modes of the cleaner to be studied under which the most high-quality work is possible when removing top residues from the surface of the root crop heads are: the speed of the forward movement of the two-shaft cleaner – 0.8…1.2 m·s^{-1}; angular speed of rotation of its drive shafts – 63...78 rad·s^{-1}; the installation height of the blades of the cleaner above the level of the ground surface – 0...2 cm.

REFERENCES

1. Bulgakov V., Adamchuk V., Ivanovs S., Ihnatiev Y. (2017). Theoretical investigation of aggregation of top removal machine frontally mounted on wheeled tractor. *Engineering for rural development.* Vol. 16, pp. 273–280.
2. Hoffmann C.M. (2018). Sugar beet from field clamps – harvest quality and storage loss. *Zuckerindustrie,* 143 (11), pp. 639–647.
3. Ivančan, S., Sito, S., Fabijanić, G. (2002). Factors of the quality of performance of sugar beet combine harvesters. *Bodenkultur,* Vol. 53(3), pp. 161–166.
4. Patent UA115404 (2017). Root head cleaner. (In Ukrainian)
5. Bulgakov V., Ivanovs S., Adamchuk V., Boris A. (2015). Mathematical model for determination of losses of sugar bearing-mass when sugar beet tops are removed. *Engineering for Rural Development*, Vol. 14, pp. 441–451.
6. Alami L., Terouzi W., Otmani M., Abdelkhalek O., Salmaoui S., Mbarki M. (2021). Effect of Sugar Beet Harvest Date on Its Technological Quality Parameters by Exploratory Analysis. *Journal of food quality.* Vol. 2, Article ID 6639612
7. Helemendik N. (1996). *Increasing the Mechanical and Technological Efficiency of the Labour Consuming Processes in Beat Growing*. Ternopol, 48 p. (In Ukrainian).
8. Montgomery D.C. (2013). *Design and Analysis of Experiments* (8th ed.). Hoboken, New Jersey: Wiley. ISBN 978-1119320937
9. Kukhmazov K., Zyabirov A. (2008). Justification of the design parameters of the comb copier of the beet harvester. *Bulletin of the Moscow Agroengineering University*. Vol. 2 (27), pp. 63 - 65. (In Russian)

Corresponding author:
Ing. Semjons Ivanovs, Ph.D., Latvia University of Life Sciences and Technologies, Liela str., 2, Jelgava, LV 3001, Latvia, phone: +37129403708, e-mail: semjons@apollo.lv

COMPARISON OF TWO METHODS FOR TREE UPROOTING FORCE MEASUREMENT

Jakub ČEDÍK[1], Radek PRAŽAN[1], Marian RYBANSKY[2], Ladislav JÍLEK[1], Vladimír ŠLEGER[3], Martin HAVLÍČEK[4]

[1]*Research Institute of Agriculture Engineering, Drnovská 507, 161 01, Prague 6, Czech Republic, email: cedikj@tf.czu.cz, radek.prazan@vuzt.cz*
[2]*University of Defence, Faculty of Military Technology, Kounicova 65, 662 10 Brno, Czech Republic, email: marian.rybansky@unob.cz*
[3]*Czech University of Life Sciences Prague, Faculty of Engineering, Department of Mechanical Engineering, Kamýcká 129, 165 21, Prague 6, Czech Republic, email: sleger@tf.czu.cz*
[4]*Czech Technical University in Prague, Faculty of Mechanical Engineering, Department of Designing and Machine Components, Technická 4, 166 07 Prague 6, Czech Republic, email: martin.havlicek@fs.cvut.cz*

Abstract
The article is focused on the measurement of uprooting force of a spruce trees of different stem diameter using two methods and their comparison. First method uses a single-axis force transducer and the tree is uprooted by pulling a steel cable with a tractor winch. Second method uses a double-frame dynamometer, mounted in the three-point hitch of the tractor and the tree is uprooted by driving a vehicle into it. 7 trees were uprooted using each method and their comparison was made. The results showed a linear dependency between maximum uprooting force and tree stem diameter.

Key words: *tractor; force measurement; three-point hitch; tree uprooting.*

INTRODUCTION

The information about the actual magnitude and layout of the traction forces evoked by a tractor or other non-road vehicle is necessary for the optimal utilization of its traction potential or in terms of strength and fatigue studies (*Roca et al., 2019*). It also carries information about the soil mechanical properties (*Novák et al., 2014*).

Measurement of force, in general, can be based on several different principles. Ştefănescu and Anghel in their study (*Ştefănescu & Anghel, 2013*) distinguished 12 main types of electrical force transducers. However, electrical resistance strain gauges are still most used currently due to its simplicity, sufficient accuracy and low cost (*Ştefănescu, 2020*). Moreover, for most applications in multi-axial force sensors the electrical resistance strain gauges are used (*Alipanahi et al., 2022; Liu & Tzo, 2002; Templeman et al., 2020*).

Measurement of traction forces is possible in one, two or three directions. In the case of one-directional force measurement only one force sensor can be used (*Kroulík et al., 2015*). The sensor can be also build in a suitable measurement frame (*Procházka et al., 2015*). This approach can offer a suitable accuracy in one axis, however, the results does not contain information about the vertical or lateral forces (*Novák et al., 2014; Roeber et al., 2017*).

The measurement of the traction forces in more directions can be done by means of single-frame or double-frame dynamometers (*Roca et al., 2019*). The frame dynamometers are usually universal and can be used on more types of vehicles, on the other hand, its dimensions and mass affect the geometry and mass distribution of the vehicle or vehicle-implement system (*Alimardani et al., 2008; Kheiralla et al., 2003; Roca et al., 2019*). Single-frame dynamometers (*Al-Jalil et al., 2001; Alimardani et al., 2008; C.G.Bowers & Jr., 1989; Kheiralla et al., 2003; Kumar et al., 2016; O'Dogherty, 1996*) are used for two-directional measurement of traction force. According to (*Roca et al., 2019*), longitudinal and vertical forces are measured using the single frame dynamometers. However, when compared to double-frame dynamometers, their mass and dimensions are smaller. The principle of double-frame dynamometers (*Askari et al., 2011; Chaplin et al., 1987; Jeon et al., 2019; Palmer, 1992; Pijuan et al., 2012; Roca et al., 2019*) is based on two frames, connected with force sensors. One frame is connected to the

vehicle and the other to the implement or other source of the measured traction force. These dynamometers offer a three-directional traction force measurement with a good accuracy, however, their dimensions and mass are higher when compared to single-frame dynamometers. Also, some dynamometer designs may suffer with cross sensitivity problems, especially when there is a separate sensor for lateral force measurement (*Palmer, 1992; Roca et al., 2019*).
The evaluation of tree uprooting force or moment (or uprooting resistance) is in literature usually evaluated due to slope stabilization, windfirmness and tree productivity (*Campbell & Hawkins, 2004; Cannon et al., 2015; Peltola et al., 2000; Rahardjo et al., 2009*). Except the tree stem diameter, there are many other factors affecting the tree uprooting force such as tree species and their condition, root system and its condition, soil type and its condition, failure mode, position of the center of mass, tree dimensions and others (*Bartens et al., 2010; Campbell & Hawkins, 2004; Cannon et al., 2015; Rahardjo et al., 2009; Ribeiro et al., 2016; Szoradova et al., 2013*). However, despite these factors, authors found in most cases linear dependency of the uprooting resistance on the tree stem diameter or stem mass (*Campbell & Hawkins, 2004; Cannon et al., 2015; Ribeiro et al., 2016*).
The objective of the paper is to determine the dependency of the tree stem diameter on the uprooting force, in order to estimate a required traction force of a vehicle crossing the forest vegetation, using a single strain gauge sensor and a double-frame dynamometer with six strain gauge sensors and compare these two methods.

MATERIALS AND METHODS

The measurement took place on the land of school forest company Masarykův Les Křtiny near the Brno city at the Czech Republic. The measurement was performed using two methods, a single axis force sensor and a double-frame dynamometer.
As a single axis sensor a HBM U10M (nominal load 125 kN, relative error 0.02%) sensor was used (Fig. 1a). The double-frame dynamometer used for measurement can be seen in Fig. 1b. Its maximal load is 400 kN and uses six half-bridge strain gauge sensors in order to obtain a three-directional results of the traction force and moment.

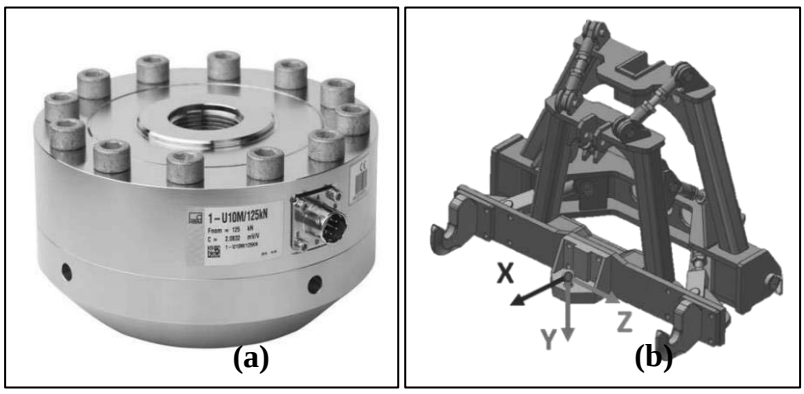

Fig. 1 Force transducers – a) HBM U10M, b) double-frame dynamometer with x, y and z axis labels

The calculation of the resultant force of the double-frame dynamometer, related to the origin of the coordinate system, is based on the coordinates of all 12 connecting points, from which the lengths of the connecting rods are calculated according to equation (1) and measured forces in these rods.

$$L_i = \sqrt{(X_{i.1} - X_{i.2})^2 + (Y_{i.1} - Y_{i.2})^2 + (Z_{i.1} - Z_{i.2})^2} \quad (1)$$

Where L_i is length of the individual connecting rod (m); $X_{i,1}$ is x–coordinates of connecting points on the implement side frame (m); $Y_{i,1}$ is y–coordinates of connecting points on the implement side frame (m); $Z_{i,1}$ is z–coordinates of connecting points on the implement side frame (m); $X_{i,2}$ is x–coordinates of connecting points on the tractor side frame (m); $Y_{i,2}$ is y–coordinates of connecting points on the tractor side frame (m); $Z_{i,2}$ is z–coordinates of connecting points on the tractor side frame (m), i=1–6.

The values of the X, Y and Z components of the forces, measured in the individual connecting rods are calculated according to equations (2), (3) and (4).

$$F_{iX} = F_i \frac{X_{i.1} - X_{i.2}}{L_i} \quad (2)$$

$$F_{iY} = F_i \frac{Y_{i.1} - Y_{i.2}}{L_i} \quad (3)$$

$$F_{iZ} = F_i \frac{Z_{i.1} - Z_{i.2}}{L_i} \quad (4)$$

Where F_{iX} *is* x–component of the measured forces in the connecting rods (N); F_{iY} *is* y–component of the measured forces in the connecting rods (N); F_{iZ} *is* z–component of the measured forces in the connecting rods (N); F_i *is* measured force in the individual connecting rod (N), i=1–6.

The X, Y and Z components of the resultant force are calculated as a sum of the components of the individual measured forces F_1-F_6 in the respective axis.
Resultant force calculation is based on its X, Y and Z components, according to equation (5).

$$F_R = \sqrt{{F_X}^2 + {F_Y}^2 + {F_Z}^2} \quad (5)$$

Where F_R is resultant force (N); F_X is the X component of the resultant force F_R; F_Y is the Y component of the resultant force F_R; F_Z is the Z component of the resultant force F_R.

Before the measurement the diameter of the tree stem was measured at the height of approx. 110 cm above the ground level. When using a single force sensor the rope was fixed at the same height and using a steel cable and a winch of the tractor the tree was uprooted while measuring the curse of the uprooting force. When using a double-frame dynamometer the device was mounted into the three-point hitch of the tractor and using a reverse gear of the tractor the tree was uprooted using the implement side of the double frame dynamometer while measuring the course of the force between tractor and the tree stem. The maximum uprooting force from the course was taken as a result. In both cases the data were recorded with a frequency of 50 Hz.
During the measurement 7 trees were uprooted using the single axis force sensor and 7 trees using the double-frame dynamometer. All uprooted trees were spruces, basic characterization of each uprooted tree can be seen in Table 1.

Tab. 1 Characterization of the uprooted trees

Sensor	Stem diame-ter (cm)	Stem circum-ference (cm)	Dry branch height (cm)	Semi-dry branch height (cm)	Green branch height (cm)	Tree height (cm)	Tree crown height (cm)	Root width (cm)	Root height (cm)	Root depth (cm)
HBM U10M	19.9	625	210	580	780	1640	260	220	155	55
HBM U10M	16.9	531	210	670	980	1650	260	310	125	90
HBM U10M	22.8	716	220	420	850	1710	330	390	120	60
HBM U10M	24.3	763	230	300	510	1620	520	350	315	100
HBM U10M	12.4	389	200	360	720	1540	250	230	160	55
HBM U10M	16.7	524	210	660	630	1630	360	310	110	65
HBM U10M	10.5	329	190	230	380	1530	230	200	130	50
Double-frame dyn.	13.4	421	220	580	750	1480	370	160	75	45
Double-frame dyn.	9.6	301	320	490	590	1110	180	40	30	45
Double-frame dyn.	11.3	355	210	500	530	1250	230	160	100	40
Double-frame dyn.	18.7	587	190	695	880	1620	310	220	215	70
Double-frame dyn.	19.7	619	260	190	620	1640	340	195	125	90
Double-frame dyn.	24.9	782	200	620	710	1670	370	250	90	40
Double-frame dyn.	20.1	631	200	360	660	1950	320	270	45	40

RESULTS AND DISCUSSION

In Figure 2 the courses of the uprooting force using the single axis sensor and the double-frame dynamometer are shown. It is evident that uprooting using a single axis force sensor takes a longer time due to the speed of the tractor winch.

In Figure 2b it can be noticed that the main component of the resultant force F_R is F_X, which was expected due to direction of the traction force, evoked by vehicle. F_Y also showed a not negligible force magnitude which is given by the stem inclination during the uprooting of the tree. However, F_Y reached in all cases its maximum after the maximum of F_X and F_R.

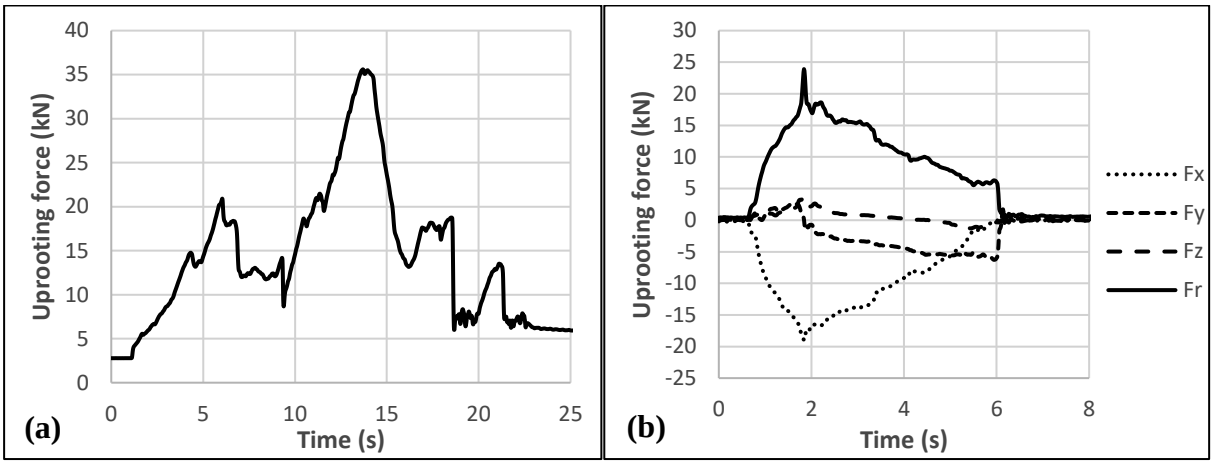

Fig. 2 The course of the forces during uprooting a tree using a single axis sensor (a) and double frame dynamometer (b) for a selected trees

In Figure 3 the overall results of both of the methods are shown. It is evident that the linear dependency between uprooting force and stem diameter was found, this trend was also found by other authors focusing on similar problematics (*Campbell & Hawkins, 2004; Cannon et al., 2015; Ribeiro et al., 2016*). For the double-frame dynamometer the resultant force F_R and its horizontal component F_X are shown, since the F_X causes the main disruption of the roots. It can be seen that only in two uprooted trees there is a noticeable difference between F_X and F_R and a slight difference in slope between the linear trend of F_R and F_X can be observed.

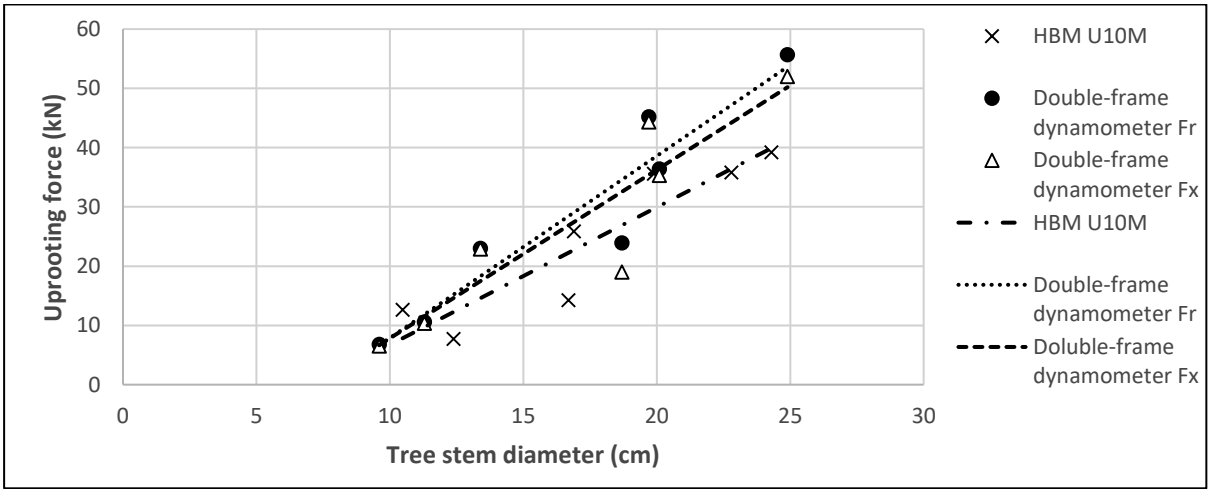

Fig. 3 The comparison of maximal reached values for both methods

From Figure 3 it is also evident that the results of both of the methods are comparable, especially when uprooting trees with the smaller stem diameter, approx. under 20 cm. The trend obtained using HBM

U10M has a lower slope in comparison with both trends obtained using the double-frame dynamometer (F_R and F_X). This is caused mainly by the variability of the actual uprooting force, which depends on many factors, as mentioned in the Introduction section. However, the method of the tree uprooting could have also affected the results into some extent. When uprooting a tree by driving a vehicle into it, higher friction between the measuring frame and the tree stem must be overcome in comparison with uprooting a tree using a steel cable and the single-axis sensor.

CONCLUSIONS

The contribution was focused on determination of dependency of tree stem diameter and uprooting force using two methods and their comparison. The study follows on from the work of Mason et al. who did similar research using a buried fence posts (*Mason et al., 2012*). From the results it can be stated that linear trend between tree stem diameter and its uprooting force was found. However, slightly higher uprooting force was obtained using a driving vehicle with double-frame dynamometer, which is mainly caused by the variability of actual uprooting force and higher friction between the frame and the tree stem. When uprooting trees with a stem diameter above approx. 20 cm using a driving vehicle, the vehicle should be able to reach the traction force of at least 50–60 kN per one uprooted tree.

ACKNOWLEDGMENT

This study was supported by the grant project of long-time development of Research Institute of Agricultural Engineering p.r.i. no. RO0621. This paper is the particular result of the defence research project DZRO VAROPS managed by the University of Defence in Brno, NATO-STO Support Project (CZE-AVT-2019), and specific research project 2021-23 at Department K-210 managed by the University of Defence, Brno.

REFERENCES

1. Al-Jalil, H. ., Khdair, A., & Mukahal, W. (2001). Design and performance of an adjustable three-point hitch dynamometer. *Soil and Tillage Research*, *62*(3–4), 153–156. https://doi.org/10.1016/S0167-1987(01)00219-7
2. Alimardani, R., Fazel, Z., Akram, A., Mahmoudi, A., & Varnamkhasti, M. G. (2008). Design and Development of a three-point hitch dynamometer. *Journal of Agricultural Technology*, *4*(1), 37–52.
3. Alipanahi, A., Mahboubkhah, M., & Barari, A. (2022). Cross-sensitivity control in a novel four-component milling dynamometer for simultaneous measurement of tri-axial forces and torque. *Measurement*, *191*, 110788.https://doi.org/10.1016/j.measurement.2022.110788
4. Askari, M., Komarizade, M. H., Nikbakht, A. M., Nobakht, N., & Teimourlou, R. F. (2011). A novel three-point hitch dynamometer to measure the draft requirement of mounted implements. *Research in Agricultural Engineering*, *57*(4), 128–136. https://doi.org/10.17221/16/2011-RAE
5. Bartens, J., Wiseman, P. E., & Smiley, E. T. (2010). Stability of landscape trees in engineered and conventional urban soil mixes. *Urban Forestry & Urban Greening*, *9*(4), 333–338. https://doi.org/10.1016/j.ufug.2010.06.005
6. C.G.Bowers, & Jr. (1989). Tillage Draft and Energy Measurements for Twelve Southeastern Soil Series. *Transactions of the ASAE*, *32*(5), 1492–1502. https://doi.org/10.13031/2013.31178
7. Campbell, K. ., & Hawkins, C. D. . (2004). Effect of seed source and nursery culture on paper birch (Betula papyrifera) uprooting resistance and field performance. *Forest Ecology and Management*, *196*(2–3), 425–433. https://doi.org/10.1016/j.foreco.2004.04.005
8. Cannon, J. B., Barrett, M. E., & Peterson, C. J. (2015). The effect of species, size, failure mode, and fire-scarring on tree stability. *Forest Ecology and Management*, *356*, 196–203. https://doi.org/10.1016/j.foreco.2015.07.014
9. Chaplin, J., Lueders, M., & Zhao, Y. (1987). Three-Point Hitch Dynamometer Design and Calibration. *Applied Engineering in Agriculture*, *3*(1), 10–13. https://doi.org/10.13031/2013.26634
10. Jeon, H.-H., Jung, Y.-J., Siddique, M. A. A.,

Nam, K.-C., Kim, T.-B., Choi, C.-H., & Kim, Y.-J. (2019). Development and Validation of simulation model for three point-hitch during agricultural operation. *ASABE 2019 Annual International Meeting*, 3–8. https://doi.org/10.13031/aim.201901032

11. Kheiralla, A. F., Yahya, A., Zohadie, M., & Ishak, W. (2003). Design and Development of A Three-Point Auto Hitch Dynamometer for An Agricultural Tractor. *ASEAN Journal on Science and Technology for Development*, *20*(3&4), 271–288. https://doi.org/10.29037/AJSTD.355
12. Kroulík, M., Chyba, J., & Brant, V. (2015). Measurement of tensile force at the fundamental tillage using tractor's build-in sensor and external sensor connected between machines and their comparison. *Agronomy Research*, *13*(2), 95–100.
13. Kumar, A. A., Tewari, V. K., & Nare, B. (2016). Embedded digital draft force and wheel slip indicator for tillage research. *Computers and Electronics in Agriculture*, *127*, 38–49. https://doi.org/10.1016/j.compag.2016.05.010
14. Liu, S. A., & Tzo, H. L. (2002). A novel six-component force sensor of good measurement isotropy and sensitivities. *Sensors and Actuators A: Physical*, *100*(2–3), 223–230. https://doi.org/10.1016/S0924-4247(02)00135-8
15. Mason, G. L., Gates, B. Q., & Moore, V. D. (2012). Determining forces required to override obstacles for ground vehicles. *Journal of Terramechanics*, *49*(3–4), 191–196. https://doi.org/10.1016/j.jterra.2012.04.001
16. Novák, P., Chyba, J., Kumhála, F., & Procházka, P. (2014). Measurement of stubble cultivator draught force under different soil conditions. *Agronomy Research*, *12*(1), 135–142.
17. O'Dogherty, M. J. (1996). The Design of Octagonal Ring Dynamometers. *Journal of Agricultural Engineering Research*, *63*(1), 9–18. https://doi.org/10.1006/jaer.1996.0002
18. Palmer, A. L. (1992). Development of a Three-Point-Linkage Dynamometer for Tillage Research. *J. Ugric. Engng Res*, *52*, 157–167.
19. Peltola, H., Kellomäki, S., Hassinen, A., & Granander, M. (2000). Mechanical stability of Scots pine, Norway spruce and birch: an analysis of tree-pulling experiments in Finland. *Forest Ecology and Management*, *135*(1–3), 143–153. https://doi.org/10.1016/S0378-1127(00)00306-6
20. Pijuan, J., Berga, J., Comellas, M., Potau, X., & Roca, J. (2012). A three-point hitch dynamometer for load measurements between tillage implements and agricultural tractors during operation. *Power and Machinery. International Conference of Agricultural Engineering*, C–1018 ref.10. https://www.researchgate.net/publication/267405934
21. Procházka, P., Novák, P., Chyba, J., & Kumhála, F. (2015). Evaluation of measuring frame for soil tillage machines draught force measurement. *Agronomy Research*, *13*(1), 186–191.
22. Rahardjo, H., Harnas, F. R., Leong, E. C., Tan, P. Y., Fong, Y. K., & Sim, E. K. (2009). Tree stability in an improved soil to withstand wind loading. *Urban Forestry & Urban Greening*, *8*(4), 237–247. https://doi.org/10.1016/j.ufug.2009.07.001
23. Ribeiro, G. H. P. M., Chambers, J. Q., Peterson, C. J., Trumbore, S. E., Magnabosco Marra, D., Wirth, C., Cannon, J. B., Négron-Juárez, R. I., Lima, A. J. N., de Paula, E. V. C. M., Santos, J., & Higuchi, N. (2016). Mechanical vulnerability and resistance to snapping and uprooting for Central Amazon tree species. *Forest Ecology and Management*, *380*, 1–10. https://doi.org/10.1016/j.foreco.2016.08.039
24. Roca, J., Comellas, M., Pijuan, J., & Nogués, M. (2019). Development of an easily adaptable three-point hitch dynamometer for agricultural tractors. Analysis of the disruptive effects on the measurements. *Soil and Tillage Research*, *194*, art. no. 104323. https://doi.org/10.1016/j.still.2019.104323
25. Roeber, J. B., Pitla, S. K., Hoy, R. M., Luck, J. D., & Kocher, M. F. (2017). Development and Validation of a Tractor Drawbar Force Measurement and Data Acquisition System (DAQ). *Applied Engineering in Agriculture*, *33*(6), 781–789. https://doi.org/10.13031/AEA.12489
26. Ştefănescu, D. M. (2020). Strain sensitivity as selection criterion for elastic elements of force transducers: a brief review. *Sensors*

and Actuators A: Physical, *315*, 112238. https://doi.org/10.1016/j.sna.2020.112238

27. Ştefănescu, D. M., & Anghel, M. A. (2013). Electrical methods for force measurement – A brief survey. *Measurement*, *46*(2), 949–959. https://doi.org/10.1016/j.measurement.2012.10.020
28. Szoradova, A., Praus, L., & Kolarik, J. (2013). Evaluation of the root system resistance against failure of urban trees using principal component analysis. *Biosystems Engineering*, *115*(3), 244–249. https://doi.org/10.1016/j.biosystemseng.2013.03.001
29. Templeman, J. O., Sheil, B. B., & Sun, T. (2020). Multi-axis force sensors: A state-of-the-art review. *Sensors and Actuators A: Physical*, *304*, 111772. https://doi.org/10.1016/j.sna.2019.111772

Corresponding author:
Ing. Jakub Čedík, Ph.D., Research Institute of Agriculture Engineering, Drnovská 507, 161 01, Prague 6, Czech Republic, phone: +420 233 022 230, e-mail: cedikj@tf.czu.cz

COMPUTATIONAL FLUID DYNAMICS ANALYSIS FOR GREENHOUSE WITH DIFFERENT VENTILATION OPENINGS AND ORIENTATIONS IN SAMSUN, TURKEY

Bilal CEMEK[1], Muminah MUSTAQIMAH[1], Erdem KÜÇÜKTOPCU[1], Gürkan Alp Kağan GURDIL[2]

[1]Department of Agricultural Structures and Irrigation, Faculty of Agriculture, Ondokuz Mayıs University, 55139 Samsun, Turkey
[2]Department of Agricultural Machinery and Technologies Engineering, Faculty of Agriculture, Ondokuz Mayıs University, 55139 Samsun, Turkey

Abstract
Airflow and air distribution are critical factors in creating the microclimatic conditions necessary for plant growth and productivity in the greenhouse. Different greenhouse models and orientations can affect airflow and ventilation rates, resulting in greenhouse microclimate variation. The aim of this study was to evaluate the microclimatic conditions in the greenhouse in Samsun under different greenhouse models and orientations using the computational fluid dynamics method (CFD). Greenhouse microclimate conditions were simulated in two different models, M1 (45° vent) and M2 (35° vent), validated with experimental data, and airflow patterns, airspeed, temperature, and relative humidity were determined for each model in different greenhouse orientations before the winding course. The statistical parameters for evaluating model performance showed good agreement between the simulation and field test data. Since the wind was from the north, there was insufficient airflow through the greenhouse in most directions. The indoor temperature ranged from 27-28°C, and the relative humidity ranged from 42-48%. Based on the simulation, the best orientation for M1 is 45^o, while M2 is close to the wind run at 75^o. This CFD method effectively provides sufficient information to determine the appropriate greenhouse model in Samsun in less time and cost.

Key words: *numeric analysis, micro-climate, model, uniformity index.*

INTRODUCTION

Greenhouse technology is developing rapidly as it helps farmers grow crops in different regions and seasons. Greenhouse microclimate analysis, such as temperature, air velocity, and humidity, is necessary to provide adequate shading and ventilation or heat or cool the greenhouse. Determining the microclimatic conditions also allows optimizing the required environment for high-quality and quantity harvests *(Akrami et al., 2020).*

The temperature inside a greenhouse is affected by several factors, including the temperature of the ambient air, the heat transfer coefficient of the covering material, and solar radiation. The amount of solar radiation received by the greenhouse depends on the angle of the sun at a given time based on a specific season, greenhouse type, location, and orientation. Most of the solar radiation hits the ground directly, which increases the temperature of the greenhouse *(Li et al., 2018).*

The orientation of the greenhouse also plays an important role in determining the entry velocity of the air. *Khaoua et al. (2006)* studied the effect of air velocity and type of roof opening on the temperature distribution inside the greenhouse. This study showed that the combination of roof opening configurations and air velocity significantly affects the microclimate inside the greenhouse.

Ventilation is a critical process that significantly impacts plant performance at all stages of the process. Due to its extreme complexity, computational fluid dynamics (CFD) techniques are particularly beneficial for mapping flows and developing a better understanding of the flow fields responsible for the evolution of the microclimate, as well as conducting sensitivity studies to improve it *(Bournet & Boulard, 2010).*

Recently, CFD has become a widely used and powerful tool for developing building plans with efficient ventilation and modeling the greenhouse under climatic conditions *(Baeza et al., 2006; Benni et al., 2016; Cemek et al., 2017; He et al., 2015; He et al., 2018; Saberian & Sajadiye, 2019; Senhaji et al., 2019).*

Given this information, the aim of this study is to determine the effects of greenhouse vents and orientation on greenhouse microclimate. For this purpose, microclimatic conditions in greenhouses in Samsun were evaluated under different greenhouse models and orientations using the CFD method. The results were used to determine the most appropriate greenhouse model and orientation.

MATERIALS AND METHODS

Field measurement

This study was conducted in an experimental greenhouse at the Faculty of Agriculture, Ondokuz Mayıs University, Samsun, Turkey. The greenhouse is 6.20 x 20 m and has a floor area of 124 m^2. A total of 42 measurements were taken inside the greenhouse, each of which included a measurement of temperature, relative humidity, wind speed, and wind direction. The temperature and wind components outside the greenhouse, within a radius of 1 m, were also considered. The wind in Samsun was mainly from the WNW and NNW directions. The average monthly wind speed is about 3.5 m/s, with the strongest wind varying between 11 and 15 m/s.

The location of measurement points is given in Fig. 1. The internal and external wall temperatures were also measured with a Testo 875-2i thermal imaging camera. All measurement parameters were measured consecutively with two repetitions to reduce possible errors. All data were measured from 10:00 am to 3:00 pm, with a total average measurement time of 1 hour for each greenhouse condition.

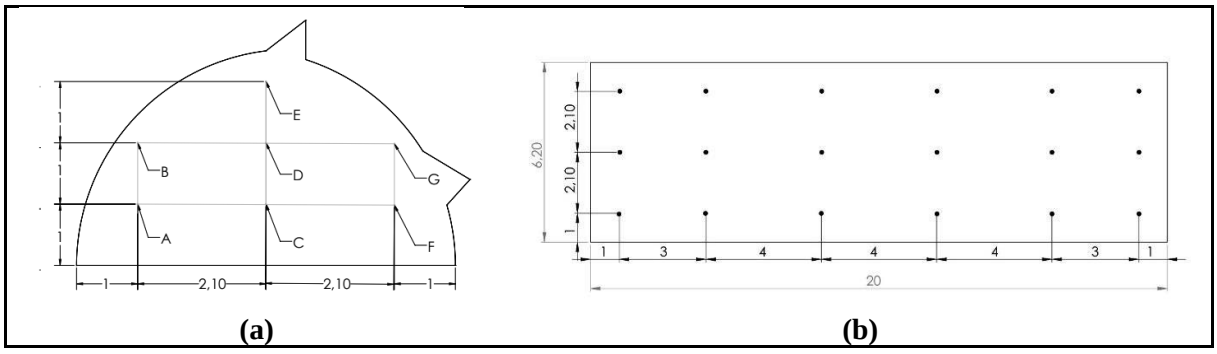

Fig. 1 Measurement points location (a) front view (b) top view

CFD Simulations

CFD is used in many disciplines worldwide *(Sørensen & Nielsen, 2003)*. With this method, a user can fully control all influencing factors for the simulation without spending much time and money. Moreover, the result of this simulation is complete and detailed information that allows the user to analyze comprehensively.

The experimental greenhouse is the same as the M1 and M2 greenhouse (Fig. 2). The models were tested in seven different directions before the wind direction (90º, 75º, 60º, 45º, 30º, 15º, 0º), as shown in Fig. 3.

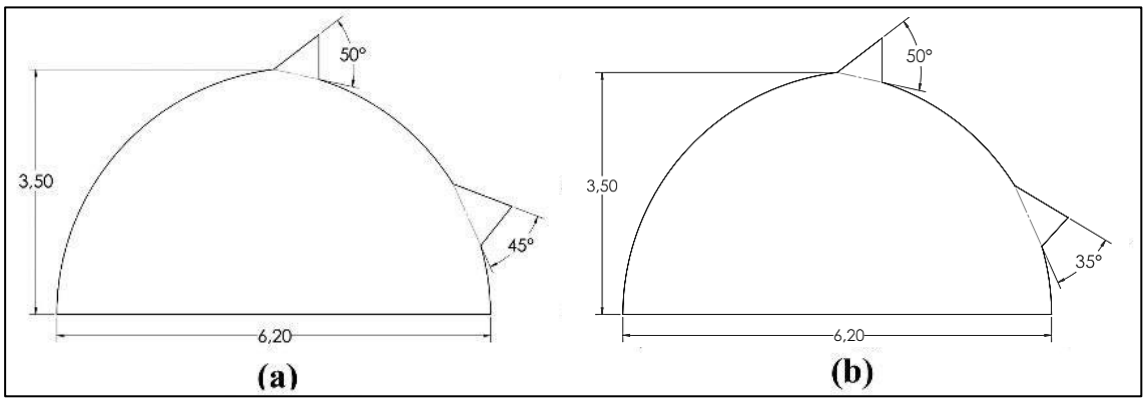

Fig. 2 Measurement points location (a) front view (b) top view

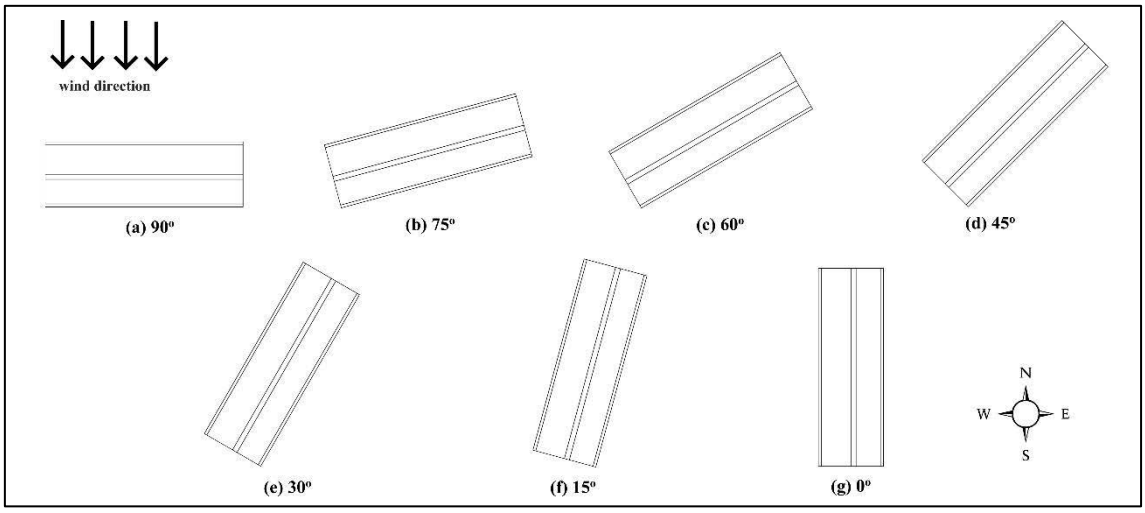

Fig. 3 Different greenhouse orientations

Solidworks was used to design the greenhouse geometry, and the simulation was performed in Ansys-Fluent. The program uses the finite volume method to numerically solve the Navier-Stokes equations, i.e., the mass, energy, and momentum balances that admit air velocity and temperature fields *(Erizal & Romdhonah, 2012)*. The geometry ratio of simulation and field experiment is 1/1. The computational domain of this CFD simulation was set to the area inside the greenhouse. The wall function used was a near-wall treatment with standard wall functions. The species transport function was used with a diffusion energy source consisting of a mixture of nitrogen, oxygen, and water vapor to simulate relative humidity.

The optimal mesh distribution and the number of cells were set in the Proximity and Curvature, Fine Relevance Center, High Smoothing, Slow Transition, and Fine Span Angle Center size functions. The minimum proximity size is 0.003 m, while the maximum area size is 0.12 m. The inlet and outlet areas have an element size of 0.05 m. The skewness of the mesh was 0.504.

There are three main methods used for fluid flow analysis: control volume or integral analysis, infinitely small element or differential analysis, and experimental study and dimensional analysis *(White, 1998)*. The second-order non-homogeneous differential solution was used for the analysis of non-compressible fluids. Some specific grid resolutions were used to maintain the accuracy of the results and reduce the calculations *(Campen & Bot, 2003)*.

Model validation

The results of the CFD model were compared with field measurements in the experimental greenhouse. Statistical parameters for model validation included fractional bias (FB), normalized mean squared error (NMSE), geometric mean bias (MG), geometric mean-variance (VG), and fraction of two (FAC2). Models were considered fit if more than half of the parameters met these criteria: |FB|<0.3, 0.7<MG<1.3, NMSE<0.25, VG<4, and 0.5<FAC2<2 *(Chang & Hanna, 2004; Küçüktopcu et al., 2022)*.

$$FB = \frac{2(\overline{C_o} - \overline{C_p})}{\overline{C_o} + \overline{C_p}} \quad (1)$$

$$NMSE = \frac{(\overline{C_o - C_p})^2}{\overline{C_o}.\overline{C_p}} \quad (2)$$

$$MG = \exp\left[\overline{\ln\left(\frac{C_o}{C_p}\right)}\right] \quad (3)$$

$$VG = \exp\left[\overline{\ln\left(\frac{C_o}{C_p}\right)^2}\right] \quad (4)$$

$$FAC = \frac{C_p}{C_o} \tag{5}$$

where C_o is the observed value and C_p is the predicted value.

Uniformity index

The uniformity index is used to represent and evaluate the uniformity of the flow distribution. It is calculated using the statistical deviation, where the γ value is between 0-1. The larger the number, the better the uniformity *(Zhang et al., 2017)*. The uniformity index used in this study is the area-weighted uniformity index. The uniformity index can be expressed as *(Tajik et al., 2017)*.

$$\gamma_v = 1 - \frac{1}{2}\left(\frac{\sum_{i=1}^{n}\left|v_i - v_{avg}\right|A_i}{A.v_{avg}}\right) \tag{6}$$

$$\gamma_T = 1 - \frac{1}{2}\left(\frac{\sum_{i=1}^{n}\left|T_i - T_{avg}\right|A_i}{A.T_{avg}}\right) \tag{7}$$

$$\gamma_{RH} = 1 - \frac{1}{2}\left(\frac{\sum_{i=1}^{n}\left|RH_i - RH_{avg}\right|A_i}{A.RH_{avg}}\right) \tag{8}$$

Where v_i, T_i, RH_i is the local velocity magnitude, temperature, and relative humidity, respectively, A_i is the local area, and A is the area where the γ is calculated. The uniformity index is calculated using ANSYS Fluent feature on the XY, YZ and XZ surface inside the greenhouse model.

RESULTS AND DISCUSSION

Validation of CFD Model

A statistical parameter for air velocity, temperature, and relative humidity in the greenhouse was determined to evaluate model performance. From Table 1, it can be seen that all the results for air velocity, temperature, and relative humidity in NMSE, FB, MG, VG, and FAC2 are within the acceptance criteria. This proves that this greenhouse model can be used to simulate indoor environmental conditions.

Tab. 1 Statistical parameters for model performance evaluation

Parameters	Air Velocity	Temperature	Relative Humidity
NMSE (< 0.25)	0.024	0.001	0.001
|FB| (< 0.3)	0.153	0.003	0.028
MG (0.7-1.3)	1.165	1.004	1.028
VG (< 4)	1.724	1.008	1.058
FAC2 (0.5-2.0)	0.858	0.996	0.972

Evaluation of the greenhouse models

Model 1

Since there was no wall opening in the northern part of the Model 1 (M1) greenhouse, there was generally an inflow at the southern roof opening and an outflow at the southern wall opening for the 90°, 75°, 60°, 45°, 30°, and 15° greenhouse orientations. Air circulated from the roof opening to the north wall and floor and exited directly through the south wall opening. For the 0° greenhouse orientation, the south roof opening and the south wall opening were parallel to the wind flow, so air flowed into both openings. This resulted in more air circulation and rotation within the greenhouse than in the others. *Khaoua et al. (2006)* also noted that there was also a countercurrent or loop in the wind flow within the greenhouse in this direction.

The magnitude of air velocity was observed in a different orientation for greenhouse M1. For the greenhouses in the 90°, 75°, 60°, 45°, and 30° orientations, the wall region tends to have a higher air velocity than the central region, as indicated by the difference in color. However, in the 15° orientation, the air

velocity in the wall and the middle of the greenhouse is slightly the same, while in the 0° orientation, the air velocity in the center area of the greenhouse is generally higher than in the wall.
The air velocity in the greenhouse with 90°, 75°, 60°, 45°, 30°, 15° and 0° orientation is 0.06-0.6 m/s, 0.02-0.45 m/s, 0.08-0.75 m/s, 0.07-0.65 m/s, 0.03-0.51 m/s, 0.07-0.35 m/s, and 0.04-0.23 m/s respectively. The greenhouse with a 60° orientation has the highest air velocity difference, 0.67 m/s, and the highest average air velocity, 0.37 m/s. This results in a relatively low uniformity index compared to the others. The greenhouse with a 0° orientation, parallel to the wind direction, has an average air velocity of 0.11 m/s and a uniformity index of 0.79. Since there is no constant inflow or outflow in this direction, the air velocity inside the greenhouse tends to be lower.
The temperature in the center of the greenhouse is constant, especially in the orientations 75° and 30°. For the greenhouses in the 90°, 60°, and 45° orientations, the wall area tends to have a lower temperature. In the 15° orientation, the temperature near the southern wall opening was slightly higher, while in the 0° orientation, the central area of the greenhouse had a higher temperature than in the other orientations. There is no difference in the uniformity index for temperature in all orientations. The temperature in the greenhouse with 90°, 75°, 60°, 45°, 30°, 15° and 0° orientation is 26.85-27.95 °C, 26.95-28.25 °C, 26.75-27.95 °C, 26.85-27.95 °C, 26.95-28.75 °C, 26.95-28.85 °C, and 26.95-29.25 °C respectively. Greenhouses with 15° and 0° orientations have a relatively higher temperature difference, 1.9 °C, and 2.3 °C, and a higher average, 28.10 °C, and 28.35 °C. This result indicates an agreement with the air velocity distribution. Since there is no constant inflow or outflow in this orientation, the air velocity inside the greenhouse tends to be lower. This results in a higher temperature. *Roy & Boulard (2004)* mentioned in their study that the temperature in the greenhouse was 5 K higher at 0° wind incidence than at 90° wind incidence. They also mentioned that the relative humidity was 20% higher at 0° incidence than at 90° incidence.
There were no significant differences in relative humidity for any of the greenhouse orientations except for the 0° orientation; the relative humidity in the western area of the greenhouse is lower than in the eastern area. The relative humidity in the greenhouse with 90°, 75°, 60°, 45°, 30°, 15° and 0° orientation is 45.15-45.77%, 44.64-45.43%, 45.37-46.2%, 45.26-45.96%, 44.87-45.48%, 42.37-45.33%, and 42.05-46.56% respectively. The greenhouse with the orientation 15° and 0° has a relative difference in relative humidity, 2.96% and 4.51%, and a lower average, 44.48%, and 43.80%. The greenhouse with orientations 15° and 0° is not as humid as the others. In all models, it was found that the lowest air temperature resulted in the highest relative humidity, mainly at the position of the air inlet *(Duong et al., 2021)*.
Overall, the highest uniformity index is seen in the greenhouse with an orientation of 0°. However, the temperature range reached in the greenhouse with this orientation is larger than the others, with a temperature difference of up to 2.3 °C. The average temperature is also higher. The same results are observed for relative humidity. The differences in relative humidity in M1 with 0° orientation are large, and the value of relative humidity is lower. Maintaining a relatively low temperature and sufficient humidity in the greenhouse to support plant growth while maintaining uniformity is essential. Therefore, the recommended values of the greenhouse can be maintained in the 45° orientation. The flow pattern, air velocity, temperature, and relative humidity for the M1 with a 45° orientation can be seen in Figures 4 and 5.

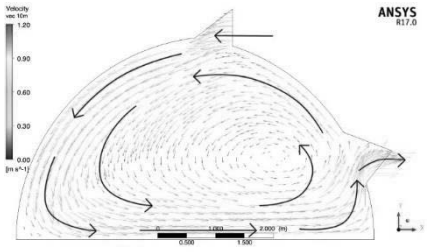

Fig. 4 Velocity flow pattern in XY and YZ plane for M1 with 45° orientation

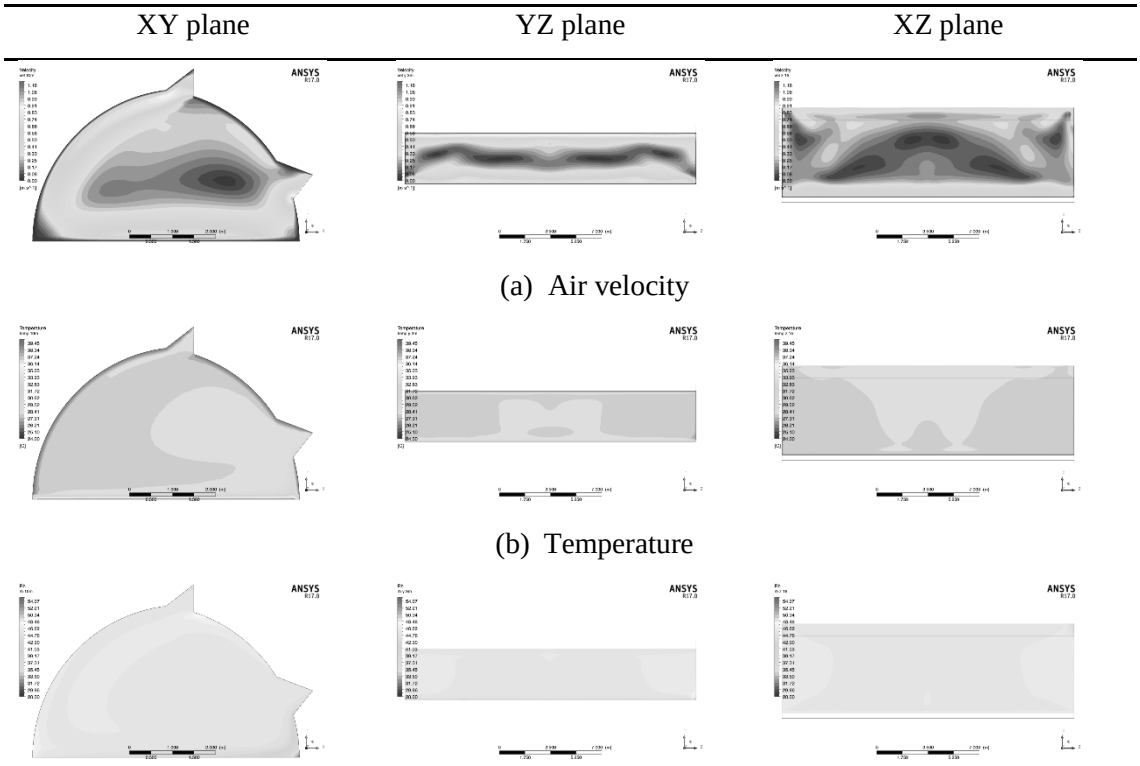

Fig. 5 Air velocity (a), temperature (b), and relative humidity (c) distribution for M1 with 45º orientation

Model 2

Since there is no wall opening in the northern part of the greenhouse, when the greenhouse was oriented 90º, 75º, 60º, 45º, 30º, and 15º, there was generally an inflow at the roof opening and an outflow at the southern wall opening, similar to the previous model. Air circulated from the roof opening to the north wall and floor and exited directly through the south wall opening. In the 0º orientation of the greenhouse, there is an inlet at the south wall opening, and the air flows directly to the roof opening.

For the greenhouses in the 90º, 75º, 60º, and 15º orientations, the wall area tends to have a higher air velocity than the center area. However, in the 45º and 30º orientations, the air velocity in the greenhouse walls and the middle area are slightly equal. In the 0º orientation, there was a large difference in velocity from the south wall opening through the roof opening compared to the other locations. This is because most of the air flows directly in this orientation. This is consistent with a study by *Shklyar & Arbel (2004)*, where a high velocity was observed near the windward corner between the sidewall and the roof. The air velocity values in the greenhouses with 90º, 75º, 60º, 45º, 30º, 15º and 0 º orientations are 0.03-0.41 m/s, 0.02-0.34 m/s, 0.03-0.33 m/s, 0.01-0.36 m/s, 0.04-0.28 m/s, 0.04-0.33 m/s and 0.02-0.44 m/s, respectively. The greenhouse with orientation 0 º has the highest average air velocity, 0.21 m/s, and the lowest uniformity index, 0.731.

The temperature in the central area of the greenhouse is largely constant in the 90º, 75º, 60º, 45º, 30º, and 15º orientations. In the greenhouse with 0º orientation, the temperature is lower around the roof from the south wall to the south roof opening. The overall temperature inside the greenhouse with 0o orientation is also lower than the others. The uniformity index of temperature does not differ for all orientations. The temperature values inside the greenhouses with 90º, 75º, 60º, 45º, 30º, 15º and 0º orientations are 26.65-28.15 ºC, 26.65-28.45 ºC, 26.65-29.25 ºC, 26.65-29.05 ºC, 26.65-29.95 ºC, 26.75-30.15 ºC and 25.55-28.15 ºC, respectively. The greenhouse with orientation 0º has the lowest average temperature, 26.57 ºC, compared to the others. This result indicates agreement with the air velocity distribution.

There is a relatively small difference in the uniformity index in all greenhouse orientations. The relative humidity values in the greenhouse with 90º, 75º, 60º, 45º, 30º, 15º and 0º orientations are 44.77-45.46%,

44.06-45.51%, 41.72-45.62%, 42.44-45.13%, 40.43-45.80%, 39.85-44.95% and 44.49-53.77%, respectively. A greenhouse with an orientation of 0º has higher relative humidity, 48.95%, and a lower uniformity index, 0.981, than the others. In contrast, a greenhouse with an orientation of 75º has the lowest average relative humidity.

The greenhouse with the 30º orientation in M2 has the highest uniformity index of 0.807. The temperature in this orientation is high, 28.23 ºC, and the relative humidity is low, 43.95%. In the greenhouses with 90º and 75º orientations, the temperature was 27 ºC. The uniformity index for a greenhouse with a 75º orientation is higher than the 90º orientation, so 75º was chosen as the most suitable orientation for the greenhouse with M2.

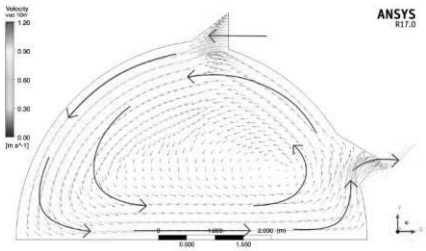

Fig. 6 Velocity flow pattern in XY and YZ plane for M2 with 75º orientation

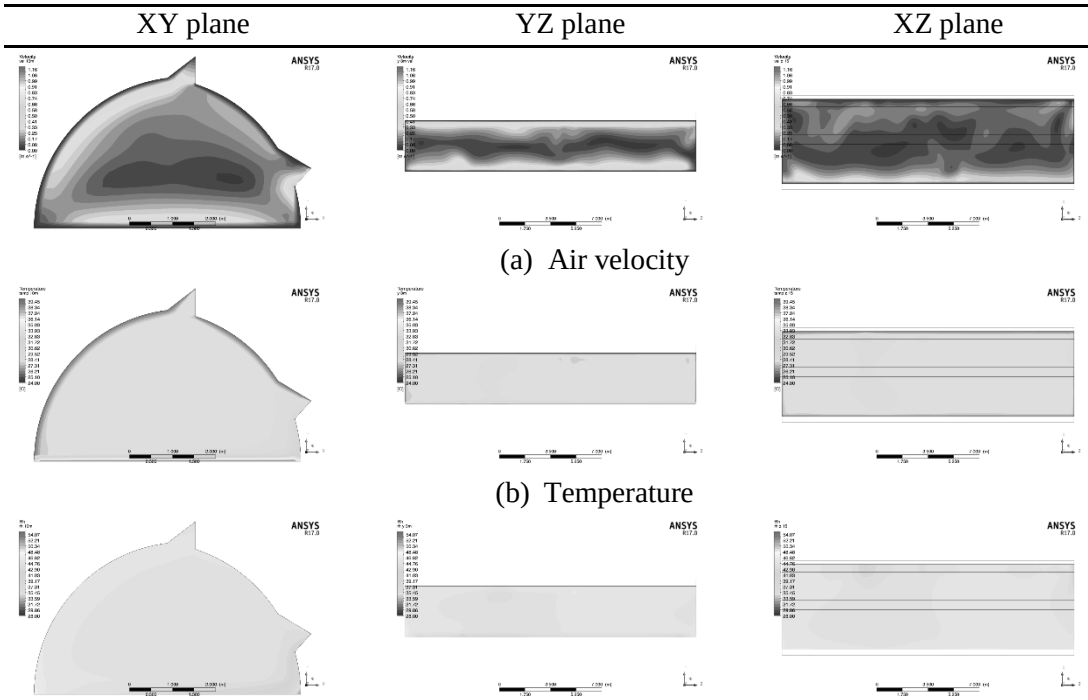

Fig. 7 Air velocity (a), temperature (b), and relative humidity (c) distribution for M2 with 75º orientation

CONCLUSIONS

The airflow pattern, air velocity, temperature, and relative humidity in two different models, M1 (45º vent) and M2 (35º vent), each with seven orientations (90º, 75º, 60º, 45º, 30º, 15º, and 0º) were investigated in this study using CFD simulation. Validation was performed using the temperature and relative humidity data set. The statistical parameters used to evaluate the model performance showed good agreement between the simulation and the field test data. Since the wind was from the north, most orientations had insufficient airflow through the greenhouse. The indoor temperature ranged from 27-28 ºC, and the relative humidity ranged from 42-48%. Based on the simulation, the best orientation for M1

is 45º and for M2 is 75º in terms of wind direction. This method effectively provides sufficient information to determine the appropriate greenhouse model in Samsun in less time and cost.

REFERENCES

1. Akrami, M., Salah, A. H., Javadi, A. A., Fath, H. E., Hassanein, M. J., Farmani, R., Dibaj, M., & Negm, A. (2020). Towards a sustainable greenhouse: Review of trends and emerging practices in analysing greenhouse ventilation requirements to sustain maximum agricultural yield. *Sustainability, 12*(7), 2794.
2. Baeza, E., Pérez-Parra, J., Lopez, J., & Montero, J. (2006). CFD study of the natural ventilation performance of a parral type greenhouse with different numbers of spans and roof vent configurations. In International Symposium on Greenhouse Cooling, ISHS Acta Horticulturae 719
3. Benni, S., Tassinari, P., Bonora, F., Barbaresi, A., & Torreggiani, D. (2016). Efficacy of greenhouse natural ventilation: Environmental monitoring and CFD simulations of a study case. *Energy and Buildings, 125*, 276-286.
4. Bournet, P.-E., & Boulard, T. (2010). Effect of ventilator configuration on the distributed climate of greenhouses: A review of experimental and CFD studies. *Computers and Electronics in Agriculture, 74*(2), 195-217.
5. Campen, J., & Bot, G. (2003). Determination of greenhouse-specific aspects of ventilation using three-dimensional computational fluid dynamics. *Biosystems Engineering, 84*(1), 69-77.
6. Cemek, B., Atiş, A., & Küçüktopcu, E. (2017). Evaluation of temperature distribution in different greenhouse models using computational fluid dynamics (CFD). *Anadolu Tarım Bilimleri Dergisi, 32*(1), 54-63.
7. Chang, J. C., & Hanna, S. R. (2004). Air quality model performance evaluation. *Meteorology and Atmospheric Physics, 87*(1), 167-196.
8. Duong, Y. H., Vo, N. T., Le, P. T. K., & Tran, V. T. (2021). Three-dimensional simulation of solar greenhouse dryer. *Chemical Engineering Transactions, 83*, 211-216.
9. Erizal, H. S., & Romdhonah, Y. (2012). Design of a sustainable greenhouse structure for the tropical regions: Applying computational fluid dynamics methods. In Proceeding of 3rd GEN Network and 4th Rispescia International Seminar: Sustainable Bio-resources for Global Welfare. Universitas Gajah Mada. Hlm,
10. He, K., Chen, D., Sun, L., Huang, Z., & Liu, Z. (2015). Effects of vent configuration and span number on greenhouse microclimate under summer conditions in Eastern China. *International Journal of Ventilation, 13*(4), 381-396.
11. He, X., Wang, J., Guo, S., Zhang, J., Wei, B., Sun, J., & Shu, S. (2018). Ventilation optimization of solar greenhouse with removable back walls based on CFD. *Computers and Electronics in Agriculture, 149*, 16-25.
12. Khaoua, S. O., Bournet, P., Migeon, C., Boulard, T., & Chasseriaux, G. (2006). Analysis of greenhouse ventilation efficiency based on computational fluid dynamics. *Biosystems Engineering, 95*(1), 83-98.
13. Küçüktopcu, E., Cemek, B., Simsek, H., & Ni, J.-Q. (2022). Computational fluid dynamics modeling of a broiler house microclimate in summer and winter. *Animals, 12*(7), 867.
14. Li, G., Tang, L., Zhang, X., Dong, J., & Xiao, M. (2018). Factors affecting greenhouse microclimate and its regulating techniques: A review. In IOP Conference Series: Earth and Environmental Science, IOP Publishing
15. Roy, J., & Boulard, T. (2004). CFD prediction of the natural ventilation in a tunnel-type greenhouse: influence of wind direction and sensibility to turbulence models. In International Conference on Sustainable Greenhouse Systems-Greensys2004 691,
16. Saberian, A., & Sajadiye, S. M. (2019). The effect of dynamic solar heat load on the greenhouse microclimate using CFD simulation. *Renewable Energy, 138*, 722-737.
17. Senhaji, A., Mouqallid, M., & Majdoubi, H. (2019). CFD assisted study of multi-chapels greenhouse vents openings effect on inside airflow circulation and microclimate patterns. *Open Journal of Fluid Dynamics, 9*(2), 119-139.

18. Shklyar, A., & Arbel, A. (2004). Numerical model of the three-dimensional isothermal flow patterns and mass fluxes in a pitched-roof greenhouse. *Journal of Wind Engineering and Industrial Aerodynamics*, *92*(12), 1039-1059.
19. Sørensen, D. N., & Nielsen, P. V. (2003). Quality control of computational fluid dynamics in indoor environments. *Indoor air*, *13*(1), 2-17.
20. Tajik, A. R., Shamim, T., Al-Rub, R. K. A., & Zaidani, M. (2017). Two dimensional CFD simulations of a flue-wall in the anode baking furnace for aluminum production. *Energy Procedia*, *105*, 5134-5139.
21. White, F. (1998). Fluid mechanics: Viscous flow in ducts Fourth Edition: New York: McGraw-Hill.
22. Zhang, H., Li, X., Wang, Y., Yao, J., Kang, Y., & Wang, Y. (2017). Evaluation and analysis of internal flow field uniformity in grain stack based on multi zone model of porous media. *Procedia Engineering*, *205*, 2164-2170.

Corresponding author:
Bilal CEMEK, Ph.D., Department of Agricultural Structures and Irrigation, Faculty of Agriculture, Ondokuz Mayıs University, 55139 Samsun, Turkey, Phone: +90 362 3121919, e-mail: bcemek@omu.edu.tr

ANALYSIS OF FLUID FLOW IN RADIAL CENTRIFUGAL PUMP

Jan ČERNÝ[1], Martin POLÁK[1]

[1]*Department of Mechanical Engineering, Faculty of Engineering, Czech University of Life Sciences Prague, Prague, Czech Republic*

Abstract

The paper presents validation of results of a numerical model of radial centrifugal pump flow using an experimental method PIV (Particle Image Velocimetry). For this purpose, a 3D model of the pump was created in Inventor, which was then used to design a numerical flow model in Ansys in the CFX module. The performance characteristics of the same pump were measured on an experimental test circuit, and vector maps of the flow in the suction pipe were obtained using the PIV method. The results of the experiment – vector fields of fluid velocity distribution in a suction pipe – were then compared with the outputs of the numerical Ansys model, namely the flow curves and pressure distribution. This comparison demonstrated that the numerical model achieves the best agreement with reality if the input variables are the pressure in front of the pump and the mass flow behind the pump. In this case, the model can calculate the pressure at the pump inlet with a deviation of 1% to 10% and create streamlines in the suction pipe corresponding to the results of PIV measurements.

Key words: *Particle image velocimetry (PIV), ANSYS, centrifugal pump, performance characteristic.*

INTRODUCTION

The more modern technologies evolve, the more the design and innovation of machine parts are transferred to the virtual environment. The programs Catia, Inventor, SolidEdge, SolidWorks, NX cad, CFturbo, and many others have been used recently for this purpose (*Chandrasekaran, Santhanam, and Venkateshwaran, 2021*). The programs Ansys, TCAE, FlexSim, AutoCAD CFD, and others are used to simulate fluid flow. They are used to verify the functionality or innovation of components (*Gülich, 2010*). For example, (*Sankar, 2018*) used Ansys to study the impact of change in the number of impeller blades and the size of their outlet angle on the efficiency and head of the pump. However, the validation of numerical models, i.e., their experimental verification, remains an issue. For example, (*Hassan, Abdallah, and Abou El-Azm Aly, 2016*) compared the numerical model of a pump in the Ansys program with experimental measurements when innovating the impeller. In their work, (*Alemi et al., 2015*) verified the numerical model with available experimental data, and there was good agreement between the model's results and reality. The pressures and flow rates of the flowing fluid can be easily verified using pressure gauges and flowmeters. The measurement is described in the standard ISO 9906 (*International Organization for Standardization, 2012*). Other more sophisticated methods for capturing fluid flow can be PIV (Particle Image Velocimetry) methods (*Corpetti et al., 2006*). PIV methods are usually used successfully to verify Ansys simulations. For example, (*Furst et al., 2021*) reached an agreement on the streamline's shapes and the fluid velocity when verifying the mathematical model with the measured values in the test laboratory using PIV. On the other hand, (*Owida et al., 2010*) compared PIV and Ansys models and did not reach an agreement. The reason was the imperfect transparency of the pump during experimental measurements. To obtain reliable results from numerical models, the setting of the density of the computational mesh is one of the most important parameters. A coarse mesh is computationally simpler but can severely skew the results. In contrast, a finer mesh gives more accurate results, but the computation time increases, and convergence becomes complicated (*Gülich, 2010*).

The aim of this research was to verify the reliability of the numerical Ansys model for predicting fluid behaviour when flowing through a radial centrifugal pump.

MATERIALS AND METHODS

Flow visualization in the suction pipe using the PIV method

Verification tests were conducted on an open hydraulic circuit in the laboratory of fluid mechanics at the Faculty of Engineering, Czech University of Life Sciences Prague. The circuit diagram is shown in Figure 1.

The test circuit consisted of a tested pump (P), a reservoir with pipes, and control and measuring devices. The motor with the momentum sensor (D) Magtrol TMB 307/41 (accuracy 0.1%) allowed for the continuous regulation of shaft speed via the frequency converter (FC) LSLV0055s100-4EOFNS. The water flow was measured using an electromagnetic flowmeter (Q) SITRANS FM MAG 5100 W (accuracy 0.5%). The pressures at pump inlet p_s (p-in) and pump outlet p_p (p-out) were measured by the pressure sensor HEIM 3340 (accuracy 0.5%), which was installed according to the first-class accuracy requirements.

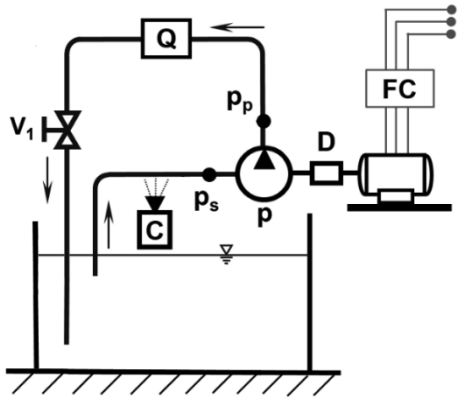

Q – flowmeter
P – tested pump
V_1 – control valve
p_p, p_s – pressure sensors
D – dynamometer
FC – frequency converter
C – camcorder PIV

Fig. 1 Hydraulic circuit for pump testing (*Polák, 2019*)

A single-stage radial centrifugal cast iron pump with a spiral casing was used for the measurement. The diagram of the pump and its performance parameters guaranteed by the manufacturer is presented in Fig. 2. The evaluation tests were based on the CSN EN ISO 9906 standard providing the tests of hydrodynamic pumps. The measurements were performed at 1,450 rpm and 2,950 rpm, which were set using a frequency converter. The torque was measured by a torque sensor on the shaft between the pump and the electric motor. The pressures were monitored by pressure sensors on the suction (p_s) and discharge pipes (p_p). The flow through the pump was measured using a flowmeter located in front of the throttle valve. Gradual closing of the throttle valve increased the head of the pump. The power parameters of the pump were measured at constant speeds, and velocity field measurement was performed synchronously using the PIV method.

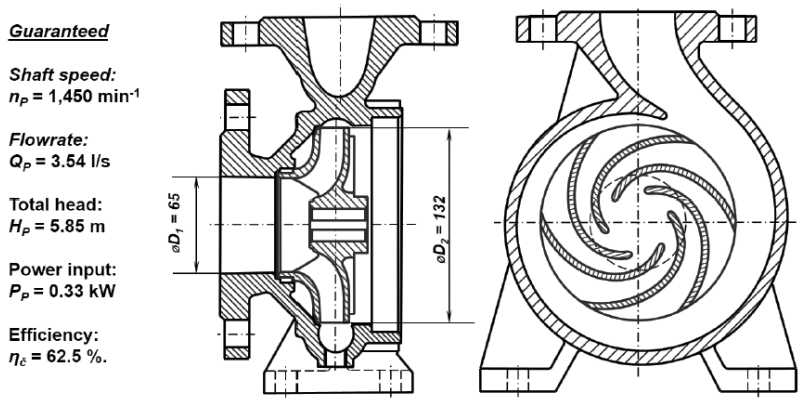

Fig. 2 Cast iron impeller in spiral casing and parameters of pump *(Polák, 2017*)

A 2D PIV set from the TSI company was used to measure the velocity fields in the pump suction pipe (see Fig. 3). The basis was a two-pulse Nd:YAG laser (YAG100-100-LIT) with a wavelength of 532 nm operating with an optical device Light Sheet Optics 610026 and a camera Powerview Cameras 630092. The set was completed by a synchronizer LaserPulse Model 610036 and COMPUTER for PIV 600054-64 with INSIGHT ™ 4G-2DTR Data Acquisition software. Fluorescent particles were dispersed in the flowing fluid –hollow glass spheres 100-SLVR with a diameter of 12 μm, silver-coated to increase the reflection of light on the surface.
A vertical plane in the axis of the transparent suction pipe at the pump inlet was selected to monitor the flow (see Fig. 3). A laser was placed above the pipe, repeatedly emitting two consecutive light pulses with a time delay of 50 μs. The optical system directed the emitting laser beam into a thin light sheet which illuminated the monitored area in the suction pipe. A high-speed camera positioned perpendicular to the plane scanned the area at the same frequency as the laser pulses. This was provided by the synchronizer. The images from the camera captured the positions of the fluorescent particles. The first image (t) displayed the initial positions of the particles and the second (t′) the final positions. The image processing was carried out by specialized software, which, by comparing the corresponding pairs, determined the directions and sizes of the velocity vectors of individual particles or flowing fluid. The Scilab program was used to visualize the measured data. The graphical form of the vector fields was created in this program.

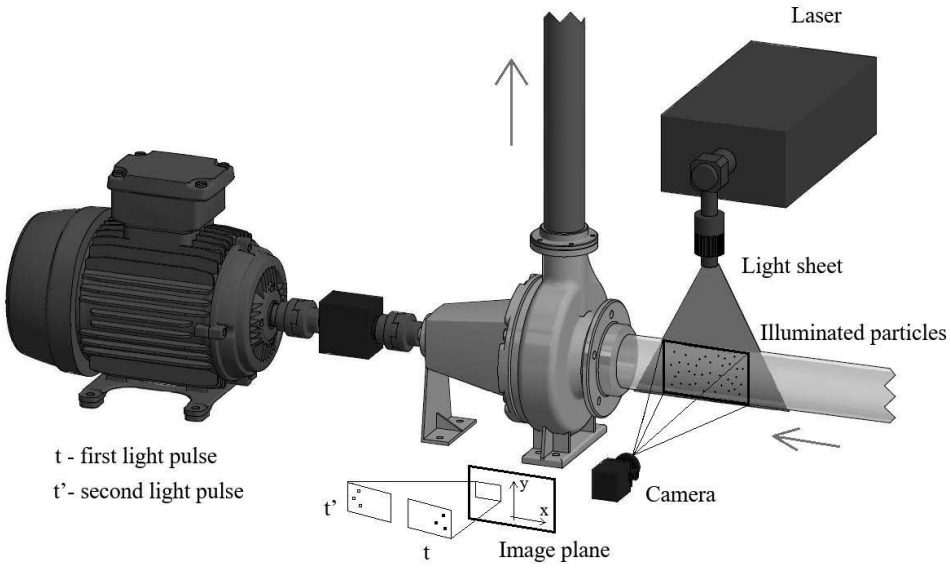

Fig. 3 Diagram of PIV method application during the experiment (*Černý and Sitte, 2020*)

Numerical model of flow in the suction pipe
The model of the pump (spiral casing, impeller, and suction pipe) was created in the Inventor 2022 program. For the purposes of numerical flow simulations in the Ansys program, the model was further modified to fill the flowing fluid space with a fine tetrahedral mesh. Two of the most important mesh quality parameters are Element Quality and Skewness. The value of Element Quality ranges from 0 to 1. A value of 1 indicates a perfect cube or square, while a value of 0 indicates that the element has a zero or negative volume. Its value is calculated according to equation (1), where parameter C corresponds to the element type. For tetrahedrons, C = 124.70765802. The frequency of mesh elements was highest in the interval of element quality values from 0.9 to 1, inclusive.

$$Element\ Quality = C\left[volume/\sqrt{(\sum(Edge\ length)^2)^3}\right] \quad (1)$$

Skewness is actually directly related to the quality of mesh structure, and it shows how close the mesh structure is to its ideal shape or form. When the Skewness decreases, it means a higher element quality.

Figure 4 presents the graphical dependence of the number of elements on the Skewness value and, at the same time, the Skewness quality spectrum (*Ansys, 2012*). The numerical model of the pump experimentally verified in this study had the majority of mesh elements in the range of Skewness value 0 – 0,25, which corresponds to excellent mesh quality.

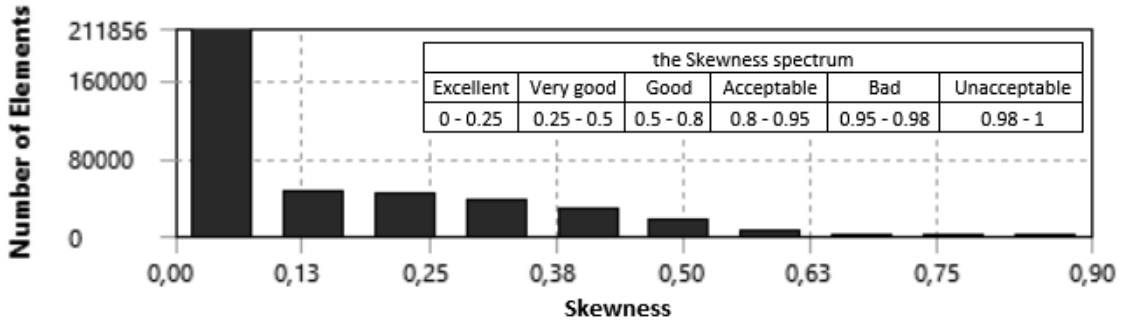

Fig. 4 Mesh quality according to skewness

To validate numerical models of flow using the PIV method, three sets of simulations were created in Ansys, which differ from each other by input parameters. The sets are marked with numbers 1 to 3, and their overview is presented in Tab. 1. For the first set of simulations, the measured pressure at the pump inlet and the mass flowrate at the pump outlet were used as input parameters. For the second set, the flowrate at the pump inlet and the pressure at the pump outlet were used. And for the third set of simulations, the velocity at the pump inlet obtained from the PIV measurement and the flowrate at the outlet were chosen. The calculated values of pressures and flowrates at the control points and graphically represented curves of the streamlines in the vertical plane in the axis of the suction pipe were the results of the numerical models. Simulations were performed at all points of the pump performance characteristics.

Tab. 1 Setting input parameters of numerical simulations

Setting No.	Input variables for numerical model
1	Pressure at the pump inlet, mass flowrates at the pump outlet
2	Mass flowrate at the pump inlet, pressure at the pump outlet
3	Velocity at the pump inlet from PIV, mass flowrate at the pump outlet

RESULTS AND DISCUSSION

The curves in the graph in Fig. 5 represent the pressure values (p-in/p-out), including the standard deviation, measured on the test circuit at 1,450 rpm. The measurement of the pump performance characteristic consisted of five partial measurements (P1 to P5). The points in the graph (Ansys out) indicate the calculated outlet pressures at setting 1 and are used for comparison with the measured outlet pressures (p-out). The points (Ansys in) are the calculated inlet pressures at setting 2 and are used for comparison with the measured values of inlet pressures (p-in).

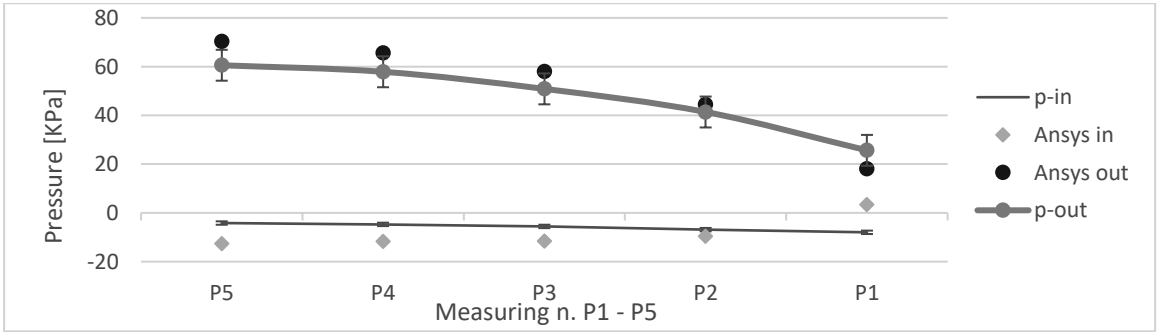

Fig. 5 Graph of measured and calculated pressures

At setting 1, the calculated pressure values are very close to the measured values – the largest deviation is 9.8%, the smallest less than 1%. At setting 2, the trend of the pressure course in Ansys was opposite to that of the measured values – i.e., the pressure at the pump inlet gradually decreased while the measured values increased. In most cases, the calculated pressure was significantly lower than the measured, even twice as much. For the calculations applied, the computation time of the numerical simulations increased with increasing head. In the first measurements (P1), the convergence occurred within 500 iterations; in the last (P5), the convergence occurred after 5000 iterations. This behaviour corresponds to the assumptions made by (*Gülich, 2010*) according to which the unsteady flow tends to converge more poorly. In setting 3, the calculation did not converge. Although this setting gave a good agreement with the shapes of the streamlines that corresponded to the PIV measurement, the results cannot be considered.

Another output of numerical models in Ansys were vector maps of fluid velocities in the suction pipe of the pump, which were compared with PIV measurements – see Fig. 6. For these purposes, vector maps were generated in Ansys in the vertical plane identical to PIV measurements, i.e., right in front of the impeller inlet. In this plane, velocity vectors were depicted only in the "tangential" direction (see Fig. 6, right). For comparison, the centre of the performance characteristic (P3) was selected, corresponding to the maximum efficiency and for which the manufacturer guarantees the parameters of the pump. The maps below indicate a steady fluid flow from the right side, which fully corresponds to the PIV measurement. The velocity increases as the fluid moves to the left towards the impeller. Both Ansys and PIV show this fact. In the lower part of the picture, PIV measurements show vectors pointing in different directions, indicating vortices' formation. A more detailed description of the PIV method results is provided by (*Černý and Sitte, 2020*). The vector field in Ansys illustrates this vortex more prominently. The vortex is not local but arises along the entire inner circumference of the suction pipe. However, a 3D PIV measurement would be needed to accurately describe it because the particles in this part of the pipe move generally in space and thus outside the monitored plane, not captured by the 2D PIV method.

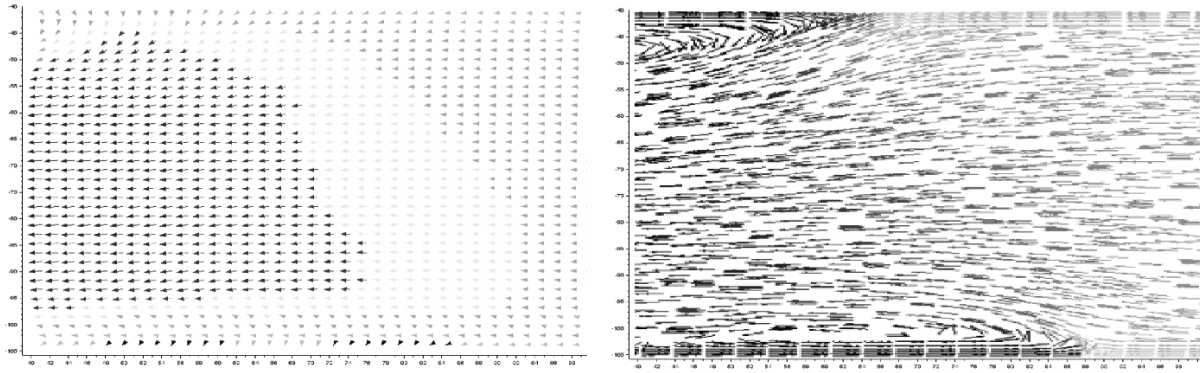

PIV method Ansys calculation

Fig. 6 Measured and calculated vector maps at 1450 rpm at measuring point P3

CONCLUSIONS

This research aimed to determine with what reliability it is possible to use a numerical model in Ansys to predict the behaviour of a fluid flowing through a radial centrifugal pump. For this purpose, the model's numerical and graphical outputs were compared with the values of measured performance characteristics and velocity fields obtained from the PIV method.

A comparison of the three different setting methods of the model in Ansys proved the best agreement of the calculation with reality when the pump inlet pressure and the pump outlet mass flowrate were set as input variables (setting 1). The calculated and measured parameters differed from 1 to 9.8% in this case. If the mass flowrate at the pump inlet and the pressure at the pump outlet (setting 2) were set as input variables, the deviations from reality were much greater. When the velocity at the pump inlet and the mass flowrate at the pump outlet were set as input variables, the calculation did not converge at all.

From the point of view of the analysis of vector maps of fluid velocities in the pump´s suction pipe, the model presents comparable shapes of streamlines at settings 1 and 2. Vector maps from the Ansys program correspond well to the outputs from PIV measurements. Possible differences are caused by the fact that 2D PIV shows vectors projected only into the measured area. Therefore, particles moving in the direction from/to the monitored plane will not be displayed in the result. In contrast, the Ansys model can display not only vectors in the area, but also their projections into all streamlines, in any cross section of the pipe. The results of this research, together with the flow model in Ansys, will be used as a basis for a more detailed flow analysis regarding the anticipated innovations of the radial centrifugal pump.

ACKNOWLEDGMENT
This study was supported by the Internal grant agency 2022 of the Czech University of Life Sciences Prague, number: 2022:31130/1312/3102

REFERENCES

1. Ansys. "ANSYS Meshing User's Guide." Release 14.5 (2012): 124-137.
2. Alemi, Hamed, Seyyed Nourbakhsh, Mehrdad Raisee Dehkordi, and Amir Najafi. 2015. 'Effects of Volute Curvature on Performance of a Low Specific-Speed Centrifugal Pump at Design and Off-Design Conditions'. *Journal of Turbomachinery* 137. doi: 10.1115/1.4028766.
3. Černý, Jan, and David Sitte. 2020. 'Analysis of the Flow of Liquid in the Suction Pipe of the Radial Centrifugal Pump'. in *Proceeding of 22nd International Conference of Young Scientists 2020*. Vol. 22. Prague: Czech University of Life Sciences Prague.
4. Chandrasekaran, M., V. Santhanam, and N. Venkateshwaran. 2021. 'Impeller Design and CFD Analysis of Fluid Flow in Rotodynamic Pumps'. *MATERIALS TODAY-PROCEEDINGS* 37(2, SI):2153–57.
5. Corpetti, T., D. Heitz, G. Arroyo, E. Memin, and A. Santa-Cruz. 2006. 'Fluid Experimental Flow Estimation Based on an Optical-Flow Scheme'. *EXPERIMENTS IN FLUIDS* 40(1):80–97.
6. Furst, Jiri, Tomas Halada, Milan Sedlar, Tomas Kratky, Pavel Prochazka, and Martin Komarek. 2021. 'Numerical Analysis of Flow Phenomena in Discharge Object with Siphon Using Lattice Boltzmann Method and CFD'. *MATHEMATICS* 9(15).
7. Gülich, Johann Friedrich. 2010. *Centrifugal Pumps*. Vol. c2010. Berlin: Springer.
8. Hassan, Ahmed, Haïscam Abdallah, and A. Abou El-Azm Aly. 2016. 'Effect of Impeller Blade Slot on Centrifugal Pump Performance'. *Global Journal of Researches in Engineerin* 16:71–85. doi: 10.17406/GJREjVol16Is4pg71.
9. International Organization for Standardization. 2012. 'ISO - ISO 9906:2012 - Rotodynamic Pumps — Hydraulic Performance Acceptance Tests — Grades 1, 2 and 3'. 59.
10. Owida, Amal, Hung Do, William Yang, and Yos S. Morsi. 2010. 'PIV MEASUREMENTS AND NUMERICAL VALIDATION OF END-TO-SIDE ANASTOMOSIS'. *JOURNAL OF MECHANICS IN MEDICINE AND BIOLOGY* 10(1):123–38.
11. Polák, Martin. 2017. 'Experimental Evaluation of Hydraulic Design Modifications of Radial Centrifugal Pumps'. *Agronomy Research* 15(Special Issue 1):1189–97.
12. Polák, Martin. 2019. 'The Influence of Changing Hydropower Potential on Performance Parameters of Pumps in Turbine Mode'. *Energies* 12(11). doi: 10.3390/en12112103.
13. Sankar, Shanmugasundaram. 2018. 'Analysis of Centrifugal Pump Impeller Using ANSYS'. *International Journal of Innovative Research in Science, Engineering and Technology* 7:5021–26.

Corresponding author:
Ing. Jan Černý, Department of Mechanical Engineering, Faculty of Engineering, Czech University of Life Sciences Prague, Kamýcká 129, Praha 6, Prague, 16521, Czech Republic, email: cernyjan@tf.czu.cz

USING ARTIFICIAL NEURAL NETWORK APPLICATION IN MODELLING THE MECHANICAL PROPERTIES OF LOADING POSITION AND STORAGE DURATION OF PEAR FRUIT

Elçin YEŞİLOĞLU CEVHER[1], Demet YILDIRIM[2], Gürkan Alp Kağan GÜRDİL[1]

[1]Department of Agricultural Machinery and Technologies Engineering, Faculty of Agriculture, Ondokuz Mayis University, Samsun, Türkiye
[2]Black Sea Agricultural Research Institute, Soil and Water Resources Department, Agricultural Irrigation and Land Reclamation, Samsun, Türkiye

Abstract
In the study, rupture energy values of Deveci and Abate Fetel pear fruits were predicted using Artificial Neural Network (ANN). The breaking energy of the pears was examined in terms of storage time and loading position, and the experiments were carried out in two stages with samples kept in cold storage immediately after harvest and 30 days later. Rupture energy values (output data) were estimated using four different single and multilayer ANN models. -Four different model results obtained using Levenberg - Marquardt, Scaled Conjugate Gradient and resilient backpropagation training algorithms were compared with the calculated values. Statistical parameters such as R^2, RMSE, MAE and MSE were used to evaluate the performance of the methods. Model 1 by ANN gave better results in network 5-1 the R^2 value is 0.90, the square of the root error is 0.018, and 0.093 in the MAE is obtained using three inputs.

Key words: *ANN, scaled conjugate gradient, rupture energy, prediction, Deveci, Abate Fetel.*

INTRODUCTION

Pear (Pyrus communis L.) is a type of fruit that was first grown in the Asian continent and spread all over the world. There are more than 5000 pear varieties in the world and about 640 of them are grown in Turkey (*Polatcı et al., 2020*). The determination of the physical and mechanical properties of the pear, which is widely produced in the world and has commercial importance, is important in the adoption and design of various unit operations. The fruit compression test simulates the static loading condition that the fruit can withstand during mechanical transport and storage (*Tabatabaekoloor, 2014*).
It is important in determining the physical, mechanical and quality characteristics of fruits under harvest and storage conditions. For this, various modeling studies are carried out. In recent years, especially soft calculation techniques have been used. Among these techniques, artificial neural networks (ANN) are widely used (*Wu et al., 2017*). The artificial neural network application is aimed to make high-accuracy predictions using a few inputs. Different input, network structure, training algorithm, number of iterations, etc. by creating different combinations, suitable ANN models were determined to be used to predict physical and mechanical properties. The ANN method was used to estimate the physiological characteristic change in pear, and it was determined that the ANN model made the best estimation based on real data (*Azadbakht et al., 2022*).
The aim of the study is to model the rupture energy of Deveci and Abate Fetel pear cultivars for loading location and storage time conditions using artificial neural network method. In the research, R^2, RMSE, MSE, MAE parameters were used as an acceptability indicator for the estimation of the rupture energy for pear.High accuracy predictions were made in the 4 ANN models created. Using these models according to the entered parameters, a high-accuracy estimation of rupture energy for pear can be made.

MATERIALS AND METHOD

Deveci and Abate Fetel pear varieties used in the research were harvested from SAMMEY fruit production farm in Samsun in October. Harvesting was done by hand. Pear varieties are divided into two groups for storage and room temperature conditions. Half of the separated pear cultivars were stored at 1˚C storage temperature and 90% relative humidity for 30 days. A refrigerator was used as a storage medium. Trials of the other half were carried out in a laboratory environment at 21±2˚C room temperature after harvest (*Yeşiloğlu et al., 2016*).

Kern brand electronic precision scales were used for mass measurements of pear varieties. Dimension measurements of fruits were made with a digital caliper (*Mohsenin, 1980; Yeşiloğlu et al., 2016*). The water-soluble dry matter content was determined digital refractometers (0.1% Bx, Davras et al., 2019). A single column Universal Tester (Lloyd Instrument LRX Plus, Lloyd Instruments Ltd, An AMETEK Company, Hampshire, UK) attached to a Magness-Taylor probe (10 mm) was used to obtain the firmness values of the fruits. Force was applied to fruit varieties with a 100 N capacity load cell at a compression speed of 10 mm/min. Data were obtained with NEXYGEN Plus Material Test Software Version 2.1 (Lloyd Instrument Ltd, An AMETEK Company) and in the force-deformation graph provided by the software was taken as the Magness-Taylor force (*Yeşiloğlu et al. 2016; Abbott et al., 1992*). With the calculation of the area under the curve, rupture energy values were obtained (*Yurtlu and Yeşiloğlu, 2011*). Estimation of the repture energy value (RE) for single and double-layer neural structures using different input combinations of length (L), thickness (T), width (W), mass (M), water soluble dry matter (WSDM), Magness-Taylor force values were made with artificial neural networks (ANN). The layers used in the study; input layer, middle layers (hidden layer) and output layer that are shown in Figure 1.

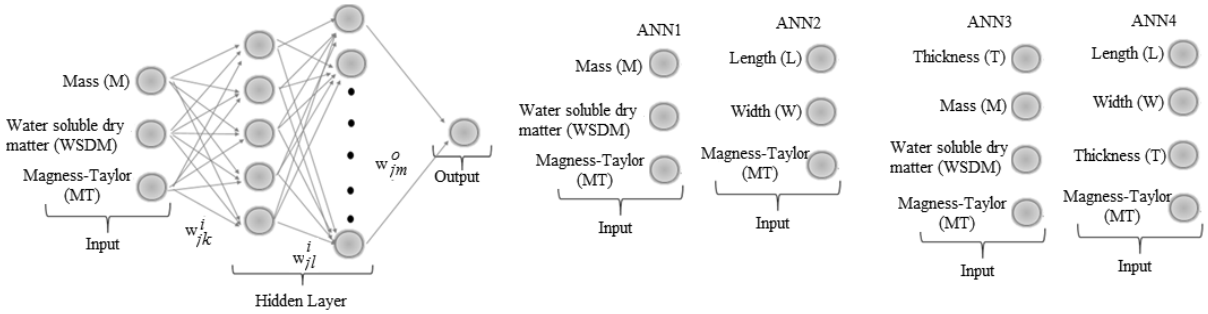

Fig. 1 Artificial neural network multi-layer structure with 3-5-8-1 and ANN models inputs

The ANN method requires adjusting the inter-network weight relationships and using a training pattern with appropriate output values. Necessary adjustments between the weights are made by adding rules to the training and thus a single information is obtained from the data. The model of a neural network is influenced by the network's topology, characteristics, and training algorithm (*Zhou and Si, 1998*) and (*Hagan and Menhaj, 1994; Parisi et al., 1996*). In this study, four different models were created with the inputs length, thickness, width, mass, and water soluble dry matterused in the study. The inputs used for the models (ANN1, ANN2, ANN3 and ANN4) are given in Fig. 1. For 4 models, estimations were made on single-layer networks as 5*1, 8*1, 10*1 and double-layer networks as 5*5*1, 5*8*1, 5*10*1. As an example, the model structure of ANN1 with 5*8*1 (double hidden layers) is shown in Figure 1. The results obtained by using three different training algorithms as Levenberg-Marquardt (LM), Scaled Conjugate Gradient (SCG) and Resilient Backpropagation (RP) were compared with the real values by performing 250-500-750 iterations. 174 (74%) of 274 data were used as training data and 60 (26%) as test data. The determination coefficient (R^2) of the data (*Azadbakht et al., 2017*), root mean square error (RMSE) (*Khoshnevisan et al., 2013; Azadbakht et al., 2018*), mean absolute error (MAE) (*Azadbakht et al., 2016*) and mean square error (MSE) (*Azadbakht et al., 2016*) values were calculated to choose the best model according to the highest R^2 and lowest RMSE, MSE, and MAE values. The aim of the study is to model the rupture energy of Deveci and Abate Fetel pear cultivars for loading location and storage time conditions using artificial neural network method. In the research, R2, RMSE, MSE, MAE parameters were used as an acceptability indicator for the estimation of the rupture energy for pear. High accuracy predictions were made in the 4 ANN models created. Using these models according to the entered parameters, a high-accuracy estimation of rupture energy for pear can be made.

RESULTS AND DISCUSSION

The descriptive statics properties of the mechanical properties measured for Deveci and Abate Fetel pear cultivars at storage and room conditions are shown in Table 2. Coefficient of variation (CV) measures the variation of an attribute. A CV ≤ 15% indicates a low variation, 16-35% a moderate variation, and a CV ≥ 36% high variation (*Wilding, 1985*). In the measured mechanical properties, CV values varied between 4.7%-39.3% in Deveci warehouse, 5.4%-37.6% in room conditions, and 3.4%-41.5% in

Abate Fetel warehouse conditions, 4.6%-41.9% in room conditions. The Skewness values for Deveci and Abate Fetel pear cultivars varied between 0 and 0.5 under storage and room conditions. It is accepted that the variables given in the table 1 show a normal distribution according to Skewness values.
In the study, 4 ANN models were created using different inputs. Using 3 inputs and 4 inputs, rupture energy was estimated for different model structures and the estimation results according to the training and testing datas, performance indicators are given in Table 2. 750 iterations were made in the SCG training algorithm, and better results were obtained than the LM and RP training algorithms. R^2 values were changed between 0.81 and 0.60 in LM and between 0.76 and 0.54 in RP for models and neural network. RMSE, MSE and MAE values higher results were obtained than the SCG training algorithms.

Tab 1 Descriptive statistical parameters for Deveci and Abate Fetel fruits

Variables		Max.	Min.	Mean	SD	CV	Skew-ness	Kur-tosis		Max.	Min.	Mean	SD	CV	Skew-ness	Kur-tosis
L	Deveci Stor-age	94.1	70.4	81.5	5.2	6.3	0.2	0.2	Abate Fetel Stor-age	130.5	117.2	122.9	4.2	3.4	0.3	-1.0
W		90.2	67.3	74.1	3.5	4.7	1.3	4.8		66.6	58.8	62.7	2.1	3.4	-0.2	0.1
T		87.8	61.4	71.2	4.0	5.6	0.4	2.7		63.8	53.5	58.7	2.8	4.8	-0.2	-0.1
M		317.5	181.8	214.6	20.6	9.6	1.3	5.6		227.1	182.3	206.2	13.8	6.7	-0.3	-1.0
WSDM		12.4	7.6	9.9	1.0	10.5	0.4	-0.1		15.3	12.9	13.9	0.7	4.8	0.5	0.0
MT		78.5	26.7	53.1	13.0	24.4	-0.2	-0.6		59.3	23.0	40.6	9.5	23.3	0.0	-0.4
RF		0.3	0.0	0.2	0.1	39.3	0.4	0.02		0.3	0.0	0.1	0.1	41.5	1.0	0.5
L	Deveci Har-vest-ing	92.2	61.2	79.3	6.5	8.1	-0.4	0.9	Abate Fetel Har-vest-ing	130.6	113.6	122.9	5.7	4.6	0.0	-1.3
W		94.0	75.4	86.2	4.8	5.5	-0.3	-0.7		66.5	53.7	58.1	3.3	5.7	1.5	2.6
T		94.8	72.7	82.9	4.4	5.4	0.1	0.8		65.1	50.1	59.2	4.3	7.2	-0.7	0.1
M		360.2	260.1	309.0	23.4	7.6	0.2	-0.5		234.9	175.7	207.8	18.3	8.8	-0.5	-0.8
WSDM		15.7	9.5	12.0	1.2	10.2	0.7	1.7		13.7	10.8	11.8	0.8	6.6	1.1	1.3
MT		67.7	20.3	40.9	10.1	24.6	0.3	-0.2		59.0	15.2	37.8	10.7	28.4	-0.3	-0.6
RF		0.3	0.0	0.1	0.0	37.6	0.6	1.1		0.3	0.0	0.1	0.1	41.9	0.2	-0.3

SD: Standard Deviation, CV: Coefficient of Variation

In ANN1, ANN2, ANN3, and ANN4 models, R^2 values in single and double-layer network structures varied between 0.86 and 0.94 and the distribution graphs are shown in Figure 2. By evaluating all data estimations, the most accurate rupture energy estimation was made using the SCG training algorithm with a single layer in the ANN1 (3*5*1) model for determining Deveci and Abate Fetel pear cultivars under storage and room conditions. Distribution and scatter graphs for rupture energy estimated storage and room conditions of Deveci and Abate Fetel pear varieties are presented in Figure 3. With the evaluation of the results, rupture energy estimation was made using the M, WSDM, and MT (ANN1) inputs. When there is missing data from the input parameters used in the study, accurate predictions can be made using the other 3 models (ANN2, ANN3, and ANN4). *Ziaratban et al., (2016)* used mathematical modeling of volume and surface area and feed-forward artificial neural network methods in Golden Delicious apples and using different training algorithms (GD, CGF, LM) 5, 10, 15 neuron structures, they predicted with high accuracy (R^2 0.99) for 15 neuron structures in the LM training algorithm. In the studies, different network neuron structures were modeled using 5, 10 (*Azadbakht et al., 2022*), between 2 and 20 neurons (*Vasighi-Shojae et al., 2020*) the and LM training algorithm (*Azadbakht et al., 2022*).

Tab. 2 Statistical results between calculated and predicted rupture energy in training and testing data

		SCG							
		Training Data				Testing Data			
Model	Model structure	R^2	RMSE	MSE	MAE	R^2	RMSE	MSE	MAE
ANN1	3-5-1	**0.94**	**0.0152**	**0.0002**	**0.1397**	**0.86**	**0.0256**	**0.0007**	**0.7853**
	3-8-1	0.91	0.0191	0.0004	0.1396	0.85	0.0270	0.0007	0.7843
	3-10-1	0.82	0.0295	0.0009	0.1391	0.80	0.0320	0.0010	0.7803
	3-5-5-1	0.88	0.0234	0.0005	0.1394	0.81	0.0259	0.0007	0.7829
	3-5-8-1	0.88	0.0238	0.0006	0.1394	0.75	0.0386	0.0015	0.7808
	3-5-10-1	0.83	0.0354	0.0013	0.1387	0.76	0.0326	0.0013	0.7784
ANN2	3-5-1	0.81	0.0287	0.0228	0.1391	0.80	0.0246	0.1061	0.7807
	3-8-1	**0.83**	**0.0266**	**0.0228**	**0.1392**	**0.91**	**0.0173**	**0.1057**	**0.7814**
	3-10-1	0.80	0.0367	0.0227	0.1386	0.87	0.0265	0.1056	0.7783
	3-5-5-1	0.83	0.0263	0.0229	0.1392	0.78	0.0434	0.1075	0.7800
	3-5-8-1	0.83	0.0273	0.0228	0.1392	0.79	0.0411	0.1072	0.7799
	3-5-10-1	0.79	0.0378	0.0227	0.1385	0.86	0.0202	0.1052	0.7782

ANN3	4-5-1	0.85	0.0268	0.0007	0.1392	0.92	0.0170	0.0035	0.7777
	4-8-1	0.80	0.0330	0.0011	0.1388	0.88	0.0244	0.0050	0.7783
	4-10-1	0.82	0.0261	0.0007	0.1392	0.82	0.0241	0.0038	0.7745
	4-5-5-1	**0.87**	**0.0250**	**0.0006**	**0.1393**	**0.94**	**0.0155**	**0.0029**	**0.7790**
	4-5-8-1	0.82	0.0282	0.0008	0.1391	0.87	0.0220	0.0043	0.7737
	4-5-10-1	0.78	0.0358	0.0013	0.1387	0.73	0.0236	0.0062	0.7763
ANN4	4-5-1	0.79	0.0291	0.0008	0.1391	0.81	0.0249	0.0045	0.7788
	4-8-1	0.81	0.0278	0.0008	0.1392	**0.90**	**0.0189**	**0.0040**	**0.7773**
	4-10-1	0.77	0.0365	0.0013	0.1386	0.84	0.0343	0.0078	0.7785
	4-5-5-1	**0.85**	**0.0241**	**0.0006**	**0.1394**	0.87	0.0238	0.0033	0.7793
	4-5-8-1	0.79	0.0409	0.0017	0.1383	0.85	0.0342	0.0086	0.7780
	4-5-10-1	0.78	0.0334	0.0011	0.1388	0.82	0.0236	0.0060	0.7761

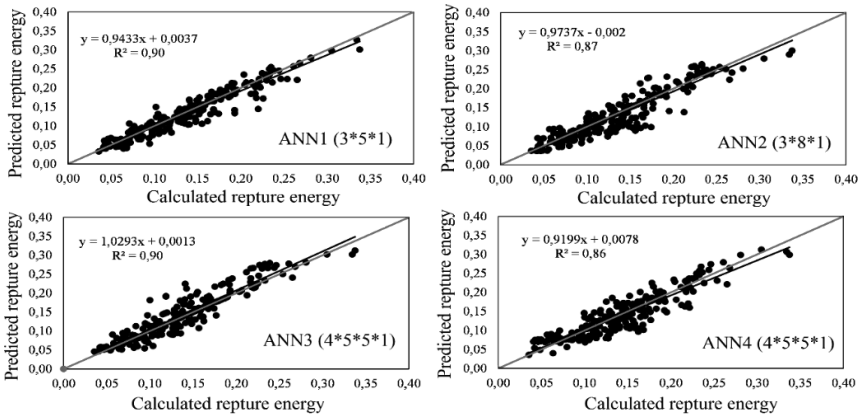

Fig. 2 Rupture energy results for all data by the best ANN models

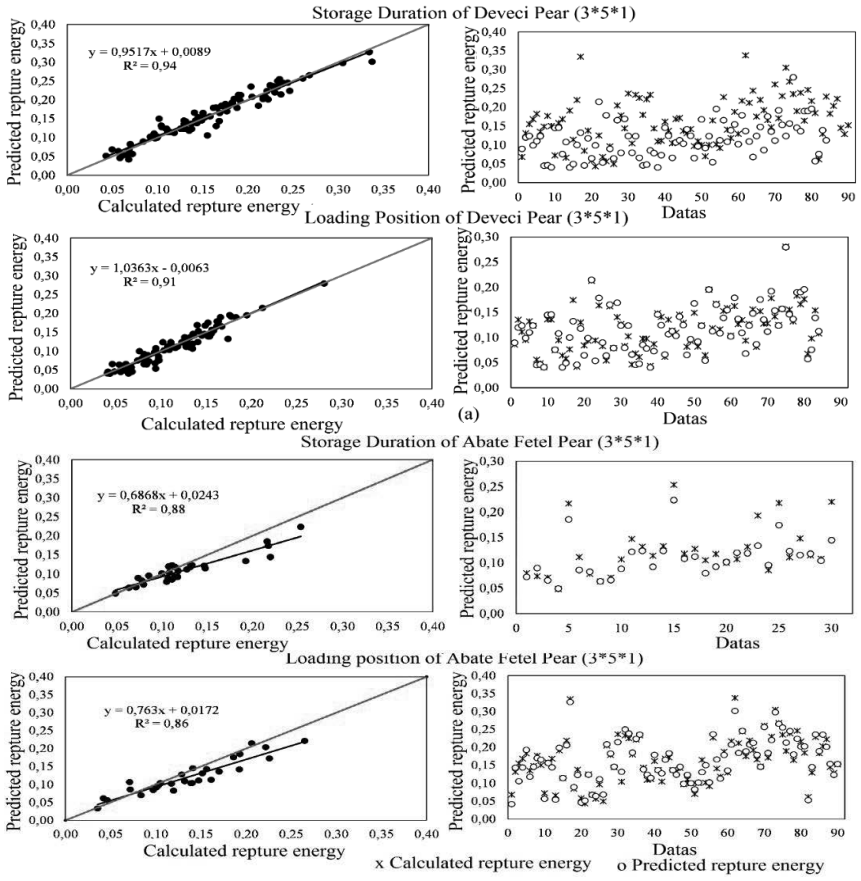

Fig. 3 Scatter plots between calculated and predicted rupture energy results by ANN1 a) storage duration and loading position of Deveci pear b) storage duration and loading position of Abate Fetel pear

Gorzelany et al., (2022) were reported to predict of mechanical properties of fresh and stored fruit of large cranberry by used artificial neural network. *Zarifneshat et al., (2012)* estimated the volume of apple fruit crunches using an artificial neural network. In the study, they concluded that the ANN model is more accurate than the regression model. The R^2 value was calculated as 0.994 for the ANN model and 0.969 for the regression model.

CONCLUSIONS

In the study, mechanical properties of rupture energy for loading position and storage time conditions of Deveci and Abate Fetel pear cultivars were modeled using artificial neural network method.
In this study, the best model (3-5-1 model structure) determined in the study was used in the estimation of the Rupture energy value. High accuracy predictions were made in the created 4 ANN models. According to the input parameters, using these models, rupture energy estimations for pear can be made with high accuracy. According to the purpose of the ANN method, it is important to obtain highly accurate predictions using how little data. Based on this and evaluating the model results in the study, a high accuracy (R^2, 0.90) estimation was made in the 3*5*1 network structure according to the highest R^2 and lowest RMSE, MSE and MAE indicators. It is thought that the results of the study will be useful in estimating the breaking energy from the mechanical properties of the fruit by using the artificial neural network method and in the development of more powerful models. The study will also enable the development of models to be used to determine the mechanical and physical properties of different fruits grown in different regions.

REFERENCES

1. Abbott, J. A., Affeldt, H. A., & Liljedahl, L. A. (1992). Firmness Measurement of Stored-Delicious' Apples by Sensory Methods, Magness-Taylor, and Sonic Transmission. *Journal of the American Society for Horticultural Science*, *117*(4), 590-595.
2. Azadbakht, M., M. Vahedi Torshizi, A. Ziaratban, and E. Ghajarjazi. (2016). Application of artificial neural network (ANN) in predicting mechanical properties of canola stem under shear loading. Agric. Eng. Int. CIGR 182:413-425.
3. Azadbakht, M., H. Aghili, A. Ziaratban, and M. Vahedi Torshizi. (2017). Application of artificial neural network method to exergy and energy analyses of fluidized bed dryer for potato cubes. Energy 120:947–958. doi: 10.1016/j.
4. Azadbakht, M., M. Vahedi Torshizi, F. Noshad, and A. Rokhbin. (2018). Application of artificial neural network method for prediction of osmotic pretreatment based on the energy and exergy analyses in microwave drying of orange slices. Energy 165:836–845. doi: 10.1016/j.energy.2018.10.017.
5. Azadbakht, M., Mahmoodi, M.J., & Abbaszadeh-Mayvan, A. (2022). Prediction of physiological characteristic changes in pears subject to dynamic loading using artificial neural network (ANN). *International Journal of Horticultural Science and Technology*, *9*(3), 275-289.
6. Neural Network (ANN). *International Journal of Horticultural Science and Technology*, *9*(3), 275-289.
7. *School of Sciences. Department of Agricultural Machinery and Technologies Engineering*. Samsun, Türkiye.
8. Davras, İ., Koyuncu, M. A., & Erbaş, D. (2019). Reducing quality losses by salicylic acid treatment in tomato during cold storage. *Uluslararasi Tarim ve Yaban Hayati Bilimleri Dergisi*, *5*(2), 176-186.
9. Du, C. J., & Sun, D. W. (2006). Learning techniques used in computer vision for food quality evaluation: a review. *Journal of food engineering*, *72*(1), 39-55.
10. Gorzelany, J., Belcar, J., Kuźniar, P., Niedbała, G., & Pentoś, K. (2022). Modelling of mechanical properties of fresh and stored fruit of large cranberry using multiple linear regression and machine learning. *Agriculture*, *12*(2), 200.
11. Hagan, M. T., & Menhaj, M. B. (1994). Training feedforward networks with the Marquardt algorithm. *IEEE transactions on Neural Networks*, *5*(6), 989-993.
12. Khoshnevisan, B., S. Rafiee, and M. Omid. (2013). Prediction of environmental indices of Iran wheat production using artificial neural networks. Int. J. Energy Environ. 42:339–348.

13. Landeras, G., Ortiz-Barredo, A., & López, J. J. (2008). Comparison of artificial neural network models and empirical and semi-empirical equations for daily reference evapotranspiration estimation in the Basque Country (Northern Spain). *Agricultural water management*, *95*(5), 553-565.
14. Lu, H., Zheng, H., Lou, H., Jiang, L., Chen, Y., & Fang, S. (2010). Using neural networks to estimate the losses of ascorbic acid, total phenols, flavonoid, and antioxidant activity in asparagus during thermal treatments. *Journal of Agricultural and Food Chemistry*, *58*(5), 2995-3001.
15. Meisami-asl, E., and S. Rafiee. (2012). Modeling of physical properties of apple slices Golab variety using artificial neural networks. Agric. Eng. Int. CIGR J. 143:175–178.
16. Parisi, R., Di Claudio, E. D., Orlandi, G., & Rao, B. D. (1996). A generalized learning paradigm exploiting the structure of feedforward neural networks. *IEEE Transactions on Neural networks*, *7*(6), 1450-1460.
17. Polatci, H., Taşova, M., & Saraçoğlu, O. (2020). Armut (Pirus communis L.) Posasının Bazı Kalite Değerleri Açısından Uygun Kurutma Sıcaklığının Belirlenmesi. *Academic Platform Journal of Engineering and Science*, *8*(3), 540-546.
18. Tabatabaekoloor, R. (2014). Bio-mechanical behavior of kiwifruit as affected by fruit orientation and storage conditions. In *Proceedings International Conference of Agricultural Engineering* (pp. 06-10).
19. Vasighi-Shojae, H., Gholami-Parashkouhi, M., Mohammadzamani, D., & Soheili, A. (2020). Predicting mechanical properties of golden delicious apple using ultrasound technique and Artificial Neural Network. *Food Analytical Methods*, *13*(3), 699-705.
20. Wilding, L. P. (1985). Spatial variability: its documentation, accomodation and implication to soil surveys. In *Soil spatial variability, Las Vegas NV, 30 November-1 December 1984* (pp. 166-194).
21. Wu, S. W., Zhou, X. G., Cao, G. M., Liu, Z. Y., & Wang, G. D. (2017). The improvement on constitutive modeling of Nb-Ti micro alloyed steel by using intelligent algorithms. *Materials&Design*, *116*, 676-685.
22. Yurtlu, Y. B., & Yeşiloğlu, E. (2011).. Mechanical Behaviour and Split Resistance of Chestnut under Compressive Loading. *Journal of Agricultural Science* 17(4):337-34
23. Yeşiloğlu, E., Yıldırım, D., & Öztekin Y. B. (2016). Effect Of Loading Position And Storage Duration On The Mechanical Properties Of Abate Fetel Pear Variety. *6th International Conference on Trends in Agricultural Engineering (TAE)*. pp.714-718
24. Zarifneshat, S., Rohani, A., Ghassemzadeh, H. R., Sadeghi, M., Ahmadi, E., & Zarifneshat, M. (2012). Predictions of apple bruise volume using artificial neural network. *Computers and electronics in agriculture*, *82*, 75-86.
25. Ziaratban, A., Azadbakht, M., & Ghasemnezhad, A. 2017. Modeling of volume and surface area of apple from their geometric characteristics and artificial neural network. *International Journal of Food Properties*, *20*(4), 762-768.
26. Zhou, G., Si, J. 1998. Advanced Neural-Network Training Algorithm with Reduced Complexity Based on Jacobian Deficiency. *IEEE Transactions on Neural Networks*, *9*(3), 448-453.
27. Zarifneshat, S., Rohani, A., Ghassemzadeh, H. R., Sadeghi, M., Ahmadi, E., & Zarifneshat, M. (2012). Predictions of apple bruise volume using artificial neural network. *Computers and electronics in agriculture*, *82*, 75-86.
28. Ziaratban A., Azadbakht M., Ghasemnezhad A. 2016. Modeling of volume and surface area of apple from their geometric characteristics and artificial neural network. International *Journal of Food Properties*. ISSN: 1094-2912 (Print) 1532-2386.

Corresponding author:
Elçin YEŞİLOĞLU CEVHER, Ph.D., Department of Agricultural Machinery and Technologies Engineering, Faculty of Agriculture, Ondokuz Mayis University, Samsun, Türkiye, phone: +90 3623121919/1258, e-mail: elciny@omu.edu.tr

SPATIO-TEMPORAL VARIABILITY OF RICE CROP FROM REMOTE SENSING

Fiorentino COSTANZA[1], Barracu FRANCESCO[2], Spanu ANTONINO[2], D'Antonio PAOLA[1*], Francesco TOSCANO[1]

[1]*Università degli Studi di Basilicata, Dipartimento di Agraria, Sezione di Meccanica e Meccanizzazione Agricola (SAFE), viale dell'Ateneo Lucano 10, Potenza, Italia*
[2]*Università degli Studi di Sassari, Dipartimento di Agraria, Sezione di Agronomia, coltivazioni erbacee e genetica, Via E. De Nicola, 1, 07100 Sassari, Italia*

Abstract
In Italy there are about 150 varieties of rice and in the world, there are more than 3 thousand, each with different properties. Predicting rice yield at panicle initiation stage would provide valuable information for future planning.
In this study, RapidEye satellite images were acquired in order to provide spatio-temporal data of canopy reflectance at high spatio-temporal resolution, allowing to identify crop differences between and within fields. The study area was located in Sardinia, in a 35ha paddy field, where rice (Oryza Sativa) has been cultivated for over 30 years. Yield maps were acquired in both study years to validate the analysis.
Spectral information and reflectance analysis from remote sensing provide information about health and growth evolution. The potential of NDVI vegetation index to be used as yield estimator was investigated. A correlation analysis was performed between NDVI maps, derived from satellite images, and yield maps respectively in both study years. Correlation analysis has shown that seeding density is a determinant of yield although the NDVI index is influenced by additional factors such as the presence of weeds and plant diseases.

Key words: *yield maps, NDVI, seeding density.*

INTRODUCTION

The agricultural sector of rice growing must be set up against a background of the new challenges facing to both cultural input competition and the increasing demand for food, linked to competition on food prices caused by the globalization of markets. Agriculture, especially in developed countries, requires an approach to sustainable production from both an economic and environmental point of view (*Coppola, 2020*).
The precision agriculture approach could benefit from the use and the convergence of several technologies among which the Global Positioning System (GPS), Geographic Information System (GIS), miniaturized computer components, automatic control, in-field and remote sensing, mobile computing, advanced information processing and, wireless data transmission (*D'Antonio 2020; Gibbons, 2000*). Previous studies using remote sensing of rice crops have demonstrated relationships between the reflectance data and biophysical parameters (*Shibayama and Akiyama, 1989; Spackman et al., 2000; Cassanova et al., 1998*). These studies are characterized by the collection of ground-based radiometric data and they have successfully estimated biomass in rice, before the heading stage, by using NDVI vegetation index values. Other studies have shown that it is possible to estimate rice yield using vegetation indices from remote sensing (*Fablo and Felix, 2001; Alvaro et al., 2007*).
Rice (Oriza Sativa L.), an essential aliment in most Asian countries, accounts for more than 40% of caloric consumption worldwide (*IRRI, 2006*). Annual rice production amounted to approximately 755 million tons (*FAOSTAT, 2019*) for a yield of around 4,88 ton/ha in Asia (*FAOSTAT, 2019*). While in 2011 (*FAOSTAT, 2012*) production reached 650 million tons.
Profit from rice production rely on crop grain yield and total biomass produced. Predicting rice yield at panicle initiation stage would provide valuable information for future planning.
Yield efficiency depends mainly on accurate site-specific management, which needs a proper delineation of homogeneous zones in the field. Homogeneous zones are the result of the analysis of the combined interaction of chemical and physical soil properties, climate and plant (*Basso et al., 2016;*

Fiorentino et al., 2020; Elsharkawy et al., 2022). Homogeneous zone definition usually requires years of studies, depending on the field complexity.
Tomography, climate and canopy reflectance data provide direct or indirect management suggestions about crop canopy, nitrogen and chlorophyll content as well as weeds density.
The objective of this paper is to investigate the potential of Normalized Difference Vegetation Index (NDVI) to estimate rice yield at different growing stages. Yield maps were acquired to validate the analysis. Rice yield is strictly related to rice seedling density (number of rice seedlings per unit area)

MATERIALS AND METHODS

Site description and agronomic management

The experiment took place in Sardinia (8°43'40"E, 39°56'44"N, WGS 84) during two consecutive growing seasons, in a 35ha paddy field, where rice (Oryza Sativa) has been cultivated for over 30 years. The study area was divided in 9 sub-areas, as shown in figure 1.
In the first experimental growing season, the "Volano" (plots D and E) and "Karnak" (plots: A, B, C, F, G, H and I) cultivars, were planted. The crop cycle length was of 150 days.
The study field was a traditional paddy area continuously flooded; the wide field had the same treatment in terms of water use, fertilization, as well as disease and pest control. Two sub-areas have required some extra treatments in graminaceae weeds control, during crop cycle.
Broadcast sowing was done on 17th May, with seed density of 500 germinables seeds m^{-2}.
"Libero" (Indica subsp., plots D and E), "Karnak" (Japonica subsp., plots B, C, F, G, H and I) and "Carnise" (Japonica, plot A) varieties were planted in the field during the second growing season. The crop cycle length was of 160 days. Broadcast sowing was done on 15th May, with a seed density of 500 germinables seeds m^{-2}. Seed density showed a noticeable variability due to a mechanical fault on broadcast sowing or environmental conditions (wind and waves, seed flotating, etc).

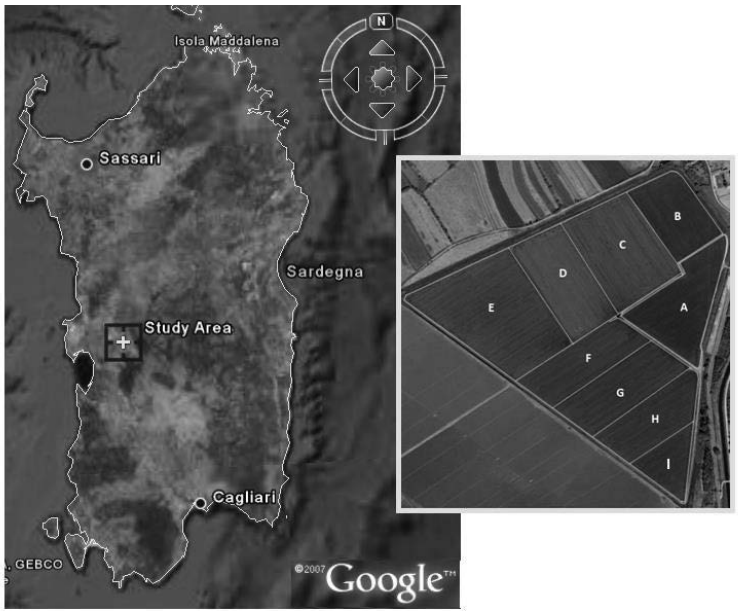

Fig. 1 Sardinia study area with the experimental plots

Field Measurements: Yield Maps

Georeferenced yield data were recorded by a New Holland combine harvester equipped with a yield monitor system (grain mass flow and moisture sensors). The data were acquired along 6 meters wide parallel transects. The average distance between two successive acquisitions was about 2 meters. Yield data were corrected based on the grain moisture content estimated by the combine harvester.
The 2 years yield maps (shown in figure 2), were obtained by plotting the yield data, elaborated by Ordinary Kriging at the nodes of a regular grid of 5 meters spatial resolution (*Goovaerts, 1997*).
It has been decided to analyzed separately the different cultivars, as a result of important discrepancies found between the mean of each yield distribution in the second year with respect to Karnak-Carmise

and Libero, while the difference was lower in the first experimental year for Volano and Karnak. The yield maps, shown in figure 2, were georeferenced and coregistrated in UTM WGS 84 zone 33N geographic reference system.

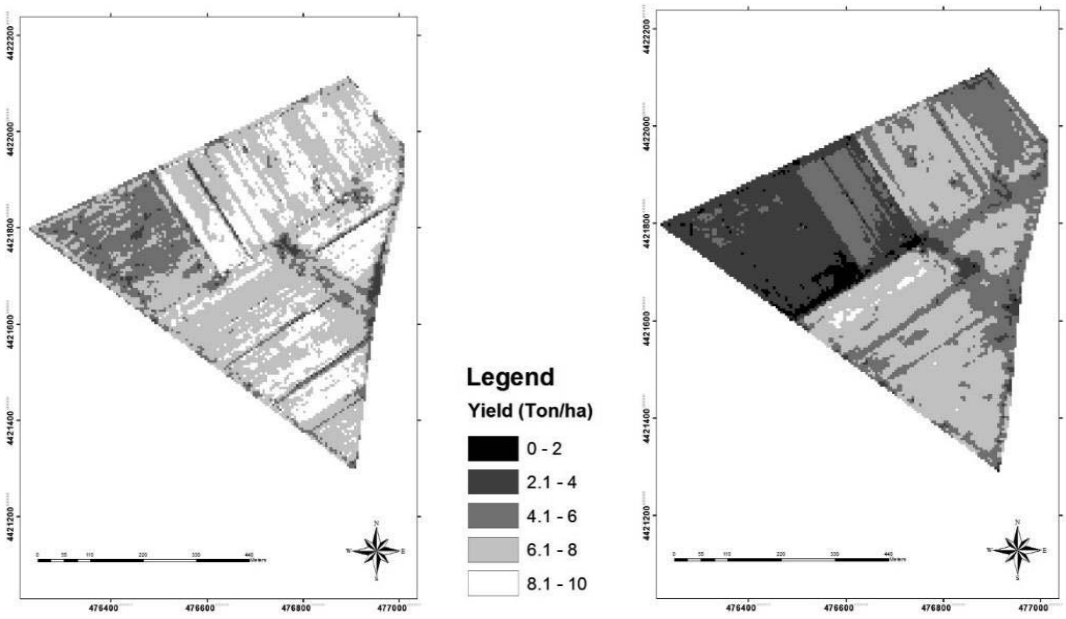

(a) (b)

Fig. 2 Yield maps for growing season 2010 (a) and 2011 (b)

Remote sensing images

A multi-temporal series of remote sensed images were acquired from the German company RapidEye A.G. (Brandeburg, DE). Satellite images were characterized by a spatial resolution of 5 meters and 5 narrow bands (spectral intervals of the electromagnetic radiation: Blue, Green, Red, Red-Edge and NearInfraRed). The images acquisition took place on 2010: 2th July, 28th July, 15th August and 10th September; and 2011: 26th June, 5th July, 16th July, 28th July 12, 20th August.

The Normalized Difference Vegetation Index (NDVI, Rouse et al., 1974) was computed as follows:

$$NDVI = (NIR - RED) / (NIR + RED) \quad (1)$$

NIR represents the wavelength in the near infrared portion of the electromagnetic spectrum (760-880 nm) and RED, the wavelength in the red portion of the spectrum (630-690 nm). All images, were geometrically and radiometrically corrected, and then, georeferenced and coregistered in UTM WGS84 coordinate system.

Correlation Analysis

A multitemporal time series of correlation maps were elaborated; the Pearson (*Hall, 1976; James, 1988*) correlation coefficients were computed at each node (5 meters equally spaced) of a regular grid associated to the corresponding pixels of the yield and the NDVI maps. The analysis has involved both studies years (2010 and 2011) at three different dates during the growing seasons. The NDVI maps involved in the analysis were: 2010 July 2nd and 2011 July 5th; 2010 July 28th e 2011 July 28th; 2010 August 15th e 2011 August 20th. The coupled dates of NDVI' maps involved in the analysis were very close, if not coincident, and relative to the same growing stage.

The spatial correlation maps, between NDVI and yield, were obtained by using a purpose-built Matlab script. Since it is not possible to consider each pixel independent from the neighbors at the spatial resolution of 5 meters, the Pearson analysis takes into account, not only of the corresponding pixels of each map, but all pixels that fall within a neighborhood centered on the pixel of interest. The neighborhood was defined as a circular moving window of a 30 meters diameter. The script produces a second output: the significance level (p-values) maps at each georeferenced location (acceptance level: p-val.<0.05).

RESULTS AND DISCUSSION

Yield maps

Figure 2 shows the yield maps for the growing season 2010 (a) and 2011(b). The average yield for the Karnak cultivar was higher in 2010 than in 2011.
In 2010 the average yield for the plots D and E, associated to the the Volano cultivar, was about 6,34 t ha^{-1}, while the remaining plots (Karnak cultivar) produced about 7,36 t ha^{-1}.
The average yields for Volano and Karnak cultivars do not show significant discrepancies.
Difference in levels of production between the fields E and D (YieldE<YieldD) (figure 2a) further supports this statement. This difference can be explained by the persistence of weeds in plot E, notwithstanding the operations of weed control.
In 2011, the average yield for the plots D and E, associated to the Libero cultivar, was about 3,31 t ha^{-1}.
From the observation of figure 2b we notice that yield in plots D and E was low, particularly in the south side of plot E. In the Karnak-Carmise plots, the average yield was about 6 t ha^{-1}, lower than the previous year because of the non-uniformity in seed density that occurred in 2011.
During both study years, the yield showed a marked spatial and temporal variability. Identification of stable zone in the field from visual inspection remains difficult.

NDVI and Yield Analysis

The number of rice seedlings in the field is one of the main agronomic components for determining rice yield and the yield is also strictly correlated to the plant growth.
In this paper, the NDVI index, acquired at different phenological stages of rice crop, was correlated to the yield map in both study years. The index allows to monitor both the distribution of plants in the field and their development over time.
The spatio-temporal correlation analysis was performed including the following NDVI dates:

- 2010 July 2nd and 2011 July 5th;
- 2010 July 28th and 2011 July 28th;
- 2010 August 15th and 2011 August 20th.

The study allows both to evaluate the behavior of a single sample point of the field, but also how it behaves with respect to its neighbors.
The correlation analysis determines the geographical relationship between NDVI and yield and highlights its distribution in the space. The correlation maps are shown in figure 3.
Figure 3a shows a high inverse correlation (p value <0.001) between yield and NDVI index in plots D and E, which was already evident from the beginning of July. This was due to the presence of weeds in both 2010 and 2011study years. A further complication occurred in 2011 with the appearance of the sterility of kernels in relation to the Libero variety. In this area, this negative correlation persists even in the analysis of the two successive dates. The infertility of kernels, that occurred in plot E in the second study year, was not detectable by the analysis of the vegetation index, but it was not influenced by nitrogen management decisions or by weeding control. It would be interesting to calibrate the index limit value beyond which the crop becomes infesting itself.
The inverse correlation will always be obtained when the density of the crop is higher than its optimum, both due to the presence of weeds, as well as to the excessive sowing density or the emission of too many adventitious stalks due to too much forced fertilization in tillering. Too many stalks imply too much flowering, too much nutrient need and increasing sterility. The crop becomes infesting itself.
In the plot B, the NDVI shows a high positive correlation with yield on July 2nd/5th (2010/2011), because during the first study year (2010), high NDVI values corresponded to good yield levels, while in 2011, the poor production was due to the low seeding density (i.e. low NDVI). At the second date the correlation is reversed and it also remained negative on the last reference date (August 15th/20th). The problem, in plot B, was the re-emergence of weeds during both study years, particularly in 2011.
In the plot C, the strong negative correlation between NDVI and yield, already evident at the first date (fig. 3a), was strongly influenced by the presence of weeds in 2011.
In the other plots (A, F, G, H and I) the significance level of correlation (pvalue> 0.05) was poor especially in the areas at the edges of the plots. This effect is more visible on July 2nd /5th while it progressively decreases at the other reference dates.

The negative correlation, in the central portion of plot A, stems from the high seeding density which occurred in 2011. Plot F shows the lowest correlation coefficients, in turn positive and negative that became quite high in some areas. It was, probably, due to the most productive zone during the first year that became the less productive in the second.
The NDVI vegetation index proved to be a good yield estimator according to *Guam et al. (2019)*.
They used small unmanned aerial vehicles (UAVs) for determining high-resolution normalized difference vegetation index. The NDVI values were used to assess their correlations with the rice yields. *Guam et al. (2019)* observed strong correlations between NDVI and yield at the early reproductive stage or the late ripening stage for the direct-seeded rice.
The limits that this methodology presents are the same as highlighted by *Wu et al. (2019)*, they proposed a method to earlier estimations of rice yield that uses computer vision to accurately count rice seedlings in a digital image.
The main cases of failure were:

- when dark areas such as shadows appeared in the image, recognized as rice areas;
- presence of weeds in images that requires more complex tecniques to be detected.

On the other hand, the use of the NDVI index from satellite requires lower spatial resolutions (5m) than the use of a UAV in the field and allows more frequent monitoring over time.

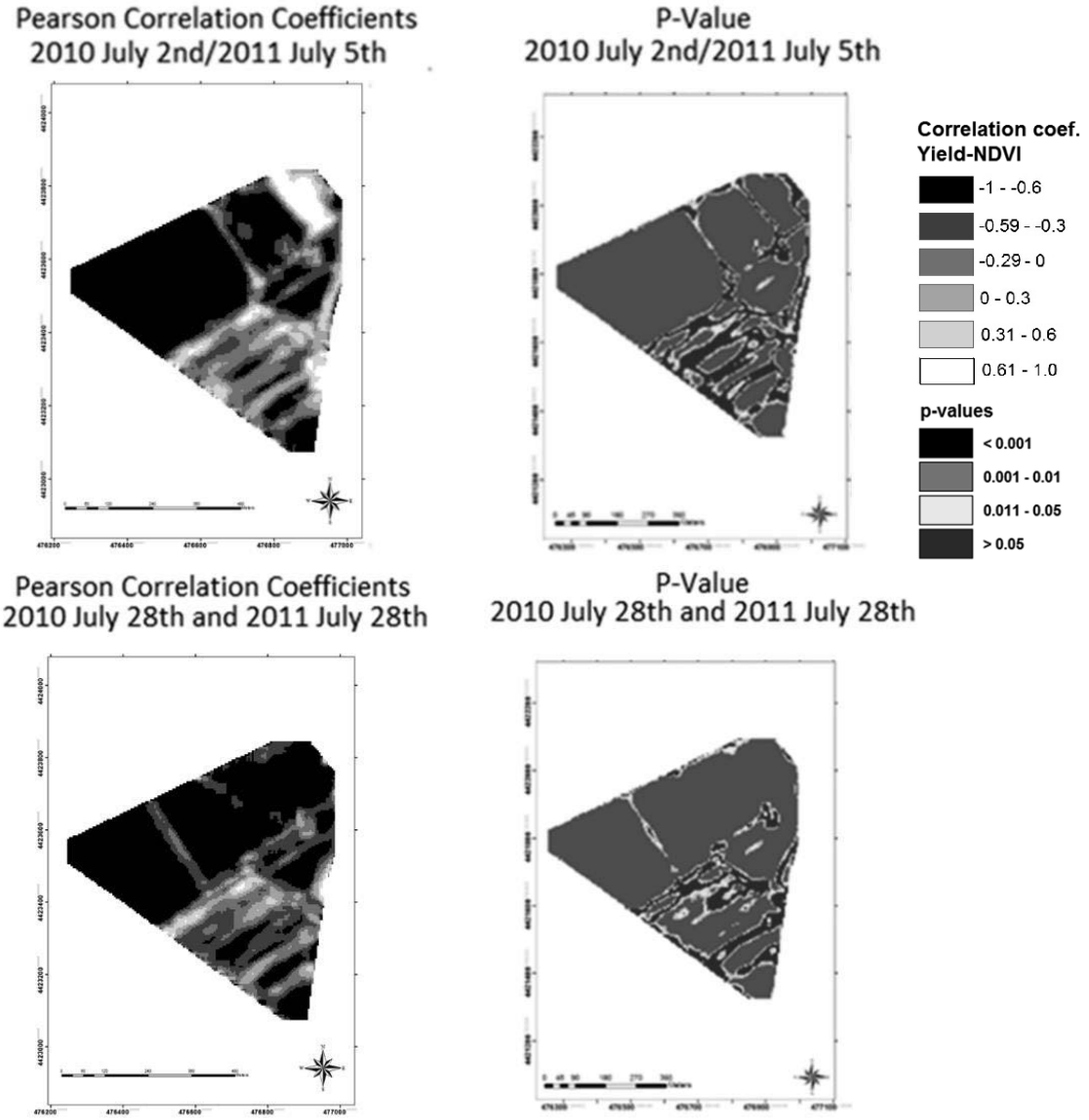

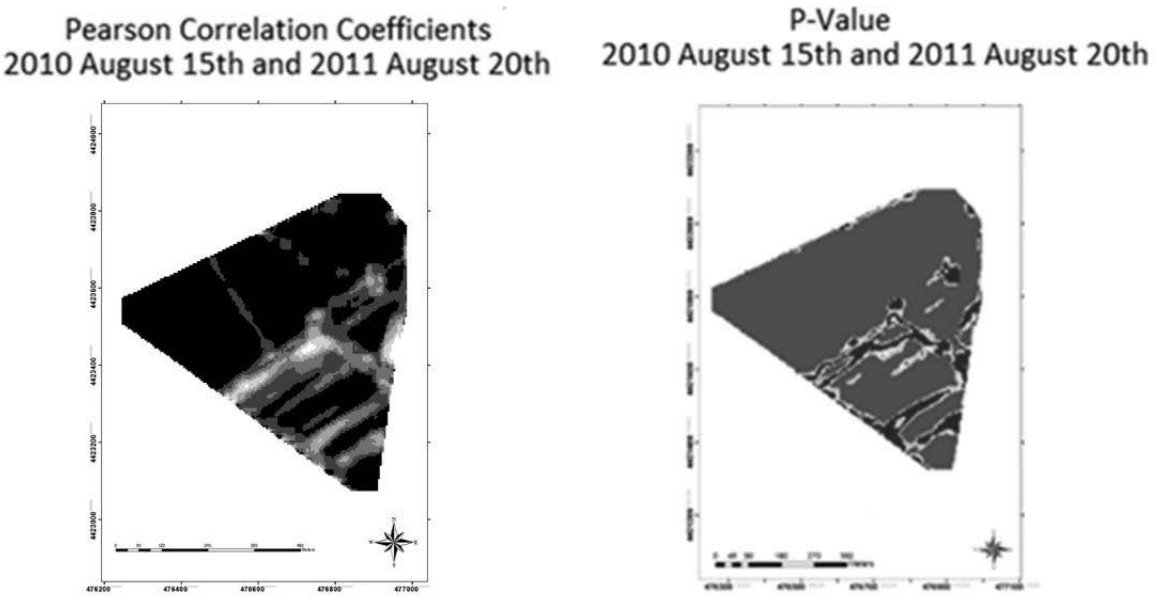

Fig. 3 Multitemporal sequence of correlation coefficients and significance maps between NDVI and yield

CONCLUSIONS

The remote sensing techniques could be an important support in the planning and management of vegetation during the growing season. They could also be used to estimate, rapidly and safely, the plant vigor and the crop potential yield.

The NDVI vegetation index, elaborated from satellite images, at different crop growing stage, was correlated with yield maps respectively in both study years. The combined study of the NDVI index and yield, has enabled the identification of potential threats related to seed density, along with the presence of pests and nutritional deficiency. Areas of high and low seeding density, as well as areas affected by weeds, were identified by

analyzing the mutual trend of NDVI index and production.

During the study years, the rice was affected by various problems, mainly the presence of weeds that made the analysis complex. In plots where no issues occurred, the NDVI index proved to be a good estimator of the yield and vegetation health during the growing season.

To address these problems, an additional analysis tool will be considered to be included in the processing chain to filter the presence of weeds from the remote sensing data.

ACKNOWLEDGMENT

This study was supported by the Italian project: CTMET – “Casa delle tecnologie emergenti” Matera-Italy.

REFERENCES

1. Alvaro, F., L. F. García del Moral, and C. Royo. 2007. Usefulness of remote sensing for the assessment of growth traits in individual cereal plants grown in the field. Intl. J. Remote Sensing 28(11): 2497-2512.
2. Basso B., Cammarano D., Fiorentino C., Ritchie J. T., 2013. Wheat Yield Response to Spatially Variable Nitrogen Fertilizer in Mediterranean Environment. *Eur. J. Agron.*.
3. Basso B., Fiorentino C., Cammarano D., Schulthess U., 2016 Variable rate nitrogen fertilizer response in wheat usingremote sensing.Precision Agriculture, DOI10.1007/s11119-015-9414-9.
4. Cassanova D., Epema G.F., and Goudriann J.. 1998. Monitoring rice reflectance at field level for estimating biomass and LAI. Field Crops Research 55:83-92.

5. Coppola A., Di Renzo G.C., Altieri G., D'Antonio P., 2020. Lecture Notes in Civil Engineering, Preface (Editorial) Volume 67, Pages v-vii.
6. D'Antonio P., Scalcione V. N., 2020. Software and satellite technologies for precision agriculture: the potential with, EPH – International Journal of Agriculture and Environmental Research.
7. Elsharkawy, M.M., Sheta, A.E.A.S., D'antonio, P., Abdelwahed, M.S., Scopa, A., 2022. Tool for the Establishment of Agro-Management Zones Using GIS Techniques for Precision Farming in Egypt. Sustainability (Switzerland), 14 (9), art. no. 5437.
8. Fablo M., and R. Felix., 2001. Analysis of GAC NDVI data for cropland identification and yield forecasting in Mediterranean African countries. Photogram. Eng. and Remote Sensing 67(5): 593-602 RRI. 2006.
9. FAOSTAT. 2019.Agricultural Statistics Yearbook: 2018.
10. FAOSTAT. 2012.Agricultural Statistics Yearbook: 2011
11. Fiorentino C., Donvito A.R., D'Antonio P., Lopinto S., 2020. Experimental Methodology for Prescription Maps of Variable Rate Nitrogenous Fertilizers on Cereal Crops Lecture Notes in Civil Engineering 2020, 67, pp. 863–872
12. Gibbons G., 2000. Turning a farm art into science */an overview of precision farming. URL: http:// www.precisionfarming.com.
13. Goovaerts P., 1997. Geostatistics for Natural Resources Evaluation. Oxford University Press, New York
14. Hall E.H., Computer Image Processing and Recognition, Academic, New York (1979), pp. 480-485.
15. Guan S., Fukami K., Matsunaka H., Okami M., Tanaka R., Nakano H., Sakai T., Nakano K., Ohdan H. and Takahashi K., 2019. Assessing Correlation of High-Resolution NDVI with Fertilizer Application Level and Yield of Rice and
16. Wheat Crops using Small UAVs. Remote Sens., 11, 112; doi:10.3390/rs11020112
17. James M., Pattern Recognition, John Wiley and Sons, New York (1988), pp. 36-40.
18. Rouse J.W., Haas R.H., Schell J.A., Deering D.W., 1974. Monitoring vegetation systems in the Great Plains with ERTS. Third ERTS Symp., NASA SP-351 1, pp. 309–317.
19. Shibusawa S., 1998. Precision Farming and Terra-mechanics. Fifth ISTVS Asia-Pacific Regional Conference in Korea, October 20 Á/22.
20. Spackman S., McKenzi G., Lamb D., and Louis J., 2000. Retrieving biophysical data from airborne multispectral imagery of rice crops. International Archives of Photogrametry and Remote Sensing B7:1447-1451
21. Tennakoon S. B., Murty V. V. N., and Eiumnoh A., 1992. Estimation of cropped area and grain yield of rice using remote sensing data. Intl. J. Remote Sensing13(3): 427-439.
22. Wu J., Yang G., Yang X., Xu B., Han L. and Zhu Y., 2019. Automatic Counting of in situ Rice Seedlings from UAV Images Based on a Deep Fully Convolutional Neural Network. Remote Sens., 11, 691; doi:10.3390/rs11060691

Corresponding author:
Prof. Paola D'Antonio, email: paola.dantonio@unibas.it

RHEOLOGICAL PROPERTIES OF FRUIT DISTILLATES

Ján CSILLAG[1], Daniela KUNECOVÁ[1], Tomáš HOLOTA[2], Matúš BILČÍK[1], Monika BOŽIKOVÁ[1]

[1]Institute of Electrical Engineering, Automation, Informatics and Physics
[2]Institute of Agricultural Engineering, Transport and Bioenergetics

Abstract
The article is focused on the experimental detection of rheological characteristics of fruit distillates. Distillates were processed with spirit of alcohol volume of 52%. 5 samples were researched. We observed dependency of dynamic viscosity, kinematic viscosity, density, and fluidity on temperature. The results were graphicly processed and regression equations, and the coefficient of determination were made. The stated courses declare strong exponential dependence of observed rheological characteristics on temperature. As different types of fruit distillates contain different additives, these may have influence on researched rheological characteristics. A specific part is devoted to thermogravimetric analysis – measures the mass (change of the mass), provides information on the content of components. Interpretation of the obtained TGA curves provides information about processes running in the materials, changes of physical and chemical properties and conditions of it, e.g., phase transitions, drying, oxidation stability, thermal stability, chemical reaction, denaturation, compositional analysis, purity, etc. Thermal analysis are respectable methods for analysis foods samples and alcohol.

Key words: *rheological properties, viscosity, thermogravimetric analysis, distillate.*

INTRODUCTION

While measuring alcohol of 99%, the density of a sample at a given temperature is same. On the other hand, as far as fruit distillates are concerned, we have alcohol volume 52 % and the left over 48 % are demineralized water and additives which are different for each sort. We can find out different courses depending on type of distillates by measuring rheological properties – density and viscosity.
Viscosity is defined by inner friction in liquid, it is the rate of resistance against mutual movement of molecules of fluid and it is the result of interaction between molecules (*Krempaský, 1982*). Viscosity can be kinematic and dynamic. Dynamic viscosity of fluids is functionally dependent on temperature and pressure, which means it decreases with increasing temperature and it increases with increasing pressure. Kinematic viscosity is determined by ratio of dynamic viscosity to density at a given temperature. Dynamic and kinematic viscosity of oils decrease considerably with increasing temperature. It is caused by aggregation of molecules at lower temperatures and by breaking up clusters at increasing temperature and by extending free volume in fluid, which means the difference between total volume of fluid and actual volume of present molecules (*Štěpina & Veselý, 1985*). Density is a quantity dependent on temperature and pressure. Density means the weight of defined volume of substance at a given temperature and pressure, usually 20 °C and 0,1 MPa. Density is an important figure for conversion units of volume and weight, and it is also important for calculating kinematic viscosity from dynamic one (*Štepina & Veselý, 1985*).
Thermogravimetric Analysis (TGA) are regarded as being the main techniques applied to improving the functional properties and process conditions. Can be investigated process of evaporation, destruction individual components and another. Effects where we can observed by TGA are compositional analysis, chemical reaction, desorption (drying, evaporation), enthalpy change, identification, oxidative stability and thermal stability. The result of the differential thermal analysis is a DTA-curve, which graphically shows the dependence of the temperature difference between the studied and reference sample (in units of electrical voltage, normally mV, since this difference is sensed as a voltage difference on the thermocouples under the studied and reference sample) on the temperature. On the DTA curve, we observe areas of zero values, when no action is taking place, and peaks. Peaks of positive values are caused by exothermic events and are called exoeffects, while peaks reaching negative values, so-called endoeffects, are caused by endothermic events (*Hrubá, 2018*). The term "differential" indicates that the difference in behaviour between the material under study and a supposedly inert reference material is

examined. In this manner the temperature at which any event either absorbs or releases heat can be found. This allows the determination of, e.g., phase transition temperatures and the study of order-disorder transitions and chemical reactions. Similarly, heat capacity measurements can be performed, although DTA and DSC differ significantly in the ease and precision of such measurements. These two methods are ideally suited for quality control, stability, and safety studies. These thermal analysis methods can be conducted simultaneously with other measurement methods to provide a greatly enhanced ability to understand material behaviour (*Lexa, 2002*). In cases blends contains starch, ethylene alcohol and water interpretation of the TGA results becomes quite difficult and usually important errors are committed in the determination of blend composition (*Vega, 1996*; *Tripodi, 2022*). Curves DTA and DTG we can help to identify exact temperature to process. The aim of the study was to detect experimentally rheological characteristics of fruit distillates. We researched five different samples with the same alcohol volume focusing on dependency of dynamic viscosity, kinematic viscosity, density, and fluidity on temperature. The second part of the research was focused on the interpretation of the obtained TGA curves.

MATERIALS AND METHODS

The measurement was carried out on five samples of distillates – cherry, plum, pear, peach, and apricot. The alcohol volume of all examined samples was 52 % at temperature 20 °C. The measurement of density was carried out on densimeter Mettler Toledo DM40. The principle of measurement of density is based on electromagnetic induced oscillation of U-shaped glass tube. Dynamic viscosity was measured on viscometer DV2T fy Brookfield. The principle of measurement is based on measurement of torque of spindle rotating in the sample at constant speed. Dynamic viscosity derived from Newton's law is characterized by a relationship:

$$\tau = \eta \; grad \; v \qquad (1)$$

where: $grad\ v = \frac{dv}{dh}$ - the size of velocity gradient (s^{-1}),
τ - shear stress (Pa),
η - dynamic viscosity (Pa.s).

The basic unit of dynamic viscosity is Pa.s., but a thousand times smaller unit mPa.s is usually used (*Krempaský, 1982*).

The temperature effect on viscosity can be described by an Arrhenius type equation:

$$\eta = \eta_0 e^{-\frac{E_A}{RT}} \qquad (2)$$

where: η – dynamic viscosity (Pa.s),
η_o – the reference value of dynamic viscosity (Pa.s),
EA – activation energy ($J.mol^{-1}$),
R – gas constant (8,314472 $J.K^{-1}.mol^{-1}$),
T – thermodynamic temperature (K).

Many authors (*Hlaváč, 2011*; *Munson et al., 2009*) explain, that the temperature dependence of viscosity may be explained by cohesive forces between molecules, too. These cohesive forces between molecules decrease with increasing temperature and flow becomes freer. As a result, viscosity of liquids decreases with increasing temperature. The fluidity of liquids in liquid state can be explained by relatively weak forces of mutual activity of molecules and their high movability. The fluidity of various liquids is different, and it equals to reciprocal of dynamic viscosity:

$$\varphi = \frac{1}{\eta} \quad (Pa^{-1}.s^{-1}) \qquad (3)$$

Kinematic viscosity can be defined as quotient of dynamic viscosity and density of liquids when measured at the same temperature:

$$\nu = \frac{\eta}{\rho}, \qquad (4)$$

where η is dynamic viscosity in Pa.s and ρ is density in $kg.m^{-3}$. The basic unit of kinematic viscosity is $m^2.s^{-1}$, but smaller unit $mm^2.s^{-1}$ is also commonly used (*Štěpina , Veselý, 1985*).

The fluidity is ability of matters to flow. Parts of liquid matters can move easily towards one another because the particles are not bounded in fixed positions. The measure of fluidity is expressed by viscosity. It is defined as reciprocal of dynamic viscosity (3).
Thermogravimetric Analysis was measured on METTLER TOLEDO. The temperature method of the experiment was set according to the needs of samples and conditions of laboratory. The temperature was increased from 25 °C to 200 °C at a heating rate of 10 °C.min^{-1}. Isothermal part of experiment was not occurred. After achieving the temperature 200 °C the sample was cooled to an operating temperature of 25 ° C. TGA was performed in nitroge atmosphere throughout the experiment.
As carrier gas was used nitrogen (purity 99 %). Gas flow was for both methods 50 ml.min^{-1}. The device TGA/DSC1 was employed to measure the changes of mass in the samples and to monitor the temperature processes. TGA measurement was realized in Alumina crucible with lids and with diameter of 6 mm and length of 4.5 mm. The total volumes of the crucibles were 70 µl and the lids were pierced. Simultaneously with the thermogravimetric analysis, DTA measurement was performed. The sample was weighed by scales KERN ABT 220-5DM version 1.2 03/2013 (Kern & Sohn GmbH, Balingen, Germany).

RESULTS AND DISCUSSION

Temperature dependence of dynamic viscosity was measured at temperatures ranging from 20 °C to 80 °C. The coefficients of regression equations and coefficients of determination are summarised in the Table 3. We can observe from Table 3 that dynamic viscosity of samples is decreasing exponentially with increasing temperature. It was expected and it corresponds with conclusions of fluid materials reported in literature (*Vozárová et al., 2015; Hlaváč et al., 2017, 2019, 2021; Trávníček et al., 2013*). The determination coefficients for all the samples are very high, what confirms strong exponentially decreasing dependence, too. The progress can be described by a decreasing exponential function, which is in accordance with Arrhenius equation.

Tab. 1 Dependences of dynamic viscosity on temperature

	Regression equation	Determination coefficient R^2
Cherry	$y = 3{,}2046e^{-0{,}011x}$	0,9542
Plum	$y = 3{,}1777e^{-0{,}011x}$	0,9556
Pear	$y = 3{,}244e^{-0{,}013x}$	0,9671
Peach	$y = 3{,}5286e^{-0{,}015x}$	0,981
Apricot	$y = 3{,}3763e^{-0{,}013x}$	0,9637

Tab. 2 Dependences of kinematic viscosity on temperature

	Regression equation	Determination coefficient R^2
Cherry	$y = 3{,}312e^{-0{,}01x}$	0,9442
Plum	$y = 3{,}3211e^{-0{,}01x}$	0,9459
Pear	$y = 3{,}381e^{-0{,}012x}$	0,9602
Peach	$y = 3{,}6979e^{-0{,}014x}$	0,9775
Apricot	$y = 3{,}7663e^{-0{,}015x}$	0,909

Tab. 3 Dependences of density viscosity on temperature

	Regression equation	Determination coefficient R^2
Cherry	$y = 0{,}9676e^{-9E-04x}$	0,9909
Plum	$y = 0{,}9568e^{-9E-04x}$	0,9921
Pear	$y = 0{,}9595e^{-9E-04x}$	0,9919
Peach	$y = 0{,}9542e^{-1E-03x}$	0,9949
Apricot	$y = 0{,}9543e^{-0{,}001x}$	0,9826

Tab. 4 Dependences of fluidity on temperature

	Regression equation	Determination coefficient R^2
Cherry	$y = 312{,}05e^{0{,}0111x}$	0,9532
Plum	$y = 314{,}7e^{0{,}0113x}$	0,9681
Pear	$y = 308{,}26e^{0{,}0129x}$	0,9689
Peach	$y = 283{,}4e^{0{,}0148x}$	0,9802
Apricot	$y = 278{,}81e^{0{,}0148x}$	0,9681

With the increasing temperature, the density decreased. We found out from the experimental measurement that the distillate of cherry has the highest density. It is caused by the fact that 30 - 40%

of the total weight of cherry is a stone which causes more oily substances. The lowest density was measured from the apricot, where the maximum of weight of the stone is only 10 %. The overall decrease of progress in curves is described by exponentially regressive equation. The coefficients of determination reached high values in all samples. We can conclude from the measurements that the regression equations describe very precisely graphically shown decreasing dependencies. Those results confirmed validity of Arrhenius exponential relation. We compared in the graphical dependence of density on temperature the coefficients of determination of linear model of regression equation with the coefficient of determination of exponential shape of curve. Similar comparison was made by (*Kumbár, 2013*) with stating that both measured coefficients reached high value. We can see that there is not a big difference between linear and exponential mathematical models – from mathematical point of view. On the other hand, from the physical point of view, better interpretation has exponential dependence of Arrhenius type.

Temperature dependencies of samples of dynamic viscosity had an exponential decreasing shape, which is in accordance with Arrhenius equation. Kinematic viscosity of samples is decreasing with increasing temperature. When heating the compared samples, their fluidity increases. Thermogravimetric (TG) curve, as a function of respective boiling temperature, where are quite like those obtained by TG curve of alcohol, performed in alumina pan with pinhole lids. All the samples were put into the similar mass from 93,70 mg to 115,60 mg. Fig. 1 shows the TGA results for at 200 °C with different composition (apricot, plum, peach, cherry and pear).

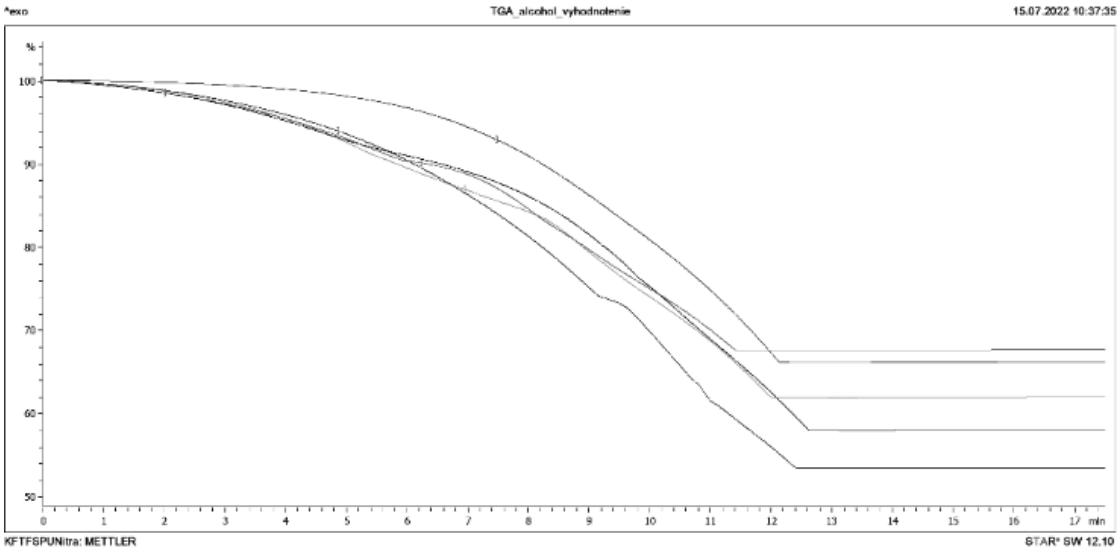

Fig.1 Thermogravimetric curves of distillate by heating rate 10 °C.min^{-1}, where blue colour is apricot, violet is plum, red is pear, black is cherry and green colour is pear distillate.

Curves are normalized and they show evident most decrease of mass by apricot and least by peach. All samples terminate yourself decreases around 150 °C. Basic information about decreases of samples are indicated in Tab. 1.

Tab. 1 Temperatures and final mass determined from analysis TG curves

	Onset (°C)	Residue (%)	Inflect. Pt. (°C)	Onset (°C)	Residue (%)	Inflect. Pt. (°C)
apricot	56.7	74.03	75.34	88.35	70.08	91.58
plum	-	-	-	85.76	91.94	102.71
peach	42.76	97.72	59.09	84.3	73.08	102.46
cherry	37.58	91.1	51.8	88	57.92	104.3
pear	43.12	87.06	55.61	92.72	61.87	103.04

TGA results show that the alcohol undergoes thermal degradation beginning around 40 °C (onset temperature), the greatest rate of change on the curve which is also known as inflection point at 102 °C and the total mass loss of 42,08 %. The residue remaining was from 57,92 % to 91,94 % at 140 °C to 150 °C. Shift of the TG curves responsible volatile melt, it is the liquid sample evaporate. All processes in this temperature range are covered by evaporation binary solution of water and ethanol.

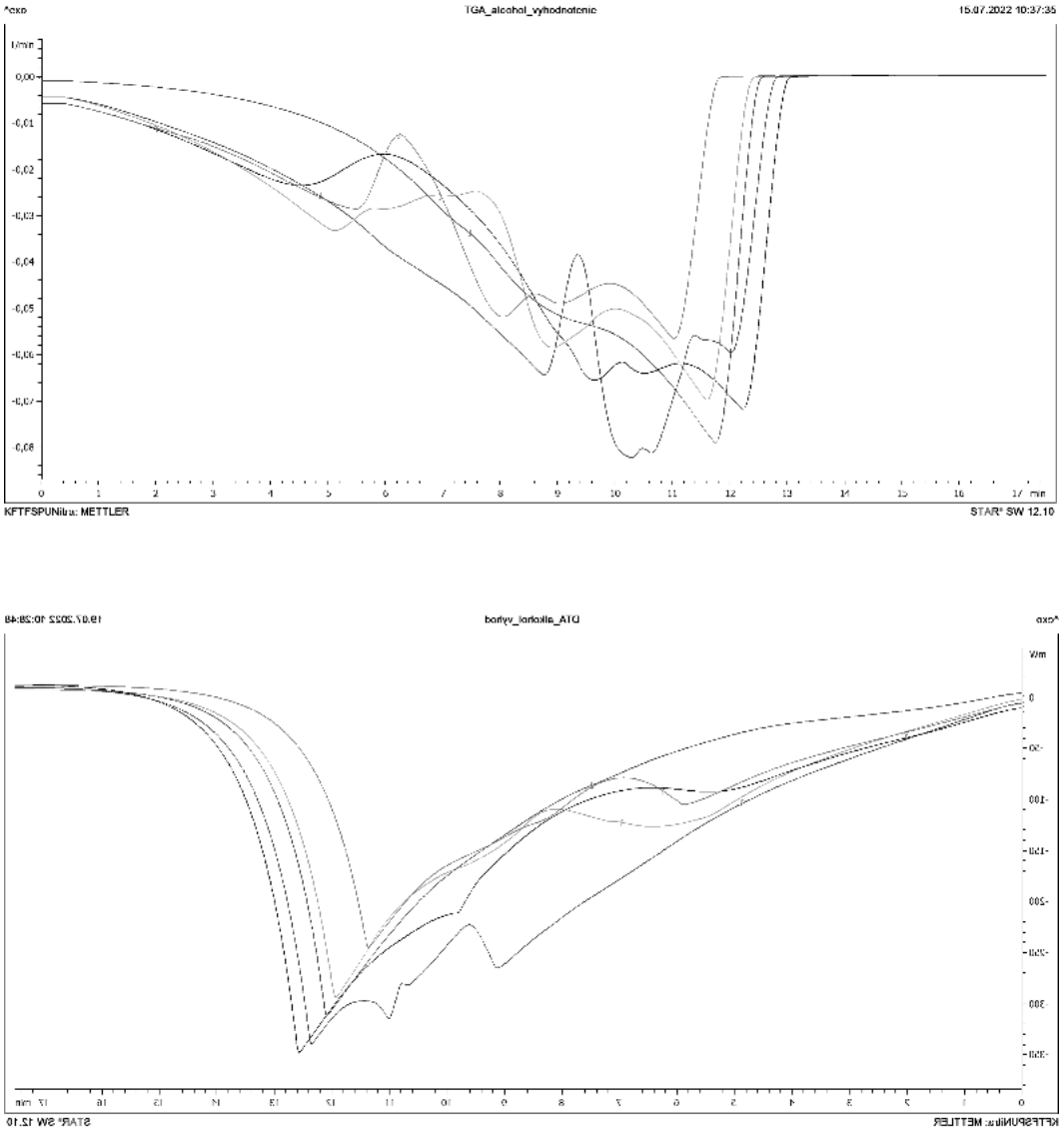

Fig. 2 DTG (left) and DTA (right) curves of distillate by heating rate 10 °C.min-1, where blue colour is apricot, violet is plum, red is pear, black is cherry and green colour is pear distillate.

To further characterize this process of samples was can the peak calculation of the 1st derivative of the mass loss curve. There is represented by DTG curves in the Fig. 2. Distinct peaks are in three samples at to temperature 55 °C (endset). Table 2 contains summary information about the individual peaks of the DTG curves. DTG curves can be divide into two parts, the first part being up to temperature 80°C and second part starting from this temperature to ending process. Peaks from first part are observable in peach, cherry and pear. It can be explained by the higher alcohol content without reaction with water and another components of distillate.

Tab. 2 Temperatures determined from analysis DTG curves

	Onset (°C)	Peak (°C)	Endset (°C)	Onset (°C)	Peak (°C)	Endset (°C)
apricot	-	-	-	63.38	103.89	120.1
plum	-	-	-	89.75	102.13	118.04
peach	35.33	59.21	66.24	74.53	101.79	111.72
cherry	31.08	50.47	62.78	86.41	103.45	121.49
pear	42.2	54.03	60.43	84.4	102.72	117.23

Main change of mass is large area of reference temperature from 80 °C to 150 °C. In peach and cherry is visible three tip at DTG curve. Two peaks are showed at temperatures (110-140) °C. One peak is observed in the plum with protracted left side peak and ending the process is determine by 149 °C. DTG curve of apricot include to the main area four peak of mass change. Peak in the main change of mass loss were match to the temperature of boil acetates. DTA curves measured concurrently with TGA as change of the heat flow determine strongly endothermic process in two curves part. One endothermic peak is visibly in firstly part of DTA curve to 80 °C in pear and peach distillate. Then follows endothermic case volatile other components of samples as aldehydes, acetates, terpenes and aromatic ingredients.

CONCLUSION

We can observe from all samples that the viscosity and density are decreasing with increasing temperature. The density and the dynamic viscosity demonstrated high temperature dependence. While distilling stone fruits, more oily substances (essential oils) are distilled and those have influence on measurement of rheological characteristics. Difference is minimal what is very suitable from the point of view of quality of distillates. The research will continue to identify tolerance limits for each distillate and based on that finding out, it will be possible to determine alcohol strength for individual produced distillate. Thermal analysis are respectable methods for analysis foods samples and alcohol. Good precondition is investigated basic composition of the samples by precisely treatment of methodology. Likeness DTA and DTG they confirm this claim. The Present peaks by temperature to 80 °C be permitted forecast change of the rheological properties (*Leonardo, 2020; Tripodi, 2022*) based on azeotropic blend water and alcohol.

ACKNOWLEDGMENT

This study was supported by project VEGA 1/0470/21: Economic aspects of the development of fruit distillate production due to climate change and socio-economic impacts of legalization of private distillate production in Slovakia.

REFERENCES

1. Albertson, W.C., Staley, D.R., Mcdonald, M.M. & Pryor, B.K. 2008. Engine oil viscosity diagnostic system and methods. United States Patent 20080223114.
2. Golles, A.(2001). Ušlechtilé destiláty: Praktická kniha o pálení. Praha: Ivo Železný. 109 s. ISBN 80-237-3642-6.
3. Hagman, Klaus & ESSICH, Birgit. Pálíme ovoce. Stuttgart: VÍKEND, 2007, 95 s. ISBN 978-80-86891-66-8.
4. Hlaváč, P. (2011). Reologické vlastnosti potravinárskych materiálov : dizertačná práca. Nitra: SPU, 2011. 135 s.
5. Hlaváč, P., Božiková, M., Ardonová, & V., Kotoulek, P.(2019). Apparent viscosity and density of chosen tomato ketchups. In BPS 2019. Gödöllő: Szent István Egyetem,, s. 20. ISBN 978-963-269-823-6.
6. Hlaváč, P., Božiková, M., Regrut, T., & Ardonová, A. (2017). Rheologic properties of selected vegetable oils. In INOPTEP 2017. Novi Sad : National society of processing in agriculture. (2017), s. 137. ISBN 978-86-7520-393-3.
7. Hlaváč, P., & Hlaváčová, Z.(2021). Comparison of apparent viscosities and densities of some mustards. In BioPhys Spring

2021. Lublin: Institute of Agrophysics Polish Academy of Sciences, s. 42--43. ISBN 978-83-89969-68-2
8. Hrubá, K., & Lapčíková, B. (2018). Thermal analysis and its use in the food industry. Univerzita Tomáše Bati ve Zlíně [internet] aviable from: http://digilib.k.utb.cz/bitstream/handle/10563/42099/hrub%C3%A1_2018_dp.pdf?sequence=1&isAllowed=y
9. Joardder (Omar), M. U.H, Karim, A., & Kumar, Ch. (2013).Better Understanding of Food Material on the Basis of Water Distribution Using Thermogravimetric Analysis. Conference: International Conference on Mechanical, Industrial and Materials Engineering 2013 (ICMIME 2013) At: RUET, Rajshahi, Bangladesh. DOI: 10.13140/RG.2.1.1508.8807
10. Krempaský, J. (1982). Fyzika. Bratislava : Alfa. 1982. ISBN 80-05-01063-X. 752 s.
11. Kumbár, V., Polcar A., & Votava, J. (2015)b. Physical and Mechanical Properties of Bioethanol and Gasoline Blends. Sugar and Sugar Beet Journal, vol. 131, no. 3, p. 112-116. ISSN 1210-3306
12. Kumbár, V., Polcar, A., & Čupera, J.(2013). Rheological profiles of blends of the new and used motor oils. Brno : Acta Universitatis Agriculturae et Silviculturae Mendelianae Brunensis,. ISSN 1211-8516, s. 115-121
13. Leonardo, R.S., Murta Valle, M.L., &Dweck, J. (2020). Thermovolumetric and thermogravimetric analysis of diesel S10. J Therm Anal Calorim 139, 1507–1514. https://doi.org/10.1007/s10973-019-08528-7
14. Lexa, D., &Leibowitz, L. (2002). Differential Thermal Analysis and Differential Scanning Calorimetry. Characterization of Materials. E.N. Kaufmann (Ed.). https://doi.org/10.1002/0471266965.com030
15. Munson, B.R., Young, D.F., & Okiishi, T.H. (2009). Fundamentals of fluid mechanics. New York:John Wiley & Sons. 783 pp.
16. Pischl J.(1997). Vyrábíme ušľechtilé destiláty. Vydavateľstvo Glos, s.r.o. 05/122. ISBN 80-237-3441-5. Leopold Stocker Verlages.
17. Škopek, J.(2003). Výroba destilátů z vlastního ovoce. 1. vyd. České Budějovice: Dona. 139 s. ISBN 80-7322-045-8.
18. Štěpina, V., & Veselý, V. (1980). Mazivá a speciální oleje. 1vyd. Slovenská akadémia vied v Bratislave : VEDA, 1980. 696 s.
19. Štepina, V., & Veselý, V. (1985). Mazivá v tribologii. Bratislava : Veda, vydavateľstvo Slovenskej akadémie vied, 1985. 408 s.
20. Thermal Analysis of Foods (2018). [internet] aviable from: http://people.umass.edu/~mcclemen/581Thermal.html
21. Trávniček, P, Valach, M., Hlaváčová, Z., Mareček, J., Vítěz, T., & Junga, P. (2013). Selected physical properties of liquid biofuels. Research in Agricultural Engineering 59(4), 121–127.
22. Tripodi, A., & Rossetti, I. (2022). Aspects of the thermogravimetric analysis of liquid mixtures as predictive or interpretation tool for batch distillation. J Therm Anal Calorim 147, 6765–6776. https://doi.org/10.1007/s10973-021-10990-1
23. Vega, D., Villar, M.A., Failla, M.D. et al. (1996). Thermogravimetric analysis of starch-based biodegradable blends. Polymer Bulletin 37, 229–235. https://doi.org/10.1007/BF00294126
24. Vozárová, V., Kardjilova, K., Híreš, Ľ., Valach, M., & Wollner, A. (2015). Temperature dependence of dynamic viscosity and DSC analysis of the Plantohyd samples. Journal of Central European Agriculture 16(2), 221–23

Corresponding author:
Ing. Tomáš Holota, PhD, Faculty of Engineering, Slovak University of Agriculture in Nitra, Tr. A. Hlinku 2, SK - 949 76 Nitra, Slovak Republic, phone: +421 37 641 4300, e-mail: tomas.holota@uniag.sk

EFFECT OF SELECTED FACTORS ON WOOD DUST EMISSION FROM CHAINSAW

Miroslav DADO[1], Marián KUČERA[2], Richard HNILICA[1]

[1]*Department of Manufacturing Technology and Quality Management, Faculty of Technology, Technical University in Zvolen, Slovak Republic*
[2]*Department of Mechanics, Mechanical Engineering and Design, Faculty of Technology, Technical University in Zvolen, Slovak Republic*

Abstract
Excessive exposure to wood dust can cause serious health problems. The aim of this study was to investigate the influence of the cutter shape and wood species on airborne wood dust concentration during chainsaw cross-cutting operations. Inhalable and respirable wood dust mass concentrations were measured using a real-time aerosol monitor DustTrak DRX. Statistical analysis was based on the Scheirer-Ray-Hare test. The results of this study indicate that both examined factors have a significant influence on respirable fraction of the wood dust mass concentration.

Key words: *wood dust; chainsaw; mass concentration; measurement.*

INTRODUCTION

Chainsaw is power-driven tool designed to cut wood with a saw-chain and consisting of an integrated compact unit of handles, power source, guide bar and saw-chain (*ISO, 2017*). Chainsaw is a source of many significant hazards (e.g. mechanical, thermal, noise, vibration, physical load, exhaust fumes, airborne wood dust). International standards *ISO 11681-1* (*2022*) and *ISO 11681-2* (*2022*) specify the safety requirements and/or measures to eliminate the hazards or reduce risks for chainsaws. A significant body of research exists regarding the exposure of chainsaw operators to noise (e.g. *Neri et al., 2018; Rukat et al., 2020; Huber et al., 2021), vibration (e.g. Kováč et al., 2018; Landekič et al., 2020; Iftime et al., 2022*), and physical load (e.g. *Cheţa et al., 2018; Arman et al., 2021; Grzywiński et al., 2022*). Several studies have been performed to determine carbon monoxide (*Lesczyński, 2014*; *Hooper, Parker & Todoroki, 2017*) and exhaust fumes (*Neri et al., 2016*) concentration within the breathing zone of chainsaw operators and explore simultaneous exposure to exhaust fumes and noise (*Schwarz et al., 2019*).

However, very few published studies have addressed the exposure of chainsaw operators to airborne wood dust. *Horvat et al. (2005)* carried out comparison between measured mass concentration of respirable particles and total dust for sample pairs collected in felling dead standing fir-trees and maximum permissible concentrations for fir-wood. In another study, *Horvat et al. (2007)* reported significant difference between mass concentrations of oak wood respirable particles in winter during the final cut and on thinning in summer, while the difference between mass concentrations of total dust was not so apparent. *Marchi et al. (2017*) found that exposure to wood dust varied widely with different silvicultural treatments, while no significant difference were found for different type of chainsaw fuel. The study (*Marenče, Mihelič & Poje, 2017*) demonstrated that cutting chain selection and proper chain preparation are crucial for achieving high productivity and reducing health risk. *Dimou et al. (2020)* showed that the concentration of inhalable dust is in inverse proportion to the increase in breast height diameter, implying that larger trees generated lower dust amounts.

Factors thought to be influencing the exposure of chainsaw operators to airborne wood dust have been explored only in several studies. Together, these studies outline that exposure of chainsaw operators to airborne wood dust was usually lower than current occupational exposure limits. Nevertheless, several authors highlight that occupational exposure limits are based on epidemiological studies from furniture industry and so it does not reflect the special conditions prevailing in the outdoor workplaces.

To the best of our knowledge, no previous studies have been undertaken to investigate influence of saw chain type and wood density on wood dust emission from chainsaw. The aim of this study is to explore the effect of the cutter shape and wood species on airborne wood dust concentration during chainsaw cross-cutting operations.

MATERIALS AND METHODS

The experiment was designed as two-factor full factorial experiment involving two levels of cutter shape and two levels of wood species. Each treatment was replicated five times so that the total number of runs was 20. The layout of experimental setup is shown in Fig. 1. In order to investigate the influence of aforementioned factors on the dust emission formation, cross-cutting experiments were carried using factory-fresh cordless chainsaw (MSA 220 C, Andreas Stihl AG & Co. KG, Weiblingen, Germany) with lithium-ion battery (Stihl AP 300 S). Battery was charged by hi-speed charger (Stihl AL 500). The chainsaw was equipped with a 35 cm length guide bar (Stihl Rollomatic E) as specified by machine manufacturer. A single individual, experienced in the use of the chainsaw, performed cross-cutting operations.

The saw chains under study were full chisel chain (Stihl Picco Super 3) and semi-chisel chain (Stihl Picco Micro 3). To avoid any effects on dust measurements due to the condition of the saw chain, only a chains originally sharpened by manufacturer were used for each test cycle. The saw chains were lubricated with chain oil (Stihl BioPlus) and tensioned according to manufacturer's recommendations.

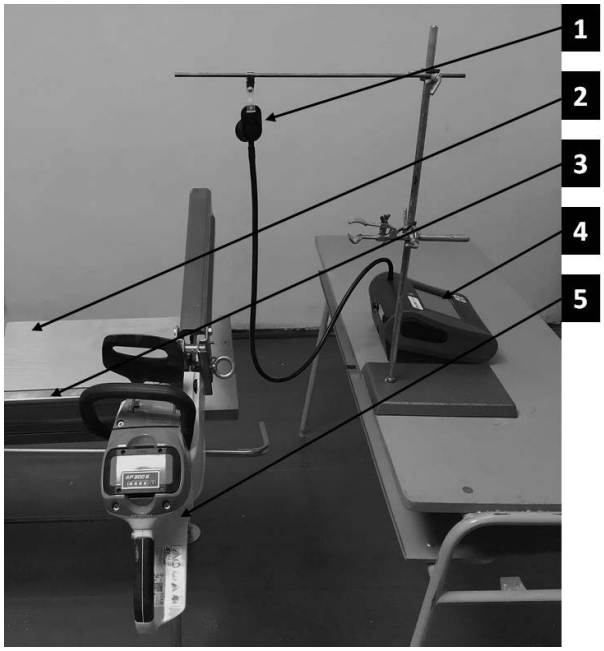

Fig. 1 Layout of experimental setup: 1- sampler, 2 - specimen, 3 - sawhorse, 4 - monitor, 5 - chainsaw

The tree species under the study were beech *(Fagus sylvatica L.)* and spruce *(Picea Abies (L.) H. Karst)*. Test specimens in the form of planks of 500 mm × 250 mm × 50 mm in dimension were conditioned to a final moisture content of 12% before experimentation. The sawhorse with chainsaw holder (Magg 120009, PHT a.s., Praque, Czech Republic) was used for clamping the test specimens.

Inhalable and respirable wood dust mass concentrations were measured using a desktop aerosol monitor (DustTrak 8533 DRX, TSI Inc., Shoreview, MN, USA). Real-time monitor measured and recorded wood dust mass concentration every second. Before each sampling event, the zero offset calibration was performed with HEPA filter, as recommended by the manufacturer. Plastic IOM sampler (IOM Multi-dust sampler, SKC Inc., Eighty-four, PA, USA) was connected to monitor inlet using conductive tubing. Fixed-point sampling was employing, the sampler was positioned at breathing zone of operator. Each sampling event lasted 5 minutes.

The temperature and relative ambient humidity was monitored using microclimatic conditions monitor (Testo 480, Testo SE & Co., Titisee-Neustadt, Germany). All tests were conducted at ambient temperature of 20 °C ± 1°C and at relative ambient humidity of 36 % ± 1 %.

In this study, data normality was tested by Shapiro-Wilk test. The Scheirer-Ray-Hare test was used to assess effects of cutter shape and wood species on airborne wood dust mass concentration. All statistical analyses were performed using a Microsoft Excel freeware add-on Real Statistics.

RESULTS AND DISCUSSION

Fig. 2 shows an example of the temporal variations in aerosol monitor response with time for generated beech dust during cross-cutting.

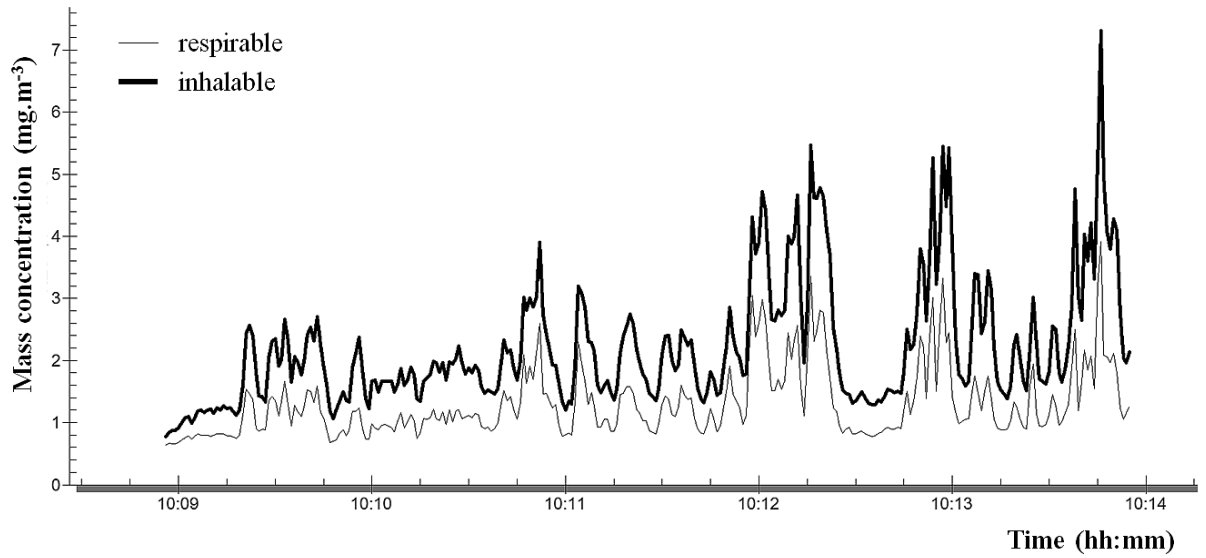

Fig. 2 Temporal variations in aerosol monitor response during cross-cutting of beech wood with semi-chisel cutter

Influence of the cutter shape and type of wood on the mass concentration of airborne dust particles emitted by chainsaw is shown in Fig. 3 and Tab.1

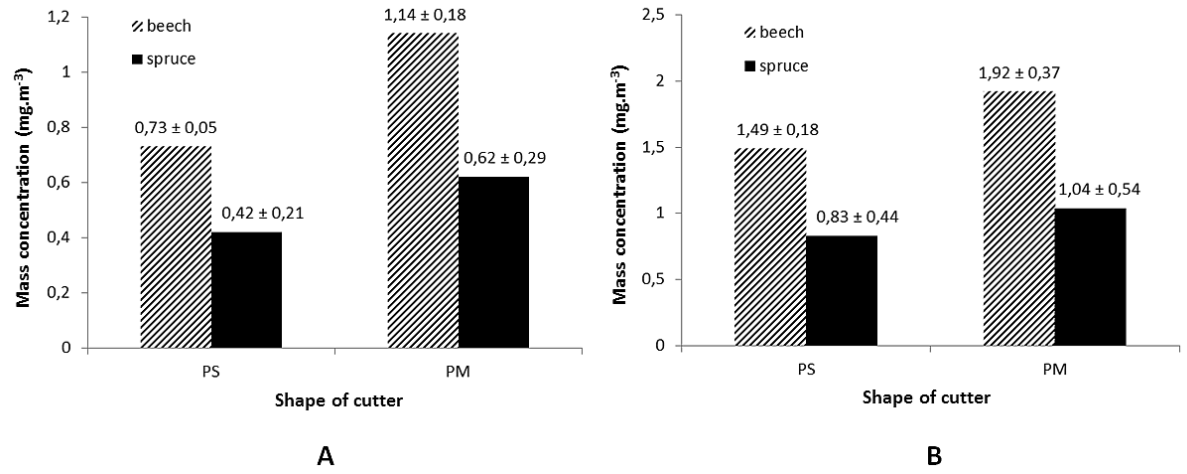

Fig. 3 Effect of cutter shape (PS - full chisel, PM - semi-chisel) and wood species on the mass concentration (arithmetic mean ± standard deviation, n=5): A – respirable fraction, B – inhalable fraction

In a case of respirable fraction, the highest average mass concentration of 1.14 mg.m^{-3} was realized using treatment beech wood and semi-chisel profile of cutter. On the other side, the minimum average mass concentration of 0.42 mg.m^{-3} was measured using treatment full chisel profile of cutter and spruce wood.

In a case of inhalable fraction, the highest average mass concentration of 1.92 mg.m^{-3} was realized using treatment beech wood and semi-chisel profile of cutter. On the other side, the minimum average mass concentration of 0.83 mg.m^{-3} was measured using treatment full chisel profile of cutter and spruce wood.

Tab. 1 Summary of the Scheirer-Ray-Hare test results. The test was performed to detect the effect of factors Wood species and Cutter shape on wood dust mass concentrations. Meaning of statistical variables: *H* refers to the value of the Scheirer-Ray-Hare test; $P < 0.05$ represents significant differences, while $P > 0.05$ represents no significant differences.

Variable	Factor	*H* statistics	*P-value*	Sign.
Respirable fraction	Wood species	7.405	0.006	Yes
	Cutter shape	4.805	0.028	Yes
	Wood species x Cutter shape	0.205	0.650	No
Inhalable fraction	Wood species	8.691	0.003	Yes
	Cutter shape	1.462	0.226	No
	Wood species x Cutter shape	0.205	0.650	No

Currently there is no specific standardized procedure for measurement the dust concentration produced by chainsaw. Real-time inhalable and respirable dust measurements in breathing zone of chainsaw's operator were used to investigate the influence of the cutter shape and wood species on airborne wood dust concentration during chainsaw cross-cutting operations.

Comparing results of airborne wood dust concentration evaluation from different experimental setups and field measurements reported in literature is very difficult. However, results of this study are consistent with results reported by several authors (*Horvat et al., 2005*; *Horvat et al., 2007*; *Marchi et al., 2017*; *Dimou et al., 2020*) in that hardwoods (angiosperms) generated higher dust concentrations than softwoods (coniferous).

Several limitations to this study need to be considered. We did not determine size and photometric calibration factors for the aerosol monitor. The DustTrak DRX monitor is factory calibrated to the respirable fraction of standard ISO 1210-1, A1 test dust. We assumed that the optical properties of beech and spruce wood aerosols are not diametrically different. Intention of this study was to investigate if there is any difference between different settings rather than to determine real occupational exposure to airborne wood dust. For this reason, it was sufficient to know relative mass concentration values. Thus we performed only zero calibration procedure for compensation of zero drift. Reported values of inhalable wood dust are underestimated due to limitation in the size range of DustTrak DRX. Feed force exerted during cross-cutting may have an effect on mass concentration and size distribution of emitted airborne wood dust. Design of the study did not allow to control the feed force. However, all the cross-cutting trials were performed by the same person using the least possible feed force to make experiments in a repeatable way. A minor limitation of this study can be considered in connection with use of safety enclosure. Safety enclosure as a part of sawhorse reduced amount of airborne dust wood which has been emitted to breathing zone of operator.

CONCLUSIONS

This paper investigated the formation of airborne wood dust emissions depending on cutter shape a wood species. Based on experimental results, the following findings are concluded for the specific case:

- In a case of respirable fraction, both the cutter shape and wood species significantly influence airborne wood dust mass concentration. For semi-chisel shaped cutter it was observed higher values of airborne wood dust mass concentrations than for cutting using full chisel chain. For cross-cutting of beech wood it was observed higher values of airborne wood dust mass concentrations than for spruce wood.
- In a case of inhalable fraction, only a type of wood significantly influences airborne wood dust mass concentration. Similarly, for cross-cutting of beech wood it was observed higher values of airborne wood dust mass concentrations than for spruce wood.

In order to extend this approach in future research, different wood species and cutter shapes should be considered. Based on further experiments with these different settings, the impact of the settings on the generation of airborne wood dust emissions can be verified and described more generally.

ACKNOWLEDGEMENT
The paper is based on work performed under research contract VEGA 1/0019/19 of the Science Grant Agency of the Ministry of Education, Science, Research and Sport of the Slovak Republic whose support is a gratefully acknowledged.

REFERENCES

1. Arman, Z., Nikooy, M., Tsioras, P. A., Heidari, M., & Majnounian, B. (2021). Physiological workload evaluation by means of heart rate monitoring during motot-manual clear-cutting operations. *International Journal of Forest Engineering*, *32*(2), 91-102.
2. Cheţa, M., Marcu, M. V., & Borz, S. A. (2018). Workload, Exposure to Noise, and Risk of Musculoskeletal Disorders: A Case Study of Motor-Manual Tree Feeling and Processing in Poplar Clear Cuts. *Forests*, *9*(6), 300.
3. Dimou, V., Malesios, C., & Chatzikosti, V. (2020). Assessing chainsaw operators' exposure to wood dust during timber harvesting. *SN Applied Science*, *2*, 1899.
4. Grzywiński, W., Turowski, R., Jelonek, T., & Tomczak, A. (2022). Physiological workload of workers employed during motor-manual timber harvesting in young alder stands in different seasons. *International Journal of Occupational Medicine and Environmental Health*, *35*(4).
5. Hooper, B., Parker, R., Todoroki, Ch. (2017). Exploring chainsaw operator occupational exposure to carbon monoxide in forestry. *Journal of Occupational and Environmental Hygiene*, *14*(1), D1-D12.
6. Horvat, D., Čavlović, A., Zečić, Ž., Šušnjar, M., Bešlić, I., & Madunić-Zečić, V. (2005). Research of fir-wood dust concentration in the working environment of cutters. *Croatian Journal of Forest Engineering*, *26*(2), 85-90.
7. Horvat, D., Kos, Ž., Zečić, Ž., Jazbec, A., Šušnjar, M., & Očkajová, A. (2007). Tree cutters' exposure to oakwood dust – A case study from Croatia. *Die Bodenkultur*, *58*(1–4), 59-65.
8. Huber, M., Hoffmann, S., Brieger, F., Hartsch, F., Jaeger, D., & Sauter, U. H. (2021). Vibration and Noise Exposure during Pre-Commercial Thinning Operations: What Are the Ergonomic Benefits of the Latest Generation Professional-Grade Battery-Powered Chainsaws? *Forests*, *12*(8), 1120.
9. Iftime, M. D., Dumitrascu, A., & Ciobanu, V. D. Chainsaw operators' exposure to occupational risk factors and incidences of profesional diseases specific to the forestry field. *International Journal of Occupational Safety and Ergonomics*, *28*(1), 8-19.
10. ISO 11681-1:2022. Machinery for forestry. Portable chain-saw safety requirements and testing. Part 1: Chain-saws for forestry service.
11. ISO 11681-2:2022. Machinery for forestry. Portable chain-saw safety requirements and testing. Part 2: Chain-saws for tree service.
12. ISO 6531:2017. Machinery for forestry. Portable chain-saws. Vocabulary.
13. Kováč, J., Krilek, J., Dado, M., & Beňo, P. (2018). Investigating the Influence of Design Factors on Noise and Vibrations in the Case of Chainsaws for Forestry Work. *FME Transactions*, *46*(4), 513-519.
14. Landekić, M., Bačić, M., Pandur, Z., & Šušnjar, M. (2020). Vibration Levels of Used Chainsaws. *Forests*, *11*(2), 249.
15. Lesczyński, K. (2014). The concentration of carbon monoxide in the breathing areas of workers during logging operations at the motor-manual level. *International Journal of Occupational Medicine and Environmental Health*, *27*(5), 821-829.
16. Marchi, E., Neri, F., Cambi, M., Laschi, A., Foderi, C., Sciarra G., & Fabiano, F. (2017). Analysis of dust exposure during chainsaw forest operations. *iForest*, *10*, 341-347.
17. Marenče, J., Mihelič, M., & Poje, A. (2017). Influence of Chain Filing, Tree Species and Chain Type on Cross Cutting Efficiency and Health Risk. *Forests*, *8*(12), 464.
18. Neri, F., Foderi, C., Laschi, A., Fabiano, F., Cambi, M., Sciarra, G., Aprea, M. C., Ceni, A., & Marchi, E. (2016). Determining exhaust fumes exposure in chainsaw operation. *Environmental Pollution*, *218*, 1162-1169.
19. Neri, F., Laschi, A., Foderi, C., Fabiano, F., Bertuzzi, L., & Marchi, E. Determining Noise and Vibration Exposure in Conifer Cross-Cutting Operations by Using Li-Ion Batteries

and Electric Chainsaws. (2018). *Forests*, *9*(8), 501.
20. Rukat, W., Jakubek, B., Barczewski, R., & Wróbel, M. (2020). The Influence of the Direction of Wood Cutting on the Vibration and Noise of Chainsaws. *Tehnički vjesnik, 27*(6), 1879-1886.
21. Schwarz, M., Salva, J., Dado, M., Vanek, M. & Borošová, D. (2019). Combined Exposure to Noise and Exhaust Fumes During Chainsaw Operation. *Akustika, 31*, 64-72.

Corresponding author:
Miroslav Dado, Department of Manufacturing Technology and Quality Management, Faculty of Technology, Technical University in Zvolen, Študentská 26, 960 01 Zvolen, Slovak Republic, phone: +421 455206864, e-mail: miroslav.dado@tuzvo.sk

INVESTIGATION OF INFRARED AND HOT AIR OVEN FOR DRYING FRESH APPLE SLICES AT DIFFERENT TEMPERATURES

Oldřich DAJBYCH[1], Abraham KABUTEY[1], Čestmír MIZERA[1], David HERÁK[1]

[1]Department of Mechanical Engineering, Faculty of Engineering, Czech University of Life Sciences Prague, Kamýcká 129, Praha 6, Prague, 165 20, Czech Republic

Abstract
This study examined infrared and hot air oven drying methods for fresh apple slices under different drying temperatures from 40 °C to 80 °C with 10 °C intervals for approximately 10 hrs drying time. The drying curves of the sample weight and moisture content versus drying time were presented. The main calculated parameters were the total colour change, chroma, colour index, whiteness index, browning index, hue angle, rehydration capacity, shrinkage (%), bulk density (g/mL), area (mm^2) and volume (mL). The correlation analysis showed that for both drying methods all the calculated parameters did not significantly ($P > 0.05$) correlate with the drying temperatures except total colour change, colour index and whiteness index which significantly ($P < 0.05$) correlated linearly with the drying temperatures. The significant correlation values were between -0.887 and 0.980. It was observed that the infrared drying showed a higher total colour change than the hot air oven drying. Future studies will consider in detail the combined drying methods, mathematical modelling of the drying curves and optimization of the operating parameters for different varieties of fresh apples and other fresh products to ensure better control of the drying operations and quality improvement of the final product for consumption and storage.

Key words: *apple slices; drying behaviour; shrinkage, rehydration capacity, colour analysis.*

INTRODUCTION

Drying has been one of the commonly used methods to preserve foods such as fruits and vegetables for human consumption (*Aral & Bese, 2016*). It is done to remove moisture through evaporating and sublimation processes including heat and mass transfer mechanisms (*Jafari, Movagharnejad & Sadeghi 2020*). Fruits and vegetables are dried to inhibit microbial, enzymatic and quality decay (*Aral & Bese, 2016*). Several authors namely but not limited to the following have studied the drying characteristics of fruits and vegetables using different drying methods (*Aidani, 2016; Karaaslan, Ekinci & Akbolat, 2017; Bozkir et al., 2019; Jafari, Movagharnejad & Sadeghi 2020*). For instance, *Aidani, (2016)* studied hayward kiwifruits by combined infrared-vacuum whereas *Jafari, Movagharnejad & Sadeghi (2020)* examined the effect of thickness of samples, air velocity and infrared power on the drying kinetics and quality attributes of blanched slices during infrared drying. Particularly, apples are cultivated in many countries of the world and can be eaten in various forms as fresh, dried, juice, jam or marmalade (*EL-Mesery, Kamel & Emara, 2021*). They provide vast health and nutritional benefits to humans like anti-inflammatory effects and chronic disease prevention (*Khudyakov, Sosnin, Shorstkii & Okpala, 2022*). In the literature, considerable studies have been performed and more are being conducted to determine the optimum drying methods, processing factors, energy consumption, physical and chemical quality characteristics of dried apple slices for their storage and reuse (*EL-Mesery, Kamel & Emara, 2021; Joardder & Karim, 2022; Khudyakov, Sosnin, Shorstkii & Okpala, 2022*). Most importantly, consumers prefer dried products according to their physical qualities such as colour, shape, aroma and appearance (*Cetin, Saglam and Demir, 2019*). The present study aimed at evaluating the colour attributes, moisture content (g/g dry basis), rehydration capacity, shrinkage (%), bulk density (g/mL), area and volume of dried apple slices under infrared and hot air oven drying methods under different drying temperatures.

MATERIALS AND METHODS

Sample and drying methods

Fresh whole red delicious apples (Fig. 1 a) were purchased from a supermarket in Prague, Czech Republic. The samples were kept in a refrigerator at 5 °C. Before the experiments, the samples were

removed and allowed to cool to a laboratory temperature of 24.26±0.50 °C and humidity of 41.6±2.42%. A slicer was used to cut the fresh apples into a cylindrical size of 10 mm. The dimensions (diameter and thickness) of the fresh and dried apple sliced samples were accurately measured using a digital calliper with an accuracy of 0.01 mm. The mass of the fresh and dried apple sliced samples was measured using a digital balance with an accuracy of 0.01. Infrared and hot air oven methods were used to dry the freshly sliced apple samples (Fig. 1 b, c and d) at different drying temperatures from 40 °C to 80 °C with 10 °C intervals.

Colour analysis

The colour values of the fresh and dried apple slices at the different drying temperatures were measured using the RGB colour analyzer (RGB-2000 Voltcraft). The RGB (Red, Green and Blue) values were converted to Lab values using an online converter. The total colour change (Δ*E*), chroma (Δ*C*), colour index (*CI*), browning index (*BI*) and hue angle (*Hue°*) of the fresh and dried sliced apples under different drying temperatures for both infrared and hot air oven methods were calculated using equations (1) to (10) according to *Aral & Bese, (2016); Bozkir & Ergun (2020); Jafari, Movagharnejad & Sadeghi (2020).*

$$\Delta E = \sqrt{(L_O^* - L^*)^2 + (a_O^* - a^*)^2 + (b_O^* - b^*)^2} \quad (1)$$

$$\Delta C = \sqrt{(a_O^* - a^*)^2 + (b_O^* - b^*)^2} \quad (2)$$

$$CI = \frac{1000 \cdot a^*}{L^* \cdot b^*} \quad (3)$$

$$WI = 100 - \sqrt{(100 - L^*)^2 + a^* + b^*} \quad (4)$$

$$BI = \frac{[100(x - 0.31)]}{0.17} \quad (5)$$

$$x = \frac{(a^* + 1.75 \cdot L^*)}{(5.645 \cdot L^* + a^* - 3.012 \cdot b^*)} \quad (6)$$

$$Hue° = tan^{-1}\left(\frac{b^*}{a^*}\right) \quad (7)$$

(when $a^* > 0$ and $b^* \geq 0; 0° < Hue < 90°$)

$$Hue° = 180 + tan^{-1}\left(\frac{b^*}{a^*}\right) \quad (8)$$

(when $a^* < 0$ and $b^* \geq 0; 90° < Hue < 180°$)

$$Hue° = 180 + tan^{-1}\left(\frac{b^*}{a^*}\right) \quad (9)$$

(when $a^* < 0$ and $b^* < 0; 180° < Hue < 270°$)

$$Hue° = 360 + tan^{-1}\left(\frac{b^*}{a^*}\right) \quad (10)$$

(If $a^* > 0$ and $b^* < 0; 270° < Hue < 360°$)

where L_O^*, a_O^* and b_O^* represent the fresh samples whereas L^*, a^* and b^* represent the dried samples. According to Aral & Bese, 2016; Bagheri & Dinani, 2019; and Jafari, Movagharnejad & Sadeghi 2020, the L^* colour parameter is in 0 (blackness) to 100 (whiteness) range. The a^* parameter is from $-a^*$ (greenness) to + a^* (redness) and the b^* parameter is in $-b^*$ (blueness) to + b^* (yellowness). The chroma (*C*) indicates the colour's saturation or purity.

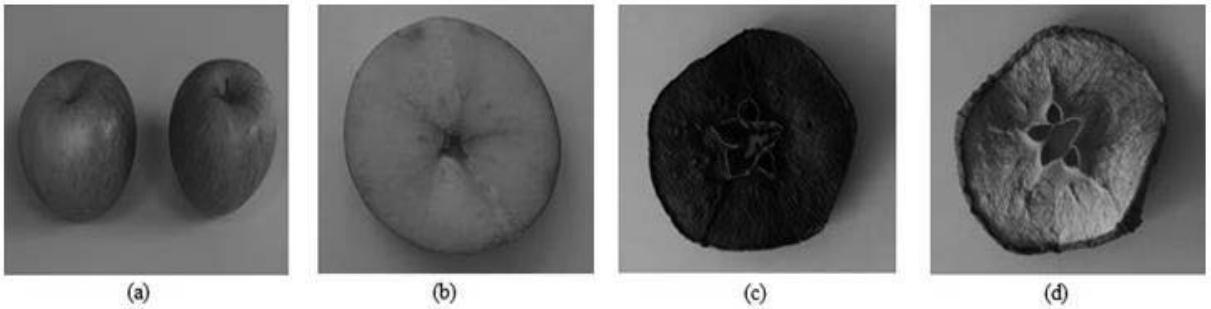

Fig. 1 Two fresh samples of whole apples (a), fresh apple slice (b), infrared dried apple slice (c) and hot air oven dried apple slice (d) at 80 °C drying temperature.

Moisture content

The moisture content MC (d.b.) of the sample during the drying process was calculated using equation (11).

$$MC = \left(\frac{W_{FS}-W_{DS}}{W_{DS}}\right) \quad (11)$$

where W_{FS} is the initial weight of the freshly sliced sample (g) and W_{DS} is the weight of the dried sliced sample (g).

Rehydration capacity

The rehydration capacity *RC* (-) was carried out according to the procedure reported by *Cui, Li, Song & Song, (2008)* cited in *Bozkir & Ergun, (2020)*. Following the procedure, the weighted dehydrated samples were dipped into a beaker of hot water at 80 °C for 15 min. The rehydrated samples were filtered over a screen for 2 min and slightly blotted with an absorbent paper thrice and then weighted again. The *RC* of the dried samples was calculated using equation (12).

$$RC = \left(\frac{W_{RS}}{W_{DS}}\right) \quad (12)$$

where W_{RS} is the weight of the rehydrated sample (g) and W_{DS} is the weight of the dried sample (g).

Shrinkage

In a drying process, the shrinkage SK (%) refers to the volume reduction or the change in selected dimensions due to the moisture removal from the sample structure (*Bozkir & Ergun, 2020*). The shrinkage of the samples was calculated using equations (13) to (15) according to *Majdi, Esfahani & Mohebbi, (2019)*.

$$SK = \left(\frac{V_O-V_f}{V_O}\right) \times 100 \quad (13)$$

where V_O is the initial volume of the fresh sample (mL) and V_f is the final volume of the dried sample (mL).

$$V_O = \pi\left(\frac{D_O}{2}\right)^2 \cdot t_O \quad (14)$$

$$V_f = \pi\left(\frac{D_f}{2}\right)^2 \cdot t_f \quad (15)$$

where D_O, t_O, D_f and t_f are the initial and final diameter (mm) and thickness (mm) of the sample.

Bulk density

The bulk density (g/mL) of the dried samples was calculated using equation (16) according to *Goula & Adamopouls, (2005)* cited in *Bozkir & Ergun, (2020)*.

$$\rho_{bulk} = \left(\frac{m}{V}\right) \quad (16)$$

where m is the weight of the dried sample (g) and V is the volume of the dried sample (mL).

Surface area

The surface area A (mm^2) of the fresh and dried sliced samples was calculated using equation (17) according to *Cetin, Saglam and Demir, (2019)*.

$$A = 2\pi r(r + h) \quad (17)$$

where r is the radius (mm) and h is the thickness (mm) of the fresh and dried samples.

Statistical analysis

The data were subjected to a correlation analysis at a 5% significance level using Statistica 13 software (*Statsoft, 2013*).

RESULTS AND DISCUSSION

The measured and calculated colour parameters of the fresh and dried sliced apple samples using the infrared (IR) and hot air oven (OV) drying methods are given in Tabs. 1 and 2. It can be seen in Tabs. 1 and 2 that the L_O^*, a_O^* and b_O^* as well as L^*, a^* and b^* values of the fresh and dried apple sliced samples increased and decreased along with the drying temperatures from 40 to 80 °C for both IR and OV. Mostly, lower values were observed at 80 °C for IR compared to OV which showed higher values.

According to *Jafari, Movagharnejad & Sadeghi (2020)*, colour is one of the major quality attributes that specifies the quality of the final product and influences consumer preference. The authors further stated that when samples of fruits and vegetables are subjected to heat treatments then non-enzymatic browning and pigment destructions can cause colour changes. In this present study, the total colour change (ΔE), chroma (ΔC), colour index (*CI*), whiteness index (*WI*) and browning index (*BI*) showed both increasing and decreasing values with the drying temperatures for IR and OV drying methods. The IR method indicated lower values among the colour indicators compared to OV. The results were similar to those reported by *Bozkir & Ergun (2020)* on persimmon cubes by ultrasound and osmotic dehydration pretreatments on the hot air drying. The correlation results (not included here) revealed that only the total colour change (ΔE) and whiteness index (WI) were significantly affected ($p < 0.05$) by the drying temperatures for IR. This means that whereas the total colour change increased along with the drying temperatures, the whiteness index decreased. Regarding the OV, the total colour change and colour index (CI) increased significantly ($p < 0.05$) with drying temperatures. The other calculated parameters as presented in Tabs. 1 and 2 for both IR and OV were not significantly affected ($p > 0.05$). Considering the rehydration capacity, it used as a measure of the physical and chemical changes that occur in the product during the drying process (*Aral & Bese, 2016*). Lower values were observed at a lower temperature of 40 °C compared to higher temperatures from 50 to 80 °C which recorded higher values. Similar results were reported by *Aral & Bese (2016)*. Finally, the obtained drying curves are described in Figs. 2a–2d. At all drying temperatures, higher moisture removal was observed for IR compared to the OV. For both IR and OV drying methods, the drying time of about 10 hrs was not enough to dry the sliced apple sample at 40 °C to reach equilibrium sample weight or moisture content. The equilibrium moisture content was reached for the drying temperatures from 50 °C to 80 °C (Figs. 2c and d). During the drying time of about 10 hr for all drying temperatures, the moisture content values were below 6 (d.b.). *Joardder and Karim (2022)* reported similar results for apple samples during convective/hot air drying.

Tab. 1 Determined parameters of sliced apple samples dried at different temperatures using IR.

Calculated parameters	Drying temperatures				
	40 °C	50 °C	60 °C	70 °C	80 °C
L_O^*	44.204	40.140	40.954	45.642	41.149
L^*	27.284	19.873	9.211	15.945	2.264
a_O^*	12.759	5.600	5.302	5.734	5.562
a^*	6.199	8.329	7.044	11.956	0.374
b_O^*	36.358	28.286	27.004	28.451	26.599
b^*	23.495	17.994	9.621	20.155	0.523
ΔE	22.244	22.894	36.233	31.456	47.105
ΔC	14.439	10.648	17.470	10.370	26.587
CI	9.670	23.292	79.486	37.203	315.859
WI	27.080	19.709	9.119	15.754	2.259
BI	172.402	200.023	270.897	385.938	37.924
$Hue°$	75.219	65.162	53.790	59.323	54.431
RC	1.542	1.798	1.676	1.772	1.616
SK	49.573	49.092	44.906	54.054	37.927
ρ_{bulk}	0.385	0.241	0.273	0.265	0.192
A_O	6833.919	8600.695	7484.533	9522.559	8347.251
A_f	4168.762	5951.719	5288.874	8957.831	8086.137
V_O	21.697	28.337	23.961	32.135	26.496
V_f	10.941	14.426	13.201	14.765	16.447

Tab. 2 Determined parameters of sliced apple samples dried at different temperatures using OV.

Calculated parameters	Drying temperatures				
	40 °C	50 °C	60 °C	70 °C	80 °C
L_O^*	28.069	46.154	47.114	42.822	48.728
L^*	24.783	34.947	24.826	16.975	19.482
a_O^*	10.112	6.601	4.661	8.031	6.391
a^*	2.651	9.154	7.41	4.519	6.596
b_O^*	22.815	30.731	28.325	29.146	30.222
b^*	20.792	27.694	21.492	24.656	17.365
ΔE	8.399	11.889	23.473	26.468	31.948
ΔC	7.730	3.968	7.364	5.700	12.859
CI	5.145	9.458	13.888	10.797	19.497
WI	24.627	34.664	24.634	16.799	19.333
BI	156.354	153.861	178.857	589.628	190.069
$Hue°$	82.734	71.709	70.977	79.614	69.201
RC	1.488	1.577	1.851	2.034	1.505
SK	52.707	57.469	50.966	55.783	53.927
ρ_{bulk}	0.434	0.468	0.344	0.331	0.344
A_O	7260.708	8429.142	7538.837	9265.871	7559.233
A_f	4626.538	5764.578	6135.093	8549.494	7039.443
V_O	21.847	25.756	24.642	30.501	24.466
V_f	10.332	10.955	12.083	13.487	11.271

IR: Infrared drying; OV: Hot air oven drying; L_O^*, a_O^* and b_O^* represent fresh samples and L^*, a^* and b^* represent dried samples as lightness, greenness/redness and blueness/yellowness; the total colour difference (ΔE), chroma (ΔC), colour index (*CI*), whiteness index (*WI*), browning index (*BI*); Hue angle (Hue^o); rehydration capacity *RC* (-); shrinkage *S* (%) and bulk density ρ_{bulk} (g/mL); A_O: initial area of the fresh sample (mm^2); A_f: final area of the dried sample (mm^2); V_O is the initial volume of the fresh sample (mL) and V_f is the final volume of the dried sample (mL).

CONCLUSIONS

Samples of dried apple slices were studied at different drying temperatures using infrared (IR) and hot air oven (OV) drying methods. Changes in high colour values were observed with the IR compared to the OV. Shrinkage values for OV were higher than the IR. Higher browning index values were obtained for IR compared to OV. Future studies would extend the results of the present study to obtain adequate information on the drying methods and their combinations by adopting a three-to-five factor with three levels using Box-Behnken design to optimize the quality parameters of dried fruits and/or vegetables.

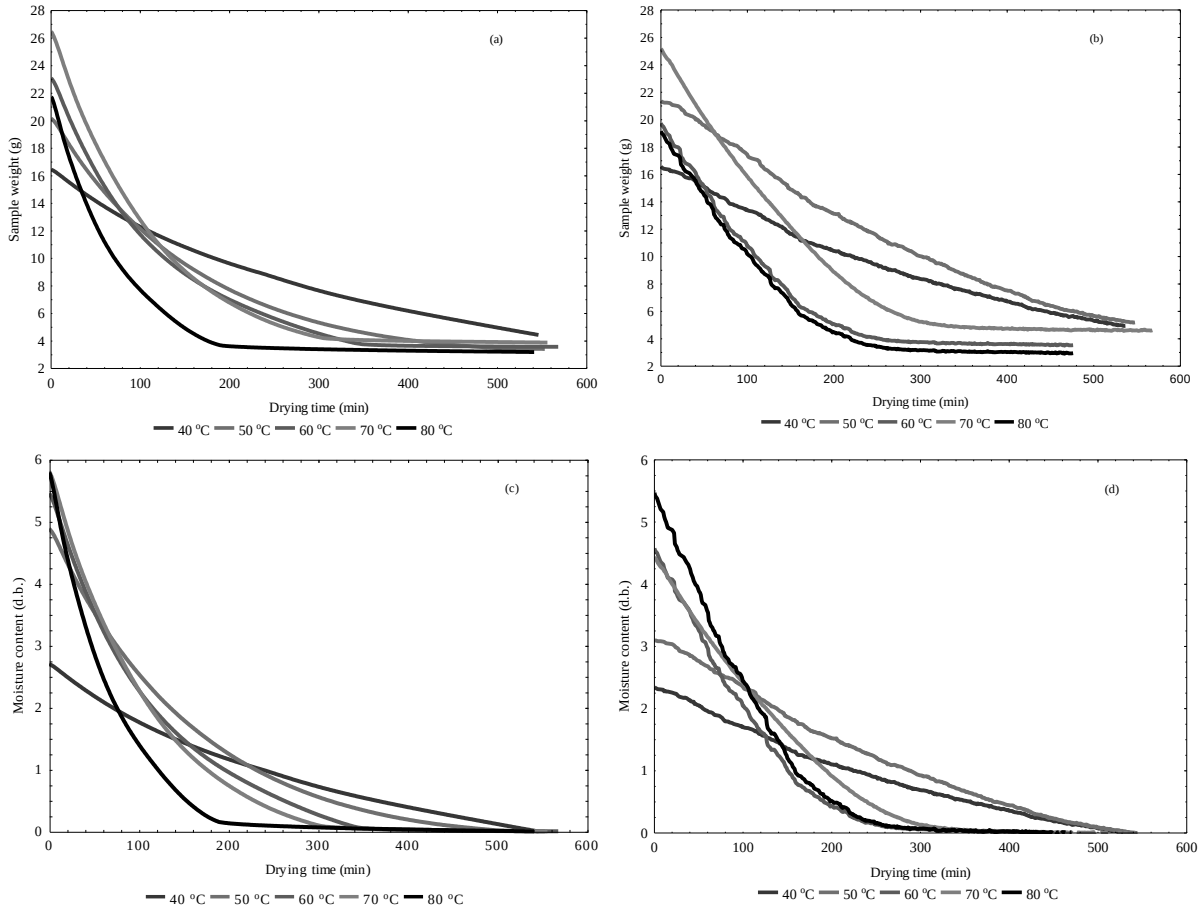

Fig. 2 Sample weight for infrared IR (a) and hot air oven OV (b) and moisture content for IR (c) and OV (d) versus drying time for different drying temperatures of a dried apple sliced samples.

ACKNOWLEDGMENT

The study was supported by the Internal Grant Agency of Czech University of Life Sciences Prague, Grant Number: IGA 2020: 31130/1312/2114.

REFERENCES

1. Aral, S. & Bese, A.W. (2016). Convective drying of hawthorn fruit (Crataegus spp.): Effect of experimental parameters on drying kinetics, color, shrinkage, and rehydration capacity. *Food Chemistry*, 210, 577-584.
2. Jafari, F., Movagharnejad, K. & Sadeghi, E. (2020). Infrared drying effects on the quality of eggplant slices and process optimization using response surface methodology. *Food Chemistry*, 127423, 1-8.
3. Aidani, E., Hadadkhodaparast, M. & Kashaninejad, M. (2016). Experimental and modeling investigation of mass transfer during combined infrared-vacuum drying of Hayward kiwifruits. *Food Science & Nutrition*, 1-7.
4. Karaaslan, S., Ekinci, K. & Akbolat, D. (2017). Drying characteristics of sultana grape fruit in microwave dryer. *Polish Academy of Sciences*, 1317-1327.
5. Bozkir, H., Ergun, A.R., Serdar, E., Metin, G. & Baysal, T. (2019). Influence of ultrasound and osmotic dehydration pretreatment on drying and quality properties of persimmon fruit. *Ultrasonics – Sonochemistry*, 54,135-141.
6. EL-Mesery, H.S., Kamel, R.M. & Emara, R.Z. (2021). Influence of infrared intensity and air temperature on energy consumption and physical quality of dried apple using hybrid dryer. *Case Studies in Thermal Engineering*, 27, 1-13.

7. Khudyakov, D., Sosnin, M., Shorstkii, I. & Okpala, C.O.R. (2022). Cold filamentary microplasma combined with infrared dryer: Effects on drying efficiency and quality attributes of apple slices. *Journal of Food Engineering*, 329, 1-11.
8. Joardder, M.U.H. & Karim, M.A. (2022). Drying kinetics and properties evolution of apple slices under convective and intermittent-MW drying. *Thermal Science and Engineering Progress*, 30, 1-7.
9. Cetin, N., Saglam, C. & Demir, B. (2019). Effects of different drying conditions on physicl changes of apple (*Malus communis* L). *Mustafa Kemal University Journal of Agricultural Sciences*, 24, 71-77.
10. Bozkir, H. & Ergun, A. R. (2020). Effect of sonication and osmotic dehydration applications on the hot air drying kinetics and quality of persimmon. *LWT – Food Science and Technology*, 131, 1-7.
11. Bagheri, N. & Dinani, S.T. (2019). Investigation of ultrasound-assisted convective drying process on quality characteristics and drying kinetics of zucchini slices. *Heat and Mass Transfer*, 55, 2123-2163.
12. Cui, Z.W., Li, C.Y., Song, C.F. & Song, Y. (2008). Combined microwave vacuum and freeze drying of carrot and apple chips. *Drying Technology*, 26(12), 1517-1523.
13. Majdi, H., Esfahani, J.A. & Mohebbi, M. (2019). Optimization of convective drying by response surface methodology. *Computers and Electronics in Agriculture*, 156, 574-584.
14. Goula, A.M. & Adamopoulos, K.G. (2005). Spray drying of tomato pulp in dehumidified air: II. The effect on powder properties. *Journal of Food Engineering*, 66, 35-42.
15. Statsoft Inc. STATISTICA for Windows; Statsoft Inc: Tulsa, OK, USA, 2013.

Corresponding author:
Ing. Oldřich Dajbych, Ph.D., Department of Mechanical Engineering, Faculty of Engineering, Czech University of Life Sciences Prague, Kamýcká 129, Praha 6, Prague, 165 20, Czech Republic, phone: +420 22438 3178, e-mail: dajbych@tf.czu.cz.

STRUCTURE AND TRIBOLOGICAL PROPERTIES OF SINGLE AND DOUBLE LAYER DEPOSITS

Róbert DRLIČKA[1], Radovan ŠOŠKA[2], Martin KOTUS[1], Peter ČIČO[1]

[1]*Institute of Design and Engineering Technology, Faculty of Engineering, SUA in Nitra, Tr. A. Hlinku 2, 949 76 Nitra, Slovakia*
[2]*Technická inšpekcia, a.s., Trnavská cesta 56, 821 01 Bratislava, Slovakia*

Abstract
The aim of the contribution was to assess the importance of the differences in the properties of single- and multi-layer coatings applicable to the renovation of elements of biomass processing equipment. The article deals with the comparison of the structure, hardness and resistance to abrasive wear in laboratory conditions of one- and two-layer hard deposits. Hardfacing powders NP 62, NP 60 WC 20 and hardfacing rod RD 571 were used for deposits. Due to the use of flame spraying technology for the first two materials, there is no significant mixing of the weld with the substrate in the first layer, therefore the differences between one- and two-layer deposits are small (in the order of one percent). We found greater differences in the layers when hardfacing the rod with an oxy-acetylene flame (up to 36.04%). However, the biggest differences naturally result from the different chemical composition and resulting structure of the deposits, while the highest wear resistance values are achieved by deposits with a high content of tungsten carbides.

Key words: *repair; hardfacing, hardness; abrasive wear resistance.*

INTRODUCTION

Biomass processing equipment is made mainly of common structural steels. The most exposed parts can be made of more resistant materials, e.g. stainless steels. In operation, due to combined biological, chemical-physical processes and mechanical effects, degradation occurs, which can lead to a reduction or loss of function. In some cases, it can also results in damages with effects on the environment and employees. Early detection using appropriate diagnostic methods (e.g. ultrasound measurement of the thickness of the vessels) makes it possible to carry out a repair by replacing the worn material with a new layer, for example by welding. Locally or even on a larger area, it is possible to apply a material with selected properties that better withstands the load.

The resulting chemical composition, mechanical properties and resistance of the weld deposit depend on the material used, the welding technology and the degree of mixing of the hardfacing material with the substrate, if it is a single-layer weld. In other layers, the composition of the deposit is close to designed, but its thickness increases, which can be limiting and costly (*Votava, 2014; Kalincová et al., 2018*).

The smallest mixing can be achieved by flame spraying, because here we can create a diffusion joint using the proper technological procedure. Welding using an electric arc leads to partial mixing of the welding material and the base material (*Ťavodová et al., 2018*).

Müller et al. (2018) in their experiment point to significant mixing of the substrate and hardfacing material of the hard deposit created by the welding rod. They state that the generally recognized fact that the higher hardness of the material also guarantees its higher resistance to wear was not demonstrably proven in the tests.

Jankura (2013) measured the hardness in laboratory tests, observed the relative wear resistance and analysed the microstructure of one-layer, two-layer and three-layer hardfacing deposits. He observed the behaviour of two additional deposits, obtained by hardfacing with welding rods E-B 508 and E-B 518. From the results, he expressed the conclusions that the optimal properties of hardness and wear of hardfacing deposits are achieved in the third layer only and it is necessary to apply the welding with parameters resulting in minimal melting of the substrate material.

The results from the authors *Zdravecká (2014), Kotus & Čičo (2005), Votava et al. (2020),* also indicate that high hardness does not automatically guarantee better wear resistance.

In this contribution, we will focus on the comparison of the chemical composition, relative wear resistance, hardness and microstructure of one- (single) layer and two- (double) layer deposits of 3 selected hardfacing materials.

MATERIALS AND METHODS

Individual single-layer and double-layer hardfacing deposits were applied to steel grade C45 substrate (samples size 150x45x10 mm) with a minimum deposit thickness of 2-4 mm.
For laboratory verification of resistance to wear, two metal hardfacing powders NP 62 and NP 60 WC 20 and filled rod RD 571 were selected.

Tab. 1 Typical chemical composition (wt.%) and hardness (HRC) of used hardfacing materials

Material	C	Si	B	Fe	Cr	WC	Ni	W_2C	Hardness
NP 62	0.9	5.5	4.0	5.0	20.0	-	rest	-	58-65
NP 60 WC 20	0.6	5.0	3.9	5.0	20.0	20.0	rest	-	75-82
RD 571	0.1	0.8	0.3	-	5.0	-	15.0	60.0	min. 65

Metal powders are highly alloyed with silicon, boron and chromium and have a higher carbon content, materials NP 60 WC 20 and RD 571 contains a significant proportion of tungsten carbide.
An NPK-3 torch with a medium neutral flame and a welding speed of 3-4 $mm.s^{-1}$ was used for the application of metal powders. The rod was hardfaced with a medium neutral oxygen-acetylene flame with a welding speed of 2-3 $mm.s^{-1}$.
After hardfacing, the samples were cut into dimensions of 25x22.5 mm using an abrasive water jet to avoid thermal effects during cutting.
Hardness measurements were realized on a HPO 250 hardness tester using Vickers method, according to the STN EN ISO 6507 standard.
The relative abrasive wear resistance measurement on the sanding cloth was realized on 24 samples, 12 of them with a single-layer deposit and 12 of them with a two-layer deposit, and each type of deposit was on 4 samples. The deposits were made in the fixture on one base of the test cylinder for tribological tests, then machined to the standardized geometric shape, size and roughness of 0.4μm.
The deposits on the faces of the rollers were aligned on a surface grinder to Ra=0.4 μm using sufficient cooling so that no heat-affected area was generated on the samples.
The tribological test was performed on the device for testing the resistance to abrasive wear on the sanding cloth according to the ČSN 01 5084 standard.
The average mass losses were determined and the relative abrasive wear resistance was calculated from them using the weight of the samples before and after the test measurement on the PRECISA 205 A device with an accuracy of 10^{-4} g.
Metallography was done on twelve samples; six of them were single-layered and six were double-layered. Before the test, the samples were cut to smaller dimensions and inserted into a resin mold, then they were polished and etched. Samples created using metal hardfacing powders were etched using a solution created from H_20, HNO_3 and HF in a ratio of 3:2:1. A light microscope AXIO OBSERVER was used to monitor the structure of the deposits. On the basis of metallographic analysis, the microstructure of welds was evaluated using the standard STN EN ISO 17 639 – Destructive tests of welds of metallic materials. Macroscopic and microscopic analysis of welds.

RESULTS AND DISCUSSION

During the laboratory tests, the hardness, relative abrasive wear resistance and the microstructure of the welds were evaluated.
As mentioned above, knowing the properties of individual deposits allows us to choose the appropriate material and technology that will ensure the resistance of the deposits applied on the surface of the part. In the laboratory, we therefore further investigated the resistance of one- and two-layer deposits by determining the relative resistance of the hardfacing materials.

Hardness values for all three hardfacing materials divided for 1-layer and 2-layer deposits are presented in Fig. 1.
The average value of the hardness of the single-layer deposit of NP 62 powder was 1095 HV30, the average value of the double-layer deposit was 1105 HV30, which represents a 0.91% increase in hardness.
The average value of the hardness of the single-layer weld from NP 60 WC 20 was 1176 HV30, the double-layer 1143 HV30, which is a decrease in hardness by 2.8%.
Filled stick for flame hardfacing in single-layer deposit reached an average hardness value of 681 HV30, double-layer reached a value of 865 HV30, which is a 27% increase in hardness.

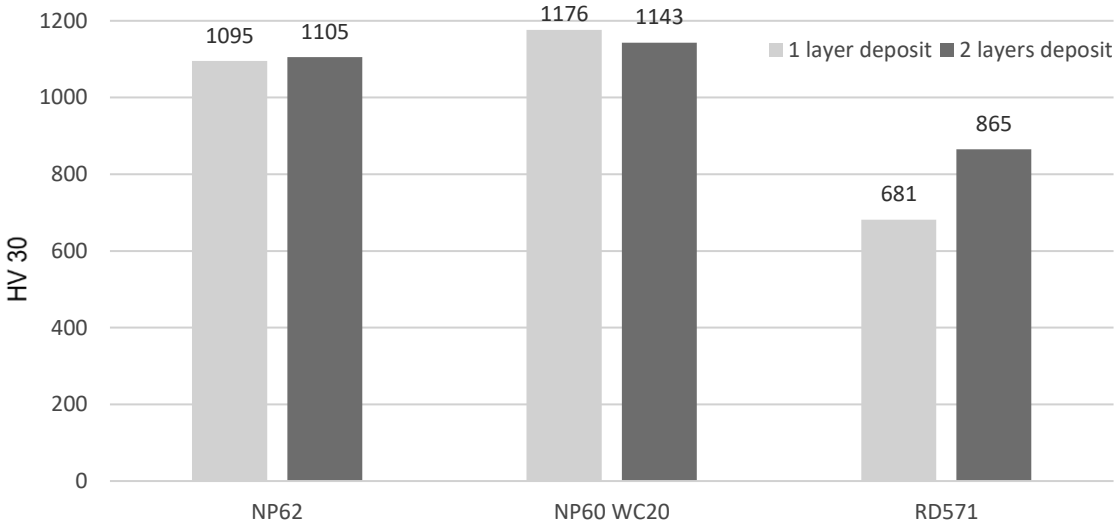

Fig. 1 Hardness of single-layer and double-layer deposits

The average mass loss and the relative wear resistance of the deposits are presented in Tab. 2.
Based on these data, relative abrasive wear resistances for the harfacing deposits are presented in the graph in Fig. 2.

Tab. 2 Average mass loss and relative abrasive material resistance

Material	Relative mass loss, g		Relative abrasive resistance, -	
	1 layer	2 layers	1 layer	2 layers
NP 62	0.9	5.5	4.0	5.0
NP 60 WC 20	0.6	5.0	3.9	5.0
RD 371	0.1	0.8	0.3	-

The relative resistance to abrasive wear on the sanding cloth for a single-layer deposit made of NP 62 was $\Psi_{abr} = 1.55$, and the double-layer one reached the value $\Psi_{abr} = 1.688$, which represents an increase of 8.9%.
The relative resistance to abrasive wear on the sanding cloth for the single-layer deposit of NP 60 WC 20 reached $\Psi_{abr} = 4.4$, for the double-layer it reached almost the same value $\Psi_{abr} = 4.38$, basically the same values.
The best result in relative resistance was achieved by the filled rod, the value of relative resistance was $\Psi_{abr} = 11.57$ for the single-layer deposit, $\Psi_{abr} = 15.74$ for the two-layer deposit, which represents an increase of 36.04%.
Nickel-based hardfacing powders has a limited ability to improve relative abrasive wear resistance, while the tungsten carbides appears to be a very effective wear propagation barrier, improving the abrasive wear resistance significantly.

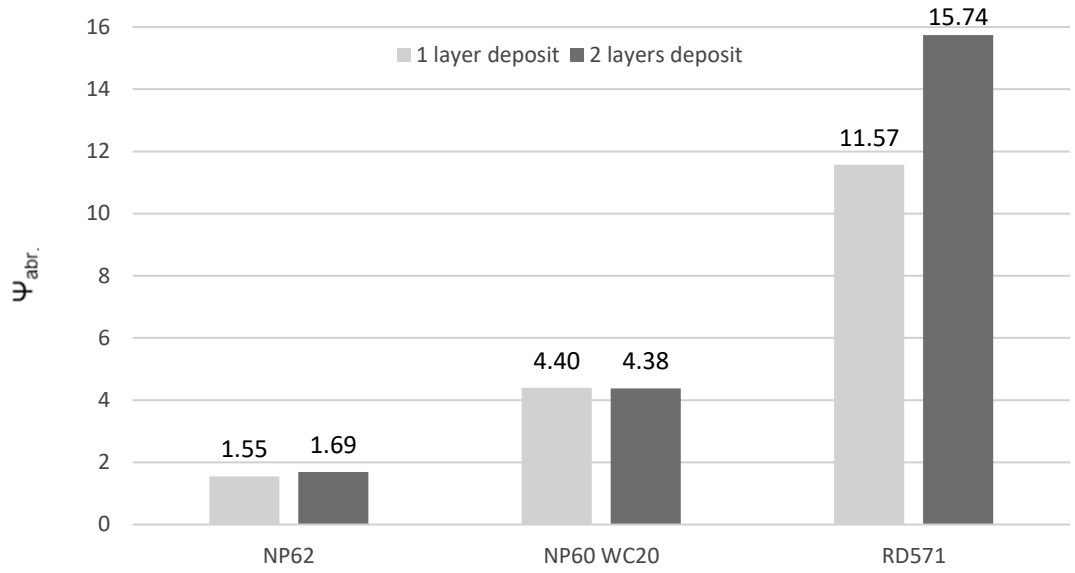

Fig. 2 Relative abrasive wear resistance of deposits

In the case of the first hardfacing material, single-layer and double-layer deposits have approximately the same chemical composition, the hardness of the coatings was also the same, but the relative wear resistance of the two-layer coating increased by only 8.9%. The microstructure of a single-layer weld is identical to the microstructure of a two-layer weld, see Fig. 3.

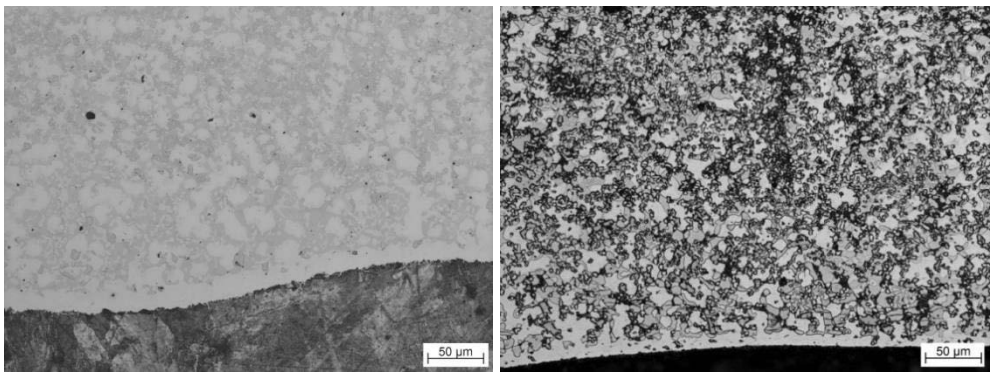

a **b**

Fig. 3 Microstructure of single-layer (a) and double-layer (b) deposits of NP 62

For the second hardfacing material NP 60 WC 20, single-layer and double-layer welds have approximately the same chemical composition, the hardness of the two-layer deposit has slightly decreased, and the relative wear resistance of the one- and two-layer deposits has reached the same value.

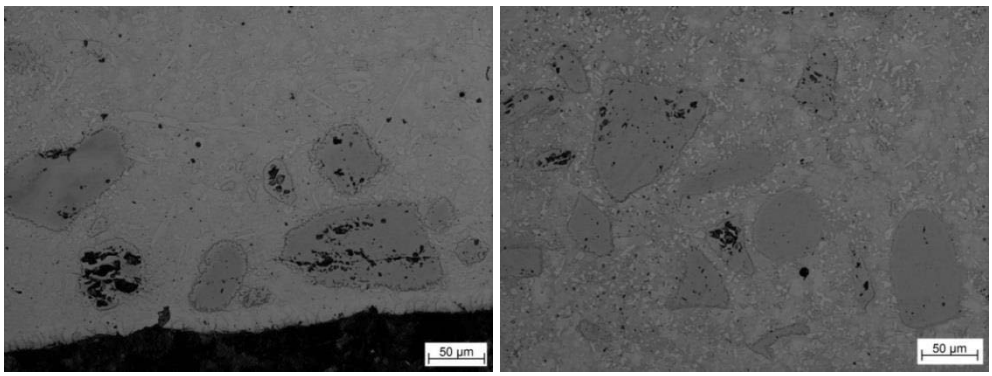

a **b**

Fig. 4 Microstructure of single-layer (a) and double-layer (b) deposits of NP 60 WC 20

In the single-layer deposit of NP 60 WC 20, we can again observe (see Fig. 4) small excluded phases together with tungsten carbide particles of size 60-80 μm. The microstructure of the NP 60 WC 20 two-layer deposit remained the same. In the microstructures, we can observe the uniform distribution of tungsten carbides and also the fact that the carbide particles do not have fused edges, which probably results in an interruption of the grooving by abrasive grains and increased resistance to wear.

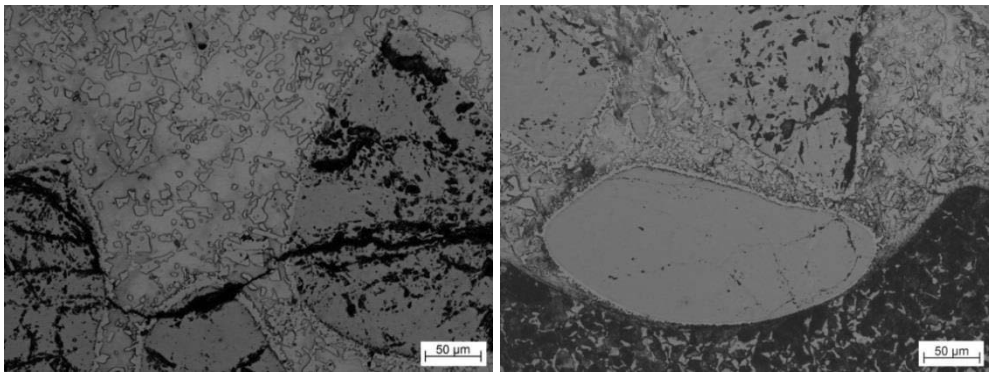

a **b**

Fig. 5 Microstructure of single-layer (a) and double-layer (b) deposits of RD 571

In the case of the third hardfacing material RD 571, it can be seen that the individual single- and double-layer deposits have almost the same chemical composition.
Compared to the two previous hardfacing materials, it reached the lowest hardness, but it can be caused by the measurement missing the carbide grains. Despite the measured lowest hardness value, the relative resistance of one and two-layer deposits was very high. It even increased by 36% for the double-layer deposit.
The microstructure of the single-layer deposit was formed by relatively large unfused tungsten carbide grains, which are embedded in the basic dendritic matrix (Fig. 5). Tungsten carbide grains reach a size of 200 to 300 μm.
According to the results of the research of *Chotěborský et al. (2009)* dedicated to the issue of the size of carbide grains for the wear of deposits, it is clear that with the increase in the size of the carbide grains stored in the basic matrix of the deposit, the resistance of the material against abrasive wear also increases.
Individual excluded phases have a small size, the NP 62 powder coating approaches nanostructured materials. It has a granular character, while the morphology is formed by austenite, as the nickel content is at the level of 65% of the total content of elements.
Tungsten carbide grains formed in RD 571 deposits are several times larger compared to NP 60 WC 20 carbide grains. The increased wear resistance was due to the uniform distribution of W_2C. These kept their size and square shape during the hardfacing process.
Until now, there is no consensus on the most advantageous type of structure in terms of resistance to abrasive wear. Some authors consider the austenitic-carbide structure to be the most advantageous, others the martensitic-carbide structure (*Chotěborský, 2019; Blaškovič, et al., 1990*)

CONCLUSIONS

The deposit of NP 62 in both single-layer and double-layer form shows approximately the same structure, which is due to the fact that the hardfacing layer – substrate binding is characterized as a diffusion and there is probably no significant mixing. In the second layer, a finer structure of globular formations can be seen.
NP 60 WC 20 the microstructure in single-layer and double-layer deposit remains the same, there is practically no mixing of the first and second layers, and no mixing with the base material in the case of the first layer, because the hardfacing material is joined by the diffusion. From the results obtained from these two materials, it can be concluded that the material NP60 WC20 could be more resistant to wear in the same operational conditions.

In the case of powder coating materials, it is a diffuse application, there is no large mixing of the coating powder with the base material, nor is there a large mixing between the one- and two-layer coating. While it is not valid for the third hardfacing material RD 571, from the results obtained from these materials, the conclusion can be drawn that the material RD 571 should be the most wear-resistant under the same operating conditions.

ACKNOWLEDGMENT
This publication was supported by the Operational Program Integrated Infrastructure within the project: Demand-driven research for the sustainable and innovative food, Drive4SIFood 313011V336, co-financed by the European Regional Development Fund.

REFERENCES

1. Blaškovič, P., Balla, J., & Dzimko, M. (1990). Tribológia. Bratislava : ALFA.
2. Chotěborsky, R. (2019). Wear resistant high boron steel for agriculture tools. In Proceeding of 7th International Conference on Trends in Agricultural Engineering 2019 (pp. 199-204). TAE 2019.
3. Chotěborský, R., Hrabě, P., Müller, M., Válek, R., Sávkova, J., & Jirka, M. (2009). Effect of carbide size in hardfacing on abrasive wear. Research in agricultural engineering, 55, 149-158.
4. Jankura, D. (2013). Vplyv počtu vrstiev na tribologické vlastnosti tvrdonávarov. Transfer inovácií, 26, 125-129.
5. Kalincová, D., Ťavodová, M., & Ľuptáčiková, V. (2018). Application of the weld deposits on function surfaces of the forest machines components. Manufacturing technology, 3, 400-405.
6. Kotus, M., & Čičo, P. (2005). Overenie návarových materiálov na plečkách v prevádzkových podmienkach. In Medzinárodní vědecká konference, Ostrava: Vysoká škola báňská, (pp. 20-25).
7. Müller, M., Novák, P., Chotěborský, R., & Hrabě, P. (2018). Reduction of ploughshare wear by means of carbide overlay. Manufacturing Technology, 18(1), 72-78.
8. Ťavodová, M., Kalincová, D., & Slováková, I. (2018). Evaluation of some parameters of hard surfacing treatment of the functional surfaces of forestry tools. Management Systems in Production Engineering, 26(4), 222-226.
9. Votava, J. (2014). Usage of abrasion-resistant materials in agriculture. Journal of Central European Agriculture, 15(2), 119-128.
10. Votava, J., Šmak, R., Polcar, A. & Kumbár, V. (2020) Využití tvrdokovu pro omezení abrazivního opotřebení pasivních částí u sklízečů cukrové řepy. Listy cukrovarnické a řepařské, 136(9-10), 313-317.
11. Zdravecká, E., Tkáčová, J., & Ondáč, M. (2014). Efect of microstructure factors on abrasion resistence of high-strenght steels. Research in agricultural engineering, 60, 192-198.

Corresponding author:
doc. Ing. Martin Kotus, PhD., Institute of Design and Engineering Technology, Faculty of Engineering, Slovak University of Agriculture in Nitra, Tr. A. Hlinku 2, Nitra, 949 76, Slovak Republic, phone: +421 37 641 5689, e-mail: martin.kotus@uniag.sk

POSSIBILITIES OF SAR IMAGES FOR POPPY EVALUATION

Jakub DVOŘÁK[1], Kristýna BALÁŽOVÁ[2], Karel STARÝ[1], Zdeněk JELÍNEK[1], Jan CHYBA[2], Jiří MAŠEK[2], Jitka KUMHÁLOVÁ[1]

[1]Department of Machinery Utilization, Faculty of Engineering, Czech University of Life Sciences Prague, Czech Republic
[2]Department of Agricultural Machinery, Faculty of Engineering, Czech University of Life Sciences Prague, Czech Republic

Abstract
Poppy (Papaver somniferum L.) is oil plant and also an export commodity of the Czech Republic. This crop is demanding to grow, especially in terms of agro-ecological conditions of the field and agricultural management. For this reason, remote sensing appears to be a suitable method for monitoring whole growth for proper treatment timing. As optical remote sensing has its limitations in the form of frequent cloud coverage, synthetic aperture radar images are becoming an alternative source of information about the crop state. The results showed that synthetic aperture radar satellite images can be helpful in case of time evaluation of poppy growth when optical images are not available. The Radar Vegetation Index could explain the yield spatial distribution from 32 % only when the crops were in elongation growing stage.

Key words: *crop production; satellite images; spectral indices, radar vegetation index.*

INTRODUCTION

Poppy belongs among the special crops grown in the Czech Republic in the area with altitude from 300 to 700 m above sea level. Poppy cultivation requires special conditions as confirmed by the study of *Hong et al. (2022)*. They stated that it is appropriate to focus on choosing a suitable place for growing poppies. Areas with strong winds are unsuitable for poppies because the crop may be uprooted. It is also not appropriate to grow poppies near forests where moisture is retained. Poppy has a small seed, so it is very demanding in the initial phenological stages. It is advisable to properly manage soil moisture and adhere to the sowing depth. Poppy is sown up to 2 cm. Like other oilseeds, poppies need little water to germinate. Subsequently, however, poppies are demanding moisture from emergence to flowering, the highest demands on moisture are 2-3 weeks before flowering. From the flowering stage to the maturity stage, the moisture requirements are reduced. Lack of water is a significant negative factor affecting poppy yields (*Makovnyka, 2020; Maurya et al., 2019*).
Poppy growth in the field is highly heterogeneous, so it requires a considerable amount of data collection to develop yield models. This phenomenon has been confirmed by several observations of poppy cultivation under controlled conditions (*Harvest et al., 2009; Kang & Primack, 1991; Lisson & Lisson, 2007*). However, few studies have used remote sensing to predict the yield (*Iqbal et al., 2017; Waine et al., 2014*). Data collected from field measurements can usually provide reference information on crop growth, but spatial coverage is often limited, so it is appropriate to use any of remote sensing methods, which can identify spatial variability of key yield indicators on a larger scale. In previous studies, various physiological indicators were evaluated to predict yield. Studies confirmed a significant correlation between Normalized Difference Vegetation Index (NDVI) and the capsule volume in the flower-to-harvest phase (*Jia et al., 2011; Mahdavi-Damghani et al., 2010*).
This article focused on exploring the potential use of the Sentinel 1 synthetic aperture radar (SAR) system to monitor the poppy growth cycle. Radar crop monitoring has several key advantages over ground-based or optical data measurements. Thanks to the use of wavelengths in the C-band, crop monitoring is not affected by clouds and the radar system provides us data for analysis at intervals without outages. This radar feature is very useful in poppies because it is important to manage soil moisture properly, especially in the early phenological stages (*Alonso-González et al., 2020*).
As the use of SAR satellite images in crop production still carries many uncertainties that need to be explored, the main aim of this study was to determine the usability of the Radar Vegetation Index (RVI)

index calculated from SAR satellite images when optical data are not available, for the purposes of poppy production management.

MATERIALS AND METHODS

The poppy was grown in 10.7 ha plot near to Kněževes (50° 7'58.65"N, 13°39'41.05"E), in the Czech Republic, during the vegetation season 2020 (sowing: March 27th to harvest on August 17th). The agro-meteorogical data (temperature and precipitation) during the poppy growing season are given in Table 1.

Tab. 1 Monthly temperatures and precipitation for the study site in growing season 2020 until August 17th 2020

Parameters/Months	April	May	June	July	August
Temperature (°C)	9.7	11.6	16.9	18.3	19.7
Precipitation (mm)	18.6	54.8	103.1	41.9	85.8

The evaluation of the whole vegetation season was carried out using satellite (optical and SAR) remote sensing, UAV scanning and crop analysis. The microwave and optical (cloud free) satellite images (Sentinel 1 and 2) were downloaded from Copernicus Open Access Hub. The images were processed in SNAP SW to the form of spectral indices. Sentinel 1 images were pre-processed by Radiometric Calibration, Multi-temporal Speckle Filtering and Range-Doppler Terrain correction (Relative Orbit 44), finally RVI was calculated. NDVI, Green NDVI (GNDVI), Triangular Greenness Index (TGI), Moisture Stress Index (MSI) and Enhanced MSI (EMSI) were calculated from Sentinel 2 images. The satellite data were complemented with images taken from drone multispectral camera. The digital elevation model (DEM) was derived from the UAV images taken on 21 May 2020. The data of acquisition and platforms with sensors used in this study are given in Table 2. Calculated spectral indices are available in Table 3.

Tab. 2 Overview of satellite and UAV data

Platform	Sensor	Calculated Index	Date (2020)
Satellite Sentinel 1	C-band SAR	RVI	15.5.; 21.5; 27.5.; 2.6.; 8.6.; 14.6.; 20.6.; 26.6.; 2.7.
Satellite Sentinel 2	MSI	NDVI, GNDVI, MSI, EMSI	18.5.; 2.6.; 12.6.;
FireFly6 Pro	Micasense RedEdge MX	NDVI, GNDVI, TGI	21.5.; 15.7.
UAV – DJI Mavic Pro	RGB	TGI	23.6.

SAR = Synthetic Aperture Radar; MSI sensor = Multispectral Instrument; RVI = Radar Vegetation Index; NDVI = Normalized Difference Vegetation Index; GNDVI = Green NDVI, MSI = Moisture Stress Index, EMSI = Enhanced MSI; TGI = Triangular Greenness Index; UAV = Unmanned Aerial Vehicle, SAR = Synthetic Aperture Radar

Tab. 3 Overview of spectral indices used in this study

Index	Equation	Reference
Radar Vegetation Index	$RVI = (4\sigma°VH)/(\sigma°VV + \sigma°VH)$	*Charbonneau et al. (2005)*
Normalized Difference Vegetation Index	NDVI = (NIR-R)/(NIR+R)	*Rouse et al. (1974)*
Green NDVI	GNDVI = (NIR-G)/(NIR+G)	*Gitelson et al. (1996)*
Triangular Greenness Index	TGI = G-0.39×R-0.61×B	*Hunt et al. (2013)*
Moisture Stress Index	MSI = SWIR1/NIR	*Rock et al. (1985)*
Enhanced MSI	EMSI = SWIR2/NIR	*Rock et al. (1985)*

R, G, B, NIR, SWIR1 and SWIR2 = reflectance in RED, GREEN, BLUE, NIR (B4, B3, B2 and B8 bands for Sentinel 2 image), SWIR1 and SWIR2 bands (B11 and B12 bands for Sentinel 2 images); σ° backscatter coefficient (sigma nought); VH polarization mode vertical/horizontal; VV polarization mode vertical/vertical.

The crop samples of poppy in the growing stage BBCH 90 (on 12 August 2020) before harvest were taken from 0.5 × 0.5 m grid for 20 selected sampling points designed according to the scale of TGI spectral index from 23 June 2020. The crop samples were analyzed for number of poppyheads and weight of seeds.
The yield was measured during the harvest with Case 8250 combine harvester equipped with yield monitor. The yield data were processed according to a common statistical workflow. All the data (crop samples, yield map and images) were converted into the shapefiles vector or geotiff raster data format with the aim to compare them on the base spatial distribution over the experimental plot. The data in such formats were then processed in QGIS (version 3.16.8) and ArcGIS Pro (version 2.9.2) SWs. The information derived from spatial formats were then analyzed in Statistica (version 13.5.0.17) SW.

RESULTS AND DISCUSSION

Coefficients of determination (R^2) between vegetation indices (NDVI, GNDVI, TGI) calculated from UAV images, number of poppyhead and weight of seeds, and RVI in individual dates of crop scanning are given in Table 4. Coefficients of determination between RVI and vegetation indices (NDVI, GNDVI, MSI and EMSI) calculated from optical satellite images are available in Table 5. The average values of selected indices (RVI, NDVI, GNDVI, MSI, EMSI) throughout the growing season of poppy in terms of Sentinel 1 and Sentinel 2 scanning can be seen in Figure 1. Figure 2 then displays selected spectral indices for individual dates: EMSI for 18 May 2020; RVI for 27 May 2020, GNDVI for 2 June 2020; and RVI for 2 June 2020.
The results showed only very low, or no dependence were found between values of RVI values and spectral indices calculated from UAV images (NDVI, GNDVI and TGI) in scanning dates. Only the date of Sentinel 1 scanning - May 27th showed relatively higher dependence between RVI and NDVI, GNDVI and TGI indices derived from UAV images on May 21st. These dates corresponded to an elongation phenological phase of poppy growth. The result showed that the TGI index can be used as alternative to NDVI or GNDVI if there is no NIR band available, as was also confirmed in the study on poppy evaluation by *Jelínek et al. (2020)*. UAV images can also sufficiently supplement crop growth information if satellite images are not or cannot be used (*Balážová et al., 2021*). The RVI index could explain the yield spatial distribution from 32 % in May 15 when the crops were in elongation phenological phase; and from 21 % (on July 2nd) in the growth phase BBCH 68 (end of flowering). Microwave radiation should carry information about moisture and roughness of canopy. These results therefore showed the possible yield variability noticeable during poppy growth, with regard to biomass increase. Coefficient of determinations 0.27 and 0.28 were found between RVI from June 20 (BBCH 58 – beginning of flowering) and number of poppy heads and weight of seeds. This result could explain the signal's ability to detect reflections from different surface types (flowers vs. canopy of green plants).

Tab. 4 Coefficients of determination (R^2) between spectral indices derived from UAV images (Normalized Difference Vegetation Index = NDVI, Green NDVI = GNDVI, Triangular Greenness Index = TGI), Digital Elevation Model (DEM), Yield, number of poppyhead (NoP) and weight of seeds (W); and Radar Vegetation Index (RVI); at 5% significance level

RVI	NDVI 21.5.	NDVI 15.7.	GNDVI 21.5.	GNDVI 15.7.	TGI 21.5.	TGI 23.6.	TGI 15.7.	DEM	Yield (t.ha^{-1})	NoP	W(g)
15.5.	0.15	0.02	0.18	0.02	0.09	0.00	0.00	0.05	0.32	0.09	0.02
21.5.	0.09	0.06	0.09	0.05	0.07	0.02	0.01	0.04	0.05	0.18	0.05
27.5.	0.28	0.11	0.35	0.13	0.24	0.05	0.07	0.05	0.15	0.02	0.00
2.6.	0.03	0.10	0.03	0.01	0.05	0.12	0.16	0.00	0.00	0.00	0.00
8.6.	0.01	0.05	0.00	0.04	0.00	0.00	0.02	0.01	0.02	0.00	0.01
14.6.	0.03	0.00	0.05	0.02	0.07	0.10	0.01	0.03	0.01	0.17	0.21
20.6.	0.01	0.02	0.01	0.10	0.00	0.05	0.16	0.11	0.03	0.27	0.28
26.6.	0.11	0.01	0.10	0.03	0.13	0.00	0.06	0.08	0.03	0.02	0.01
2.7.	0.04	0.00	0.06	0.01	0.04	0.00	0.01	0.00	0.21	0.00	0.01

Tab. 5 Coefficients of determination (R^2) between spectral indices derived from satellite images in optical (Normalized Difference Vegetation Index = NDVI, Green NDVI = GNDVI, Moisture Stress Index = MSI, Enhanced MSI = EMSI) and microwave (RVI) part of electromagnetic spectra I given dates; at 5% significance level

RVI	NDVI 18.5.	NDVI 2.6.	NDVI 12.6.	GNDVI 18.5.	GNDVI 2.6.	GNDVI 12.6.	MSI 18.5.	MSI 2.6.	MS 12.6.	EMSI 18.5.	EMSI 2.6.	EMSI 12.6.
15.5.	0.06	0.00	0.01	0.06	0.00	0.04	0.32	0.01	0.00	0.28	0.00	0.01
21.5.	0.02	0.00	0.00	0.02	0.00	0.00	0.09	0.01	0.01	0.07	0.01	0.00
27.5.	0.30	0.05	0.00	0.37	0.04	0.00	0.40	0.07	0.00	0.41	0.05	0.00
2.6.	0.07	0.22	0.17	0.15	0.29	0.24	0.10	0.25	0.21	0.09	0.24	0.20
8.6.	0.01	0.07	0.07	0.01	0.06	0.04	0.08	0.10	0.09	0.07	0.08	0.08
14.6.	0.00	0.02	0.03	0.00	0.03	0.04	0.10	0.08	0.09	0.06	0.05	0.06
20.6.	0.09	0.03	0.01	0.06	0.05	0.03	0.00	0.02	0.02	0.00	0.04	0.02
26.6.	0.02	0.01	0.01	0.01	0.02	0.02	0.05	0.06	0.07	0.04	0.04	0.05
2.7.	0.10	0.03	0.00	0.16	0.04	0.01	0.26	0.08	0.07	0.24	0.01	0.00

The dependency between RVI and optical indices was also relatively low. The RVI values are generally in relation to the water content of the canopy and the increase in biomass, which finally corresponded to the higher R^2 on May 27th and June 2nd. The similar results confirmed *Tůma el al. (2021)*. The higher dependence of the MSI / EMSI indices at the beginning of growth rather corresponded to the low moisture content in the soil. The MSI and EMSI values decreased as the biomass increased during the very rainy growing season (see Table 1). The RVI curve followed the tendency of the NDVI and GNDVI indices, although the optical indices were less useful due to frequent clouds. *Gonenc et al. (2019)* found out similar trend in NDVI and RVI curves. The RVI curve clearly showed an increase in values at the end of May, when there was an elongation growth stage during a relatively humid spring and then also a sudden decrease in values during flowering (June 8th). This was followed by an increase and decrease in values from the beginning of plant maturation and death (see Table 5, Fig. 1 and 2).

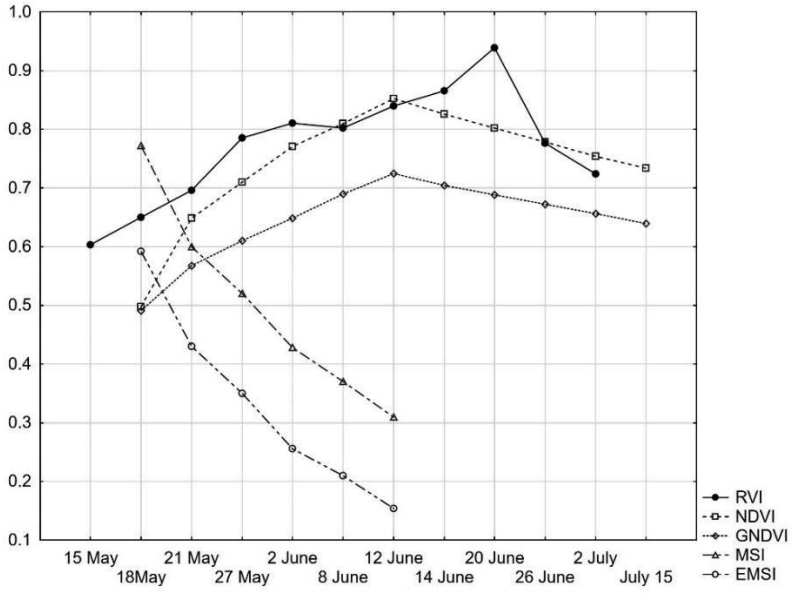

Fig. 1 The average values of selected indices (RVI, NDVI, GNDVI, MSI, EMSI) throughout the growing season of poppy

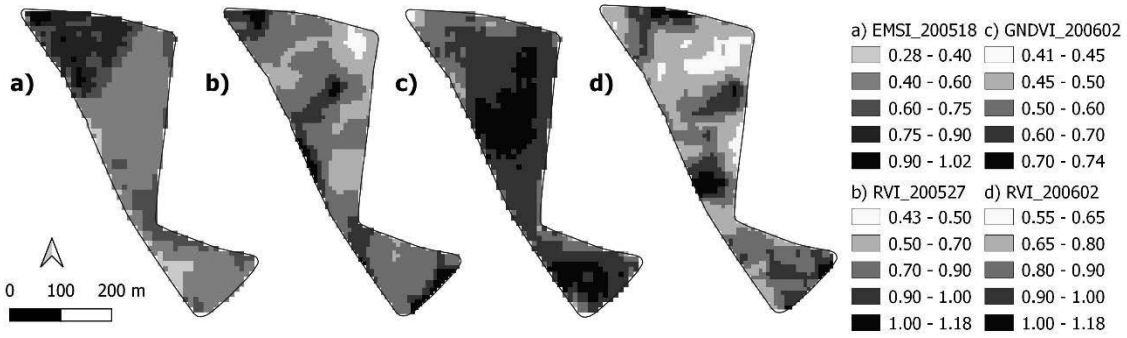

Fig. 2 Selected spectral indices for individual dates: Enhanced Moisture Stress Index (EMSI) for 18 May 2020 (a); Radar Vegetation Index (RVI) for 27 May 2020 (b); Green Normalized Difference Vegetation Index (GNDVI) for 2 June 2020 (c); and RVI for 2 June 2020 (d)

CONCLUSIONS

The poppy was monitored with optical and synthetic aperture radar sensors during 2020 vegetation season. The results showed that development of calculated RVI values in time, can be very helpful in assessing the condition of the poppy stand, especially in cases where optical satellite images are missing, and the stand cannot often be scanned using UAVs. It has been also confirmed that if a common RGB camera is available on the UAV, it is sufficient to calculate the TGI index as an alternative to NDVI or GNDVI. RVI index was also evaluated in terms of use for yield estimation. The spatial distribution of final yield was explained from 32 % by RVI index when the crops were in elongation phenological phase and from 21 % in growing phase at the end of flowering. Future research should focus not only on the use of RVI in poppy stands, but also on other crops commonly grown in the Czech Republic, including the implementation of the RVI index into common agricultural practice.

ACKNOWLEDGMENT

This study was supported by grants: IGA (Geoinformatics as a tool for optimization and efficiency of production and operational processes in Agriculture 4.0.) and NAZV no. QK22010014.

REFERENCES

1. Alonso-González, A., López-Martinez, C., Papathanassiou, K., Hajnsek, I. (2020). Polarimetric SAR Time Series Change Analysis Over Agricultural Areas. *IEEE Transactions on Geoscience and Remote Sensing 58*(10), 7317-7330.
2. Balážová, K., Chyba, J., Kumhálová, J., Mašek, J., Petrásek, S. (2021). Monitoring of Khorasan (Triticum turgidum ssp. Turanicum) and Modern Kabot Spring Wheat (Triticum aestivum) Varieties by UAV and Sensor Technologies under Different Soil Tillage. *Agronomy, 11*(7), 1347.
3. Gonenc, A., Ozerdem, M. S., & Acar, E. (2019). Comparison of NDVI and RVI vegetation indices using satellite images. In *8th International Conference on Agro-Geoinformatics (Agro-Geoinformatics)*, Istanbul, Turkey, pp. 1–4.
4. Harvest, T., Brown, P., Fist, A., Gracie, A. J., Gregory, D., Kotoulis, A. (2009). The latex capacity of opium poppy capsules is fixed early in capsule development and is not a major determinant in morphine yield. *Annals of Applied Biology 154*(2), 251-258.
5. Hong, U. V. T., Tamiru-Oli, M., Hurgobin, B., Okey, Ch. R., Abreu, A. R. Lewsey, M. G. (2022). Insights into opium poppy (Papaver spp.) genetic diversity from genotyping-by-sequencing analysis. *Scientific Reports 12*(111).
6. Jelínek, Z., Starý, K., Kumhálová, J., Lukáš, J., Mašek, J. (2020). Winter wheat, winter rape and poppy crop growth evaluation with the help of remote and proximal sensing measurements. *Agronomy Research 18*(3), 2049-2059.
7. Jia, K., Wu, B., Tian, Y., Li, Q., Du, X. (2011). An effective biophysical indicator for

opium yield estimation. *Computers and Electronics in Agriculture 75*(2), 272-277.
8. Kang, H., Primack, R., 1991. Temporal variation of flower and fruit size in relation to seed yield in celandine poppy (Chelidonium majus papeveraceae). *American Journal of Botany 78*(5), 711-722.
9. Lisson, S. N. (2007). Temperature and photoperiod effects on the growth and development of opium poppy (Papaver somniferum). *Australian Journal of Experimental Agriculture 47*(6), 742-748.
10. Mahdavi-Damgahani, A., Kamkar, B., Al-Ahmadi, M., Testi, L., Muñoz-Ledesma, F. J., Villalobos, F. J. (2010). Water stress effects on growth, development and yield of opium poppy (Papaver somniferum L.). *Agricultural Water Management 97*(10), 1582-1590.
11. Makovnyka, J. (2020). Opium Poppy Agriculture and Consumption. *The Arbutus Review 11*(2), 91-101.
12. Maurya, K., Pal, P., Shukla, S. (2019). Relationship of opium yield with yield contributing traits in segregating populations derived through biparental mating in opium poppy (Papaver somniferum L.) *Industrial Crops and Products 139*, 111557.
13. Tůma, L., Kumhálová, J., Kumhála, F., Krepl, V. (2021). The noise-reduction potential of Radar Vegetation Index for crop management in the Czech Republic. *Precision Agriculture 23*(2), 450-469.
14. Waine, T. W., Simms, D. M., Taylor, J. C., Juniper, G. R. (2014). Towards improving the accuracy of opium yield estimates with remote sensing. *International Journal of Remote Sensing 35*(16), 6292-6309.

Corresponding author:
Ing. Jakub Dvořák, Department of Machines Utilization, Faculty of Engineering, Czech University of Life Sciences Prague, Kamýcká 129, Praha 6, Prague, 16521, Czech Republic, phone: +420 22438 3148, e-mail: jakubdvorak@tf.czu.cz

A META-ANALYSIS ON INFLUENCE OF OXIDIZED-BIOCHAR ON CROP YIELD

Mohammad GHORBANI[1], Petr KONVALINA[1], Marek KOPECKÝ[1], Ladislav KOLÁŘ[1]

[1]*Department of Agroecosystem, Faculty of Agriculture, University of South Bohemia, Czech Republic*

Abstract
Application of oxidized-biochar as one of the most controversial issues of sustainable agriculture and consequently improving crop production needs to a meta-analysis investigation due to conflicting studies that covers representative crop yields datasets. Based on results, crop yields increased by 6.7%, 11.8%, and 18.1% in low (<15 ha), medium (15-25 ha), and high (>25 ha) rates of oxidized-biochar, respectively. While produced-biochar at 350-500 °C and >500 °C temperature significantly enhanced crop yield by 20.2% and 15.7%, respectively, there wasn't a significant change in yield with biochar pyrolyzed at < 350 °C. Also, using oxidized biochar caused to increase crop yield in soils with high value (>2.5% kg^{-1} soil) of organic matter and clay texture by 23% and 22% increase, respectively. Overall, altering these factors can notably boost crop yield efficiency, because they play important roles in nutrient, water and air supply as well as in biogeochemical cycling in agricultural ecosystems.

Key words: *soil organic carbon, pyrolysis temperature, aging, oxidation.*

INTRODUCTION

In recent decades, special attention has been paid to increasing crop production efficiency by application of biochar in the direction of sustainable agriculture (*Asadi et al., 2021*). Due to its porous structure and creating a suitable substrate to retain water, nutrients (*Ghorbani et al., 2019*) and prevent the absorption of contaminants such as heavy metals by plant roots (*Amirahmadi et al., 2020*), the crop yield has been significantly enhanced (*Ghorbani et al., 2021*). Recently, this attention has been enhanced by boosting the surface properties of biochar, such as the cation exchange capacity (CEC) due to oxidation (*Yang et al., 2019; Li et al., 2020*). Most scientific publications refer to the initial properties of fresh biochars. However, these properties are changing over time when biochars have been exposed to a moisture-containing environment, as it is the case after application to soil. This process is referred to as "ageing (oxidation)" (*Beusch, 2021*). Oxidation of biochar can be defined as dissociation in biochar structure and altering in its biochemical characteristics. These basic changes can be effectively caused to the dissolution of organic compounds, absorption of dissolved compounds from the soil, and the neutralization of alkaline conditions in soil over time (*Mia et al., 2017*; *Hung et al., 2021*). It has been studied that the degradation of biochar due to the aging process can be derived into two-part as follows; a) biotic oxidation (activities and respiration of microorganisms) and abiotic oxidation (chemical aging in lab, and photooxidation) (*Bakshi et al., 2016*; *Feng et al., 2018; Yang et al., 2019*). The addition of oxidized-biochar in soils may be more advantageous than fresh biochars, because the degradation in characteristics of the biochars during oxidation may extent the capacity of water and nutrient sustain in soils (*Shi et al., 2015*; *Mia et al., 2017*).

It has been demonstrated that oxidized-biochar can improve soil water storage in drought conditions (*Mia et al., 2017*; *Hung et al., 2021*). Meanwhile, oxidized-biochar can improve carbon sequestration due to the mineralization of organic carbon (*Li et al., 2020*). Surface characteristics of biochar are playing important roles in altering absorption behavior in soil (*Asadi et al., 2021*; *Hung et al., 2021*). Organic matter in biochar tends to be converted to low molecular weight compounds by chemical interactions over a long period of time (*Pan et al., 2021*). The chemical oxidation of biochar is one of the best promising ways to degradation of physicochemical characteristics of biochar and thus, enhance the CEC of biochar as the result of more negatively charge and oxygen-containing functional groups on the surface (*Huff et al., 2018*; *Yang et al., 2019*). On the other hand, it has been shown that using oxidized-biochar without fertilization may even diminution crop yields due to immobilization of N (*Tam-meorg et al., 2014*). A considerable increment in quinoa (*Chenopodium quinoa L.*) yield was reported (*Kammann et al. 2015*) when a mix of compost and biochar was applied to the soil. The substance of compost-biochar was significantly nutrient-loaded and had absorbed substantial amounts of nitrate. Also, there wasn't a significant improvement in maize yield when oxidized-biochars were applied for two years'

field study (*Rogovska et al., 2014*). A labile fraction of oxidized-biochar which is rapidly mineralized by the extension of soil respiration is the main reason (*Haider et al., 2017*). Therefore, it's hypothesized that decreasing nutrient availability may also be correlated with the complex absorbent behavior of biochar (*Kanthle et al., 2016*).
Increment of phenolic hydroxyl groups and aromatic ethers on biochar surface due to oxidation is inevitable (*Li et al., 2020*). However, the magnitude of degradation on the surface area isn't clear, and different studies have reported conflicting findings of either enhancement or a scarce reduction in functional groups. Notwithstanding, the manipulating of oxidized-biochar in agricultural systems has been implemented by many studies, it seems existence of contradictory data regarding the changes in crop yields needs a meta-analysis study. Therefore, the aim of this meta-analysis is clarification the role of oxidized biochar in crop efficiency influenced by pyrolysis condition and soil properties.

MATERIALS AND METHODS

Literature survey and selection criteria

Based on published literature, this meta-analysis was implemented. We identified papers that reported agricultural crop yield in non-oxidized (control) and oxidized (treatment) biochar using the online database search engines Web of Science and Google Scholar. Keywords used for literature search were combinations of terms such as biochar, pyrolysis, feedstock, oxidation, aged biochar, soil, surface area, porosity, functional groups, CEC and crop yield. Also, two criteria were considered to select proper studies as follows: a) all studies were conducted in agricultural environments, and b) all studies reported results from a non-oxidized (control) and oxidized (treatment) biochar.

Collection of data

We reviewed over 50 papers and found that 12 of them met our selection criteria. In total, 864 observations or 432 pairs of observations (effect sizes) were extracted from those studies meeting our criteria and were used in this meta-analysis. These datasets consisted of crop yield in t ha^{-1} affected by oxidized and non-oxidized biochar, pyrolysis temperature, and soil texture and soil organic carbon (SOC).
The rate of biochar application was grouped as low for <15 ha, medium for 15-25 ha, high for >25 ha. Pyrolysis temperature were classified as low (<350 °C), medium (350-500 °C), and high (>500 °C). Soils with the texture of sandy loam, loamy sand, and sand were categorized as sandy. Also, studies that contained soils with the texture of loam, silt loam, clay loam, and silty clay loam were categorized as loamy, as well as, clay and silty were grouped as clay texture. SOC was categorized as low (<1 %), medium (1-2.5 %), and high (>2.5 %).

Meta-data analyses

Meta-analysis calculates the magnitude of change of a variable and the significance of this change in response to a treatment. The natural logarithm of the response ratio (RR) was used to evaluate the value of change which defines as effect size (*Hedges et al., 1999*):

$$\ln(RR) = \ln\frac{X_T}{X_C}$$

where X_C and X_T represent the average of the variable in the control and treatment, respectively. The RR can be considered as the percentage change after applying oxidized-biochar as $(e^{\ln(RR)} -1) \times 100$ (*Nave et al., 2010*). For generating confidence intervals (CIs) around effect sizes, we recorded standard deviation (SD) and number of replicates (n) of crop yield for the control and treatment. The statistical significance was tested using 95% CI for each effect size. If the 95% CIs didn't overlap with the zero line, the change was statistically significant at $P \leq 0.05$. Also, doesn't overlap between groups represent significant differences. A non-linear regression test was used for SOC versus biochar rate and for soil texture versus biochar rate, because the data were not normally distributed. Data collection and organization as well as all calculations (i.e., effect size and CIs), regression analyses and creation of forest plots were performed by Microsoft Excel 2020.
For assessing the presence of publication bias, the Spearman rank correlation test in order to clarify the correlation between the replicates of each study and the effect size was conducted (*Holden and Treseder, 2013*). No publication bias was inspected in the crop yield data for any of the factors.

RESULTS AND DISCUSSION

Based on meta-analysis of data, oxidized-biochar caused crop yield changes across all investigated influencing factors and in total significantly increased crop yields up to 14% at $\alpha = 0.05$ (Fig. 1).

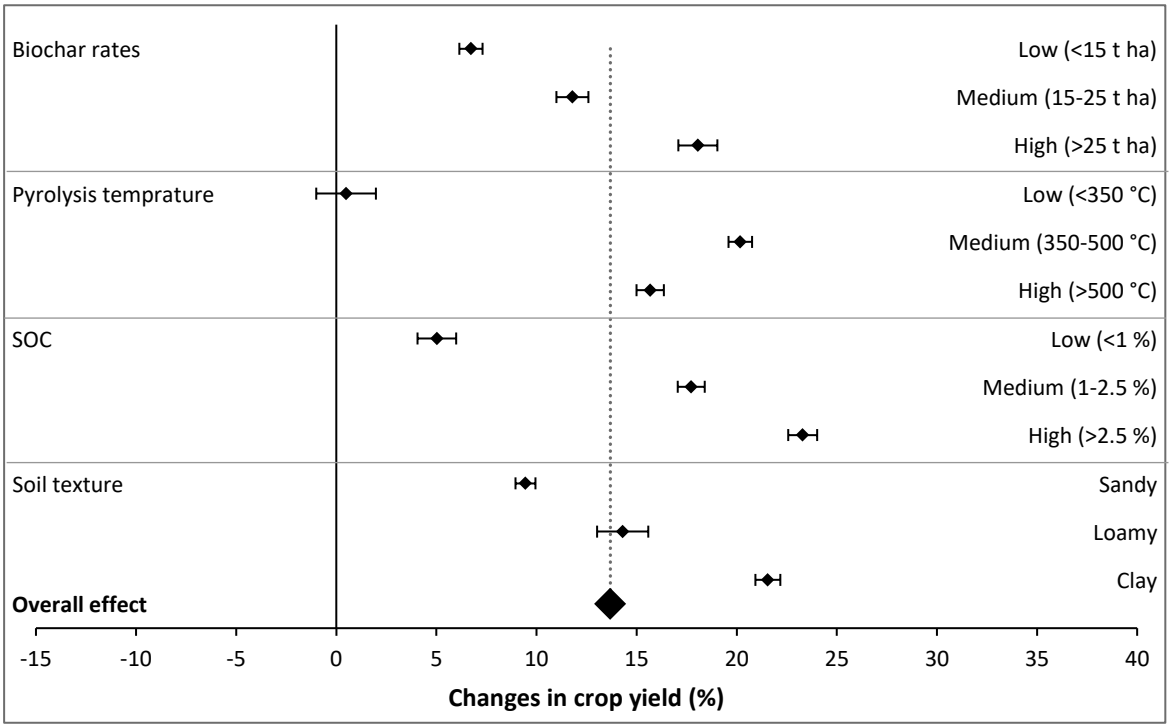

Fig. 1 Crop yield changes due to application of oxidized biochar, influenced by biochar rate, pyrolysis temperature, SOC, and soil texture. Results are presented as mean effect sizes ± 95% confidence intervals. Groups with confidence intervals overlapping the reference line (0% change) indicate no statistically significant change in crop yield due to using oxidized biochar at $\alpha = 0.05$.

Influence of biochar application rates

Crop yields increased by 6.7%, 11.8%, and 18.1% in low, medium, and high rates of biochar, respectively, due to oxidation, which were significantly different from each other. Greater effectiveness in higher grades means more porosity and negative charges on the biochar surface, resulting in more water and nutrients available to the plant's roots. Adding oxidized-biochar to the soil stimulates the development of acidic functional groups (*De la Rosa et al., 2018*), and the accumulation of basic functional groups on the biochar surface will decline for the long term (*Rechberger et al., 2017*). Furthermore, the negative surface charge is increasing with oxidation, leading to a high surface charge density and enhanced CEC (*Mia et al., 2017*). One of the main reasons for the increase in crop yields at higher rates of oxidized-biochar is adding nutrients and required ions to the soil than furthermore. Enhancement in atomic concentrations of sulfur (S), N (nitrogen), sodium (Na), aluminum (Al), calcium (Ca), manganese (Mn), and ferric (Fe) was detected at the surface of oxidized-biochar (*Mia et al., 2017*; *De la Rosa et al., 2018*). In particular, the changes in the surface chemistry may alter the adsorption properties of oxidized-biochars and consequently more nutrient retention in soil (*Ren et al., 2016*). However, due to the increment in CEC, oxidized-biochars may provide a superior potential to sustain cations and elevate crop yields (*Mia et al., 2017*).

Influence of pyrolysis temperature

Oxidized biochar which produced at medium (350-500 °C) and high (>500 °C) pyrolysis temperature significantly enhanced crop yields by 20.2% and 15.7%, respectively. While adding oxidized biochar that derived from low pyrolysis temperature (< 350 °C) wasn't significantly affected by oxidation. In general, ageing processes are enhanced with increasing temperatures and duration of exposure (*Heitkötter & Marschner, 2015*) and in particular affect the biochar surface (*Sorrenti et al., 2016*). Pyrolysis

temperature is a key factor that most of the biochar characteristics are depending on its changes (*Ippolito et al., 2020*; *Das et al., 2021*). Higher temperatures caused to increment of C content (*Yuan et al., 2011*), specific surface area, and porosity (*Al-Wabel et al., 2013*), inorganic element concentrations (*Chen et al., 2019*), ash content (*Ippolito et al., 2020*), CEC (*Zhao et al., 2013*), and aromaticity (*Chen et al., 2019*). With the rising temperature, more volatile ingredients have been lost, and as a result, the value of biochar yield will be diminution (*Al-Wabel et al., 2013*). Moreover, higher temperatures foster decomposition of acidic functional groups like phenolic hydroxyl and carboxyl groups, while carbonyl groups form (*Chen et al., 2019*). Also, decreasing zeta potential with increasing pyrolysis temperatures has been reported, which indicating less negative surface charges for high-temperature biochars than for low-temperature biochars (*Yuan et al., 2011*). This is the main reason that biochar divided from 350-500 °C had the best result in oxidized-biochar efficiency.

Influence of soil organic matter and texture

Application of oxidized biochar significantly increased crop yields up to 5%, 18%, and 23% in soils with low (<1%), medium (1-2.5%), and high (>2.5%) values of SOC, respectively, which have shown significant differences from each other. Crop yields significantly increased by 22%, 14%, and 9% in clay, loamy and sandy soils, respectively, due to oxidation. Also, there were significantly different between soil textures. It has been widely corroborated that biochar significantly affects the accumulation of organic carbon and nitrogen at soil aggregate fractions (*Xiu et al., 2019*; *Ghorbani et al., 2019*; *Joseph et al., 2020*). After adding oxidized-biochar to the soil biochar surface is coated and the pores are linked with organic and mineral components of soils (*Ren et al., 2016*; *De la Rosa et al., 2018*), leading to an increase of aggregation and improving soil structure (*Xiu et al., 2019*). The clay particles apparently play the main role in formation of soil aggregates through binding organic molecules by bi- and trivalent cations (e.g. Ca^{2+}, Fe^{3+} and Al^{3+}) (*Juriga et al., 2018*). That is why soils with clay texture showed the best perform in increasing crop yields. Regarding Fig. 2, a significant positive correlation between changes in biochar rate and SOC (R^2= 0.49), as well as, biochar rate and soil texture (R^2= 0.56) in response to adding oxidized-biochar proves that claim.

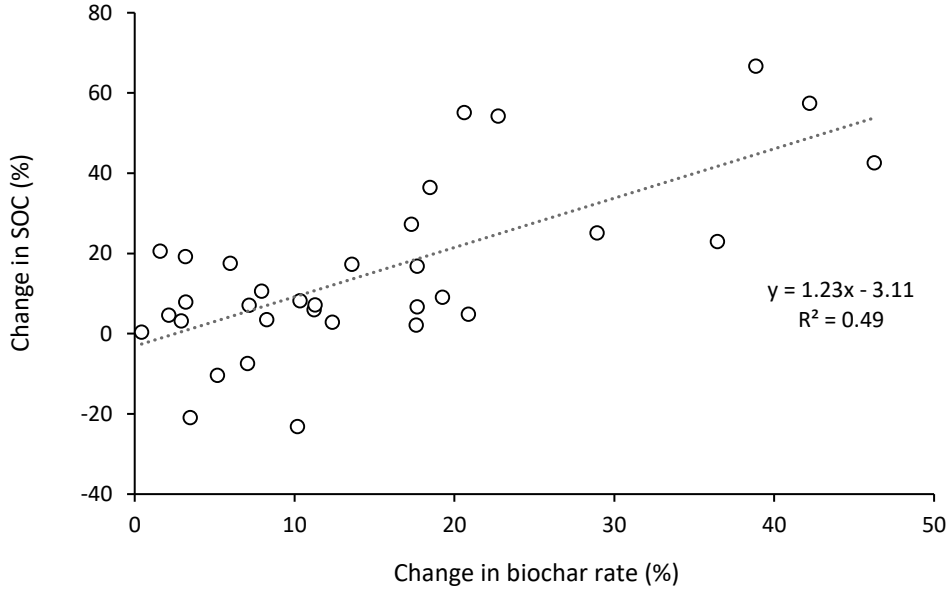

Fig. 2 The correlation between the percentage changes in biochar rate (n = 33) and soil organic carbon (SOC). The correlation was statistically significant at $\alpha = 0.05$.

CONCLUSIONS

This meta-analysis evaluated the impact of oxidized-biochar on crop yields in agricultural ecosystems affected by two amendment factors (biochar rate and pyrolysis temperature and two soil factors (SOC and texture). Despite contradictory reports in previous literature, the meta-analysis showed that the application of oxidized-biochar significantly increased crop yields up to 14%. The positive effect of oxidized-biochar on efficiency of crop yield is largely depends on the pyrolysis temperature. This means that increasing the pyrolysis temperature increases the porosity of biochar structure. This helps to increase the specific surface area and oxygen-contained functional groups during the oxidation and then supply more nutrients, water and air for plant root's area. Accompanied with the fact that clay texture soils hold more water and create organo-mineral bridges with soil organic matter, specific consideration should be paid when oxidized-biochar are used, with the intention to improve the efficiency of strategic agricultural products.

ACKNOWLEDGMENT

This study was supported by the University of South Bohemia in České Budějovice, project GAJU 085/2022/Z.

REFERENCES

1. Al-Wabel, M.I., Al-Omran, A., El-Naggar, A.H., Nadeem, M. & Usman, A.R. (2013). Pyrolysis temperature induced changes in characteristics and chemical composition of biochar produced from conocarpus wastes. *Bioresource Technology*, *131*, 374-379.
2. Amirahmadi, E., Mohammad Hojjati, S., Kammann, C., Ghorbani, M. & Biparva, P. (2020). The potential effectiveness of biochar application to reduce soil Cd bioavailability and encourage oak seedling growth. *Applied Sciences*, *10*(10), 3410.
3. Asadi, H., Ghorbani, M., Rezaei-Rashti, M., Abrishamkesh, S., Amirahmadi, E., Chengrong, C.H.E.N. & Gorji, M. (2021). Application of Rice Husk Biochar for Achieving Sustainable Agriculture and Environment. *Rice Science*, *28*(4), 325-343.
4. Bakshi, S., Aller, D.M., Laird, D.A. & Chintala, R. (2016). Comparison of the physical and chemical properties of laboratory and field-aged biochars. *Journal of Environmental Quality*, *45*(5), 1627-1634.
5. Beusch, C. (2021). Biochar as a Soil Ameliorant: How Biochar Properties Benefit Soil Fertility—A Review. *Journal of Geoscience and Environment Protection*, *9*(10), 28-46.
6. Chen, W., Meng, J., Han, X., Lan, Y. & Zhang, W., 2019. Past, present, and future of biochar. *Biochar*, *1*, 75-87.
7. Das, S.K., Ghosh, G.K., Avasthe, R.K. & Sinha, K. (2021). Compositional heterogeneity of different biochar: Effect of pyrolysis temperature and feedstocks. *Journal of Environmental Management*, *278*, 111501.
8. De la Rosa, J.M., Rosado, M., Paneque, M., Miller, A.Z. & Knicker, H. (2018). Effects of aging under field conditions on biochar structure and composition: Implications for biochar stability in soils. *Science of the Total Environment*, *613*, 969-976.
9. Feng, Y., Sun, H., Xue, L., Wang, Y., Yang, L., Shi, W., & Xing, B. (2018). Sawdust biochar application to rice paddy field: reduced nitrogen loss in floodwater accompanied with increased NH3 volatilization. *Environmental Science and Pollution Research*, *25*(9), 8388-8395.
10. Ghorbani, M., Amirahmadi, E. & Zamanian, K. (2021). In-situ biochar production in paddies: direct involvement of farmers in greenhouse gases reduction policies besides increasing nutrients availability and rice production. *Land Degradation & Development*, *32*(14), 3893-3904.
11. Ghorbani, M., Asadi, H. & Abrishamkesh, S. (2019). Effects of rice husk biochar on selected soil properties and nitrate leaching in loamy sand and clay soil. *International soil and water conservation research*, *7*(3), 258-265.
12. Haider, G., Steffens, D., Moser, G., Müller, C. & Kammann, C.I. (2017). Biochar reduced nitrate leaching and improved soil moisture content without yield improvements in a four-year field study. *Agriculture, Ecosystems & Environment*, *237*, 80-94.
13. Hedges, L.V., Gurevitch, J. & Curtis, P.S., (1999). The meta-analysis of response ratios

in experimental ecology. *Ecology*, *80*(4), 1150-1156.
14. Heitkötter, J. & Marschner, B. (2015). Interactive effects of biochar ageing in soils related to feedstock, pyrolysis temperature, and historic charcoal production. *Geoderma*, *245*, 56-64.
15. Holden, S.R. & Treseder, K.K. (2013). A meta-analysis of soil microbial biomass responses to forest disturbances. *Frontiers in Microbiology*, *4*, 163.
16. Huff, M.D., Marshall, S., Saeed, H.A. & Lee, J.W., 2018. Surface oxygenation of biochar through ozonization for dramatically enhancing cation exchange capacity. *Bioresources and Bioprocessing*, *5*(1), 1-9.
17. Hung, C.M., Huang, C.P., Chen, C.W., Hsieh, S.L. & Dong, C.D. (2021). Effects of biochar on catalysis treatment of 4-nonylphenol in estuarine sediment and associated microbial community structure. *Environmental Pollution*, 268, 115673.
18. Ippolito, J.A., Cui, L., Kammann, C., Wrage-Mönnig, N., Estavillo, J.M., Fuertes-Mendizabal, T., Cayuela, M.L., Sigua, G., Novak, J., Spokas, K. & Borchard, N., 2020. Feedstock choice, pyrolysis temperature and type influence biochar characteristics: a comprehensive meta-data analysis review. *Biochar*, *2*, 421-438.
19. Joseph, U.E., Toluwase, A.O., Kehinde, E.O., Omasan, E.E., Tolulope, A.Y., George, O.O., Zhao, C. & Hongyan, W. (2020). Effect of biochar on soil structure and storage of soil organic carbon and nitrogen in the aggregate fractions of an Albic soil. *Archives of Agronomy and Soil Science*, *66*(1), 1-12.
20. Juriga, M., Šimanský, V., Horák, J., Kondrlová, E., Igaz, D., Polláková, N., Buchkina, N. and Balashov, E. (2018). The effect of different rates of biochar and biochar in combination with N fertilizer on the parameters of soil organic matter and soil structure. *Journal of Ecological Engineering*, *19*(6), 153-161.
21. Kammann, C.I., Schmidt, H.P., Messerschmidt, N., Linsel, S., Steffens, D., Müller, C., Koyro, H.W., Conte, P. & Joseph, S. (2015). Plant growth improvement mediated by nitrate capture in co-composted biochar. *Scientific Reports*, *5*(1), 1-13.
22. Kanthle, A.K., Lenka, N.K., Lenka, S. & Tedia, K. (2016). Biochar impact on nitrate leaching as influenced by native soil organic carbon in an Inceptisol of central India. *Soil and Tillage Research*, *157*, 65-72.
23. Li, K., Yin, G., Xu, Q., Yan, J., Hseu, Z.Y., Zhu, L. & Lin, Q. (2020). Influence of Aged Biochar Modified by Cd2+ on Soil Properties and Microbial Community. *Sustainability*, *12*(12), 4868.
24. Mia, S., Dijkstra, F.A. & Singh, B. (2017). Long-term aging of biochar: a molecular understanding with agricultural and environmental implications. Advances in agronomy, 141, 1-51.
25. Pan, S.Y., Dong, C.D., Su, J.F., Wang, P.Y., Chen, C.W., Chang, J.S., Kim, H., Huang, C.P. & Hung, C.M. (2021). The Role of Biochar in Regulating the Carbon, Phosphorus, and Nitrogen Cycles Exemplified by Soil Systems. *Sustainability*, *13*(10), 5612.
26. Rechberger, M.V., Kloss, S., Rennhofer, H., Tintner, J., Watzinger, A., Soja, G., Lichtenegger, H. and Zehetner, F. (2017). Changes in biochar physical and chemical properties: Accelerated biochar aging in an acidic soil. *Carbon*, *115*, 209-219.
27. Ren, X., Sun, H., Wang, F. & Cao, F. (2016). The changes in biochar properties and sorption capacities after being cultured with wheat for 3 months. *Chemosphere*, *144*, 2257-2263.
28. Rogovska, N., Laird, D.A., Rathke, S.J. & Karlen, D.L. (2014). Biochar impact on Midwestern Mollisols and maize nutrient availability. *Geoderma*, *230*, 340-347.
29. Shi, K., Xie, Y. & Qiu, Y. (2015). Natural oxidation of a temperature series of biochars: opposite effect on the sorption of aromatic cationic herbicides. *Ecotoxicology and Environmental Safety*, *114*, 102-108.
30. Sorrenti, G., Masiello, C.A., Dugan, B. & Toselli, M. (2016). Biochar physico-chemical properties as affected by environmental exposure. *Science of the total Environment*, *563*, 237-246.
31. Tammeorg, P., Simojoki, A., Mäkelä, P., Stoddard, F.L., Alakukku, L. & Helenius, J., (2014). Biochar application to a fertile sandy clay loam in boreal conditions: effects on soil properties and yield formation of wheat, turnip rape and faba bean. *Plant and Soil*, *374*(1), 89-107.
32. Xiu, L., Zhang, W., Sun, Y., Wu, D., Meng, J. & Chen, W. (2019). Effects of biochar and straw returning on the key cultivation limitations of Albic soil and soybean growth over 2 years. *Catena*, *173*, 481-493.

33. Yang, X., Zhang, S., Ju, M. & Liu, L. (2019). Preparation and modification of biochar materials and their application in soil remediation. *Applied Sciences*, *9*(7), 1365.
34. Yuan, J.H., Xu, R.K. & Zhang, H. (2011). The forms of alkalis in the biochar produced from crop residues at different temperatures. Bioresource Technology, *102*(3), 3488-3497.
35. Zhao, L., Cao, X., Mašek, O. & Zimmerman, A. (2013). Heterogeneity of biochar properties as a function of feedstock sources and production temperatures. Journal of *Hazardous Materials*, *256*, 1-9.

Corresponding author:
Ing. Mohammad Ghorbani, Ph.D., Department of Agroecosystem, Faculty of Agriculture, University of South Bohemia, Studentská 13, 370 05 České Budějovice, Czech Republic, e-mail: ghorbm00@zf.jcu.cz

WATER TREATMENT TECHNOLOGY SUPPLEMENTED BY ELEMENTS FROM INDUSTRY 4.0 – A REVIEW

David Guth[1]

[1]*Department of Mechanical Engineering, Faculty of Engineering, Czech University of Life Sciences Prague, Czech Republic*

Abstract
This review deals with the issue of water and its filtering. Among others, the effects on human health, in the case of consumption of contaminated water, are also mentioned. The main parameters are the implementation of modern elements (pH meter, flow meter, thermometer, filter pollution meter, UV lamp, reverse osmosis and cameras) to the existing water treatment plant and their subsequent use. The result should be an independent, modern treatment plant that should be able to filter clean drinking water for final consumers without bacteria or discoloration.

Key words: *water treatment plant, filtration, drinking water, industry 4.0*

INTRODUCTION

In today's modern times, the quality of drinking water is a very discussed, important and current topic, especially in the developing countries of the world was mentioned by *Sutherland, K. (2008).* Providing high-quality drinking water for the population to their homes without any pollution is a basic condition for developed countries described by *Mallik, A., & Arefin, M. A. (2018)*. In order to meet these conditions, it is required to improve the microbiological quality of the water, control of undesirable substances, chemicals and metals that may be contained in the water, reported by *Fewtrell, L. et al. (1997)*. Secondary steps are the maintenance and sufficient protection of the water pipeline and the complete system, management and control of the content and aesthetic quality of the water, which include color, hardness, smell and taste, these steps are reported by *Martynov, S.et al. (2020)*. Polluted and contaminated water is the main carrier of many water-borne diseases, including typhoid, cholera, salmonellosis, hepatitis, viral infections and many others reported by *Deflorio-Barker, S. et al. (2016)*. These diseases cause a noticeable weakening of the human organism and can lead to the complete failure of the human body, both men and women, but also children mentioned by *Momba, M. N. B. et al. (2009)*. Water industry-specific structures and functioning provide the perfect environment for improvements in efficiency, quality, and availability using Industry 4.0 principles. The water industry is represented by highly heterogeneous and geographically dispersed processes and technical solutions that are described by *Nicolae, A. et al. (2019)*. These include legacy systems and new structures that are in stringent need of connecting the digital and the physical worlds in the context of highly functional process dependencies with interoperation reported by *Nicolae, A. et al. (2019)*. In todays world, there is very many modern elements and filtration methods that are used in the water treatment plants. One of the most common used elements is reverse osmosis or UV (ultra-violet) purification which is described by *Piferi, C. et al. (2021)*. Study by *Rao, S. M. (2007)* describes that reverse osmosis process involves the use of membrane technology which allows to remove dissolved salts and other impurities in water. The radiations function by irradiating the water and piercing through the cells of the microorganisms and viruses. Study by *Pinto et al. (2012*) describes that among the generally accepted methods of purifying drinking water is the addition of chlorination to the filtration process, which results in a dramatic decrease in the amount of bacteria in the water. Study by *Liao, X., et al. (2015)* describes that filtration by dual media rapid sand filters in a drinking water plant played a primary role in shaping the bacterial community. If residents decide to draw and consume water from their own sources, ensuring sufficient filtration to prevent possible diseases is a necessary step. Drinking water filters differ according to the technologies used, filter materials and purpose. Study by *Poitelon, J. B. et al. (2010)* describes the most common are mechanical filters and filters with active carbon. Mechanical filtration can be mesh or membrane. Membrane filtration is generally more effective, but it is not suitable for drinking water. The membrane captures vital substances that the organism would miss, which is reported by *Nagakura, (2015)*. Chemical filtration is not filtration in the true sense of the word, but water treatment, where unwanted

chemical or organic substances are removed from the water. For these purposes, granulated activated carbon is most often used, which, thanks to its surface and sorption properties, can capture the entire range of harmful substances dissolved in water – from heavy metals to chlorine and other chemicals to viruses and bacteria. Granulated activated carbon absorbs or captures these substances and organisms on its surface. Based on this, it removes unpleasant odors from the water and improves its taste which was reported by *Tang, H. L., & Xie, Y. F. (2016)*. Study by *T. Eisenberg, E. Middlebrooks (1986)* describes that reverse osmosis processes can simultaneously remove hardness, color, many types of bacteria, viruses and organic contaminants. Contaminants, as agricultural chemicals reviewed the effectiveness of reverse osmosis on drinking water and reported that it can successfully remove a wide range of contaminants that are often found in drinking water which was reported by *T. Eisenberg, E. Middlebrooks (1986)*. The aim of this study is to create a water treatment plant based on industry 4.0. By combining mechanical filtration and chemical filtration, using modern elements to maximize unit self-automatization. By using pH meter, water flow calculator, thermometer, filter pollution meter and install the cameras to simply prevent a possible problem that could arise as a result of neglect. The water entering the treatment plant will undergo treatment using several modern elements, and the main goal of this work is clean treated water at the exit.

MATERIALS AND METHODS

In order to create and maximize the automatization and modernization of the water treatment plant, a treatment plant named Oaza 100 was selected. The treatment plant is equipped with a pre-filter with an ABS (acrylonitrile butadiene styrene) and nylon filter insert, composite fiberglass, reverse osmosis module and its membrane, pump and UV lamp. All the data were collected from the manual of the water treatment itself and from the articles uploaded to Web of Science, Scopus, IWA (International Water Association). A large part of the obtained data and knowledge was obtained through an interview with the creator of the water treatment plant, and its subsequent maintenance and the possibility of modernization was solved with a specialist company dealing with this issue. Other technical parameters are mentioned in the Tab.1. All the technological equipment of the water treatment plant are fixed in a stainless steel frame so that all parts of the technological unit can be easily serviced while maintaining the smallest possible space. All materials used must meet certification for contact with food, respectively drinking water. To achieve the modernization of the water treatment plant, a pH meter, flow meter, thermometer, filter pollution meter, and cameras will be purchased. All these mentioned elements will be installed on the water treatment plant and tested. The water will be entering the water treatment plant in three different flows 0,2; 0,4 and 0,6 liters per minute. Subsequently, the water values at the inlet and outlet will be compared and the efficiency of the treatment plant will be evaluated by an expert laboratory dealing with water analysis.

Tab.1 Operational - technical parameters

Working pressure range	6-10 bars
Optimal working pressure	7-8 bars
Permeate performance at optimum pressure	100 l/hod
Weight of the body of the treatment plant approx.	500 kg
Body dimensions (height × width × depth)	2000 × 1100 × 1720mm

RESULTS AND DISCUSSION

This review is focused on, how the treatment plant will be able to filter the water that will be admitted to the treatment plant at the entrance and will pass through all the installed elements and come out at the exit. Colored water with added bacteria and then with cyanobacteria will be fed into the treatment plant. Assuming that disinfection is sufficient in the treatment plant and suspended and colloidal solids are sufficiently removed in preceding steps, the main controlled parameters for a treatment plant are chemical stability (saturation index SI), biological stability (assimilable organic carbon AOC), disinfection by-products (bromate) and organic micro-pollutants (pesticides) which was reported by *Rietveld, L. et al. (2008)*. The expected results are that the treatment plant will be able to fully remove all undesirable

elements from the water and at the exit the water will be clean and drinkable meeting WHO requirements. The process revealed that the system which combines NF and UV disinfection is ranked first for all the different stakeholder weightings reported by *Bouchard, et al. (2010)*. All three investigated flow rates should be able to filter water equally well, as they are below the limit of the maximum flow rate of the treatment plant. The most suitable filter cleaning process is the backwash, which is the most effective, which is confirmed by *Arendze, S., & Sibiya, M. (2014)*. Although it may seem that the control of the treatment plant is relatively complicated, but it is not. The treatment and its controls are set up so that even quickly trained personnel can control it easily. No same or similar works to this were found, and therefore does not have the possibility to compare the results with other works. This is one of the reasons and motivations why this topic was chosen.

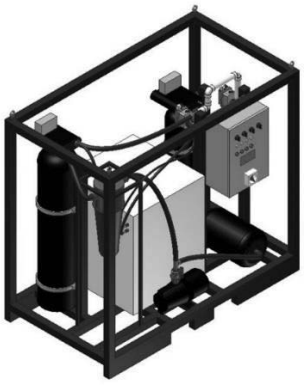

Fig. 1 Animation of Oasa 100 water treatment plant

Fig.2 Real picture of Oasa 100 water treatment

CONCLUSIONS

Water takes an essential part of human daily lives that's mostly not even being considered where it´s being sourced or the quality of the water. For many people, tap water is deemed as undrinkable. That's why it´s very important to take care of the water and filter it. The importance of water filtration is that it gives people access to clean water that is free of contaminants, that tastes good, and is a reliable source of hydration. The implementation of the modern elements into the water treatment plant would bring lots of benefits. Using the elements mentioned above would save time on operating the water treatment plant. Some of the negatives of implementing the modern elements into the water treatment may be reflected in the purchase price of the water treatment. The main positives of implementing the modern elements based on industry 4.0 into the existing water treatment plant is remote controlling the treatment by experts and educated workers. Which means measuring the pollution of the filters, checking if the filling of the filters was changed and measuring the pH and temperature. Based on these, the water treatment plant would provide filtering to the final consumers.

REFERENCES

1. Mallik, A., & Arefin, M. A. (2018). Clean water: Design of an efficient and feasible water treatment plant for rural South-Bengal. Journal of Mechanical Engineering Research and Developments, 41(1), 156–167. https://doi.org/10.7508/jmerd.2018.01.019
2. Martynov, S. et al. (2020). Modern trends at natural and wastewater treatment plants reconstruction. IOP Conference Series: Materials Science and Engineering, 907(1), 0–8. https://doi.org/10.1088/1757-899X/907/1/012083
3. Momba, M. et al. (2009). Survey of disinfection efficiency of small drinking water treatment plants: Challenges facing small water treatment plants in South Africa. Water SA, 35(4), 485–494. https://doi.org/10.4314/wsa.v35i4.76795
4. Liao, X., et al. (2015). Bacterial community change through drinking water treatment processes. International Journal of Environmental Science and Technology, 12(6), 1867–1874. https://doi.org/10.1007/S13762-014-0540-0/FIGURES/7

5. Poitelon, J. B. et al. (2010). Variations of bacterial 16S rDNA phylotypes prior to and after chlorination for drinking water production from two surface water treatment plants. Journal of Industrial Microbiology and Biotechnology, 37(2), 117–128. https://doi.org/10.1007/s10295-009-0653-5
6. Rao, S. M. (2007). Reverse osmosis. Resonance 2007 12:5, 12(5), 37–40. https://doi.org/10.1007/S12045-007-0048-8
7. Pinto, A. J. et al. (2012). Bacterial community structure in the drinking water microbiome is governed by filtration processes. Environmental Science and Technology, 46(16), 8851–8859. https://doi.org/10.1021/ES302042T/SUPPL_FILE/ES302042T_SI_001.PDF
8. Tang, H. L., & Xie, Y. F. (2016). Biologically active carbon filtration for haloacetic acid removal from swimming pool water. Science of The Total Environment, 541, 58–64. https://doi.org/10.1016/J.SCITOTENV.2015.09.059
9. Nagakura, Y., et al. (2015). Modern Electrical Technology for Water Treatment Plants. 45(4), 110–121.
10. Sutherland, K. (2008). Water filtration: Bulk water filtration techniques. Filtration & Separation, 45(10), 17–19. https://doi.org/10.1016/S0015-1882(08)70496-8
11. Nicolae, A. et al. (2019). Identifying data dependencies as first step to obtain a proactive Historian: Test scenario in the water industry 4.0. Water (Switzerland), 11(6). https://doi.org/10.3390/w11061144
12. Fewtrell, L. et al. (1997). Microbiological quality of bottled water. Water Science and Technology, 35(11–12), 47–53. https://doi.org/10.2166/WST.1997.0708
13. Deflorio-Barker, S. et al. (2016). Water recreation and illness severity. Journal of Water and Health, 14(5), 713–726. https://doi.org/10.2166/WH.2016.002
14. Piferi, C. et al. (2021). Intensity comparison between UV lamps and plasma emission for air purification studies. AIP Advances, 11(8), 085209. https://doi.org/10.1063/5.0057033
15. Kahdim, A. S. et al. (2003). Modeling of reverse osmosis systems. Desalination, 158(1–3), 323–329. https://doi.org/10.1016/S0011-9164(03)00471-5
16. Sun, M. et al. (2021). Electrified Membranes for Water Treatment Applications. ACS ES&T Engineering, 1(4), 725–752. https://doi.org/10.1021/ACSESTENGG.1C00015
17. Bouchard, C., Beauchamp, N., Abi-Zeid, I., Lamontagne, L., Desrosiers, J., & Rodriguez, M. (2010). Multicriteria decision analysis for the selection of a small drinking water treatment system. Journal of Water Supply: Research and Technology-Aqua, 59(4), 230–242. https://doi.org/10.2166/AQUA.2010.071
18. Arendze, S., & Sibiya, M. (2014). Filter backwash water treatment options. Journal of Water Reuse and Desalination, 4(2), 85–91. https://doi.org/10.2166/WRD.2013.131
19. Rietveld, L., Van Der Helm, A., Van Schagen, K., Van Der Aa, R., & Van Dijk, H. (2008). Integrated simulation of drinking water treatment. Journal of Water Supply: Research and Technology-Aqua, 57(3), 133–141. https://doi.org/10.2166/AQUA.2008.098
20. T. Eisenberg, E. Middlebrooks, Reverse osmosis treatment of drinking water, (1986), 1–271, doi:10.1016/B978-0-250-40617-3.50004-4

ACKNOWLEDGEMENT
This study was supported by CZU Faculty of Engineering *IGA 2022 – 31130 30103 1312*

Corresponding author:
Ing. David Guth, Department of Mechanical Engineering, Faculty of Engineering, Czech University of Life Sciences Prague, Kamýcká 129, Praha 6, Prague, 16500, Czech Republic, phone: +420 224 383 181, e-mail: guthd@tf.czu.cz

ACQUISITION OF 3D MODELS OF PARTS BY REVERSE ENGINEERING PROCESS

Martina HAJKOVÁ[1], Róbert DRLIČKA[1], Martin KOTUS[1], Monika TÖRÖKOVÁ[2], Juraj CANDRÁK

[1]Institute of Design and Engineering Technology, Faculty of Engineering, SUA in Nitra, Tr. A. Hlinku 2, 949 76 Nitra, Slovakia
[2]Department of Computer Aided Manufacturing Technologies, Faculty of Manufacturing Technologies of the Technical University of Kosice with a seat in Prešov, Bayerova 1, 080 01 Prešov, Slovakia

Abstract
Currently, there are many situations in which we do not have documentation for some element, object, and we need it for various reasons. The article describes the procedure of using data from 3D scanning in a non-contact way for the reconstruction of a 3D model in modeling CAD software. The degree of approximation is determined by comparing the 3D model and the 3D scan. The accuracy of the work is checked by comparing the 3D model with the original CAD data. Obtained models can serve as data for computer-aided production, or digital imaging, for example, in virtual reality.

Key words: *object; 3D scanning, CAD software; data inspection.*

INTRODUCTION

Reverse engineering is a common approach in many fields, such as software engineering, computer, electronics, chemical industry. It is also used in automotive or general engineering production (*Babjak, 2006*). Reverse engineering does not only apply to processes working with material objects, but its application is known primarily in the areas of software, where it involves the examination of codes and processes through analytical procedures.
In engineering, we understand that reverse engineering (RE) as the process of duplicating an existing component, assembly or product, without drawings, documentation or a computer model being available However, the possibilities of using RE technologies go beyond the scope of product design, with appropriate application they can also be used as a tool for design, safety and production management (*Dado et al., 2018*). A typical example is the use of 3D scanners in production lines as a tool for quality control when comparing actually produced parts with production documentation, or 3D CAD models. In this way, it is then possible, for example, to determine the rate of tool wear in a quick way, moreover, without the need to interrupt the production process. Suitable device with advanced software support can scan the physical product within a few minutes, compare it with the CAD model and even automatically generate an inspection report (*Babjak, 2006*). 3D scanning processes can be used to generate inspection reports, verify CAD models, create digital objects for virtual and mixed reality.
The aim of the paper is to describe the process of creating a digital 3D model of a component using reverse engineering technologies.

MATERIALS AND METHODS

Engineering is the process of designing, manufacturing and maintaining products, assemblies and systems. Standard engineering („forward engineering“) is the traditional process of moving from high-level abstractions and logical designs to the physical system implementation. Definition of reverse engineering is the process of obtaining a geometric CAD model from 3D points acquired by scanning existing parts/products. In reverse engineering, the physical model is the source of information for the CAD model (Fig. 1).

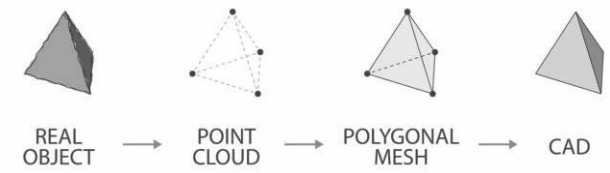

Fig. 1 3D Reverse engineering from real object to CAD

The starting point for creating any model using RE is to obtain input data in the form of spatial coordinates of the surfaces of the object (cloud of points). There are many principles, procedures and devices for obtaining this geometric data. Currently, non-contact optical 3D scanners are readily available, most often working on the principle of triangulation, optical interferometry, or measuring the time of flight of modulated light (*Telíšková et al., 2018*). The light source can project light patterns or lines and have the nature of structured ambient light or laser beams of different colours and intensities. The simplest devices are starting at the price of several hundred euros, while serious quality can be obtained with devices costing couple of thousand euros.
For our experimental work, we used a dual-camera HP 3D SLS PRO S3 device using 3D triangulation using a structured light beam emitted by a projector and captured on a surface by 2 industrial cameras. It is a static system requiring subsequent positioning of the object and scanning in these positions, followed by combining individual scans. By merging these scans in the program, a closed polygon is created. The system offers the possibility of using interpolation of gaps and smoothing filters, which can make scanning even more accurate. The 3D model obtained in this way can be saved, including the scanned texture, in various formats, e.g. stl, obj, plt.
We used Rhinoceros 3D software to create a CAD model from the scanned data. It is a middle-range 3D CAD system with a wide application area, including mechanical engineering. Rhinoceros specializes in free-form non-uniform rational B-spline (NURBS) modelling. There is also over 100 third-party plug-ins available, including rendering plug-ins for Maxwell Render, V-Ray, Thea and lots of other engines. Additional plug-ins for CAM and CNC milling are available as well. Its advantages are an affordable price and a favourable licensing policy for schools and students, allowing keep a full license even after the end of the academic career. We used the Mesh2Surface plugin to work with the point cloud. Mesh2Surface simplifies reverse engineering in Rhinoceros and helps convert digitized objects from non-contact scanners to CAD models. The typical workflow comprises importing data into Rhinoceros and Mesh2Surface, alignment, creating shapes, splitting surfaces, creating a solid model, rounding edges and exporting CAD model. The plugin offers a number of useful functions: extraction of shapes such as surfaces, spheres, cones, cylinders and free-form surfaces, object symmetry search, object alignment to a coordinate system. To obtain the geometric elements of the model, we combined the use of automated recognition and creation of geometric primitives with manual creation of geometry by translating the forming curve of the surface by cutting a polygonal mesh of points. We supplemented the basic shape with shape and cosmetic elements using standard modelling tools.
We compared the model created in this way with the original CAD data using the freely available version of the GOM Inspect software for 3D point cloud inspection and mesh processing enabling dimensional analysis of 3D point clouds obtained from optical scanners, laser scanners, computed tomography CT and other sources.

RESULTS AND DISCUSSION

Basic shape of the selected part (Fig. 2a) combines a simple cylindrical surface and a shaped rotary surface. It was manufactured by machining and has a smooth and shiny surface. The latter is problematic for scanning with normal structured light due to unwanted light reflections. Therefore we covered it with white chalk spray for scanning purposes (Fig. 2b). The spray adds a layer to the surface causing a uniformly distributed systematic change in dimensions of the order of thousandths to hundreds of mm, which is bellow or on par of the level of the best accuracy of the scanner.

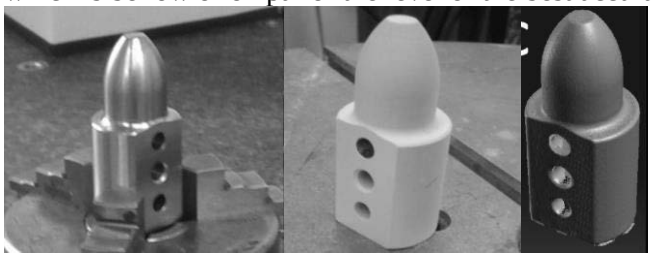

a b c

Fig. 2 Machined sample (a), coated sample (b), scanned sample (c)

After a successful scan (Fig. 2c), we imported the data in the .obj format into the Rhinoceros program.

Work with the mesh is handled by the Mes2Surface plug-in module, simplifying the initial alignment of the scan with the CAD coordinate system. Adjustment of the position was done by aligning the selected or created element with the selected plane of the modeller (Fig. 3a).

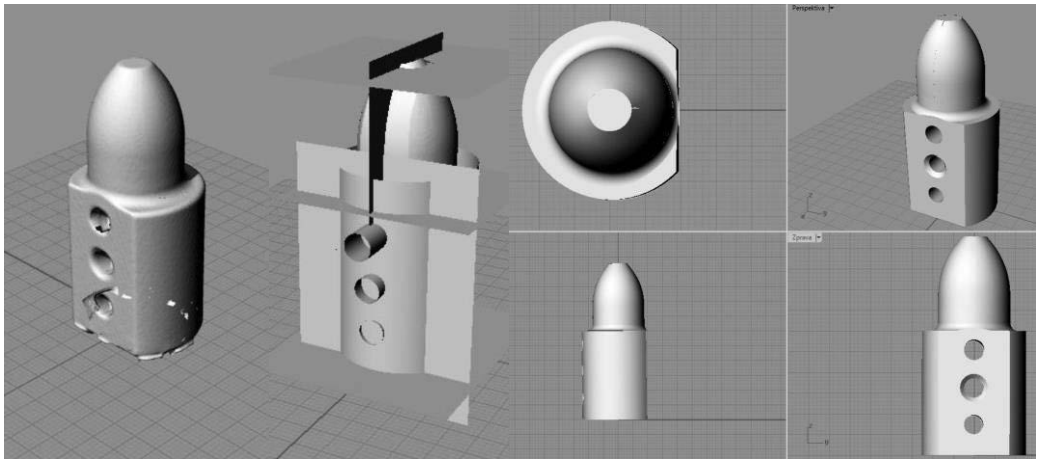

a b c

Fig. 3 Polygonal mesh aligned to WCS in Rhinoceros (a), surfaces wrapping the mesh (b), resulting 3D model (c)

Designing on the basis of a polygonal mesh starts in selection of the area for translation of the basic geometric entity. The surface creation wizard (Magic Wang) then allows the selection of the type of geometric element to be created, in our case a cylindrical surface, the shape and dimensions of which can be modified interactively. To create a continuous model, it is optimal to generate the basic surfaces so that they intersect each other and later cut them at the intersections. The surface is then created with the Create Surface tool. In addition to the cylindrical surface, we used plane surfaces (Plane) for design and the Free Form tool for the shaped surface.
The result of these steps can be seen in Fig. 3b. The last step is to trim the protruding parts forming the surfaces in the intersections, which is a routine matter. The resulting model is shown in Fig. 3c.
Comparing the created model with the source CAD data, we found a complex deviation consisting mainly of deviations of the physical object manufacturing, errors created in the process of scanning and scan processing, as well as errors in the creation of geometry based on the scan. The comparison process in the GOM Inspect program includes the definition of the nominal geometry (of the original CAD model), loading of the compared model (created by the reverse engineering process), the choice of the model alignment method and conditions. We can see the result in Figs. 4a, 4b.

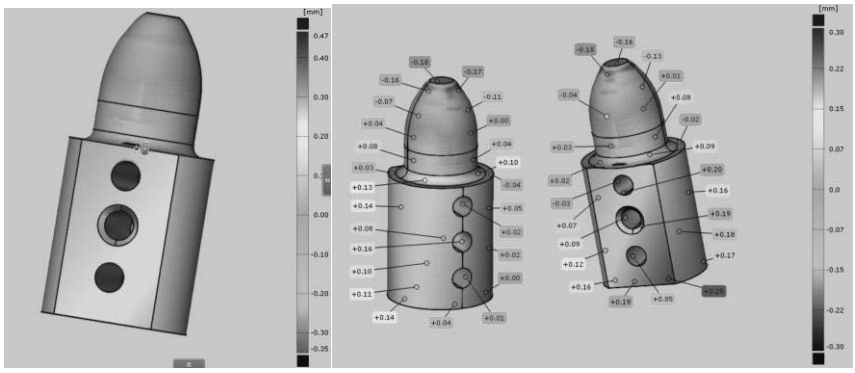

a b

Fig. 4 Colour coded differences of original CAD model and RE acquired model surfaces (a) with error values labels (b).
Before the scanning process, we applied two coats of chalk spray to the part. This layer had a certain thickness. According to *Dokoupil (2013),* who dealt in his work with the determination of measurement

deviations due to the use of chalk and titanium matting powder, the value of the thickness of one layer of chalk spray was 0.003 mm. However, with the second layer of spray, the thickness increased largely and reached a value of 0.031 mm. The scanning device itself has a certain value of accuracy (0.1% of the object size, up to 0.05 mm). Another source for the inaccuracies generation was the composition process of scans and the design process. In his work, *Grujičić (2014)* investigated the accuracy of the designing itself on the obtained cloud of points. The maximum value of deviations in his case reached -0.14 mm and +0.12 mm. However, when considering the digitization of objects for graphic use, for example in virtual and mixed reality, the use of special metrology scanners is unnecessarily expensive (*Török et al., 2017*).

CONCLUSIONS

Based on the output of the GOM Inspect program in the form of a colour scheme of the part with tolerances, we found largest cumulative upward deviation value of +0.25 mm and the largest downward deviation value of -0.18 mm. It can be stated we have created a fairly accurate 3D model with very small values of deviations compared to the real part. These deviation values are within the general tolerances according to STN EN 22768-1 and STN EN 22768-2 standards.

In addition to the above-mentioned shortcomings, scanning with the mentioned technology also has a problem with uniform shapes due to a small number of reference points for composing scans, which then need to be added by as reflecting scanning targets. Higher class hand scanners with blue laser usually perform better in direct light conditions and/or reflective surface due to better contrast. The means and procedure presented in the paper are completely sufficient for obtaining sufficiently accurate models for virtual environments. Considering the number of objects, the efficiency of the mesh-based design process is rather important. There are also more advanced software tools with more sophisticated algorithms for automated recognition of elementary elements in scans, but they are an order of magnitude more expensive. However, currently there is no tool for fully automated RE process available. Nevertheless, the RE process remains very important, since the mesh files are usually several orders of magnitude larger than the corresponding CAD model files.

ACKNOWLEDGMENT

This publication was supported by the KEGA project nr. 004TUKE-4/2020 Kreovanie nových vzdelávacích nástrojov pre oblasť počítačového modelovania s implementáciou prvkov virtuálnej a rozšírenej reality.

REFERENCES

1. Babjak, Š. (2006). Plánovanie reverzného inžinierstva v procese rýchleho vývoja výrobkov II. In Transfer inovácií, 62-64.
2. Dokoupil, F. (2013). Stanovení odchylek měření 3D optického skeneru. Brno : Vysoké učení technické v Brně.
3. Grujičić, D. (2014). Data processing of 3D measurements. Nitra : SPU v Nitre.
4. Telíšková, M., Török, J., Baron, P., Pollák, M., Kaščák, J. & Mezencevová, V. (2018). Implementation of Innovative D igitalization Methods in Reverse Engineering. 5th International Conference on Industrial Engineering and Applications, 406-409.
5. Török, J., Kočiško, M, Telíšková, M., Petrus, J. & Cuma, M. (2017). Alternative methods of three dimensional data obtaining for virtual reality and aufmented reality. In Acta Technica Corviniensis, 10, 51-54.
6. Dado, M., Kotek, L., Hnilica, R. & Tůma, Z. (2018). The Application of Virtual Reality for Hazard Identification Training in the Context of Ma-chinery Safety: A Preliminary Study. In Manufacturing Technology, 18 (5), 732-736.

Corresponding author:
doc. Ing. Martin Kotus, PhD., Institute of Design and Engineering Technology, Faculty of Engineering, Slovak University of Agriculture in Nitra, Tr. A. Hlinku 2, Nitra, 949 76, Slovak Republic, phone: +421 37 641 5689, e-mail: martin.kotus@uniag.sk

STUDY OF CONTINUOUS SENSING OF THE SPEED OF BELTS IN A HOP DRYER

Petr HEŘMÁNEK, Adolf RYBKA, Ivo HONZÍK

Department of Agricultural Machines, Faculty of Engineering, Czech University of Life Sciences Prague, Czech Republic

Abstract
The article is focused on hop belt dryer and study of sensing of the speed of belts. It contains a schema of the belt dryer and a description of the device for sensing the speed of the belt in the dryer. In measurement was found that the speed of the belts in the dryer is from 0 to 6 mm.s^{-1}. Simultaneously was found that the 3rd belt achieved approximately 66 % of the speed of the second belt all the time. The speed of the first and the second belts was different in both hop dryers. From meteodata was found that for belt speed comparison and thereby setting off the hop dryer is the most suitable parameter for humidity. In conclusion, are indicated directions for further research.

Key words: *speed, hop, belt, dryer.*

INTRODUCTION

Drying is the extensively used method of the conservation of agricultural materials and food. The success and sustainability of the drying process are assessed based on the quality of the dried products, the specific energy consumption and costs (*Kudra, 2004; Lewicki, 2006; Mujumdar et al., 2014; Myllymaa et al., 2019; Myllymaa et al., 2020; Ziegler et al., 2021*). During drying, water is removed from the dried material as quickly as possible while maintaining product quality and minimizing energy consumption. A universal dryer was not developed because every material insists on specific drying conditions. Many types of dryers (over 400) are used in industry and agriculture, which use different drying methods (*Guine et al., 2011; Tarhan et al., 2011; Mujumdar et al., 2014*). Theoretical and practical aspects of drying various materials are described in the literature. Many studies were accomplished to mathematically model drying and determine the drying kinetics of various vegetables, fruits and medicinal plants. *Zhang et al.* (*2015*) suggested a method of controlling the temperature and relative humidity of the drying medium for the dryer controls system. The topic of numerical models and networks during drying was also deal with, for example, by *Chokphoemphun & Chokphoemphun (2018), Youssefi et al. (2009), Guine et al. (2015), Şahinbaşkan & Köse (2010), Kaveh et al. (2018), Kaveh et al. (2019), KirbaŞ et al. (2019) and Holowaty et al. (2022).*
Vasiliev et al. (2020) mention in their contribution that it is necessary to further deal with the issue of drying hops in belt dryers, especially in the area of airflow. In Germany *Raut et al. (2020), Sturm et al. (2020) and Raut et al. (2021)* studied the drying of hop in the dryers.
Hop drying is the last stage of the grower's hop production. The belt dryers are the most widespread among growers in the Czech Republic, which represent 60 % of their total number (approx. 200 units), built mainly in the 1970s. The total capacity of the drying facilities is 9,500 tons of dry hops. However, the growers' production is lower, with approximately 6,000 tons of dry hops. For this reason, it is not worthwhile to build new drying operations, but instead to modernize and innovate existing capacities. This article aimed to provide a method to monitor the average speed of the belt. Information on the speed of the belt together with other data (the hop moisture, the temperature of the drying medium, etc.) will allow the operator to appropriately regulate the drying process of the belt dryer.

MATERIALS AND METHODS

The belt dryer (Fig.1) contains, among other things, 3 drying belts on which the hops are dried from an input humidity of approx. 80 % to an output humidity of approx. 10 %. The quality of the hops (over-drying or under-drying) depends on the speed of the drying belts, and thus the energy requirement. In older dryers, we often encounter slippage of drying belts. If the movement of the drying belts stops, there is no signalling on the dryer for the operator of the dryer, and the dried product – hops – can thus deteriorate.

One of the key parameters for the drying process is the speed of the drying belt. The principle of sensing the feed rate is known and used. However, in this case, it is a very slow speed of the drying belts up to 10 mm.s^{-1}.
It is known from earlier experiments *(Rybka et al. 2017 and Hermanek et al. 2018)* that hops, depending on the variety, are dried to a greater extent on the second belt, while the third belt only tempers the hops. Therefore, it is necessary to focus on monitoring and automating the drying process.

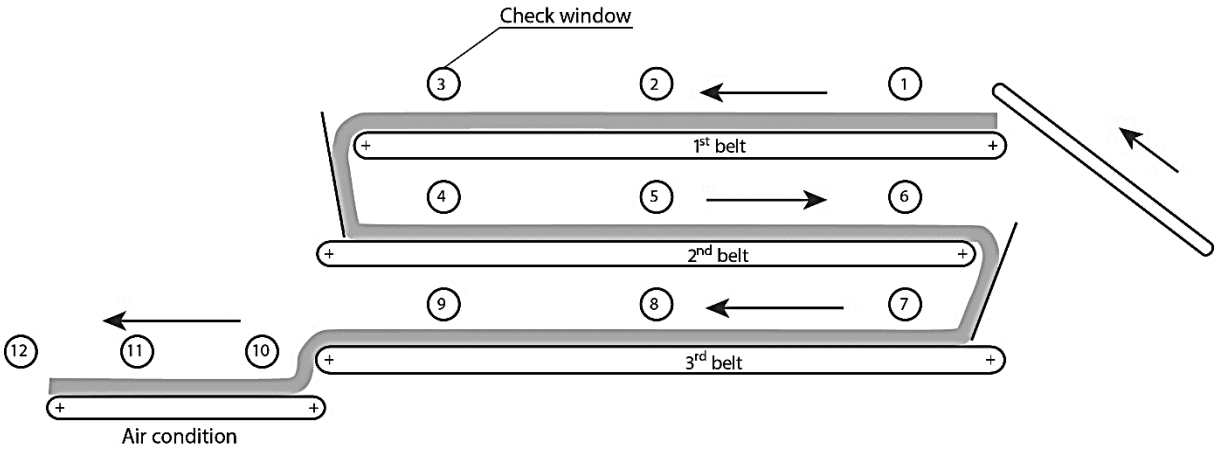

Fig. 1 The scheme of belt dryer PCHB 750

Measurements were carried out on two belt dryers PCHB 750 in companies – Lupofyt Co., Ltd. in Chrášťany and Agrospol Velká Bystřice Co., Ltd. The Saaz variety, the leading variety of Czech hop growing, was mainly used during the measurements. As a delicate aromatic variety, it requires specific drying conditions that differ from hybrid varieties.
During the experiments, the following equipment was installed in the PCHB 750 dryer:

- the sensor (wheel) of the speed of the drying belts (for the speed from 0 to 10 mm.s^{-1}) in the belt dryer of hops (Fig. 2), which was manufactured by SKV Co., Ltd. in Dvůr Králové nad Labem according to the suggestion of the authors of the article,
- the evaluation centre (Fig. 3) for continuous sensing and evaluation of the speed of all drying belts in the belt dryer of hops, the manufacturer was SKV Co., Ltd. in Dvůr Králové nad Labem according to the specifications and parameters of the authors of the article,
- the device for fastening to a belt dryer, which was designed and manufactured at the Czech University of Life Sciences in Prague,
- the connecting and electrical material.

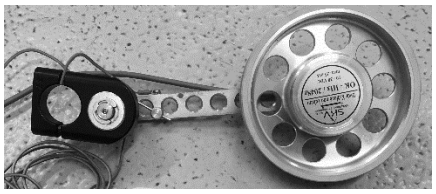

Fig. 2 The sensor (wheel) of the speed of the drying belts

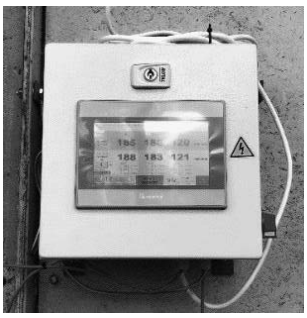

Fig. 3 The evaluation centre

The methodology of the experiment was based on the collection of process parameters from sensors installed on the hop dryer, i.e., the instantaneous and average speed of the belt. Furthermore, available meteorological data from individual areas – Chrášťany near Rakovník and Velká Bystřice – were used. Subsequently, the values were analysed.

RESULTS AND DISCUSSION

According to measurements at the belt dryer in 2020, the speed of the second belt varied between 2.4 and 3.8 mm.s^{-1}. For the experiments that were carried out during the drying period in 2021, we used a modified device. The modification consisted of the possibility of choosing a period for which the average speed of the belt will be measured. This value is adjustable in the range from 0 to 600 s. When measuring in 2021, we looked for a suitable setting for the average belt speed per time interval (60 s, 120 s, 300 s and 600 s). For our measurements on both dryers, we set the measurement for 60 s. An example of measured data is shown in Table 1. The measured data from the speed sensors are displayed as the current instantaneous belt speed and the average belt speed.

Tab. 1 An example of measured data of average belt speed in a hop dryer (Agrospol Velká Bystřice Co., Ltd.)

date	time	speed of belt 1	speed of belt 2	speed of belt 3
month.day.year	h:min:s	mm.s^{-1}	mm.s^{-1}	mm.s^{-1}
08.23.2021	13:00:57	4.57	1.58	1.03
08.23.2021	13:02:57	4.57	1.58	1.03
08.23.2021	13:04:57	4.55	1.57	1.03
08.23.2021	13:06:57	4.53	1.55	1.03
08.23.2021	13:08:57	4.53	1.57	1.03
08.23.2021	13:10:57	4.55	1.58	1.03

We obtained meteorological data from the harvest period: temperature [°C], dew point [°C], humidity [%], speed of wind [m.s^{-1}] and pressure [hPa].

In the analysis, we examined and compared various meteorological data with belt speed values. Firstly, we removed the stopping, standing, and starting motion of the belts. We did not include the results of the measured values of the average speed of all three belts in the graphs below for the sake of clarity. From a technological point of view, the inclined belt for the supply of fresh hops and the first belt of the dryer are driven from one source. The second and third belts are driven from the second source. The third belt reached approximately 66 % speed of the second belt. The speed of the second belt was different for both dryers. Compared to the speed of the first belt, the speed of the second belt in the dryer Lupofyt Co., Ltd. was 98 % and, in the dryer Agrospol Velká Bystřice Co., Ltd. was approximately 30 %.

For comparison, we selected humidity from all meteodata. The results of the speed of the first belt and the humidity of the air for the entire period of drying of hops after their harvest are shown in the graphs in Figure 4 (Lupofyt Co., Ltd.) and Figure 5 (Agrospol Velká Bystřice Co., Ltd.).

The graphs in Fig. 4 and 5 show the dependence of the average speed of the first belt of the hop dryer on humidity. The interpretation of the measured values shows that when the humidity increased, the speed of the belt decreased and vice versa. The dependence is most evident in the graph in Fig. 5. Belt speed regulation was not based on automatic regulation of the drying process but based on manual control by the operator of the dryer, which we want to eliminate in the future and fully replaced with automation. Manual control has so far been based on the experience of the operator and is implemented based on the moisture of the hops leaving the dryer and with a certain time delay. The obtained data were not subjected to a statistical evaluation, as only the results for one year of measurement are available so far. According to the measured values, it is also possible to conclude that speed sensors only on the first and second belt are sufficient. However, in the case of the third belt, the malfunction will not be signalled, and the operator must find out by looking into the control windows.

J. Münsterer (2020) dealt with a detailed study of drying hops in chamber and belt dryers. In the study, he states that it is necessary to change the speed of the belts in the dryer in order to regulate the hop layer. However, there was no published article about measuring and visualizing the speed of the belts during drying of hops in a belt dryer.

For further measurements, it will be necessary to obtain current meteorological data and compare them with measured data from speed sensors during the drying period on individual days. This assesses the

effect of humidity and speed of belts in the dryer. The next task will be to solve the visualization of the measured values in the control device in the dryer. Next, we will focus on the possibility of monitoring the passage of the hop mass through the dryer when changing varieties, plots, etc.

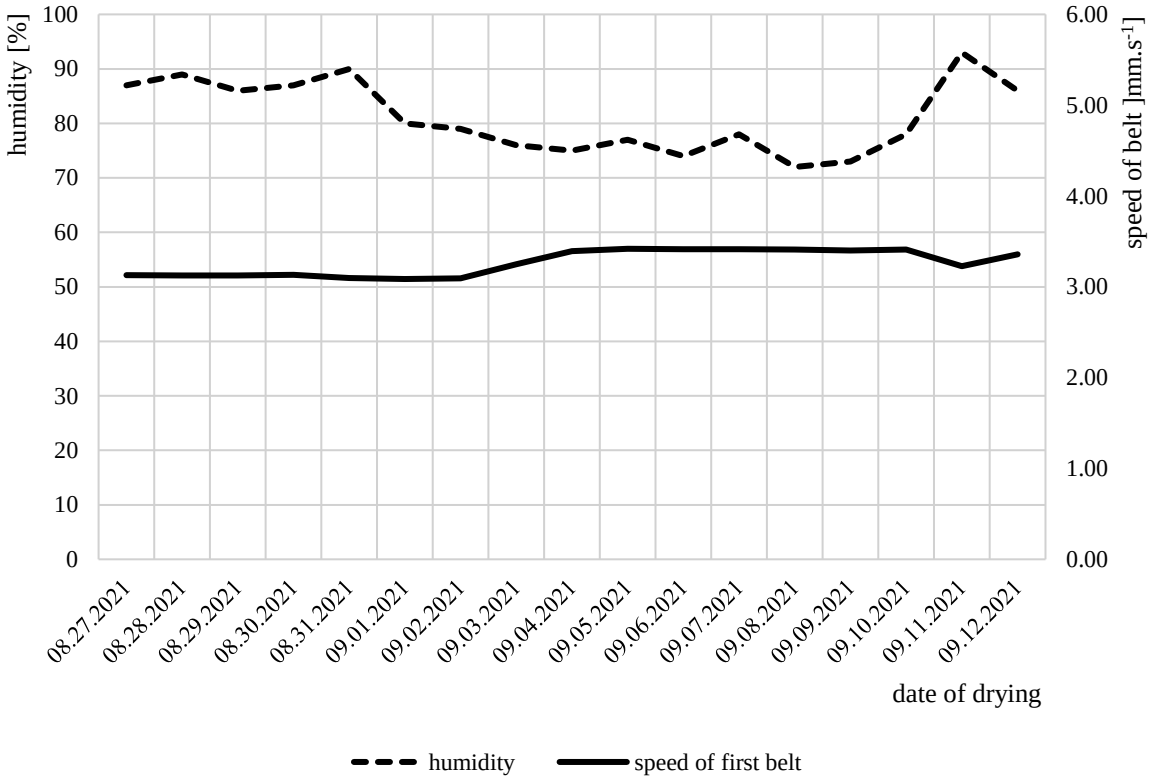

Fig. 4 Measured data from Lupofyt Co., Ltd.

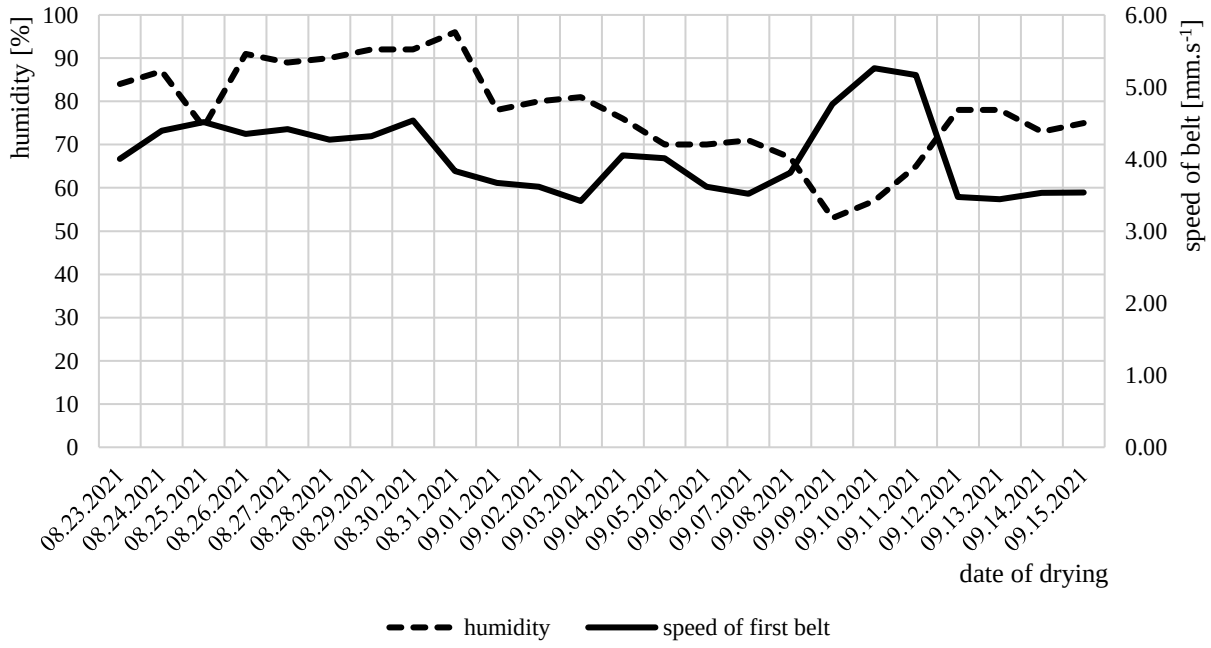

Fig. 5 Measured data from Agrospol Velká Bystřice Co., Ltd.

CONCLUSIONS

Continuous sensing of the speed of the dryer belts will help to signal slippage or unexpected stoppage of the dryer belts. The advantage of continuous sensing of the speed of the drying belts is an increase in

the quality of hops, safety when working in the dryer, the introduction of signalling for the operator and subsequent use for the automation of the hop drying process. The speed data will be transmitted to the computer and subsequently, it will be possible to use it for precise adjustment of the movement of the drying belts of the belt dryer. Another advantage lies in the possibility of using motion sensing devices in post-harvest technologies of other crops, e.g., when processing vegetables and sensing slow speeds of various mechanisms. The uniqueness of the solution results from the fact that there is no mechanism or device used in hop dryers to continuously monitor the speed of the drying belts. The automation of the drying process is achieved by mounting the designed sensor and connecting it to the control of the dryer.

ACKNOWLEDGMENT

This study was supported by Technology Agency CZ TG03010020 Proof-of-Concept 2 at the Czech University of Life Sciences in Prague the sub-project: The equipment for automating the process of drying hops on a belt dryer. It is also necessary at this point to thank the representatives of Lupofyt Co., Ltd. in Chrášťany and Agrospol Velká Bystřice Co., Ltd. for their willingness and helpfulness during experiments in their dryers.

REFERENCES

1. Guiné, R., P., F. (2011). Influence of Drying Method on Some Physical and Chemical Properties of Pears, International Journal of Fruit Science, 11:3, 245-255, DOI: 10.1080/15538362.2011.608295.
2. Guiné, R., P., F., Barroca, M., J., Gonçalves, F., J., Alves, M., Oliveira, S., & Mendes, M. (2015). Artificial neural network modelling of the antioxidant activity and phenolic compounds of bananas submitted to different drying treatments. Food Chemistry, 168, 454-459. DOI:10.1016/j.foodchem.2014.07.094.
3. Hermanek, P., Rybka, A., & Honzik, I. (2018). Determination of moisture ratio in parts of the hop cone during the drying process in belt dryer. Agronomy Research, 16 (3), 723 – 727. DOI: 10.15159/AR.18.076
4. Holowaty, S., A., Schmalko, M., E., & Schvezov, C., E. (2022). Modeling of a double pass belt conveyer dryer of yerba mate, Drying Technology, 40:5, 938-947. DOI: 10.1080/07373937.2020.1839488
5. Chokphoemphun, S., & Chokphoemphun, S. (2018). Moisture content prediction of paddy drying in a fluidized-bed drier with a vortex flow generator using an artificial neural network. Applied Thermal Engineering, 145, 630-636. DOI:10.1016/j.applthermaleng.2018.09.087.
6. Kaveh, M., Amiri Chayjan, R., Taghinezhad, E. et al. (2019). Modeling of thermodynamic properties of carrot product using ALO, GWO, and WOA algorithms under multi-stage semi-industrial continuous belt dryer. Engineering with Computers, 35, 1045–1058. DOI: 10.1007/s00366-018-0650-2
7. Kaveh, M., Sharabiani, V., R., Chayjan, R., A., Taghinezhad, E., Abbaspour-Gilandeh, Y., & Golpour, I. (2018). ANFIS and ANNs model for prediction of moisture diffusivity and specific energy consumption potato, garlic and cantaloupe drying under convective hot air dryer. Information Processing in Agriculture, 5(3), 372-387. DOI: 10.1016/j.inpa.2018.05.003.
8. Kırbaş, İ., Tuncer, A., D., Şirin, C., & Usta, H. (2019). Modeling and developing a smart interface for various drying methods of pomelo fruit (Citrus maxima) peel using machine learning approaches. Computers and Electronics in Agriculture, 165. DOI: 10.1016/j.compag.2019.104928.
9. Kudra, T. (2004). Energy Aspects in Drying. Drying Technology, 22:5, 917-932. DOI: 10.1081/DRT-120038572.
10. Lewicki, P. (2006). Design of hot air drying for better foods. Trends in Food Science & Technology, 17:4, 153-163. DOI: 10.1016/j.tifs.2005.10.012.
11. Mujumdar, A., S. et al. (2014). Handbook of Industrial Drying. CRC Press.
12. Münsterer, J. (2020). Trockung und Konditionierung von Hopfen. LFL Information. Wolnzach. (in Germany).
13. Raut, S., Gersdorff, G., J., E., Münsterer, J., Kammhuber, K., Hensel, O., & Sturm, B. (2020). Impact of Process Parameters and

Bulk Properties on Quality of Dried Hops. Processes, 8(11), 1507. DOI: 10.3390/pr8111507.
14. Raut, S., Gersdorff, G., J., E., Münsterer, J., Kammhuber, K., Hensel, O. & Sturm, B. (2021). Influence of pre-drying storage time on essential oil components in dried hops (Humulus lupulus L.). Journal of The Science of Food Agriculture, 101, 2247-2255. DOI: 10.1002/jsfa.10844.
15. Rybka, A., Hermanek, P., Honzik, I., Krofta, K. (2017). Parameters of the drying medium and dried hops in belt dryer. Research in Agriculture Engineering, 63, 24–32. DOI:10. 17221/35/2017-RAE.
16. Sturm, B., Raut, S., Kulig, B., Münsterer, J., Kammhuber, K., Hensel, O., & Crichton, O., J., S. (2020). In-process investigation of the dynamics in drying behavior and quality development of hops using visual and environmental sensors combined with chemometrics. Computers and Electronics in Agriculture, 175. DOI: 10.1016/j.compag.2020.105547.
17. Myllymaa, T., Holmberg, H., & Ahtila, P. (2019) Techno-economic evaluation of biomass drying in moving beds: The effect of drying kinetics on drying costs. Drying Technology, 37:10, 1201-1214. DOI: 10.1080/07373937.2018.1492615.
18. Myllymaa, T., Holmberg, H., & Ahtila, P. (2020). Economic Evaluation of Drying of Soot Sludge and Sawdust Mixture at Low Temperatures Using the Characteristic Drying Curve Method. ChemEngineering, 4(1):6. DOI: 10.3390/chemengineering4010006.
19. Şahïnbaşkan, T., & Köse, E. (2010). Modelling of time related drying changes on matte coated paper with artificial neural networks. Expert Systems with Applications, 37(4), 3140-3144. DOI: 10.1016/j.eswa.2009.09.068.
20. Tarhan, S., Telci, I., Tuncay, M., T., & Polatci, H. (2011). Peppermint Drying Performance of Contact Dryer in Terms of Product Quality, Energy Consumption, and Drying Duration. Drying Technology, 29:6, 642-651. DOI: 10.1080/07373937.2010.520421.
21. Vasiliev, A., O., Andreev, R., V., Smirnov, M., P., Pushkarenko, N., N., & Zaitsev, P., V. (2020). Hop Drying process Research in industrial dryer. IOP Conference Series: Earth Environmental Science, 433. DOI: 10.1088/1755-1315/433/1/012032.
22. Youssefi, S., Emam-Djomeh. Z., & Mousavi, S., M. (2009) Comparison of Artificial Neural Network (ANN) and Response Surface Methodology (RSM) in the Prediction of Quality Parameters of Spray-Dried Pomegranate Juice, Drying Technology, 27:7-8, 910-917. DOI: 10.1080/07373930902988247.
23. Zhang, W., Ma, H., & Yang, S., X. (2015). A neuro-fuzzy decoupling approach for real-time drying room control in meat manufacturing. Expert Systems with Applications, 42(3), 1039-1049. DOI: 10.1016/j.eswa.2014.09.013.
24. Ziegler, T., Jubaer, H., & Teodorov, T. (2021). Bottlenecks in continuous hops drying with conveyor-belt dryer, Drying Technology. DOI: 10.1080/07373937.2021.1950168.

Corresponding author:
Petr Heřmánek, Department of Agricultural Machines, Faculty of Engineering, Czech University of Life Sciences Prague, Kamýcká 129, Praha 6, Prague, 16521, Czech Republic, phone: +420 22438 3126, e-mail: hermanek@tf.czu.cz

TEMPERATURE RELATIONS OF SOME MUSTARDS RHEOLOGIC PROPERTIES

Peter HLAVÁČ

Institute of Electrical Engineering, Automation, Informatics and Physics, Faculty of Engineering, Slovak University of Agriculture in Nitra, Tr. A. Hlinku 2, SK- 949 76 Nitra, Slovak Republic

Abstract
In this article we compared apparent viscosity and density of three types of whole mustards from different producers (Boneco, SNICO, COOP). We performed measurements of both parameters in the temperature range (5 – 25) °C. Apparent viscosity was measured on rotational viscometer Anton Paar DV-3P and density was determined according to definition (exact volume of sample was weighted). We have found that apparent viscosity is decreasing exponentially, while the density decreases polynomially with increasing of temperature. Highest apparent viscosity was obtained for the mustard Boneco and lowest for the mustard SNICO. Highest density had mustard COOP, while other two samples had similar densities. We had also investigated the effect of storing on mustards apparent viscosity and all samples had a bit lower values after storing. Changes of rheological properties with temperature and storing time could be caused by internal structural changes and by destruction of bonds.

Key words: *whole mustards; apparent viscosity; density; storing; temperature.*

INTRODUCTION

One of the most used materials from mustard seeds is oil, which could be used in many areas e.g. in industry as a lubricant or diesel fuel additive, in traditional medicine as antitumor, antiviral and analgesic agent, as well as in food preparation as a condiment and a preservative (*Kostić et al., 2018*). *Rapp et al.* (*2021*) have reported the properties of biofuels and biolubricants made from Indian mustard.
Mustard paste is a non-Newtonian material for which must be applied apparent viscosity, defined as a ratio of shear stress and corresponding shear rate. It is expressed in physical unit Pa·s. Viscosity changes with temperature, for most of the liquids decreases with increasing temperature and can be described by an Arrhenius type equation

$$\eta = \eta_0 \, e^{-\frac{E_A}{RT}} \qquad (1)$$

where η_0 is reference value of viscosity, E_A is activation energy, R is gas constant and T is absolute temperature (*Figura & Teixeira, 2007*).
According to *Juszczak et al.* (*2004*) mustard is a pungent, spicy-tasting paste which is usually used as a condiment, and it is made from party deoiled mustard flour or mustard seeds, water, food acids, vinegar, salt, sugar and flavouring additives. There are many types of mustards that differ in its composition, for example: whole mustard, whole grain mustard, honey mustard, spicy mustard, American mustard (from yellow mustard), horseradish mustard, Dijon mustard, English mustard, French mustard, hot pepper mustard, etc.
Juszczak et al. (*2004*) had mentioned that the rheological properties of processed mustard are influenced by the size of solid phase particles, which could be controlled during the manufacturing (e.g. at the milling process). The rheological properties of mustard are also affected by other factors such as its dry matter content, the presence of oil fraction and the addition of thickeners (*Juszczak et al., 2004*). Authors studied the temperature relation of mustard apparent viscosity in the temperature range (8 – 30) °C and described this dependency with an Arrhenius equation. Authors (*Aguilar & Ziegler, 1990*) found that viscosity of dispersions of mustard seeds had decreased with increased temperature. *Aguilar et al. (1991)* compared mustards with different particle sizes obtained by milling (slightly coarse, standard, and fine). They observed higher apparent viscosity in no-mixing variants of mustard. Higher apparent viscosity of the fine milling variant, authors (*Aguilar et al., 1991*) explained by greater surface area and by increased chemical related particle-particle interactions due to the smaller particles. In case of slightly coarse milling variant, the higher apparent viscosity may be related to packing density or due to physical interactions between large particles of irregular shape (*Aguilar et al., 1991*). Differences in apparent viscosity after mixing could not be detected because the mixing had disturbed the formation of a soft structure or network of particles (*Aguilar et al., 1991*). Flow behaviour of processed mustard was described with

Herschel-Bulkley model by *Aguilar et al. (1991). Bhattacharya et al. (1991)* had observed pseudoplastic behaviour with yield stress for three types of mustard pastes (paste with whole mustard seeds; paste with dehulled kernels; paste from meal). Authors used Herschel–Bulkley model for all three types of mustard pastes. *Bhattacharya et al. (1991)* found that yield stress, consistency index and apparent viscosity of the mustard pastes increased, but the flow behaviour index decreased with a moisture content decrease. Authors identified that the mustard pastes from meal showed the highest apparent viscosity, followed by the pastes with whole mustard seeds, and lowest apparent viscosities were observed for pastes with dehulled kernels (*Bhattacharya et al., 1991*). *Kang et al. (2020)* had analysed the flow profiles of yellow mustard mucilage and its two fractions (water soluble and water insoluble fraction). Authors had observed shear-thinning flow behaviour. *Cui et al. (1994)* investigated rheologic behaviour of water-soluble yellow mustard and observed pseudoplastic (shear thinning behaviour). *Repin et al. (2018)* studied the flow behaviour of yellow mustard mucilage at different concentrations. Authors observed shear thinning behaviour in all cases.
Similar observations were performed on various materials. *Ahmed et al. (2013)* had analysed flow properties of purees from rocket leaves. From their research is clear that the flow behaviour of puree sample could be well described by the Herschel–Bulkley model. *Baslingappa Swami et al. (2004)* investigated flow characteristics of black gram batter and found that batters exhibited shear thinning behaviour, and it could be described by the Herschel–Bulkley model. Authors also determined the bulk density of the batters by weighing the exact volume of sample. *Morales-Tovar et al. (2020)* observed that the chan mucilage exhibits a non-Newtonian behaviour of the pseudoplastic type. Authors applied the Ostwald de Waele equation for characterising the flow behaviour of the chan mucilage. *Oliveira et al. (2019)* indicated that the flow behaviour of biodegradable films based on Pereskia aculeata Miller mucilage exhibited shear thinning behaviour and described it by power law model (Ostwald – de Waele equation). Decrease in the apparent viscosity caused by increased shear rate authors explained by the fact that when stress is applied the molecules of the solution begin to become ordered, thus, high applied stress produces higher ordering, and consequently, lower apparent viscosity (*Oliveira et al., 2019; Steffe, 1996*). *Orcajo et al. (2013)* had compared flow curves for hydrolysed and non-hydrolysed granules mayonnaise with the commercial mayonnaise sample. Authors observed that the apparent viscosity decreases with increments in the shear rate, which is a feature of shear thinning products. *Orcajo et al. (2013)* found that non-hydrolysed granules mayonnaise reached highest values of apparent viscosity, while hydrolysed granular and commercial mayonnaise had comparable values. *Jouki et al. (2014)* mentioned that apparent viscosity besides the temperature depends also on chemical composition and structure. *Kishk & Elsheshetawy (2013)* also observed decrease of apparent viscosity during the storage of mayonnaise. *Hakimian et al. (2022)* had examined microbial and physicochemical properties of mayonnaise. Authors investigated the effect of storing time on these properties and found that apparent viscosity had decreased with storing time.
It is very hard to find information about physical properties of mustards and how are they affected by selected properties. That is why the aim of this article was to investigate the effect of temperature and storing time on the rheologic properties of mustards.

MATERIALS AND METHODS

In our article we compared apparent viscosity and density of three types of whole mustards from different producers (Boneco, SNICO, COOP). Composition of mustards was similar, only small differences were in used ingredients like vinegar and sugar. We performed measurements of both parameters in the temperature range (5 – 25) °C. Apparent viscosity was measured on rotational viscometer Anton Paar DV-3P and density was determined according to definition (exact volume of sample was weighted on scales with precision 0,0001 g). Presented are averages of two values. Sample cooling was performed in cooling box and measurements were realized after the temperature stabilization. Heating of the sample was performed in water bath. Measurements of apparent viscosity were repeated also after three weeks of storing. There were constructed dependencies of rheological properties on temperature and storage time and evaluated by the regression equations and the coefficients of determination.
Temperature dependency of mustard apparent viscosity can be modelled by decreasing exponential function (2).

$$\eta_a = A\, e^{-B\left(\frac{t}{t_0}\right)} \qquad (2)$$

where η_a is apparent viscosity (Pa·s), t is temperature (°C), t_0 is 1 °C, A and B, coefficients of regression equation (2), are constants dependent on kind of material, and on ways of processing and storing. Similar dependency of mustard density can be characterized by decreasing polynomial function of second degree (3)

$$\rho = C\left(\frac{t}{t_0}\right)^2 - D\left(\frac{t}{t_0}\right) + E \quad (3)$$

where ρ is density (kg·m^{-3}), C, D and E, coefficients of regression equation (3), are constants dependent on kind of material, and on ways of processing and storing.

RESULTS AND DISCUSSION

In this article we compared apparent viscosity and density of three types of whole mustards from different producers (Boneco, SNICO, COOP). Temperature dependencies of mustards apparent viscosity is presented on Fig. 1.

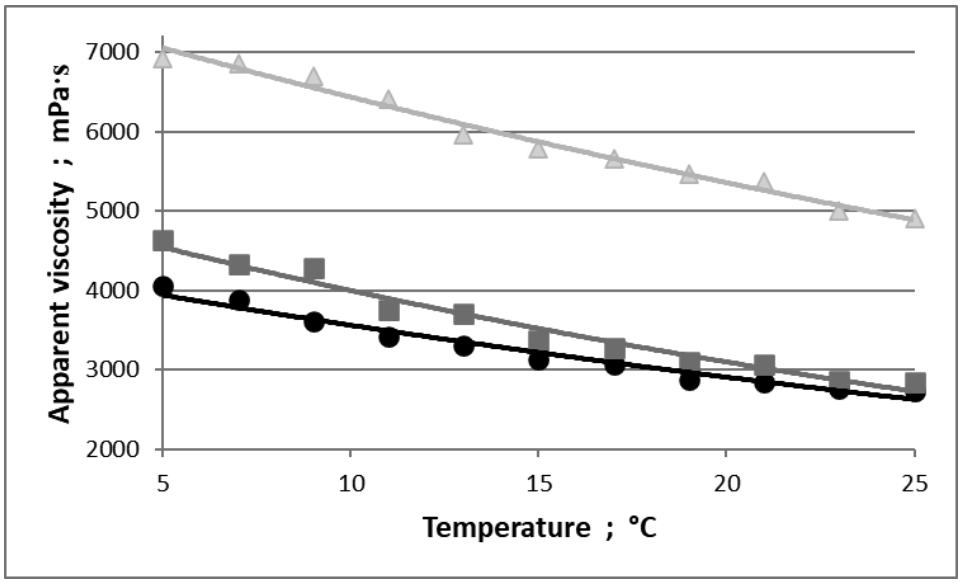

Fig. 1 Temperature dependency of mustard apparent viscosity: Boneco (▲), COOP (■), SNICO (●)

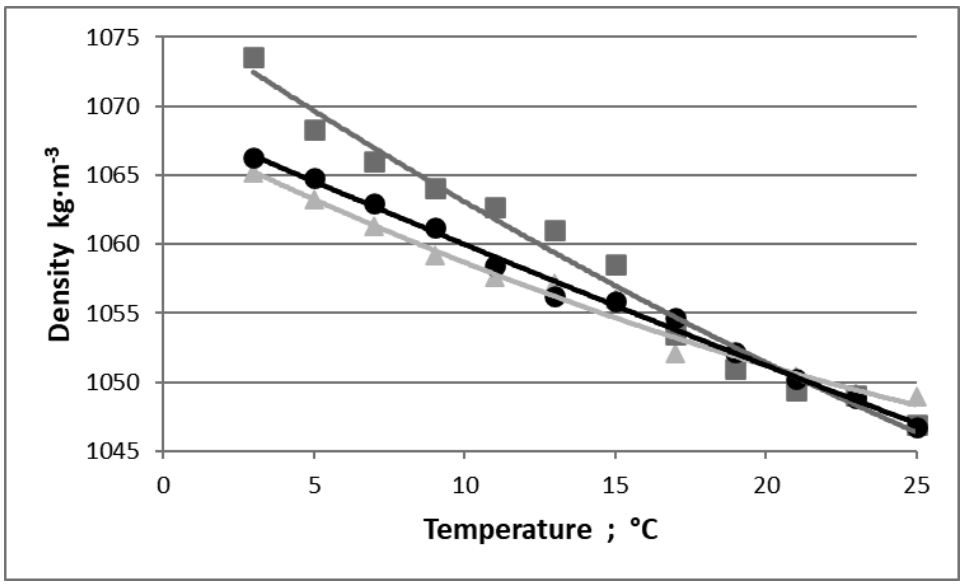

Fig. 2 Temperature dependency of mustard density: Boneco (●), COOP (■), SNICO (▲)

It could be seen that for all examined samples the apparent viscosity decreases with increment of temperature. This is in accordance with the Arrhenius equation (1). Coefficients of regression equation (2) and coefficients of determination are summarized in Tab. 1. Similar observations were obtained by other authors (*Aguilar & Ziegler, 1990*; *Juszczak et al., 2004*). Highest apparent viscosities were observed for mustard Boneco, lowest values for sample SNICO.

Effect of temperature on mustard density is shown on Fig. 2. For all samples was applied decreasing polynomial function of second degree. Decreasing of density with temperature were also obtained for other materials *(Kumbár & Nedomová*, 2015; *Thomas et al., 2015*). Density of the mustard COOP was highest, while other two samples had similar densities. Coefficients of regression equation (3) and coefficients of determination are summarized in Tab. 1.

We had also investigated the effect of storing on apparent viscosity of mustards. Samples of mustards were stored in cooling box and next measurements were performed after three weeks. On Fig. 3 are shown differences in apparent viscosity of mustard Boneco caused by storing. For all three samples we obtained a bit lower values after storing. Changes of rheological properties with temperature and storing time could be caused by internal structural changes and by destruction of bonds. Decrease of apparent viscosity after storing was observed by other authors (*Hakimian et al., 2022*; *Kishk & Elsheshetawy, 2013*).

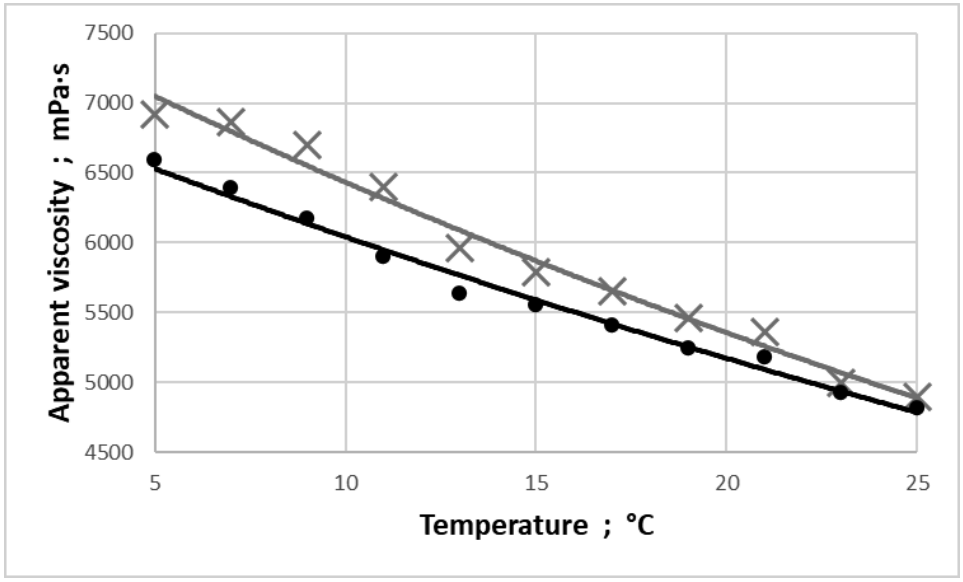

Fig. 3 Temperature dependency of mustard Boneco apparent viscosity: first measurement (×), next measurement after three weeks of storing (●)

Tab. 1 Coefficients of regression equations (2 – 3) and coefficients of determination

Mustard / measurement	A mPa·s	B mPa·s	R^2
SNICO / first	4360.8	0.020	0.9685
SNICO / next	4031.3	0.016	0.9748
COOP / first	5158.5	0.025	0.9724
COOP / next	4478.4	0.018	0.9676
Boneco / first	7724.7	0.018	0.9821
Boneco /next	7056.8	0.016	0.9889

Mustard	C $kg \cdot m^{-3}$	D $kg \cdot m^{-3}$	E $kg \cdot m^{-3}$	R^2
SNICO	0.0113	1.0855	1068.4	0.9846
COOP	0.0102	1.4718	1076.8	0.9808
Boneco	0.0023	0.9452	1069.2	0.9938

CONCLUSIONS

Food materials composition is different, so their physical properties are very complex. Physical properties of food materials depend on the manipulation, external conditions and on other factors, which determine their behaviour. Rheological properties of whole mustard were measured and analysed in this paper. Mustard paste is a non-Newtonian material, so for this material is relevant apparent viscosity. Effect of temperature and storing time on measured samples of whole mustard was investigated and comparison of used samples was made. We found out that apparent viscosity of samples decreased exponentially with increasing temperature, so the Arrhenius equation is valid. Coefficients of determination reached high values in the range (0.967 – 0.994). Comparable rheological results for mustard were reported by *Juszczak et al. (2004)*. Proportion of the curves in Fig. 1 could be caused by different composition of analysed samples (*Aguilar et al., 1991*). Apparent viscosity had decreased with storage time, which can be caused by structural changes in samples during storing (*Hakimian et al., 2022*; *Kishk & Elsheshetawy, 2013*). The rheological characteristics can be used for designing of technological equipment or containers for distribution of the product to the final users. The knowledge of flow behaviour is also important for the development of new recipes and direct qualitative assessment of the products. Further analysis of samples is needed for the characterization of mustard flow behaviour.

ACKNOWLEDGMENT

This publication was supported by the Operational Program Integrated Infrastructure within the project: Demand-driven research for the sustainable and innovative food, Drive4SIFood 313011V336, co-financed by the European Regional Development Fund.

REFERENCES

1. Aguilar, C. A., & Ziegler, G. R. (1990). Effect of temperature and electrolytes on the viscosity of aqueous dispersions of mustard seed (Sinapsis alba) mucilage. *Food Hydrocolloids*, 4(2), 161-166.
2. Aguilar, C., Rizvi, S. S. H., Ramirez, J. F. & Inda, A. (1991). Rheological behavior of processed mustard. I. Effect of milling treatment. *Journal of Texture Studies*, 22, 59-84.
3. Ahmed, J., Al-Salman, F., & Almusallam, A. S. (2013). Effect of blanching on thermal color degradation kinetics and rheological behavior of rocket (Eruca sativa) puree. *Journal of Food Engineering*, 119, 660-667.
4. Baslingappa Swami, S., Das, S. K., & Maiti, B. (2004). Effect of water and air content on the rheological properties of black gram batter. *Journal of Food Engineering*, 65, 189-196.
5. Bhattacharya, S., Vasudha, N. & Krishna Murthy, K. S. (1991). Rheology of mustard paste: a controlled stress measurement. *Journal of Food Engineering*, 41(3–4), 187-191.
6. Cui, W., Eskin, N. A. M., & Biliaderis, C. G. (1994). Yellow mustard mucilage: chemical structure and rheological properties. *Food Hydrocolloids*, 8(3–4), 203-214.
7. Figura, L. O., & Teixeira, A. A. (2007). Food Physics, Physical properties – measurement and applications (1st ed.), Verlag, Berlin, Heidelberg, New York: Springer
8. Hakimian, F., Emamifar, A., & Karami, M. (2022). Evaluation of microbial and physicochemical properties of mayonnaise containing zinc oxide nanoparticles. *LWT - Food Science and Technology*, 163, 10 p.
9. Jouki, M., Mortazavi, S. A., Tabatabaei Yazdi, F., & Koocheki, A. (2014). Optimization of extraction, antioxidant activity and functional properties of quince seed mucilage by RSM. *International Journal of Biological Macromolecules*, 66, 113-124.
10. Juszczak, L., Witczak, M., Fortuna, T., & Banyś, A. (2004). Rheological properties of commercial mustards. *Journal of Food Engineering*, 63(2), 209-217.
11. Kang, J., Guo, Q. & Cui, S. W. (2021). Other emerging gums: Flaxseed gum, yellow mustard gum, and psyllium gums (Chapter 20). In *Handbook of Hydrocolloids* (Third Edition) (pp. 597-624), Elsevier Ltd.
12. Kishk, Y. F. M., & Elsheshetawy, H. E. (2013). Effect of ginger powder on the mayonnaise oxidative stability, rheological measurements, and sensory characteristics. *Annals of agricultural science*, 58(2), 213-220.
13. Kostić, M. D., Djalović, I. G., Stamenković, O. S., Mitrović, P. M., Adamović, D. S., Kulina, M. K., & Veljković, V. B. (2018). Kinetic

modeling and optimization of biodiesel production from white mustard (Sinapis alba L.) seed oil by quicklime-catalyzed transesterification. *Fuel*, 223, 125-139.
14. Kumbár, V. & Nedomová, Š. (2015). Viscosity and analytical differences between raw milk and UHT milk of Czech cows. *Scientia Agriculturae Bohemica*, 46, 78-83.
15. Morales-Tovar, M. E., Ramos-Ramírez, E. G., & Salazar-Montoya, J. A. (2020). Modeling and optimization of the parameters affecting extraction of the chan seed mucilage (Hyptis suaveolens (L.) Poit) by mechanical agitation (MA) and ultrasound-assisted extraction (UAE) in a multiple variables system. *Food and Bioproducts Processing*, 120, 166-178.
16. Oliveira, N. L., Rodrigues, A. A., Oliveira Neves, I. C., Teixeira Lago, A. M., Borges, S. V., & de Resende, J. V. (2019). Development and characterization of biodegradable films based on Pereskia aculeata Miller mucilage. *Industrial crops and products*, 130, 499-510.
17. Orcajo, J., Marcet, I., Paredes, B., & Díaz, M. (2013). Egg yolk hydrolysed granules: Characteristics, rheological properties and applications. *Food and bioproducts processing*, 91, 457-463.
18. Rapp, G., Garcia-Montoto, V., Bouyssiere, B., Thiebaud-Roux, S., Montoya, A., Trethowan, R., Pratt, P., Mozet, K., Portha, J. F. & Coniglio, L. (2021). Indian mustard bioproducts dry-purification with natural adsorbents - A biorefinery for a green circular economy. *Journal of cleaner production*, 286, 18 p.
19. Repin, N., Cui, S. W., & Goff, H. D. (2018). Rheological behavior of dietary fibre in simulated small intestinal conditions. *Food Hydrocolloids*, 76, 216-225.
20. Steffe, J. F. (1996). Rheological method in food process engineering, 2nd ed., Freeman Press, East Lansing (USA), 428 p.
21. Thomas, M. J., Bramblett, K. A., Green, B. D., & West, K. N. (2015). Thermophysical and absorption properties of brominated vegetable oil. *Journal of Molecular Liquids*, 211, 647 – 655.

Corresponding author:
doc. Mgr. Peter Hlaváč, Ph.D., Institute of Electrical Engineering, Automation, Informatics and Physics, Faculty of Engineering, Slovak University of Agriculture in Nitra, Tr. A. Hlinku 2, SK- 949 76 Nitra, Slovak Republic, phone: +421 37641 4749, e-mail: Peter.Hlavac@uniag.sk

WHEAT AND LEGUMES MIXTURES INFLUENCE GRAIN QUALITY

Trong Nghia HOANG[1, 3], Marek KOPECKÝ[1], Mohammad GHORBANI[1], Yves Theoneste MURINDANGABO[1], Dang Khoa TRAN[3], Karel SUCHÝ[2], Petr KONVALINA[1]

[1]*Department of Agroecosystems, Faculty of Agriculture and Technology, University of South Bohemia in Ceske Budejovice, Studentska 1668, 37005 Ceske Budejovice, Czech Republic.*
[2]*Department of Biological Disciplines, Faculty of Agriculture and Technology, University of South Bohemia in Ceske Budejovice, Studentska 1668, 37005 Ceske Budejovice, Czech Republic.*
[3]*Faculty of Agronomy, University of Agriculture and Forestry, Hue University, 102 Phung Hung Street, Hue City, Vietnam.*

Abstract
This study aims to evaluate the effect of the mixture of winter wheat and legumes cultivars on grain yield and wheat rheological quality properties. The experiment was conducted in an organically certified field at Zvikov, Ceske Budejovice, to compare grain yield, baking quality, and rheological quality analyzed by Mixolab of wheat flour. Based on results, grain yield showed range from 7.03 to 8.31 t ha^{-1} and there were no significant differences under winter wheat and legumes cultivars mixtures. Productivity wheat quality was significantly different between wheat variety and legumes mixtures in terms of protein content ($P < 0.05$), wet gluten ($P < 0.01$), sedimentation value, and falling number ($P < 0.001$). There was a significant difference in rheological quality analyzed by Mixolab as stability, weakening of protein, and starch characteristics under growing winter wheat and legumes mixtures. Wheat and legumes mixtures may offer a small yield and grain quality advantage.

Key words: *baking quality, yield, Mixolab, organic farming, winter wheat.*

INTRODUCTION

Wheat (Triticum aestivum L.) is one of three main kinds of cereals consumed worldwide *(Aune et al., 2016*). Products of wheat, particularly those from organic farming, have been interesting and developing in recent years (*Mie et al., 2017*). Organic farming systems are characterized by limited soluble nitrogen. Especially, nutrient uptake and use in early spring are important in winter wheat cultivation because it affects not only growth and grain yield but also baking wheat flour quality (*Konvalina et al., 2009*). On the other hand, organic yields are often 14% lower (*Mäder et al., 2007*), 20 – 30% less, and the protein content 10 – 25% lower than conventional farming *(Konvalina et al., 2009; Osman et al., 2012*).

Organic winter wheat cultivation is limited by the low input, especially the addition of nitrogen to the soil. Additionally, wet soil and low temperatures conditions in early spring reduce microbial activity and the process of mineralization in soil affects the development of plants, particularly in the early stage. The main priorities in organic agriculture are improving grain yield, increasing grain quality, and productivity of rheological characteristics. Protein content, wet gluten, gluten index, sedimentation value (Zeleny test), falling number, and rheological quality analyzed by Mixolab are characterized for high baking quality of the organic wheat varieties. Efforts to boost grain yield and quality include breeding and selection. However, these take a long time and cost. Designing cultivation practices could be a complementary strategy in grain yield and quality improvement of grain wheat in organic farming *(Konvalina et al., 2009)*.

Mixtures of wheat varieties or wheat and legumes are a viable strategy for sustainable products to help greater stability or no reduced yield, which is promoting to achieve high yields in bread quality in organic farming compared to single systems (*Kaut et al., 2009*). Mixing varieties of wheat improves baking quality (*Aart, 2006*), growing multiline cultivars and cultivar mixtures between wheat and legumes would complement properties of grain yield, grain bulk density, protein content, and also economic efficiency (*Vrtilek et al., 2016*), yield stabilization and pathogen spread in plant populations reduction (*Vidal et al., 2020*). In addition, growing mixtures of pure varieties or annual arable crop species is a promising way to improve crop productivity and complementary N accumulation, decreasing agricultural inputs, especially without chemicals use (*Borg et al., 2018; Chen et al., 2020; Dahlin et al., 2020; Gaudio et al., 2019*). The main objective of the research was to evaluate wheat yield, rheological technological quality characteristics of winter wheat flour under mixtures of winter wheat and legumes mixtures in organic farming.

MATERIALS AND METHODS

Field Experiment

The small plot experiment was carried out in the certified organic field (48.973995N, 14.612085E) at Zvikov, Ceske Budejovice, Czech Republic in vegetation season 2020. The soil texture was loamy soil. The weather condition was mild warm climate, at an altitude of 460 m. Experiments were started using the method of randomized complete block design with three replicates. Trial variants were evaluated in experiments with mixtures of winter wheat varieties (Butterfly) and different legumes (field bean – Vicia faba L., incarnate clover - Trifolium incarnatum L., spring pea Pisum sativum L. and winter pea - Pisum sativum L.).

Evaluation of Qualitative Parameters

Grain wheat was harvested from treatments without legumes seeds. The wheat flour samples were milled by PSY 20 (Mezos, Hradec Kralove, Czech Republic) and Quadrumat Junior machine (Brabender, Duisburg, Germany). Protein content (PC) was estimated by Kjeltec 1002 System (Tecator AB, Hoganas, Sweden), based on N * 5.7 (in dry matter). Wet gluten (WG) was measured by Glutomatic 2200 and Centrifuge 2015 (Perten Instruments, Hägersten, Sweden), according to ICC Standard No. 137/1. Falling number (FN) was determined on FN 1100 (Perten Inst., Sweden) according to AACC/No. 56-81B, ICC/No. 107/1, ISO/No. 3093. Sedimentation value (Zeleny test) (ZSV) was measured by using SDZT4 apparatus according to the ICC standard No. 116/1.

Rheological properties of wheat flour such as dough stability or weakening during mixing, as well as the quality of starch and protein were assessed by Mixolab (CHOPIN Technologies, France) according to the ICC standard method No. 173 - ICC 2006. Mixolab curves made from wheat flour. Amplitude: Elasticity of the dough. Higher the value, the more elastic the flour; Stability: Resistance to dough kneading. The longer the duration, the stronger the flour; C1: Dough development; Torque C2: Attenuation of protein due to mechanical work and temperature; Torque C3: The gelatinization of starch; Torque C4: Stability of hot gel; Torque C5: Measured retrogradation of starch in the cooling phase; Slope α: Attenuating rate of protein in warming; Slope β: starch gelatinization rate; Slope γ: enzymatic degradation rate.

Statistical Analysis

For the analysis of measured data, the STATISTICA program (version 13.2, StatSoft, Inc., California, USA) was used. One-way ANOVA was used for variance analysis. Tukey's honest significant difference (HSD) was used to identify significantly different mean values, $P < 0.05$; $P < 0.01$; and $P < 0.001$, probability level.

RESULTS AND DISCUSSION

Grain Yield

Productivity is an important indicator to evaluate manufacturing efficiency. Wheat grain production is influenced by agronomic features, cultivation practices, and environmental conditions. The addition of legumes in our experiment aimed to increase soil nutrients, resulting in increased wheat output and quality. Fig. 1 shows that grain yield did not differ statistically between combinations of Butterfly variety and legumes cultivars. The grain yield varied from 7.03 to 8.31 t ha^{-1}. The mixtures of winter wheat and legumes were not effective on yield. On the other hand, although there is no difference between the treatments when compared with the results of other studies, it shows the potential and achieves higher yield as *Tran et al., (2020)* found that grain yield ranged from 4.07 t ha^{-1} to 4.28 t ha^{-1} lower, compared to 7.78 t ha^{-1} in our experiment. *Lacko-Bartošová et al., (2021)* and *Jablonskytė-Raščė et al., (2013)* reported in their paper the grain yield of 6.7 t ha^{-1} and 4.95 t ha^{-1}, respectively, which are lower than our study. *Buraczyńska et al., (2011)* found that winter wheat mixed legumes yielded higher yields than mono cultivar cereals. Hence, cultivating mixtures of winter wheat and legumes positively impacted, potentially improving grain yield in low-input agricultural systems.

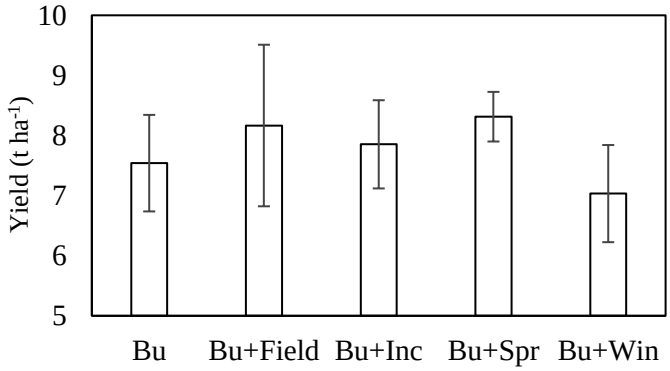

Fig. 1 Grain yield under mixtures of winter wheat variety and legumes (Bu: Butterfly, Field: Field beans, Inc: Incarnate clover, Spr: Spring pea, Win: Winter pea). Means ± standard deviation (SD), *P < 0.05*, N = 24

Wheat Quality

The highly significant statistical difference in the productivity of wheat quality in terms of protein content (*P < 0.05*), wet gluten (*P < 0.001*), sedimentation value (*P < 0.001*), falling number (*P < 0.001*). Protein content ranged from 9.83 to 10.61%. The highest number of protein content under Butterfly and field bean mixtures, differed significantly compared to Butterfly single by 0.76%. There was no difference between Butterfly and other combinations. *Krejčířová et al., (2008)* showed that the protein content was higher than in conventional farming (11.04%) compared to organic farming (9.48%). The number of protein content in their paper under organic farming cultivar is close to our results (10.09%). *Buraczyńska et al., (2011)* found that total N content in winter wheat grain of grown single crop was lower than crop mixtures (winter wheat and legumes).

Tab. 1 Baking quality, rheological parameters evaluation by Mixolab of winter wheat and legumes mixtures

Treatment	Protein (%)	Wet gluten (%)	ZSV (mL)	FN (s)
Bu	9.85 ± 0.25^{b}	16.66 ± 1.14^{c}	28.42 ± 0.80^{b}	310.00 ± 6.08^{b}
Bu+Field	10.61 ± 0.43^{a}	18.83 ± 0.01^{ab}	27.38 ± 0.38^{bc}	304.67 ± 6.43^{b}
Bu+Inc	9.83 ± 0.27^{b}	17.43 ± 0.08^{bc}	27.00 ± 0.00^{c}	309.00 ± 4.36^{b}
Bu+Spr	9.97 ± 0.10^{ab}	18.99 ± 0.30^{a}	30.00 ± 0.00^{a}	297.33 ± 2.52^{b}
Bu+Win	10.26 ± 0.19^{ab}	19.06 ± 0.16^{a}	26.50 ± 0.00^{c}	335.00 ± 3.00^{a}
P	*	**	***	***
Treatment	Torque C2 (Nm)	Torque C3 (Nm)	Torque C4 (Nm)	Torque C5 (Nm)
Bu	0.42 ± 0.00^{ab}	1.55 ± 0.01^{b}	0.74 ± 0.52	1.57 ± 0.02^{b}
Bu+Field	0.42 ± 0.01^{ab}	1.57 ± 0.01^{b}	0.89 ± 0.01	1.50 ± 0.03^{b}
Bu+Inc	0.45 ± 0.02^{a}	1.69 ± 0.02^{a}	1.02 ± 0.04	1.75 ± 0.08^{a}
Bu+Spr	0.41 ± 0.01^{b}	1.48 ± 0.02^{c}	0.95 ± 0.09	1.51 ± 0.03^{b}
Bu+Win	0.43 ± 0.01^{ab}	1.54 ± 0.01^{b}	0.93 ± 0.03	1.55 ± 0.00^{b}
P	**	***	*NS*	***
Treatment	Alfa	Beta	Gamma	Stability (min)
Bu	-0.07 ± 0.00	0.44 ± 0.02^{b}	-0.13 ± 0.06	6.20 ± 0.20^{c}
Bu+Field	-0.08 ± 0.01	0.47 ± 0.02^{b}	-0.10 ± 0.02	5.80 ± 0.10^{c}
Bu+Inc	-0.08 ± 0.00	0.54 ± 0.03^{a}	-0.08 ± 0.03	8.53 ± 0.06^{a}
Bu+Spr	-0.08 ± 0.01	0.45 ± 0.01^{b}	-0.12 ± 0.02	5.27 ± 0.06^{d}
Bu+Win	-0.08 ± 0.01	0.48 ± 0.03^{ab}	-0.07 ± 0.02	6.77 ± 0.32^{b}
P	*NS*	**	*NS*	***

Means ± standard deviation (SD), Tukey HSD test, influence of mixtures of winter wheat and legumes provable at *$P < 0.05$, ** < 0.01, *** < 0.001, NS – Non significant; different letters within the column shown statistically significant difference at *P < 0.05*. Bu: Butterfly, Field: Field beans, Inc: Incarnate clover, Spr: Spring pea, Win: Winter pea, FN: Falling number, ZSV: Sedimentation value (Zeleny test).

Wet gluten results were also significantly different, with the highest wet gluten under intercropping with field beans (18.83%), spring pea (18.99%), and winter pea (19.06%), higher than sowing only Butterfly seed variety (16.66%), and no difference between winter wheat and incarnate clover (17.43%). A lower number on wet gluten of 6.34% compared to *Jablonskytė-Raščė et al., (2013)* results and similar to *Krejčířová et al., (2008)*, gluten content stood at 18.59%. There is a correlation positively between sedimentation value with protein content and loaf volume, with the higher sedimentation value, the greater the baked bread volume. The evaluation of sedimentation value characteristics indicated a significant difference, sedimentation value was highest when growing winter wheat with spring beans (30.00 mL), however, incarnate clover (27.00 mL) and winter pea (26.50 mL) were lower than single grown Butterfly (28.42 mL), field bean mixes (27.38 mL) were not statistically different from single Butterfly.

Testing of falling number is used to evaluate the amount of sprout damage wheat and correlates negatively with alpha-amylase (an enzyme found in sprout-damaged wheat), with a large increase in this enzyme if the germination occurs. The decreasing number test will be reduced when the amount of alpha-amylase in the wheat increases. A high falling number or the longer indicates that the wheat is more suitable for most baking quality, with an ideal falling number range of 250 - 280 s. There was a considerable variation between winter wheat and legume cultivar mixes. Winter wheat and winter pea mixes produced a greater result (335.00 s) than the other treatments, which ranged from 297.33 to 310.00 s. Our falling number is higher than an ideal falling number, however, it is 140 s slower than the results of *Lacko-Bartošová et al., (2021)*. The baking quality of winter wheat flour was improved by combining winter wheat and legumes.

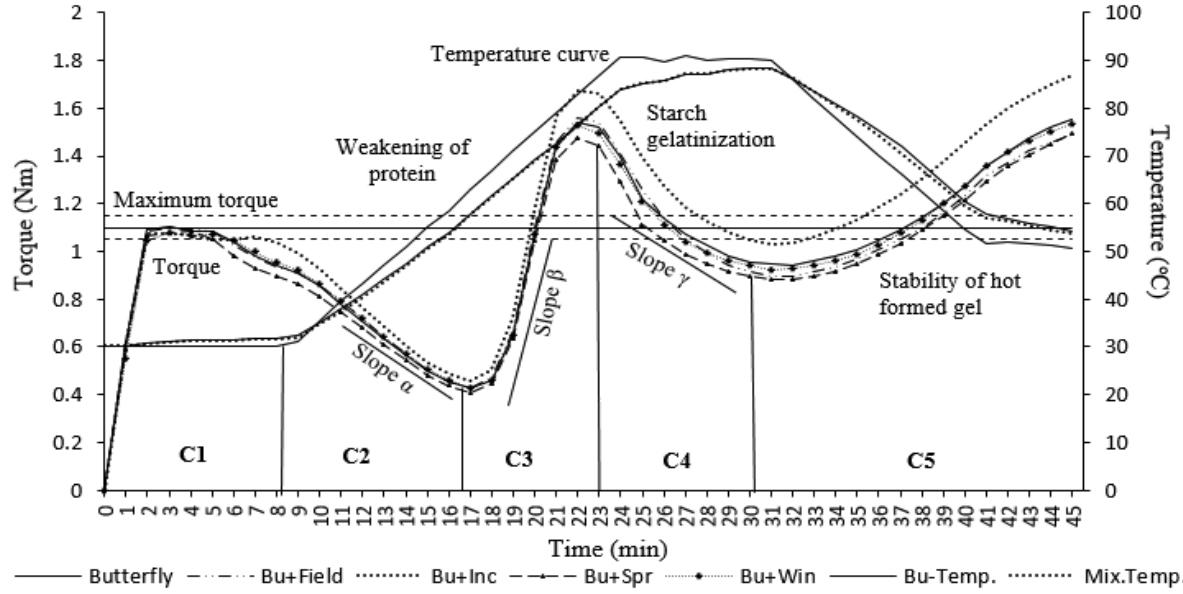

Fig. 2 Mixolab curve of flour milled under mixtures of winter wheat variety and legumes (Bu-Temp.: Butterfly dough temperature, Mix-Temp.: Mixtures of Butterfly and legumes dough temperature, Bu: Butterfly, Field: Field beans, Inc: Incarnate clover, Spr: Spring pea, Win: Winter pea)

Mixolab Analysis

The advantage of Mixolab is being able to measure cereals flour characteristics in one test as proteins, starch, and associated enzymes. The mean values of each treatment for stability, Torque C2, Torque C3, Torque C4, Torque C5, and slope alfa, beta, gamma are displayed in Tab. 1 and Fig. 2. The mixing of dough against evaluation is indicated in the first phase. Mixing resistance of dough, the longer this time is, the more the flour will be strong. The value of stability normally ranges from 4.96 to 11.42 minutes. Tab. 1 shows that the stability assessed by Mixolab under growing winter wheat Butterfly variety and different types of legumes mixtures between 5.27 and 8.53 minutes, was high significantly statistically different ($P < 0.001$). The value of stability of mixtures of Butterfly with incarnate clover, and Butterfly with winter pea, respectively, was 2.33 and 0.57 minutes longer, however, Butterfly intercropping with field beans (5.80 minutes), and Butterfly with spring pea (5.27 minutes) was shorter compared to singly Butterfly (6.20 minutes). The mixtures of winter wheat and legumes were effected on stability of winter wheat flour, intercropping with legumes systems (6.59 minutes) longer, and related to the high gluten in

mixtures compared with only winter wheat (6.20 minutes). Growing winter wheat in organic farming with fertilizer (8.83 minutes) is higher than growing winter wheat organically without fertilizer, according to *Lacko-Bartošová et al., (2021)* (3.19 minutes). Addition of organic fertilizer or mixtures with legumes positively affected the baking quality of wheat flour. Torque C2 measures protein weakening as a function of mechanical work and temperature. The weakening of protein was significantly different in growing seed mixtures of winter wheat and legumes. Despite the fact that there was a significant difference ($P < 0.01$) between the treatments, however, there was no significant difference when comparing the intercropping of each type to the control (no intercropping). Torque C2 ranged from 0.41 Nm to 0.45 Nm, the highest being a mixture of Butterfly with incarnate clove and the lowest being a mixture of Butterfly with spring pea (0.41 Nm).

Starch characteristics were significantly different in growing seed combination of winter wheat namely Butterfly with different types of legumes (except Torque C4). Torque C3 measures starch gelatinization indicated the mixtures reached highest by Butterfly intercropping with incarnate clover (1.69 Nm) and was significantly different compared to Butterfly, followed by Butterfly with field bean and winter pea stood at 1.57 Nm, 1.54 Nm, respectively. Butterfly and spring pea (1.48 Nm) were less than sown single Butterfly (1.55 Nm). Torque C5 under sowing seed Butterfly variety mixtures incarnate clover (1.75 Nm) was higher than other treatments, which ranged from 1.50 to 1.57 Nm. Torque C4, the number of measures of hot gel stability between 0.74 and 1.02 Nm, there was no difference. There was no effect under mixtures of winter wheat with legumes on slope alfa, which ranged from -0.08 to -0.07, and slope gamma from -0.13 to -0.07. On the other hand, the difference in wheat flour starch gelatinization speed was significant for factors of winter wheat varieties and legumes mixtures. The highest number of slope beta of the curve between C2 and C3 was Butterfly and incarnate clover (0.54), similar to Butterfly and winter pea, the number was higher than control (Butterfly variety only). Tab. 1 shows that almost rheological characteristics analyzed by Mixolab were higher under mixtures of Butterfly and incarnate clover compared to other mixtures or grown single Butterfly variety. However, comparison to *Lacko-Bartošová et al., (2021)* research reported torque C2, C3, C4, and C5 values of 0.51, 1.91, 1.94, and 3.82 Nm, respectively, which was higher than rheological quality characteristics of winter wheat flour in our site.

CONCLUSIONS

The current research aims to give an understanding of the effects of changing cultivation practices on grain production, wheat quality, and rheological quality features analyzed by Mixolab evaluation in organic farming. Four percent of average grain yield under mixtures of winter wheat and legumes was higher than the single winter wheat variety. Winter wheat variety and legume cultivar mixtures impacted grain wheat quality. The highest protein content was under Butterfly and field bean mixtures, while there was no difference between Butterfly and other combinations. The highest wet gluten under intercropping with field beans, spring pea, and winter pea was higher than sowing a single Butterfly variety. The rheological properties evaluation of grain wheat in Mixolab yielded the same findings. The mixtures of winter wheat and legumes were a potential method for better winter wheat quality. Therefore, improving the grain dough and baking properties under combinations of winter wheat and legumes should be additional research for adaptation to low input cultivations conditions.

ACKNOWLEDGMENT

This study was supported by research project No. NAZV QK1910046 of the Ministry of Agriculture of the Czech Republic.

REFERENCES

1. Aart, O. (2006). The Effect of Growing Cultivar Mixtures on Baking Quality of Organic Spring Wheat. In *Proceedings of the COST SUSVAR Workshop on Cereal Crop Diversity: Implications for Production and Products. Presented at the Crop Diversity and Quality of end Product – Involving Farmers and end Users*, (pp. 17–22). La Besse, France.
2. Aune, D., Keum, N., Giovannucci, E., Fadnes, L.T., Boffetta, P., Greenwood, D.C., Tonstad, S., Vatten, L.J., Riboli, E., & Norat, T. (2016).

Whole Grain Consumption and Risk of Cardiovascular Disease, Cancer, and all Cause and Cause Specific Mortality: Systematic Review and Dose-response Meta-analysis of Prospective Studies. *BMJ*, 353, i2716.
3. Borg, J., Kiær, L.P., Lecarpentier, C., Goldringer, I., Gauffreteau, A., Saint-Jean, S., Barot, S., & Enjalbert, J. (2018). Unfolding the Potential of Wheat Cultivar Mixtures: A Meta-analysis Perspective and Identification of Knowledge Gaps. F*ield Crops Research*, 221, 298-313.
4. Buraczyńska, D., Ceglarek, F., Gąsiorowska, B., Zaniewicz-Bajkowska, A., & Płaza, A. (2011). Cultivation of Wheat Following Pea and Triticale/pea Mixtures Increases Yields and Nitrogen Content. *Acta Agriculturae Scandinavica, Section B - Soil & Plant Science*, 61(7), 622-632.
5. Chen, H., Nguyen, K., Iqbal, M., Beres, B.L., Hucl, P.J., & Spaner, D. (2020). The Performance of Spring Wheat Cultivar Mixtures under Conventional and Organic Management in Western Canada. *Agrosystems, Geosciences & Environment*, 3(1).
6. Dahlin, I., Kiær, L.P., Bergkvist, G., Weih, M., & Ninkovic, V. (2020). Plasticity of Barley in Response to Plant Neighbors in Cultivar Mixtures. *Plant and Soil* 447(1-2), 537–551.
7. Gaudio, N., Escobar-Gutiérrez, A.J., Casadebaig, P., Evers, J.B., Gérard, F., Louarn, G., Colbach, N., Munz, S., Launay, M., Marrou, H., Barillot, R., Hinsinger, P., Bergez, J.-E., Combes, D., Durand, J.-L., Frak, E., Pagès, L., Pradal, C., Saint-Jean, S., Van Der Werf, W., & Justes, E. (2019). Current Knowledge and Future Research Opportunities for Modeling Annual Crop Mixtures. A Review. *Agronomy Sustainable Development*, 39, 20.
8. Jablonskytė-Raščė, D., Maikštėnienė, S., & Mankevičienė, A. (2013). Evaluation of Productivity and Quality of Common Wheat (*Triticum aestivum* L.) and Spelt (*Triticum spelta* L.) in Relation to Nutrition Conditions. *Zemdirbyste Agriculture* 100(1), 45-56.
9. Kaut, A.H.E.E., Mason, H.E., Navabi, A., O'donovan, J.T., & Spaner, D. (2009). Performance and Stability of Performance of Spring Wheat Variety Mixtures in Organic and Conventional Management Systems in Western Canada. *The Journal of Agricultural Science*, 147(2), 141-153.
10. Konvalina, P., Moudry, J. (Jr), Capouchova, I., & Moudry, J. (2009). Baking Quality of Winter Wheat Varieties in Organic Farming. *Agronomy Research*, 7(2), 612–617.
11. Krejčířová, L., Capouchová, I., Petr, J., Bicanová, E., & Faměra, O. (2008). The Effect of Organic and Conventional Growing Systems on Quality and Storage Protein Composition of Winter Wheat. *Plant, Soil Environment*, 53(11), 499–505.
12. Lacko-Bartošová, M., Lacko-Bartošová, L., & Konvalina, P. (2021). Wheat Rheological and Mixolab Quality in Relation to Cropping Systems and Plant Nutrition Sources. *Czech Journal of Food Sciences*, 39(4), 265–272.
13. Mäder, P., Hahn, D., Dubois, D., Gunst, L., Alföldi, T., Bergmann, H., Oehme, M., Amadò, R., Schneider, H., Graf, U., Velimirov, A., Fließbach, A., & Niggli, U. (2007). Wheat Quality in Organic and Conventional Farming: Results of a 21 Year Field Experiment. *Journal of the Science of Food and Agriculture*, 87(10), 1826–1835.
14. Mie, A., Andersen, H.R., Gunnarsson, S., Kahl, J., Kesse-Guyot, E., Rembiałkowska, E., Quaglio, G., & Grandjean, P. (2017). Human Health Implications of Organic Food and Organic Agriculture: A Comprehensive Review. *Environmental Health*, 16(1).
15. Osman, A.M., Struik, P.C., & Bueren, E.T.L. van. (2012). Perspectives to Breed for Improved Baking Quality Wheat Varieties Adapted to Organic Growing Conditions. *Journal of Science of Food and Agriculture*, 92(2), 207–215.
16. Tran, K.D., Konvalina, P., Capouchová, I., Janovská, D., Lacko-Bartosova, M., Kopecký, M., & Phương, T. (2020). Comparative Study on Protein Quality and Rheological Behavior of Different Wheat Species. *Agronomy*, 10(11), 1763.
17. Vidal, T., Saint-Jean, S., Lusley, P., Leconte, M., Krima, S.B., Boixel, A.-L., & Vallavieille-Pope, C. de, (2020). Cultivar Mixture Effects on Disease and Yield Remain Despite Diversity in Wheat Height and Earliness. *Plant Pathology*, 69 (6), 1148–1160.
18. Vrtilek, P., Handlirova, M., & Smutny, V. (2016). Growing Winter Wheat Varieties and Their Mixtures on Different Sites of Yields, Quality, and Economy. In *MendelNet 2016 Conference on Plant Production* (pp. 183-188). Mendel University in Bruno.

Corresponding author:
Trong Nghia Hoang, PhD. Student, Department of Agroecosystems, Faculty of Agriculture and Technology, University of South Bohemia in Ceske Budejovice, Studentská 1668, České Budějovice 37005, Czech Republic, phone: +420 387772446, e-mail: hoangn00@fzt.jcu.cz.

ENERGY ANALASIS OF COOLING SOURCES IN DISTILLATION COLUMN

Tomáš HOLOTA[1], Mária HOLOTOVÁ[3], Ján CSILLAG[2], Matúš BILČÍK[2], Peter KUCHAR[1]

[1]Institute of Agricultural Engineering, Transport and Bioenergetics, Slovak University of Agriculture in Nitra, Faculty of Engineering, Tr. A. Hlinku 2, 949 76 Nitra, Slovakia
[2]Institute of Electrical Engineering, Automation, Informatics and Physics, Slovak University of Agriculture in Nitra, Faculty of Engineering, Tr. A. Hlinku 2, 949 76 Nitra, Slovakia
[3] Institute of Marketing, Trade and Social Studies, Slovak University of Agriculture in Nitra, Faculty of Economics and Management, Tr. A. Hlinku 2, 949 76 Nitra, Slovakia

Abstract
The world is making great progress in technological field, and this is exactly what create new opportunities to reduce costs. One of the ways is to design an appropriate cooling of the distillation column, which ultimately contributes to positive economical results in distillery operating. The aim of the article is to propose the most efficient cooling method in distillation. The cooling sources described in the methodology were selected on the basis of cooling water flow measurement, implementation costs and annual operating costs. This data was evaluated by using the FDMM method. We found out by a more detailed comparison that at a flow of 400 m3 per year it is most worthwhile to cool with public water system until the fourth year of operation. From the fourth year of operation, cooling costs are lower at a given flow rate if we use a pumped groundwater with a frequency converter or pressure tank.

Key words: *distillation, cooling, distillation column, cooler.*

INTRODUCTION

Distillation equipment are used in the food industry as well as in the chemical industry in ethanol distillation process from prepared fermented mash (*Vogelpohl, 2015*). For these processes various distillation methods are used as well as different related distillation technologies. In the case of the use of distillation equipment in the food industry, the primary focus is on the processing of mash prepared from fruit and agricultural crops. Ethanol from agricultural crops can be divided into consumable and bioethanol as an ecological fuel additive (*Turner, 2006*).In the food industry, two basic types of distillation equipment are used, namely a double distillation boiler and a distillation column (*Holota, 2019*).

Quality and effective distillery equipment provide a prerequisite for ensuring proper production techniques and the opportunity to consume quality spirits for the wide public. These processes are greatly influenced by the correct choice of distillation equipment (*Holota, et al., 2021*). The technological equipment of distilleries must be also adapted to the requirements of growers, who process fruit and agricultural crops (*McHarry, 2012*). The input costs represent a costly item for each organization at the establishment of the distillery. The current requirement for quality products in the best price range, encourages distillery owners to find the most efficient ways to operate them. One of the ways is selected method of cooling during distillation. The profitability of the process and time-acceptable return on input costs can only be achieved by using the device effectively. One such way to reduce costs is to apply the most efficient cooling in distillation equipment while maintaining the quality of the final distillates.

The purpose of cooling is to remove heat from materials or liquid substance, which are either cooled to a temperature lower than the surroundings, or their state changes, or reaction heat is removed (*Clark, 2008*).The vapors from the distillation pot pass through the vapor pipe and enter the cooler. The task of the cooler is to condense these vapors and cool down to a temperature of 10°C to 20°C. The temperature of the distillate flowing out of the cooler should be the same or just a little higher than the cooling water temperature (*Opáth, 2007*). Cooling is a very important element that affects the result of the distillation process in a fundamental way. It is important not only to choose the right volume of the cooler, which depends on the distillation pot volume but also the type of distillation equipment (*Fekete, et al., 2007*).

In the presented paper, we emphasized the reduction of energy consumption of the production of fruit distillates and therefore the main aim of the study was to propose the most efficient cooling method in distillation.

MATERIALS AND METHODS

The research is focused on various types of cooling medium in the coolers of distillation column with a nominal volume of 300 l. The measurements were carried out on 3 identical distillation equipment with the same amounts per distillation batch (i.e. 300 l of fruit mash) at the same time.
One distillation process of 300 liters of mash takes 3 hours, using a coolant with an inlet temperature of 12°C and a coolant volume of 205 liters per production batch of 300 liters of mash. It is possible to process up to 2400 liters of mash in 8 batches within 24 hours.

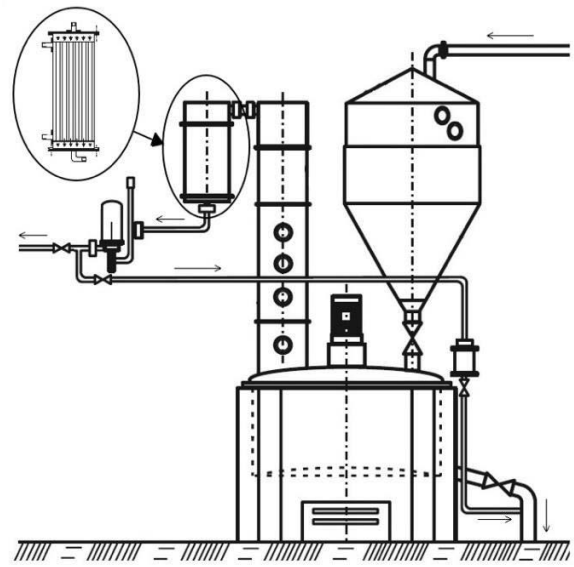

Fig. 1 Schematic diagram of distillation column with tube cooler

A tube exchanger/cooler is installed on the distillation equipment (see Figure 1). The cooler has 4 holes, where 2 serve for the inlet and outlet of the coolant and other 2 serve as the inlet of distilled vapors and the outlet of condensed distillate. Tube heat exchangers are the most common type used in industry. The tube diameters vary from 0.625" to 1.5" (~16 mm to 38 mm) in conventional heat exchangers. These heat exchangers have very low surface area to volume ratio. Since this type of heat exchanger can handle more severe conditions and higher pressures and temperatures, it can be used in differently systems if there is no space limitation (*Chordia, et al., 2017*). The tube cooler is one of the most effective coolers as regards consumed amount of cooling medium required for the condensation of vapors produced during distillation and at the same time contributes to a higher quality of the final distillate (*Pischl, 1997*). Three basic sources of cooling medium were involved in the research. In the case of using underground water sources, we compared two methods of obtaining water, namely by using a pump with pressure vessel and by using a pump with a frequency converter. Based on selected cooling sources, we created the following research elements (Tab. 1). The temperature of coolant supplied to the cooler was the same for all cooling sources, namely 12°C. We ensured the same inlet temperature due to the relevant results of comparing the volume of consumed coolant from various sources during distillation. The temperature of 12°C was ensured with the mixing valve at the entrance to the cooler. It is an automatic valve for coolant control with return flow to the dephlegmator. The mixing valve can be adjusted in the range of 10°C to 80°C.

Tab. 1 Characteristics of research elements

Research elements			
V1	V2	V3	V4
Water from public water supply	Groundwater with using a pump and frequency converter	Groundwater with using a pump and a pressure vessel	Coolant with using a cooling tower
Water connection water meter shaft 10 micron filter siliphos filter	20 m well bore water meter shaft submersible pump Pedrollo 4SR 4/14 frequency converter GD10 pressure sensor tank ZILMET 24 liter 10 micron filter 6x siliphos filter stainless particulate filter plastic plate particulate filter	20 m well bore water meter shaft submersible pump Pedrollo 4SR 4/14 stainless steel tank 500l Aquatrading AISI 304/500 10 micron filter 6x siliphos filter stainless particulate filter plastic plate particulate filter	cooling tower PMS 9/85 K12 ATT BIF Pump 0,55 kW Electroinstalation, pipe connection Water chemical treatment

When comparing cooling sources, we applied the multi-criteria FDMM method (Forced Decision Matrix Method) with the following procedure (*Holota, et al., 2021*):

1. Determine the compared properties (criteria) of cooling sources and write them in the table.
2. Carry out a pairwise comparison of the criteria in a matrix plotted in tabular form. When comparing, rate the more significant criterion as "1" and rate the less significant criterion as "0".
3. Based on the criteria comparison, determine the appropriate weights for the criteria.
   $$weight_n = \frac{\sum_{n=1}^{n} H_n}{\sum_{k=1}^{k}\sum_{n=1}^{n} H_n}, - \quad (1)$$
   kde: H_n - evaluation of the criterion,-;
   n - number and ordinal number of the criteria;
   k - ordinal number of the evaluation of the criterion.
4. Create a decision matrix for separate assessment of materials and individual criteria.
5. Compare variants with regard to a specific criterion. We rate a more suitable variant as "1" and worse as "0".
6. Define the respective ratings using the equation based on the comparison of the variants:
   $$H_v = \frac{\sum_{i=1}^{i} H_{vi}}{\sum_{j=1}^{j}\sum_{i=1}^{i} H_{vi}}, - \quad (2)$$
   kde: H_{vi} - evaluation of the variant,-;
   i - number and ordinal number of the variant;
   j - ordinal number of the evaluation of the variant.
7. Create a decision table from the received weights and evaluations of the variants.
8. Define the weighted sum (S_v) using the equation:
   $$S_v = \sum_{n=1}^{n} weight_n \times H_v, - \quad (3)$$
   kde: $weight_n$ - weight value,-;
   H_v - variant value,-;
   n - number and ordinal number of the criteria.
9. Determine the order of the variants based on the calculated weighted sum.

RESULTS AND DISCUSSION

Cooling as the final process in the distillation of fruit distillates is carried out in tube coolers, by using 4 various cooling sources. In the first phase, we focused on the economic effectiveness of individual cooling sources, what can be seen in Figure 2, where cumulative price increase for procurement and operation in years is displayed while keeping the prices in 2021 and an average coolant flow rate of 400 m3/year. In the first year of operating costs, the input prices for the construction of individual cooling sources are also included according to the equipment price survey and the average price per 1 m3 of water in the year 2021. The lowest price of construction and the first annual operation, i.e., €1,640.56 can be seen in the case of using public water supply (potable water) and the highest €7,484.55 in the case of using a cooling tower. A very important moment occurs in the 4th year, when so far, the cheapest variant using public water supply is priced higher than the well source of cooling even with using both a tank and a frequency converter.

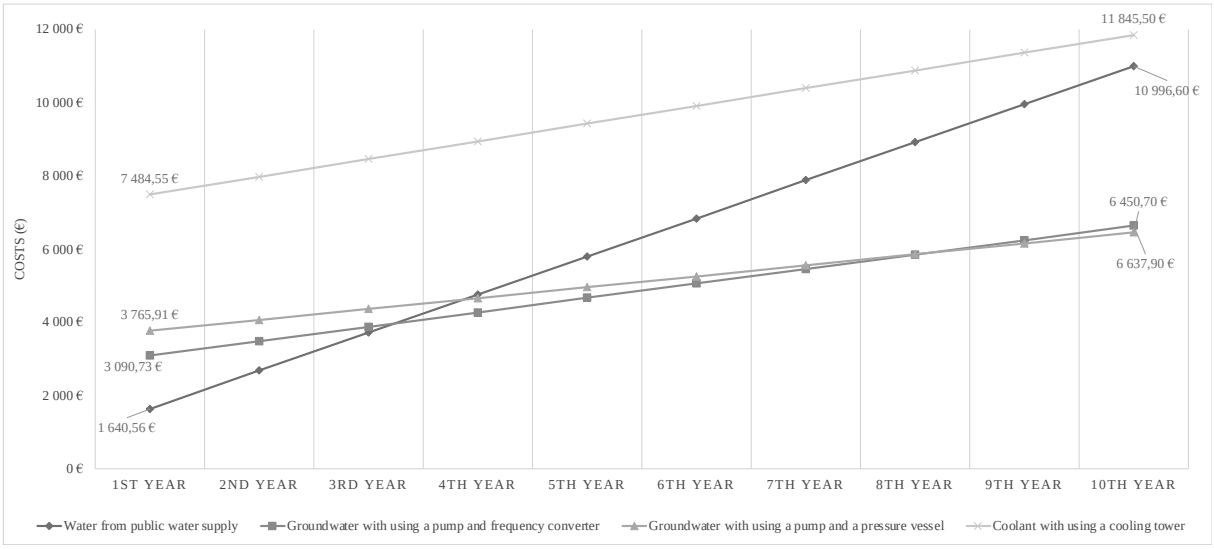

Fig. 2 Economy effectiveness of cooling sources

In the second phase, we focused on applying the multi-criteria method FDMM (Forced Decision Matrix Method) according to the procedure described in Materials and Methods. We decided on the FDMM method based on the requirement to eliminate subjective interventions into the process of choosing the most effective and efficient cooling source. At first, we proceeded to determine the weights using a pairwise comparison of criteria (establishment – K1, operating costs – K2, eco-friendly – K3, effectiveness – K4) in Table 2.

Tab. 2 Pairwise comparison of criteria

Criteria	K1	K2	K3	K4	Sum	wise
K1 – establishment	-	0	1	1	2	0,333
K2 – operating costs	1	-	1	1	3	0,500
K3 – eco-friendly	0	0	-	1	1	0,167
K4 – effectiveness	0	0	0	-	0	0,000

We applied a similar evaluation procedure in variants evaluation of cooling source for each selected criterion separately. We evaluated the compared variants of cooling sources "1" if it suited better the selected criterion, if it suited worse, we rated it "0". Pairwise comparisons of the variants were recorded in tables 3-6. We recorded pairwise comparisons of variants (V1 - Water from public water supply, V2 - Groundwater using a pump and a pressure vessel, V3 - Groundwater using a pump and frequency converter, V4 - Coolant using a cooling tower) in Tables 3-6.

Tab. 3 Pairwise comparison of variants according to criterion K1

Variant	V1	V2	V3	V4	súčet	váha
V1	-	1	1	1	3	0,500
V2	0	-	1	1	2	0,333
V3	0	0	-	1	1	0,167
V4	0	0	0	-	0	0,000

Tab. 4 Pairwise comparison of variants according to criterion K2

Variant	V1	V2	V3	V4	súčet	váha
V1	-	0	0	0	0	0,000
V2	1	-	1	1	3	0,500
V3	1	0	-	1	2	0,333
V4	1	0	0	-	1	0,167

Tab. 5 Pairwise comparison of variants according to criterion K3

Variant	V1	V2	V3	V4	súčet	váha
V1	-	0	0	0	0	0,000
V2	1	-	1	0	2	0,333
V3	1	0	-	0	1	0,167
V4	1	1	1	-	3	0,500

Tab. 6 Pairwise comparison of variants according to criterion K4

Variant	V1	V2	V3	V4	súčet	váha
V1	-	1	1	1	3	0,500
V2	0	-	0	0	0	0,000
V3	0	1	-	0	1	0,167
V4	0	1	1	-	2	0,333

Tab. 7 Decision table of the FDMM method

Criteria	Weight	Evaluated variants of the material			
		V1	V2	V3	V4
K1 – establishment	0,333	0,500	0,333	0,167	0,000
K2 - operating costs	0,500	0,000	0,500	0,333	0,167
K3 – eco-friendly	0,167	0,000	0,333	0,167	0,500
K4 – effectiveness	0,000	0,500	0,000	0,167	0,333
Weighted sum		0,167	0,417	0,250	0,167
Rank		3.	1.	2.	3.

As we can see from table 7, after taking into account the weights and values of individual variants using the weighted sum, we get a clear determination of the order of individual variants of cooling sources. Cooling using a pump and frequency converter is in the first place in the rating. Both cooling with water from public water supply and cooling with a closed cooling tower system are in the third place, their position was significantly affected by higher operating costs in the case of potable water and higher procurement costs in the case of a cooling tower. Based on the results of the FDMM method we decided that the most effective source of cooling in a still with a nominal volume of 300 liters is cooling provided by groundwater using a pump and frequency converter, which will ensure the fluidity and stability of the flow of coolant to the cooler. In the case of the FDMM method, we are talking about a modified decision matrix (FDMM - Forced Decision Matrix Method). The decision matrix provides an effective way to prioritize a particular item among many competing items. It's a process where we compare items

on an individual base, on every other item with preference given to one over the other. Prioritization is defined according to weights (*Bhushan & Kanwal, 2004*).

CONCLUSIONS

Distilleries currently have high-level technological equipment. Just like any business, distillery also tries to manage its finances as the most effective as possible. In this step, it is important to determine how and where the economic costs can be minimized and thus ultimately make the work of the distillery more efficient. Currently, companies are trying to achieve a greater degree of sustainability and thus, in addition to the economic side, they must also focus on greater eco-friendly production and workplace processes in the company. The aim of the study was to propose the most efficient method of cooling during the distillation of fruit distillates in distilleries with a nominal capacity of the raw material boiler of 300 liters. In the first step, we visualized the economic side of individual cooling sources from their establishment to operation with a 10-year development prediction. The lowest initial costs together with operating costs in the first year were in the case of using public water supply and potable water, on the other side, the highest input costs together with operating costs were with the cooling tower. When we analyzed the ecological aspect of individual cooling sources, we can conclude that the use of potable water for cooling is the worst option from an ecological point of view.

When choosing the most appropriate cooling, we set criteria important for the right selection and applied the multi-criteria statistical method FDMM. The method showed that the most effective cooling of the distillation column at the determined flow rate is using groundwater transported by a pump with a frequency converter. This cooling method is also the most economically effective from the 4th year of operation, and until in the 9th year changes its position with groundwater transported by a pump with a pressure vessel.

ACKNOWLEDGMENT

This study was supported by project VEGA 1/0470/21: Economic aspects of the development of fruit distillate production due to climate change and socio-economic impacts of legalization of private distillate production in Slovakia.

REFERENCES

1. Bhushan, N. & Kanwal R. (2004). Strategic decision making: Applying the Analytic Hierarchy Process. London: Springer-Verlag.
2. Chordia, L., Portnoff, M. A., & Green, E. (2017). High Temperature Heat Exchanger Design and Fabrication for Systems with Large Pressure Differentials. Pittsburgh: Thar Energy LLC.
3. CLARK, S. (2008). Elements of Fractional Distillation. United Kingdom: Read Books.
4. Fekete, R., Peciar, M. & Gužela, Š. (2007). Procesné strojníctvo. Bratislava: STU v Bratislave.
5. HOLOTA, T. (2019). Destilačné technológie a ich výhody a nevýhody. Sady a vinice, 14(2), 32-33.
6. Holota, T., Holotová, M. & Csillag, J. (2021). Klasifikácia a hodnotenie technológií na výrobu destilátov na Slovensku Ostrava: Key Publishing.
7. McHarry, S. (2012). The Practical Distiller. United Kingdom: Start Publishing LLC.
8. Opáth, R. (2007). Výroba ovocných destilátov. Topoľčany: Prima Print.
9. Pischl, J. (1997). Vyrábíme ušlechtilé destiláty. Semily: Ivo Železný.
10. Turner, W., C. (2006). Energy management handbook. London: Taylor and Francis Ltd.
11. Vogelpohl, A. (2015). Distillation. Germany: CPI books GmbH

Corresponding author:
Ing. Mária Holotová, PhD., Department of Marketing and Trade, Faculty of Economics and Management, Slovak University of Agriculture in Nitra, Tr. A. Hlinku 2, Nitra, 949 76, Slovakia, phone: +421 907 560 780

DESIGN OF A LABORATORY TEST EQUIPMENT FOR MEASURMING AND TESTING MOBILE ENERGY MEANS WITH SIMULATION OF OPERATING CONDITIONS

Ľubomír HUJO[1], Jozef NOSIAN[1], Sylwestwer BOROWSKI[2], Marietta MARKIEWICZ-PATALON[2], Milan TOMIČ[3], Peter KOŽUCH[1]

[1]Department of Transport and Handling, Faculty of Engineering, SUA in Nitra, 949 76 Nitra, Slovakia
[2]Department of Machinery, Faculty of Mechanical Engineering, Politechnika Bydgoska, 85 795 Bydgoszcz, Poland
[3]Department of Agricultural Engineering, Faculty of Agriculture, University of Novi Sad, 21 102 Novi Sad, Serbia

Abstract
The designed laboratory equipment is used for measuring and testing hydrostatic transducers and properties of hydraulic fluids. A verification measurement of the flow of the hydrostatic transducer was performed on the proposed laboratory equipment. The output of the measurements is a confirmation of the functionality of the designed equipment. The results of the verification measurement were compared with the data obtained during the simulations in the computer program FluidSIM 5. The flow data obtained by the simulation show higher values than in the verification measurement. Specifically, at 250 rpm it was an increase of 3.21%, at 500 rpm by 0.39%, and at 750 rpm by 3.14%.

Key words: *laboratory test equipment, flow, hydrostatic transducers, simulation.*

INTRODUCTION

The use of hydraulic equipment is increasing across all industries, which is mainly due to the advantages and large range of their use. In agricultural machinery, hydrostatic transducers are widely used as part of the hydraulic circuit. These transducers have the main function of supplying the hydraulic circuit with hydraulic fluid as well as generating pressure energy in the hydraulic circuit. It is therefore necessary to maintain the exact mechanical production of the individual elements of the entire hydraulic circuit, by monitoring the accuracy of CNC machine tools (*Košinár, et al. 2011; Kuric, et al. 2016*). Due to the high demands, especially on hydrostatic transducers used in the agricultural industry, there is a need to test them. It is for these reasons that the design of a laboratory equipment is created, which allows testing the parameters of hydrostatic transducers and hydraulic fluids. Operating fluid is also an important part of hydraulic mechanisms. The author *Kučera et al. (2016)* claims that based on the analysis of the operating fluid, we can determine the technical condition of hydraulic elements located in hydraulic systems. At the same time, it is important to monitor the contamination of the working fluid. According to author *Zastempowski et al. (2013)*, the physico-chemical properties of hydraulic fluids are also affected by pollution, which results in degradation processes. Oil contamination is the most common and serious source of machine failure (*Kučera et, al. 2016*). The article also performs a simulation of the verification measurement in the simulation program, which was compared with the values obtained during the verification measurement at the laboratory equipment. The aim of the study was to design laboratory test equipment for measuring parameters of hydrostatic transducers and energy carriers with subsequent verification measurement and comparison of results with simulation.

MATERIALS AND METHODS

According to the author *Simikič et al. (2014)* machines which are used in agriculture and forestry are characterized by demanding operational hours and often work in dusty and humid environments. This has negative consequences on the proper functioning of hydraulic systems. Agricultural engineering requires continuous improvement of the service life and reliability of machinery (*Tóth et al. 2019*). Laboratory testing device allows to simulate the variable testing conditions of the real conditions under which the hydraulic system of agricultural wheel tractor operates (*Hujo, et al. 2019*). The proposed device consists of two hydraulic circuits. One circuit of the measuring chain is primary while the other circuit is secondary, due to the possibility of continuously testing two hydrostatic transducers or two

types of hydraulic fluids concurrently under the same or different conditions. Using verification measurements and their results, we demonstrated the suitability of the proposed laboratory test equipment for measuring the parameters of hydrostatic transducers.. The importance of monitoring the operating parameters of hydraulic pumps is also confirmed by the authors *Majdan et al. (2016, 2017)* who consider the values of flow and flow efficiency as important indicators of the assessment of hydraulic transducers. Flow and flow efficiency values are used to create dynamic flow models in hydrostatic transducers using numerical simulation to protect the environment *Puškár et al. (2015)*. We'll perform flow measurements from which we'll determine three critical values, which will be compare and evaluate. Subsequently, we'll simulate the same conditions as when measuring on a laboratory equipment in the program FluidSim 5. We compare the values obtained during the measurements. Mathematical relations necessary for dimensioning of individual elements of the proposed laboratory equipment:

Hydrostatic transducer flow: $Q = \frac{V_g.n}{1{,}000}.\eta_{pr}$, dm^3.rpm, (1)

Power of hydrostatic transducer: $P = \frac{V_g.n.p}{60.1{,}000.\eta_c}$,W, (2)

Cooling power: $P_0 = P_{01}.1.1, \quad W.°C^{-1}$ (3)

Inner diameter of the pipe: $d = \sqrt{\frac{4.Q}{\pi.w}}$, mm, (4)

where: $V_g -$ volume of hydrostatic transducer, dm^3; $n -$ speed of rotation hydrostatic transducer, rpm; $\eta_{pr} -$ flow efficiency of the hydrostatic transducer; $p -$ pressure, MPa; $\eta_c -$ overall effectiveness; $w -$ resistance to flow rate, m.s^{-1} (*Hujo, et al. 2017*).

Prior to the actual measurements on the designed laboratory equipment, it is necessary to heat the working fluid in the measuring chain to a temperature of 50° C based on the SAE J745 standard (Hydraulic Power Pump Test Procedure). The SAE J745 standard deals with test procedures for hydrostatic transducers. PARAMO HM 46 oil will be used as the hydraulic charge when measuring the flow of the hydrostatic transducer at the designed laboratory equipment, its parameters are in Table 1. According to authors *Halenár et al. (2017)* and *Kumbár et al. (2013)*, the results of measurements affect the physico-chemical properties, pollution and temperature of the working fluid.

Tab. 1 Basic characteristics of PARAMO HM 46 oil

Parameter	Unit	PARAMO HM 46
Point of fluidity	° C	-27
Flash point	° C	Over 190
Vapor pressure at 20 ° C	Pa	<10
Relative density at 15 ° C	kg.m^{-3}	865
Kinematic viscosity at 40 ° C	mm^2.s^{-1}	41.4-50.6

We'll monitor gear hydrostatic transducer UD-25R, which technical parameters are given in table 2.

Tab. 2 Technical parameters of hydrostatic transducer UD–25 R

Parameter	Unit	Value
Rated/Maximum/Minimum rotation	rpm	1 500/3 200/450
Nominal outlet pressure/ Maximum outlet pressure	MPa	20/23
Geometric volume	dm^3	0.02546
Maximum oil viscosity/ Minimum oil viscosity	mm^2.s^{-1}	1 200/10
Maximum oil temperature/ Minimum oil temperature	° C	80/ -20

Part of hydraulic circuit are associated sensors, through which we can measure pressure, temperature and flow. In the proposed laboratory equipment, a associated EVS 3 100 sensor is used to measure physical quantities. Authors *Kopiláková et al. (2017) and Csillag et al. (2019)* in their work state, that the operating parameters, especially temperature and pressure, have an impact on the measuremets, as well as the thermophysical properties of the used fluid. We use the HYDAC HMG 3010 unit to record and display quantities from sensors, the maximum inaccuracy of which is $\pm$ 1 %.

RESULTS AND DISCUSSION

Design of laboratory test equipment

Figure 1 shows the scheme of the designed laboratory equipment. The measurement of the characteristics of hydraulic elements in laboratory conditions also dealt with the author *Kopiláková et al. (2019)*.

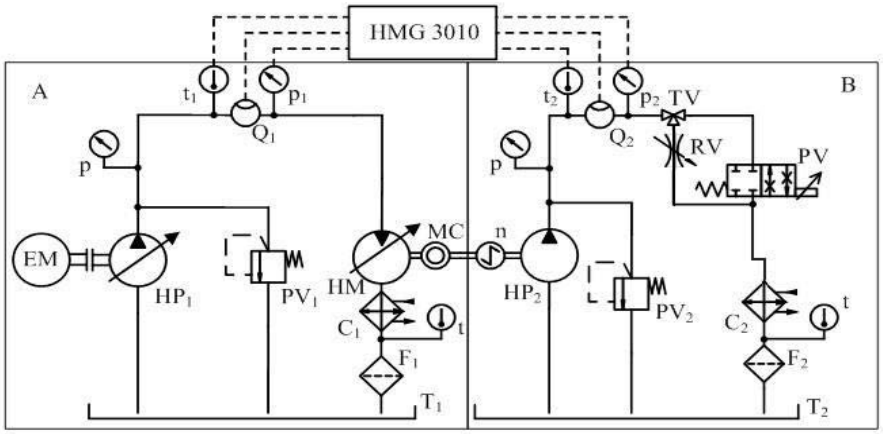

Fig. 1 Laboratory equipment for measuring the parameters of hydrostatic transducers
Legend: A-primary hydraulic circuit, B-secondary hydraulic circuit, EM-electromotor, HP_1-regulatory hydrostatic transducer, PV_1, PV_2-pressure valve, HM-regulatory hydraulic motor, HP_2-tested hydrostatic transducer, C_1, C_2-cooler, t-temperature sensor for tanks,T_1, T_2-tanks, F_1, F_2-filters, p-pressure gauge, RV-reducing valve, TV-three-way valve, PV-proportional reducing valve, MC-mechanical coupling, n-rpm sensor, t_1, t_2-temperature sensors, Q_1, Q_2- flow rate sensors, p_1, p_2-pressure sensors, HMG 3010-recording unit.

The equipment consists of two circuits (labeled A and B) due to parallel the simultaneous testing of two hydrostatic transducers or two energy carriers under the same or different operating conditions. The primary circuit is located next to a three-phase asynchronous electric motor EM. In front of the electric motor there is a frequency converter, which is used to set the speed on the electric motor EM. The electric motor supplies mechanical energy to the hydrostatic transducer HP_1. Furthermore, there is a pressure valve PV_1 in the primary circuit, which performs a safety function. When the set pressure is exceeded, the pressure valve releases the fluid back into the tank, thus protecting the hydraulic circuit from a dangerous condition. The pressure valve is also located in the PV_2 secondary circuit. In both circuits of the designed device there are also filters F_1 and F_2. According to *Kaszkowiak et al. (2015)* filters and filtration system affect the operation and technical condition of the machines and equipment of which they are a part. T_1, T_2 serve as reservoirs of hydraulic fluid located in both hydraulic circuits. Thanks to two tanks, we can test two types of hydraulic fluids simultaneously under the same or different conditions. In the primary circuit there is a hydraulic motor HM, which is used to convert pressure to mechanical energy. The HM hydraulic motor is connected to the HP_2 hydrostatic transducer through a mechanical coupling. HP_2 is a hydrostatic transducer UD-25R. We will monitor the change in flow depending on the rotation speed on the mentioned transducer. In the secondary hydraulic circuit there is a three-way valve TV. The three-way valve has two positions, in the first position the liquid flows into the reducing valve RV, while in the second position the liquid flows through the proportional valve PV. The reducing valve is used to load the elements of the hydraulic circuit and to heat the working fluid. When measuring on the designed device, it is possible to derive a load (pressure) by means of a proportional PV valve, which we use to simulate operating conditions. The proportional valve is located in the secondary circuit and by loading the secondary circuit, we also load the primary circuit, as the given hydraulic circuits are mechanically connected. The proportional valve can be able connected to a computer and a set of pressures obtained in the operating conditions can be loaded into it, and used to creation the required load. Another part of the proposed laboratory equipment is the Hydac HMG 3010 recording unit, in which they are connected to sensors (Q,p,t).

Measurement of hydrostatic transducer flow on the designed laboratory test equipment

During the verification measurement, we will monitor the flow of the hydrostatic transducer UD-25 R. Measurment procedure for measuring the flow of hydrostatic transducer UD-25R: We set the required rotation speed on the electric motor through the frequency converter. We need to heat the working fluit to working temperature, which is 50° C. When measuring the hydrogenerator flow, we set the following rotation speed values: 250, 500 and 750 rpm. At each of the set rotation speeds, the HYDAC HMG 3010 records the measured values from the sensors. During measurement, it is necessary to ensure a stable temperature value at 50° C. The author *Kopiláková et al. (2019)* also stated in her work that it is important to monitor the temperature of the working fluid, due to its influence on the resulting values of measurements. We will process and evaluate the obtained data.

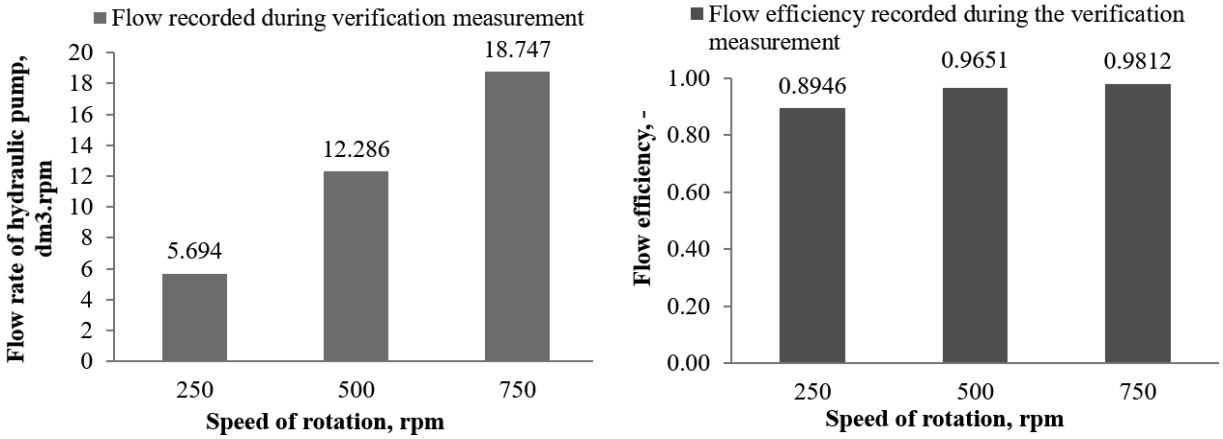

Fig. 2 Hydrostatic transducer flow and flow efficiency values recorded during the measurements

It is the oil flow that is important for the life of the hydraulic system (*Kosiba, et al., 2016*).

Hydrostatic transducer flow measurement – simulation

The flow measurement of the UD-25R hydrostatic transducer was performed in the FluidSIM5 computer simulation program. During the simulations, we tried to approach the conditions and technical parameters of individual hydraulic elements, which contains the proposed laboratory equipment.

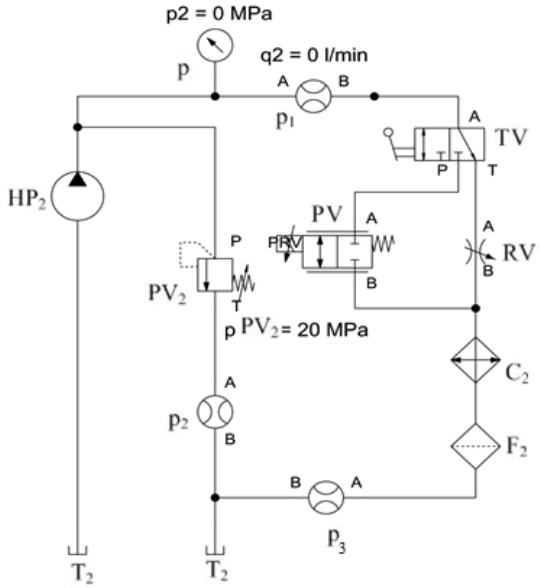

Fig. 4 Scheme of secondary hydraulic circuit of laboratory test equipment

Legend: HP_2-hydrostatic transducer UD-25R, p-pressure gauge, p_1, p_2, p_3-flow rate sensors, PV_2-pressure valve, F_2-filtes, C_2-cooler, RV-reducing valve, TV-three-way valve, PV-proportional reducing valve.

Tab. 4 Recorded values of the hydrostatic transducer flow during the simulation

Rotation speed, n, rpm	Arithmetic mean flow rate, Q, dm^3.rpm	Flow efficiency, η, –
250	5.877	0.9233
500	12.334	0.9688
750	18.806	0.9848

The values recorded during the simulation show (Table 4) higher flow as a values recorded during the verification measurement, where the increase of the flow value is by 3.21% at the converter speed n_1 = 250 rpm, by 0.39% at the speed n_2 = 500 rpm and by 3.14% at the speed n_3 = 750 rpm. Differences can be caused, for example, by leaks, seepage or changes in the viscosity of the liquid during measurements on laboratory equipment.

DISCUSSION

The proposed laboratory equipment in article is used to measure and test mobile energy means with simulation of operating conditions. We declared the suitability of the design by verification measurements on the proposed equipment. Laboratory equipment allows repeatability of measurements in laboratory conditions by simulating operating conditions. Author *Tkáč et al. (2008)* focused on the design of laboratory equipment for measuring the parameters of mobile energy means. In his work, he stated that there is an increased interest in testing methods in laboratory conditions. Based on the designed laboratory test equipment, it is possible to shorten the testing time of hydrostatic transducers, hydraulic fluids and hydraulic elements. Thanks to the results obtained in the measurement of the hydrostatic transducer, it is possible to make changes in the design of the subject equipment before their introduction into the production process. It is also possible to test environmentally degradable fluids in the proposed equipment, which according to the author *Tkáč et al. (2017)* must meet the requirements for the operation of hydraulic equipment in terms of low impact on the wear of hydraulic components. Author *Hujo et al. (2021)* states in its work that testing under laboratory conditions is appropriate mainly for reasons of repeatability of tests and also because of shortening of testing time.

CONCLUSIONS

The need to test energy carriers and transducers used in hydraulic mechanisms is increasing due to environmental requirements. The analysis of hydraulic fluids in operating conditions and its influence on the operating parameters of individual elements of the hydraulic system has already been dealt with in the work of the authors *Čorňák (2018)* and *Kučera et al. (2013)*. At the same time, it is important to perform a comprehensive analysis of the effect of fluids and their mixtures, which was dealt with in his work by the author *Puškár et al. (2019)*. Thanks to its modularity, the designed laboratory equipment also enables testing of other types of hydrostatic transducers used in hydraulic mechanisms. In the presented article, a verification measurement and simulation of hydrostatic transducer flow measurements with data comparison is performed.Minimal deviations were recorded in hydrostatic transducer flow measurements's comparation between the data obtained on the proposed device and the data obtained during the simulation in program, we recorded minimal deviations.

ACKNOWLEDGMENT

This publication was supported by the Operational Program Integrated Infrastructure within the project: Demand-driven research for the sustainable and innovative food, Drive4SIFood 313011V336, cofinanced by the European Regional Development Fund.

REFERENCES

1. Csillag, J., Petrovič, A., Vozárová, V., Bilčík, M., Božiková, M., & Holota, T. (2019). Comparasion of rheological properties of new and used biolubricants, Praha. In *Proceedings of 7th International Conference on Trends in Agricultural Engineering* (pp. 103-108). TAE.
2. Čorňák, Š. (2018). Identification of Operating Fluids with Fingerprint Method Utilization, Jelgava. In *Proceedings of 17th International Scientific Conference Engineering for Rural Development* (pp. 2048-2053). Latvia University of Agriculture.

3. Halenár, M., & Kuchar, P. (2017). Research of biodegradable fluid during operating test, Brno. In *MendelNet 2017* (pp. 784-788). Mendel University in Brno.
4. Hujo, Ľ., Čorňák, Š., Tkáč, Z., & Jánošová, M. (2019). Laboratory Research of Transmission-Hydraulic Fluid, Praha. In *Proceedings of 7th International Conference on Trends in Agricultural Engineering* (pp. 17-20). TAE.
5. Hujo, Ľ., Jablonický, J., & Tkáč, Z. (2017). Návrh inovatívneho laboratórneho simulačného zariadenia na skúšanie hydrostatických prevodníkov a hydraulických kvapalín. Nitra: SUA.
6. Hujo, Ľ., Nosian, J., Zastempowski, M., Kosiba, J., Kaszkowiak, J., & Michalides, M. (2021). Laboratory Test of the Hydraulic Pump Operating Load with Monitoring of Changes in the Physical Properties. *Measurement and Control, 54*, 243-251.
7. Kaszkowiak, J., Borowski, S., Kaszkowiak, E., Dulcet, E., Zastempowski, M., & Hujo, Ľ. (2015). Systemy filtrowania spowietrza w układach zasilania silników spalinowych maszyn roboczych. *Logistyka, 4*, 1893-1898.
8. Kopiláková, B., Turza, J., Hujo, Ľ., & Kosiba, J. (2017). Evaluation of Hydraulic Resistance in Various Liquids and Temperature. *Tribology in Industry, 39,* 129-135.
9. Kopiláková, B., Zápotočný, J., & Eckert, M. (2019). Methodology for measuring and assessing static characteristics of liquid elements. *University Review, 13,* 8-15.
10. Kosiba, J., Čorňák, Š., Glos, J., Jablonický, J., Vozárová, V., Petrovič, A., & Csillag, J. (2016). Monitoring Oil Degradation During Operating Tests. *Agronomy Research, 14,* 1626-1634.
11. Košinár, M., & Kuric. (2011). Monitoring of CNC machine tool accuary. In *New product development in business to business marketing a relational perspective* (pp. 115-118). Proceedings of the 1st International Conference on Quality and Innovation in Engineering and Management.
12. Kučera, M., Aleš, Z., Ivandič, Z., & Hujo, Ľ. (2013). Possibility of Hydraulic Fluids with a Low Environmental Impact Application in Agricultural and Transport Machinery. *Journal of Central European Agricultural, 14*, 1592-1601.
13. Kučera, M., Aleš, Z., & Pexa, M. (2016). Detection and Characterization of Wear Particles of Universal Tractor Oil Using of Particles Size Analyser. *Agronomy research, 14*, 1351-1360.
14. Kučera, M., Majdan, R., Abrahám, R., Kučera, M., & Hass, P. (2016). Analysis of the effect of loading process on tribological system properties. *Acta Universitatis Agriculturae et Silviculturae Mendelianae Brunensis, 64*, 825-833.
15. Kumbár, V., & Dostál, P. (2013). Oils degradation in agricultural machinery. *Acta Universitatis Agriculturae et Silviculturae Mendelianae Brunensis, 61*, 1297-1303.
16. Kuric, I., Zajačko, I., & Císar, M. (2016). Analytical Intelligence tools for multicriterial of CNC machines. *Advances in Science and Technology research journal, 10,* 59-64.
17. Majdan, R., Tkáč, Z., Abrahám, R., Kollárová, K., Vitázek, I., & Halenár, M. (2017). Filtration systems design for universal oils in agricultural tractors. *Tribology in industry, 39,* 547-558.
18. Majdan, R., Tkáč, Z., Abrahám, R., Szabó, M., Halenár, M., & Rášo, M. (2016). Proposal for filtration system for biodegradable lubricants in agricultural tractors. *Agronomy Research, 14,* 1395-1405.
19. Puškár, M., Brestovič, T., & Jasminská, N. (2015). Numerical simulation and experimental analysis of acoustic wave influences on brake mean effective pressure in thrust-ejector inlet pipe of combustion engine. *International Journal of Vehicle Design, 67,* 63-67.
20. Puškár, M., Jahnátek, A., Kuric, I., Kádárová, J., Kopas, M., & Šoltésová, M. (2019). Complex analysis focused on influence of biodiesel and its mixture on regulated and unregulated emissions of motor vehicles with the aim to protect air quality and environment. *Air Quality, Atmosphere and Health, 12,* 1-10.
21. Simikič, M., Dedovič, N., Savin, L., Tomič, M., & Ponjičan, O. (2014). Power delivery efficiency of a wheeled tractor at oblique drawbar force. *Soil and Tillage Research, 141,* 32-43.
22. Tóth, F., Fürstenzeller, A., Rusnák, J., Bošanský, M., & Kadnár, M. (2019). The possibilities of using ecological liquids in tribological gliding systems with a selected surface created by the radial welding technology. *Acta technologica agriculturae, 22*, 134-139.
23. Tkáč, Z., Čorňák, Š., Cviklovič, V., Kosiba, J., Glos, J., Jablonický, J., & Bernát, R. (2017). Research of biodegradable fluid impacts on

operation of tractor hydraulic system. *Acta technologica agriculturae, 20*, 42-45.

24. Tkáč, Z., Drabant, Š., Majdan, R., & Cvíčela, P. (2008). Testing stands for laboratory tests of hydrostatic pump of agricultural machinery. *Resarch in Agricultural Engineering, 54*, 127-141.
25. Zastempowski, M. (2013). Test Stands with Energy Recovery System for Machines and Hydraulic Transmission. *Journal of Research and Application in Agricultural in Agricultural Engineering, 58*, 188-191.

Corresponding author:
Ing. Jozef Nosian, PhD., Department of Transport and Handling, Faculty of Engineering, Slovak University of Agriculture in Nitra, 949 76 Nitra, Slovakia, phone: +421 37 641 4537, e-mail: jozef.nosian@uniag.sk

CHARACTERISTICS OF ECOLOGICAL ENERGY CARRIERS USED IN AGRICULTURAL TECHNOLOGY

Ľubomír HUJO[1], Romana JANOUŠKOVÁ[1], Mirko SIMIKIĆ[2], Marcin ZASTEMPOWSKI[3], Matej MICHALIDES[1], Monika HAJDÁKOVÁ[1]

[1]*Department of Transport and Handling, Faculty of Engineering, Slovak University of Agriculture in Nitra, Slovakia*
[2]*Faculty of Agriculture, University of Novi Sad, Serbia*
[3]*Faculty of Mechanical Engineering, University of Science and Technology, Poland*

Abstract
The article focuses on the properties of ecological energy carriers, which are used in agricultural and forestry technology. The aim of the article is to describe the degradation of the working fluid from the point of view of the atomic emission spectrometer, which is used for the purpose of monitoring contaminants and additive elements. The working fluid examined was Shell Naturelle HF-E 46, a universal ecological transmission-hydraulic fluid, which was tested on laboratory test equipment. The laboratory measurement was performed for 200 hours, during which the gear hydraulic pump with external gearing was cyclically loaded, according to the Vickers standard. The analysis of the transmission-hydraulic fluid was performed after every 50 working hours, where the analysis of the working fluid showed, that there were no significant changes in the properties of the working fluid and fluid is suitable for work in agricultural and forestry machines operating in environmentally sensitive environments.

Key words: *ecological transmission-hydraulic fluid, atomic emission spectrometry, laboratory test equipment.*

INTRODUCTION

Environmental pollution is not a new phenomenon and a problem of the present, but its roots go back to the first human communities (*Janoško et al., 2016*). Therefore, working fluids used in agricultural and forestry machinery are currently subject to increased requirements in terms of reducing environmental pollution. For this reason, the research deals with the use of such liquids, which will not have a negative impact on the environment, the cultivation of healthy food, water pollution, but will also meet the demanding requirements of use in energy devices. The research of degradation of working fluids and their effects on changes of machine parts was dealt with by author *Tkáč, et. al (2014)*, *Hujo (2021)* and *Nosian (2021)*. In our work we focus on the research of the properties of ecological energy carriers, which are used in transmission-hydraulic systems of agricultural and forestry machines, where the impact of working fluids on the environment in the event of a machine failure is significant. At present, it is not uncommon for modern types of tractors to be equipped with a three-point hitch control (*Turza, Kopiláková, 2011*). It is important to notice, that tractors use various types of lubricating oils, which can be contaminated by different ways. That depends on how, and where the whole system's works (*Majdan et al., 2019*). Ecological transmission-hydraulic fluids do not always achieve the properties required for safe and reliable operation of a given mobile handling equipment at higher outputs and higher operating temperatures. The aim of the study was research of changes in the individual properties of transmission-hydraulic fluids, as well as to monitor their impact on individual elements of the hydraulic circuit.

MATERIALS AND METHODS

The measurement was performed on a laboratory test equipment, designed to test the service life of hydrostatic transducers and to test various types of hydraulic fluids. The scheme of hydraulic circuit of laboratory test equipment is shown in Fig. 1 (*Hujo et al., 2017*). The methodology for measuring the working fluid by loading the gear hydraulic pump was implemented according to the Vickers standard at 200 operating hours and corresponded to a dynamic load of 480,000 cycles during which the GHD1-17R-S2D1-SG05G04-N hydraulic pump was loaded with pressure of 22.5 MPa for 0.5 second, with pressure of 18.5 MPa for 0.5 second and with pressure of 0 MPa also for 0.5 second. The system itself was thus cyclically loaded. A similar approach was used in the work of the author *Majdan et al. (2018)*.

After 50 working hours, corresponding to 120,000 cycles, a sample of the working fluid was taken. The temperature of the working fluid during the measurement reached a value of 90-95 °C and the speed was set at 1,600 rpm. Liquid sampling was performed based on the methodology specified in the standard STN 65 6207.

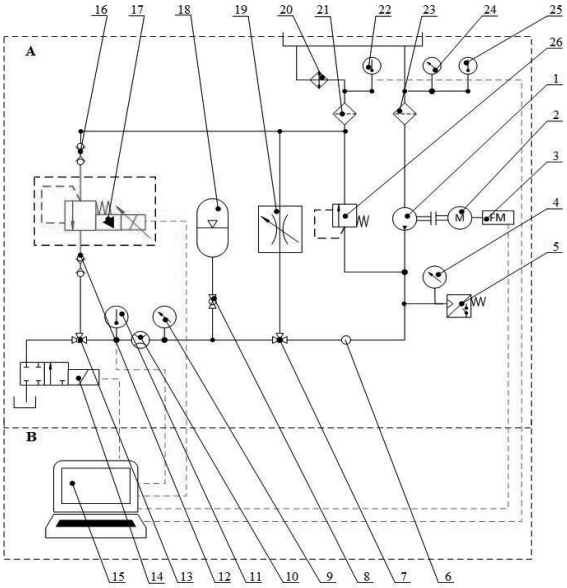

A – hydraulic circuit; B – control and evaluation circuit; 1 – hydraulic pump; 2 – electric motor; 3 – frequency converter; 4, 9, 24, 5 – pressure sensors; 6 – measuring point of evaluation of the fluid indicator; 7, 13 – three-way valves; 8 – ball valve; 10 – flow sensor; 11, 22, 25 – temperature sensors; 12, 16 – quick couplers; 14 – hydraulic switchboard; 15 – computer; 17 – electro-hydraulically operated proportional pressure valve; 18 – accumulator; 19 – throttle valve with stabilization; 20 – cooler; 21, 23 – filters; 26 – pressure valve

Fig. 1 Scheme of hydraulic circuit for testing a hydrostatic transducers and hydraulic fluid (*Hujo et al., 2017*)

Atomic emission spectrometry was performed on a Spectroil Q^{100} device. The standard configuration is equipped and calibrated for 32 abrasive metals, contaminants, and additives. Additional elements can be added at any time, even directly at the place of use. Its great advantage is that it can analyse all elements simultaneously and the analysis process itself takes only about 30 seconds. Fig. 2 shows Spectroil Q^{100} devices in laboratory.

Dimensions (HxDxL) – 706x384x66 mm
Weight – 70 kg
Methodology – ASTM D6595, D6728
Optic system – Pashen-Runge polychromator
Spectral range – 203 – 810 mm
Temperature control – temperature stabilization, 40 °C ± 1 °C
Detectors – CCD detectors
Relative humidity – 0 – 90 %
Temperature requirements – 0 – 40 °C
Sample volume – 1 ml
Data storage – external PC
Software - Windows

Fig. 2 Spectroil Q^{100}

As mentioned at the beginning, tested working fluid was Shell Naturelle HF-E 46, the properties of which is given in Tab. 1.

Tab. 1 Basic properties of the tested transmission-hydraulic fluid Shell Naturelle HF-E 46

Parameter	Unit	Value
Density at 15 °C	$kg.m^{-3}$	921
Viscosity at 40 °C	$mm^2.s^{-1}$	47,2
Viscosity at 100 °C	mPa.s	9,41
Viscosity index	-	188
Flash point	°C	322
Pour point	°C	-42
Biodegradability according to OECD 301 B	%	>60
Biodegradability according to CEC L-33-A 93	%	90
Water hazard class WGK	-	0

RESULTS AND DISCUSSION

Based on the obtained results of atomic emission spectrography of the tested transmission-hydraulic fluid after 200 working hours, there is an increase in chemical elements: lead, potassium, iron. The mentioned chemical elements in the working fluid are evaluated as contaminants, however, despite the loading of the working fluid with a temperature in the range of 90 to 95 °C, the limit values set by the ASTM D6595 standard were not exceeded.

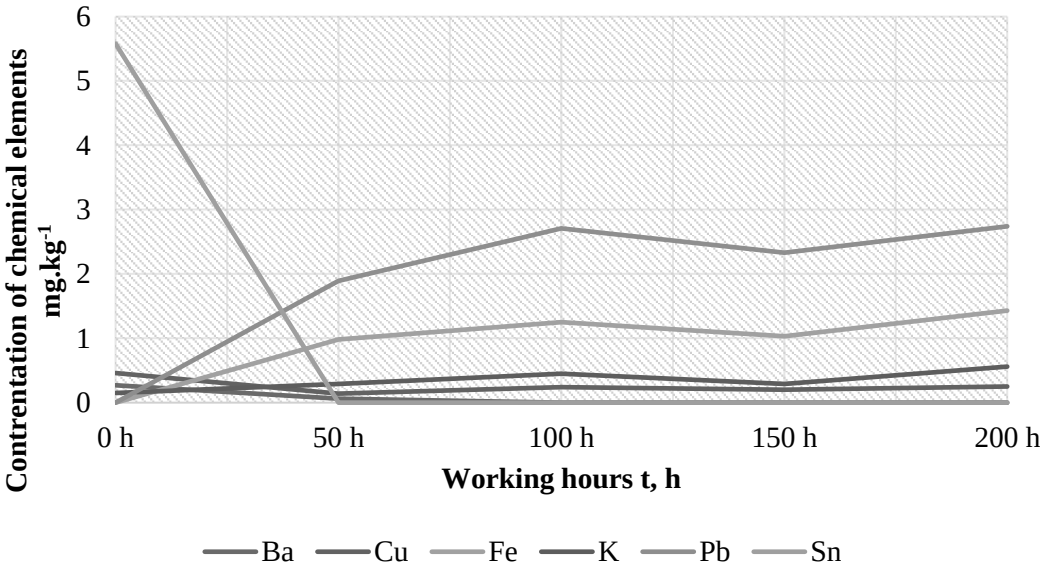

Fig. 3 Graph of atomic emission spectrometry after 200 h from the point of view of contaminants

Tab. 2 Atomic emission spectrometry from the point of view of contaminants

Contrentation of chemical elements $mg.kg^{-1}$	Barium Ba	Copper Cu	Iron Fe	Potassium K	Lead Pb	Tin Sn
0 h	0.27	0.46	0	0.15	0	5.58
50 h	0.06	0.14	0.98	0.29	1.89	0
100 h	0	0.24	1.25	0.45	2.71	0
150 h	0	0.20	1.03	0.29	2.33	0
200 h	0	0.25	1.43	0.56	2.74	0

Gradually, after 50 to 200 working hours, individual chemical elements are involved as additives in the working fluid, where there was an increase in the values of boron, calcium, zinc, silicon, while the value of phosphorus increased within 50 hours and then the values starting to decrease. Nevertheless, the value of phosphorus increased by 15.04 mg.kg^{-1} in total, in 200 working hours. The analysis shows that the individual additive elements of the working fluid were gradually activated and increased depending on the number of hours worked. Activation of the additive elements was carried out gradually, without increasing the pressure and temperature determined by the Vickers method.

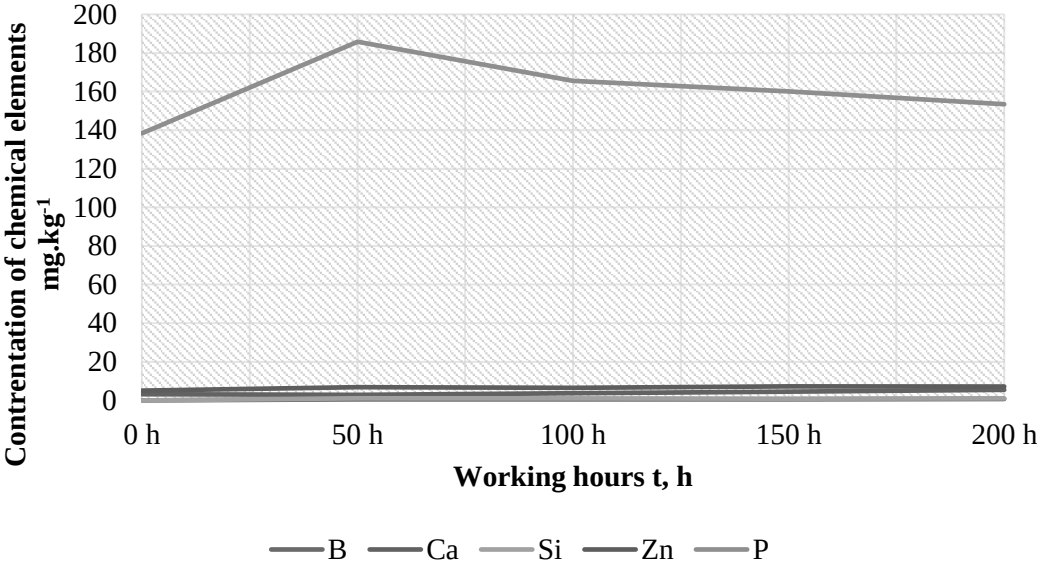

Fig. 4 Graph of atomic emission spectrometry after 200 h from the point of view of additives

Tab. 3 Atomic emission spectrometry from the point of view of additives

Concentration of chemical elements mg.kg^{-1}	Boron B	Calcium Ca	Silicon Si	Zinc Zn	Phosphorus P
0 h	0	3.22	0	5.07	138.35
50 h	0.52	2.87	1.01	6.92	185.79
100 h	0.52	3.72	1.08	6.49	165.54
150 h	0.58	4.53	0.96	7.27	160.02
200 h	0.77	5.49	1.02	7.23	153.39

Comparing obtained results given in Tab. 2 and Tab. 3, with the measurements performed by the author *Pochi et al. (2020)* it can be stated that ecological transmission hydraulic fluid is suitable for use in hydraulic systems of machines and equipment operating in an environmentally sensitive environment. On the other hand, author *Kučera et al. (2016)* states, that for a more accurate evaluation of the results, it would be appropriate to perform an experiment that would include both approaches, i.e., chemical-physical analysis, as well as determining the technical condition of the machine based on component analysis in universal tractor transmission oil.

CONCLUSIONS

Laboratory measurements of hydraulic fluid transmissions show that the content of contaminants increased at lead 2.74 mg.kg^{-1} and potassium 0.41 mg.kg^{-1}. Barium, which can be considered as an additive or as a contaminant, appeared immediately at the beginning of the measurement, but only with a low concentration of 0.27 mg.kg^{-1} and after 50 hours one value decreased to 0 mg.kg^{-1}. Based on the performed analysis, it can be stated that the new working fluid has probably been contaminated, which is

stated in the work of the author *Kosiba et al., (2017),* and during the work in the hydraulic circuit it was gradually filtered out. The same situation occurred with the chemical element tin, where its value at the beginning of the measurement was 5.58 mg.kg^{-1} and at the next measurement was already 0 mg.kg^{-1}. The observation did not show that the limit values for chemical elements given in ASTM D6595 were exceeded. During the measurement, there was also a decrease, but also an increase of individual chemical elements, which can be attributed to a measurement error or an inhomogeneous sample during testing. It should be noted that some additive elements may also act as contaminants, which can be observed on the element boron, whose value at the beginning of the measurement was 0 mg.kg^{-1} and gradually began to increase to 0.77 mg.kg^{-1}. Also, for the element silicon, which can also act as a contaminant, where at the beginning of the measurement the value was 0 mg.kg^{-1} and at the end of the measurement it was 1.02 mg.kg^{-1}. Silicon is used as an antifoam additive, but from the point of view of the contaminant it is a dust particle or seal. The gradual increase in the value of the additives can be attributed to the activation, after which the value stabilizes and gradually begins to decrease. In the case of phosphorus, an increase in concentration can be seen within 50 hours worked, and after exceeding it, the value began to slowly decrease. For zinc, the value increased until interval 175 hours worked, and then the value began to decrease. Calcium concentration fluctuated during the measurement, but at the end of the measurement the value was higher by 2.27 mg.kg^{-1} compared to the value at the beginning of the measurement. According to author *Deustra et al. (2021)* environmentally friendly hydraulic fluids offer great potential due to their thermal properties in terms of temperature dependence of viscosity (viscosity index). Author *Kosiba et al. (2017)* and *Halenár et al. (2018)* states that ecological hydraulic fluids are biodegraded by microorganisms in the presence of oxygen, phosphorus, nitrogen as well as trace amounts of minerals. Tested working fluid is suitable for use in agricultural and forestry machines operating in an environmentally sensitive environment.

ACKNOWLEDGMENT

This publication was supported by the Operational Program Integrated Infrastructure within the project: Demand-driven research for the sustainable and inovative food, Drive4SIFood 313011V336, cofinanced by the European Regional Development Fund.

REFERENCES

1. Deuster, S., Schmitz, K. (2021) Bio-Based Hydraulic Fluids and the Influence of Hydraulic Oil Viscosity on the Efficiency of Mobile Machinery. *Sustainability*, 13 (14)
2. Halenár, M., & Nosian, J. (2018). Laboratory equipment for testing hydrostatic transducers. In *MendelNet* (pp. 418-423).
3. Hujo, Ľ., Jablonický, J., & Tkáč, Z. (2017). Návrh inovatívneho laboratórneho simulačného zariadenia na skúšanie hydrostatických prevodníkov a hydraulických kvapalín. Nitra: SPU. 140 s. ISBN 978-80-552-1645-4.
4. Hujo, Ľ., Nosian, J., Zastempowski, M., Kosiba, J., Kaszkowiak, J., & Michalides, M. (2021). Laboratory test of hydraulic pump operating load with monitoring of changes in the physical properties. *Measurement & Control*, 54 (3-4), 243-251.
5. Janoško, I., Černecký, J., Brodnianska, Z. & Hujo, Ľ. (2016). Environmentálne technológie a technika. 1. vyd. Nitra. Slovenská poľnohospodárska univerzita, 2016. 306 s. ISBN 978-80-552-1604-1.
6. Kosiba, J., & Hujo, Ľ. (2017). Výskum degradačných procesov ekologických kvapalín v procese prevázdkových skúšok. Nitra: SPU, ISBN 978-80-552-1733-8.
7. Kučera, M., Aleš, Z., & Pexa, M. (2016). Detection and charac-terization of wear particles of universal tractor oil using of particles size analyser. *Agronomy Research*, 14 (4), 1351 – 1360.
8. Majdan, R., Olejár, M., Abrahám, R., Šarac, V., Uhrinová, D., Jánošová, M., & Nosian, J. (2018). Pressure surge analysis of a test bench for biodegradable hydraulic oil. Tribology in *Industry*, 40 (2), 183-194
9. Majdan, R., Abrahám, R., Uhrinová, D., & Nosian, J. (2019). Contamination of transmission and hydraulic oils in agricultural tractors and proposal of by-pass filtration system. *Agronomy Research*, 17 (1), 1107-1122.

10. Nosian, J., Hujo, Ľ., Zastempowski, M., & Janoušková, R. (2021). Design of laboratory test equipment for testing the hydrostatic transducers. *Acta Technologica Agriculturae*, 24 (1), 35-40.
11. Pochi, D, Fanigliulo, R., Bisaglia, C., Cutini, M., Grilli, R., Fornaciari, L., Betto, M., Pari, L., Gallucci, F., Capuzzi, L., Sagliano, A., Palmieri, F., & Chiatti, G. (2020). Test Rig and Method for Comparative Evaluation of conventional and Bio-Based Hydraulic Fluids and Lubricants for Agricultural Transmissions. *Sustainability*, *12* (20).
12. Tkáč, Z., Majdan, R., & Kosiba, J. (2014). Výskum vlastností ekologických kvapalín a nových testovacích metód mazacích olejov. Nitra: SPU, ISBN 978-80-552-1140-4.
13. Turza, J., & Kopiláková, B. (2011). Kombinovaný stand pre meranie hydraulických prvkov. Hydraulicka a pneumatika. In *Časopis pre hydrauliku, pneumatiku a automatizačnú techniku* (pp. 60-64).

Corresponding author:
doc. Ing. Ľubomír Hujo, PhD., Department of Transport and Handling, Faculty of Engineering, Slovak University of Agriculture in Nitra, Tr. A. Hlinku 2, Nitra 949 76, Slovak Republic, phone: +421 376414128, e-mail: lubomir.hujo@uniag.sk

DISCRETE ELEMENT MODELS OF A COHESIVE SOIL

Rostislav CHOTEBORSKY[1], Jiří KURE[2], Egidijus KATINAS[2]

[1]*Department of Material Science and Manufacturing Technology, Faculty of Engineering, Czech University of Life Sciences, Kamýcká 129, 165 21 Prague – Suchdol, Czech Republic*
[2]*Department of Electrical Engineering and Automation, Faculty of Engineering, Czech University of Life Sciences, Kamýcká 129, 165 21 Prague – Suchdol, Czech Republic*

Abstract
The soil tensile test was performed to analyze the cohesive soil model. The results were obtained experimentally and from the simulation using the discrete element method with the new bond model suggested by the Rocky DEM software. The simulated tensile test results showed good agreement with the experimental results done in the laboratory. Thereafter, the effect of Young's modulus, normal stiffness, normal stress limit, tangential stiffness, and tangential stress limit was analyzed to generate maximal force, power, and stiffness during the simulation. As well as, multivariate equations were suggested to describe the influence of previously mentioned properties.

Key words: *soil; discrete element method; mechanical properties; cohesion.*

INTRODUCTION

Tillage or non-tillage operations are carried out using mechanical energy, commonly using a tractor-drawn tool to achieve cutting, inversion, pulverization, and other types of soil movement. The energy required for soil processes accounts for a significant proportion of total energy used in crop production. With high fuel prices and increasing pressure on emissions, minimizing the energy used in crop production is essential. In soil processing, decreasing the draught forces and optimizing vertical forces are desired to reduce energy consumption. However, the experimental procedures involved have a high cost, and the extrapolation of the results to all conditions is uncertain (*Mattetti, Varani, Molari, & Morelli, 2017*). With the rapid development in computer technology, researchers have employed numerical methods to model the soil-tool interaction.

Numerical methods (*Mouazen & Neményi, 1999*), including the finite element method (FEM) and discrete element method (DEM), were also used to simulate the interaction between cohesionless soil and tillage tools (*Asaf, Rubinstein, & Shmulevich, 2007*). These methods could calculate tool forces and simulate soil loosening (*Mouazen & Neményi, 1999*). In DEM simulation, mixing and cracking propagation can be simulated. It is well-known that cohesive forces exist between soil particles, which are attributed to liquid bridges and living organisms with very complex behaviors (*Cundall & Hart, 1992*). Although these forces must be accounted in the DEM simulations, a few reports about this point can be found in the literature on soil–tool interaction, where is presented chisel motion in the soil (*Du et al., 2022; Katinas, Chotěborský, Linda, & Jankauskas, 2019; Kešner et al., 2021; Mak, Chen, & Sadek, 2012; Tamás, Jóri, & Mouazen, 2013; Ucgul, Saunders, & Fielke, 2018)*.

Tsuji's report (*Tsuji et al., 2012*) included several models for cohesion are classified into non-physical, microscopic, and macroscopic models. The latter describes models that are not derived from a micromechanical origin of cohesion, but their formulation is oriented on the macroscopic effect of cohesion. The studies mentioned above about capillary cohesion are examples of the microscopic approach. It is suggested (*Obermayr, Vrettos, Eberhard, & Däuwel, 2014; Tsuji et al., 2012*), to use models derived from macroscopic considerations for practical engineering problems, while the microscopic models may serve for calibration purposes.

Currently, the DEM method is widely used in the study of rocks (*Liu et al., 2022*), soils *(Ding, Song, & Yue, 2022; Dun, Yue, Huang, & Zhang, 2022; Foldager et al., 2022; Gao, Yu, Wang, Li, & Shi, 2022; P. Wang & Yin, 2022; J. Wu, Shen, Yang, & Feng, 2022*), powders, grains *(Guo, Zheng, Zang, & Chen, 2022; M. Wu & Wang, 2022*) or agriculture (*Guo et al., 2022*) because it can adequately describe discrete behaviors of these materials.

The present paper investigates cohesion soil model by Discrete Element Method, considering the prestress and the cohesive forces formed by bond bridges among neighboring soil grains. The aim is to

explore the evolution of the behavior of soil grains and their relationship with the mechanical properties of cohesive soil.

MATERIALS AND METHODS

Discrete element model for cohesive soil

This contribution is focused on the model for cohesive soil. The adhesive force is added to the adhesionless material interaction. For the discrete element model shown here, only forces laws for the contacts between adjacent particles are given. Used software RockyDEM provides all other necessary steps in the simulation, like contact detection, overlaps, and time integration of the particle dynamics and takes care of input and output operations. The description of these steps is omitted here for brevity.

Normal force model

The normal force model is described as a hysteretic linear spring model. This model, proposed by Walton & Braun (*Walton & Braun, 1986*), was referred to as the linear hysteresis model. This elastic-plastic (repulsive and dissipative) normal contact model allows simulation of the plastic energy dissipation on contact without introducing the overhead of long simulation time. In addition, since no viscous damping term is used, the energy dissipation is not dependent on the relative velocities of neighboring particles, making the energy dissipation insensitive to other contacts. An additional advantage of this model is that compressible materials can be accurately modeled because the contact forces can be almost zero even at residual overlaps.

$$F_n^t = \begin{cases} min\left(K_{nl}s_n^t, F_n^{t-\Delta t} + K_{nu}\Delta s_n\right) & if\ \Delta s_n \geq 0 \\ max\left(F_n^{t-\Delta t} + K_{nu}\Delta s_n, \lambda K_{nl}s_n^t\right) & if\ \Delta s_n < 0 \end{cases} \quad (1)$$

$$\Delta s_n = s_n^t - s_n^{t-\Delta t} \quad (2)$$

where F_n^t and $F_n^{t-\Delta t}$ are normal elastic-plastic contact forces at the current time t and at previous time $t - \Delta t$, respectively, where Δt is the time step, Δs_n is the change in the normal contact overlap during the current time. It is assumed positive as particles approach each other and negative when they separate. s_n^t and $s_n^{t-\Delta t}$ are normal overlap values at the current and previous time, respectively. K_{nl} and K_{nu} are the values of loading and unloading contact stiffness, respectively. A typical cycle of loading/unloading is placed in Fig. 1.

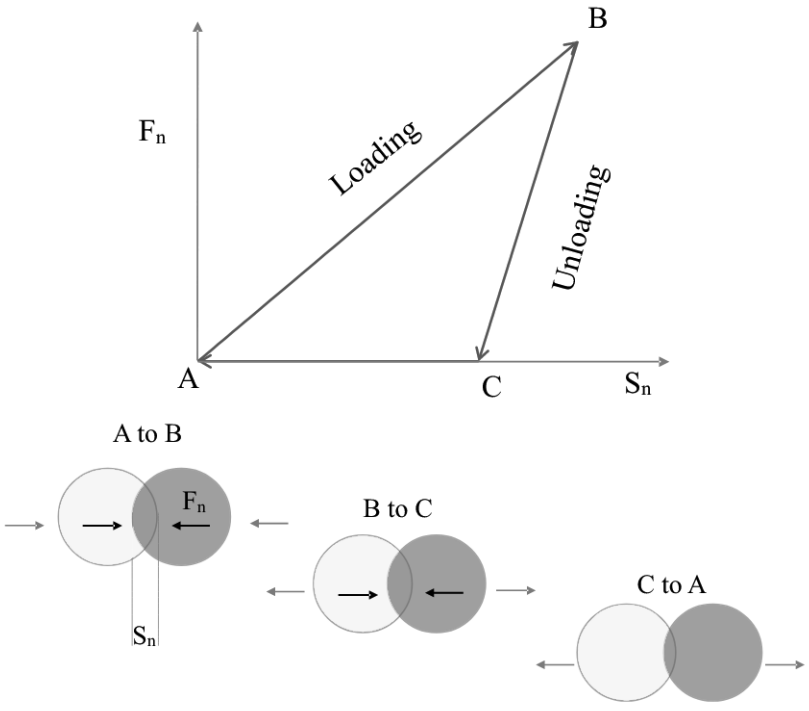

Fig. 1 Walton & Braun normal contact model.

The loading and unloading stiffnesses are defined by the particle size, the bulk Young's modulus, and the restitution coefficient of contacting materials. The last two are the user inputs into RockyDEM. The coefficient of restitution ε in Rocky is a measure of energy dissipation for the contacting pair of materials. For the contact of two particles or a particle with a boundary, the loading and unloading equivalent stiffnesses are defined, respectively, as

$$\frac{1}{K_{nl}} = \begin{cases} \frac{1}{K_{nl,p1}} + \frac{1}{K_{nl,p2}} & for\ particle\text{–}particle\ contact \\ \frac{1}{K_{nl,p}} + \frac{1}{K_{nl,b}} & for\ particle\text{–}boundary\ contact \end{cases} \quad (3)$$

$$K_{nu} = \frac{K_{nl}}{\varepsilon^2} \quad (4)$$

The individual stiffnesses corresponding to a particle and a boundary are computed, respectively, as

$$K_{nl,p} = E_p L \quad (5)$$

$$K_{nl,b} = E_b L \quad (6)$$

where E_p is bulk Young's or elastic modulus of the particle material, E_b is Young's modulus of boundary material, L is the particle size. In long-term contacts, for instance, among particles in a stockpile, the hysteretic linear spring model can give rise to oscillations of very small amplitudes on the normal force and the overlap.

Tangential force model

The tangential force model is the linear spring coulomb limit model. In this model, tangential force is elastic-frictional force. If the tangential force were considered purely elastic, the value at time *t* would be:

$$F_{t,e}^{t} = F_t^{t-\Delta t} + K_t \Delta S_t \quad (7)$$

Where $F_t^{t-\Delta t}$ is the value of the tangential force at a previous time, ΔS_t is the tangential relative displacement of the particles during the timestep, K_t is tangential stiffness (calculated as loading stiffness times tangential stiffness ratio) – this calculation included Young's modulus of particles and their diameter (*Yeom et al., 2019*).

Adhesive (cohesion) force model

In the macroscopic scale, cohesive materials are characterized by having shear strength even at minimal confining pressure. It is described by a cohesive intercept ***c*** of the shear strength envelope.

The bond model implemented similar models described in the papers of Gimenez and Potyondy *(Potyondy & Cundall, 2004; Sangrós Giménez, Finke, Nowak, Schilde, & Kwade, 2018*). In this model, a bond is a massless entity of cylindrical shape attached to a pair of neighbor particles that exerts elastic and viscous forces and moments on them as a reaction to deformations caused by their relative motion. If the external load acting on a bond exceeds its specified strength, it will break, and its bonding action over the particles will be the case. The two particles are located at a distance *h* lower than the activation distance given by eq (8)

$$h_{ac} = f_{ac}(r_i + r_j) \quad (8)$$

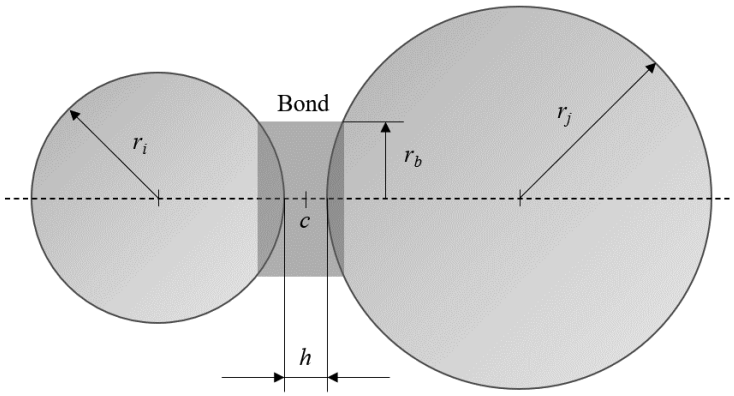

Fig. 2 Geometry of the bond model between two spherical particles of different sizes

where r_i (m) and r_j (m) are the radii of the bonded particles, as shown in Fig. 2, while f_{ac} (-) is an input parameter as "distance factor". The activation of bonds happens only once at a specific time during a simulation. The radius of the bond between two particles depends only on the radii of those particles

$$r_b = \frac{r_i r_j}{r_i + r_j} \quad (9)$$

The bond model implemented in this module also includes the possibility of adding particle-boundary bonds to the simulation. Those bonds share all characteristics described earlier for particle-particle bonds, except the activation distance, in this case, is given simply by

$$h_{ac} = 2 f_{ac} r_p \quad (10)$$

where f_{ac} is the corresponding "distance factor" and r_p is the radius of the bonded particle. Similarly, the radius of the corresponding bond will be directly $r_b = r_p$ in that case.

At the time of its activation, a bond is undeformed. From that time on, any relative motion of the bonded particles will cause deformation on the bond, to which it will react exerting forces and moments opposing to that relative motion. The bond deformation can be linear or angular, the former caused by both the translational and rotational motion of the bonded particles. At the same time, the latter is only a consequence of their rotational motion. In the module, both types of deformation are calculated incrementally, starting from the time of bond activation, t_{ac}. Thus, the linear deformation of a bond at any given time t is provided by

$$s^b = \sum_{t_{ac}}^{t} v_c^{rel} \Delta t \quad (11)$$

where v_c^{rel} is the instantaneous relative velocity at the center point of the bond c, while dt is the simulation timestep. The relative velocity v_c^{rel} is calculated as

$$v_c^{rel} = v_i - v_j + \omega_i \times \Delta r_{i-c} - \omega_j \times \Delta r_{j-c} \quad (12)$$

where v_i and v_j are the translational velocities of the bonded particles, ω_i and ω_j are the rotational velocities of the bonded particles, $\Delta r_{i\text{-}c}$ is the vector that joints the centroid of the particle i to the bond's center point c. The definition is equivalent to the vector $\Delta r_{j\text{-}c}$. The bond in the considered model will oppose the linear deformation s^b by exerting an elastic force on both bonded particles. The normal and tangential components of this force will be given, respectively, by:

$$F_n^b = -K_n^{"} A_b s_n^b \quad (13)$$

$$F_\tau^b = -K_\tau^{"} A_b s_\tau^b \quad (14)$$

where $K_n^{"}$ and $K_\tau^{"}$ are the normal and tangential stiffnesses per unit area, respectively. A_b is the cross-sectional area of the bond, s_n^b and s_τ^b are the normal and tangential components of the bond's linear deformation s^b. The decomposition of the vector s^b is carried out by using the following simple expressions

$$s_n^b = s^b \cdot \hat{n} \quad (15)$$

$$s_\tau^b = s^b - s_n^b \cdot \hat{n} \quad (16)$$

in which $\hat{n}$ is the normal unit vector parallel to the bonds axis.

The breakage criterion is based on the maximum values of the tensile and shear stresses acting on the periphery of the bond. Those values are given, respectively, by

$$\sigma^{max} = -\frac{F_n^b}{A_b} \quad (17)$$

$$\tau^{max} = \frac{|F_\tau^b|}{A_b} \quad (18)$$

During a simulation, the maximum tensile and shear stresses values are constantly monitored for all active bonds. When the tensile strength limit exceeds σ^{max} or the shear strength limit exceeds τ^{max}, the bond breaks and, consequently, is deactivated immediately. After such a breakage, a bond cannot be reactivated again during the simulation.

Tested soil

The soil tests were conducted in Prague-Suchdol, Czech Republic (50°12'78.51″N, 14°37'58.01″ E). The soil of the experimental field was classified as Haplic Chernozem, including clay (6.52%), sand (29.32%), and silt loam soil (64.16%) (*Kodešová et al., 2016*). The average moisture content was 14.3 wt. %.

Model calibration

The Rocky DEM software (version 2022R1, ESSS company, Florianopolis, Brazil) was used for the simulation. The NVIDIA Quadro GV100 graphic card was used to operate Rocky DEM software. The DEM analysis and post-processing were performed with an Intel Xeon Gold 6244 (3.6 GHz) computer, 128 GB RAM, and 2x1TB PCIe SSD.

Tab. 1 Variables setup for cohesive discrete element model

Material interaction	Normal stiffness (NS)	Normal stress limit (NSL)	Tangential stiffness (TS)	Tangential stress limit (TSL)	Bulk young modulus (YM)
	$N \cdot m^{-3}$	kPa	$N \cdot m^{-3}$	kPa	MPa
Particle-particle	$1 \cdot 10^{10}$	1000	$1 \cdot 10^{10}$	1000	20
	$1 \cdot 10^{9}$	500	$1 \cdot 10^{9}$	500	40
	$1 \cdot 10^{8}$	100	$1 \cdot 10^{8}$	100	60
Totally 256 tasks	Static friction 0.7				
	Dynamic friction 0.6				
Particle-boundary	Static friction 0.4				
	Dynamic friction 0.3				

A DEM calibration was performed based on a tensile test of the soil (Fig. 3). The tensile test was conducted in the laboratory. Afterward, the value of the soil strength was used in the evaluation model for the DEM tensile test model. The values from the model were compared with those from the experiment. Iterations were compiled for the subsequent model until the course of the curves showed deviations. The setting of the iterations was performed using a DoE approach, and the effects of the DEM parameter's dependency on the cohesive soil properties were determined. The parameters were obtained by optimization of the model results and validated based on the experimental results.

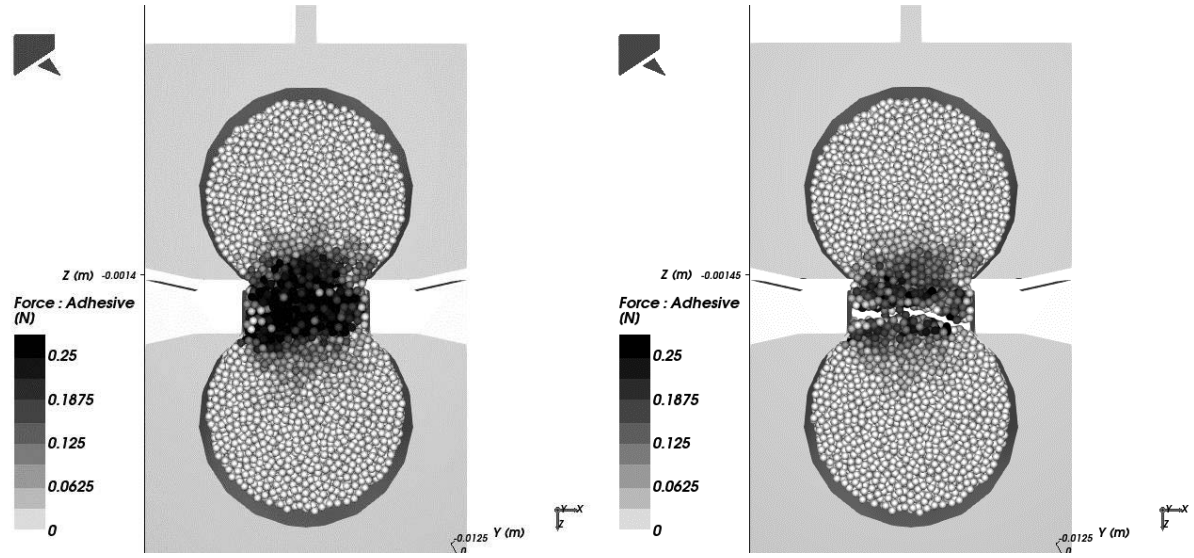

a) b)

c)

Fig. 3 Tensile test of simulated (a and b) and measured (c) samples. Adhesive force distribution in soil sample before rupture (a) and after that (b) with fracture line.

RESULTS AND DISCUSSION

The simulated maximal forces and stiffness agreed with experimental data in all cases. A typical comparison is presented in Fig. 4. Simulated maximal forces of the tensile test were within the limits of experimental test values. Power, calculated like area under the tensile curve, seems to show different values, and relationships between simulated and experimental data are too difficult. Because the power is calculated with deformation, the size of discrete elements can probably play a role in the model's accuracy.

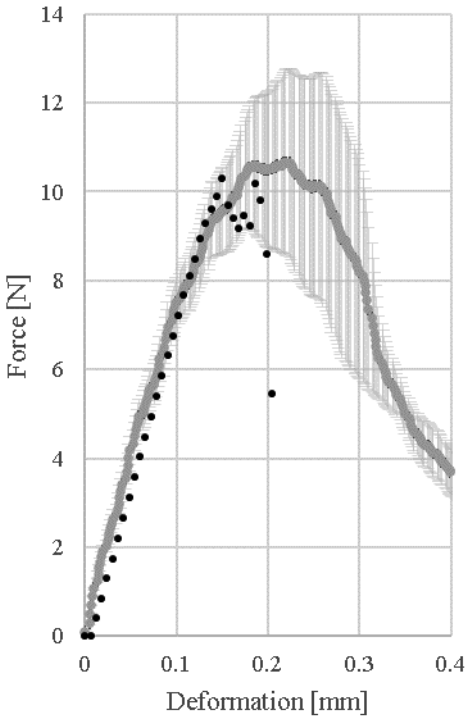

Fig. 4 Simulated (black) and measured (grey) data from the tensile test, mean and standard deviations are represented by limits.

Good practice models need relative accuracy variables for a simulation setup. The results of the ANOVA multi-criteria analysis of the simulations (Fig. 5) were carried out using the DoE approach. This approach creates a relevant response sensitivity to changes in input variables. In other words, how can the model's input data affect the observed result? The effects analysis shows that the most significant influence on the results of the strength model (maximum strength) has the variable "normal stress limit" and "normal stiffness" and their interaction (Fig. 5a). The model is less influenced by the tangential input parameters. In the case of stiffness, however, the model's sensitivity is also affected by Young's modulus and, after that, by the "tangential stress limit" (Fig. 5c). The energy (Fig. 5b) output cannot be adequately interpreted due to the high error rate compared to the experiments. Still, it seems that it will correlate with the force model and its sensitivity.

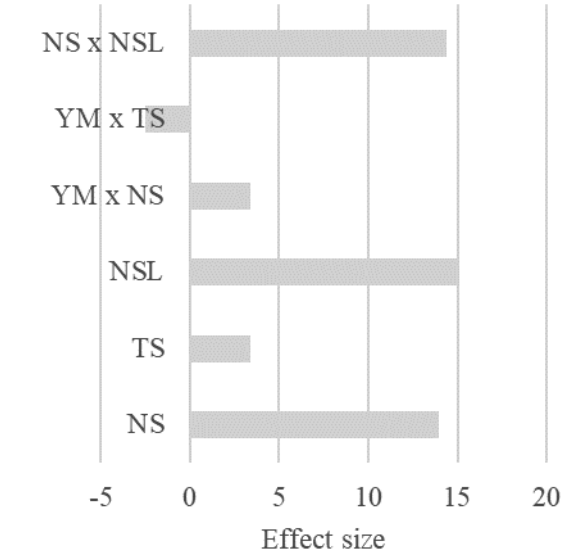

a)

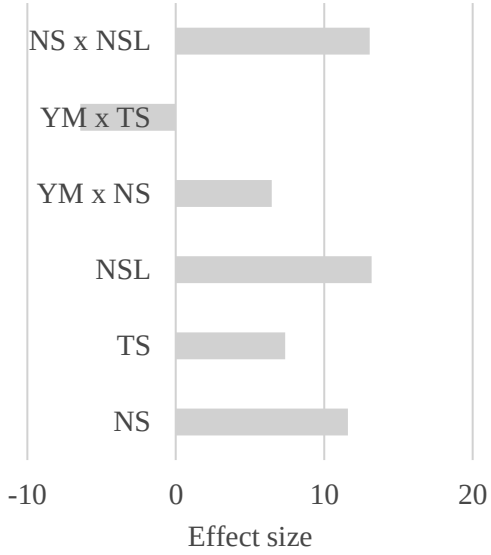

b)

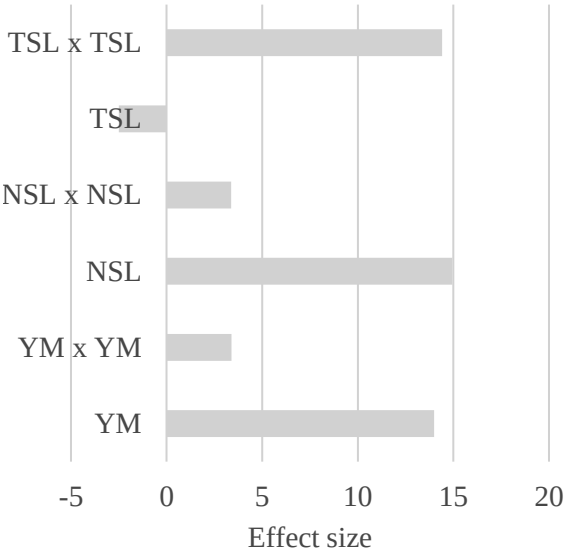

c)

Fig. 5 Effect of variables (Young's modulus, normal stiffness, normal stress limit, tangential stiffness, tangential stress limit) on responses, (a) – maximal forces, (b) – power, (c) stiffness.

Data from 256 models can be generalized in multivariate linear equations. The results of these statistical models are presented below. The determination index shows a close dependence between the phenomenological model and the simulation results, i.e., the experimentally measured values.

$$F_{max} = 16.3 - 7 \cdot 10^{-5} NS + 7.6 \cdot 10^{-5} TS - 4 \cdot 10^{-9} NSL + 9.5 \cdot 10^{-7} YM \cdot NS - 1.2 \cdot 10^{-6} YM \cdot TS + 1.6 \cdot 10^{-14} NS \cdot NSL$$

$$R^2 = 0.93$$

$$Power = 9.5 \cdot 10^{-1} - 2.7 \cdot 10^{-5} NS + 2.6 \cdot 10^{-5} TS - 6 \cdot 10^{-10} NSL + 4.2 \cdot 10^{-7} YM \cdot NS - 4.4 \cdot 10^{-7} YM \cdot TS + 2.4 \cdot 10^{-15} NS \cdot NSL$$

$$R^2 = 0.94$$

$$Stiffness = 16 + 6.2 \cdot 10^{-1} YM - 5.7 \cdot 10^{-3} YM^2 + 2.4 \cdot 10^{-9} NSA - 2.9 \cdot 10^{-20} NSA^2 + 5 \cdot 10^{-9} TSA - 2.2 \cdot 10^{-20} TSA^2$$

$$R^2 = 0.99$$

The literature does not often describe the cohesive soil model for simulations of agricultural tasks. Most researchers (*Tsuji et al., 2012; X. Wang, Zhang, Huang, & Ji, 2022; Zhang, Zhai, Chen, Zhang, & Huang, 2022)*use cohesionless models or models involving the adhesive properties of discrete elements. Probably one of the reasons is the high sensitivity of the cohesion model to the results of the solution and, therefore, the high demands on the accuracy of the obtained values of the mechanical properties necessary for setting the model. Another disadvantage can be the computational complexity of a model with cohesive properties; compared to a model without cohesion, the computational complexity increases so that the computational time increases up to 10 times. Nevertheless, the cohesive model is more reliable for the soil model within DEM calculations, especially for analyzing the processing of soil and plant residues, than the adhesive or non-cohesive model.

CONCLUSIONS

The simulations and measurement results show the suitability of using a cohesive soil model for DEM. However, by appropriately setting of cohesion model, it is possible to obtain very accurate output values of the model, which is more suitable for agricultural tasks than the cohesion-less or adhesion models.

ACKNOWLEDGMENT

This study was supported by the Internal Grant 2020:31200/1312/3109 agency of the Faculty of Engineering, Czech University of Life Sciences in Prague with the name: Model of bulk matter for interaction solution between agriculture tool and soil.

REFERENCES

1. Asaf, Z., Rubinstein, D., & Shmulevich, I. (2007). Determination of discrete element model parameters required for soil tillage. *Soil and Tillage Research, 92(1–2),* 227–242.
2. Cundall, P. A., & Hart, R. D. (1992). Numerical modelling of discontinua. *Engineering Computations, 9(2),* 101–113.
3. Ding, F., Song, L., & Yue, F. (2022). Study on Mechanical Properties of Cement-Improved Frozen Soil under Uniaxial Compression Based on Discrete Element Method. *Processes 2022, Vol. 10,* Page 324, 10(2), 324.
4. Du, J., Heng, Y., Zheng, K., Luo, C., Zhu, Y., Zhang, J., & Xia, J. (2022). Investigation of the burial and mixing performance of a rotary tiller using discrete element method. *Soil and Tillage Research, 220,* 105349.
5. Dun, H., Yue, P., Huang, N., & Zhang, J. (2021). Discrete Element Simulation on Sand-Bed Collision Considering Surface Moisture Content. *Processes 2022, Vol. 10,* Page 52, 10(1), 52.
6. Foldager, F. F., Munkholm, L. J., Balling, O., Serban, R., Negrut, D., Heck, R. J., & Green, O. (2022). Modeling soil aggregate fracture

using the discrete element method. *Soil and Tillage Research, 218*, 105295.
7. Gao, Y., Yu, J., Wang, Y., Li, W., & Shi, T. (2022). Breakage effect of calcareous sand on pile tip resistance and the surrounding soil stress. *Energy Reports, 8*, 183–190.
8. Guo, X., Zheng, Z., Zang, M., & Chen, S. (2022). A multi-sphere DE-FE method for traveling analysis of an off-road pneumatic tire on irregular gravel terrain. *Engineering Analysis with Boundary Elements, 139*, 293–312.
9. Katinas, E., Chotěborský, R., Linda, M., & Jankauskas, V. (2019). Wear modelling of soil ripper tine in sand and sandy clay by discrete element method. *Biosystems Engineering, 188*, 305–319.
10. Kešner, A., Chotěborský, R., Linda, M., Hromasová, M., Katinas, E., & Sutanto, H. (2021). Stress distribution on a soil tillage machine frame segment with a chisel shank simulated using discrete element and finite element methods and validate by experiment. *Biosystems Engineering, 209*, 125–138.
11. Kodešová, R., Kočárek, M., Klement, A., Golovko, O., Koba, O., Fér, M., … Grabic, R. (2016). An analysis of the dissipation of pharmaceuticals under thirteen different soil conditions. *Science of The Total Environment, 544*, 369–381.
12. Liu, Z., Li, J., Zhao, Q., Wang, J., Liu, T., & Zhang, Q. (2022). Gradation Design of Phosphorus Tailing–Graded Waste Rock Subgrade Filling Using Discrete Element Method. *Minerals, 12(5)*, 573.
13. Mak, J., Chen, Y., & Sadek, M. A. (2012). Determining parameters of a discrete element model for soil–tool interaction. *Soil and Tillage Research, 118*, 117–122.
14. Mattetti, M., Varani, M., Molari, G., & Morelli, F. (2017). Influence of the speed on soil-pressure over a plough. *Biosystems Engineering, 156*, 136–147.
15. Mouazen, A. M., & Neményi, M. (1999). Finite element analysis of subsoiler cutting in non-homogeneous sandy loam soil. *Soil and Tillage Research, 51(1–2)*, 1–15.
16. Obermayr, M., Vrettos, C., Eberhard, P., & Däuwel, T. (2014). A discrete element model and its experimental validation for the prediction of draft forces in cohesive soil. *Journal of Terramechanics, 53(1)*, 93–104.
17. Potyondy, D. O., & Cundall, P. A. (2004). A bonded-particle model for rock. International *Journal of Rock Mechanics and Mining Sciences, 41(8)*, 1329–1364.
18. Sangrós Giménez, C., Finke, B., Nowak, C., Schilde, C., & Kwade, A. (2018). Structural and mechanical characterization of lithium-ion battery electrodes via DEM simulations. *Advanced Powder Technology, 29(10)*, 2312–2321.
19. Tamás, K., Jóri, I. J., & Mouazen, A. M. (2013). Modelling soil–sweep interaction with discrete element method. *Soil and Tillage Research, 134*, 223–231.
20. Tsuji, T., Nakagawa, Y., Matsumoto, N., Kadono, Y., Takayama, T., & Tanaka, T. (2012). 3-D DEM simulation of cohesive soil-pushing behavior by bulldozer blade. *Journal of Terramechanics, 49(1)*, 37–47.
21. Ucgul, M., Saunders, C., & Fielke, J. M. (2018). Comparison of the discrete element and finite element methods to model the interaction of soil and tool cutting edge. *Biosystems Engineering, 169*, 199–208.
22. Walton, O. R., & Braun, R. L. (1986). Viscosity, granular-temperature, and stress calculations for shearing assemblies of inelastic, frictional disks. *Journal of Rheology, 30(5)*, 949–980.
23. Wang, P., & Yin, Z.-Y. (2022). Effect of particle breakage on the behavior of soil-structure interface under constant normal stiffness condition with DEM. *Computers and Geotechnics, 147*, 104766.
24. Wang, X., Zhang, Q., Huang, Y., & Ji, J. (2022). An efficient method for determining DEM parameters of a loose cohesive soil modelled using hysteretic spring and linear cohesion contact models. *Biosystems Engineering, 215*, 283–294.
25. Wu, J., Shen, Y., Yang, S., & Feng, Z. (2022). Simulation of Track-Soft Soil Interactions Using a Discrete Element Method. *Applied Sciences 2022, Vol. 12*, Page 2524, 12(5), 2524.
26. Wu, M., & Wang, J. (2022). Constitutive modelling of natural sands using a deep learning approach accounting for particle shape effects. *Powder Technology, 404*, 117439.
27. Yeom, S. Bin, Ha, E., Kim, M., Jeong, S. H., Hwang, S. J., & Choi, D. H. (2019). Application of the Discrete Element Method for Manufacturing Process Simulation in the Pharmaceutical Industry. *Pharmaceutics 2019, Vol. 11*, Page 414, 11(8), 414.

28. Zhang, L., Zhai, Y., Chen, J., Zhang, Z., & Huang, S. (2022). Optimization design and performance study of a subsoiler underlying the tea garden subsoiling mechanism based on bionics and EDEM. *Soil and Tillage Research*, *220*, 105375.

Corresponding author:
Asc. Prof. Ing., Rostislav Choteborsky, Ph.D., Department of Material Science and Manufacturing Technology, Faculty of Engineering, Czech University of Life Sciences Prague, Kamýcká 129, Praha 6, Prague, 16521, Czech Republic, phone: +420 22438 3274, e-mail: choteborsky@tf.czu.cz

APPLICATION OF DIGITAL TECHNOLOGY IN AGRICULTURE: POTENTIAL SUPPORT FOR WINEGROWERS

Oskars JAVA[1], Bernward ASPRION[2], Torsten PRIEBE[2], Eszter SÁRKÖZI[3], Rui Neves MADEIRA[4]

[1]*Institute of Social, Economic and Humanities Research, Vidzeme University of Applied Sciences, Latvia*
[2]*Center for Artificial Intelligence, St. Pölten University of Applied Sciences, Austria*
[3]*Institute of Technology, Hungarian University of Agriculture and Life Sciences, Hungary*
[4]*Sustain.RD, Escola Superior de Tecnologia de Setúbal, Inst. Politécnico de Setúbal, Portugal*

Abstract
In agriculture, disease and pest infestation are normal phenomenon, but they reduce the quality of the crop. Likewise, wrong irrigation or fertilization may damage the yield or lead to inefficient use of resources. Lack of adequate decision support tools and user-friendly interaction with advanced technologies are the most critical barriers that prevent the adaption of Precision Agriculture by farmers. In this article, we review the state-of-the art of digital technology in agriculture and present requirements for an ecosystem that goes even further than Precision Agriculture and reaches up to Digital Agriculture. Given the wide coverage of the agricultural sectors, the authors focus on grapevine in this article.

Key words: *digital agriculture; IoT sensors; sensor system; digital twin, grapevine.*

INTRODUCTION

Modern agricultural production is not possible without reliable and up-to-date information about farm operations (*Verdouw et al., 2021*). IoT sensors are increasingly used to collect information about farm operations and the situation in the fields. The collection of data from sensors creates new opportunities for innovation in the field of prediction systems in the vineyard (*European Commission, 2017*). Using IoT sensors leads to large-scale big data that provides valuable information (*Muangprathub et al., 2019*). Big data-driven agriculture offers opportunities to transform traditional decision-making into data-based decision-making (*Sarker et al., 2020*). Traditional agriculture with manual labour and low productivity is being transformed into sustainable, intelligent, efficient, and eco-friendly agriculture by using technologies (*Mitra et al., 2022*). Thanks to modern analysis systems and deep learning techniques, for example, it is possible to identify the changes of a plant being infected and thus notify the farmer in advance (*Udutalapally et al., 2021*). In addition, controlled usage of pesticides and fertilizers helps to increase the crop quality as well as minimizing farming costs (*Nabi et al., 2022*).

The modernization of agriculture is reflected in the application of digital technologies and the development of new agricultural concepts such as Precision Agriculture, Smart Farming and Digital Agriculture. Although these concepts may seem to be similar, there are significant differences between them.

Precision Agriculture is a modern farming management concept using digital technologies to monitor and optimize agricultural production processes (*Schrijver et al., 2016*).

Smart Farming is the use of information and communication technologies for optimization of complex farming/agriculture systems (*Udutalapally et al., 2021*). Smart Farming goes beyond the concept of Precision Agriculture by basing management tasks not only on location but also on data, enhanced by context and simulation awareness, triggered by real-time events (*Sundmaeker et al., 2016*).

In the agricultural sector, digitization is considered as a function of four components, including: Smart Agriculture, Smart Technology, Smart Design and Smart Business (*Elijah et al., 2018*). As a holistic approach, Digital Agriculture uses the knowledge of information science, environmental science, computer and software engineering, system science, GIS (Geographical Information System), GPS (Global Position System), remote sensing technology, and virtual satellite imaging for better integration of soil, climate and environment information with agriculture (*Sarker et al., 2020*).

With proper resource management, technology may be sound, feasible, relevant and quite useful to measure factors like climatic changes, undefined rainfall and high temperature and humidity, therefore helping the farmers to save the cost and time spent upon dangerous fungicide sprays (*Nabi et al., 2022*).

This article aims to identify the needs of winegrowers in particular and reviews the state-of-the-art for addressing these needs through the use of a combination of digital tools and technologies, which includes the identification of technological capabilities. In conclusion, we offer a – work-in-progress – concept for an extensible Digital Agriculture ecosystem for farm monitoring using a Digital Twin and Mixed Reality for data representation and interaction with a simulation model to test different farm management scenarios.

MATERIALS AND METHODS

During the Living Labs of the Erasmus+ project "Engaged and Entrepreneurial European University as Driver for European Smart and Sustainable Regions (E^3UDRES^2)" in Spring 2021, a group of researchers focused on developing a Digital Agriculture solution for winegrowers. The idea of the Living Labs was to bring researchers from the six universities of E^3UDRES^2 initiative together with regional stakeholders. During the Living Labs a research group called "Human Contribution to Artificial Intelligence" was formed, comprising researchers with background in simulation modelling, IoT, machine learning, statistics and big data management. From the challenges and needs submitted by stakeholders it became clear that in each of the six countries (Austria, Belgium, Hungary, Latvia, Portugal, and Romania) grapevine is one of the agricultural sectors and all countries are facing similar problems (e.g., lack of tools and methods to deal with pests and diseases).

In order to examine in detail what has previously been done in the field of applying of digital technology in grapevine, the Scopus and Web of Science databases, and the World Wide Web were used to search for articles containing keywords, such as, Precision Agriculture, Smart Farming, Digital Farming, IoT sensors, sensor system, grapevine, Digital Twin.

Furthermore, in order to specify the requirements of the winegrowers from the perspective of the user, in-depth interviews and workshops were held. The questions were focusing on problems, challenges and needs regarding the cultivation processes that can be addressed by technological solutions. During a structured interview the following work processes were reviewed: canopy, soil, water, nutrient management; weed, disease, pest, insect, fungus and wild life management; weather forecast and frost protection; grapevine management, crop estimation and harvesting. Besides challenges and needs questions were also included to clarify what traditional, Precision Agriculture, Smart Farming and Digital Farming tools have already been used, what are the experiences of the utilization, what is not working and needs to be improved. The survey was carried out through highly different regions of Europe, we got answers from Austria, Hungary, Latvia and Portugal. For instance, in Portugal two interviews were conducted with representatives and members of Association of Wine Growers of the Municipality of Palmela (AVIPE), in Austria with the Federal Office of Viticulture and Pomology (Wein und Obst Klosterneuburg RTD).

RESULTS AND DISCUSSION

Results are divided into subsections where the authors conclude what is discovered from the literature review, what is discovered from in-depth interviews with winegrowers and what kind of Digital Agriculture ecosystem is proposed to make it easier for winegrowers to work using big data-driven disease detection and optimal resource-utilization tool.

Literature review

When considering Digital Agriculture, farmers' needs as well as their attitudes or perceptions towards these technologies play a crucial role. This can be done by drawing on published surveys and/or asking individual farmers.

In a survey by Kernecker et al. (*2020*), 287 farmers (from the arable, orchard, vegetable and vineyard sectors) from 7 EU countries and 22 experts from the agricultural knowledge and innovation system were asked about smart farming technologies (SFT). Winegrowers indicated that among the listed smart farming technologies (recording and mapping technologies, GPS based steering tools, apps and farm management information system (FMIS), and autonomous machines) apps and FMIS are most useful for their farm (*Kernecker et al., 2020*).

Also interesting are the findings that there is a large discrepancy between the daily work requirements and the ability of new technologies and their users to meet these requirements (*Kernecker et al., 2020*).

Users of SFT are frequently confronted with the challenge to interpret data and to assure devices' connectivity and preciseness. Farmers tend to support a positive assessment of SFT in general, but looking at impacts on economic profitability as well as on environmental performance of SFT, the level of conviction is clearly moderate (*Kernecker et al., 2020*).
Kaňovská (*2021*) conducted a survey of 22 small and medium winegrowers from the Czech Republic regarding the benefits and barriers of using of sensors and weather stations. Unfortunately, the needs of the winegrowers were not directly inquired there. The obstacles of using sensors were that it is not necessary to measure so much data or that the usefulness of this information is not clear (*Kaňovská, 2021*).
Methods made available to winegrowers should predict as far in advance as possible, must be as simple as possible, and work with as little data as possible, preferably with data that farmers can access quickly, easy, and cheaply and, if possible, without the need for intensive training. The best approach must consider the availability and/or possibility to have required inputs (required data is sometimes not available), the adequate spatial resolution (field level or regional level), the necessary granularity (information regarding the spatial variability in each area) and required precision (e.g., a simple smartphone camera, despite the loss in quality, can be in many cases a cost-effective alternative to hyper and multispectral cameras, LiDAR, ultrasonic and radar sensors) (*Barriguinha et al., 2021*).
Recently, several studies have looked at the problems of managing and effectively using large numbers of heterogenous devices, and have found a solution in the use of social networking principles and technologies. The guiding motivation is that a social-oriented approach is intended to aid in the discovery, collection, and composition of resources and knowledge offered by distributed objects and networks (*Delnevo et al., 2021*).

In-depth interviews
To understand what are the most urgent needs of the farmers, we conducted several informal in-depth interviews: with a technical adviser of AVIPE, with farmers associated to AVIPE, with a researcher for viticulture and orcharding of Wein und Obst Klosterneuburg RTD, and with a horticultural engineer of MATE Hungarian University of Agriculture and Life Sciences.
From the interviews was learned that the used technologies are well-known, well-adapted, but they are highly labour-demanding and require expertise. The main problem is the shortage of financial resources (high personnel costs) and manpower (unwillingness to work in the agriculture), which causes a critical overload of the present employees. Under these circumstances there is often no capacity for finding, learning and trying out the new technologies, even though it is highly needed and this need is identified. The knowledge base and expertise (and intention) are given even for research, development and innovation, but there is no free capacity for it. To summarize, new technologies are needed to reduce winegrowers' dependency on traditional labour-demanding agriculture management methods, but informative and financial support should be appropriate to implement them.
From the consumer's perspective, the required Digital Agriculture ecosystem:

- brings together different systems making them available to winegrowers,
- is user-friendly and easy to adapt,
- gives information on the management practices,
- suggests appropriate decisions or prevention measures to be taken,
- informs about when and where operations should be performed,
- conveys information on time,
- creates awareness among winegrowers so that only necessary plant protection is carried out,
- measures correctly so that it could give accurate information about, e.g., level of infection or possible emergence of a disease.
- is capable of identifying the situation in each row, individually for each plant,
- supports reliable means of communication with the farmer,
- allows networking (sharing experience and sensor data with other winegrowers),
- is cost effective, and
- reflects independently host, pathogen, and environmental interaction, etc.

A Digital Agriculture ecosystem

In view of the variety of crops, the group of researchers chose to create a Digital Agriculture ecosystem specifically for winegrowing purposes, with a potential to extending its use in future to other plant species that are grown in lines between which a self-driving drone can drive through. The principle of an on-surface-driving drone, to the contrary to a flying drone, was chosen (1) to allow it to move autonomously in closed areas, thereby (2) removing the need for a licensed drone pilot, while (3) complying with existing legislative requirements allowing the use of self-driving drones, such as lawn mowers and vacuum cleaners, in most countries.

To meet the demands arising from our literature review and in-depth interviews, the group of researchers propose a Digital Agriculture ecosystem using a Digital Twin concept and Mixed Reality applied to the grapevine field. A Digital Twin is a dynamic representation of a real-life object that mirrors its states and behaviours across its lifecycle and that can be used to monitor, analyse and simulate current and future states of and interventions on these objects, using data integration, artificial intelligence and machine learning (*Verdouw et al., 2021*). Basically, a Digital Twin architecture is composed of a physical object in real space, a digital representation of this object in the virtual space and the connection between the virtual and real space for transferring data and information (*Grieves & Vickers, 2017; Redelinghuys et al., 2019; Verdouw et al., 2021*). The Digital Twin would allow observing, and ultimately simulation of the various internal and external influence factors with a focus on pest and disease detection (and ultimately prediction). Another ambition is to contribute to optimal resource-utilization, e.g., irrigation, fertilization. These solutions lead not only to reducing the costs and necessary resources such as water and chemical pesticides, but also to minimizing pressure on the environment (*Sarker et al., 2020*). Soil health is yet another application of the planned monitoring and prediction capabilities.

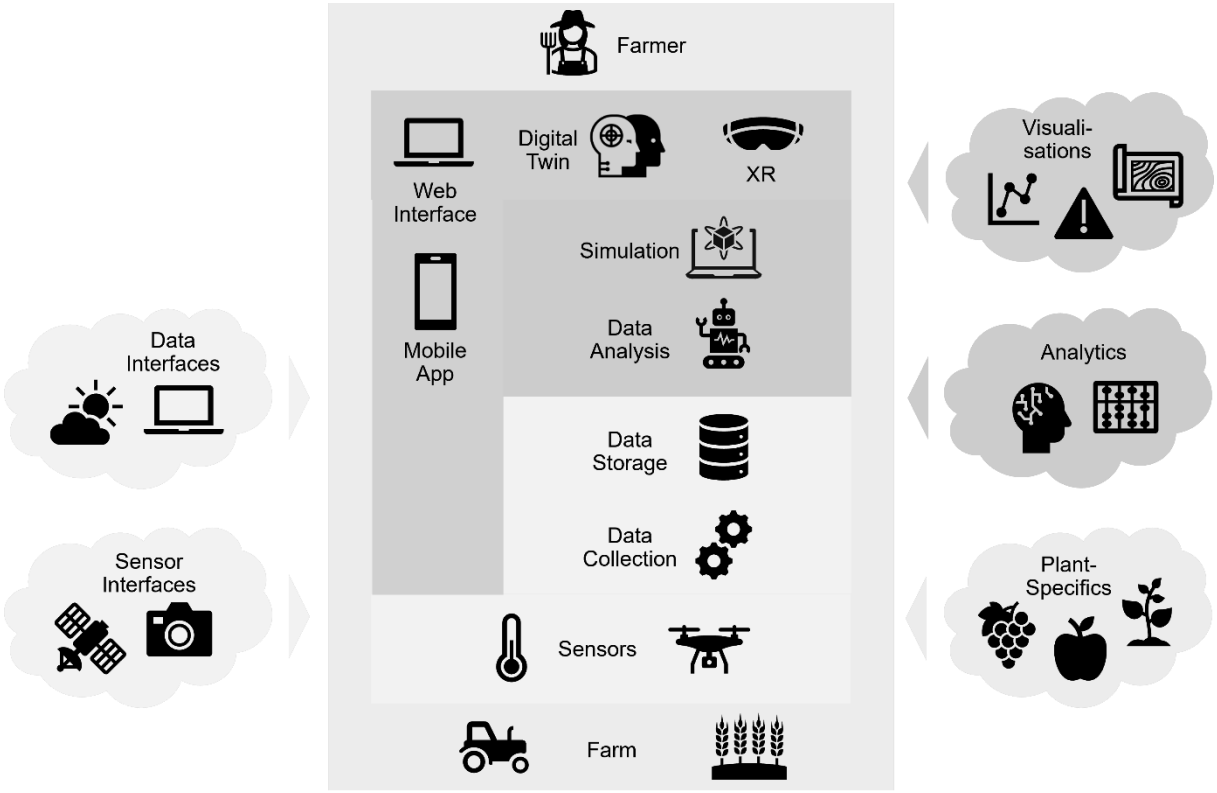

Fig. 1. Proposed Digital Agriculture ecosystem overview and extensibility

Figure 1 shows a high-level representation of the proposed Digital Agriculture ecosystem. It includes the following key solutions based on preliminary concepts (*Ojha et al., 2015*), which should be easily replaceable and extendable due to the modular nature of the proposed ecosystem:

- Wide range of sensors and other input data;
- Wide range of analytics tools and visualization outputs.

Given that not all farmers have applied SFT to manage their fields, it is intended to establish a three-level engagement where each subsequent one requires greater involvement of the farmer, while providing more detailed feedback:

- Smartphone mode. A user-friendly toll-free mobile app and only external data are used. The user receives rather general alerts and management recommendations from the data analysis service.
- Stationary sensor mode. A mobile or web app, external data and IoT sensor measurements from the field are used. More detailed data enables the data analysis service, thus providing the user with more detailed, tailor-made intervention proposals.
- Virtual twin mode. A mobile or web app, external data, IoT sensor measurements and a mobile sensor system are used. The mobile sensor system provides the possibility to generate a Digital Twin, thus the user can interact with the simulation service, test different management scenarios and consider strategic intervention proposals.

Various levels of the Digital Agriculture ecosystem are necessary at the first stage to enable productivity to be improved and environmental impacts to be reduced without financial contribution. After gaining trust in the system, acquiring additional IoT sensors enables productivity to be further improved and environmental impacts to be made even more neutral.

One impact of using the proposed system would be larger yields, since it will be possible to deal with pests and diseases in early stage, which leads to less pesticides and fungicides, which leads to clean and healthy food. It would also help to make more efficient use of resources such as water and fertilizer, thereby reducing the costs of winegrowers.

CONCLUSIONS

Literature review and in-depth interviews shows that the team of researchers is on the right track and that the job started on the Digital Agriculture ecosystem during the Living Labs is the right way to go. Considering the development of IoT sensors, data mining, machine learning etc., technological capabilities are available to establish an extensible ecosystem which helps winegrowers to deal with agricultural issues.

Farmers do not need general management advices, but a notification system that would warn of potential problems on their farm, explicitly providing their location and advising a possible solution.

A Digital Agriculture ecosystem consisting of sensitive and specific sensor devices allowing an automated non-stop monitoring of vineyards would (1) allow a temporally and spatially precise application of plant protection products and, in consequence, (2) allow a reduction of pesticides and thus their impact on the environment, as well as (3) reduce the winegrower's risk of economic losses due to plant diseases and pests, (4) it would also help to make more efficient use of resources such as water and fertilizers, thereby reducing the costs of winegrowers.

Next steps in further research are (1) to identify existing databases worldwide that collect information to be included in the Digital Agriculture ecosystem (e.g., meteorological data, disease and pest distribution, multispectral data, land surface data etc.), (2) to identify sensor capabilities to create a mobile sensor system for local information acquisition, (3) to adapt the Digital Twin approach to bog ecosystem management *(Cirulis et al., 2022)* for agricultural use, (4) to run first case studies to test the prototype and get feedback from winegrowers.

ACKNOWLEDGMENT

This study was supported by Erasmus+ project "Engaged and Entrepreneurial European University as Driver for European Smart and Sustainable Regions (E^3UDRES^2)" no 101004069.

REFERENCES

1. Barriguinha, A., de Castro Neto, M., Gil, A. (2021). Vineyard yield estimation, prediction, and forecasting: A systematic literature review. *Agronomy*, *11*(9), 1789, 1-27.
2. Cirulis, A., Taube, L., Erics, Z. (2022). Automated Generation of Digital Twin in Virtual Reality for Interaction with Specific Nature Ecosystem. *Lecture Notes in Computer*

Scinece, 13309, 187-202, doi:10.1007/978-3-031-05039-8_13.

3. Delnevo, G.; Girau, R.; Ceccarini, C.; Prandi, C. (2021). A Deep Learning and Social IoT approach for Plants Disease Prediction toward a Sustainable Agriculture. *IEEE Internet Things J., 14(8),* 1-8 doi:10.1109/JIOT.2021.3097379.
4. Elijah, O., Rahman, T.A., Orikumhi, I., Yen Lee, C., Hindia, N. (2018). An Overview of Internet of Things (IoT) and Data Analytics in Agriculture: Benefits and Challenges. *IEEE Internet of Things Journal, 5(5),* 3758-3773, doi:10.1109/JIOT.2018.2844296.
5. European Commission (2017). Smart vineyard: management and decision making support for wine producers. *Digital Transformation Monitor*, 1-6.
6. Grieves, M., Vickers, J., (2017). Digital twin: Mitigating unpredictable, undesirable emergent behaviour in complex systems. In Transdisciplinary Perspectives on Complex Systems (pp. 85-113). Springer International Publishing.
7. Kaňovská, L. (2021) "Barriers to and Benefits of the Use of Smart Farming Technologies for Small and Medium Winemakers, Specifically Sensors and Weather Stations: A Pilot Study", AGRIS on-line Papers in Economics and Informatics, Vol. 13, No. 1, pp. 71-85. ISSN 1804-1930, doi:10.7160/aol.2021.130106.
8. Kernecker, M., Knierim, A., Wurbs, A. *et al.* (2020). Experience versus expectation: farmers' perceptions of smart farming technologies for cropping systems across Europe. *Precision Agric, 21,* 34–50, doi:10.1007/s11119-019-09651-z.
9. Mitra, A., Vangipuram, S.L.T., Bapatla, A.K., Bathalapalli, V.K.V. V., Mohanty, S.P., Kougianos, E., Ray, C. (2022). Everything You wanted to Know about Smart Agriculture. 1-45, doi:10.48550/arXiv.2201.04754.
10. Nabi, F.; Jamwal, S.; Padmanbh, K. (2020). Wireless sensor network in precision farming for forecasting and monitoring of apple disease: a survey. *Int. J. Inf. Technol.*, 1-12, doi:10.1007/s41870-020-00418-8.
11. Ojha, T., Mirsa, S., Raghuwanshi, N.S. (2015). Wireless sensor networks for agriculture: The state-of-the-art in practice and future challenges. *Computers and Electronics in Agriculture, 118,* 66-84, doi:10.1016/j/compag.2015.08.011.
12. Redelinghuys, A., Basson, A., Kruger, K., (2019). A six-layer Digital Twin architecture for a manufacturing cell. In Service Orientation in Holonic and Multi-Agent Manufacturing (pp. 412-423). Springer International Publishing, Cham.
13. Sarker, N.I., Islam, S., Murmu, H., Rozario, E. (2020). Role Of Big Data On Digital Farming. *Artic. Int. J. Sci. Technol. Res., 9(04),* 1222-1225.
14. Schrijver, R., Poppe, K., Daheim, C. (2016). Precision agriculture and the future of farming in Europe. Brussels: European Union, ISBN 978-92-846-0475-3, doi:10.2861/020809.
15. Sundmaeker, H., Verdouw, C., Wolfert, S., Pérez-Freire, L. (2016). Internet of Food and Farm 2020. In Digitising the Industry. Internet of Things Connecting the Physical, Digital and Virtual Worlds (pp. 129-150). River Publishers. ISBN: 978-87-93379-82-4.
16. Udutalapally, V., Mohanty, S. P., Pallagani, V., Khandelwal, V. (2021). sCrop: A novel device for sustainable automatic disease prediction, crop selection, and irrigation in internet-of-agro-things for smart agriculture. *IEEE Sensors Journal, 21(16),* 17525-17538.
17. Verdouw, C., Tekinerdogan, B., Beulens, A., Wolfert, S. (2021). Digital twins in smart farming. *Agric. Syst., 189(2021),* 1-19, 103046, doi:10.1016/j.agsy.2020.103046.

Corresponding author:
Ing. Oskars Java, Ph.D., Institute of Social, Economic and Humanities Research, Vidzeme University of Applied Sciences, LV-4201, Latvia, phone: +371 28678558, e-mail: oskars.java@va.lv

A REVIEW OF ENVIRONMENTAL IMPACT OF MOTORIZED VEHICLE ON HUMAN

Debela JIMA[1], Tibor SIPOS[2], Retta ZEWDIE[3]

[1]Budapest University of Technology and Economics, Department of Transportation and Vehicle Engineering, Ph.D. Student, Debela.Jima@edu.bme.hu
[2]Budapest University of Technology and Economics, Department of Transport Technology and Economics, senior lecturer, sipos.tibor@kjk.bme.hu
[3]Departments of Vehicles and Ground Transport, Faculty of Engineering, Czech University of Life Sciences in Prague, Czech Republic, zewdie@tf.czu.cz

Abstract
Globally, around 7 million people die annually due to air pollution. The aim of this review was to define the impact of motorized vehicles on humans due to air pollution. Using 1995 as a baseline, the increase in death and disability due to air pollution was discussed over a five-year period. The review showed that of global death and disability, on average, around 13% and 5% were registered due to air pollution. In total air pollution deaths, motorized vehicles contribute around 7% annually. It shows that air pollution caused by motor vehicles accounts for less than 1% of global deaths. Unprocessed biomass fuel, diesel, and older motorized vehicles are still widely used in developing countries. These contribute to more than half of the air pollution in developing countries. As a result, stakeholders must deal with motorized vehicle air pollution.

Keywords: *air pollution; developing country; diesel effects; motorized vehicle; old vehicle*

INTRODUCTION

Toxic substances emitted from indoor or outdoor sources are a factor in causing environmental degradation. A particulate pollutant is a mixture of microscopic liquid droplets and solid particles found in the air that are generated by vehicle emissions, smoke particles, dust particles, and ash from industries (*World Health Organization, 2020*; *toppr, 2020*). Approximately; half of the world population and up to 90% of rural households in developing countries still rely on unprocessed biomass fuels (*World Resources Institute (WRI), 1998*). In 2020, around 7 million people died due to air pollution; of this, around 0.5 million were caused by motorized vehicles (*World Health Organization, 2020*). This shows 1 out of 14 air pollution deaths occur due to motorized vehicles. In low-income countries, 6% of all deaths are the result of indoor air pollution (*Hannah and Max, 2019*). Motorized vehicles are one of the outdoor air pollutants that emit toxic gases into the environment (*Ostro, 2004*). Emissions and the toxic nature of the gas can vary based on the type and nature of power consumed (*Union of Concerned Scientists, 2014*). The aim of this review is to define the effect of motorized vehicles on air pollution and its severity level on humans. For further consideration and analysis, the review was presented as follows:

EFFECTS OF ENVIRONMENTAL AIR POLLUTION

Climate change is one of the most serious health threats of the twenty-first century. That was caused by air pollution, which is the single largest environmental health risk (*World Health Organization, 2016*). Of the total world population, around 90% of the population breathes polluted air (*World Health Organization, 2018*). Actually, the air quality inside a home can be worse than the air quality outside (*Robert, 2016*; *Budget Home Services, 2020*).

The levels of indoor air pollutants are often 2 to 5 times higher than outdoor (*Medical Associates of Northwest Arkansas, 2020*; *Victoria, 2019*). The most common indoor pollutants and sources are asbestos, biological pollutants, carbon monoxide (CO), pressed wood products, nitrogen dioxide (NO2), indoor particulate matter, etc. (*United State Environmental Protection Agency, 2020*). However, the most common sources of outdoor air pollution are emissions caused by combustion processes from motor vehicles, solid fuel burning, and industry (*Department of Pediatrics, 2019*).

Air pollution can cause human deaths; long-term health effects include heart disease, lung cancer, respiratory disease, birth defects, and damage to other organs *(Texas A & M University, 2019; Lili et*

al., 2019). Air pollution is linked to 9% of global deaths (*Hannah and Max, 2019*). Death rates from air pollution are highest in low-to-middle income countries (*Jos et al., 2018*; *Dr. Susanne, 2018*).

Tab.1 Global number of Death and Disability

	Year	1995	2000	2005	2010	2015	2020	Avg.
Total Population	Death (million)	51.34	52.98	54.02	54.5	56.33	59.3	54.75
	Disability (billion.)	2.55	2.55	2.51	2.47	2.43	2.62	2.52
Air Pollution	Death (million)	7.38	7.32	7.23	7.02	6.9	6.7	7.09
	Disability (million)	130.3	124.4	119.4	116.6	107.6	98.8	116.2

Source: *(United Nations (UN), 2019; Global Burden of Disease Collaborative Network., 2018)*

As shown in Tab.1, globally on average, around 55 million and 2.5 billion people die and become disabled annually. Air pollution contributes to 7 million (13%) and 116 million (5%) of global deaths and disabilities annually. It also shows the total number of deaths and disabilities gradually increases and decreases.

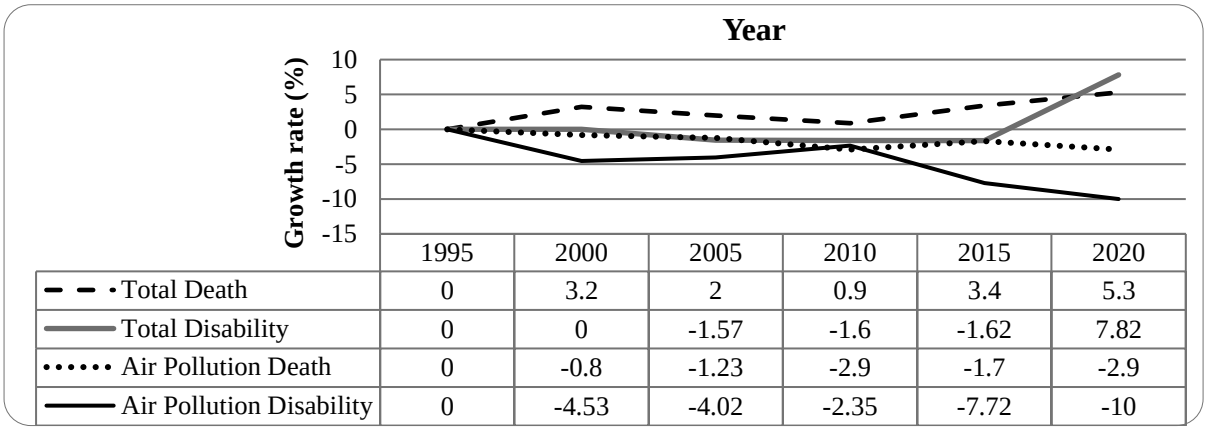

	1995	2000	2005	2010	2015	2020
Total Death	0	3.2	2	0.9	3.4	5.3
Total Disability	0	0	-1.57	-1.6	-1.62	7.82
Air Pollution Death	0	-0.8	-1.23	-2.9	-1.7	-2.9
Air Pollution Disability	0	-4.53	-4.02	-2.35	-7.72	-10

Fig. 1 Annual Growth Rate of Death and Disability

According to Fig. 1, the maximum death and disability growth rates were observed in 2020, using 1995 as a base year within a five-year interval. Relatively, due to air pollution, the maximum reduction in death and disability growth rate was also observed in 2020.

EFFECTS OF MOTORIZED VEHICLE AIR POLLUTION

Motor vehicles emit toxic and carcinogenic compounds *(American Cancer Society, 2020)*. Hydrocarbons and nitrogen oxides contribute to smog, which damages the lungs and aggravates respiratory disease *(Dasom et al., 2018)*. In 2018, diesel vehicles were responsible for nearly half of the health impacts of air pollution from vehicles worldwide, and two-thirds of the impact in India, France, Germany, and Italy *(Joshu, 2019)*. It was estimated that over 80% of people living in urban areas were exposed to motorized air pollution that exceeded the WHO limit. In 2016, over 95% of the world's population was breathing unhealthy air. From this, transportation emissions contributed 32% (*Susan et al., 2019*). Recent evidence indicates that the health problems caused by air pollution may be greater at high concentrations than previously estimated; this would likely happen due to vehicle exhaust emissions increasing *(Joshu, 2019*).

The principal emissions from motor vehicles are greenhouse gases. In vehicles, the principal greenhouse gas is carbon dioxide (CO2), but vehicles also produce other greenhouse gases such as nitrous oxide and methane. For example, diesel vehicles have a higher emission limit for nitrogen oxides than petrol vehicles have a higher emission limit for carbon monoxide (*İbrahim et al., 2014*; *An Australian Government Initiative, 2021*). Once greenhouse gases are released, they can stay in the atmosphere for more than 100 years (*National Academies of Sciences, 2021*). It acts like a blanket around the Earth, trapping energy in the atmosphere and causing it to warm. In 2019, the total CO2 emissions from aviation and motor gasoline combustion were about 22% of the total US energy related CO2 emissions. This resulted in 9% of greenhouse gas emissions from the tailpipe (*U.S. Energy Information Administration, 2020)*.

Vehicle age, type, power consumption, tonnage, speed, etc. play a critical role in defining the amount of gas emitted to the environment. Transportation contributed more than half of the carbon monoxide and nitrogen oxides emitted into the atmosphere in 2013, as well as nearly a quarter of the hydrocarbons (*Union of Concerned Scientists, 2014*). The valuation of health effects associated with diesel vehicles is at least 5 times greater than those associated with petrol vehicles, and around 20 times greater than battery electric vehicles (*Dr. Christinian, 2018*). Close to half of all deaths by transport air pollution are caused by diesel road vehicles (*BreatheLife Campaign, 2019*). By removing cars from cities, it's difficult to reduce emissions (*Audrey, 2018*).

Tab.2 Death due to Total Air Pollution and Motorized Vehicle air pollution

Year	1995	2000	2005	2010	2015	2020	Avg.
Total Air Pollution Death (million)	7.38	7.32	7.23	7.02	6.9	6.7	7.09
Motorized Vehicle Air Pollution Death (million)	0.51	0.7	0.4	0.2	0.4	0.5	0.45

Source: *(Clean Air Coaliation (CCAC) secretariat, 2020; Global Burden of Disease Collaborative Network, 2017; ScienceX Network, 2019)*

As shown in Tab.2, the number of deaths caused by air pollution gradually decreases, but the number of deaths due to motorized vehicle air pollution oscillates up and down. Motorized vehicles contribute approximately 6.5% of all air pollution deaths on an annual basis. It shows a reduction in deaths. It needs special care by the stakeholders.

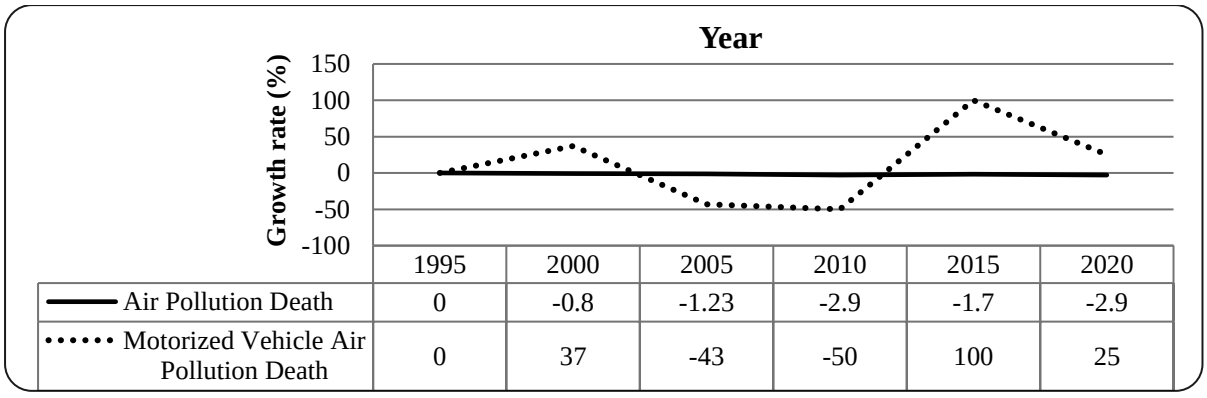

Fig. 2 Death Annual Growth Rate due to Air Pollution

As shown in fig. 2, referencing 1995 as the base year, over a five-year interval the maximum total motorized vehicle air pollution growth rate in deaths was observed in 2015. In consideration of global death, motorized vehicle air pollution contributes around 1% on average annually. This shows that out of 100 people killed, 1 person died due to air pollution resulting from motorized vehicles.

EFFECT OF MOTORIZED VEHICLE AIR POLLUTION IN DEVELOPING NATION

The benefits of motorized vehicles are countless, but the disadvantages are more pollution and energy use *(Daniel, 2004*). The number of motorized vehicles in the world is expected to reach about 1.3 billion by 2020 (*Andrew, 2018*). Between 1990 and 2020, emission reductions from road transport have been lower than originally anticipated over the last two decades due to transport having grown more than expected (*Susan and Timothy, 2007*; *European Environment Agency, 2019*).

China and the USA are the leading polluters in the world in terms of motor vehicles. America generates more than 25% of global warming emissions that come from the transportation sector (*United States Environmental Protection Agency, 2018*). The U.S. has 30% of the world's automobiles, yet contributes to about half of the world's car emissions (*Howstuffworks, 2020*). Air pollution accounts for about 6% of deaths in Austria, France, and Switzerland annually (*World Health Organization Regional Office for Europe, 2015*). European citizens still breathe harmful air, mostly due to weak legislation and poor policy implementation (*European Court of Auditors, 2018*).

Atmospheric pollution has emerged as one of the primary environmental issues in developing countries. China has become the world's largest vehicle market. Vehicle emissions have become a significant

source of air pollution and are ranked 109th out of 180 countries (*Wu et al., 2016*; *Liu et al., 2017*). Globally, the top ten countries with the highest mean exposure to outdoor air pollution include Nepal, India, Niger, Cameroon, Nigeria, and Chad; and Qatar, Saudi Arabia, Egypt, and Bahrain in the Middle East (*Florina and Wendy, 2019*). This shows most developing countries are more responsible for environmental air pollution.

In India, 12.5% of deaths were attributable to air pollution (*India State-Level Disease Burden Initiative Air Pollution Collaborators, 2020*). India has 18.1% of the global population but contributes 26.2% of the global air pollution (*Sahana, 2019*). In Delhi, diesel vehicles were responsible for 62.5% of the total particulate load coming from all vehicle emissions (*Yewande et al., 2015*).

Most African countries import a large number of used vehicles that account for around 40% of the world (*United Nation Environmental Program, 2020*). The poor quality of used vehicles was not only a cause of environmental pollution; it was also a cause of road traffic accidents (*Peter, 2020*). Developing countries are exporting air pollution by importing used vehicles (*Sophie Edwards, 2017*). Even if the number of vehicles were small in developing countries, those tend to have worse air pollution than developed nations. Lack of technology and resources aggravates air pollution (*Nationwide Air Filter Company, 2017*). Vehicles with an age of 5 and above pollute the environment more (*Peter, 2020*; *Cathryn et al., 2014*). The age of the vehicle is a concern and defines the amount of gas emitted to the environment in connection with its power traction type.

CONCLUSION

Air pollution has killed or disabled millions of people worldwide. Motorized vehicle emissions are an outdoor (ambient) air pollutant that causes a large number of deaths and disabilities. Referring to 1995 as a base with an interval of 5 years, the maximum growth rate of global death and disability was registered in 2020. This review indicated that of global death and disability, air pollution contributes around 13% and 5% of death and disability, respectively. From the total global deaths caused by air pollution, vehicle emissions on average contribute to around 0.5 million (7%) deaths on an annual average. Even if the global death rate gradually increases, deaths due to air pollution and disability slightly decrease, and the number of deaths due to motorized vehicle air pollution oscillates up and down. Even so, the number of deaths caused by motorized vehicle air pollution accounted for around 1% of global deaths.

Approximately half of the world's population, as well as up to 90% of rural households in developing countries, are still subjected to air pollution caused by unprocessed biomass fuels. Even though developed nations use more motorized vehicles, the damage caused by vehicle emissions is much worse in developing nations. The reason behind it was that more than half of used vehicles with an age of 5 years and above are dumped in developing nations and most of them consume diesel. As a result, motorized vehicle emissions account for more than half of all air pollution in developing countries. Therefore, in order to overcome these problems, stakeholders must focus on the age of imported vehicles and the type of power consumption they consume in developing countries.

ACKNOWLEDGMENTS

It gives us great pleasure to honor those who contributed their precious time in reviewing and commenting on the report while conducting this review article. The research was supported by OTKA - K20 - 134760 - Heterogeneity in user preferences and its impact on transport project appraisal led by Adam TOROK.

REFERENCE

1. America Cancer Society. (2020). *Diesel Exhaust and Cancer.* USA.
2. An Australian Goverment Initiative. (2021). Vehicle emissions. Australia: Commonwealth of Australia.
3. Andrew Chesterton. (2018). How many cars are there in the world? Urban Guide.
4. Audrey de Nazelle. (2018). What would happen if we removed cars from cities? London: World Economic Forum.
5. BreatheLife Campaign. (2019). Short Lived Climate Pollutants. Bangkok, Thialand: Climate and Clean Air Coalition.

6. Budget Home Services. (2020). *The Air in Your Home is Dirtier than Outside (and What You Can Do About it).* Budget Home Services.
7. Cathryn Tonne et al. (2014). Traffic-related air pollution in relation to cognitive function in older adults. *25(5)*, 674-81. London: Epidemology.
8. Clean Air Coaliation (CCAC) secretariat. (2020). Air pollution is cutting years off lifespans, diesel trucks and buses are a major cause. Nework: UN Environment Programme.
9. Daniel Spreling. (2004). Motorizing the Developing World. California: Transportation Finance.
10. Dasom Kim et al. (2018). Air pollutants and early origins of respiratory diseases. *4(2)*, 75-94. USA: Chronic Dis Transl Med.
11. Department of Pediatrics. (2019). Outdoor Air Pollutants. Georgia: Emory University School of Medicine.
12. Dr. Christinian Brand. (2018). *Cars and vans are responsible for 10,000 early deaths each year.* UK Energy Research Centre. Oxford : Enviromental Change Institute.
13. Dr. Susanne Benner. (2018). Air Pollution Significantly Increases Mortality in Low-Income Countries. Max Planck Institute: SciTechDaily.
14. Europian Court of Auditors. (2018). *Air pollution: Our health still insufficiently protected.* Curia Rationum.
15. Europian Environment Agency. (2019). Emissions of air pollutants from transport. Copenhagen: European Environment Information and Observation Network (Eionet).
16. Florina Pirlea and Wendy Ven-dee Huang. (2019). The global distribution of air pollution. World Bank Group.
17. Global Burden of Disease Collaborative Network. (2017). *Global Burden of Disease Study 2016 (GBD 2016) Results.* Seattle, United States: Institute for Health Metrics and Evaluation (IHME).
18. Global Burden of Disease Collaborative Network. (2018). *Global Burden of Disease Study 2017 (GBD 2017) Results.* Seattle, United States: Institute for Health Metrics and Evaluation (IHME),.
19. Hannah Ritchie and Max Roser. (2019). *The global distribution of deaths from indoor air pollution.* England: Our World In Data.
20. Howstuffworks. (2020). How much air pollution comes from cars?
21. İbrahim Aslan Reşitoğlu et al. (2014). The pollutant emissions from diesel-engine vehicles and exhaust aftertreatment systems. *17*, 15-27. Turkey: Clean Technologies and Environmental Policy.
22. India State-Level Disease Burden Initiative Air Pollution Collaborators. (2020). Health and economic impact of air pollution in the states of India: the Global Burden of Disease Study 2019. *5(1)*, 25-38. India: The Lancet Planetry Health.
23. Jos Lelieveld et al. (2018). Age-dependent health risk from ambient air pollution. London: London School of Hygiene and Tropical Medicine.
24. Joshu Miller. (2019). New study quantifies the global health impacts of vehicle exhaust. *A global snapshot of the air pollution-related health impacts of transportation sector emissions in 2010 and 2015*. The International Council on Clean Transportation,.
25. Lili Xiong et al. (2019). The association between ambient air pollution and birth defects in four cities in Hunan province, China, from 2014 to 2016. *98(4)*. Baltimore: Medicine.
26. Liu et al. (2017). The drivers of local environmental policy in China: an analysis of Shenzhen's environmental performance management system, 2007–2015. *Journal of Cleaner Production., 165*(b), 656–666.
27. Medical Associates of Northwest Arkansas. (2020). Indoor Air vs. Outdoor Air. Northwest Arkansas: Mana Medical Association.
28. National Academies of Sciences. (2021). Policy Implications of Greenhouse Warming: Mitigation, Adaptation, and the Science Base. Washington DC: Sciences Engineering Medicine.
29. Nationwide Air Filter Company. (2017, 10 30). How To Fight Air Pollution In Developing Countries. USA: Camfil.
30. Ostro Bart. (2004). *Out Door Air Pollution: Assessing the enviromental burden disease at national and local level.* Geneva: World Health Organization.
31. Peter Muiruri. (2020, 10 27). Old and unsafe' cars sent to developing world fuelling air pollution, report finds. *Global Development*. The Guardian.

32. Robert Ferris. (2016). *Indoor air can be deadlier than outdoor air, research shows.* CNBC.
33. Sahana Ghosh. (2019). Air pollution major, underappreciated contributor to ill health in India. India: Mongabay.
34. ScienceX Network. (2019). Nearly 50% of transport pollution deaths linked to diesel: study. Physiogory.
35. Sophie Edwards. (2017, January 26). Inside Development. *Unban Sustainability*. Devex.
36. Susan A.Shaheen and Timothy E.Lipman. (2007). Reducing Greenhouse Emissions and Fuel Consumption: Sustainable Approaches for Surface Transportation. *31(1)*, 6-20. California: International Association of Traffic and Safety Sciences (IATSS).
37. Susan Anenberd et al. (2019). A Global Snapshot of the Air Pollution Related Health Impacts of Transportation Sectors Emission in 201 and 2015.
38. Texas A & M University. (2019). Severe air pollution can cause birth defects, deaths. (EurekAlert, Ed.) Texas: American Association for the Advancement of Science (AAAS).
39. toppr. (2020). *Environmental Chemistry.* toppr.
40. U.S Energy Information Administration. (2020, 11 19). Gasoline and the Enviroment. *Gasoline Explained*. USA, USA: Independent Statistics and Analysis.
41. Union of Concerned Sceintists. (2014, July 18). Vehicles, Air Pollution, and Human Health. *Cars and trucks are one of the leading causes of air pollution.* Cambrige, USA.
42. Union of Concerned Scientists. (2014). *Environmental Impacts of Natural Gas.* Cambridge: Union of Concerned Scientists.
43. United Nation Enviromental Program. (2020). Environmental impacts of export of used vehicles to developing world. Niarobi: United Nation.
44. United Nations (UN). (2019). *World Population Prospects.* Nework: Department of Economic and Social Affairs.
45. United State Enviromental Protection Agency. (2020). Indoor Air Quality (IAQ). USA: An official website of the United States government.
46. United States Environmental Protection Agency. (2018). *Greenhouse Gas Emissions from a Typical Passenger Vehicle.* Washington DC: Environmental Protection Agency.
47. Victoria Allen. (2019). *Indoor air pollution is 3.5 times worse than outdoor air pollution and at its peak can be up to 560 times higher, study finds.* UK: Associated Newspapers Ltd.
48. World Health Organization. (2016). A global assessment of exposure and burden of disease. *Ambient air pollution*. Geneva: World Health Organization (WHO).
49. World Health Organization. (2020). *Types of pollutants.* World Health Organization (WHO).
50. World Health Organization Regional Office for Europe. (2015). Economic cost of the health impact of air pollution in Europe. Copenhagen: World Health Oroganization (WHO).
51. World Health Organization,. (2018). 9 out of 10 people worldwide breathe polluted air, but more countries are taking action. Geneva: World Health Organization (WHO).
52. World Health Organozation. (2020). *Air Pollution.* Geneva: World Health Organization (WHO).
53. World Resources Institute (WRI). (1998). *World resources: a guide to the global environment.* Oxford: Oxford University Press.
54. Wu X et al. (2016). Assessment of vehicle emission programs in China during 1998-2013: Achievement, challenges and implications. *Environment Pollution, 2014*, 556-567.
55. Yewande Awe et al. (2015). Clean Air and Healthy Lungs. Delhi: World Bank Group.

Corresponding Author:
Debela Jima, Budapest University of Technology and Economics, Department of Transportation and Vehicle Engineering, Műegyetem rkp. 3, 1111, Budapest, Hungary, phone: +36205815441, email: Debela.Jima@edu.bme.hu

ASSESSMENT OF THE POSSIBILITY OF EXTENDING THE INTERVALS BETWEEN ENGINE OIL CHANGES ON BIOGAS POWERED UNITS

Jerzy KASZKOWIAK[1], Marcin ZASTEMPOWSKI[2], Lubomir HUJO[3]

[1]*Department of Mechanical Engineering,Bydgoszcz University of Science and Technology*
[2]*Department of Mechanical Engineering,Bydgoszcz University of Science and Technology*
[3]*Department of Transport and Handling, Slovak University of Agriculture in Nitra*

Abstract
Intervals between subsequent oil changes in combustion engines are usually specified in operating hours and for most units an oil change is carried out after this period. The possibility of a controlled extension of the oil service life until the next oil change on the one hand reduces engine operating costs, but on the other hand may have a negative effect on engine lifetime.
It is also important to reduce the environmental impact resulting from the reduced consumption of engine oil. Checking the quality of oil may allow you to safely extend oil service life without the risk of reducing an engine lifetime. The article presents the results of a study of selected oil parameters at excessive usage times. It was found that for the engines powered by biogas it is possible to extend the oil change interval by 200 hours.

Key words: *engine oil, biogas, durability.*

INTRODUCTION

Spark-ignition internal combustion engines powered by biogas are not only used in electricity production systems. Despite the use of such solutions, e.g. in buses, this is still the predominant use of internal combustion engines in biogas. Biogas can be produced from biological material. These can include both crops grown specifically for biogas production, organic waste from agricultural production and waste from storage facilities. In addition, sewage, municipal waste and, increasingly, marine algae are used to produce biogas (*Kaszkowiak et al., 2017; Czekała, et al., 2016*). Biogas is produced from renewable sources, which reduces the balance of CO_2 emissions. Due to the diversified raw materials from which biogas is produced, its composition varies (*Bilcan, Le Corre & Delebarre, 2003; Kosiba et al., 2016*). The approximate composition of biogas depending on the substrate from which it is produced is presented in Table 1.

Tab. 1 Selected components of biogas depending on the substrate from which it is produced (*Kwaśny, Banach & Kowalski, 2012*)

Component/substrate	units	Waste from households	Sludge from sewage treatment plant	Waste from agricultural production	Wastes from the agro-food industry
Methane CH_4	[%]	50-60	60-75	60-75	68
Carbon dioxide CO_2	[%]	34-38	19-33	19-33	26
Nitrogen N_2	[%]	0-5	0-1	0-1	-
Hydrogen sulphide H_2S	[ppm]	100-900	1000-4000	3000-10000	100
Oxygen	[%]	0,1-2,0	0,5-1,0	0,5-1,5	1,-1,5

Particularly high differentiation in the composition of biogas can be seen for hydrogen sulphide and methane content. At the present time, the production of biogas as a fuel is becoming particularly profitable, because in addition to waste utilization (as is the case with the use of sewage, municipal waste and waste from the agro-food industry as a substrate), a fuel can be obtained at a relatively low cost. Moreover, the fuel is treated as generated from renewable sources. Furthermore, the fuel is treated as originating from renewable sources. This consequently affects the profitability of using biogas as fuel. It

should be mentioned that biogas used as a fuel is exposed to continuous monitoring of the methane content and volume of impurities.
Specially developed engine oils are most often used to lubricate engines powered by biogas. Biogas as a fuel is characterised by a higher auto-ignition temperature and usually a longer combustion time. This results in more intense heating of the engine oil (*Górniak et al., 2014*). As previous studies have shown, the composition of the biogas feeding the engine also has a significant influence on the condition of the engine oil (*Kaszkowiak et al., 2017*).

MATERIALS AND METHODS

Three spark ignition, supercharged, 380 kW each, type MAN E2842LF322 internal combustion engines were used in the tests. They powered the power generators. The engines were of identical design, powered by biogas. They powered electric generators with a capacity of 340 kW, loaded with an average power of 300 kW. Their load varied only slightly (±5%). They operated at a speed of 1500 rpm [157 rad/s]. The engines were in very good technical condition. The engines had had their engine oil changed before the commencement of the tests. The biogas used to power the engines was purified. The biogas's parameters were monitored systematically with the use of the biogas analyzer BIOTEX MultiPoint. The changes in the content of individual components were slight (less than 1%). The composition of biogas is presented in table 2.

Tab. 2 Composition of biogas powering engines

Component	Content
Methane [%]	65
Hydrogen sulphide [ppm]	17
Carbon dioxide [%]	34,5
Ammonia [ppm]	0

The engine was lubricated with Shell - Mysella S5 S 40, a low ash oil with extended durability, dedicated for engines fuelled with gaseous fuels. Its basic nominal properties are presented in table 3.

Tab. 3 Selected properties of the new Shell – Mysella S5 S 40 oil

Properties	Unit	Value
Kinematic viscosity 100^0C	[mm^2/s]	13,5
Density (15^0C)	[kg/m^3]	890
Flash point	[^{0}C]	230
Ash content	[%wt]	0,48
Alkaline number TBN	[mg KOH/g]	4,5
Acid number TAN	[mg KOH/g]	4,0

The oil change frequency recommended by the manufacturer for the tested engines is 500 operating hours. However, it is suggested that oil parameters should be continuously monitored and, should they deteriorate, an earlier oil change should be carried out. Such a period between oil changes affects the maintenance of the good condition of the engine, but it should be noted that the condition of the oil also affects fuel consumption (*Macian et al., 2015*). The oil condition was monitored in the tests after every 100 hours of operation. Oil change criteria were as follows: silicon increase above 70 ppm, iron increase above 10ppm, potassium increase above 4 ppm, TBN above 5.50 and TAN below 5.00 or viscosity increase above 14.5 or decrease below 13 mm^2/s. Exceeding the permissible value of one of the monitored components is considered as a necessity to change the oil. The tested oil parameters were statistically analysed using the Tukey test at the significance level of 0.05. These values are recommended by the oil producer. The average values of the obtained results are presented in table 4.

Tab. 4 The average values of the selected oil parameters in relation to the operating time

Operating time [h]	100	200	300	400	500	600	700
Si content [ppm]	55^{a}	64^{b}	64^{b}	65^{b}	64^{b}	67^{c}	70^{d}
Fe content [ppm]	5^{a}	7^{b}	7^{b}	9^{bc}	9^{bc}	10^{c}	13^{d}
K content [ppm]	0^{a}	0^{a}	1^{b}	1^{b}	1^{b}	2^{c}	2^{c}
TBN [mgKOH/g]	$4,5^{a}$	$4,7^{b}$	$4,7^{b}$	$4,6^{ab}$	$5,0^{c}$	$5,4^{d}$	$5,7^{e}$
TAN [mgKOH/g]	$2,08^{b}$	$2,01^{ab}$	$2,03^{b}$	$2,4^{c}$	$1,85^{a}$	$2,12^{b}$	$2,38^{c}$
Viscosity [cSt]	$13,9^{a}$	$13,8^{a}$	$13,9^{a}$	$14,1^{b}$	$14,0^{ab}$	$14,2^{b}$	$14,5^{c}$

RESULTS AND DISCUSSION

The content of silicon, iron and potassium in the oil showed an initial slight increase (silicon after 100h, iron after 200h and potassium after 300h of operation) and then remained at a slightly varying level until 500 hours of operation. From 600 hours onwards, a statistically significant increase in both silicon, iron and potassium contents was observed. However, only the iron content exceeded the limit values at 700 hours of work. The course of the changes in the content of the above-mentioned elements is presented in figure 1.

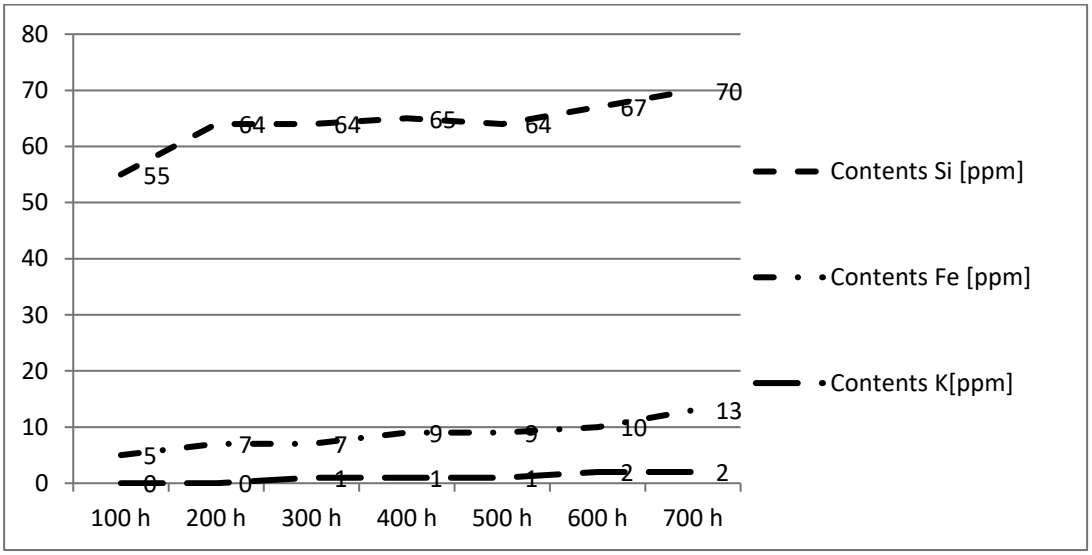

Fig. 1 Changes in silicon, iron and potassium content of oil as a function of operating time.

The changes in the acid and base numbers followed a similar pattern and remained stable after an initial increase up to 500 hours of operation. The acid value did not reach the limit value over the entire test range. The alkaline number only exceeded the limit value after 700 hours of operation. Similar results were obtained by (*Knopik et al., 2016*).The changes in the acid and alkaline values are shown in figure 2.

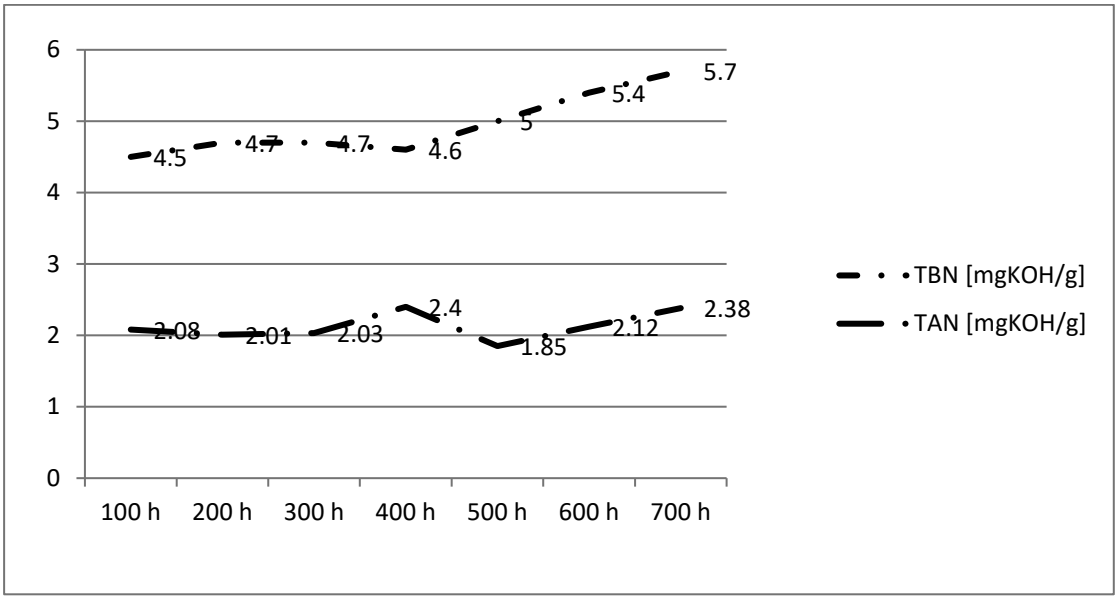

Fig. 2 The course of the changes in the acid and alkaline values as a function of operating time.
The viscosity value measured at 100 °C up to a running time of 500 h did not change in a statistically significant manner. At an operating time of 600 hours, a statistically significant increase in viscosity occurred, and at an operating time of 700 hours, the viscosity reached a limit of 14.5 cSt.

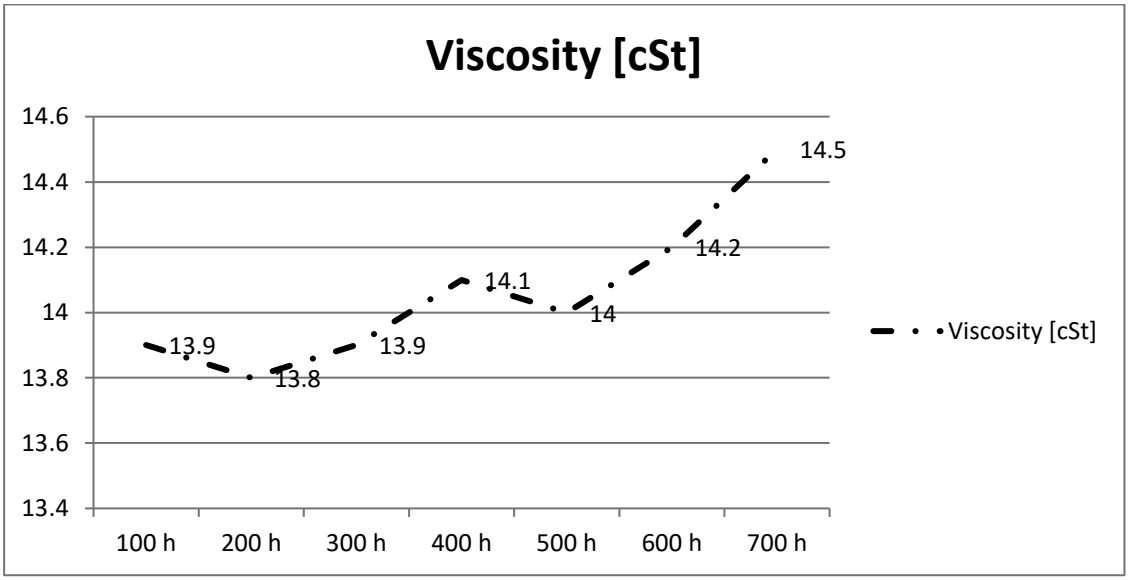

Fig. 3 The course of the changes in the viscosity at 100°C depending on oil operating time.

CONCLUSIONS

On the basis of the conducted tests it can be stated that extending the interval between engine oil changes in biogas-fuelled units is possible. In the cases studied, the factors deciding about the necessity of oil replacement were: alkaline number, iron content and viscosity. On the basis of previous tests, it should be noted that the composition of biogas has a significant impact. At the same time, according to the recommendations of the oil manufacturer, it is necessary to control the condition of the engine oil.

REFERENCES

1. Bilcan, A., Le Corre, O. Delebarre, A. (2003), Thermal efficiency and environmental performances of a biogas-diesel stationary engine *Environmental Technology* Vol. 24 , No. 9, 49-57,
2. Czekała, W., Bartnikowska S., Lewicka A., Bugała A., Zbytek Z., Lewicki A., (2016) Economic and energy efficiency of the solid biofuels produced from digested pulp *3RD International Conference on Chemical and Biological Sciences* Amsterdam, 135-139,
3. Górniak A., Midor K., Kaźmierczak J., Kaniak W. (2014) Advantages and Disadvantages of Using Methane from CNG in Motor Vehicles in Polish Conditions,
4. Guangqing L., Ruihong Z., Hamed M. El-Mashad, Renjie D., (2009) Effect of feed to inoculum ratios on biogas yields of food and green wastes *Bioresource Technology* Vol. 100, No 21, 80-86.
5. Kaszkowiak J., Borowski S., Dorszewski P., Markiewicz M., (2017) Influence of Composition of Biogas on Selected Engine Oil Values, Proceedings of 58th International Conference of Machine Design Departments - ICMD 2017 150-154
6. Knopik, L., Migawa, K. & Kolber, P. (2016). Statistical analysis of parameters of rail vehicles. *22nd International Conference on Engineering Mechanics Location: Svratka, CZECH REPUBLIC*, 286-289
7. Kosiba J., Uhrinova D., Jablonicky J., Majdan R., (2016) Alternatívne palivá a pohony motorových vozidiel Nitra 2016
Multidisciplinary Aspects of Production Engineering 241-248,
8. Kwaśny J., Banach M., Kowalski Z., (2012). Technologies of biogass produktion from diferent suorces, Chemistry, No 17, 83-88
9. Macian V., Tormos B., Miro G., Perez T., (2015) Assessment of low-viscosity oil performance and degradation in a heavy duty engine real-world fleet test, Proceedings of the Institution of Mechanical Engineers, Part J: Journal of Engineering Tribology, Volume: 230 issue: 6, page(s): 729-743,

Corresponding author:
Eng. Jerzy Kaszkowiak, Ph.D., , Faculty of Mechanical Engineering, Bydgoszcz, University of Sciences and Technology, Poland, phone: +48 374- 82-08 e-mail: jerzy.kaszkowiak@pbs.edu.pl

EFFECT OF MAP-BASED SITE-SPECIFIC SEEDING USING PROXIMAL SENSING DATA ON WHEAT YIELD PARAMETERS AND ECONOMY

Marius KAZLAUSKAS[1], Egidijus ŠARAUSKIS[1], Kęstutis ROMANECKAS[2], Vilma NAUJOKIENĖ[1], Indrė BRUČIENĖ[1], Sidona BURAGIENĖ[1], Dainius STEPONAVIČIUS[1], Algirdas JASINSKAS[1], Dovydas VAICEKAUSKAS[1], Abdul Mounem MOUAZEAN[1,3]

[1]Department of Agricultural Engineering and Safety, Faculty of Engineering, Agricultural Academy, Vytautas Magnus University, Lithuania
[2]Department of Agroecosystems and soil Sciences, Faculty of Agronomy, Agricultural Academy, Vytautas Magnus University, Lithuania
[3]Department of Environment, Faculty of Bioscience Engineering, Ghent University, Belgium

Abstract
Different areas of the field may support different numbers of winter wheat plants. It depends on the properties of the soil. The use of proximal sensor data for site-specific seeding can make better usage of the soil potential to increase yields and their quality parameters for greater cost-effectiveness. The aim of this work was to determine the influence of different soil granulometric composition based on electrical conductivity measurements on winter wheat yield by applying a variable seeding rate (VRS) in different soil management zones, derived from apparent electrical conductivity (ECa) maps. The results of the study showed that VRS resulted in average a 3.27% higher yield and a 3.95% higher relative profit than the control with a fixed seeding rate (FRS).

Key words: *variable rate seeding, soil management zones, winter wheat yield, soil electrical conductivity, grain protein, economic efficiency.*

INTRODUCTION

In order to optimize seed consumption and adapt to field variability, soil type, soil structure differences and to maintain the profitability of crop production, precision seeding or variable rate seeding (VRS) technologies are already being introduced in modern agriculture. Seed germination, crop development and yield potential can vary from field to field. Precision seeding is a way to link seed quantities to a specific site to increase plant yield and production efficiency (*Fulton, 2019; Šarauskis et al., 2022*). The variability of the precision seeding rate is usually determined by the apparent electrical conductivity (ECa) of the soil measurements, which are closely related to changes in soil moisture and the granulometric composition of the soil (*Grisso et al., 2009; Griffin et al., 2013*).
Winter wheat is most popular cereal crop grown in Lithuania (*Statistics Lithuania, 2022*), therefore the application of precision seeding technology to this crop in Lithuanian farms is very important. The aim of this work was to determine the influence of different soil granulometric composition based on ECa measurements on winter wheat yield by applying a VRS in different soil management zones.

MATERIALS AND METHODS

The research was carried out in 2020–2021 Panevėžys district, Naujamiestis on a commercial farm. The research field coordinates are 55.674734, 24.145607, the field area is 22.37 ha. At the beginning of the study on precision seeding technology, on 11th August 2020 the determination of the ECa of the soil was performed in the study field. The ECa of the soil was determined using an EM38-MK device by pulling it on the surface every 24 m between parallel neighboring tram lines. The soil ECa was scanned at a depth from 0 to 1.5 m. After measurement the ECa of the soil and determination the values of it, the whole study field was divided into 5 different soil management zones (MZ) from the highest to lowest accordingly the ECa (MZ1 – 28.6; MZ2 – 27.3; MZ3 – 25.7; MZ4 – 24.2; MZ5 – 22.6 $mS \cdot m^{-1}$).
On 16th September 2020 winter wheat was seeded in two variants: fixed seeding rate (control – FRS) and variable seeding rate (VRS) according to the seeding recommendation map in four repetitions. The width of one repetition was 36 m. Winter wheat (variety Skagen) was seeded, whose weight of 1000 grain was 44.8 g and a germination rate was 95%. In the control FRS technology, the seeding rate was 180 $kg \cdot ha^{-1}$. In the VRS, the seeding rate varied from 146 to 214 $kg \cdot ha^{-1}$ (MZ1 – 146; MZ2 – 153; MZ3

– 180; MZ4 – 197; MZ5 – 214 kg·ha^{-1}). In both treatments the same 6 m working width direct seeding using a drill Horsch Avatar 6.16SD (Germany) with coulter spacing of 16.7 cm and a seeding depth of 3 cm were used.
On 27th July 2021 plant samples were taken to determine yield. The samples were taken by cutting winter wheat plants with a knife from a 1.0 m long row. A total of 60 samples were taken, representing 5 replicates of each variant, depending on the EC zones of the soil. From the collected samples the mass of 1000 grains and the grain yield of wheat per hectare were determined.
The economic evaluation of the VRS technology was performed by determining the relative profit difference of this technology and it was compared to the control variant. The relative profit on seeding technology, excluding other costs, was calculated as follows: relative profit = income – (seed price + fertilization costs + plant protection products). The income of winter wheat yield was 240 EUR·t^{-1}. The price of winter wheat seed used for the research was 370 EUR·t^{-1}. Fertilizers and plant protection products were used at the same rates in both seeding treatment. Costs on fertilizers amounted to about 233 EUR·ha^{-1} and on plant protection products – 65 EUR·ha^{-1}. These calculations did not take into account farming equipment fuel consumption, operating costs, operator costs, etc.
Data from the experimental study were processed using the one-way ANOVA. Data were calculated using the smallest significance difference ($p < 0.05$) using the T-test. In Figures 2 and 3 the columns marked with the same letter do not differ significantly.

RESULTS AND DISCUSSION

After scanning the ECa of the soil map of the electrical conductivity of the soil was created and a map of the precision seeding of winter wheat with a variable seeding rate was prepared Fig. 1.

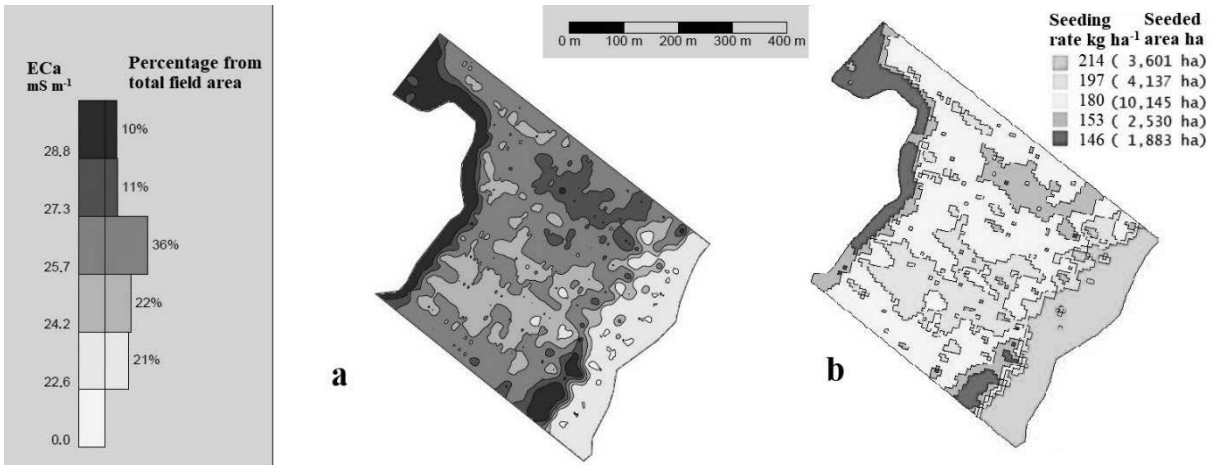

Fig. 1 Maps: a – soil electrical conductivity; b – variable rate seeding

The map of soil ECa distinguishes 5 different soil MZs,, which reflect 5 different seeding rates on the seeding map. The highest ECa of the soil indicates the maximum amount of clay particles corresponding to heavy soils, and these soils are able to retain moisture better (*Grisso et al., 2009*). In such soils, it is possible that the plants will have more tillers, which allow for a smaller amount of seeds to be sown, e.g. MZ1 – 146 kg·ha^{-1}. In the areas of the lowest ECa of the soil, low tillering of the plants and lower amount of developed ears are expected. Therefore, the highest seeding rate of 214 kg·ha^{-1} has been chosen in MZ5. In the control FRS treatment with a an average FRS of 180 kg·ha^{-1} was seeded.
The weight of 1000 grains of winter wheat was calculated and the obtained results are presented in Fig 2. Comparative calculations showed that a significant difference was found in the FRS of zone MZ5 compared to all other zones. The maximum weight of 1000 grains (37.44 g) was found in the VRS treatment in MZ4 zone and there was a significant difference in comparison with all other zones. Zones MZ1 and MZ2 of the VRS have significant differences with zones MZ3, MZ4 and MZ5. The VRS technology avoided significant areas of separation and the average weight of 1000 grains was about 35.1 g, while the average weight of 1000 grains in the FRS variant was about 34.0 g. The difference between the seeding variants was about 3.1%.

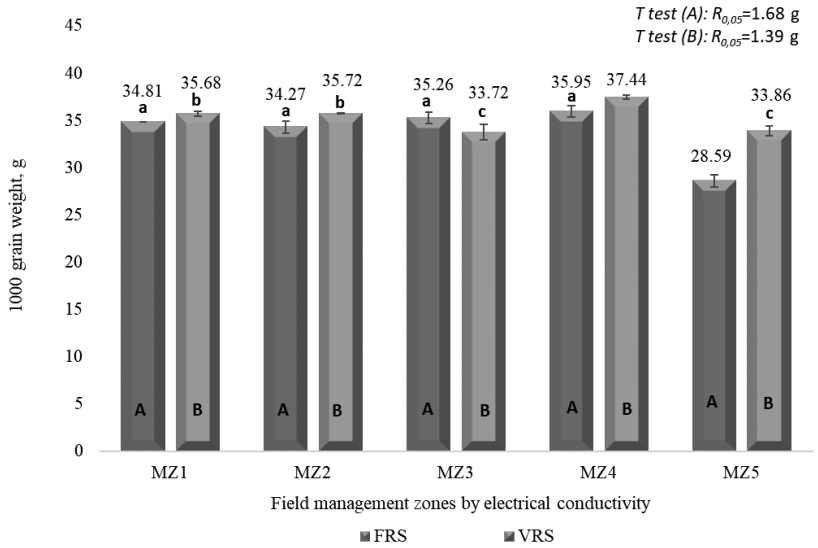

Fig. 2 Mass of 1000 grains (g) in different soil management zones: MZ1–MZ5 – soil management zones; FRS – fixed rate seeding; VRS – variable rate seeding

The biological yield of winter wheat was determined by laboratory tests. The obtained results are presented in Fig 3.

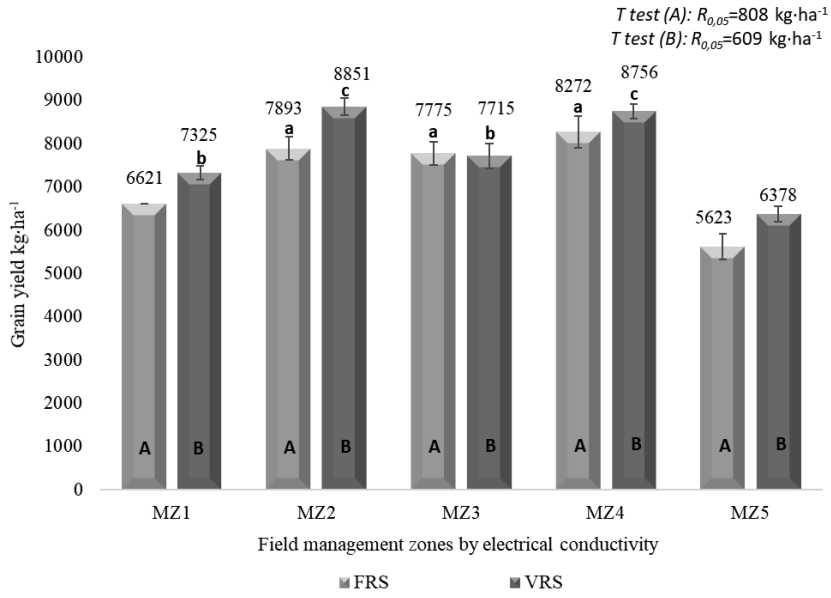

Fig. 3 Grain yield in different soil management zones: MZ1–MZ5 – soil management zones; FRS – fixed rate seeding; VRS – variable rate seeding

In the control treatment the significant differences of the yield were determined between zones MZ1 and MZ5 and these zones were compared to other zones. The lowest yield (5623 kg·ha^{-1}) was obtained in the MZ5 zone of the FRS variant. Although the seeding rate was the same (180 kg·ha^{-1}), lower grain yields were achieved in poorer sandy soils under the VRS. The VRS variant in the MZ5 zone had significantly lower yields in comparison to the other zones. Significantly the highest grain yields were achieved in MZ2 and MZ4 zones, where seeding rates were 153 and 197 kg·ha^{-1}. The yield of the VRS and the FRS variant in the MZ3 zone was very similar, because in this zone the seeding rate was the same – 180 kg·ha^{-1}. The average grain yield of the VRS, regardless of MZ, was 7782 kg·ha^{-1}, while in the FRS variant it was 7536 kg·ha^{-1} (246 kg·ha^{-1} less). Precision VRS technology resulted in average 3.27% increase in winter wheat yield. This study showed that many of the yield quality parameters were more homogeneous with VRS compared to FRS.

The economic indicators of traditional fixed rate and precision seeding technologies are presented in Tab. 1.

Tab. 1 Economic evaluation of different seeding technologies (FRS – fixed rate seeding; VRS – variable rate seeding)

Replications	Relative profit, FRS (Eur·ha^{-1})	Relative profit, VRS (Eur·ha^{-1})	Relative profit difference VRS to FRS %
1	1336.33	1382.05	3.42%
2	1303.76	1297.03	-0.52%
3	1604.43	1669.33	4.05%
4	1533.84	1658.12	8.10%
Average	1444.59	1501.63	3.95%

An economic evaluation of the traditional fixed rate and precision seeding technologies showed that the precision seeding technology resulted 3.95% higher relative profit per hectare in comparison to the traditional fixed rate technology. Economic profit can be a key for farmers interested in VRS (*Šarauskis et al., 2022*).

CONCLUSIONS

1. The weight of 1000 grains seeding winter wheat at a variable rate was 3.1% higher than seeding at a fixed rate.
2. The precision seeding technology has resulted in 3.27% increase in winter wheat yields over conventional seeding.
3. The precision seeding technology with a variable seeding rate has in average a 3.95% higher relative profit in comparison to traditional seeding technology at a fixed seeding rate.

ACKNOWLEDGMENT

This study was supported by European Regional Development Fund (project No. 01.2.2-LMT-K-718-03-0041) under a grant agreement with the Lithuanian Science Council (LMTLT)

REFERENCES

1. Fulton, J. (2019). Variable-rate seeding systems for precision agriculture. In Precision agriculture for sustainability. Stafford J., Ed.; Burleigh Dodds Science Publishing Limited, Silsoe Solutions, UK, 297p.
2. Griffin, S., Hollis, J. (2013). Using profile soil electrical conductivity survey data to predict wheat establishment rates in the United Kingdom. In Precision agriculture'13. Wageningen Academic Publishers, Wageningen. 491–497.
3. Grisso, R.B., Alley, M., Wysor, W.G., Holshouser, D., Thomason, W. (2009). Precision farming tools: Soil electrical conductivity. Virginia Cooperative Extension, 1–6.
4. Lietuvos statistikos departamentas. (2022). Žemės ūkio augalų pasėtas plotas. Prieigą per internetą: https://osp.stat.gov.lt/statistiniu-rodikliu-analize?hash=36784441-a07f-4c39-9946-774b5c062973#/
5. Šarauskis, E., Kazlauskas, M., Naujokienė, V., Bručienė, I., Steponavičius, D., Romaneckas, K., Jasinskas, A. (2022) Variable Rate Seeding in Precision Agriculture: Recent Advances and Future Perspectives. Agriculture, 2022, 12(2), 305, 1–24.

Corresponding author:
Ing. Marius Kazlauskas, Doctoral student, Department of Agricultural Engineering and Safety, Faculty of Engineering of Agriculture Academy, Vytautas Magnus University, Studentu 15A, LT-53362 Akademija, Kaunas Reg., Lithuania, phone: +370 612 40119, e-mail: marius.kazlauskas@vdu.lt

DIGESTATE APPLICATION RATES WITH REGARD TO EMISSION OF GREENHOUSE GASES

Jaroslav KORBA[1], Petr ŠAŘEC[1], Václav NOVÁK[1], Pavel BROŽ[2], Antonín DOLAN[3]

[1]*Department of Machinery Utilization, Czech University of Life Sciences Prague, Kamýcká 129, CZ165 00 Prague 6, Czech Rep.*
[2]*Department of Agricultural Machines, Czech University of Life Sciences Prague, Kamýcká 129, CZ165 00 Prague 6, Czech Rep.*
[3]*Department of Technology and Cybernetics, Czech University of Life Sciences Prague, Branišovská 1645/31a, CZ370 05 České Budějovice, Czech Rep.*

Abstract
The article focuses on the method and on the rate of digestate application with respect to the environment at impact, especially to the air pollution. Two methods of applying digestate were selected that were performed after harvesting rye as the pre-crop, and before sowing maize. Digestate is a waste product of biogas plants and contains a large amount of nutrients, therefore it is very often used as fertilizer in agriculture. It is not only when it is applied that greenhouse gases are released into the atmosphere, so it is necessary to find an ideal application method that minimizes the release of gases while providing sufficient nutrition for the crop. In this paper, the emissions from two methods of digestate application were compared. For each application technology, emissions at different application rates were assessed. The emissions of ammonia and carbon dioxide increased with higher rates of digestate. This finding was not confirmed for methane emissions though.

Key words: *disc slurry injector; strip-till slurry injector; ammonia; methane; carbon dioxide.*

INTRODUCTION

Climate change and global warming are increasing the pressure on all fossil fuel industries (*Jacob et al., 2018*). This issue has been addressed by the European Commission when it set a mandatory share of energy from renewable sources. Biogas produced in agriculture can help to meet these targets (*Mamica et al., 2022*). Because intensive farming is now the predominant way of managing agricultural land, mankind grows enough food and feed on a smaller area than before. Higher yields would not be possible without major advances in plant breeding (*Frei, 2000*). Appropriate fertilization management also contributes substantially. Chemical plant protection is another important aspect, without which intensive farming would not succeed *(Birkhofer et al., 2008)*. On the remaining area of agricultural land, crops including energy crops suitable as the main feedstock for biogas plants (*Voltr et al., 2021*) can be grown. Furthermore, biological waste from crop and livestock production in agriculture is most commonly used as feedstock (*Priekulis et al., 2016*). Anaerobic digestion is the controlled microbial conversion of organic matter without access to air to produce biogas and digestate (*Pain & Hepherd, 1985*). After removal from the digester, the biogas is free of undesirable elements and compounds, and its final quality is specified by a standard. The biogas is then burned in a cogeneration unit which produces electricity by means of a generator. Part of the waste heat is used to heat the fermenter. A large amount of digestate is produced during the production of the gas and is considered a waste product. It is most often used in agriculture as a liquid organic fertilizer, because it contains a large amount of nutrients (*Szymańska et al., 2022*). But there is a reduction of carbonaceous matter. Consequently, digestate contains mainly less decomposable organic matter, so it can sometimes be referred to more as a mineral fertilizer (*Möller & Müller, 2012*). Digestate is continuously discharged from the digester into storage tanks, from which it is then taken to the field according to agronomic deadlines. The digestate contains large amounts of nitrogen, mainly in the form of ammonia. Not only ammonium nitrogen but other elements contained in the fertilizer are lost to the air. The gases monitored in this experiment are among the gases that increase the greenhouse effect of the atmosphere (*Lamolinara et al., 2022*). The most important greenhouse gas monitored is carbon dioxide, whose concentration is steadily increasing in the atmosphere. The burning of fossil fuels contributes in a major way to this increase *(Lamb et al., 2021)*. Methods for measuring greenhouse gas emissions in livestock production are well established, but methods for measurement in

field after application are not uniform. In livestock production, concentrations are higher and easier to measure because of the steady production of emission gases, and a stable environment that is not affected by weathering. The concentration of the monitored gases above the surface of the land where the application took place decreases with time (*Dietrich et al., 2020*). For these reasons, it is advisable to carry out measurements as soon as possible after fertilizer application. In the search for the optimal method and rate at which the least release of greenhouse gases into the atmosphere occurs, the sufficient supply of the necessary nutrients to the plants must not be forgotten. The aim of the experiment was to compare the amount of emissions released after application of different doses by two application methods.

MATERIALS AND METHODS

The measurement field was located near the village of Čechtice in the Central Bohemia Region, Czech Republic (49.6049206 N, 15.0815178 E), with an average altitude of 550 m above sea level. According to the USDA, the soil texture of the field was sandy loam. Digestate application was carried out using two different implements, i.e. disk injector and strip-till injector. The application of digestate took place on 25 May 2021, approximately one week after the harvest of rye for silage. Maize was then seeded four days after application. In the first part of the experimental plot, the digestate was applied using a self-propelled tanker equipped with a disc injector with a soil cover of approximately 12 cm. In the second part of the plot, the same self-propelled machinery was used but equipped with an injector that applied digestate and processed the soil in a strip-till only manner. The depth of tillage was approximately 16 cm in the latter case. The application at both parts of the plot differing by the injector used was carried out on four variants with different digestate rates. The rates chosen were 10, 20, 30 and 40 $m^3.ha^{-1}$. On the fifth variant considered as the control, only tillage was carried out without any digestate application. Each variant for the disk-applied technology was 24 m wide and 100 m long; for the strip-applied technology, the width was 12 m, and the length 200 m. Measurements of emissions and physical properties of the soil were carried out after application. The monitored emission gases were CO_2, CH_4, NH_3. INNOVA 1412 (LumaSense Technologies A/S, Denmark) was used for the measurement of gas concentrations, linked to the replicator INNOVA 1309 (LumaSense Technologies A/S, Denmark) that enabled to measure all the variants simultaneously. A wind tunnel (CZU Prague, Czech Rep.) was placed on each variant, from which special air tubes led to the measuring equipment. The wind tunnel was a plastic hollow block that did not have a wall at the bottom, the dimensions of which were 50 x 35 cm. There were ventilation openings on the two sides facing each other. One opening was fitted with a fan to provide the required airflow velocity for the wind tunnel, which was around 0.8 $m.s^{-1}$. The second opening carried air into the wind tunnel and was fitted with an anemometer. A thermometer was placed inside to record the temperature during the measurement. The wind tunnels were moved to a different location within a variant after one hour, for a total of three repetitions. All data were recorded with simultaneous transfer to a PC. Furthermore, the concentration of each gas in the ambient air was subtracted from the measured concentrations for each variant. These adjusted concentrations were converted from the area covered by the wind tunnel to an area of one square meter. Finally, the recalculated concentrations were converted to theoretical emissions released during one day. Statistical analysis of the data was performed using Statistica 12 software. ANOVA test was used to evaluate the gas emission differences

RESULTS AND DISCUSSION

The highest rate of 40 $m^3.ha^{-1}$ was chosen because it contained the maximum recommended nitrogen dose for a single application. The measured methane values for both injectors used were very similar. Concerning digestate rates, statistical difference can be seen (Fig. 1) between the variant without fertilizer dose (control) and all the variants with any digestate dose applied, i.e. with the doses of 10, 20, 30 and 40 $m^3.ha^{-1}$. Otherwise, the measured emissions did not differ significantly among the variants. When compared at the same time interval after the application, the measured emissions of the variants with applied fertilizer were higher than those found by *Czubaszek & Wysocka-Czubaszek (2018)*. Furthermore, it is noticeable that there are no significant differences between the application methods. Similar values were obtained by *Koga et al. (2022)* after application of liquid fertilizer to the experimental post-emergence crop. Methane emissions were higher than measured by *Šařec et al. (2021)*, which may be partially attributed to a different composition of the digestate.

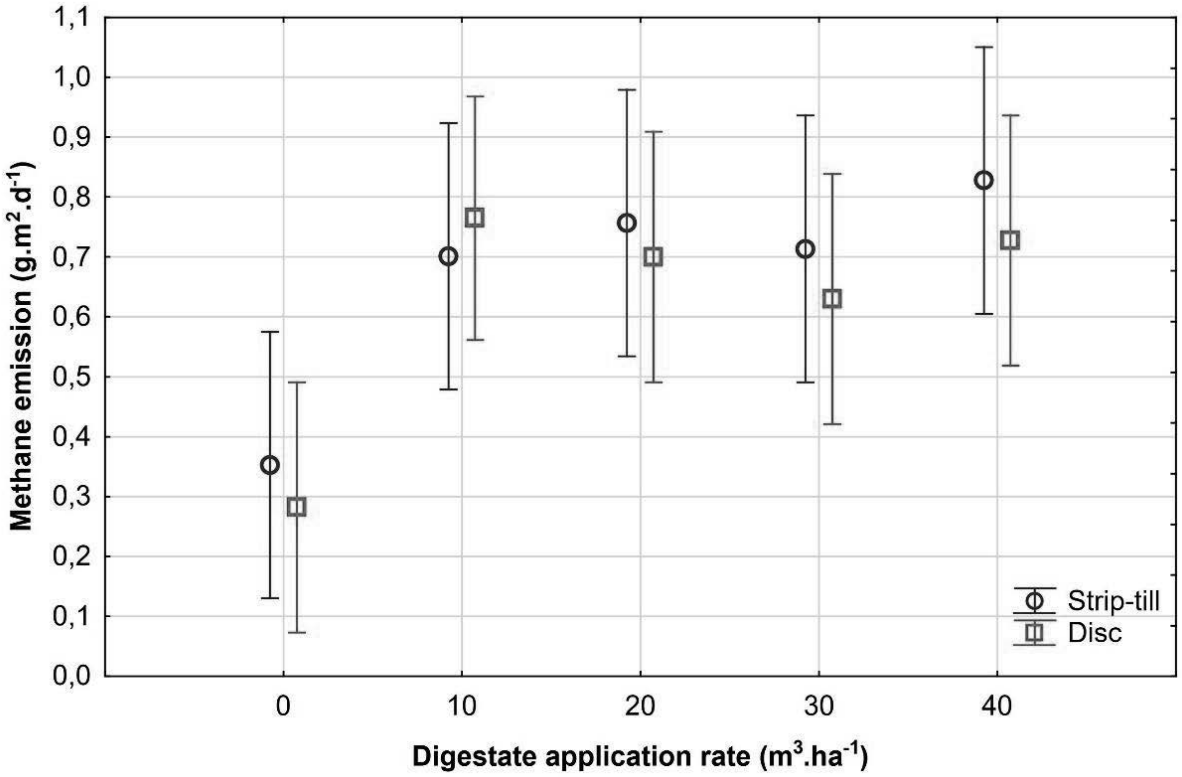

Fig. 1 Methane emission for different digestate doses and injectors used

According to Fig. 2, the measured carbon dioxide emissions increased also with increasing fertilizer rate. No significant differences were found concerning injectors used. Statistically significant differences were obtained when having compared the control variant and the lowest dose of 10 $m^3.ha^{-1}$ to the doses of 30 and of 40 $m^3.ha^{-1}$. The measured values for all the variants were higher than those of *Rosace et al. (2020)*. This difference may be affected by a different measurement method, although the time development of the emission release is similar.

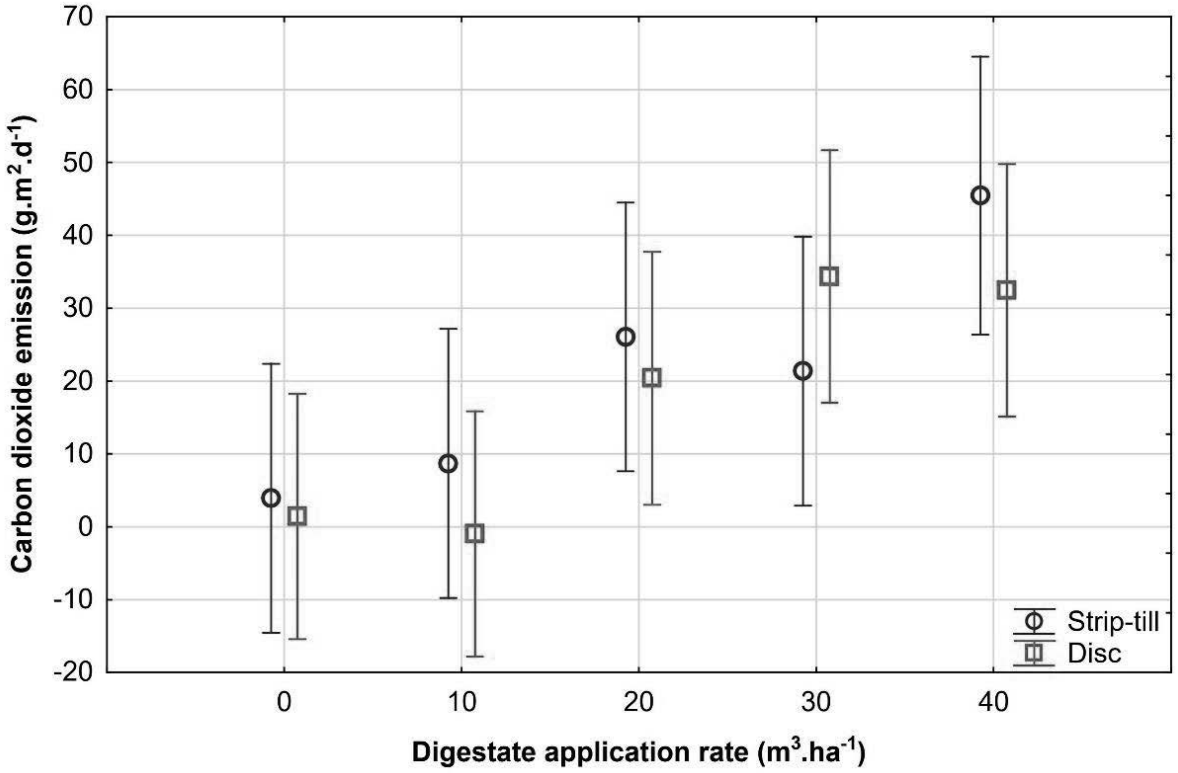

Fig. 2 Carbon dioxide emission for different digestate doses and injectors used

The Fig. 3 shows some differences between the injectors used, but these were not statistically significant. Concerning digestate rates, statistical difference can be seen (Fig. 3) only between the variant without fertilizer dose (control) and the variant with the maximum dose of 40 $m^3.ha^{-1}$. Otherwise, the measured emissions did not differ significantly among the variants. The measured NH_3 concentration is significantly lower than that by *Wolf et al. (2014)*, where digestate was incorporated in a slightly different way.

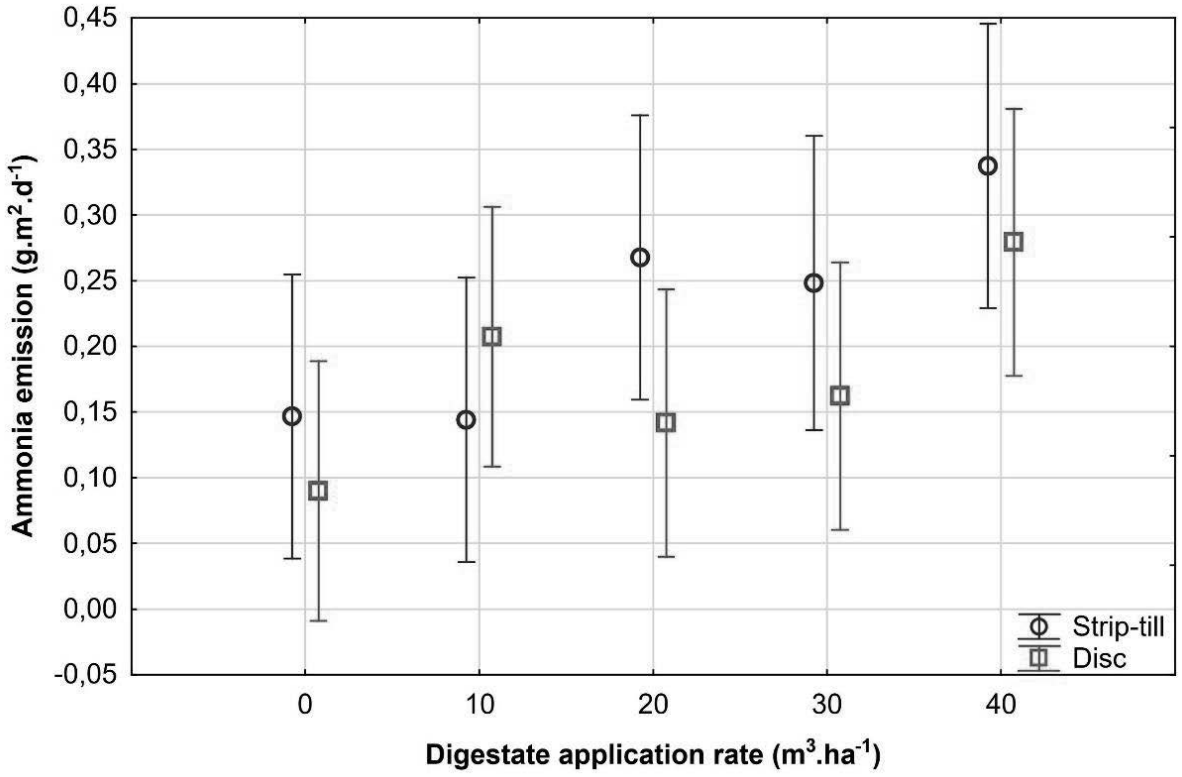

Fig. 3 Ammonia emission for different digestate doses and injectors used

CONCLUSIONS

Measurements showed that the digestate dose applied had an effect on the amount of gases released into the air. This was confirmed particularly for carbon dioxide and ammonia emissions. In the case of methane, the measurements suggested that the application of digestate led to the methane released into the air, but the amount of it did not depend on the amount of digestate. Concerning disk and strip-till injectors, no statistically significant differences in emissions were recognized for either of the three measured gasses. Probably the key aspect was that both methods incorporated the digestate into soil.

ACKNOWLEDGMENT

Supported by the project TAČR TH04030132 of the Technology Agency of the Czech Republic, and by the Czech University of Life Sciences, Faculty of Engineering in the frame of the internal project IGA 2022: 31180/1312/3106.

REFERENCES

1. Birkhofer, K., Bezemer, T., Bloem, J., Bonkowski, M., Christensen, S., Dubois, D., Ekelund, F., Fließbach, A., Gunst, L., Hedlund, K., Mäder, P., Mikola, J., Robin, C., Setälä, H., Tatin-Froux, F., Van der Putten, W., & Scheu, S. (2008). Long-term organic farming fosters below and aboveground biota: Implications for soil quality, biological control and productivity. *Soil Biology and Biochemistry, 40(9),* 2297-2308. https://doi.org/10.1016/j.soilbio.2008.05.007
2. Czubaszek, R., & Wysocka-Czubaszek, A. (2018). Emissions of carbon dioxide and methane from fields fertilized with digestate from an agricultural biogas plant. *International Agrophysics, 32*(1), 29-37. https://doi.org/10.1515/intag-2016-0087
3. Dietrich, M., Fongen, M., & Foereid, B. (2020). Greenhouse gas emissions from digestate in soil. *International Journal of Recycling of Organic Waste in Agriculture, 2020*(9), 1 - 19.

4. Frei, O. (2000). Changes in yield physiology of corn as a result of breeding in northern Europe. *Maydica*, *3*(45), 173 - 183.
5. Jacob, D., Kotova, L., Teichmann, C., Sobolowski, S., Vautard, R., Donnelly, C., Koutroulis, A., Grillakis, M., Tsanis, I., Damm, A., Sakalli, A., & van Vliet, M. (2018). Climate Impacts in Europe Under +1.5°C Global Warming. *Earth's Future*, *6*(2), 264-285. https://doi.org/10.1002/2017EF000710
6. Koga, N., Ihara, H., Yamane, T., Yamaguchi, C., & Kobayashi, S. (2022). Soil greenhouse gas emissions from an animal excrement-based forage cropping system. *Nutrient Cycling in Agroecosystems*, *123*(3), 153-167. https://doi.org/10.1007/s10705-022-10214-4
7. Lamb, W., Wiedmann, T., Pongratz, J., Andrew, R., Crippa, M., Olivier, J., Wiedenhofer, D., Mattioli, G., Khourdajie, A., House, J., Pachauri, S., Figueroa, M., Saheb, Y., Slade, R., Hubacek, K., Sun, L., Ribeiro, S., Khennas, S., de la Rue du Can, S. et al. (2021). A review of trends and drivers of greenhouse gas emissions by sector from 1990 to 2018. *Environmental Research Letters, 16(7)*. https://doi.org/10.1088/1748-9326/abee4e
8. Lamolinara, B., Pérez-Martínez, A., Guardado-Yordi, E., Guillén Fiallos, C., Diéguez-Santana, K., & Ruiz-Mercado, G. (2022). Anaerobic digestate management, environmental impacts, and techno-economic challenges. *Waste Management*, (140), 14-30. https://doi.org/10.1016/j.wasman.2021.12.035
9. Mamica, Ł., Mazur-Bubak, M., & Wróbel-Rotter, R. (2022). Can Biogas Plants Become a Significant Part of the New Polish Energy Deal? Business Opportunities for Poland's Biogas Industry. *Sustainability*, *14*(3). https://doi.org/10.3390/su14031614
10. Möller, K., & Müller, T. (2012). Effects of anaerobic digestion on digestate nutrient availability and crop growth: A review. *Engineering in Life Sciences*, *12*(3), 242-257. https://doi.org/10.1002/elsc.201100085
11. Pain, B., & Hepherd, R. (1985). Anaerobic digestion of livestock wastes. *Anaerobic digestion of livestock wastes, 1985*, 9 - 14.
12. Priekulis, J., Aplocina, E., & Laurs, A. (2016). Chemical composition of digestate. *15th International Scientific Conference on Engineering for Rural Development, 2016*, 381 - 386.
13. Rosace, M., Veronesi, F., Briggs, S., Cardenas, L., & Jeffery, S. (2020). Legacy effects override soil properties for CO2 and N2O but not CH4 emissions following digestate application to soil. *GCB Bioenergy*, *12*(6), 445-457. https://doi.org/10.1111/gcbb.12688
14. Szymańska, M., Ahrends, H., Srivastava, A., & Sosulski, T. (2022). Anaerobic Digestate from Biogas Plants—Nuisance Waste or Valuable Product?. *Applied Sciences*, *12*(8). https://doi.org/10.3390/app12084052
15. Šařec, P., Korba, J., Novák, V., & Křížová, K. (2021). Digestate application with regard to greenhouse gases and physical soil properties. *Agronomy Research*, *19*(4), 1929 - 1937. https://doi.org/10.15159/AR.21.125
16. Voltr, V., Hruška, M., & Nobilis, L. (2021). Complex Valuation of Energy from Agricultural Crops including Local Conditions. *Energies*, *14*(5). https://doi.org/10.3390/en14051415
17. Wolf, U., Fuß, R., Höppner, F., & Flessa, H. (2014). Contribution of N2O and NH3 to total greenhouse gas emission from fertilization: results from a sandy soil fertilized with nitrate and biogas digestate with and without nitrification inhibitor. *Nutrient Cycling in Agroecosystems*, *100*(1), 121-134. https://doi.org/10.1007/s10705-014-9631-

Corresponding author:
Ing. Jaroslav Korba, Department of Machinery Utilization, Czech University of Life Sciences Prague, Kamýcká 129, CZ165 00 Prague 6 Czech Republic, Czech Republic, e-mail: korba@tf.czu.cz

USE OF AERIAL APPLICATION OF POD SEALANTS IN CANOLA CROPS

František KUMHÁLA[1], Jitka KUMHÁLOVÁ[2], David BEČKA[3], Martin MADĚRA[1]

[1]Czech University of Life Sciences Prague, Faculty of Engineering, Department of Agricultural Machines
[2]Czech University of Life Sciences Prague, Faculty of Engineering, Department of Machinery Utilization
[3]Czech University of Life Sciences Prague, Faculty of Agrobiology, Food and Natural Resources, Department of Agroecology and Crop Production.

Abstract
Canola is important and widely grown agricultural crop. When growing canola, a losses caused by pod shattering are a problem. These losses can be reduced by applying pod sealant. Two methods of pod sealant application, aerial and ground, were compared in 2021 growing season. A pilot experiment was set up for this purpose. The results showed that in the conditions of the Czech Republic, the use of pod sealing technology is advantageous when using both ground and aerial applications. However, the use of an aerial application is more advantageous than a ground application, because it does not cause losses due to damage to the vegetation by the crossing of agricultural machinery.

Key words: *aerial spraying; ground spraying; effectiveness of spraying; canola losses; economic evaluation.*

INTRODUCTION

Canola, or rapeseed (Brassica napus) is an important and widely grown agricultural crop. Current world production is around 70 million tons out of around 35 million hectares, with canola being grown on around 5.3 million hectares in the European Union, producing approximately 17 million tons *(USDA, 2022*). For example, in the Czech Republic, in the period between 2016 and 2020, canola was grown on an average of 368,000 hectares of arable land per year and its average annual production was 1.26 million tons (*Czech Statistical Office, 2021*).

Losses caused by pod shattering are problem in canola growing and harvesting (*Child et al., 2003; Gulden, Shirtlie & Thomas, 2003; Zhu et al., 2012*). In order to reduce these losses, canola crops are now commonly treated with pod sealants with different results (*Kosteckas et al., 2009; Nunes et al., 2015; Bauša et al., 2018; Steponavičius et al., 2019*). According to *Bauša et al. (2018),* the application of acrylic- and trisiloxane-based pod sealant is the most promising method of pod shattering control. The essence of the function of these substances lies in the physical prevention of valve separation by gluing them together and in altering the pod moisture regime (sealant allows moisture to leave the pod but prevents getting into it).

A common way of treating canola crops by pod sealant is to apply it by spraying (*Bauša et al., 2018; Steponavičius et al., 2019*). There are various methods of spraying. Probably the most common and widely researched method of spraying is ground application using a tractor operated or self-propelled sprayer (e.g. *Anthonis, Audenaert & Ramon, 2005; Wrest Park History Contributors, 2009; Faiçal et al., 2017; Penney et al., 2021;* and many others). Another possibility is aerial application, both when using a pilot-controlled aircraft (e.g. *Viret et al., 2003; Hevitt, 2008; Jiao et al., 2021; Penney et al., 2021*; etc.) or an unmanned aerial vehicle (e.g. *Qin et al., 2016; Faiçal et al., 2017; Gibbs, Peters & Heck, 2021; Zhan et al., 2022;* and others). All spraying methods have its advantages and disadvantages. Terrestrial spraying is based on ground vehicles. Paths are needed within the crop field. Therefore, this method is usually slow and has contact with the culture, which decreases the production area and can damage healthy plants. On the other hand, small distance of spraying system and treated crop reduces the drift of chemicals to neighboring areas - terrestrial application is able to reach relatively high accuracy of spraying (*Faiçal et al., 2017)*. In contrast, according to *Nádasi and Szabó (2011)*, the aerial spraying is faster without the need for paths. However, the larger distance between the spraying system and the cultivated area increases protective substance drift to neighboring areas.

Nevertheless, the advantages and disadvantages of pod sealant aerial and ground applications have not been compared in the past. That is why the main aim of this contribution is to compare ground and aerial way of pod sealant application on the basis of a field experiment carried out on a common agricultural holding in the Czech Republic in the growing season 2021.

MATERIALS AND METHODS

A pilot experiment was set up in order to compare different technologies of canola crops treatment against spontaneous pods shattering. The experiment was established on the land block 3901 "K Břišťanům" of the Agricultural Joint Stock Company Mžany. Track lines for application technology with a working width of 30 m were used. Five test plots 60 m wide and approximately 740 m long were created on the land block. The first plot was a control and was not treated. The second plot was treated with a tractor set with a trailed sprayer, the third with a self-propelled sprayer, the fourth by aerial application using an atomizer and the last fifth by conventional aerial spraying. Arrest Plus® protective substance was used in all cases at a rate of 1 l per hectare. The application was carried out in the interest of the greatest possible objectivity of the measurement within one day, June 29, 2021. Detailed information on application technology and application is given in Tab. 1.

Tab. 1 Used application technique and amount of applied spray mixture on individual plots.

Plot No.	Method of treatment	Machinery used	Applied dose of spray mixture
1	Control	-	-
2	Trailed tractor sprayer	Case 160 CVX +Agrio Mamut Topline (30 m)	200 l/ha
3	Self-propelled sprayer	Tecnoma (30 m)	200 l/ha
4	Aerial application using atomizer	Agricultural aircraft Čmelák Z 37 T equipped by atomizer	2 x 5 l/ha (2 x flight over the plot, there and back)
5	Conventional aerial spraying	Agricultural aircraft Čmelák Z 37 A equipped by sprayer	110 l/ha

On June 29, 2021, the day of the protective substance application, the first experiments were performed for the purpose of visual evaluation of the test plots. The pictures of the test plots were taken with the eBee X unmanned system (fixed wing) equipped with an RGB camera S.O.D.A. working in the visible part of the spectrum (senseFly SA, Cheseaux-Lausanne, Switzerland). The unmanned vehicle mission was carried out after the treatment of the canola crop with all compared application technologies.

Further measurements were focused on the effectiveness of the application of the protective substance in order to reduce pre-harvest and harvest losses of rape. Land block with pilot experiment was harvested on 30-31 July 2021 by Claas Lexion 580 combine harvester using an adapter V 900 with 9 m width. The machine was equipped with a yield mapping device. A yield map of the entire soil block with test plots was subsequently created in SW ArcGIS Pro and QGIS using the Kriging method. The individual recorded relative yield values were recalculated so that the average yield on the land block corresponded to the actually determined yield. Subsequently, individual test plots were delimited in the QGIS software. Its average yield was calculated on each of the plots. The average yields from individual plots were then compared with the average yield of the entire land block.

On July 20, 2021, 15 samples of whole plants were taken to determine the yield in the footsteps of agricultural machinery in the track lines. Three samples with an area of 3 m^2 were taken on each of the test plots. Samples were taken from an area 1 m wide across the track line and 3 m long in the direction of the track line at a distance of about 100 m from the headland. The track width of agricultural machinery was 0.5 m. During storage in the laboratory, the samples were naturally dried evenly to the same moisture of 7.2%. In order to calculate the effect of the change in yield in the track lines using different application technologies, the effect of the change in yield in the track lines on the total yield from 1 ha was compared. It was calculated with a measured average track width of 0.5 m and an area of 1 ha (100 x 100 m). To treat this area by ground application at a width of 30 m, 3.3 rides are required, i.e. 6.7 feet of agricultural machinery with a length of 100 m. In this area, there may have been a change in yield due to crossings of agricultural machinery and the total canola yield from 1 ha of area could be affected.

On August 20, 2021, the germinated canola plants from the losses were also counted. The germinated plants were counted not behind the combine's straw walkers, but only in the area behind the cutting bar. Quarter meters were used to determine the number of germinated plants. On each plot, this number was counted at 4 different locations. The average of these 4 measurements was calculated and then recalculated to the average germination from 1 m^2 area. The germinated canola plants can be considered as losses, so they were converted to 1 ha. To calculate the loss estimate, it was assumed that about 90% of rapeseed would germinate.

RESULTS AND DISCUSSION

From the visual comparison, at first glance, the damage to the canola crop in the wheel tracks in the track lines after the passage of agricultural machinery and partly also in the space between the wheels was obvious. The vegetation collapsed here, especially in the case of the passage of a trailed sprayer, due to the low ground clearance of the tractor chassis. After the passage of the self-propelled sprayer, the situation was significantly better, especially between the wheels, compared to the set with a trailed tractor sprayer. In both of these monitored variants, however, the traces of the passage of agricultural machinery were quite obvious in comparison with the control plot. On the headlands, this fact became even more significant. When visually comparing the plots treated by aerial spraying with the control plot, no change in the track lines was observed.

Already during the visual evaluation of the yield map obtained, it was observed that the lowest yield was achieved on control plot which were not treated by pod sealants. Everything is clear from Tab. 2, where the yields on the individual test plots are compared.

Tab. 2 Measured canola yield on the soil block and yields calculated from the measured yield map on the test plots.

Plot No.	Method of treatment	Yield on soil block (t/ha)	Yield on individual plots (t/ha)
1	Control		3,19
2	Trailed tractor sprayer		3,46
3	Self-propelled sprayer	3,67	3,8
4	Aerial application using atomizer		4,06
5	Conventional aerial spraying		3,8

When comparing the yield on individual test plots, Tab. 2 shows that the worst average yield from the treated plots was achieved on plot 2 treated with a trailed tractor sprayer. Plots 3 and 5 treated with a self-propelled sprayer and a conventional aerial spraying showed the same yield. The aerial application with an atomizer on plot 4 came out as the best.

Tab. 3 Table of the number of germinated plants from canola losses and canola losses derived from emerged seeds.

Plot No.	Method of treatment	Number of emerged canola seeds per ¼ m^2				Average on ¼ m^2	Number of emerged canola seeds per m^2	% of losses reduction	*Losses. (kg/ha)
		A	B	C	D				
1	Control	156	262	412	480	328	1310	100	69,5
2	Trailed tractor sprayer	344	308	203	182	259	1037	79	55,0
3	Self-propelled sprayer	208	108	252	128	174	696	53	36,9
4	Aerial application using atomizer	108	124	182	148	141	562	43	29,8
5	Conventional aerial spraying	102	96	143	98	110	439	34	23,3

*Losses were calculated on the base of the weight of a thousand canola seeds, which was 4.82 g. The calculation assumed that about 90% of all lost seeds germinated.
Tab. 3 shows the values of germinated canola seeds after harvest. Based on these values, losses on individual plots were estimated.
The largest amount of germinated plants (and therefore also losses) was found on the control plot, which was not treated. This is a clear argument in favor of treatment with pod sealants in order to reduce pre-harvest and harvest canola losses. It was also found that the effectiveness of aerial application of the preservative is quite comparable, if not better than the effectiveness of ground application. According to the results of our measurements, the conventional aerial application came out best, when the amount of losses compared to the control decreased to 34% (from 100% losses on untreated plots). Ground applications also had a positive effect on the amount of losses found, but not as significant as in the case of aerial applications. The values measured for the trailed tractor sprayer were the worst (decrease to 79% of losses only), which corresponds to the increased damage to the vegetation in the track lines, found both in the visual evaluation and in the evaluation of losses in track lines (see below).
The values of the total measured and calculated rapeseed yield and the yield measured in traces of agricultural machinery on all monitored plots are given in Tab. 4.

Tab. 4 Measured yield in track lines of agricultural machinery. Calculated reduced yield on trial plots due to lower yield in track lines.

Plot No.	Method of treatment	*Measured average yield from 3 m^2 (g)	*Measured average yield (t/ha)	Reduced yield (t/ha)	Difference in yield (kg/ha)
1	Control	1069,5	3,57	3,67	0
2	Trailed tractor sprayer	580,4	1,93	3,61	60
3	Self-propelled sprayer	769,3	2,56	3,63	40
4	Aerial application using atomizer	880,6	2,94	3,65	20
5	Conventional aerial spraying	884,4	2,95	3,65	20

*Yield measured in track lines after the crossing of agricultural machinery.

For each of the variants, the difference in yield compared to the average hectare yield of the entire land block was calculated. The average yield on this land block was 3.67 t/ha. The difference in yield was calculated on the basis of a comparison of the size of the track lines area to the area of 1 ha. Based on the data described in the methodology, the track lines area represents 3.3% of 1 ha area. Therefore, a weighted average was used to calculate the reduction in yield per hectare due to the reduction in yields in the tramlines. The average plot yield of 3.67 t/ha on the area of 9,667 m^2 was calculated and on the rest up to 1 ha (333 m^2) it was calculated with the average yield measured in the track lines given in Tab. 4.
Although the visual comparison showed exactly the same condition of the track lines in comparison with the control plot, in the case of both air-treated test plots a slightly lower yield was measured in the track lines. In our opinion, there is no objective reason for this reduction in yield. This situation could be due to the small number of yield measurements repetitions or due to different yields at yield sampling points (we could not consider the differences in yield; the yield map was not available at the time of yield sampling). Nevertheless, in the case of the control plot, the reduction in yields due to lower yields in the track lines was negligible, in the case of aerial treatment, in both cases (atomizer and conventional), the yield decreased by 20 kg/ha.
However, the reduction of yields due to the crossing of the sprayers during ground application was even more significant. In the case of a self -propelled sprayer, based on our measurements, we have determined a reduction in yields by an average of 40 kg/ha and in the case of tractor trailed sprayer, this

reduction on average was 60 kg/ha. This measured result is fully in agreement with the visual evaluation of the status of canola crop after aerial and ground application.
In 2021, in the Czech Republic, the cost of self-propelled sprayers working in services was in the range of CZK 250-270 per hectare, plus approximately 2 l/ha of consumed diesel (additional CZK 50), which in total is approximately 320 CZK/ha. The price of the aviation application was between 311 and 339 CZK/ha. The price for the treatment of one ha of canola crop was in both cases (ground x air application) approximately the same (about 320 CZK/ha). Service work (water, filling) is also approximately comparable for both applications. The price for the chemical preservative Arrest Plus® is approx. 500 CZK/ha (1 liter of the product). In the summer of 2021, the price of rapeseed was about 11,500 CZK/t. It is clear from Tab. 2 that the average yield on untreated control plots 1 was 3.19 t/ha, while the average yield on treated plots 2-5 was 3.78 t/ha. This means a difference in yield of 0.59 t/ha. Due to treatment of the canola crop by pod sealants, the revenue from one hectare was approx. CZK 6,800 more than in comparison with untreated crop. Based on the results of our measurements, it can be stated that the savings by reducing losses far exceed the price of treatment per hectare, which will be up to 1,000 CZK/ha, even with services works. The treatment of the canola crop by pod sealants it is therefore clearly advantageous and can be recommended. Similar results were obtained by the authors *Nunes et al. (2015)*, who recommended the use of pod sealant as effective in the case of later than ideal time harvesting of canola crops by various methods. *Bauša et al. (2018)* reported beneficial effect in reducing canola seed yield losses using pod sealant. Also, *Steponavičius et al. (2019)* reported 20-70% canola seeds losses reduction using pod sealant.
Based on our results, it can also be stated that the air application of pod sealant is more advantageous than the ground application. The crop undamaged by agricultural machinery showed a higher yield of another 40-60 kg/ha, which means revenue higher by another 460-690 CZK/ha. *Nádasi and Szabó (2011)* also pointed out this advantage of the aerial application. *Antuniassi (2015)* then pointed out the development of aerial applications in Brazil.

CONCLUSIONS

Based on the results of our pilot experiment, it has been shown that the use of pod sealing technology to reduce rapeseed harvest losses is recommended and it is also financially beneficial for farmers. It has also been shown that pod sealant aerial application is more advantageous than ground application because it does not cause any damage to the vegetation.

ACKNOWLEDGMENT

This study was supported by Agroair, Ltd. Company and Agricultural Joint Stock Company (ZAS) Mžany. Special thanks to Mr. Ing. Jan Vratislav, agronomist of ZAS Mžany.

REFERENCES

1. Anthonis, J.; Audenaert, J.; Ramon, H. (2005). Design Optimisation for the Vertical Suspension of a Crop Sprayer Boom. *Biosystems Engineering 90(2)*, 153–160.
2. Antuniassi, U.R. (2015). Evolution of Agricultural Aviation in Brazil. *Outlooks on Pest Management 26(1)*, 12-15.
3. Bauša, L.; Steponavičius, D.; Jotautienė, E.; Kemzūraitė, A.; Zaleckas, E. (2018). Application of rape pod sealants to reduce adverse environmental impacts. *Journal of the Science of Food and Agriculture 9*, 2428–2436.
4. Child, R.D.; Summers, J.E.; Babij, J.; Farrent, J.W.; Bruce, D.M. (2003). Increased resistance to pod shatter is associated with changes in the vascular structure in pods of a resynthesized Brassica napus line. *Journal of Experimental Botany 54(389)*, 1919 – 1930.
5. Czech Statistical Office 2022. Statistical Yearbook of the Czech Republic – 2021. Accessed on May 6, 2022. Available online https://www.czso.cz/csu/czso/13-agriculture-rz0mwsbjrn
6. Faiçal, B.S. Freitas H.; Gomes, P.H.; Mano, L.Y.; Pessin, G.; de Carvalho, A.C.P.L.F.; Krishnamachari, B.; Ueyama, J. (2017). An adaptive approach for UAV-based pesticide spraying in dynamic environments. *Computers and Electronics in Agriculture 138*, 210-223.
7. Gibbs, J.; Peters, T.M.; Heck, L.P. (2021). Comparison of droplet size, coverage and drift

potential from UAV application methods and ground application methods on row crops. *Transactions of the ASABE 64(3)*, 819-828.
8. Gulden, R.H.; Shirtlie, S.J.; Thomas, A.G. Harvest losses of canola (Brassica napus) cause large seedbank inputs. (2003). *Weed Science 51*, 83–86.
9. Hewitt, A.J. (2008). Droplet size spectra classification categories in aerial application scenarios. *Crop Protection 27*, 1284– 1288.
10. Jiao, L.; Dong, D.; Feng, H.; Zhao, X.; Chen, L. (2021). Monitoring spray drift in aerial spray application based on infrared thermal imaging technology. *Computers and Electronics in Agriculture 121*, 135–140
11. Kosteckas, R.; Liakas, V.; Šiuliauskas, A.; Rauckis, V.; Liakien, E.; Jakien, E. (2009). Efect of pinolene on winter rape seed losses in relation to maturity. *Agronomy Research 7*, 347–354.
12. Nádasi, P., Szabó, I. (2011). On-board applicability of mems-based autonomous navigation system on agricultural aircrafts. *Hungarian Journal of Industrial Chemistry 39 (2)*, 229–232.
13. Nunes, A.L.; Ascari, J.; Pereira, L.; Sossmeier, S.G.; Bispo, N.B. Pod sealant and canola harvest methods for pod shattering mitigation. (2015). *Australian Journal of Crop Science* 9, 865–869.
14. Penney, A.J.; Kandel, Y.R.; Josh N. Viggers, J.N.; Robertson, A.E; Mueller, D.S. (2021). Comparison of aerial and ground sprayer fungicide application technologies on canopy coverage, disease severity, lodging, and yield of corn. *Crop Protection 139*, 105393.
15. Qin, W.-C.; Qiu, B.-J.; Xue, X.-Y.; Chen, Ch.; Xu, Z.-F.; Zhou, Q.-Q. (2016). Droplet deposition and control effect of insecticides sprayed with an unmanned aerial vehicle against plant hoppers. *Crop Protection 85*, 79-88.
16. Steponavičius, D.; Kemzūraitė, A.; Bauša, L.; Zaleckas, E. (2019). Evaluation of the Effectiveness of Pod Sealants in Increasing Pod Shattering Resistance in Oilseed Rape (*Brassica napus L.*). *Energies 12*, 2256.
17. USDA. World Agricultural Production. 2022. Accessed on May 6, 2022. Available online https://apps.fas.usda.gov/psdonline/circulars/production.pdf
18. Viret, O.; Siegfried, W.; Holliger, E.; Raisigl, U. (2003). Comparison of spray deposits and efficacy against powdery mildew of aerial and ground-based spraying equipment in viticulture. *Crop Protection 22*, 1023–1032.
19. Wrest Park History Contributors. (2009). Chapter 6 Crop protection. *Biosystems engineering 103 (Supplement 1)*, 70-78.
20. Zhan, Y.; Chen, P.; Xu, W.; Chen, S.; Han, Y.; Lan, Y.; Wang, G. (2022). Influence of the downwash airflow distribution characteristics of a plant protection UAV on spray deposit distribution. *Biosystems Engineering 216*, 32-45.
21. Zhu, Y.M.; Li, Y.D.; Colbach, N.; Ma, K.P.; Wei,W.; Mi, X.C. Seed losses at harvest and seed persistence of oilseed rape (Brassica napus) in different cultural conditions in Chinese farming systems. (2012). *Weed Research 52*, 317–327.

Corresponding author:
prof. Dr. Ing. František Kumhála, Department of Agricultural Machines, Faculty of Engineering, Czech University of Life Sciences Prague, Kamýcká 129, Praha 6, Prague, 16521, Czech Republic, phone: +420 22438 3135, e-mail: kumhala@tf.czu.cz

A QUALITATIVE AND ECONOMIC EVALUATION OF THE SPREADING OF DIFFERENT ORGANIC FERTILIZERS

Kristina LEKAVIČIENĖ[1], Raimonda ZINKEVIČIENĖ[1], Eglė JOTAUTIENĖ[1], Vilma NAUJOKIENĖ[1], Zita KRIAUČIŪNIENĖ[2], Algirdas JASINSKAS[1], Egidijus ŠARAUSKIS[1]

[1]Department of Agricultural Engineering and Safety, Faculty of Engineering, Agriculture Academy, Vytautas Magnus University, Lithuania.
[2]Department of Agroecosystems and Soil Sciences, Faculty of Agronomy, Agriculture Academy, Vytautas Magnus University, Lithuania

Abstract
Recently, the use of granular fertilizers in agriculture has been expanding rapidly due to their favorable properties in improving the environment and increasing operational efficiency. Therefore, a qualitative and economic evaluation of the precise application of granular and non-granular organic fertilizers has been performed in this work. The evaluation of the uneven application of organic fertilizers was performed by spreading cattle manure, manure granules, and lime in the spreading spreader "Rollforce" 5517. The economic evaluation was performed for mechanized technological operations of loading, transportation, and distribution of organic fertilizers, estimating the price of used aggregates and consumed fuel, the cost of individual technological operations, and other indirect costs. Studies have shown that manure is easier to spread over a wider area than pellets and lime, as manure particles are much larger and heavier. The lowest costs (180 Eur ha^{-1}) for the purchase of organic fertilizers are incurred using manure, but in the evaluation of mechanized technological operations, the lowest costs (2.32 Eur ha^{-1} and 6.65 Eur ha^{-1}) are obtained for fertilization with meat and bone meal pellets, and manure pellets.

Key words: *cattle manure; granulated fertilizers; lime fertilizers; costs; spreading.*

INTRODUCTION

To obtain an optimal yield, it is very important to provide growing plants with the necessary nutrients (*Schmitt & Vries, 2020; Sikora et al., 2020*). *Stewart et al.* (2005) states that crop fertilization increases crop production by 30-50%. The scientific literature states that there are many crops and plants with different growing habits as well as different nutrient needs. Fertilizers containing measured nutrient mixtures, which give plants access to potential nutrients, accelerate growth and provide higher yields than usual, help to meet these needs (*Hazra, 2016*). The main means of building up good quality humus are fertilization with organic fertilizers such as manure, compost, peat, straw (*Čiuberkis, 2005; Pranckietienė & Dromantienė, 2017; Jonikaitė, 2018*). Organic fertilizers are also defined as those derived exclusively from the remains of decayed or decaying plants or animals (*Khandaker et al., 2017*). The use of organic fertilizers not only saves on mineral fertilizers but also contributes to the preservation of the environment (*Jonikaitė, 2018).*
Manure has been used around the world for centuries as the optimal fertilizer for farming (*Chew et al., 2019*). Recently, the production of granular organic fertilizers manufacturing popularity, the main purpose of which is to convert organic substances with a high moisture content (manure, manure mixtures, meat, bone waste, or other organic substances) into convenient pellets. The granules are usually made in such a way that they can be spread with mineral fertilizer spreaders, preferably 4 or 6 mm (*Staugaitis et al., 2016*). This technology can be applied to manure processing to facilitate the export of manure nutrients to the market (*Sharara et al., 2018*). The main advantage of granular organic fertilizers is that they contain 50-75% organic matter. It is a very good tool for restoring the amount of humus in the soil (*Staugaitis et al., 2016*).
The efficiency of fertilizers is determined by many factors, but the focus is on fertilization rates and forms of fertilizer and the timing of fertilizer application, considering into account the stages of plant development. However, another important factor is the quality of the fertilizer application. Poor quality spreading of even the best fertilizers can have a negative impact on economic performance, increase environmental pollution and reduce plant quality (*Zinkevičius, 2004; Ştefan et al., 2019; Sikora et al.,*

2020). Equal the application of organic fertilizers is a complex process, as the consistency and size, and shape of fragments are not homogeneous, so the movement of fertilizers on the surface of the spreading (metal) and in the air is uneven (*Ştefan et al., 2019*). The dynamics of the spread of fertilizer particles are influenced by the fixed and changing technical specifications of the spreader. The point of descent of a particle on the soil depends on the trajectory of the particle itself, which is ejected by the rotating disk (*Pocius et al., 2014*).
To find the best technological solution for the application of various organic fertilizers, it is very important to carry out experimental studies of the properties of fertilizers and their application under real conditions in the field. It is equally important to carry out an economic assessment that would justify the cost-effectiveness of the use of different organic fertilizers. The aim is to perform a qualitative and economic assessment of the precise application of granular and non-granular organic fertilizers.

MATERIALS AND METHODS

Experimental research methods and parameters for the application of granular organic fertilizers to soil were selected and determined according to the relevant standards ISO 5690 and ASAE S314.2. The assessment of the uneven the transverse application of organic fertilizers was performed by spreading cattle manure, manure pellets, and lime in the spreading spreader "Rollforce" 5517. The unevenness of the fertilizer application is assessed by the coefficient of variation of the distribution of the fertilizer mass determined by collecting the spreading fertilizer over the entire working width of the fertilizer machine. For this purpose, in a line perpendicular to the direction of movement of the fertilizer implement, special boxes with dimensions of 500x400x10 mm are placed on the field surface over the entire working width of the fertilizer (Fig. 1). For spreading lime and granular fertilizer, cardboard partitions are placed in the trays so that the fertilizer does not bounce off the bottom of the tray and is evenly collected in the box.

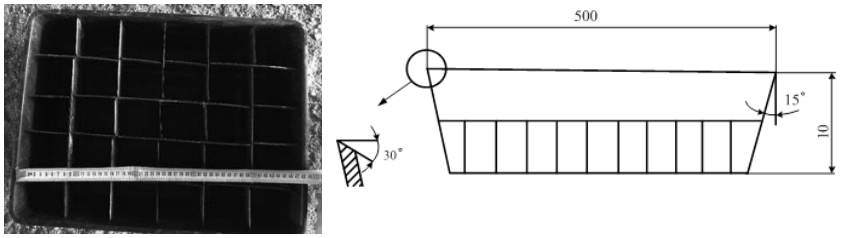

a) b)

Fig. 1 Experimental research boxes, used to determine the irregularities in the transverse application of the fertilizer: (a) general top view; (b) box scheme from the side

For one measurement, special boxes for collecting fertilizers are arranged in one row with a gap of at least one meter between them. The row of boxes is arranged so that the direction of movement of the machine coincides with the prevailing wind direction. 3 replicates were performed for each experiment. An example of the arrangement of the boxes is given in Fig. 2.

Fig. 2 Arrangement of boxes to determine the evenness of organic fertilizers

Fertilizers were spread while driving at a speed of 12 km h^{-1}. All fertilizers were spread with the same fertilization rate, 200 kg ha^{-1}.

The economic evaluation was performed for mechanized technological operations of loading, transportation, and spreading of organic fertilizers, estimating the price of used aggregates and consumed fuel, the cost of individual technological operations, and other indirect costs. Expenses affecting the change of economic costs in technological operations, calculated according to the rates of mechanized work services prepared by the Lithuanian Institute of Agrarian Economics (*LIAE, 2018*). Nitrogen N, phosphorus P_2O_5 and potassium K_2O fertilizer prices were selected according to the literature (*Kazlauskas et al., 2021*), accordingly N – 0,90 Eur kg^{-1}, P_2O5 – 0,8 Eur kg^{-1} ir K_2O – 0,5 Eur kg^{-1}.

Arithmetic means of the data, their standard deviations and confidence intervals at the probability level of 0.95 were determined.

RESULTS AND DISCUSSION

Experimental studies have shown that the lowest amount of lime fertilizer entered the boxes furthest from the spreading discs of the fertilizer machine. Box 6, meanwhile, has a maximum amount of fertilizer. It should be noted that this box was placed in the center between the tractor and the fertilizer wheels during the studies (Fig. 3a.). Studies on the uniformity of manure spreading with a manure spreader showed that the amount of manure in the test boxes ranged from 491 g to 982 g (Fig. 3a). The results of the study were evaluated by calculating a Gaussian coefficient that is less than 0, suggesting that the uniformity of distribution is greater than that of lime. This is because the manure particles are much larger and heavier, making it easier to spread them over a wider area during spreading.

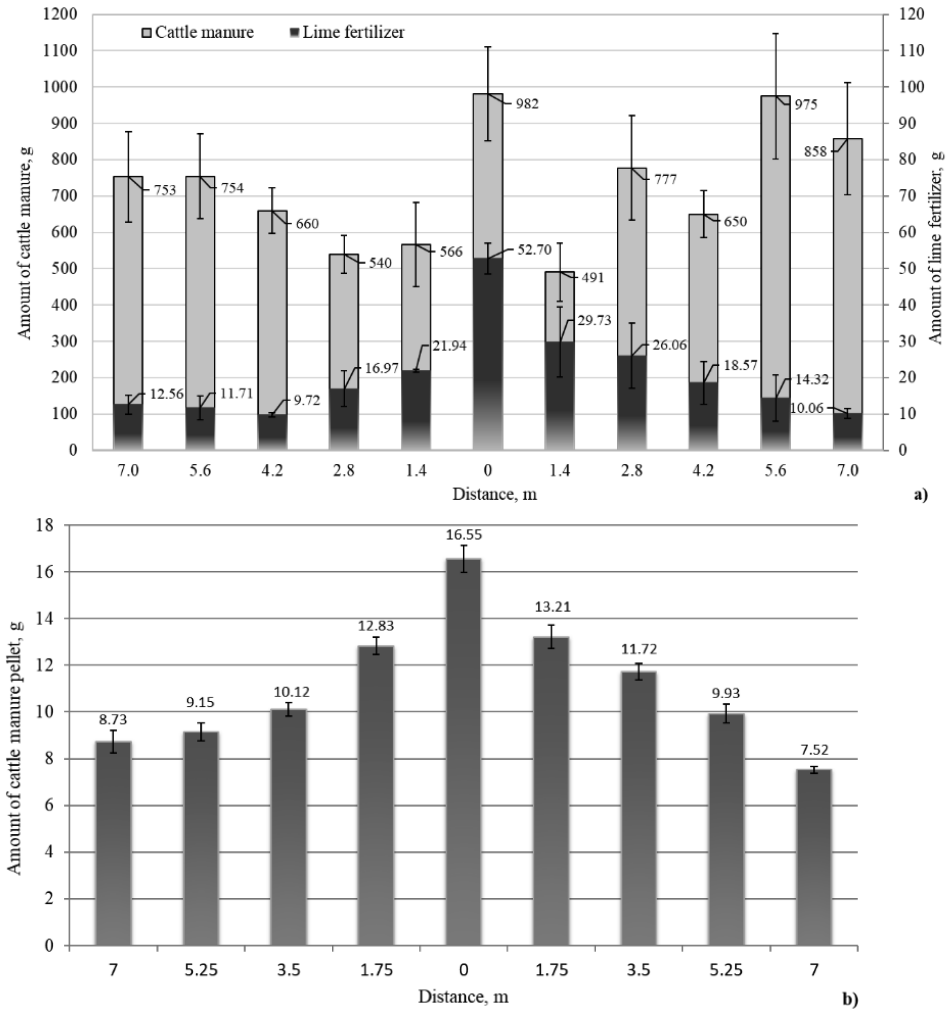

Fig. 3 Quality of organic fertilizer spreading: a – cattle manure and lime fertilizer; b – cattle manure pellet

As can be seen in Fig. 3b., the amount of organic granular fertilizer in the test boxes varied from 7.52 g to 16.55 g. The box in the center, which was in the middle of the fertilizer, had the highest amount of granular fertilizer falling between the tractor and the manure spreader wheels, reaching 16.55 g. The spreading of granular fertilizers was not uniform. In order to improve the spreading uniformity, it is necessary to increase the number of cross conveyor belts and the corps must not be fully no unloaded in order to ensure a smooth and even supply of pellets.
Analyzing the value of one tonne of organic fertilizer by individual elements, it was found that manure pellets and meat and bone meal pellets have significantly higher NPK levels than manure, so the rate of manure pellets or meat and bone meal pellets can be many times less that to provide similar economic benefits to the soil. However, in assessing the cost of organic fertilizers, it has been found that the cheapest organic fertilizer is manure (Tab. 1), as it is used for livestock production, and manure pellets or meat and bone meal pellets still have to go through a certain technological process before they become pellets form. As a result, their price per tonne is several times higher.

Tab. 1 Costs of organic fertilizers spreading

Organic fertilizers quantity	Costs on organic fertilizers, Eur ha^{-1}	Loading, Eur ha^{-1}	Transportation, Eur ha^{-1}	Spreading, Eur ha^{-1}	All costs, Eur ha^{-1}
Manure (16 t ha^{-1})	180	4.64	22.24	26.3	233.18
Manure pellet (2 t ha^{-1})	400	0.58	2.78	3.29	406.65
Meat and bone meal pellet (0.7 t ha^{-1})	273	0.20	0.97	1.15	275.32

An analysis of the costs of loading, transporting, and spreading different types of organic fertilizers has shown that the highest costs per hectare are incurred when manure is applied, 53.18 Eur ha^{-1} is spent. This is because is not enough for manure one spreader to in the spreading of one hectare. Depending on the capacity of the manure spread, you may need to drive several times. Distance also has a significant effect. In our case, the distance to the field was 7.5 km. The further away the field is fertilized from the livestock complex, the higher the transport costs. Fertilization with manure pellets with one load of spreader can fertilize several hectares and fertilization with meat and bone meal pellets - a dozen hectares. And this, of course, significantly reduces costs.
Organic fertilizer pellets have several other advantages over manure that are not always easy to evaluate money. Dry organic fertilizer pellets are much easier, cleaner, and safer to transport than wet manure (*Jotautienė et al., 2021*). The high temperature of pellet production allows the removal of all harmful pathogens or microorganisms, so safe and nutritious fertilizers reach the soil and plants. The granulation process also reduces unpleasant odors, which is very important during the transport and fertilization of fields (*Klyosov & Orekhovskaya, 2021*). Other authors state that the yield of spring wheat is significantly higher when using organic granular fertilizers compared to non-granular fertilizers (*Apaeva et al., 2021*).

CONCLUSIONS

The spreading of the pellets was influenced by the pulsating supply of pellets by the conveyor towards the spreading discs. To improve the uniformity of the spreading of the pellet's fertilizer by the spreader, it is necessary to increase the number of cross conveyor belts and to always have a not fully discharged corps to ensure a smooth and even supply of pellets. The effect on the uniformity of manure spreading is that the manure particles are much larger and heavier, which makes it easier to spread over a wider area during spreading, which is the opposite compared to lime fertilizers.
Fertilization costs for loading, transport, and spreading are several to dozen times higher than for manure pellets (8 times) and meat and bone pellets (23 times). Assessing the total costs, including the price of fertilizers, fertilization with manure results in only 42.14 Eur ha^{-1} lower costs compared to fertilization with meat and bone meal pellets, but significantly lower (173.47 Eur ha^{-1}) compared to fertilization with manure pellets. However, granular fertilizers are more easily compatible with modern agricultural machinery used for precision farming.

REFERENCES

1. Apaeva, N.N.; Yamalieva, A.M. & Manishkin, S.G. (2021) Ecologized technology of spring wheat cultivation with application of granular organic fertilizers. *Earth Environ. Sci*. 624, 012217.
2. Chew K.W., Chia S.R., Yen H.W., Nomanbhay S., Ho Y.C. & Show P.L. (2019). Transformation of Biomas Waste into Sustainable Organic Fertilizers. *Sustainability. MDPI*. 2266, p. 1–19.
3. Čiuberkis S., Čiuberkienė D., Končius D., Lapinskas E., Ambrazaitienė D. & Piaulokaitė-Motuzienė L. (2005). Effects of liming and fertilization systems on soil properties and agrocenosis productivity. *Agricultural sciences*. 2, 1–12.
4. Hazra G. (2016). Different types of Eco-Friendly Fertilizers: An Overwiew. *Sustainability in Environment*. Vol. 1, No. 1.
5. Jotautienė, E.; Mieldazys, R.; Gaudutis, A. & Aboltins, A. (2021) Granulation of poultry manure and biochar for production of organic fertilizers. *In Proceedings of the International Scientific Conference Engineering for Rural Development*, Jelgava, Latvia, 26–28 May 2021; p. 431–436.
6. Jonikaitė J. (2018). Why choose organic fertilizers? *Agroacademy*. 2018-03-13.
7. Kazlauskas, M.; Bručienė, I.; Jasinskas, A. & Šarauskis, E. (2021) Comparative Analysis of Energy and GHG Emissions Using Fixed and Variable Fertilization Rates. *Agronomy*. 11, 138
8. Khandaker M.M., Jusoh N., Ralmi N.H.A. & Izmail S.Z. (2017). The Effect of Different Types of Organic Fertilizers on Growth and Yield of Abelmoschus Esculentus L. Moench (Okra). *Bulgarian Journal of Agricultural Science. Agricultural Academy*. 23(1), p. 119–125.
9. Klyosov, D.N. & Orekhovskaya, A.A. (2021) On the development of technology for obtaining organomineral fertilizers. *Earth Env. Sci.*, 723, 032024.
10. LIAE. Prices of Mechanized Agricultural Services, Part 1, Main tillage. Vilnius, Lithuania. 2018. Available online: https://www.laei.lt/?mt=leidiniai&metai=201
11. Pocius, A.; Jotautienė, E.; Pekarskas, J.; Mieldažys, R. & Jasinskas, A. (2014). Research of particle geometrical parameters and aerodynamic features of granular organic compost fertilizers. In Engineering for Rural Development, Proceedings of the 13th International Scientific Conference Proceedings, Jelgava, Latvia, 29–30 May; Latvia University of Agriculture: Jelgva, Latvia, 2014; pp. 401–406.
12. Pranckietienė I. & Dromantienė R. (2017). Organic fertilizers. *My farm*, 2017/12. https://manoukis.lt/mano-ukis-zurnalas/2017/12/organines-trasos/
13. Schmitt, E. & Vries, W. (2020). Potential benefits of using Hermetia illucens frass as a soil amendment on food production and for environmental impact reduction. *Current Opinion in Green and Sustainable Chemistry*. 25, 100335.
14. Sharara M.A., Runge T., Larson R. & Primm J.G. (2018). Techno-economic Optimisation of Community-based Manure Processing. Agricultural Systems. Elsiever. 161. p. 117–123
15. Sikora, J., Niemiec, M, Tabak, M., Gródek-Szostak, Z., Szeląg-Sikora, A., Kuboń, M. & Komorowska, M. (2020). Assessment of the Efficiency of Nitrogen Slow-Release Fertilizers in Integrated Production of Carrot Depending on Fertilization Strategy. *Sustainability*. 12(5), 1982.
16. Staugaitis G., Masevičienė A., Mažeika R. & Arbačiauskas J. (2016). Granular organic fertilizers. *Peasant newspaper*. 2016-10-31.
17. Stewart, W.M., Dibb, D.W., Johnston, A.E. & Smyth., T.J. (2005). The Contribution of Commercial Fertilizer Nutrients to Food Production. *Agronomy Journal*, 97(1), 1–6.
18. Ştefan, V., Sfîru, R. & Popa L. (2019). Experimental results on the solid organic fertilizer machine MG 5. E3S Web of Conferences 112, 03007, TE-RE-RD 2019.
19. Zinkevičius. R. (2004). Requirements for modern organic fertilizer application techniques. *My farm*. 2004/12.

Corresponding author:
Kristina Lekavičienė, Ph.D., Department of Agricultural Engineering and Safety, Faculty of Engineering, Agriculture Academy, Vytautas Magnus University, Studentu Str. 15A, LT-53362 Akademija, Kaunas District, Lithuania, e-mail: kristina.lekaviciene@vdu.lt

INNOVATIONS OF BARN CONSTRUCTIONS FOR BETTER PARAMETERS OF THE BREEDING ENVIRONMENT

Jana LENDELOVÁ[1], Ingrid KARANDUŠOVSKÁ[1], Milada BALKOVÁ[1], Miroslav ŽITŇÁK[1]

[1]Institute of Agricultural Engineering, Transport and Bioenergetics, Faculty of Engineering, Slovak University of Agriculture in Nitra, Tr. A. Hlinku 2, 949 76 Nitra, Slovakia

Abstract
The aim of this study was to determine the concentrations of harmful gases and microclimate parameters of the indoor air in two different building and construction types of dairy housing in the summer season with an emphasis on evaluating the effect of structural innovation, air chemistry and animal thermal load indices, as well as parameters of the quality of the employees' environment. The results consisting of measurements of microclimatic parameters, measurements of pollutant concentrations and calculation of the heat load indexes THI and ETIC, showed a partial reflection of various building and construction solutions for the quality of the breeding environment. During hot summer days, no significant differences in heat load indices were detected between the low-volume object (where VA=34.3 m^3 per animal) with 5 basket sliding fans (total output 82500$m^3.h^{-1}$) compared to the index values in the large-volume object with natural ventilation (where VB =82.5 m^3 per animal). The concentrations of CO_2, NH_3, CH_4 and H_2S were significantly lower in the large-volume object (P<0.01), which, including the design conditions, predicts more effective conditions for ensuring the required environmental hygiene.

Key words*: cattle housing, gas concentrations, temperature-humidity index, equivalent temperature index.*

INTRODUCTION

Agriculture and animal husbandry are important sources of greenhouse gas (GHG) emission and contribute to climate change (*Li et al., 2021*). Emissions of ammonia (NH_3) and greenhouse gases, e.g. methane (CH_4), carbon dioxide (CO_2) and nitrous oxide (N_2O), from livestock production systems are of great concern to livestock producers, environmentalists, and governments due to their negative impact on surrounding environment and global climate (*Kavanagh, 2019*). Their high concentration in production buildings has a negative effect on both livestock and livestock breeders. Poor ventilation can increase the relative humidity and the concentration of harmful gases such as carbon dioxide and ammonia. The concentration of carbon dioxide depends to a large extent on the type of building, the ventilation system and the density of the animals. Many factors influence the concentrations of harmful gases, in especially high temperature, emitting area and emission source, etc. Due to climate change, even in temperate climates, the issue of high air temperatures and increased heat load is increasingly becoming more common and affects high producing dairy cows the most (*Herbut, 2021*). One option to reduce heat load in dairy cows is by using flow cooling through natural and forced ventilation. Natural ventilation is dependent on weather and structural design and is often not adequate in summer. Then it is required to provide cooling by forced ventilation or by a combination of several methods - evaporative cooling, shading, spraying of animals, etc. (*Fournel, 2017; Doležal, 2010*). To assess the quality of the environment, in scientific practice, combined methods are used - part of practical measurements and part of theoretical calculations, or the detection of production or health indicators. The worst combination is when extremes in both high concentration of pollutants and high heat load of animals occur. The article is devoted to the comparison of the state of air chemistry and the level of heat load in two structurally different types of housing buildings.

MATERIALS AND METHODS

The study was performed during the summer season in two types of dairy cattle barns with different process and technical systems, in the old (A) and new building (B) in the same farm. The barns differed in herd size, housing system, and manure management. The older three-row building A (Fig. 1) was 11.5 m wide and 70 m long, with a side (longitudinal) wall height of 4.3 m and a total height of 9.7 m

at the ridge. The building had 3 rows of diagonally arranged cubicles for free housing of 158 dairy cows. One row of cubicles was oriented directly to the wall, and it was separated from the double-row cubicles by an internal movement corridor 2.45 m wide. An outdoor feeding area with a length of 70 m and a width of 3.25 m was added to the building. The ceiling parts were removed due to an increase in the volume of the building from the original 2,329.6 m^3 to 5,154.1 m^3. The ridge of the roof was opened to at a width of 350 mm and parts of the roof covering were illuminated by five vertical strips 1 m wide. Milking took place twice a day, ad libidum feeding with supplementary feeding twice a day. There were 34.3 m^3 per animal in the building, area of 4.85 m^2 per animal in the interior and 6.37 m^2 per animal including the outdoor covered feeding area. Five basket fans were installed in the longitudinal axis above the double-row of cubicles, each with a capacity of 16,500 m^3h^{-1} (total 82,500 m^3h^{-1}). Cleaning of cubicles and corridors was carried out twice a day, coordinated to milking time. Fresh litter up to 100 mm thick was spread daily during morning milking.

The new eight-row building B (Fig. 2) for 444 dairy cows (Czech spotted cattle) had two internal feeding corridors, the length of the building was 85.4 m with the height of the 3-sector counter roof in the ridge of 18.2 m. The height of the wall was h_s=8 m on the south side, h_n=6.5 m on the north side. The front walls were made of Agropanels with a thickness of 40 mm, 8 gates for the entry of the mechanisms were made up of remote-controlled green plastic blinds. The roller shutter system was also used on the side walls, where a fully openable roller shutter 85 m long and 4.8 m high was made above the 2.1 m high fixed wall. The roof area was composed of three roof boards - the southern area made of Agropanels 1,500 m^2, the middle area made of double-cavity polycarbonate corrugated roofing 1,865 m^2 at a slope of 15° and the northern Agropanel-roof area of 1,440 m^2 at a slope of 24°. Two large vertical slits were made along the entire roof, which ensure the removal of air through natural ventilation. The upper continuous intermediate opening in the ridge was 3.3 m high, the second roof opening was 1.5 m high. The deepened cubicles were 2,700 mm long in a single-row and double-row arrangement (head-to-head) with a depth of 0.3 m in the filling area. This part of the bed was made of moistened and compacted straw and limestone, which was leveled with the height of the litter threshold. A fresh layer of chopped wheat straw (approximately 100 mm thick) was applied daily to this permanent foundation. This layer was cleaned twice a day with subsequent removal of all excrement.

The concentrations of CH_4, NH_3, N_2O, and CO_2 were measured using a photo-acoustic multi-gas analyser 1309 (Inova, Denmark). The measurement of gas concentrations inside the breeding environments was located on the sampling points according to Fig.1 and Fig. 2 at a height of 1.8 m above the floor. The outdoor location was chosen along either side of the barn at the height of about 2 m above the ground. The average air temperature and relative humidity were measured every 5 min using datalogger Comet. Three data loggers were placed close to the gas sampling locations inside the barn, and two data loggers were placed outside the barn. The two types of indexes were used to evaluate the heat load of animals. The temperature humidity index (THI) was calculated according to *Kelly & Bond, (1971)*. There are four load levels: mild heat stress 72 < THI < 79, moderate stress 80 < THI < 89 and severe heat stress THI > 89 (*Hoffmann et al., 2020*). The Equivalent Temperature Index for Dairy Cattle (ETIC - calculated according to *Wang et al., 2018*) takes into account - in addition to temperature and relative air humidity - air velocity and solar radiation (*Hempel et al., 2019*). There are also four load levels: mild category 18 ≤ ETIC < 20, moderate category 20 ≤ ETIC < 25, severe category 25 ≤ ETIC < 31, emergency category 31 ≤ ETIC (*Hempel et al., 2019*). The quality of the workers' working environment was evaluated according to Act No. 355/2007 and Decree No. 99/2016. The aim of this study was to determine the concentrations of harmful gases and microclimatic properties of indoor air in two different building and construction types of dairy housing in the summer season with an emphasis on the evaluation of the effect of structural innovation on air chemistry and animal heat load indexes, as well as parameters of the quality of the employees' environment.

Statistical analysis

Data on climatic parameters, gas concentrations in two barns with different housing systems were processed statistically. Since all variables had a normal distribution, single factor ANOVA was performed. The significance of differences between the mean values of gas concentrations in barns was determined by Tukey's test. All calculations were made using Statistica 10 for Windows (StatSoft, CZ).

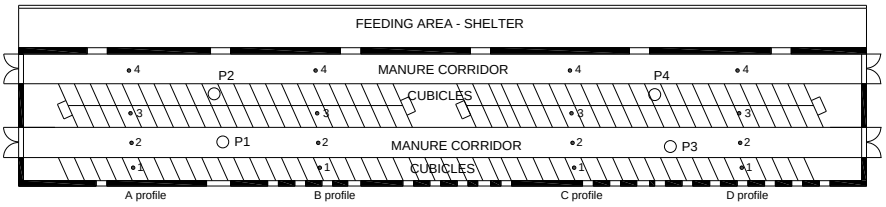

Fig. 1 Floor plan of object A with measuring points P1 – P4 of gases and points 1 - 4 of measuring microclimate parameters

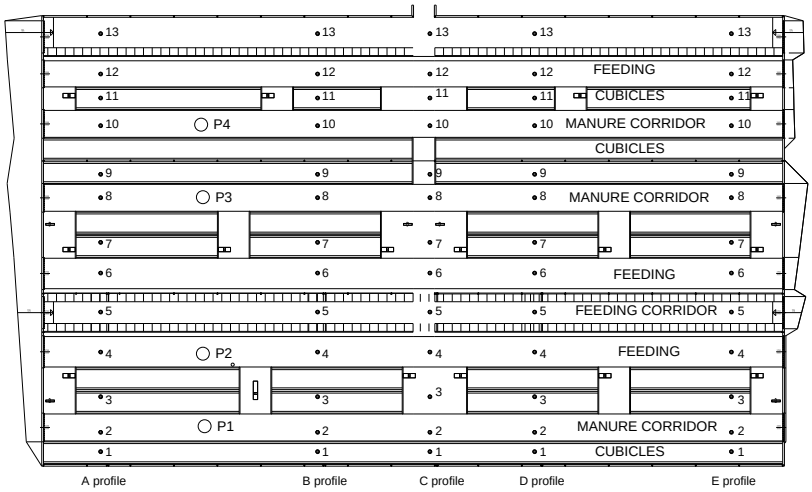

Fig. 2 Floor plan of object B with measuring points P1 – P4 of gases and points 1 - 13 of measuring microclimate parameters

RESULTS AND DISCUSSION

The results of the on-farm measurements and climate index calculations are shown in Figures 3 and 4. The optimum temperature in dairy cow housing is 8-16°C (*Gálik et al., 2015*). As aspected - in neither building was the optimal temperature ensured. In the location of Central Europe, this is almost impossible during the day in summer. Moreover, the methodology of the experiment was aimed at monitoring situations during days with extremely high outdoor air temperatures, so that air chemistry and heat load were assessed for critical cases. The climatic data was recorded during the period with outdoor air temperature 30°C<T_{ext}<32°C, relative humidity 47%<RH_{ext}<53% and airflow velocity 0.2 m.s^{-1}<v_{ext}<1.2 m.s^{-1}. During the assessment of indoor climate parameters, no significant differences were found between objects A and B (P>0.05), however, in accordance with the methodology - fans were not installed in building B. The intention of the breeder was to provide the new building with a large-cubicle space with low-energy, quiet and low-emission operation. Mean concentrations of greenhouse gases and ammonia differed significantly (P<0.01) between facilities. Building B (new) was characterized by lower (P<0.01) mean concentrations of GHGs and ammonia compared to Building A (Table 1). The detected amounts of all gases were lower than the recommended environmental limits for workers and animals during the experiment. The microclimate in the stables has both direct and indirect effects on animal health, as it significantly influences the emissions and concentrations of ambient gaseous gases such as greenhouse gases, ammonia and VOCs. The release of NH_3 and CO_2 from manure is determined by the temperature and moisture content of the straw, among other factors (*Witkowska & Sowinska, 2017*). The observed differences in GHG concentrations can be attributed to the different technological systems in the analysed barns. According to *Dimov et al. (2019)*, temperature and relative humidity are related to CO_2 levels. In the study (*Dimov et al., 2019*), the lowest CO_2 concentrations and the smallest variations in CO_2 levels were recorded in barns with automated and robotic cleaning systems. In our experiment, the average CO_2 concentration in the new barn (B) was 9.8% lower than in barn A. The most significant improvement in chemistry was observed for NH_3, which was 34.2% lower in the new facility, and CH_4

concentrations were 41.5% lower than in the old facility. Microclimatic parameters are an important physical factor of the working environment that affects working conditions in workplaces. For this reason, in our legislation (§ 37 of Act No. 355/2007) lays down the basic obligations of employers to protect the health of employees against the burden of heat and cold at work, and Decree No. 99/2016 of the Ministry of Health of the Slovak Republic lays down details related to the protection of the health of employees against the burden of heat and cold at work. For working class "1b", the optimum temperature is T_{op}=22-25°C (T_{min}=19°C, T_{max}=27°C), permissible relative humidity RH=30-70% and permissible air velocity v≤0.3 m.s^{-1}. However, the daily tasks of the staff working to provide the necessities of life and hygiene in the housing facilities are not continuously tied to their permanent performance only in those facilities during working hours. Especially in a new facility, the working time in the barn is reduced to the time necessary for the operation of machinery, possible repairs and maintenance. The longest stays are for the treatment of animals, part of which is usually carried out by external staff - the veterinary service. The construction of the building with a new structural design and innovative housing technology has increased the comfort of the housed animals and the air quality in terms of ammonia production, greenhouse gases as well as microclimatic parameters.

Tab. 1 The minimum, maximum values and average values of all measurements of gases, temperature and relative humidity

	old three-row building A				new eight-row building B				Limit values mg.m^{-3}
gas con-centr. mg.m^{-3}	average	min	max	st. dev.	average	min	max	st. dev.	
CO_2	1422.9	852.1	2619.7	290.6	1295.3	912.5	2045.8	170.7	4582
NH_3	2.5	1.1	5.1	0.6	1.8	0.7	4.1	0.4	17.6
CH_4	22.9	6.8	60.4	9.1	16.2	7.9	76.8	5.0	666
N_2O	0.9	0.6	3.7	0.1	0.8	0.5	1.3	0.1	180
H_2S	1.5	0.7	3.3	0.2	1.3	0.4	2.7	0.3	14

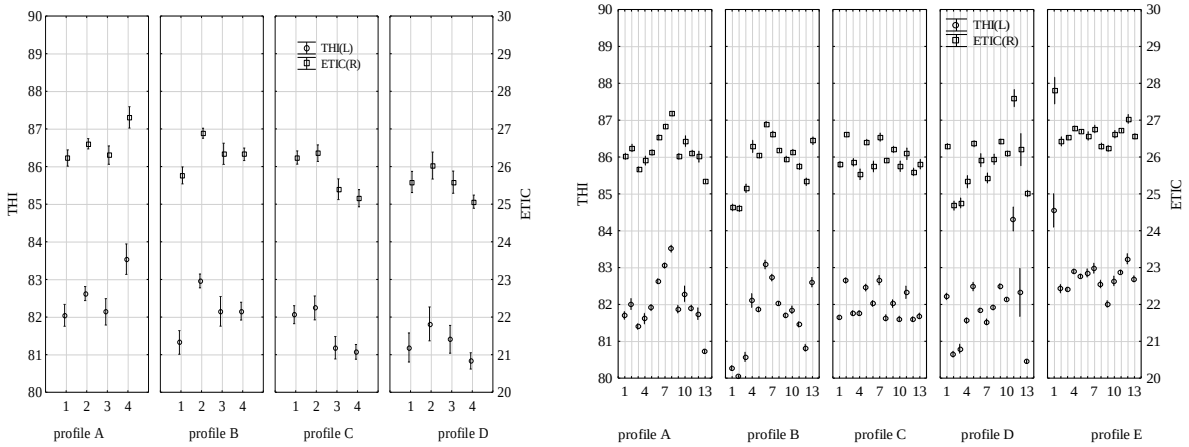

Fig. 3 left: results of the evaluation of the THI and ETIC heat load indexes in building A. The average values found by measurements and calculation from the 16 measurement locations in the old building were: THIA,AVG=81.93±0.87 and ETICA,AVG=26.09±0.71; right: results of the evaluation of the THI and ETIC heat load indexes in building B. The average values found by measurements and calculation from 65 measurement locations in the old building were: THIB,AVG=82.09±0.89 and ETICB,AVG=26.12±0.71.

The productivity of labour has also increased, the cubic volume of the environment has increased from the original V_A=34.3m^3 to the new V_B=82.5 m^3 per cow. These results are in accordance with the statement of *Pogran et al. (2011)* that the construction-technological design of buildings for livestock production has a significant impact on the formation of the indoor environment, which is formed by the air content of the housing space, the temperature and humidity of the air, its movement and stratification,

the amount of solid, gaseous (CO_2, NH_3, H_2S) and bacterial parts. Long heat waves have a strong influence on the impairment of welfare and reduced performance of dairy cows (*Herbut et al., 2021*). Management strategies for cows against heat stress can be summarized into the following components: physical environmental modification, genetic development of heat-tolerant breeds, and improved nutritional management practices (*Johnson, 2018*). Construction parameters are also essential in the context of ventilation (*Drewry et al., 2018*). Air quality variability also influences the quality of the animal environment and the working environment of caregivers, as well as the quality of bedding, which secondarily also influences animal welfare (*Némethová et al., 2020*). The design of ventilation openings in buildings with natural ventilation is also an important element subject to beneficial innovative changes *Li et al. (2021)*. In accordance with his testing, the design of the side walls of barn B of our experimental farm stands out, where the wall openings occupied the area, protected by a controllable roller shutter system, $A_{B,w}$=882 m^2. The vertical openings between the roof slabs with the area of the upper opening $A_{B,1}$=280 m^2 and the lower vertical opening $A_{B,2}$=127 m^2 effectively helped the flow regime. In total, there were 2.7 m^2 of structural openings per animal in barn B.

CONCLUSIONS

On the dairy farm located 287 m above sea level, during hot summer days with an indoor air temperature T_{avg} > 32°C in a three-row barn with a lower cubic capacity (V_{Aa} = 34.3 m^3 per animal) with motoric ventilation and a total capacity of 82,500 $m^3.h^{-1}$ (Q = 522 m^3 per animal) – there were THI_{avg} = 81.93±0.87 and $ETIC_{avg}$ = 26.09±0.71. According to our measurements, the installation of more powerful fans would be necessary, and especially the installation of fans even in the single row of cubicles along the wall, which is technically difficult. If an increase in air velocity by 1 $m.s^{-1}$ is achieved, theoretically the air exchange in the building could be increased from 28.4 h^{-1} to 68.9 h^{-1}, where the recommended value of ACH>80 h^{-1}. This solution would help in moisture reduction, but according to THI calculations, even with a 10% drop in relative humidity, this would not be able to adjust the degree of heat load to the required level (THI<72). The ETIC index responds more flexibly not only to relative humidity but also to an increase in flow velocity, but to achieve the required value of ETIC = 20, it would be necessary to ensure an average airflow velocity of v>7.1 $m.s^{-1}$, which is irrational. Also the additional cooling of the animals by evaporative cooling has limitations in this building due to the necessary ventilation of the additional humidity and it would be more rational to use it in an outdoor feeding area, where - it does not affect the interior effect, however. Moreover, even with the use of motorized ventilation, the NH_3 and CH_4 levels were more than 34.2% and 41.5% higher, respectively, than in the new eight-row large cubicle building without the use of fans. The investment of the new building was increased by the higher cubature (V_{Ba}=82,5 m^3 per animal), mainly by the size of the openings. These are advantageously used during the whole year with a natural ventilation system that works cost-free, without additional energy and noise. The large openings in the wall are covered with plastic roller shutters with adjustable height up to 4.8 m, which is not a costly element at the prices of building components. The openings in the roof are uncovered, thus at no cost. In a large cubature building, in addition to lower concentrations of harmful gases, we found spatial and installation advantages of using cyclonic fans, which, with unit capacities of 55,000 $m^3.h^{-1}$ to 85,000 $m^3.h^{-1}$ and their regulatability, would increase heat removal in the summer and, in the case of increased humidity, from the elements of evaporative cooling. To make the effect of the ventilation technique more effective, it would be advisable to prepare simulations of the distribution of fans using baffle shutters and subsequent more detailed research to assess the balance of the benefits of using forced ventilation in such a building design.

ACKNOWLEDGMENT

This study was supported by the Operational Programme Integrated Infrastructure within the project: Sustainable smart farming systems taking into account the future challenges 313011W112, co-financed by the European Regional development fund.

REFERENCES

1. Dimov, D., Marinov, I., Penev, T., Miteva, Ch. & Gergovska, Z. (2019). Animal hygienic assessment of air carbon dioxide concentration in semi-open freestall barns for dairy cows. *Bulgarian Journal of Agricultural Science, 25*(2), 354-362.
2. Drewry, J.L., Mondaca, M.R., Luck, B.D. & Choi, C.Y. (2018). A computational fluid dynamics model of biological heat and gas generation in a dairy holding area. *Transactions of the ASABE, 61*(1), 449–460.
3. Doležal, O. (2010). Methods of eliminating heat stress - a significant breeding reserve. Praha: IAS
4. Fournel, S., N. Rousseau, A. & Laberge, B. (2017). Rethinking environment control strategy of confined animal housing systems through precision livestock farming. *Biosystems Engineering, 155*, 96-123.
5. Gálik, R., - Mihina, Š., Boďo, Š., Knížková, I., Kunc, P., Celjak, I., Šístková, M., Botto, Ľ. & Brestenský, V. (2015). Technique for animal husbandry. Nitra: SUA
6. Herbut, P., Hoffmann, G., Angrecka, S., Godyń, D., Vieira, F. M. C., Adamczyk, K. & Kupczyński, R. (2021). The effects of heat stress on the behaviour of dairy cows. *Annals of Animal Science, 21*(2), 385-402.
7. Hempel, S., Menz, C., Pinto, S., Galan, E., Janke, D., Estelles, F., Müschner-Siemens, T., Wang, X., Heinicke, J., Zhang, G., Amon, B., Del Prado, A. & Amon, T. (2019). Heat stress risk in European dairy cattle husbandry under different climate change scenarios - uncertainties and potential impacts. *Earth Syst. Dynam. Discuss. 10*(4), 859–884.
8. Hoffmann, G., Herbut, P., Pinto, S., Heinicke, J., Kuhla, B. & Amon, T. (2020). Animal-related, non-invasive indicators for determining heat stress in dairy cows. *Biosystems Engineering, 199*, 83 -96.
9. Johnson, J.S. (2018). Heat stress: Impact on livestock well-being and productivity and mitigation strategies to alleviate the negative effects. *Animal production science journal, 58*, 1404-413.
10. Kavanagh, I., Burchill, W., Healy, M.G., Fenton, O., Krol, D.J. & Lanigan, G.J. (2019). Mitigation of ammonia and greenhouse gas emissions from stored cattle slurry using acidifiers and chemical amendments. *J. Clean Prod., 237*, 117822.
11. Kelly, C.F. & Bond, T.F. (1971). Bioclimatic factors and their measurements. Washintong: National Academy of Sciences.
12. Li, M., Liu, Sh., Sun, Y. & Liu, Y. (2021). Agriculture and animal husbandry increased carbon footprint on the Qinghai-Tibet Plateau during past three decades. *Journal of Cleaner Production, 278*, 123963.
13. Némethová, M., Lendelová, J., Šranková, V., Žitňák, M. & Botto, Ľ. (2020). Verification of thermo-technical characteristics of selected floor constructions for dairy cows. Acta technologica agriculturae, *23*(2), 87-91.
14. Pogran, Š., Bieda, W., Gálik, R., Lendelová, J. & Švenková, J. (2011). The quality of the indoor environment of housing facilities. Nitra: SUA.
15. Wang, X., Gao, H., Gebremedhin, K. G., Bjerg, B. S., Van Os, J., Tucker, C. B. & Zhang, G. (2018). A predictive model of equivalent temperature index for dairy cattle (ETIC). *Journal of Thermal Biology, 76*, pp. 165–170.
16. Witkowska, D. & Sowinska, J. (2017). Identification of microbial and gaseous contaminants in poultry farms and developing methods for contamination prevention at the source. *Poultry Science*, London: IntechOpen.
17. Act No. 355/2007 *Coll. Act on the Protection, Support and Development of Public Health and on Amendments to Certain Acts*
18. DECREE 99/2016 *Collections of laws of the Ministry of Health of the Slovak Republic on details on health protection against heat and cold stress at work*

Corresponding author:
doc. Ing. Ingrid Karandušovská, PhD. Institute of Agricultural Engineering, Transport and Bioenergetics, Faculty of Engineering, Slovak University of Agriculture in Nitra, Tr. A. Hlinku 2, 949 76 Nitra, Slovakia, phone: +421 37 641 5691, e-mail: ingrid.karandusovska@uniag.sk

DYNAMIC BIAXIAL LOADING OF CAR SEATS

Petr LEPŠÍK[1], Vítězslav FLIEGEL[2], Aleš LUFINKA[3]

[1]*Faculty of Mechanical Engineering, TU of Liberec, Studentska 2, Liberec 1*
[2]*Faculty of Mechanical Engineering, TU of Liberec, Studentska 2, Liberec 1*
[3]*Faculty of Mechanical Engineering, TU of Liberec, Studentska 2, Liberec 1*

Abstract
Testing of car seats and evaluation of their quality depends on the testing technology used. Basically we have two options to test the car seat in the car in a real ride or laboratory. Both methods have their advantages and disadvantages. Testing a car seat in a car has a great advantage in performing the test. You just need to sit on the driver's or passenger's seat, choose the right route for driving and the whole test is set, unfortunately the big disadvantage is the repeatability of such a test, e.g. there must always be the same the "test" person is preferably at the same time of the day and the same driver, i.e. the same driving style on a given route in the same weather conditions. From experience, we can say that it will never be possible to 100% reproduce the test. The advantage of laboratory testing is the almost perfect reproducibility of test conditions, but the great disadvantage is the high time required for preparation, e.g. measurement of test signals from real driving, reproducibility of these signals by the control system of the laboratory test equipment.

Key words: *car seat; testing; biaxial loading, measurement standards.*

INTRODUCTION

Testing of car seats in laboratory conditions is performed according to the relevant standards (*ASTM D3574-11; JASO B407-87; DIN EN ISO 3385; JASO B407-871978*). Each standard specifies a test method that corresponds to a particular car seat load regime. The comfort of sitting and the level of fatigue after a long drive with the car depend on the interaction properties of the car seat with the human body at the point of contact with the seat. Reproduction of seat testing in real operation in laboratory conditions requires strict adherence to prescribed standards, i.e., simultaneous multi-axis loading in the vertical and two horizontal directions. Therefore, the test equipment must be increasingly sophisticated, enabling the implementation of load signals in multiple axes. The possibility of comparing tests from real operation and their uniform evaluation also depends on the method of realization of test signals. Of course, the signals must be recorded correctly in the actual driving of the car along the specified route. A number of studies have already been carried out in the area of loading PU foams describing its specific properties (*Han et al., 2011; Werner & Daniel, 2014; Yang et al., 2021*) and describing properties under uniaxial loading (*Fliegel & Martonka, 2015; Martonka & Fliegel, 2016b*). The aim of this paper is to compare influence of one- and two-axes dynamic loading of car seat.

MATERIALS AND METHODS

Testing device

The current test facility was created as an innovation of the existing facility, which allowed the performance of load tests of car seats in only one axis, i.e. vertical in the "z" axis. However, current normative legislation requires testing in two axes, i.e. in the vertical axis and in the anteroposterior axis at the same time. In order to meet the requirements of the standard, we have added a horizontal actuator to the existing equipment, which serves as an exciter in the “x” axis (Fig.1). The excitation range in the vertical axis is plus / minus 200mm and the anteroposterior axis is plus / minus 50mm. These ranges richly cover the requirements of currently valid standards as well as the ranges of measured values of excitation signals in real driving. A great advantage of said test device is the overall energy consumption for the test. Because the exciters are electric, their consumption is an order of magnitude lower than that of their hydrodynamic analogist. A sufficient amount of oil with the required pressure is required for the hydrodynamic hexapod to function properly, but this is created in the unit with the required power. This increases the price of individual tests many times over. There is an expert discussion about the economy

and ecology of the laboratory tests performed. Optimization of energy intensity of laboratory tests determines the possibilities of their practical use. The signals required by the test methodology, both measured and generated, will used as test signals. The spatial movement of the seat or the load is then composed of the realized excitation signals. From the preferred fluctuations and frequencies of the excitation signal, we can prioritize the "force" of excitation in individual directions.

Fig. 1 Original test equipment for biaxial loading

Testing loading

Fittings corresponding to the EuroSit III test dummy were used as test loads. The existing test equipment was used to perform the dynamic test. Loads differ in their design. The first type is very similar to the human body, i.e. it is shaped like a moderately static person. This manikin is used both in testing in a moving car as a "passenger" and in static testing of the seat, e.g. for measuring the H-point. The second type of load used is a European copy of a medium-sized statistical person (Fig. 2). It is mainly used for dynamic tests, both with free load, e.g. for determining transmission characteristics, ie dynamic load, and with vertically guided load for determining, for example, seat creep. In this study we used the second manikin.

Fig. 2 Original loading

Principles of control

The actuator is basically an electric motor with a gearbox and a motion screw. This converts the rotary motion of the motor into a sliding motion. The actuator is also equipped with a position sensor which is used for position feedback control. An integral part of the actuator is an external control unit that provides power to the electric motor and implements the position feedback control. The actuator control unit is connected to the user computer in several ways. The RS 485 serial line and software supplied by the actuator manufacturer are used for basic parameter settings. The user application created in the Labview environment is then used to control the movement of the actuator during testing. It uses logical lines for communication, which are used for basic commands and status signals (eg start, ready, etc.). The value of the desired position of the actuator is transmitted by an analog signal, so the speed is not limited, for example, by the transmission speed of the serial line, and position changes can be very fast.

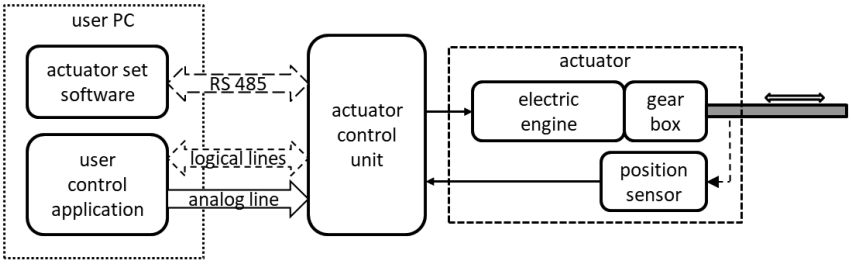

Fig. 3 Block diagram of the basic actuator connection

The test device allows movement in two axes Z and X. It therefore has two actuators, which are controlled simultaneously by the user application. A connection block diagram is shown in the following figure.

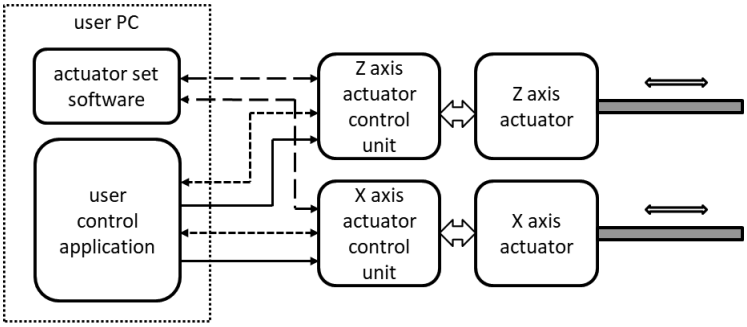

Fig. 4 Block diagram of the testing device actuators connection

The user control application can to use an external file with time record of the excitation signal for the actuator control or can directly generate fundamental harmonic signals. These methods can also be combined, for example the Z axis can be controled with an external file and harmonic signal can to be add to the X axis. This control method was also used for this testing, the Z axis was always excited by the same signal from the file and harmonic signals with different amplitude and frequency were gradually added to control the X axis.

Test signals and measurement

The resonant frequency of passive car seats is usually around 6 Hz. Therefore, an excitation signal in the range of 0.5 to 16 Hz is usually used for the measurement. The frequency increases continuously during the measurement in the specified range and the amplitude of the oscillations is usually set so that the acceleration value of the excitation signal remains constant. Therefore, the amplitude must decrease with increasing frequency of the excitation signal. Such a signal was created for the basic excitation in the Z axis, the value of acceleration amplitude was set to 0.1 G. Its example is shown in the following figure.

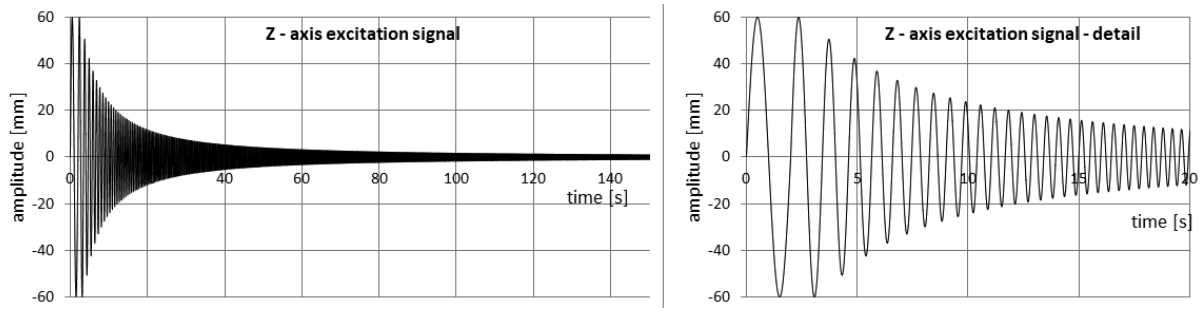

Fig. 5 Test signal for Z-axis excitation

Harmonic excitations in the X-axis direction with different amplitudes and frequencies were then added to this basic Z-axis excitation signal during testing. An example of such a compound excitation is shown in the following figure.

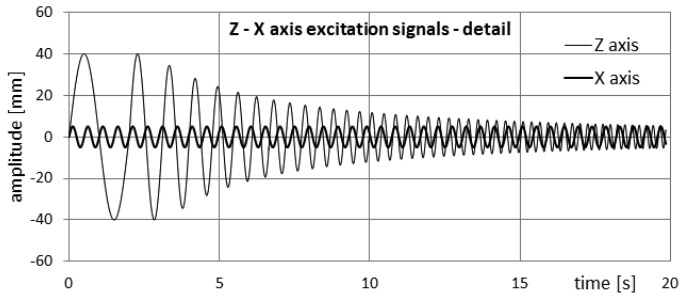

Fig. 6 The example of the compound Z–X axis excitation

The Dewe 5000 measuring device was used for the measurement. Non-contact laser position sensors were used to measure table and mass movements in the Z-axis direction. Two accelerometers simultaneously measured the acceleration of the table and the mass again in the direction of the Z axis. The experiment was further captured by a camera, the image recording is synchronized with the measured data. The sampling frequency of the data was 500 Hz, the camera took 100 images per second.

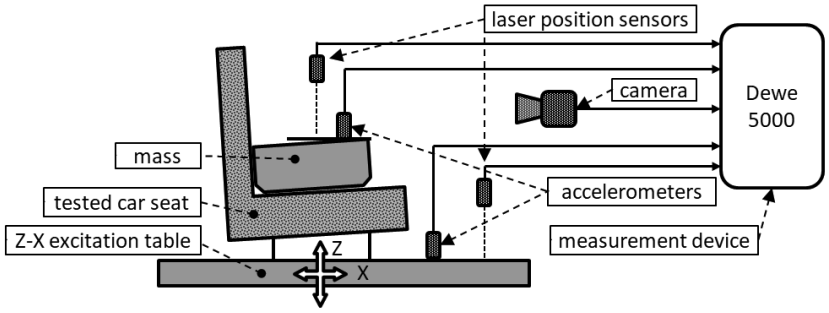

Fig. 7 Block diagram of the measurement arrangement

Mathematical channels for automatic calculation of the amplitude transmission characteristic in real time were defined in the measuring device. In the first step, the amplitudes of the measured signals are detected and the transmission value is calculated as the ratio of the amplitude of the signal from the mass and the signal of the excitation table. Two transfer functions are calculated, one from movements and the other from the accelerations. The result is therefore two transmission characteristics, which should, however, be essentially the same. The double measurement and calculation method was chosen to refine

the results and eliminate possible errors. In addition, the course of the amplitude transmission characteristic is synchronized with the image recording. When analyzing the results, the shape of the characteristic can be assigned to the visible oscillations of the mass.

RESULTS AND DISCUSSION

The tests carried out show a significant influence of loading in the horizontal direction on the size of the natural frequency and the size of the transmission. The magnitude of the transmission from the acceleration as well as the values of the natural frequencies for excitation in the Z-axis (5 to 11Hz) and the X-axis with frequencies of 0Hz, 2Hz, 5Hz, 8Hz and 11Hz at 0.1G are shown in Fig. 8.

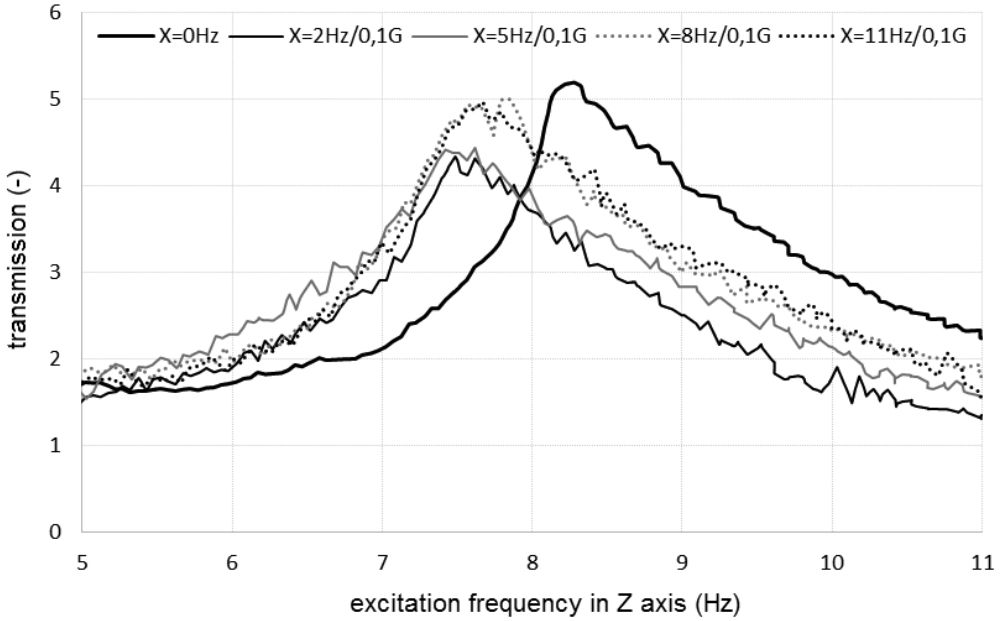

Fig. 8 Test results – Transmission from acceleration for Z-axis excitation 5 to 11Hz and 0.1 G

It can be seen from the figure that there are two effects if we introduce excitation in the X axis. The first effect is that the natural frequency is reduced (from 8.2Hz to 7.8 or 7.4Hz). The second effect is that the transmission value is reduced. A more pronounced drop in transmission was seen at lower frequencies (a drop of 26.5% at 2Hz and 24.5% at 5Hz), at higher excitation frequencies the drop was smaller, 3.8% for 8Hz and 4.4% for 11Hz. The described effects of biaxial loading extend the knowledge gained from uniaxial loading described in the studies (*Fliegel & Martonka, 2015; Martonka & Fliegel, 2016b*) using device (*Martonka & Fliegel, 2016a*). In addition to the above, the performed tests showed the functionality of the developed device (*Fliegel et al., 2019*), which make it possible to carry out tests according to the relevant standards for biaxial loading of car seats (*ASTM D3574-11; JASO B407-87; DIN EN ISO 3385; JASO B407-871978*).

CONCLUSIONS

The aim of the research was to perform initial measurements on the developed device *(Fliegel et al., 2019*) and to compare the influence of one- and bi-axial dynamic loading of a car seat. The results showed a significant effect of horizontal excitation on the transmission in the car seat, when both the transmission and the resonance of the car seat were reduced. In real operation, the car seat is exposed to multi-axial loads, for this reason a 3-axis test device was designed *(Fliegel et al., 2021; Lepsik et al., 2021*), which should bring further refinement of the behavior of the car seat. The subject of further work will be the execution of a more extensive set of measurements at different input parameters (amplitude, frequency) as well as a set of seats made of different foam stiffness and foam thickness. Knowledge of natural frequencies must be taken into account when designing the seats so that there is no unwanted strain on the human body of the crew.

ACKNOWLEDGMENT
This work was supported by the Ministry of Education, Youth and Sports of the Czech Republic and the European Union - European Structural and Investment Funds in the frames of Operational Programme Research, Development and Education - project Hybrid Materials for Hierarchical Structures (HyHi, Reg. No.CZ.02.1.01/0.0/0.0/16_019/0000843).

REFERENCES

1. Standard: ASTM D3574-11. Standard Test Methods for Flexible Cellular Materials—Slab, Bonded, and Moulded Urethane Foams.
2. Standard JASO B407-87: Test code of seating comfort for automobile seats.
3. Standard DIN EN ISO 3385: Flexible cellular polymeric materials - Determination of fatigue by constant-load pounding.
4. Standard JASO B407-871978: Test code of seating comfort for automobile seats
5. Fliegel, V., Lepšík, P., & Martonka, R. (2019). Innovation measurement device of car seats. *7th International Conference on Trends in Agricultural Engineering 2019*, *7*, 127–132.
6. Fliegel, V., Lepšík, P., & Martonka, R. (2021). *A device for simulating a moving vehicle.* UPV. https://isdv.upv.cz/doc/FullFiles/UtilityModels/FullDocuments/FDUM0035/uv035663.pdf
7. Fliegel, V., & Martonka, R. (2015). Characteristics of PU Foam at Long Term Static and Dynamic Loading. *Applied Mechanics and Materials*, *732*, 149–152.
8. Han, S. H., Lu, Z. H., & Liu, Y. J. (2011). Study on Multi-Axial Mechanical Properties of a Polyurethane Foam and Experimental Verification. *Advanced Materials Research*, *311–313*, 301–308.
9. Kia, K., Johnson, P. W., & Kim, J. H. (2021). The effects of different seat suspension types on occupants' physiologic responses and task performance: Implications for autonomous and conventional vehicles. *Applied Ergonomics*, *93*, 103380.
10. Lepsik, P., Fliegel, V., & Lufinka, A. (2021). Innovation of Car Seat Testing Device with Three Axes of Loading. *AD ALTA: Journal Of Interdisciplinary Research*, *11*(2), 331–335.
11. Martonka, R., & Fliegel, V. (2016a). Analysis and construction of measurement device, EAN 2016—54th International Conference on Experimental Stress Analysis. *EAN 2016 - 54th International Conference on Experimental Stress Analysis*, 242–248.
12. Martonka, R., & Fliegel, V. (2016b). Live tests of car seats. *Vibroengineering PROCEDIA*, *7*, 138–141.
13. Werner, B. T., & Daniel, I. M. (2014). Characterization and modeling of polymeric matrix under multi-axial static and dynamic loading. *Composites Science and Technology*, *102*, 113–119.
14. Yang, L., Li, X., Zi, F., Yang, S., Zhang, Z., Qu, J., Dong, Y., & Wu, L. (2021). Dynamic response of graded PVC foam sandwich panel under air blast loads. *Mechanics of Advanced Materials and Structures*, 1–15.

Corresponding author:
doc. Ing. Petr Lepšík, Ph.D., Department of Mechine Parts and Mechanisms, Faculty of Mechanical Engineering, Technical University of Liberec, Studentska 2, 461 17 Liberec 1, Czech Republic, phone: +420 48535 3326, e-mail: petr.lepsik@tul.cz

COMBINING THE SURVEILLANCE OF UNMANNED AERIAL VEHICLE AND DEEP LEARNING METHODS IN SAGO PALM DETECTION

Sri Murniani Angelina LETSOIN[1,2], Ratna Chrismiari PURWESTRI[3,4], David HERÁK[1]

[1]Department of Mechanical Engineering, Faculty of Engineering, Czech University of Life Sciences Prague,
Kamýcká129, 16500 Praha-Suchdol, Czech Republic; letsoin@tf.czu.cz (S.M.A.L.), herak@tf.czu.cz (D.H.)
[2]Faculty of Engineering, University of Musamus, Merauke Regency, Papua 99611, Indonesia
[3]Faculty of Forestry and Wood Sciences, Czech University of Life Sciences Prague, Kamýcká 129, 16500 Praha-Suchdol, Czech Republic, purwestri@fld.czu.cz (R.C.P.)
[4]Institute of Nutritional Science (140a), University of Hohenheim, Garbenstrasse 30, 70599 Stuttgart, Germany; rc.purwestri@uni-hohenheim.de (R.C.P.)

Abstract
The study concerns on the detection of sago palm tree based on Unmanned Aerial Vehicle (UAV) images. Sago palm (Metroxylon Sagu Rottb) lives ecologically in Indonesia, particularly in Papua and Papua Barat. However, our previous study in Papua, especially in Merauke Regency convinced us that 12 of 20 regions tend to lose the potential area of sago palm. To support the detection process from higher spatial data resolution of UAV, we applied a deep learning model based on Convolutional Neural Network (CNN). Although existing studies have implemented a deep learning model based on CNN, rare immersion has been delivered by using deep learning networks, such as mobile net V2 in sago palm detection. Therefore, this study aims to detect sago palms from UAV imagery, and to examine the performance of mobile net V2 in detection tasks. As a result, the metric performance demonstrates good potential as a classifier and predictor.. To add this, as shown by the independent t-test of sago trees (58.3±6.8%) compared to other vegetations (27.4±13,4%) ($p<0.001$), prompting to become more rigid in sago palm detection.

Key words: *sago; classification; UAV; mobile net V2.*

INTRODUCTION

Sago palm was affiliated with palmae family known as Metroxylon Sagu Rottb., grows in swamps or salty areas of tropic lowlands in South East Asia, particularly in Thailand, Malaysia, Papua New Guinea, and about 85% of world's sago area is in Indonesia (*Hidayat et al., 2018; Lim et al., 2019*) , specifically in Papua, and Maluku (*Sidiq et al., 2021*). The potential use of sago were introduced these days, especially the primary product of sago palm which is sago starch. Numerous earlier studies have found that the primary product of this palm, which is sago starch, used as a food substance in traditional cakes, or as a raw material for agro industry, and others aspect of sago can be refer to (*Karim et al., 2008*). Sago pith waste (SPW) or 'Sago hampas' can be used for Bio-ethanol production (*Thangavelu et al., 2014*). Other product of Sago palm determined by study of fermentable sugars from enzymatic hydrolysis of sago pith residues were transformed to acetone-butanol-ethanol (*Linggang et al., 2013*). In Papua, sago plays an important role as a staple food and also a part of indigenous costumes (*Sidiq et al., 2021*), thus, sago waste is used as livestock feed or as bio-energy alternative (*Jonatan et al., 2017*). However, our previous study found that the potential habitat of sago palm in the area of Merauke Regency of Papua Province of Indonesia was decreased, twelve of twenty regions of the area tend to lose over time. On the other hand, other sectors such as the settlement areas, and agricultural regions were significantly increased during 29 years of study (*Letsoin et al., 2020, 2022*). Therefore, our current study focuses on the detection of sago palm trees in the selected area. During the last decades, various approaches have been investigated and applied for palm detection purposes, for instance, airborne and ground-based multispectral data combined with spatial and spectral information. Thus, different algorithm classifiers such as image processing methods, machine learning and deep learning methods have applied. Classical image processing methods consists of, for example, template matching, image binarization. Furthermore, machine learning that contains of two general ways, likewise feature

extraction by using HOG; and classifier prediction by using Support Vector Machine (SVM), Random Forest (RF), Artificial Neural Network (ANN), etc. Today, several studies elaborated deep learning by semantic segmentation, object detection and Convolutional Neural Network (CNN). CNN architectures are now extensively developed in various studies, such as AlexNet, ResNet, Inception or mobile net (*Hidayat et al., 2018; Zheng et al., 2021*). Hence, our study concerns on the detection of sago palm by applying mobile net V2 as a classifier, in addition, to assess the characteristic of the classifier in discovering sago palm area and other vegetation based on metric performance as well as analyzed statistically.

MATERIALS AND METHODS

The specific multirotor platform is accustomed as unmanned device to capture images over the sago fieldwork within the specification as follows; Autel Robotics version 2 (EVO II Pro 6K), equipped with advance camera of 12 computer vision sensors, thus, two sonar sensors, two LED landing lights. This drone product also consisting of ultra-HD with a 1-inch sensor, supports range of f2.8 to f11, also JPEG/RAW format of data types with a resolution of 5472 x 3648 pixel. The Autel drone flights flew over the sago field area of a double grid via 70% and 80% of forwarding overlap, 70% and 60% of side overlap, with 60.3 m of altitude. The drone systems have integrated with mission flight planner around the area of 74.600 m^2.

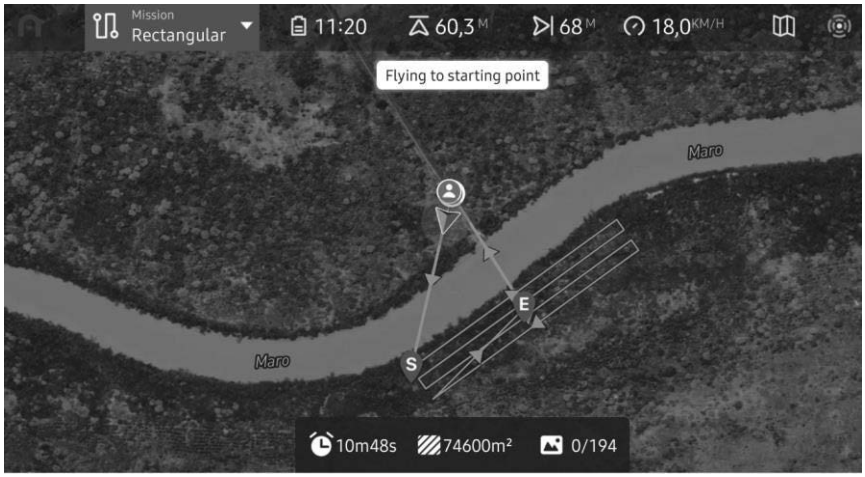

Fig. 1 Mission flight planner

The study area is in Merauke Regency, Papua Province of Indonesia which is positioned between Mappi Regency and Boven Digoel Regency at the North, the Arafuru Ocean at the South and West, and Papua New Guinea to the East. This regency is considered as the Easternmost city in Indonesia that consists of 20 districts. Merauke Regency also known as the largest area of paddy field approximately 91% over Papua Province of Indonesia. Within the area of 46.074.63 km^2/sq.km, the Regency becomes the largest area around Papua Province. Due to the temperature humidity and air temperature about 80.5% and 2.40-32.06 ℃ respectively; are generally preferred for paddy field and maize, different vegetables, and plantation crops, for example mustard green, and coconut tree. The Regency also recognized as the three largest maize producers after Nabire Regency and Biak Numfor Regency (*BPS, 2015*). Considering the sago palm habitat in our field work is typically around primary dryland, secondary dryland, primary swamp forest, secondary swamp forest, bush/shrub, grassland, swamp shrub, and swamp area (*Letsoin et al., 2020*), as captured in this study, natural sago forest in this area is lives together with other vegetation along the river and swamp area (Fig. 3).

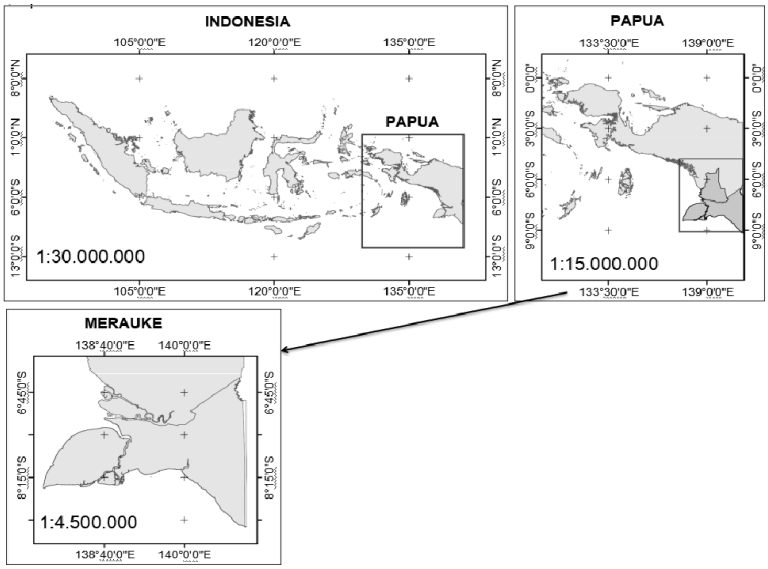

Fig. 2 Study area positioned in Merauke Regency of Papua Province of Indonesia (137°38'52.9692"E - 141°0'13.3233"E and 6°27'50.1456"S - 9°10'1.2253"S)

The proposed methods to define sago areas from the acquired spectral imagery; consists of three stages, I.e., (1) pre-processing, (2) dataset preparation that contains of data train and data test, and (3) deep learning-based CNN classification. In pre-processing stage, all the images are downloaded from UAV to computer data storage, then all the images are assessed geometrically by using pix4dmapper software. The purpose of the stage is to generate a mosaic of all acquired images to prepare them ready and accurately read as dataset of deep learning model. A classification based on CNN architecture model were designed to detect sago palm area and not sago palm area; for this purpose, mobile net v2 was applied. After the data pre-processing step, all data images were labelled, re sized, and augmented by using MATLAB software. The most common augmentation contains of rotation, cropping, zooming, and flipping. Further, the dataset was divided into two groups namely data train and data test that obtained from the previous step. To train the models, we collect 114 images of sago palm area and other vegetation.

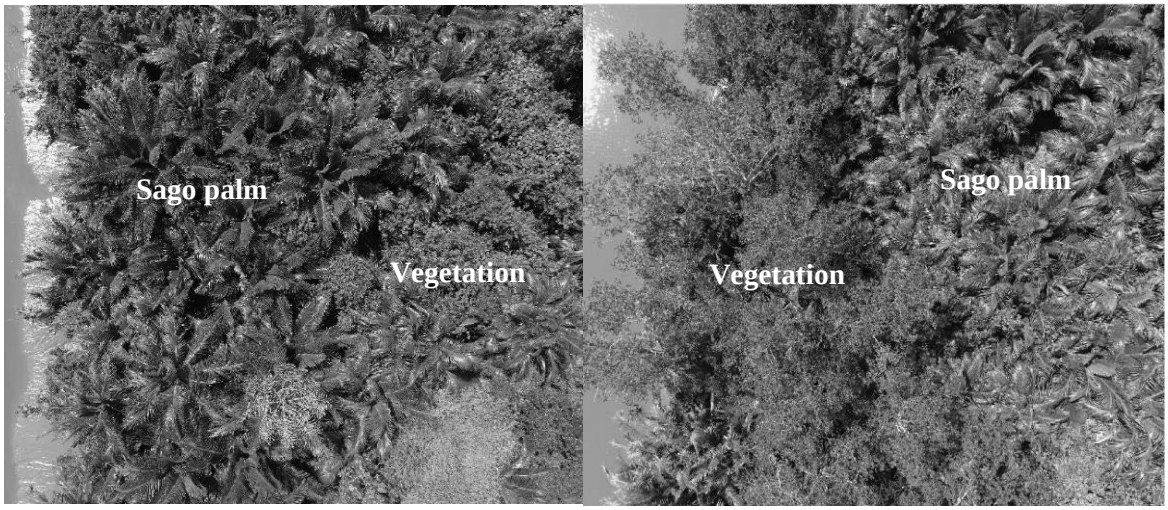

Fig. 3 Sago Forest in Merauke Regency of Papua Province of Indonesia

In accordance with the requirements of the Mobile Net V2 model, the size of input images is adjusted to 224x224. The architecture of Mobile Net V2 mainly consists of two blocks namely linear bottleneck

and inverted residual. Conv2d is standard convolution, then avgpool is the average pooling, *c* is the number of output channels and *n* is restated times. Mobile Net V2 has a total layer of 19 residual bottleneck layers, the middle layer used to feature extraction while the last layer is served for classification.

Tab. 1 Network structure of Mobile Net V2

Input	Operator type	T	C	N	S
224 x 224 x 3	Conv2d	-	32	1	2
112 x 112 x 32	Bottleneck	1	16	1	1
112 x 112 x 16	Bottleneck	6	24	2	2
56 x 56 x 24	Bottleneck	6	32	3	2
28 x 28 x 32	Bottleneck	6	64	4	2
14 x 14 x 64	Bottleneck	6	96	3	1
14 x 14 x 96	Bottleneck	6	160	3	2
7 x 7 x 160	Bottleneck	6	321	1	1
7 x 7 x 320	Conv2d 1x1	-	1280	1	1
7 x 7 x 1280	Avgpool 7x7	-	-	1	-
1 x 1 x 1280	Conv 1x1	-	k	-	-

Regenerating characteristics from *N* to *M* channels, with stride *s* and expansion factor *t*. The bottleneck attaches a 1x1 convolution layer in front of the depth-wise convolutional layer and applies linear activation after the pointwise convolutional layer, also obtains the aim of down sampling by designing the parameter *s* in the depth-wise convolutional layer (*Goceri, 2021; Phan et al., 2020; Sandler et al., 2018*).

Tab. 2 Bottleneck structure of Mobile Net V2

Input	Operator	Output
H x W x N	1x1 Conv2d, ReLU	H x W x tN
H x W x tN	3x3 dwise s = *s*, ReLU	H/s x W/s x tN
H/s x W/s x tN	Linear 1x1 conv2d	H/s x W/s x M

to examine the performance of deep learning model, we applied metrics evaluation specifically to evaluate the accuracy of the model on data set. The accuracy is estimated as (*Chen et al., 2021*):

$$Accuracy = \frac{TP+TN}{TP+TN+FP+FN} \quad (1)$$

$$F1\ score = \frac{2\times(Sensitivity \times Precision)}{Sensitivity + Precision} \quad (2)$$

Whereas TP, TN, FP, FN, represents the number of true positives, true negatives, false positives and false negatives. The number of images predicted to be correct or positive and the number of samples predicted negative were both calculated. To add this, percentage of correctly identified (true positive) sago trees was compared to the proportion of false positive and analyzed statistically using the independent t-test. The p-value >0.05 was determined as a statistical significance difference between variables. Statistical analysis was performed using the IBM SPSS software version 26.

RESULTS AND DISCUSSION

Based on equations (1) and (2), measured data are presented in Table 3, it represents the precision of the model distinguishing the object.

Tab. 3 Metric evaluation

Image Input	Sensitivity	Precision	F1-Score
Sago	0,72	0,72	0,72
Vegetation	0,68	0,68	0,68

Generally, the model was able to identify the object whether sago palm or other vegetation. However, considering the training accuracy of the model which is 97%, and 19 mins of time training; the metric performance was expected to be higher than 0.72. Nonetheless, optimized parameters, mobile net V2 network layer designed in this study, and training time, are needed to be considered. Mobile Net V2 has utilized in classification or detection matters, specifically in embedded platform or mobile devices. To increase the efficiency and time cost this model was enabled to be integrated with other deep learning method such as Faster R-CNN or Long Short-Term Memory (LSTM) (*Hartanto & Wibowo, 2020; Srinivasu et al., 2021*). Comparing the network layer designed, particularly last stage used in this study i, e., after bottleneck residual block and depth-wise convolution, then, global pooling average. Followed by fully connected layer, thus, logits SoftMax and at the final layer is classification output. Nevertheless, adding other deep learning model or techniques between the convolution layer and global pooling average layer could be enhanced the identification result as done by (*Chen et al., 2021*). The training performance for ten epochs as follows: training accuracy, test accuracy, training loss of 98,31%, 91,07, 1,3224 respectively. Also, both F1 score, and sensitivity was around 89%, however, as shown by table 3, the performance result of the mobile network V2 is about17% lower than the earlier study. In addition, the training validation, training loss in this study was 97.05%, 0,20% subsequently. On one hand, attaching a shape detector as output, for example box regressor, is helpful to identify the object properly (*Hartanto & Wibowo, 2020*). Although based on our statistical analysed, the results presented a significantly higher proportion of the machine correctly identifying sago trees (58.3±6.8%) compared to other vegetations (27.4±13,4%) ($p<0.001$, Independent t-test). Nevertheless, integrating the mobile network layer as used in this study within other deep learning techniques, and fine-tuned parameters such as epoch, learning rate, L2 regulation, and validation frequency are required in our future work.

CONCLUSIONS

The study has utilized mobile network V2 in sago palm detection based on an UAV RGB imagery. According to the experiments with seven epochs, initial learn rate and L2 regulation = 0.0001, the data training accuracy is 97%. Although, the metric performance was not significantly higher compared to several earlier studies, the statistical analyzed has shown the model is quite representative in classifying the sago palm or vegetation. As further work to our research, we would like to improve the current result by integrating the network layer designed with other deep learning techniques.

ACKNOWLEDGMENT

The data presented in this article in the form of figures and tables are a part of ongoing research being undertaken for PhD work of the first author.

REFERENCES

1. Chen, J., Zhang, D., Suzauddola, M., & Zeb, A. (2021). Identifying crop diseases using attention embedded MobileNet-V2 model. *Applied Soft Computing*, *113*, 107901. https://doi.org/10.1016/j.asoc.2021.107901
2. Goceri, E. (2021). Diagnosis of skin diseases in the era of deep learning and mobile technology. *Computers in Biology and Medicine*, *134*, 104458. https://doi.org/10.1016/j.compbiomed.2021.104458
3. Hartanto, C. A., & Wibowo, A. (2020). Development of Mobile Skin Cancer Detection using Faster R-CNN and MobileNet v2 Model. *2020 7th International Conference on Information Technology, Computer, and Electrical Engineering (ICITACEE)*, 58–63. https://doi.org/10.1109/ICITACEE50144.2020.9239197
4. Hidayat, S., Matsuoka, M., Baja, S., & Rampisela, D. A. (2018). Object-Based Image Analysis for Sago Palm Classification: The Most Important Features from High-Resolution Satellite Imagery. *Remote Sensing*, *10*(8), 1319. https://doi.org/10.3390/rs10081319

5. Jonatan, N. J., Ekayuliana, A., Dhiputra, I. M. K., & Nugroho, Y. S. (2017). The Utilization of Metroxylon Sago (Rottb.) Dregs for Low Bioethanol as Fuel Households Needs in Papua Province Indonesia. *KnE Life Sciences*, *3*(5), 150. https://doi.org/10.18502/kls.v3i5.987
6. Karim, A. A., Tie, A. P.-L., Manan, D. M. A., & Zaidul, I. S. M. (2008). Starch from the Sago (*Metroxylon sagu*) Palm TreeProperties, Prospects, and Challenges as a New Industrial Source for Food and Other Uses. *Comprehensive Reviews in Food Science and Food Safety*, *7*(3), 215–228. https://doi.org/10.1111/j.1541-4337.2008.00042.x
7. Letsoin, S. M. A., Herak, D., & Purwestri, R. C. (2022). Evaluation Land Use Cover Changes Over 29 Years in Papua Province of Indonesia Using Remote Sensing Data. *IOP Conference Series: Earth and Environmental Science*, *1034*(1), 012013. https://doi.org/10.1088/1755-1315/1034/1/012013
8. Letsoin, S. M. A., Herak, D., Rahmawan, F., & Purwestri, R. C. (2020). Land Cover Changes from 1990 to 2019 in Papua, Indonesia: Results of the Remote Sensing Imagery. *Sustainability*, *12*(16), 6623. https://doi.org/10.3390/su12166623
9. Lim, L. W. K., Chung, H. H., Hussain, H., & Bujang, K. (2019). *Sago Palm (Metroxylon sagu Rottb.): Now and Beyond*. 18.
10. Linggang, S., Phang, L. Y., Wasoh, H., & Abd-Aziz, S. (2013). Acetone–Butanol–Ethanol Production by Clostridium acetobutylicum ATCC 824 Using Sago Pith Residues Hydrolysate. *BioEnergy Research*, *6*(1), 321–328. https://doi.org/10.1007/s12155-012-9260-9
12. BPS. Papua Province in Figures 2015.BPS-Statistics of Papua Province
13. Phan, H., Huynh, D., He, Y., Savvides, M., & Shen, Z. (2020). MoBiNet: A Mobile Binary Network for Image Classification. *2020 IEEE Winter Conference on Applications of Computer Vision (WACV)*, 3442–3451. https://doi.org/10.1109/WACV45572.2020.9093444
14. Sandler, M., Howard, A., Zhu, M., Zhmoginov, A., & Chen, L.-C. (2018). MobileNetV2: Inverted Residuals and Linear Bottlenecks. *2018 IEEE/CVF Conference on Computer Vision and Pattern Recognition*, 4510–4520. https://doi.org/10.1109/CVPR.2018.00474
15. Sidiq, F. F., Coles, D., Hubbard, C., Clark, B., & Frewer, L. J. (2021). Sago and the indigenous peoples of Papua, Indonesia: A review. *Journal of Agriculture and Applied Biology*, *2*(2), 138–149. https://doi.org/10.11594/jaab.02.02.08
16. Srinivasu, P. N., SivaSai, J. G., Ijaz, M. F., Bhoi, A. K., Kim, W., & Kang, J. J. (2021). Classification of Skin Disease Using Deep Learning Neural Networks with MobileNet V2 and LSTM. *Sensors*, *21*(8), 2852. https://doi.org/10.3390/s21082852
17. Thangavelu, S. K., Ahmed, A. S., & Ani, F. N. (2014). Bioethanol production from sago pith waste using microwave hydrothermal hydrolysis accelerated by carbon dioxide. *Applied Energy*, *128*, 277–283. https://doi.org/10.1016/j.apenergy.2014.04.076
18. Zheng, J., Fu, H., Li, W., Wu, W., Yu, L., Yuan, S., Tao, W. Y. W., Pang, T. K., & Kanniah, K. D. (2021). Growing status observation for oil palm trees using Unmanned Aerial Vehicle (UAV) images. *ISPRS Journal of Photogrammetry and Remote Sensing*, *173*, 95–121. https://doi.org/10.1016/j.isprsjprs.2021.01.008

Corresponding author:
Sri Murniani Angelina Letsoin, ST., M.Eng (S.M.A.L), Department of Mechanical Engineering, Faculty of Engineering, Czech University of Life Sciences Prague, Kamýcká 129, Praha 6, Prague, 16521, Czech Republic, phone: +420 776569772, e-mail: letsoin@tf.czu.cz

THE TEMPERATURE OF PHOTOVOLTAIC PANELS AND THE EFFECT ON THEIR EFFICIENCY

Martin LIBRA[1], Sona GRIGORYAN[1], Vladislav POULEK[1], Tomáš PETRÍK[1], Pavel KOUŘÍM[1], Jan SEDLÁČEK[1], Václav BERÁNEK[2]

[1]*Department of Physics, Faculty of Engineering, Czech University of Life Sciences Prague, Czech Republic*
[2]*Solarmonitoring, Ltd., Czech Republic*

Abstract
When photovoltaic systems operate in areas with extreme climatic conditions, their characteristics can change significantly during operation. The temperature mainly affects the open circuit voltage and the efficiency of the photovoltaic system. Therefore, it is necessary to pay particular attention to the fact that the connected devices can work in the given range of parameters of the photovoltaic power source.

Key words: *photovoltaic system; semiconductor diode; data monitoring; carbon footprint.*

INTRODUCTION

Today, photovoltaic energy conversion has an important place in the energy mix. They are also important in terms of reducing the carbon footprint. Many photovoltaic power plants operate worldwide (*Božiková et al., 2021; Poulek et al., 2021*). Many of them are directly building integrated (*Libra et al., 2016; Pokorný & Matuška, 2020*), including our photovoltaic system on the roof of the Faculty of Engineering (*Libra et al., 2019*) (see Fig. 1). The temperature of photovoltaic panels changes during the year. In Central Europe, the air temperature can change by up to about 60°C during the year, but there are places on Earth (for example in Siberia), where the air temperature changes by up to 100°C.

Fig. 1 Photovoltaic system (P_{max} = 10 kW_p) on the roof of the Faculty of Engineering in Prague

It is known, that the temperature of photovoltaic cells significantly affects the efficiency of energy conversion. It follows from the semiconductor theory. A photovoltaic cell is essentially a planar semiconductor diode. Photovoltaic panels with silicon-based photovoltaic cells are commonly used on Earth and photovoltaic panels with GaAs-based photovoltaic cells are commonly used in space. Photovoltaic voltage arises at the PN junction due to the different distribution of significant energy levels in areas P and N. If the irradiation is constant, the increasing temperature causes a shift of Fermi energy towards the center of the band gap and a decrease in photovoltaic voltage. However, the increasing temperature also reduces the width of the band gap and increases the electric current. For example, in (*Meral & Dincer, 2011*) the results of measuring *I-V* characteristics of a photovoltaic cell based on monocrystalline silicon were presented and discussed, but the temperature range was relatively small (20°C ÷ 60°C).

We performed similar measurements in the maximum possible temperature range of photovoltaic systems, which can work even in extreme climatic conditions or in space (-170°C ÷ +100°C) and we presented the results in (*Libra et al., 2021*). In this article, we discuss in more details the influence of temperature dependences of important characteristics of photovoltaic cells and panels on photovoltaic systems.

MATERIALS AND METHODS

Using our monitoring system Solarmon (*Beránek et al., 2018*), we evaluate data from 85 photovoltaic power plants in the Czech Republic, Slovakia, Romania, Hungary, Chile. The dispatching center is at the Czech University of Life Sciences Prague, Faculty of Engineering. We compare the results with the assumed values according to the solar calculator (Photovoltaic Geographical Information System). Description of the activity associated with high technologies of real-time monitoring of the Earth surface and solar energy conversion is in the work (*Rezk et al., 2015*). A data acquisition system has designed and implemented with facilities for monitoring meteorological data and solar radiation. The system of our colleagues uses photovoltaic monitoring equipment and was developed for taking images of the Earth from satellites. It can forcast meteorological parameters and incoming solar radiation.
When photovoltaic modules operate on the Earth's surface without radiation concentration, their temperature can change from about -100°C to +100°C. When using a photovoltaic system in space, temperature can change over an even larger temperature range during one Earth orbit.

RESULTS AND DISCUSSION

Fig. 2 shows the most important characteristics of the electricity source (in this case an irradiated photovoltaic cell based on monocrystalline silicon) at three selected temperatures. We measured similar characteristics at other temperatures in the above mentioned temperature range (*Libra et al., 2021*). Temperature dependences of the efficiency of photovoltaic energy conversion were measured in (*Gordon et al., 2021*) as well.
If the photovoltaic system operates in places with extreme climatic conditions, especially with extreme temperature changes during the year, the electrical voltage of the photovoltaic panels will change significantly. This can be seen in Fig. 3 and there is also a decrease in the energy conversion efficiency with increasing temperature. Thus, in the stated temperature range, the open circuit voltage can up to double. This must be taken into account when designing a photovoltaic system, including connected devices. If the photovoltaic system is connected to the network, the stability of the grid can also be affected (*Petrík et al., 2020*).
For example, in Oymyakon, (Siberia, 63° north latitude, 750 m altitude), the lowest temperature was - 72°C (on 26th January 1926) and the highest temperature was +35°C (on 28th July 2010). At night, the temperature of the photovoltaic panels is usually lower than the air temperature due to radiation. In the winter morning at sunrise, the temperature of the photovoltaic panels can approach up to the value - 100°C. When using a photovoltaic system in space, temperatures can be even lower in the Earth's shadow, and our measurements are very important especially for these applications. Conversely, the use of radiation concentrators can significantly increase maximum operating temperatures. In this case, it is necessary to assess whether the increased radiation intensity on the photovoltaic panels pays off in comparison with the reduced energy conversion efficiency at the higher temperature of the photovoltaic panels. The decrease in the efficiency of photovoltaic energy conversion with increasing temperature shows an approximately linear dependence, as can be seen in Fig. 3. At the temperature 25°C, the decrease is 0.36 %/°C. These values differ slightly for different PV cell designs and different irradiation.

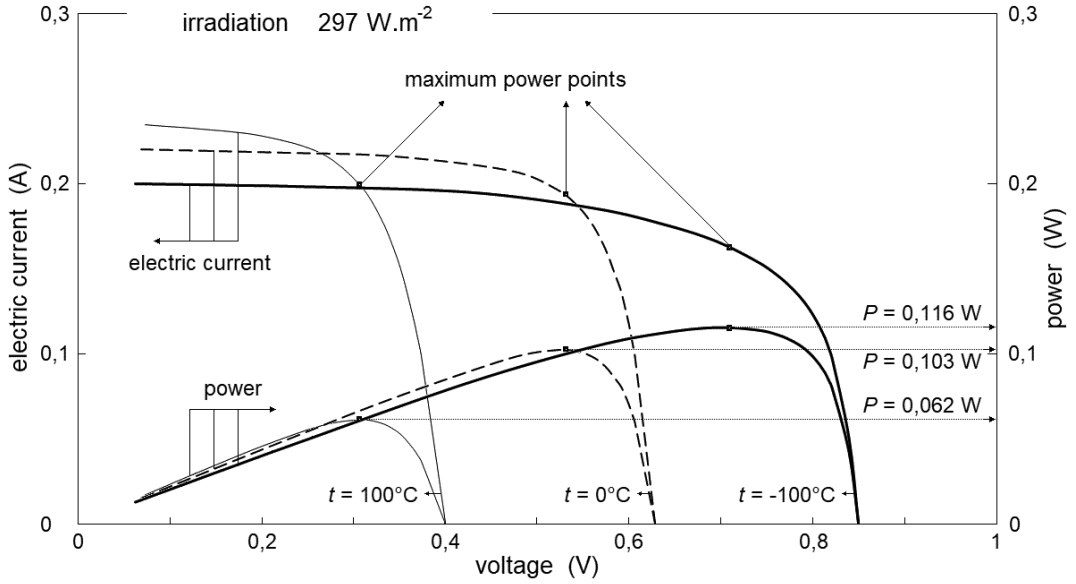

Fig. 2 Important characteristics of an irradiated photovoltaic cell at three different temperatures

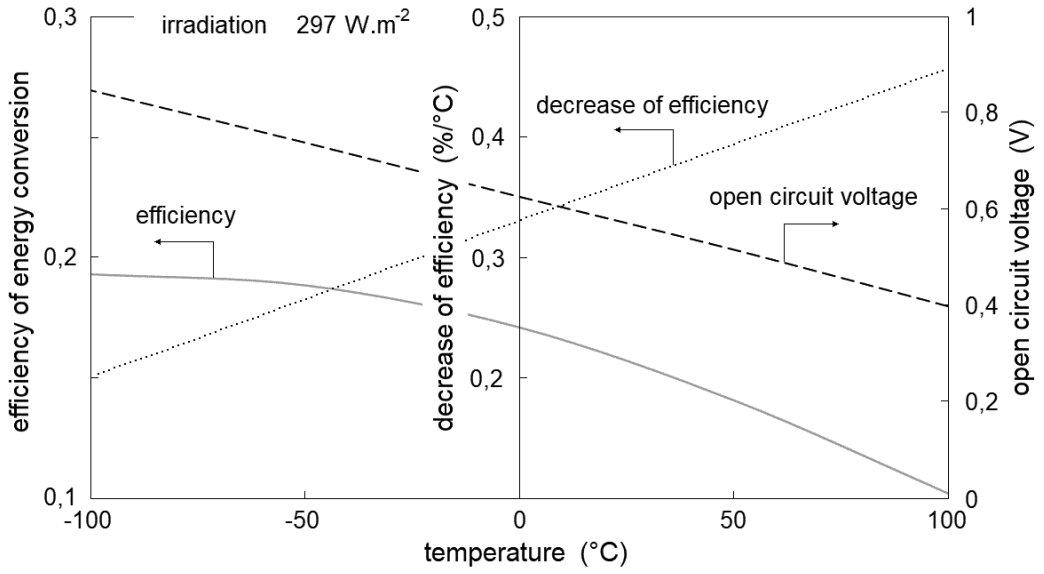

Fig. 3 Dependences of open circuit voltage and energy conversion efficiency on temperature

This mentioned effect of temperature on the efficiency of photovoltaic energy conversion means that extreme values of solar radiation do not necessarily mean extreme yield of the photovoltaic power plant. Tropical areas have a high intensity of sunlight (especially in Africa, Australia and Central America). The yield of photovoltaic power plants is here good but not top, because the efficiency of energy conversion is lower at higher temperatures. The highest yields are achieved in the much more northern and cold regions of Tibet, Mongolia and Siberia with higher altitudes. The plateaus of Chile in the Atacama Desert are also excellent locations. Also on the coast of Antarctica, there can be achieved similar annual yields as in subtropical areas.

For example, we have been operating the photovoltaic system in Fig. 1 (P_{max} = 10 kW_p) at the Faculty of Engineering in Prague (50° north latitude, 300 m altitude) since 2015, we collect data using our monitoring system Solarmon (*Beránek et al., 2018*). Fig. 1 shows the photovoltaic system in winter period. The yield of electricity produced slightly exceeds the expected values according to the solar calculator

(Photovoltaic Geographical Information System). We achieved the highest energy yield in 2019, as shown in Fig. 4.

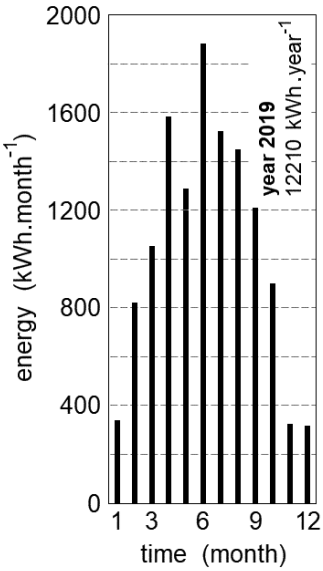

Fig. 4 Electricity produced in the photovoltaic system at the Faculty of Engineering in 2019

CONCLUSIONS

Photovoltaic systems are an important part of the energy mix also with regard to reducing the carbon footprint.

Measurement of important characteristics of photovoltaic cells shows a significant dependence on temperature. The decrease in the efficiency of photovoltaic energy conversion with increasing temperature shows an approximately linear dependence as can be seen in Fig. 3.

Thus, the efficiency of energy conversion and open circuit voltage can up to double on Earth in extreme climatic conditions during the year. In space applications, these values can triple in a single satellite orbit around the Earth. This must be taken into account when designing photovoltaic systems. The individual components and especially the overvoltage protectors must be carefully selected so as not to damage or destroy the connected equipment.

REFERENCES

1. Beránek, V., Olšan, T., Libra, M., Poulek, V., Sedláček, J., Dang, M-Q., Tyukhov, I.I. (2018). New Monitoring System for Photovoltaic Power Plants' Management. *Energies*, 11(10), 2495, doi: 10.3390/en11102495.
2. Božiková, M., Bilčík, M., Madola, V., Szabóová, T., Kubík, L'., Lendelová, J., Cviklovič, V. (2021). The Effect of Azimuth and Tilt Angle Changes on the Energy Balance of Photovoltaic System Installed in the Southern Slovakia Region. *Applied Sciences*, 11(19), 8998, doi: 10.3390/app11198998.
3. Gordon, J.M., Moses, G., Eugene A. Katz, E.A. (2021). Boosting silicon photovoltaic efficiency from regasification of liquefied natural gas. *Energy*, 214, 118907, doi: 10.1016/j.energy.2020.118907.
4. Libra, M., Beránek, V., Sedláček, J., Poulek, V., Tyukhov, I.I. (2016). Roof photovoltaic power plant operation during the solar eclipse. *Solar Energy*, 140, 109-112, doi: 10.1016/j.solener.2016.10.040.
5. Libra, M., Daneček, M., Lešetický, J., Poulek, V., Sedláček, J, Beránek, V. (2019). Monitoring of Defects of a Photovoltaic Power Plant Using a Drone. *Energies*, 12(5), 795, doi: 10.3390/en12050795.
6. Libra, M., Petrík, T., Poulek, V., Tyukhov, I.I., Kouřím, P. (2021). Changes in the Efficiency of Photovoltaic Energy Conversion in Temperature Range With Extreme Limits. *IEEE Journal of Photovoltaics*, 11(6), 1479-1484, ISSN 2156-3403, doi: 10.1109/JPHOTOV.2021.3108484.

7. Meral, M.E., Dincer, F. (2011). A review of the factors affecting operation and efficiency of photovoltaic based electricity generation systems. *Renewable and Sustainable Energy Reviews*, 15, 2176–2184, doi: 10.1016/j.rser.2011.01.010.
8. Petrík, T., Daneček, M., Uhlíř, I., Poulek, V., Libra, M. (2020). Distribution Grid Stability - Influence of Inertia Moment of Synchronous Machines. *Applied Sciences*, 10(24), 9075, doi: 10.3390/app10249075.
9. Photovoltaic Geographical Information System (PVGIS), [online] (2021). Available from https://re.jrc.ec.europa.eu/pvg_tools/en/tools.html. Accessed 10.12.2021.
10. Pokorný, N., Matuška, T. (2020). Glazed Photovoltaic-thermal (PVT) Collectors for Domestic Hot Water Preparation in Multifamily Building. *Sustainability*, 12(15), 6071, doi: 10.3390/su12156071.
11. Poulek, V., Šafránková, J., Černá L., Libra, M., Beránek, V., Finsterle T., Hrzina, P. (2021). PV Panel and PV Inverter Damages Caused by Combination of Edge Delamination, Water Penetration, and High String Voltage in Moderate Climate. *IEEE Journal of Photovoltaics*, 11(2), 561-565, doi: 10.1109/JPHOTOV.2021.3050984.
12. Rezk, H., Tyukhov, I., Raupov, A. (2015). Experimental implementation of meteorological data and photovoltaic solar radiation monitoring systém. *Int. Trans. Electr. Energ. Syst*. 25, 3573–3585, doi: 10.1002/etep.2053.

Corresponding author:
Prof. Ing. Martin Libra, CSc., Department of Physics, Faculty of Engineering, Czech University of Life Sciences Prague, Kamýcká 129, Praha 6, Prague, 16500, Czech Republic, phone: +420 22438 3284, e-mail: libra@tf.czu.cz

LOADING ACCURACY OF TOTAL MIXED RATION COMPONENTS AS A DIGITAL TOOL ENSURING THE OPTIMAL BREEDING CONDITIONS AND WELFARE IN DAIRY FARMING

Gabriel LÜTTMERDING[1], Roman GÁLIK[1], Štefan BOĎO[1], Jana LENDELOVÁ[1]

[1]Institute of Agricultural Engineering, Transport and Bioenergetics, Faculty of Engineering, Slovak University of Agriculture in Nitra, Tr. A. Hlinku 2, 949 76 Nitra, Slovakia

Abstract
The paper is focused on the total mixed ration and it's components, which are used in order to create the best possible mix of ingredients for the feeding of dairy cows. For the experiment a mixer feed wagon with an external loader was selected from an agricultural holding in the Slovak Republic. The total mixed ration consisted of five components, delivered to the wagon via the external loader. The loading accuracy was calculated and evaluated from the extracted data from the wagon's own data software. The data shown there were found some significant differences in the loading of these five components. The average loading accuracy of the TMR was 99.23 %.

Key words: *data digitalization, loading accuracy, mixerfeed wagon, total mixed ration, dairy cows*

INTRODUCTION

The total mixed ration (TMR) is a feeding system, used to provide consistent feed to animals and to stabilize rumen conditions as desired. Feeding activities have an important place in terms of animal health, performance, milk yield or meat production. The very each mouthful of the mixture consumed by an animal, must be homogenous and balanced, otherwide the animal can be negatively affected (*Sova et al., 2014*). Several manufacturers have introduced automatic feeding systems (AFS) during the past decade (*Belle et al., 2012; Unal & Kuraloglu, 2015*). The main advantage of the AFS is the possibility to supply a total mixed ration (TMR) with a high frequency and a low labour requirement, whilst farms which feed with conventional feeding systems (CFS) commonly supply TMR only once or twice a day and require more labour with a rigid work schedule. (*DeVries et al., 2005*). TMR production is formulated to obtain a homogeneous and balanced ratio of all components in one solution. Many strategies can be used in TMR systems. These mixtures can be formulated for fresh cows, early lactation cows, mid-lactation as well as late-lactation, or close-up dry cows. Cows can be placed in groups created, which are based on actual or fat-corrected milk, days in milk, reproductive status, age, nutrient requirements and health (*Baumgard et al., 2017*). Together with the balance between dietary components that allow for good rumen status, feed particle size distribution and physical efficiency of the diet lead to adequate chewing stimulation mechanisms and rumen fermentation intensity (*Zebeli et al., 2011*). The airm of this paper was to evaluate the precision of loading various TMR components into the chosen mixer feed wagon, as well to evaluate the total precision of the TMR. A hypothesis was established that the weight differences between all the TMR components will not be greater than ± 5 %.

MATERIALS AND METHODS

Farms and animals

The study was performed at a dairy farm located in the Slovak Republic. For the privacy of the selected farm, only the basic information were provided. Only the TMR of the group with the highest milk yield was selected. The TMR consisted of following components: core concentrate, corn silage, lantern silage, wet destillery grain, water. The TMR was fed to the dairy cows twice a day. The weight of the TMR was irregular during the study, varing from 3 672 kg to 4 504 kg per feeding. The milk yield of the selected group of dairy cows was over 35 liters.

Data collection

The study lasted in May 2022. The monitored parameters included: total set weight of TMR components (kg), total loaded weight of TMR components (kg) and the difference of total set weight and total loaded

weight (%). Data were extracted from the farm's TMR report and then evaluated in selected statistical software. The selected mixer feed wagon was a Trioliet Solomix 2 1200 ZK with 1 wheel axle (Trioliet, Oldenzaal, The Netherlands).

Figure 1 provides an illustration of the selected mixer feed wagon and Table 1 provides the wagon' basic technical specifications.

Fig. 1 Trioliet Solomix 2 1200 ZK (1 wheel axle)

Tab. 1 Basic technical specifications of Trioliet Solomix 2 1200 ZK (1 wheel axle)

Parameter	Specification	Parameter	Specification
Age	6 years	Height when unloading	0.82 m
Volume	6 m^3	Unloading width	0.92 m
Length	6 m	Payload	4 500 kg
Width	2.24 m	Knives/counter-blades	4/2
Height	2.50 m	Tires	2x 400/45 L 17.5
External width on wheels	1.71 m	Tractor	82 HP

The following formula (1) was used for the calculations of the weight differences between the set and the loaded weight of the TMR components

$$w_d = \frac{w_{l_t} - w_{s_t}}{w_{a_t}} . 100 \quad (1)$$

where w_d is weight difference (%), w_{l_t} is the total loaded weight (kg), w_{s_t} is the total set weight (kg)

Data analysis
The data from May 2022 were used for the evaluation. Each component was assessed separately and also the total precision of all five components was calculated. An acceptable permissible limit of ± 5 % was chosen.

Statistical analysis
The data from the TMR report were imported in to Microsoft Office Excel (Microsoft, Redmond, the United States of America). For the purposes of plotting the graphs, the Microsoft Office Excel and a statistical software Statistica 12.5 (TIBCO, Palo Alto, the United States of America) were utilized. Resulting data were given as means ± SD (standard deviation).

RESULTS AND DISCUSSION

Figure 2 shows the weight differences of core concentrate during the period of study. The minimum value was -0.50 %, the maximum value was 14.27 %, the average value was 1.50 %. As the figure 2 shows, there were only 2 of 31 (6.45 %) exceedings bigger than the permissible limit ± 5 %.

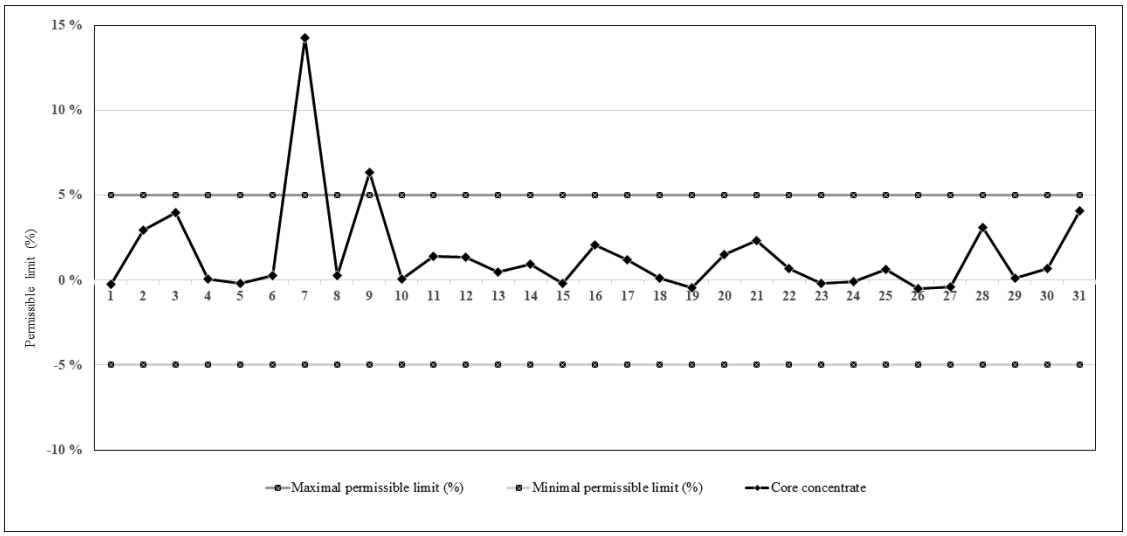

Fig. 2 Core concentrate

Figure 3 shows the weight differences of corn silage during the period of study. The minimum value was -0.24 %, the maximum value was 3.15 %, the average value was 0.60 %. As the figure 3 shows, there were no exceedings bigger than the permissible limit ± 5 %.

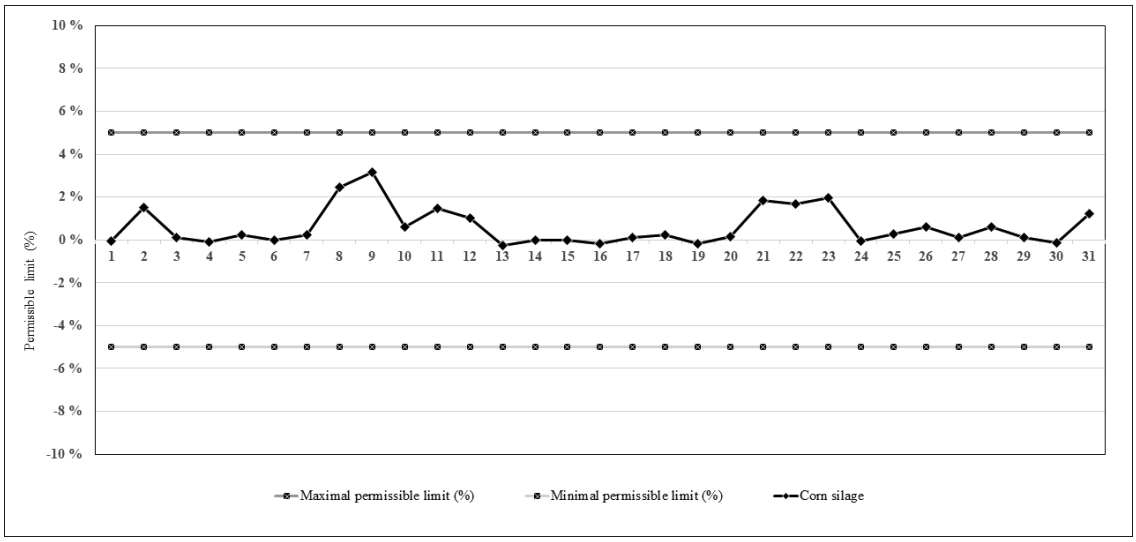

Fig. 3 Corn silage

Figure 4 shows the weight differences of lantern silage during the period of study. The minimum value was -0.91 %, the maximum value was 4.81 %, the average value was 0.81 %. As the figure 4 shows, there were no exceedings bigger than the permissible limit ± 5 %.

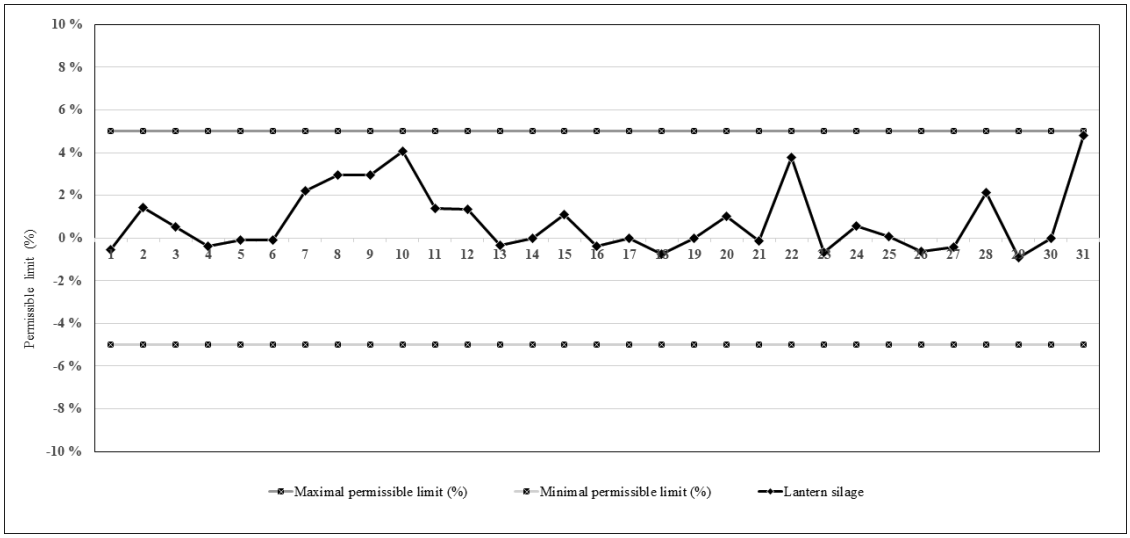

Fig. 4 Lantern silage

Figure 5 shows the weight differences of water during the period of study. The minimum value was -0.18 %, the maximum value was 7.91 %, the average value was 2.55 %. As the figure 5 shows, there were only 3 of 31 (9.68 %) exceedings bigger than the permissible limit ± 5 %.

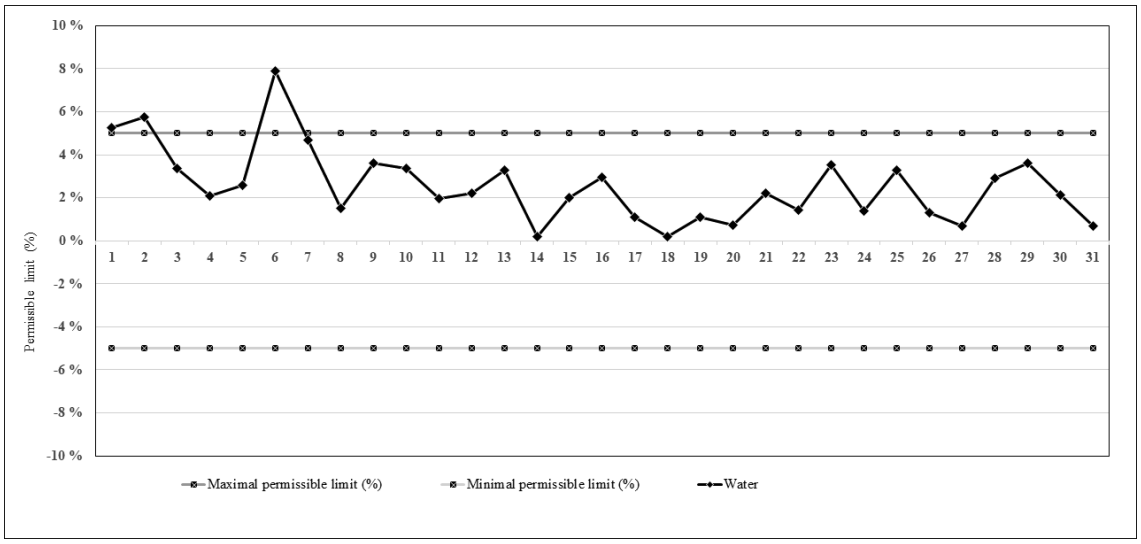

Fig. 5 Water

Figure 6 shows the weight differences of wet destillery grain during the period of study. The minimum value was -49.52 %, the maximum value was 7.54 %, the average value was -2.55 %. As the figure 6 shows, there were only 6 of 31 (19.35 %) exceedings bigger than the permissible limit ± 5 %.

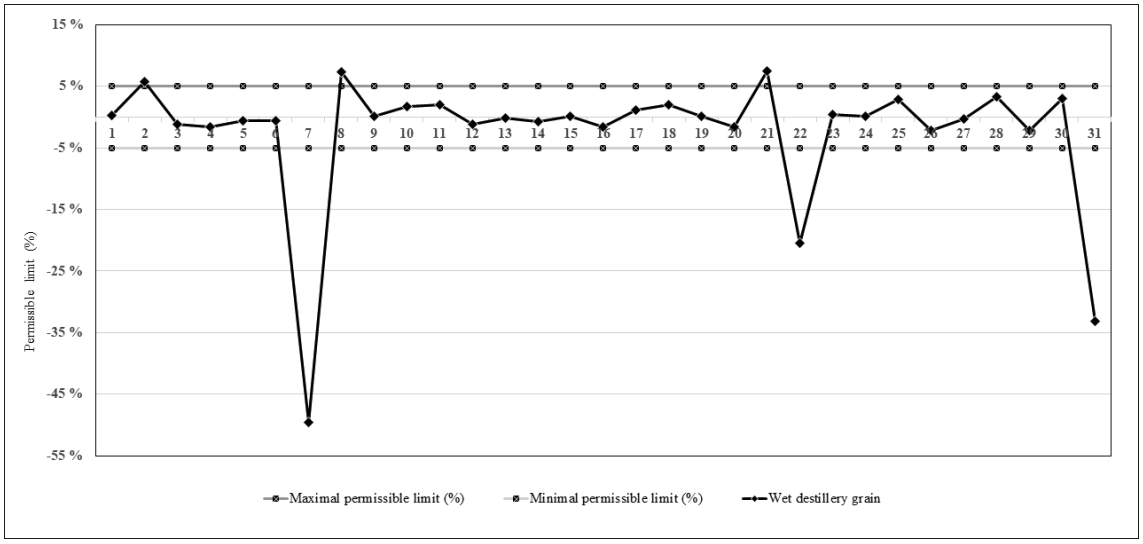

Fig. 6 Wet destillery grain

Figure 7 shows the weight differences of the TMR during the period of study. The minimum value was -0.09 %, the maximum value was 3.68 %, the average value was 0.75 %. As the figure 7 shows, there were no exceedings bigger than the permissible limit ± 5 %. The loading accuracy of the TMR was 99.23 %.

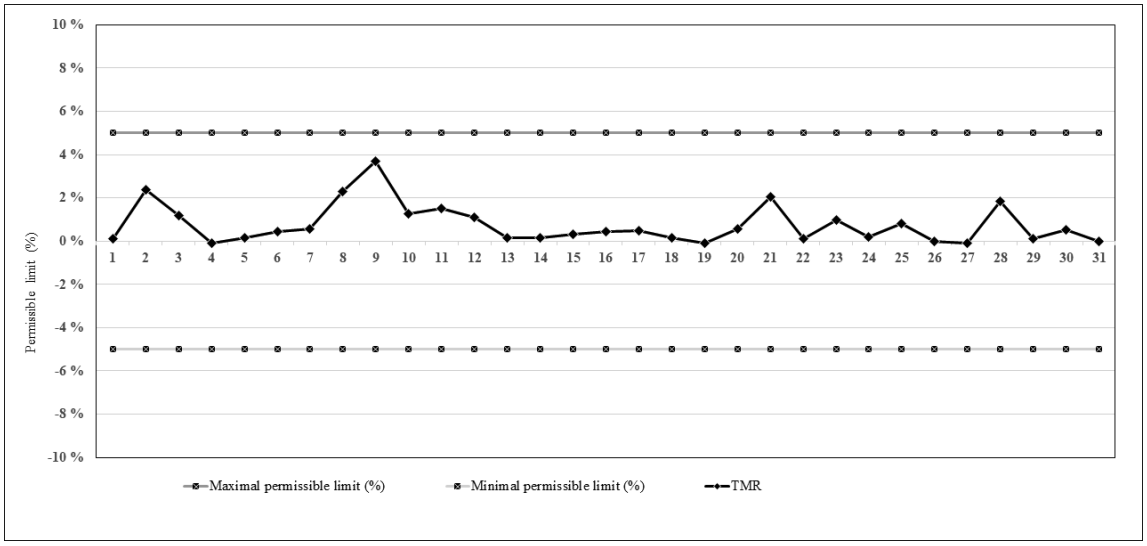

Fig. 7 Total mixed ration

Some authors also achieved similar results, when the quality of the work of feed mixer wagons with both horizontal and vertical augers was compared. In their research they assessed the accuracy of loading the TMR components. They did use three mixer feed wagons with the vertical augers, one mixer feed wagon with a horizontal crushing & mixing system and a self-loader, as well as one self-propelled mixer feed wagon with a vertical crushing & mixing system and a self-loading equipment. Whilst in our TMR we only had 1 TMR with 5 components available, the cited author had 2 TMRs available, the first one with 7 components and the second one with up to 10 components (*Kowalik et al., 2018*).

In another study the authors also dealed with a similar topic, examining the accurate and over-limit and under-limit loadings of each component of two mixer feed wagons with two different TMRs. The first wagon was equipped by a loading cutter integrated in the vehicle, and the second wagon was loaded by an external loader with a loader bucket. The authors used for the study four TMR components: CCM, haylage, silage and straw. It was concluded that the precision did depend not only on the method or used

technique, but also on the kind, i.e. properties of loaded components. Loading of TMR components with the loading cutter was considerably more even than with the loader (*Šístková et al., 2015*).

CONCLUSIONS

To put everything into the conclusion, the precision of loading the TMR components into the chosen mixer feed wagon was almost excellent, with the value of 99.23 %. The established hypothesis was confirmed. Three of five TMR components were loaded over the established permissible limit, however the other two TMR components were always loaded under the established limit. The chosen mixer feed wagon does not provide any internal loader, which means it has to be loaded with an external loading machine, guided by the precise information provided by the wagon's own weighing system. Although the mixer feed wagon we used the data from has no loader, and the loading is based on the manual external loading machine, we can say the feeding system works better than we expected. Thanks to the data transferbetween the mixer feed wagon and the local network on the farm we had the data from, it is now easier than ever to use the numbers to create these inputs in a matter of minutes.

ACKNOWLEDGMENT

This research presented in this scientific paper is supported by the Ministry of Education, Science, Research and Sport of the Slovak republic, by the project VEGA 1/0709/21: „Scientifically justified proposals for technological solutions of housing facilities ensuring optimal microclimatic conditions for livestock and their practical verification“.

REFERENCES

1. Baumgard, L. H., Collier, R. J., Bauman, D. E. (2017). A 100-Year review: Regulation of nutrient partittioning to support lactation. In. *Journal of Dairy Science*, 100, 10353-10366.
2. Belle, Z., André, G., Pompe, J. C. A. M. (2012). Effect of automatic feeding of total mixed rations on the diurnal visiting pattern of dairy cows to an automatic milking system. In *Biosystems Engineering*, 111, 33-39.
3. DeVries, T. J., Keyserlingk, M. A. G., Beauchemin, K. A. (2005). Frequency of feed delivery affects the behaviour of lactating cows. In *Journal of Dairy Science*, 88(10), 3553-3562.
4. Kowalik, I., Grześ, Z., Rybacki, P., Michalski, T. (2018). A comparison of quality of work of the feed mixer wagons with vertical and horizontal mixing systems. In *Journal of Research and Applications in Agricultural Engineering*, 63(2), 124-128.
5. Sova, A. D., LeBlanc, S. J., McBride, B. W., DeVries, T. J. (2014). Accuracy and precision of total mixed rations fed on commercial dairy farms. In *Journal of Dairy science*, 97(1), 562-571.
6. Šístková, M., Pšenka, M., Kaplan, V., Potěšil, J., Černín, J. (2015). The effect of individual components of total mixed ration (tmr) on precision dosing to mixer feed wagons. In *Journal of Microbiology, Biotechnology and Food Sciences*, 05(01), 60-63.
7. Trioliet. (2020). Solomix 2 ZK. In *Solomix 2 feed mixers with two vertical augers*, 42.
8. Unal, H., Kuraloglu, H. (2015). Determination of operating parameters in milking robots with free cow traffic. In *Engineering for Rural Development*, 14, 234-240.
9. Zebeli, Q., Dunn, S. M., Ametaj, B. N. (2011). Perturbations of plasma metabolites correlated with the rise of rumen endotoxin in dairy cows fed diets rich in easily degradable carbohydrates. In *Journal of Dairy Science*, 94(5), 2374-2382.

Corresponding author:
Ing. Gabriel Lüttmerding, Institute of Agricultural Engineering, Transport and Bioenergetics, Faculty of Engineering, Slovak University of Agriculture in Nitra, Tr. A. Hlinku 2, 949 76 Nitra, Slovakia, phone: +421 37 641 4304, e-mail: xluttmerding@uniag.sk

GEOSPATIAL DATASET FOR EVALUATION OF FIELD SCALE EXPERIMENT

Miroslav MACÁK[1], Jitka KUMHÁLOVÁ[2], Jana GALAMBOŠOVÁ[1], František KUMHÁLA[3], Marek BARÁT[1], Vladimír RATAJ[1], Jan CHYBA[3]

[1]Institute of Agricultural Engineering, Transport and Bioenergetics, Faculty of Engineering, Slovak University of Agriculture in Nitra, Tr. A. Hlinku 2, 949 76 Nitra, Slovak republic; miroslav.macak@uniag.sk; jana.galambosova@uniag.sk; vladmir.rataj@uniag.sk; marek.barat@uniag.sk;
[2]Department of Vehicles and Ground Transport, Faculty of Engineering, Czech University of Life Sciences Prague, 10 Kamýcká 129, 165 21 Suchdol - Prague, Czech Republic; kumhalova@tf.czu.cz
[3]Department of Agricultural Machines, Faculty of Engineering, Czech University of Life Sciences, Kamýcká 12 129, 165 21 Suchdol - Prague, Czech Republic; kumhala@tf.czu.cz; chyba@tf.czu.cz

Abstract
Successful implementation of precision agriculture technologies is subject of reliable experimental data. Field scale experimentation plays an important role as a source of information for farmers. Due to the inherent spatial variability of the field, this type of research, requires use of robust methods to ensure the statistical significance. Geospatial multidataset offers advantages compared to traditional data collection methods. Presented paper shows on an example of long-term field scale experiment on CTF technology, benefits of using geospatial dataset. Results showed that combining the satellite data and the combine harvester yield monitoring data help to assess the field scale experiment outputs during the growing season as well as at the harvest stage. Beneficial is most of all the overall view across long term period comprising weather extremes as well as typical years.

Key words: *traffic management, CTF, yield, remote sensing, cereal.*

INTRODUCTION

The technologies of precision agriculture have been the subject of scientific research for last decades (*Gebbers & Adamchuck, 2010; Shafi et al., 2019; Galambosova et al., 2020*). All scale of experiments has been established, however, to provide a realistic view of a technology implementation in practical farming conditions, long term field scale experiments play an important role (*Godwin et al., 2015; Kravchenko et al., 2017*). According to *Godwin et al. (2015)* a robust experimental design and adequate replication is necessary when field studies are undertaken. Hence, limitations in terms of statistical significance are present. Author claims that the experiment layout often cover big areas and so inherent field variability effects the data and causes variability of the data obtained (*Godwin et al., 2015*).
Traditional hand sampling and ground-based sensing might be challenging from the time as well as financial considerations, therefore non-contact methods offer potential advantages. Free satellite data are reliable tool to assess the field variability (*Skakun et al., 2021*)
The aim of this paper was to show the possibility of use of geospatial multidata sets obtained from remote sensing and combine yield monitoring systems to assess the crop yield of selected cereals at two experimental fields: a controlled traffic farming (CTF) field and a random traffic farming (RTF) field. Accent was placed to comparison in several seasons with different climate conditions.

MATERIALS AND METHODS

Experimental site
To evaluate the differences between selected traffic treatments, two fields were selected (Fig. 1). This fields are situated close together (4 km away by bee line) at the University farm of the Slovak University of Agriculture in Kolinany, located in south-west of Slovakia.
Field A: CTF system with 6m OutTrac modul (63,8% non-compacted soil, 36,2% compacted soil) was established in 2009 on 16 ha field "A" (48°22'16.97" N, 18°12'25.43" E). Commercially available machinery with standard wheel spacing (as they are manufactured) is used for all work operations. Since 2009, this field (A) is cultivated within soil conservation tillage technology (without ploughing) up to depth of 15 cm. In 2021 no till technology was used and the crop was drilled directly into the previous crop stubble. On this field ("A") the tree band areas were established in 2010, by reason of modelling

RTF traffic management in the same field. This bands were generated by wheel-by-wheel movement of tractor (JD 8230 with RTK guidance system) in right angle to direction of CTF lines, ones pre year, after harvest annually from 2010 (Fig. 1). More detailed information is available in published papers *Macák, et al. (2018) ; Galambošová et al. (2017); Barát et al. (2017), Goodwin et al. (2015).*
Field B: As a reference field a 23ha field (48°20'36.61" N, 18°13'39.15" E) with conventional management system (random traffic during all field operations) and conventional tillage technology with ploughing (up to depth 30 cm) was selected.
According to soil classification (BPEJ units), the soil type at both experimental fields is classified as loamy soil (*Džatko, et al., 2009*), and the elevation ranged from 178 to 212 m a.s.l. with average slope about 6%.
For this study, barley and wheat crops were selected and seasons where these two crops were grown at the two fields were selected. Choice of crop and their variety was done by the agronomist´s best practice in each year and the overview is provided in Results (Tab. 1). Year average precipitation throughout the assessed time period (2009-2021) is displayed in Fig. 2. Source data sets were obtained from meteorological station situated in university farm (in Kolinany), between the fields A and B.

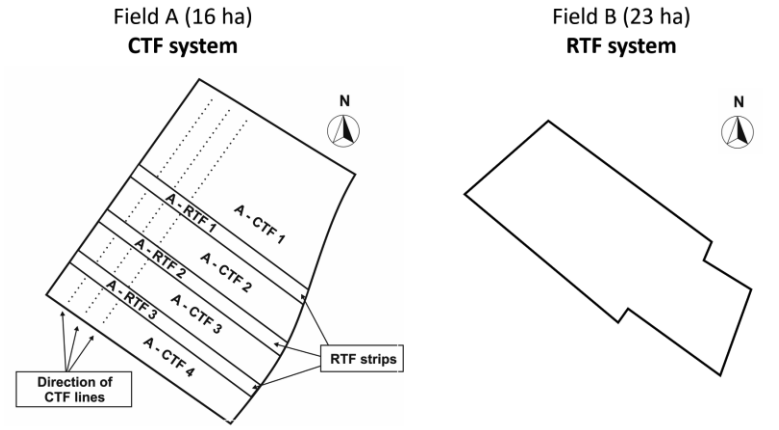

Fig. 1 Experimental site and detail pattern of the fields; (field "A": areas of CTF system: A - CTF1, A - CTF2, A-CTF3, A-CTF4; and areas with modelling RTF traffic system = RTF strips labelled as A-RTF1, A-RTF2, A-RTF3; field "B" – whole of parcel is defined as area named B – RTF)

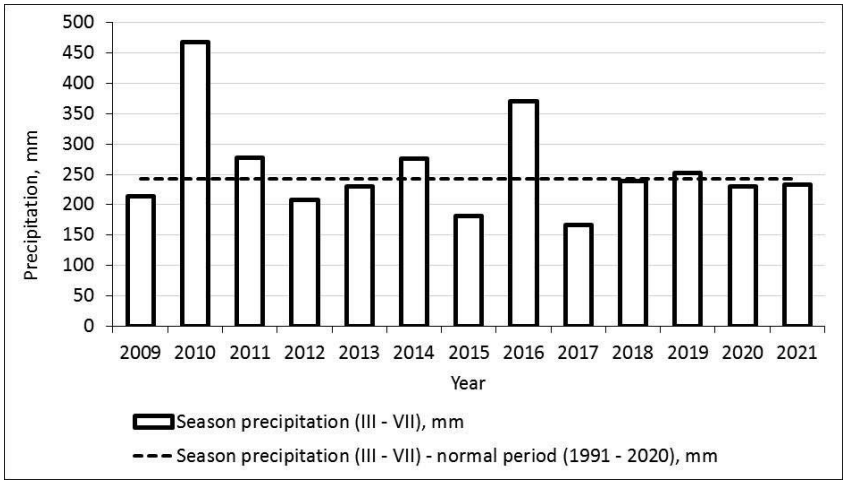

Fig. 2 Seasonal (March-July) average of precipitation thought the assessed period of time (2009-2021) for location of university farm - Kolinany (data source climate normals: SHMU, 2020)
Multiannual data used from Remote sensing and yield monitoring
Experimental fields were monitored by satellite images and yield mapping. Evaluation was done with multiannual data sets for selected cereal crops (field "A" was monitored from 2009 and yield "B" from

2007). Calculation of Normalized Vegetation Index (NDVI) was carried out for every downloaded satellite image by SNAP (version 8.0.7) and ENVI (version 5.6.1) software. Detail overview of used satellite platforms is listed in Table 1.
For yield mapping the John Deere combine with impact sensor or Claas harvester with optical sensor were used too. Available yield maps (in selected years, see Table 1) were processed by ArcGIS Pro software (version 2.8.3) by geostatistical methodology (detailed described at Kumhálová et al., 2011) to the resulting kriging maps. Yield maps obtained from yield monitoring systems were available for seasons from 2011 to 2021 (field A), and for 2014, 2017, 2019 and 2021 (field B). In other monitoring years (when the map is not available), the yield was calculated as average from data available only from cargo balance.
In order to standardize the data, NDVI and yield data were transformed to relative numbers. Then the frequency maps (FM) were computed by "Cell Statistics tool" (in ArcGIS Pro software). Thus, calculated frequency maps allow view areas with potential of crop vitality and structure (in the event of NDVI maps) and yield (in the event of using yield maps).

RESULTS AND DISCUSSION

Relative yield and relative NDVI values for targeted seasons is summarised in Table 1. When assessing performance of given technology, many factors effect the yield and yield potential. Crop varieties and agroecological conditions of the fields are very important for the resulting yields and yield potential (*Jelínek et al., 2020; Balážová et al., 2021*). From the results it is evident that conversion of the conventional technology to soil conservation brought decrease on yield in the first years of the experiment in "field A" with relative improvements further after season. A drop in yield was detected on 2021 season, when no-till drill was used for the first time.

Tab. 1 Crop, average yield and mean relative values of NDVI and yield for fields A and B

Field	Year	Remote sensing platform**	Crop and variety	Yield - field average ($t.ha^{-1}$)	CTF Yield (%)	CTF NDVI (%)	RTF Yield (%)	RTF NDVI (%)
A	2009	L5 TM	Spring barley cv. Kango	5.01*	-	101.35	-	100.97
	2011	L5 TM	Winter wheat cv. Augustus	6.17	94.58	100.23	98.43	101.17
	2014	L8 OLI	Spring barley cv. Kango	4.8	95.85	99.98	98.47	101.37
	2016	L8 OLI	Winter wheat cv. HYFI	7.94	101.00	100.95	100.77	100.20
	2017	L8 OLI	Winter barley cv. Wintmalt	6.73	105.35	100.93	104.80	100.37
	2019	S2 MSI	Winter wheat cv. RGT Reform	7.8	103.23	100.60	101.87	100.47
	2021	S2 MSI	Spring barley cv. IS Maltigo	3.04	99.18	96.73	102.53	99.4
B	2007	L5 TM	Spring barley cv. Ebson	4.81*	-	-	-	98.36
	2008	L5 TM	Winter wheat cv. Armelis	5.77*	-	-	-	100.44
	2010	L5 TM	Winter wheat cv. Vendur	2.47*	-	-	-	99.74
	2014	L8 OLI	Winter wheat cv. Globus	5.80	-	-	101.90	100.11
	2017	L8 OLI	Winter wheat cv. Fabius	4.66	-	-	98.26	99.96
	2019	S2 MSI	Winter wheat cv. Genius	7.37	-	-	100.86	100.06
	2021	S2 MSI	Spring barley cv. IS Maltigo	4.5	-	-	106.08	100.39

Note: parameters: CTF Yield (%), CTF NDVI (%), RTF Yield (%) and RTF NDVI (%) are calculated from remote sensing data as mean relative value
* data is available only from weighting whole grain mass by cargo balance; symbol " – " indicates that data are not available
** satellite images were downloaded from USGS archive (*https://earthexplorer.usgs.gov/*) and Open Access Hub of ESA Copernicus program (*https://scihub.copernicus.eu/dhus/#/home*)

Use of geospatial datasets make it possible to compare the A-CTF with A-RTF areas with sufficient data robustness. It is obvious from the data, that the A-CTF outperformed the A-RTF after initial 5 years (in seasons 2016, 2017, 2019). These results are of great importance as the 2016 was the extremely wet season and as opposite 2017 was extremely dry season (Fig. 2). As the yields are calculated as relative values – A-CTF area can be compared also with field B. Relative yields were higher at A-CTF up to 7.09 % in comparison with B-RTF system in the dry season 2017 when the total precipitation during main growing season was lower by 32% compared to long term average. This increase of yield (favour of CTF system) was observed despite that, in the 2017 the winter barley (crop incoherent to soil air

deficiency and sensitive to soil compaction) was growing on field A and winter wheat (specie "Fabius" with middle drought tolerance) has been sowed on field B. The CTF method seems to be more appropriate and gentler in this respect. *Busari et al. (2015)* also concluded that for dry years, it might be better to implement tillage management avoiding soil compaction and support its conservation.
In normal precipitation year (e.g., 2019) when winter wheat was growing on both fields, difference in mean relative values of yield was up to 2,37 % for benefit of field A (managed under CTF system). When comparing real measured yields (from cargo balance) the increase of the yield is up to 5,8% for CTF field in 2019. It can be stated that over the years, the field managed by the CTF traffic systems has stabilize yields of cereals with potential for their growth in drier years and compared with compacted soil at A-RTF areas the benefit is visible also during extremely wet yeas (season 2016).
Data from Yield monitoring systems always follows the NDVI data. This is an important information as yield monitoring data are not always available or are not correct and hand sampling might be non-efficient for such a type of experiment.
Use of satellite data in 2021, no till drill was used for the first time at the CTF field, what was reflected in lower yield, this effect was clearly detected by the NDVI as well as yield monitoring system. The reduction was present at CTF as well as RTF areas of the field A, compared to the RTF at field B.
To have an overview of the whole time period, summary statistics of relative yield and NDVI frequency maps for different management systems (CTF and RTF) is provided in Table 2. The results show that different mean values were found between the relative yield and NDVI frequency maps for yield potential estimation. While the mean value for NDVI frequency maps was around 110 %, for yield frequency maps it was around 120 %. The difference in the results is due to the different way of obtaining the source data. While the Yield frequency map is based on the yield maps of the monitored years derived from the final harvest data, NDVI frequency maps are averaged images of the current state of the stand in each year captured in the pre-ripening phase.

Tab. 2 Summary statistics of relative (%) frequency maps (FM) for NDVI index and yield on both experimental fields (A and B) characterized by different management system: controlled traffic farming (CTF) and random traffic farming (RTF), α=0.05

Parameter	A-CTF		A-RTF (modelled RTF)		B-RTF	
	FM NDVI	*FM yield*	*FM NDVI*	*FM yield*	*FM NDVI*	*FM yield*
Mean	110.39	119.95	110.76	121.27	109.54	119.94
Error of mean value	0.31	0.58	0.27	0.52	0.38	0.66
Median	107.02	114.73	106.94	115.03	109.85	114.14
Modus	111.82	113.85	104.71	115.07	109.96	107.23
St.Dev.	9.72	18.23	10.49	20.31	5.78	30.23
Variance	94.80	336.18	110.11	412.70	33.38	914.04
Kurtosis	0.47	2.10	0.36	1.55	2.34	11.96
Skewness	1.19	1.49	1.21	1.40	0.92	3.19
Difference max. min.	41.57	112.19	42.74	126.74	37.13	244.29
Minimum	97.78	83.73	97.78	76.32	99.59	61.92
Maximum	139.35	195.92	140.52	203.06	136.72	306.21
Sum	113750.52	123845.96	169474.69	185553.02	25084.95	250547.06
Count	1029.50	1029.50	1530.00	1530.00	229.00	2089.00
level of sign. (95.0%)	0.61	1.13	0.53	1.02	0.75	1.30

FM – frequency map, NDVI -Normalised Difference Vegetation Index, sign. – significance, St.Dev. – Standard Deviation

CTF management has generally proved to be a management method that is able to provide stable yields on the whole plot in the long run (see individual measured years in Table 1), especially in dry years. Although the mean value of the relative yield potential was relatively lower, compared to the RTF field B management. As Table 2 shows, Yield_CTF was 119.95%, while Yield_RTF was 121.27% on field A. On the field B, where RTF management was fully operated, the value of the relative yield frequency map reached 119.94 %. The values related to NDVI frequency maps had the same trend, where field B

with complex RTF management showed the worst mean values. NDVI as a green crop vitality indicator can show current state of the canopy related to a certain date or period of the growth stage and is usually related to the agroecological conditions of the field.
The standard deviation and variance also differed with presented management methods. CTF management in field A showed lower values of standard deviation and variance for both: Yield and NDVI frequency maps than for modelled RTF management. Field B showed relatively large differences between yield and NDVI in this respect, with the resulting yield potential achieving high variability on this field. Again, when looking at the variability of the CTF field (*Galambošová et al., 2017*), decrease of the standard deviation at A-CTF an areas throughout the seasons (*Rataj et al., 2022*) and overall (Tab. 2) compared to A-RTF and B-RTF shows the potential for management the variability and stabilisation of yields via avoiding soil compaction.

CONCLUSIONS

In this study we used multiannual datasets to assess the vitality of selected cereals growing under two different traffic management systems (CTF and RTF). Combining the satellite data and the combine harvester yield monitoring data help to assess the field scale experiment outputs during the several growing seasons as well as at the harvest stage.
Results showed that performance of a tested technology (CTF) can be reliably evaluated after each growing season and relative yield and NDVI data enable to compare the performance with a technology where random traffic is used.
Data confirmed the potential of CTF technology to stabilise the yield during extremely weather conditions and given them potential for growth in drier years (up to 7%). Beneficial is most of all the overall view across long term period of time comprising weather extremes as well as typical years.

ACKNOWLEDGMENT

This publication was supported by the Operational Programme Integrated Infrastructure within the project: Sustainable smart farming systems taking into account the future challenges 313011W112, financed by the European Regional Development Fund.
This publication is the result of the project implementation: „Scientific support of climate change adaptation in agriculture and mitigation of soil degradation" (ITMS2014+ 313011W580) supported by the Integrated Infrastructure Operational Programme funded by the ERDF.
The authors are grateful to the staff at the University Farm in Kolinany, Slovakia, for technical and operational support to conduct this research.

REFERENCES

1. ArcGIS Pro 2.8.3, Esri Inc. CA, USA, 2021. (GIS SW)
2. Balážová, K.; Chyba, J.; Kumhálová, J.; Mašek, J.; Petrásek, S. (2021). Monitoring of Khorasan (Triticum turgidum ssp. Turanicum) and Modern Kabot Spring Wheat (Triticum aestivum) Varieties by UAV and Sensor Technologies under Different Soil Tillage. In *Agronomy* 11(7), 1348, https://www.mdpi.com/2073-4395/11/7/1348.
3. Barát, M., Rataj, V., Týr, Š., Macák, M. & Galambošová, J. (2017). Effect of controlled traffic farming on weed occurrence. In *Agronomy Research* 15(4), 1484–1490, https://doi.org/10.15159/AR.17.005.
4. Busari, M.A.; Kukal, S.S.; Kaur, A. Bhatt, R.; Dulazi, A.A. (2015). Conservation tillage impacts on soil, crop and the environment. In *International Soil and Water Conservation Research* 2015, 3(12), 119–129, https://doi.org/10.1016/j.iswcr.2015.05.002.
5. Džatko, M. & Sobocká, J.; et al. (2009). Handbook for using maps of soil-environmental units. Innovative handbook for agricultural land evaluation of Slovakia (In Slovak: Príručka pre používanie máp pôdno-ekologických jednotiek. Inovovaná príručka pre bonitáciu a hodnotenie poľnohospodárskych pôd). (2009). Soil science and conservation research institute, Bratislava, (pp. 102) ISBN 978-80-89128-55-6. http://www.podnemapy.sk/portal/verejnost/bpej/prirucka_BPEJ.pdf

6. ENVI 5.6.1 (API version 3.7), Harris Geospatial Solution, Inc., Broomfield, USA, 2021
7. Galambošová, J.; Macák, M.; Rataj, V.; Antille, D. L.; Godwin, R. J.; Chamen, W. C. T.; Žitňák, M.; Vitázková, B.; Ďuďák, J. & Chlpík, J. (2017). Field evaluation of controlled traffic farming in central Europe using commercially available machinery. In *Transaction of ASABE* 60(3), 657-669. https://doi.org/10.13031/trans.11833
8. Galambosova, J.; Macák, M.; Rataj, V.; Barát, M., & Misiewicz, P. (2020). Determining Trafficked Areas Using Soil Electrical Conductivity – A Pilot Study. In *Acta Technologica Agriculturae* 23(1), 1-6. https://doi.org/10.2478/ata-2020-0001
9. Gebbers, R. & Adamchuck, V. I. (2010).Precision Agriculture and Food Security. In *Science* 327(5967), 828-831, https://www.science.org/doi/10.1126/science.1183899
10. Godwin, R., Misiewicz, P., White, D., Smith, E., Chamen, T., Galambošová, J. & Stobart, R. (2015). Results from recent traffic systems research and the implications for future work. In *Acta Technologica Agriculturae* 18(3), 57–63, https://doi.org/10.1515/ata-2015-0013
11. Jelínek, Z.; Kumhálová, J.; Chyba, J.; Wohlmuthová, M.; Madaras, M.; Kumhála, F. (2020). Landsat and Sentinel-2 images as a tool for the effective estimation of winter and spring cultivar growth and yield prediction in the Czech Republic. In *International Agrophysics*, 34(3), 391–406, https://doi.org/10.31545/intagr/126593 .
12. Kravchenko, A.N.; Snapp, S.S. &Robertson, G.P. (2017). Field-scale experiments reveal persistent yield gaps in low-input and organic cropping systems. In *PNAS* 114 (5) 926-931. https://doi.org/10.1073/pnas.1612311114
13. Kumhálová, J.; Kumhála, F.; Kroulík, M. & Matějková, Š. (2011). The impact of topography on soil properties and yield and the effects of weather conditions. In *Precision Agriculture* 12, 813–830. http://dx.doi.org/10.1007/s11119-011-9221-x
14. Macák, M., Rataj, V., Barát, M. & Galambošová, J. (2018). Comparison of two sowing systems for CTF using commercially available machinery. In *Agronomy Research* 16(2), 523-533, https://doi.org/10.15159/AR.18.060
15. Rataj, V., Kumhálová, J. Macák, M., Barát, M., Galambošová, J., Chyba, J. & Kumhála, F. (2022). Long-Term Monitoring of Different Field Traffic Management Practices in Cereals Production with Support of Satellite Images and Yield Data in Context of Climate Change. In *Agronomy* 12(1), 128, https://doi.org/10.3390/ agronomy12010128
16. Shafi, U., Mumtaz, R.; García-Nieto, J.; Hassan, S.A.; Zaidi, S.A.R. & Iqbal, N. (2019). Precision Agriculture Techniques and Practices: From Considerations to Applications. In *Sensors* 19(17) 3796, https://doi.org/10.3390/s19173796
17. SHMU. Climate normals of atmospheric rain fall for period 1981–2010 in Slovakia. (2020). In Slovak Hydrometeorological Institute, National Climatologic Program–Roll 15; Ministry of environment of Slovak Republic: Bratislava, Slovakia, ISBN 978-80-99929-04-4.
18. Skakun, S.; Kalecinski, N.I.; Brown, M.G.L.; Johnson, D.M.; Vermote, E.F.; Roger, J-C. & Franch, B. (2021). Assessing within-Field Corn and Soybean Yield Variability from WorldView-3, Planet, Sentinel-2, and Landsat 8 Satellite Imagery. In *Remote Sensing* 13(5), 872. https://doi.org/10.3390/rs13050872
19. SNAP 8.0.7 Desktop, ESA - European Space Agency, 2021. (Open-source SW)

Corresponding author:
doc. Ing. Miroslav Macák, PhD., Institute of Agricultural Engineering, Transport and Bioenergetics, Faculty of Engineering, Slovak University of Agriculture in Nitra, Tr. A. Hlinku 2, 949 76 Nitra, Slovak republic; phone: +421 6414797, miroslav.macak@uniag.sk

ANALYSIS OF ULTRASOUND SIGNAL ON REFLECTION FROM A SHARP CORNER SURFACE

Vladimír MADOLA, Vladimír CVIKLOVIČ, Stanislav PAULOVIČ

Institute of Electrical Engineering, Automation, Informatics and Physics, Slovak University of Agriculture in Nitra, Tr. A. Hlinku 2, 949 76 Nitra, Slovak Republic, e-mail: xmadolav@uniag.sk (V. M.), vladimir.cviklovic@uniag.sk (V. C.), stanislav.paulovic@uniag.sk (S. P.)

Abstract
The article deals with the analysis of ultrasonic signal amplitudes when the reflecting surface changes from the planar case to the sharp corner case. The distance between the transmitter and the reflecting surface was varied in steps in the interval 100 mm ÷ 215 mm. Statistically significant differences between the planar reflection and the reflection from the corner surface were demonstrated in the case of the ultrasound signal amplitudes at each distance as well as in the cases of the maximum components of the frequency analysis of the ultrasound signal. The statistically non-significant difference between the amplitude of the ultrasound signal and the amplitude of the simulated transfer function gives an indication of the universal description of the ultrasound signal on complex variable modelling in the case of reflection from a planar and corner surface.

Key words: *distance, measurement, transfer function, ultrasound amplitude, ultrasound reflection.*

INTRODUCTION

The measurement of position has fundamental place in the industry. Not only accuracy and scale but also the economics of the measurement system are addressed. Ultrasonic waves are widely used for object distance measurement, distance measurement in robots, robot (vehicle) navigation and so on in industrial applications (*Naba et al., 2015*). A typical system for distance measurement using ultrasound includes ultrasonic transducers for generating and sensing ultrasonic pulses, a microcontroller for controlling the measurement system, a temperature compensation for the accuracy of the measured distance, and a unit for processing the measured data (*Qiu et al., 2022*). The basic distance measurement method is the impulse method. Measurement systems using correlation for distance measurement, the generated ultrasonic signal is compared with the reflected ultrasonic signal from the object. The maximum of the correlation function over time gives a more accurate time indication for distance measurements relative to the impulse method. Compared to the impulse method, the correlation method requires a higher number of iterations of cross-correlations by convolution (*Hirata et al., 2008*). The authors (*Vogt et al., 2014*) report the application of ultrasonic water flow measurement. They note that the use of the correlation method improves the accuracy of flow measurement in turbulent flow media. In (*Blasina et al., 2017*), the authors subjected ultrasonic reflections from steel rods to correlation at specific times to which it was exposed to external heat. The method is used in monitoring temperature characteristics in food production. The measurement of the position of an object can also be obtained by integrating two ultrasonic sensors and identifying the position vector by triangulation. In applying the triangulation method, the authors (*Moreira et al., 2019*) used the standard deviation to quantify the deviations between the actual and the measured position vector. The authors (*Martínez et al., 2004*) used a nonlinear regression method to estimate the shape of the reflection surface between the planar case and the sharp edge. The aim of this article is the frequency analysis of an ultrasonic signal reflected from a sharp corner, representing a simulated edge in space. The results are compared with the reflection of the ultrasonic signal from a planar surface with unchanged characteristics.

MATERIALS AND METHODS

Measurement system

The animal positional identification logging system (*Lendelová et al., 2017*) was used as the measurement system. The block diagram of the measurement system is shown in Fig. 1. A 400ST160 piezoelectric transmitter was used as the source of ultrasonic impulses. The transmitter had a resonant frequency of 40 kHz ± 1 kHz according to (*Pro-Wave, 2005*). A 400SR160 piezoelectric sensor was used

for ultrasonic reflection sensing. The electrical signal from the ultrasonic transducer was amplified with an operational amplifier with an input impedance of 1 kΩ and a gain of 25 dB. One transmitter and one ultrasonic impulse sensor were used.

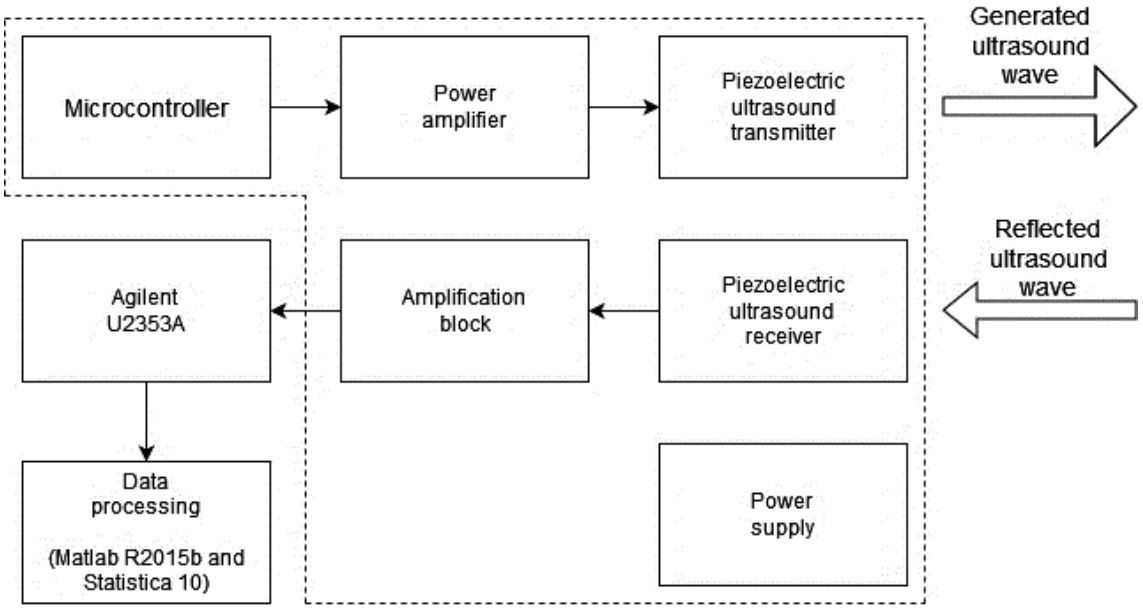

Fig. 1 Block diagram of measurement system

The electrical signal was measured with an Agilent U2353A data logger in differential mode of the analog inputs. The sampling frequency was determined 200 kHz heuristically. Selected characteristics of the datalogger used are shown in Tab. 1.

Tab. 1 Selected characteristics of U2353A dataloger (*Keysight, 2021*)

Parameter	**Value**
Resolution, bit	16
Number of analog channels, -	16
Input impedance, GΩ / pF	1 / 100
Uncertainty of measure, μV (at selected range: a) ± 10 V, b) ± 5 V, c) ± 2,5 V, d) ± 1,25 V)	± 305.2 a)
	± 152.6 b)
	± 76.3 c)
	± 38.2 d)
Sampling, MSa · s^{-1}	max. 1
Offset error, mV	± 1
Gain error, mV	± 2
System noise, mV	1
Slew rate, V · $(\mu s)^{-1}$	19

Agilent Measurement manager 1.2 software was used to acquire the measured signals. An electrical signal with an effective value of 3 mV was interpreted as noise. We cleaned the measured sample from the noise defined in this way, taking into respect the amplitude of the acquired signal in the Matlab environment.

Conditions of experiment

As a reflective surface we used a metal profile of 'L' shape with a thickness of 1.5 mm. The surfaces which were perpendicular to each other have the dimensions 230 mm x 110 mm. The reflecting normal was exposed to ultrasonic impulses in the planar case (Fig. 2, a) and in the corner case (Fig. 2, b). During the experiment, we changed the geometrical conditions of the measurement, namely: the distance

between the transmitter and the reflecting surface was changed stepwise in the interval 100 mm to 215 mm. For the corner case, the transmit vector guide made a mid-angle with the reflection corner (45°). The ultrasound transducer and receiver were positioned at the geometric centre in the X-axis direction (Fig. 2).

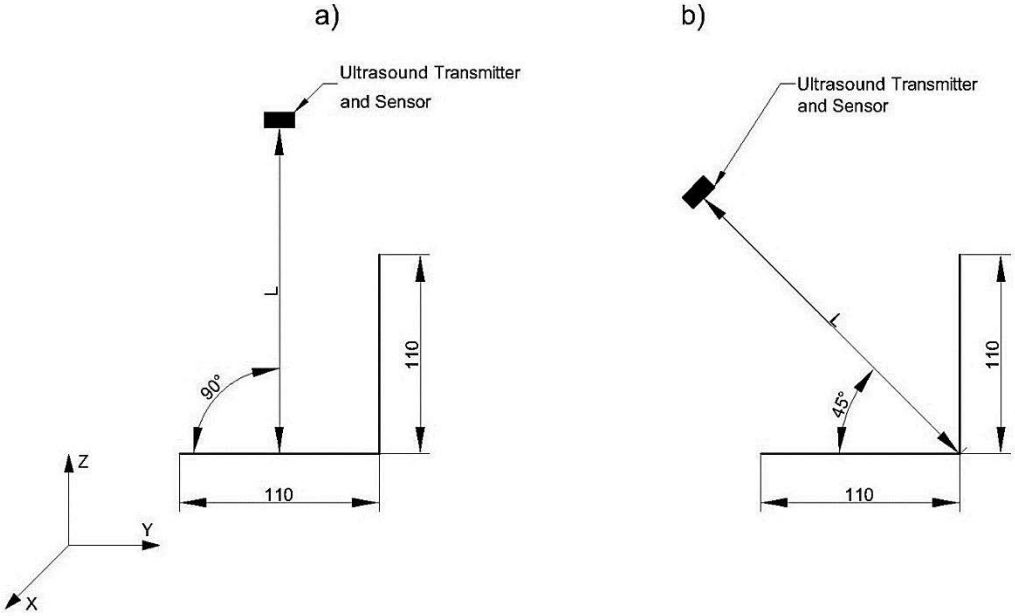

Fig. 2 Measurement geometric conditions (all length dimensions are in millimetres)

Data processing and used software

For statistical processing of observed data, STATISTICA 10 software was used. Results are presented as mean ± standard deviation. Statistically significant differences ($p \leq 0.05$) were obtained by Sidak's test in one-factor analysis of variance at the significance level of $\alpha = 0.05$. The normality of the measured data was verified by the Shapiro-Wilk test at a significance level of $\alpha = 0.05$. The experimental measurement was performed 4 times at a given distance L. Frequency analysis of the measured samples from the ultrasound sensor and modelling in the complex variable were performed by Discrete Fourier Transform in Matlab R2015b environment. The maximum frequency component was chosen as the quantifier of the frequency analysis result. We determined the correlation between the selected parameters by Pearson's correlation coefficient r.

RESULTS AND DISCUSSION

Analysis of ultrasound signal amplitudes

The statistical evaluation of the mean amplitudes of the ultrasonic signals at given distances L is presented in Fig. 3. The correlation between the average amplitudes and the distance L shows a nonlinear characteristic in the planar case with a coefficient of $r = -0.595$. The normality of the measured amplitudes was verified in favour of the Normal probability distribution with a maximum coefficient of variation which equal to 2.239 % for the condition $L = 200$ mm. In the corner case, the measured data showed statistically significant similarity to the Normal probability distribution with a maximum coefficient of variation of 2.393 % at the $L = 215$ mm condition. The correlation between the average ultrasound signal amplitudes and the distance L shows a non-linear characteristic in the corner case with a coefficient of correlation $r = -0.640$. By Sidak's test of statistically significant difference, we obtained statistically significant differences between the amplitudes of similar dimensions ($p \leq 0.05$). The non-linearity of the signal amplitude with distance is consistent with the authors (*Martínez et al., 2004*), who modelled the amplitude function of ultrasound on distance with the exponential regression equation.

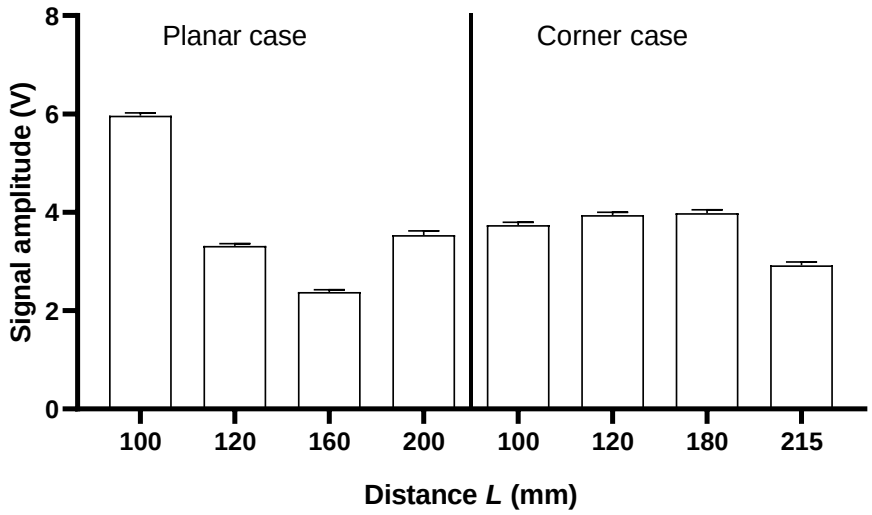

Fig. 3 Statistical evaluation of ultrasound signal amplitudes

Analysis of ultrasound signal frequency spectra

A statistical evaluation of the mean amplitudes of the ultrasound signal spectra at given distances L is shown on Fig. 4. By identifying the maximum amplitude component of the signal spectra at the ultrasound sensor, we determined the maximum frequency component, which was in the interval 40.039 kHz ÷ 40.625 kHz for both planar and corner cases. The normality of the identified spectra amplitudes was verified in favour of the Normal Probability Distribution for all measured samples with a maximum coefficient of variation of 2.746 % for the L = 200 mm condition. The correlation between the average spectral amplitudes of the ultrasound signal and the distance L shows a nonlinear characteristic with a coefficient r = - 0.635 on the planar case and a nonlinear characteristic with a coefficient r = - 0.195 on the corner case. By Sidak's test of statistically significant difference, we obtained statistically significant differences between the amplitudes of the spectra of similar dimensions ($p \leq 0.05$).

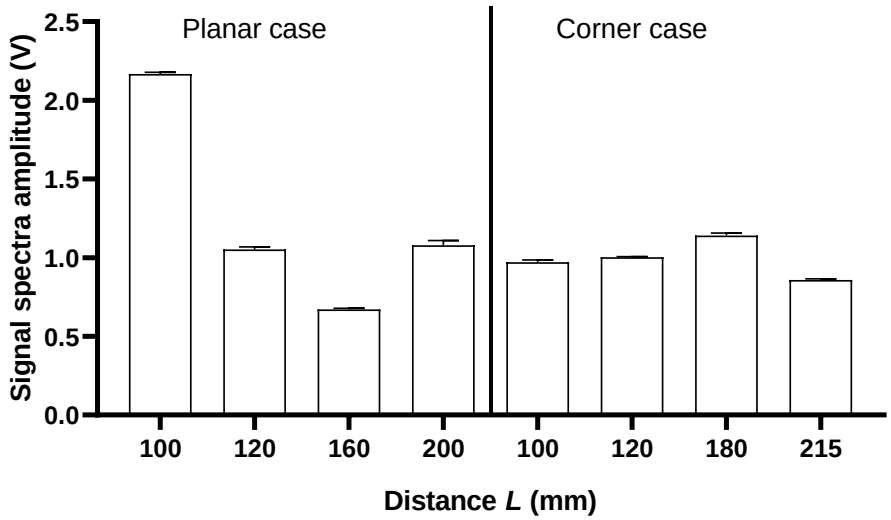

Fig. 4 Statistical evaluation of ultrasound frequency component amplitudes from signal spectra

Analysis of ultrasound signal by modelling on complex variable

By modelling the transfer functions of the measured ultrasound signals with maximum amplitudes of voltage on ultrasound sensor, we obtained third-order dynamic systems. The coefficient of determination was up to 85.86 % for the planar case and up to 83.99 % for the corner case.

Tab. 2 Poles and zeros of modelled dynamic systems

Parameter		Value
Poles, -	Planar case	- 1564 - 2249 ± i 3721
	Corner case	- 1196 - 1395 ± i 3885
Zeros, -	Planar case	8943 ± i 8997
	Corner case	6383 ± i 6368

The settlement time of the complex function shows an increase of 25.40 % in the corner case compared to the planar case. The increase indicates longer duration transient phenomenon in the case of reflection from a non-planar surface. The statistically significant difference between the transfer function amplitude and the experimental amplitudes was statistically significant ($p \leq 0.05$) in the planar case and statistically insignificant ($p > 0.05$) in the corner case. By comparing the chosen level of statistical significance and identified statistically significant differences, we can obtain similar distance measurement deviations, as the authors (*Moreira et al., 2019*) when interpreting the ultrasound signal amplitude at the level of threshold by voltage. Based on the amplitude of the ultrasound signal, we can correlate the dependence between the shape of the reflecting surface and the distance between the transmitter and the reflecting surface, which is nonlinear (*Yata et al., 2000*). The increase in transient phenomena for the corner case correlates with the multiple reflection from sharp edges as has been the result of the authors (*Martínez et al., 2004*). The authors (*Chen & Chou, 2008*) used the triangulation method to identify the corner reflective surface. Evaluating the influence of additional reflections on the frequency domain of the signal gives a direction to classify the acquired signal as time-varying, which will be reflected in quantifying the impulse duration over time as an n-th order dynamic system. It can be stated that according to the authors (*Qiu et al., 2022*), when cross-correlation is used to increase the accuracy of the distance measurement, at the same time, the computation duration requirements increase significantly due to the possibility of the presence of higher frequency significantly. The decrease in ultrasound signal amplitude in the corner case can be compared with the article (*Yata et al., 2000*), where the authors present a power function for the ultrasound amplitude as a function of the characteristics and distance from the reflecting surface.

CONCLUSIONS

The evaluation of correlation between the distance between object and the amplitude of ultrasonic signal is indicating a strong nonlinear dependence. The statistically significant difference between the planar reflection case of the ultrasound pulse versus the corner case suggest a possible correlation between the reflection case and the signal amplitude. Frequency analysis of the ultrasound signal showed identically statistically significant differences between the planar case and the corner case. The correlation between the amplitudes of the ultrasound signal spectra showed a poor nonlinear dependence to distance vector. In terms of transient effects, modelling the ultrasonic pulse is more guided by a complex model versus regression model.

ACKNOWLEDGMENT

The article was realized with the support of the project of Ministry of Education, Science, Research and Sport of the Slovak Republic: KEGA 006SPU-4/2021 Implementation of technology of Industry 4.0 in education process in study program ‘Control Systems in Production Engineering’.

REFERENCES

1. Blasina, F., Perez, N., Budelli, E., Lema, P., Kiri Ing, R., & Negreira, C. (2017). Development of a multiple-scattering acoustic sensor for process monitoring: Application to monitoring milk coagulation. 2017 IEEE International Instrumentation and Measurement Technology Conference. DOI: 10.1109/i2mtc.2017.7969965.
2. Hirata, S., Kurosawa, M. K., & Katagiri, T. (2008). Cross-Correlation by Single-bit Signal Processing for Ultrasonic Distance Measurement. IEICE Transactions on Fundamentals of Electronics, Communications and Computer Sciences. DOI: 10.1093/ietfec/e91-a.4.1031.
3. Chen, B. Ch. & Chou, J. (2008). A corner differentiation algorithm by a single sonar sensor for mobile robots. Asian Journal of Control. DOI: 10.1002/asjc.42.
4. Keysight. (2021). Keysight U2300A Series USB Multifunction Data Acquisition Devices. © Keysight Technologies.
5. Lendelová, J., Cviklovič, V., Olejár, M., & Pogran, Š. (2017). Animal position identification logging system. SK patent 288467.
6. Martínez, M., Benet, G., Blanes, F., Simó, J., Pérez, P., & Poza, J. (2004). Wall/corner classification. A new ultrasonic amplitude-based approach. IFAC Proceedings Volumes. DOI: 10.1016/s1474-6670(17)32054-2.
7. Moreira, T., Lima, J., Costa, P., & Cunha, M. (2019a). Low Cost Binaural System Based on the Echolocation. Advances in Intelligent Systems and Computing. DOI: 10.1007/978-3-030-36150-1_6.
8. Moreira, T., Lima, J., Costa, P., & Cunha, M. (2019b). Low-cost Sonar based on the Echolocation. Proceedings of the 16th International Conference on Informatics in Control, Automation and Robotics. DOI: 10.5220/0008119108180825.
9. Naba, A., Khoironi, M. F., & Santjojo, D. D. H. (2015). Low cost but accurate ultrasonic distance measurement using combined method of threshold-correlation. 2015 International Conference on Quality in Research. DOI: 10.1109/qir.2015.7374887.
10. Pro-Wave. (2005). Air Ultrasonic Ceramic Transducers: 400ST/R160. © Pro-Wave Electronic corp.
11. Qiu, Z., Lu, Y., & Qiu, Z. (2022). Review of Ultrasonic Ranging Methods and Their Current Challenges. Micromachines. DOI: 10.3390/mi13040520.
12. Vogt, M., Gevers, M., & Musch, T. (2014). Evaluation of transducer configurations for ultrasound cross-correlation flowmeters. 2014 IEEE International Instrumentation and Measurement Technology Conference Proceedings. DOI: 10.1109/i2mtc.2014.6860519.
13. Yata, T., Ohya, A., & Yuta, S. (2000). Use of amplitude of echo for environment recognition by mobile robots. Proceedings. 2000 IEEE/RSJ International Conference on Intelligent Robots and Systems. DOI: 10.1109/iros.2000.893198.

Corresponding author:
Ing. Vladimír Madola, Institute of Electrical Engineering, Automation, Informatics and Physics, Faculty of Engineering, Slovak University of Agriculture in Nitra, Tr. A. Hlinku 2, 949 76 Nitra, Slovak Republic, phone: +421 37 641 4723, e-mail: xmadolav@uniag.sk

INFLUENCE OF HEAT PUMP CONTROL ON PERFORMANCE PARAMETERS

Pavel MÍŠEK[1], Radomír ADAMOVSKÝ[1], Pavel NEUBERGER[1]

[1]*Department of Mechanical Engineering, Faculty of Engineering, Czech University of Life Sciences*

Abstract
The aim of the verification was to gain knowledge about the energy balance, performance, and operating parameters of gas absorption heat pumps with equithermal heating water temperature control and fixed heating water temperature control. Four ROBUR air-water gas absorption heat pumps (GAHP) A with outputs of 50 kW and 100 kW were tested in operation in various modes. During equithermal control of heat pump operation, 6.5-18.2% higher values of SCOP, SGUE and SPER performance parameters were achieved. The performance parameters SCOP, SGUE and SPER were 8.4-9.1% higher in equithermal control and the requirement of 16-hour active control than in the requirement of 24-hour active control. When using equithermal control, the specific CO_2 production resulting from natural gas consumption was lower by 6.84 kg CO_2/GJ and from electricity consumption by 0.32 kg CO_2/GJ compared to fixed heating water temperature control. A lower defrost frequency of the heat pump evaporator was found during the fixed heating water temperature control.

Key words: *absorption heat pump; natural gas; energy balance; COP; GUE; PER; CO_2 emission.*

INTRODUCTION

Gas Absorption Heat Pump (GAHP) operation control has a major impact on its performance parameters, namely Coefficient of Performance (COP), Gas Utilization Efficiency (GUE), and Primary Energy Ratio (PER). (*Fumagalli, 2017*) indicated that performance parameters determine global performance. However, it is important to analyse performance parameters together with other parameters characterising GAHP operating conditions. They included external conditions (ambient temperature and humidity), operating conditions (heating water temperatures), number of burner ignitions, cycle time, and defrost frequency. They considered PER to be the performance parameter with the highest definition. (*Janssen, 2020*) indicated that the key parameter is the cycle time, which significantly affects the overall efficiency. They supported this statement by the results of verification showing that the start-up time is about 8 minutes. At the 15-minute cycle, the actual efficiency was 22% lower than the steady-state efficiency. When the cycle lasted 35 minutes, the efficiency reached a value higher than 90% of the steady state. (*Corrales Ciganda, 2015*) studied GAHP efficiency in real applications. They observed the poor impact of incorrect design and control strategies, which caused excessive power consumption and frequent ON-OFF cycles (cycling). They also considered the PER performance parameter to be the most important.

(*Famiglietti, 2021*) studied the environmental aspects of GAHP applied to space heating and domestic hot water heating. They carried out evaluations in three buildings located in three representative European climatic conditions. CO_2 emissions were specified per 1 kWh produced by these sources. (*Charlick, 2014*) performed detailed dynamic tests of air/water GAHP at ambient air temperatures of 0 °C and 7 °C and heating water temperatures of 40 °C and 60 °C. CO_2 production ranged from 0.185 kg CO_2/kWh to 0.202 kg CO_2/kWh.

It is indicated in the report for Sustainable Energy Authority of Ireland (*Heat Pumps Technology Guide, 2020*) that the equithermal control is the most commonly used to manage GAHP operations. Equithermal temperature control consists in setting the heating water temperature of the heat source based on the outdoor temperature. At a lower outdoor temperature, a higher heating water temperature is required to balance the supplied heat with the heat loss of the building and vice versa. A set of equithermal curves can be determined for a given building, which describes the interdependence of the heating water temperature, the temperature in the building, and the outdoor temperature. Based on the required temperature in the building, a particular curve can be selected, and the heating water temperature can be regulated according to the outdoor temperature. The disadvantage of GAHP equithermal control is the slow response to rapid changes in outdoor temperatures (*Heat Pumps Technology Guide, 2020*).

The output of systems integrating several heat pumps, or heat pumps containing several cooling circuits, is controlled by switching the individual circuits on or off. This control method reduces the number of starts required, which means getting the system components less worn out and lowering the requirements for the balancing capacity (*Heat Pumps Technology Guide, 2020*).
The verification aimed to gain knowledge about the energy balance and values of the GAHP seasonal performance parameters, i.e., Seasonal Coefficient of Performance (SCOP), Seasonal Gas Utilization Efficiencies (SGUE), Seasonal Primary Energy Ratio (SPER), and values of GAHPs operating parameters (time of one cycle τ_c, total operating times $\Sigma\tau_o$, number of burner ignitions n_c, defrost frequency n_d) at two different control modes. It also aimed to specify the impact of the verified type of regulation on specific CO_2/GJ production resulting from natural gas and electricity consumption.

MATERIALS AND METHODS

The verification was carried out on ROBUR air-water GAHPs A in 4 boiler rooms in a cascade with gas condensing boilers (CB) with outputs of 50 kW and 100 kW in the period of 1.9.2019 to 31.8.2020. The basic description of individual installations is presented in Tab. 1. The column "control" specifies the GAHP and CB operation control method. Abbreviation "Fix." indicates fixed required heating water temperatures. GAHP operation at heating water temperatures of 60/50 °C and 55/45 °C was verified. Abbreviation "Eq." stands for the control of the required heating water temperature based on the outdoor temperature, and the subsequent value indicates the slope of the equithermal curve. The value after the dash indicates the number of hours during the day when the request was active in comfort mode. The note "in" and "out" indicates the position of the reference sensor of the setpoint temperature, i.e., whether the cascade is controlled according to the temperature of the inlet or outlet water from the unit. The following column specifies the heat loss of the building $Q_{\square,h.l.}$ at the calculated temperature of -15 °C. The penultimate column shows the installed capacity of GAHP and peak CB sources, and the last column presents the average ambient temperature t_e during the verification.

Tab. 1 Specification of parameters of verified operations

	Type of building	Type of source control	Heat loss $Q_{\tau,h.l.}$ [kW]	Installed power $Q_{\tau,i.c.}$ GAHP/CB [kW]	t_e [°C]
A	Primary school	Fix. 60/50 - 16 - out	50	1x35/1x30	3.6
B	Primary school	Eq. 1,0 - 16 - in	100	2x35/1x35	3.2
C	Primary school	Fix. 55/45 - 24 - out	50	1x35/1x30	3.6
D	Municipal authority	Eq. 1,0 - 24 - in	100	2x35/1x50	3.0

Heat production Q_C from GAHP condensers, natural gas consumption $Q_{gen.}$ in the generators, and the unit electricity consumption $Q_{e.e}$ in the monitored period were measured. The total operating times of GAHP $\Sigma\tau_o$, average operating times of the cycle τ_c, numbers of ignitions of generator gas burners n_c, and defrost frequency of evaporators n_d were also recorded.
The efficiency of the cycle operation was evaluated by the standard seasonal performance parameters SCOP, SGUE, and SPER, and by the average cycle time τ_c calculated according to the following relations:

$$SCOP = \frac{Q_{C.}}{Q_{gen.}+Q_{e.e}} \quad [-] \quad (1) \qquad SGUE = \frac{Q_{C.}}{Q_{gen.}} \quad [-] \quad (2)$$

$$SPER = \frac{Q_{C.}}{Q_{gen.}.f_{gen.}+Q_{e.e.}.f_{e.e.}} \quad [-] \quad (3) \qquad t_c = \frac{St_o}{n_c} \quad [s] \quad (4)$$

Factors of primary energy from non-renewable sources in the sense of the (*Directive EU 2018/844, 2018*) for the Czech Republic are considered $f_{gen.}$ = 1.0 for natural gas and $f_{e.e}$ = 2.6 for electricity.

RESULTS AND DISCUSSION

The verification results are summarized in the graphs in Fig. 1 and 2 and in Tab. 2.

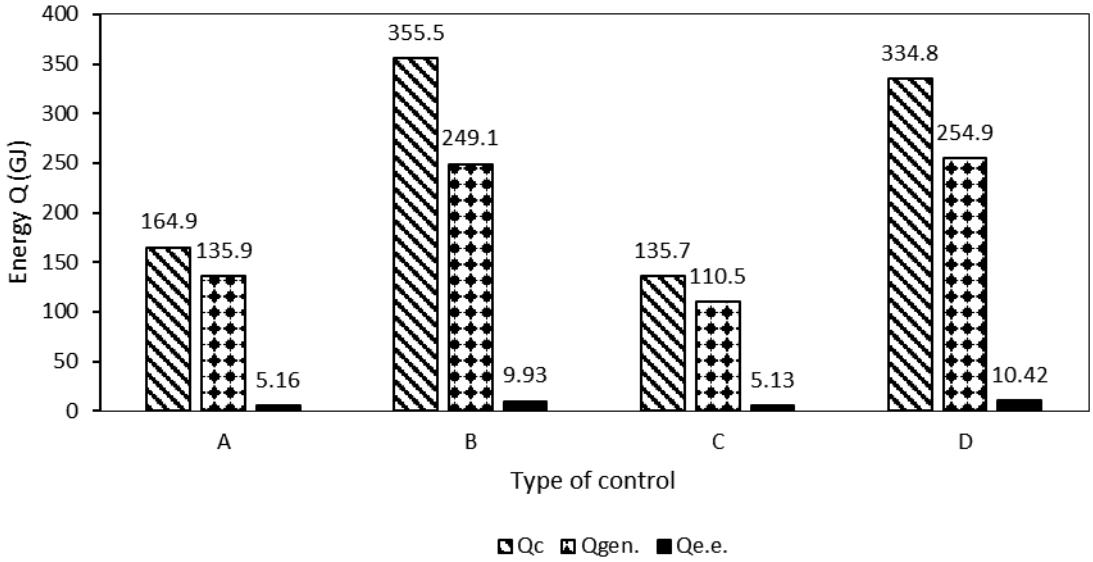

Fig. 1 GAHP energy balance

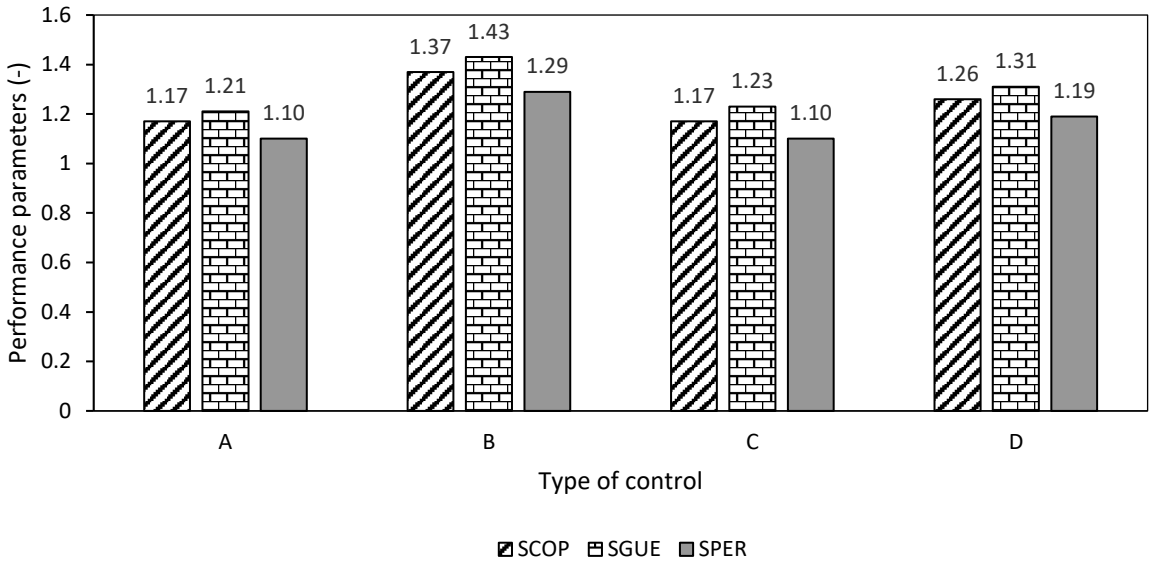

Fig. 2 GAHP performance parameters

Due to different operational and external conditions, the calculated values of SPER performance parameters in the primary school building were 15-25% higher than reported by (*Fumagalli, 2017*). They were in conformity in the municipal authority building.

Tab. 2 Heat pump operating times and switch-on and defrost frequencies

	Type of building	Total operating time $\Sigma\tau_o$ [h]	Average time of cycle τ_c [s]	Number of cycles n_c [-]	Defrost frequency n_d [-]
A	Primary school	1 863	4 132	1 623	59
B	Primary school	1 788/1 795	8 164	742/838	181/140
C	Primary school	1 924	1 399	4 950	0
D	Municipal authority	1 852/1 861	1 538	4 403/4 288	44/39

The verification results confirmed the conclusions reported by (*Corrales Ciganda, 2015*). A higher number of ON/OF cycles caused dynamic losses leading to lower SPER and SGUE values. Higher electricity consumption affected the SPER values negatively.
At the requirement of 16-hour active control, the average cycle times τ_c during control Eq. and Fix. were significantly longer than the cycle time limits specified in (*Janssen, 2020*). It was not the case during the 24-hour active control.

The operational verifications resulted in the following:

1. Despite the significantly higher defrost frequency n_d, higher values of the performance parameters SCOP, SGUE, and SPER were achieved when the control of GAHP operation was based on outdoor air temperature Eq. than when it was based on the fixed outlet water temperature Fix.
2. The average cycle times τ_c were longer during Eq. control, especially when 16-hour active control was required. When 24-hour active control was required, the cycle times were significantly shorter and almost identical for both types of control.
3. Total operating times $\Sigma\tau_o$ did not differ significantly at Eq. or Fix. control. They increased slightly with 24-hour active control.
4. The number of starts (cycling) n_c was higher during control Fix., especially when 16-hour active control was required. When 24-hour active control was required, the number of starts in both types of control increased significantly.
5. The performance parameters SCOP, SGUE, and SPER during Eq. control were higher when 16-hour active control was required than during the 24-hour active control requirement. The performance parameters during control Fix. were almost identical.
6. The number of defrost cycles was significantly higher during Eq. control than during Fix. control.

The seasonal energy efficiency of the device equivalent to our measured SPER value calculated by the manufacturer according to the NK 811/2013 methodology (*Eur-lex, 2013*) indicated its value for Robur GAHP A device 1.13 in average climatic conditions (CR), 1.09 in colder climates, and 1.17 in warmer climates. Higher SPER values were reached during Eq. control, both at the request of 16- and 24-hour active control, and lower during Fix. control.
Tab. 3 presents specific heat consumption in the generator $q_{gen.}$, specific electricity consumption $q_{e.e.}$, and low-potential energy q_{air} in the air fed to the GAHP evaporator needed to produce 1 GJ of energy in the GAHP condenser.

Tab. 3 GAHP specific heat and electricity consumption for the production of 1 GJ

	Type of source control	Heat production in condenser q_C [GJ]	Heat consumption in generator $q_{gen.}$ [GJ]	Electricity consumption $q_{e.e.}$ [GJ]	Heat at the evaporator $q_{air.}$ [GJ]
A	Fix. 60/50 - 16 - out	1.0	0.824	0.031	0.145
B	Eq. 1.0 - 16 - in	1.0	0.701	0.028	0.271
C	Fix. 55/45 - 24 - out	1.0	0.814	0.038	0.148
D	Eq. 1.0 - 24 - in	1.0	0.761	0.031	0.208

The processed verification results indicated the highest specific energy consumption 60/50 - 16 – "out" (A) during Fix. control and the lowest 1.0 - 16 – "in" (B) during Eq. control. The difference between specific heat and electricity consumption was $\Delta q_{gen} = 0.123$ GJ and $\Delta q_{e.e.} = 0.003$ GJ.
According to (*NIR, 2021*), the emission factor 0.2 t CO_2/MWh (55.6 kg/GJ) and the electricity generation factor 0.382 t CO_2/MWh (106.1 kg/GJ) are used to calculate CO_2 emissions from natural gas combustion in the Czech Republic. Average emissions production of 43.78 kg CO_2/GJ was calculated during Eq. control and 49.20 kg CO_2/ GJ during Fix. control. It is evident from the above that the application of control type Eq. 1.0 - 16 – "in" compared to Fix. control 60/50 - 16 – "out" will reduce specific CO_2 production resulting from natural gas consumption by 6.84 kg CO_2/GJ and electricity consumption by 0.32 kg CO_2/GJ. (*Charlick, 2014*) considered emission factors for natural gas 0.1841 kg CO_2/kWh (51.14 kg CO_2/GJ), and for electricity 0.5173 kg CO_2/kWh (143.69 kg CO_2/GJ). For control Fix., they stated average emission values of 0.187 kg CO_2/kWh (51.94 kg CO_2/GJ) for a heating water temperature of 40 °C, values of 0.201 kg CO_2/kWh (55.84 kg CO_2/GJ) for a heating water temperature of 60 °C. The recalculation indicated that the production of CO_2/GJ in our verifications during control Fix. was lower by 16.1%.

CONCLUSIONS

The goals presented in the introduction to the article were achieved. The verification results showed that the Eq. control, i.e., the setting of the heating water temperature based on the outdoor temperature, was more effective than the Fix. control (setting fixed heating water temperatures) in terms of performance and operating parameters of the GAHP.
The results also showed that the heat balance and performance and operating parameters of GAHP achieved better values at the requirement of 16-hour than at 24-hour active control.
Higher performance and operating parameters of GAHP at Eq. control also brought positive environmental aspects of reducing CO_2 emissions.

REFERENCES

1. Corrales Ciganda, J. L., Graf, R., Kühn, A., Schmitt-Gehrke, P., & Ziegler, F. Opertional experiences and system improvement measures for gas absorption heat pump systems. In: 6th IIR Conference: Ammonia and CO2 Refrigeration Technologies, Ohrid, 2015. 9 p.
2. Directive (EU) 2018/844 of the European Parliament and of the Council of 30 May 2018 amending Directive 2010/31/EU on the energy performance of buildings and Directive 2012/27/EU on energy efficiency.
3. Eur-lex (2013), COMMISSION DELEGATED REGULATION (EU) No 811/2013 of 18 February 2013. Available online at https://ec.europa.eu/eurostat/statistics-explained/index.php?title=Archive: Consumption_of_energy
4. Fumagalli, M., Sivieri, A., Aprile, M., Motta, & M., Zanchi, M. Monitoring of gas driven absorption heat pumps and comparing energy efficiency on primary energy. *Renewable Energy*, 110, 2017, 115-125.
5. Famiglietti, J., Toppi, T., Pistocchini, L., Scoccia, R., & Motta, M. A comparative environmental life cycle assessment between

a condensing boiler and a gas driven absorption heat pump. *Science of the Total Environment*. 762 (144392), 2021.
6. Heat Pumps Technology Guide. Report prepared for SEAI by: Ricardo Energy & Environment, 2020, Available online: https://www.seai.ie/business-and-public-sector/business-grants-and-supports/support-scheme-renewable-heat/Heat-Pump-Technology-Guide.pdf
7. Charlick, H., Crowther, M., Dennish, T., & Thomas, J. *Comparative testing of a gas absorption heat pump on the dynamic test rig*. Cheltenham UK: Kiwa Ltd, 2014, 56 p.
8. Janssen, E., Brookson, A., Amdurski, G., Nixon, D., Brown, R., & Hilaire. L. S. Gas Absorption Heat Pump Performance Mapping and Projections of Energy, Cost, and Carbon Savings, for Different heating Apllications in a Cold-Climate. *International Journal of Energy Managment*. 1 (2020) 8-24.
9. National Greenhouse Gas Inventory Re-port of the Czech Republic (reported in-ventories1990- 2019). Published by Czech Hydrometeorological Institute, April 2021, 526 p. ISBN 978-80-7653-015-7

Corresponding author:
Assoc. Prof. Ing. Pavel Neuberger, Ph.D., Department of Mechanical Engineering, Faculty of Engineering, Czech University of Life Sciences Prague, Kamýcká 129, Praha 6, Prague, 16521, Czech Republic, phone: +420 224383179, e-mail: neuberger@tf.czu.cz

MODELLING OF COMPOSITE REINFORCEMENTS IN AGRICULTURAL EQUIPMENT

Jaroslav MLÝNEK[1], Michal PETRŮ[2], Roman KNOBLOCH[1]

[1]Department of Mathematics, FP, Technical University of Liberec, Liberec 1, Studentská 2, Czech Republic
[2]Institute for Nanomaterials, Advanced Technologies and Innovation, Technical University of Liberec, Studentská 2, Czech Republic

Abstract
The article is focused on the technology of polymer composite frame production by winding fibres on a non-load-bearing frame and their possibilities of use in the development of new agricultural machinery and equipment. An industrial robot and a winding head are used in the process of winding the fibres onto the frame. The main focus is attended on the process of winding fibres on a frame consisting of several parts with different cutting radii and the requirement to wind these parts at different angles due to the different loads of the future composite frame. The lengths of the individual parts of the frame, the radii of their circular cross-sections, and the required winding angles are determined on the basis of composite load modeling in some software systems. This type of composite frames has a wide range of applications in the production of agricultural machinery and equipment.

Key words: *agricultural machinery; polymer composite frame; model of composite load; composite lifespan; machine reinforcement.*

INTRODUCTION

At present, the production of modern agricultural machinery is focused primarily on increasing their power, reduction of fuel consumption, and reducing the machine weight. At the same time, a sufficiently long lifespan of the agricultural machine and its production at an acceptable financial cost is required. The use of composite materials in the production of many machine components significantly helps to meet the stated production requirements (*Gay, 2014; Agaroal, Broutman & Chandrashekhara, 2017*). Composites are increasingly replacing conventional materials in production. Composite materials increase the resistance of the machine to the stresses of its individual parts (elasticity, tensile strength, pressure, and torsion). Furthermore, the composites enable low machine weight (preventing of soil compaction, see Fig. 1) and weather resistance.

Fig. 1 Agricultural machines previously produced were constructed mainly of classic materials (iron, steel, aluminum, various metal alloys). Their weight was therefore significantly greater than the current machines. The two-row potato harvester is shown on the left, the grain harvester on the right.

The application of composite materials to the renovated surfaces of machines due to their wear (e.g. plowing parts of the machine) was used already in the past (*Mùller, Chotěborský & Hrabě, 2009*). At present, composite materials are increasingly used in agriculture (*Chen, G., 2018*). Polymer composite frames occupy an important place in the use of new materials.

Polymer composite frames are often used as machine chassis reinforcements, reinforcements of cargo space, doors, and driver's cabs. Composite frames are also applied as load-bearing structures for various agricultural machines and devices (e.g. trucks) and also as mechanical protective equipment for machines (for example external safety frames at the tractor cab, see Fig. 2).
The aim of this contribution is to describe the technology of winding several layers of fibres onto a non-load bearing composite frame. The winding process is implemented by using a mathematical model of winding, a winding head, and an industrial robot.

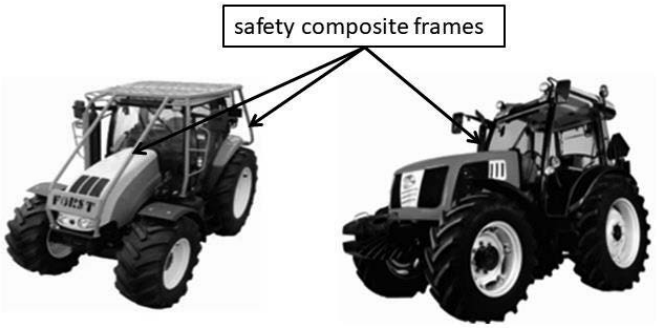

Fig. 2 Safety composite frames for the tractor cab.

MATERIALS AND METHODS

One of the possibilities for the production of composite frames is fibre winding technology. The non-load-bearing frame (usually made from polyurethane) is attached to the end of the working arm of the industrial robot (robot-end-effector). Based on a suitably determined trajectory of the robot (in more detail see (*Siciliano, Sciavicco, Villani, & Oriolo,2010; Martinec, Mlýnek & Petrů, 2015*)), the frame passes through the winding head, see Fig. 3 on the right and Fig. 4 on the right. The winding head comprises three rotating annular rings with spools of fibres. One layer of fibre windings is gradually formed by each annular ring as the frame passes through the winding head and the annular ring rotates. The technology of winding the fibres on the frame is described in detail in (*Mlýnek, Koloor, Martinec & Petrů, 2021*; *Mlýnek, Petrů & Martinec, 2019*). Composite frames have different geometric shapes, often highly 3D ragged (see Fig. 3 on the left). Frames can be closed (see Fig. 3 on the right) or open (see Fig. 3 on the left and Fig. 4 on the right) and have different cross-sections (e.g. circular, elliptical, trapezoidal).

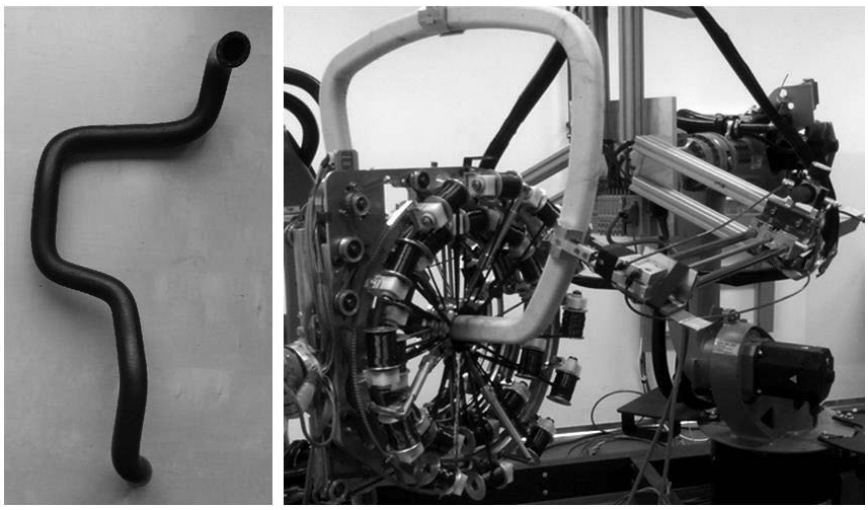

Fig. 3 Example of a 3D multi-shaped non-bearing hollow frame with circular cross-section (on the left). Closed non-bearing frame prepared to winding process. Frame is connected to robot working arm and goes through winding head (on the right).

In the remaining part of the article we will focus on the issue of winding frames consisting of several parts with different cross-sectional radii and the need to wind these parts in general at different angles (see Fig. 5 on the left). The parameters of such a frame and the required winding angles can be obtained on the basis of modeling the planned composite load, e.g. in the ANSYS and ABAQUS software tools.

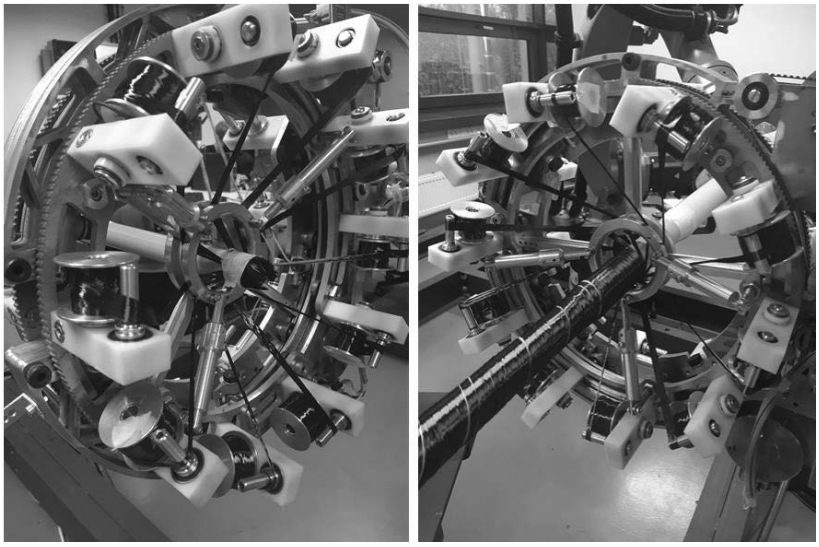

Fig. 4 Preparation of a winding head with three rotating rings with carbon fibre spools to start the winding process is shown on the left. The actual process of winding the fibres on a polyurethane frame, which is attached to the end of the working arm of the industrial robot, is displayed on the right. The frame passes through the winding head based on the movement of the robot arm, and at the same time three layers of fibres are wound simultaneously (each rotating annular ring winds one layer).

A mathematical model of the winding process is shown in Fig. 5 on the right. One rotating annular ring *k* with its center *S* and radius *R* is depicted in this figure. The annular ring is part of the winding head and lies in plane orthogonal to axis *s* of winding head.

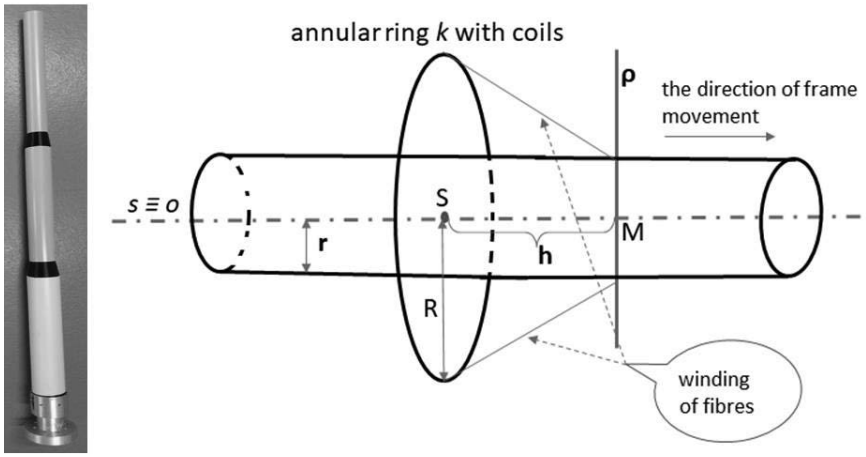

Fig. 5 Example of a straight-line frame with three parts with different radii of their circle cross-sections on the left. The mathematical model of annular ring *k* of the winding head, straight-line frame and winding plane ρ is shown on the right.
Central axis *o* of frame is identical with axis *s* of the winding head (see Fig. 5 on the right). Radius of cylindrical frame is denoted *r*. We suppose constant speed *w* of the passage of the frame through the winding head. Annular ring *k* with coils is rotated around axes *s*, frame goes through annular ring *k* by

speed *w* and on frame is created layer of wound fibres under winding angle α in distance *h* from the annular ring *k* (in plane ρ).
We need to determine the angular speed ω of the annular ring *k* so that the fibres are wound at the prescribed angle α. The angular speed ω is controlled by the external axis of the robot during the winding process.
It is also necessary to know at what distance *h* from the annular ring *k* the fibres are wound on the frame when winding at an α angle is specified. The procedure for deriving the calculation of required angular speed ω and the winding distance *h* at the required winding angle α is described in detail in (*Mlýnek, Koloor, Martinec & Petrů, 2021*).
The wound fibre (usually from carbon, glass or aramid) forms a helix on the surface of the frame with circular cross-section. The fibre forms a right-handed helix (positive winding angle α) or a left-handed helix (negative winding angle α). Winding angle $\alpha \in (0, \frac{\pi}{2})$ in positive winding orientation corresponds to the pitch angle α of the right-handed helix.
Pitch of helix *v* (height of helix when is created one thread at an α angle) is given by relation $v = 2\pi r.tg\alpha$ (see (*Pressley, 2010*)). To ensure winding at an α angle, the annular ring have to make one turn in the same amount of time as the frame travels the distance v.
Peripheral speed *u* of the annular ring *k* is given by relation $u = \omega.R$. Based on the validity of the relation

$\frac{u}{w} = \frac{2\pi R}{v} = \frac{2\pi R}{2\pi r.tg\alpha} = \frac{R}{r.tg\alpha}$, we can express angular speed ω in the form

$$\omega = \frac{1}{r.tg\propto} \cdot w \,. \qquad (1)$$

Distance *h* of winding the fibre onto the frame from the annular ring *k* can be derived from the parametric equation of the helix and the expression of the equation of the tangent of the helix at a given point. Distance *h* is given by relation (derivation is described in detail in (*Mlýnek, Koloor, Martinec & Petrů, 2021*))

$$h = tg\alpha \,.\sqrt{R^2 - r^2} \,. \qquad (2)$$

Based on the use of equations (1) and (2), the desired winding angle of the fibres can be continuously and repeatedly changed. From relation (1) it can be seen that angular speed ω of the annular ring *k* depends on radius *r* of frame, at required winding angle α and constant movement *w* passage of the frame through winding head. Distance *h* in relation (2) depends on winding angle α, on radius *R* of annular ring *k*, and radius *r* of frame.

RESULTS AND DISCUSSION

Braiding technology and filament winding are the most used manufacturing procedures of composite frames productions. The advantage of braiding is the high adhesion of the fibres to the frame surface (see (*Eschler, Miadowitz, Zaremba, & Dreschsler, K., 2020*)). The main advantage of filament winding is the possibility of winding a closed frames and performing a continuous change of filament winding angle (see (*Mlýnek, Koloor, Martinec & Petrů, 2021*)). Relationships (1) and (2) make it possible to continuously wind frame parts with different radii of their circular cross-sections. Using relation (2), it is possible to determine at what distance from the annular ring the fibres are wound on the frame. At the same time, relation (1) provides us information on what angular speed ω the annular ring must rotate in order for the fibres to be wound at the desired angle α on a given part of the frame. Thus, assuming a constant speed *w* of the passage of the frame through the winding head, we know how it is necessary to ensure the angular speed of the annular ring at a given moment in order for the winding of the fibres to meet the requirement of winding angles. When the winding transition between two parts of the frame, it is necessary that the transition of the frame radius changes continuously (i.e. without a jump).
Three layers of fibre windings for the described frame type can be performed simultaneously in one pass of the frame through the winding head. If a larger number of fibre windings is required, the frame needs to pass through the winding head repeatedly.

Values of angular speed ω of annular ring depending on the parameters in relation (1) are shown in Tab. 1. This table shows that with increasing value of the winding angle $\alpha \in (0,\ \pi/2)$ (trigonometric function *tg* is increasing on this interval) and radius *r* of the frame, the angular speed ω of the rotating ring *k* decreases. Conversely, as the constant speed *w* of passage of the frame through the winding head increases, the angular speed ω increases

Tab. 1 Calculation of angular speed ω of ring rotation depending using relation (1)

w [mm/s]	*r*[mm]	α [°]	α [rad]	*tg* α	ω [rad/s]
20	20	30	0.5235	0,577 3	1,7322
		45	0.7853	1,000 0	1,0000
		60	1.0471	1,732 0	0,5773
	40	30	0.5235	0,577 3	0,8661
		45	0.7853	1,000 0	0,5000
		60	1.0471	1,732 0	0,2886
50	20	30	0.5235	0,577 3	4,3305
		45	0.7853	1,000 0	2,5000
		60	1.0471	1,732 0	1,4432
	40	30	0.5235	0,577 3	2,1652
		45	0.7853	1,000 0	1,2500
		60	1.0471	1,732 0	0,7215

Values of distance *h* of winding fibres on frame from annular ring depending on the parameters in relation (2) are shown in Tab. 2.

Tab. 2 Calculation of distance winding *h* of fibres on the frame from rotating ring *k* using relation (2)

R [mm/s]	*r*[mm]	α [°]	α [rad]	*tg* α	*h*[mm]
50	20	30	0.5235	0,5773	26,4403
		45	0.7853	1,0000	45,8000
		60	1.0471	1,7320	79,3256
	40	30	0.5235	0,5773	17,0319
		45	0.7853	1,0000	30,0000
		60	1.0471	1,7320	42,9600
100	20	30	0.5235	0,5773	56,5632
		45	0.7853	1,0000	97,9795
		60	1.0471	1,7320	169,7004
	40	30	0.5235	0,5773	52,9101
		45	0.7853	1,0000	91,6510
		60	1.0471	1,7320	158,7395

Tab. 2 indicates the values of distance *h* of winding fibres on the frame from the rotating annular ring *k* with the fibres for specific input parameters in relation (2). Distance *h* increases with growing of annular ring radius *R* and winding angle α, on the contrary it decreases with increasing value of frame radius *r*.

CONCLUSIONS

At present, composite materials are increasingly used in the production of agricultural machinery. Polymer composite frames have an irreplaceable place in production. The procedure described in this article allows the application of fibre winding technology to more complicated shapes of frames composed of several parts with different radii of circular cross-section. Different parts of the composite frame can be significantly loaded in different ways during the operation of an agricultural machine or equipment.

Based on modelling the planned load of the developed composite frame using a software tool, it is possible to determine the appropriate shape and radius of the cross-section of individual frame parts as well as the required fibre winding angle on individual frame parts for each fibre winding layer. The positive and negative winding orientations usually alternate between successive layers of fibres. The quality of winding fibres on the frame is addressed in this article mainly from a geometric point of view. The quality of the fibres used to winding also plays an important role. But the correct winding of fibres from a geometric point of view is a necessary prerequisite for the production of a high-quality composite frame.
The results and conclusions of this article can be successfully used in the development of polymer composite frames in agriculture when designing new machines and equipment.

ACKNOWLEDGMENT

This study was supported by the project "Modular platform for autonomous chassis of specialized electric vehicles for freight and equipment transportation", Reg. No CZ.02.1.01/0.0/0.0/16_025/0007293.

REFERENCES

1. Agarwal, B., D., Broutman, L., J., & Chandrashekhara, K. (2015). *Analysis and Performance of Fiber Composites*. John Wiley & Sons. New York, NY, USA. ISBN: 978-81-265-3636-8.
2. Chen, G. (2018). *Advances in Agricultural Machinery and Technologies*. CRC Press. Boca Raton, FL, USA. ISBN: 9781498754125.
3. Eschler, E., Miadowitz, T., Zaremba, S., & Dreschsler, K. (2020). Design optimization of a braided roof frame reinforcement by process-integrated local customization of component properties. *Applied composite materials*, Volume 27, pp. 75-91.
4. Gay, D. (2014). *Composite Materials: Design and Applications*. CRC Press. Boca Raton, FL, USA.
5. Martinec, T., Mlýnek, J., & Petrů, M. (2015). Calculation of the robot trajectory for the optimum directional orientation of fibre placement in the manufacture of composite profile frames. *Robotics and Computer-Integrated Manufacturing*, Volume 25, pp. 42-54. ISSN: 0736-5845, DOI: 10.1016/j.rcim.2015.02.004, https://www.sciencedirect.com/science/article/pii/S0736584515000228
6. Mlýnek, J., Petrů, M., & Martinec, T. (2019). Design of Composite Frames Used in Agricultural Machinery. *Proceedings of the 7th International Conference on Trends in Agricultural Engineering 2019*, Herák, D. (Ed.), Czech University of Life Sciences Prague, Prague, September 2019, pp. 396-401, ISBN: 978-80-213-2953-9.
7. Mlýnek, J., Koloor, S., S., R., Martinec, T., & Petrů, M. (2021). Fabrication of High-Quality Straight-Line Polymer Composite Frame with Different Radius Parts Using Fiber Winding Process. *J. Polymers*, Volume 13(4), 497, 2021, 18 pages. https://doi.org/10.3390/polym13040497, Open Access.
8. Mùller, M., Chotěborský. R., & Hrabě, P. (2009). Degradation processes influencing bonded joints. *Research in Agricultural Engineering*, 55(1), 29-34.
9. Pressley, A., N. (2010). *Elementary differential geometry*. Springer Science & Business Media. ISBN: 9781848828902.
10. Siciliano, B., Sciavicco, L., Villani, L., & Oriolo, G. (2010). *Robotics: Modelling, Planning and Control*. Springer-Verlag London Limited. ISBN: 978-1-84628-641-4.

Corresponding author:
doc. RNDr. Jaroslav Mlýnek, CSc., Department of Mathematics, FP, Technical University of Liberec, Studentská 2, Liberec, 46117, Czech Republic, phone:+420 485352847, e-mail: jaroslav.mlynek@tul.cz

EVALUATION OF ELECTRODES WITH CONDUCTIVE INK FOR FLEXIBLE TACTILE SENSOR

Viktor NOVÁK[1], Jaromír VOLF[1], Vladimír RYŽENKO[1], Stanislava PAPEŽOVÁ[1]

[1]Czech University of Life Sciences Prague, Faculty of Engineering, Department of Electrical Engineering and Automation, Kamýcká 129, 165 21 Prague 6, Czech Republic

Abstract
This paper presents the ongoing research which aims to determine suitable combinations of dimensions of electrodes and of mixtures of conductive inks in the design of planar pressure transducers, and particularly in the design of the currently developed flexible tactile sensor SITSCAN CS. Here we continue in our previous work on planar pressure transducers by evaluating conductive inks. Due to the only partial results in this research field, we decided to perform an extensive and original measurement of totally 162 combinations of different electrode sizes, various conductive ink mixtures and ink layer thicknesses. Thanks to this, it will be possible to design various tactile sensors without the need to perform time-consuming preparatory measurements. The aim of the measurement is also to determine the usable working range of pressures and the corresponding sensitivity for certain combinations of electrodes and inks, and also to exclude those variants which are unsuitable for the given purposes. In the paper, we present the impact of the electrode dimensions on the measured electrical resistance.

Key words: *tactile sensor; communication bus; pressure; electrode; Sitscan; conductive ink.*

INTRODUCTION

In our previous work, we developed a planar measuring system PLANTOGRAF which evaluates the pressure distribution between the road, the soil and the tyre, or even within the soil itself; but the measuring system found its use in the medicine, too. Its current version consists of a large number of 16 400 individual sensors, that change their electrical resistance due to the applied pressure. Its predecessors also used individual electrodes to convert pressure into electric signals, however, they used different technology (originally conductive rubber, further conductive ink on a separate foil layer), for more detailed information about the previous research see e.g. (*Volf et al., 2015; Koder et al., 2019*). The main difference represents another method of applying ink to the electrodes and the flexibility of the transducer; any individual sensor represents a circle electrode with conductive ink applied directly to it, unlike previous solutions, where the ink was applied on a separate layer, more discussion about the application of the ink is described by (*Volf et al., 2019*). This was possible using a different ink type, namely polymer-based instead of water-based that did not adhere to the electrode. Now we are developing a new measuring system labelled SITSCAN CS, which is primarily designed to development of ergonomically shaped chairs. The main difference to its predecessors is the flexibility, i.e. its possibility to adopt to uneven surfaces, such as chair seats. This brings some innovative techniques of the design, such as using the printing technology by creating the sensor matrix.

A planar pressure transducer consists of a matrix of individual sensors, that are covered with the piezoresistive material. They originally came with conductive rubber based on the experiences described (*Barman & Guha, 2005*). As we focused our research to create a flexible transducer, we also reflect newer experiences teams experimenting with piezoresistive materials, e.g. by the design of FSR sensors discussed by (*Giovanelli. & Farella, 2016*) with lower pressure range. The properties of conductive inks are extensively described by (*Dimitriou E. & Michailidis, 2021*). The authors also focus on the electrical conductivity of conductive inks, which we will also reflect in further parts of our research, where different ink mixtures will be evaluated.

Before the final design of the new transducer SITSCAN CS, individual characteristics of various combinations of inks and different electrodes have to be measured; subsequently, their suitability for the intended use will be evaluated and the most suitable one will be implemented into the measuring system. The main motivation of our research is to perform the time-consuming preparatory measurements of the ink characteristics only once and to efficiently use the results in the design of a wide range of planar pressure transducers. This includes an extensive and original measurement of several combinations of

different electrode sizes, various conductive ink mixtures and ink layer thicknesses. The aim of the study is to present the first part of the measurement, namely on the test sample plates Nr. 3 to Nr. 5 and to use the results to create a preliminary mathematical model that describes the relation between the electrodes and the electrical resistance.

MATERIALS AND METHODS

As we started the development of the new transducer, we ordered at the Faculty of Chemical Technology, University of Pardubice, Czech Republic, 2 + 9 individual samples (see Fig. 1) in shape of a plate, that includes 18 individual circular electrodes with different dimensions. The samples were made using printing technology and each one has a unique combination of thickness of the ink layer and the ratio of the inks in the mixture. The electric output signal is obtained via three busses that are connected to the electrodes. As the piezoresistive layer were selected conductive inks HENKEL NCI 7002 and ECI 7004HR in the specified ratios in the mixture. The ink 7002 is non conductive, whereby the ink 7004 is conductive with carbon particles as filler. The inks are designed to blend with each other to obtain the required level of resistivity, they are suitable for the printing technology (LOCLITE NCI 7002 and LOCLITE NCI 7002 product sheets).

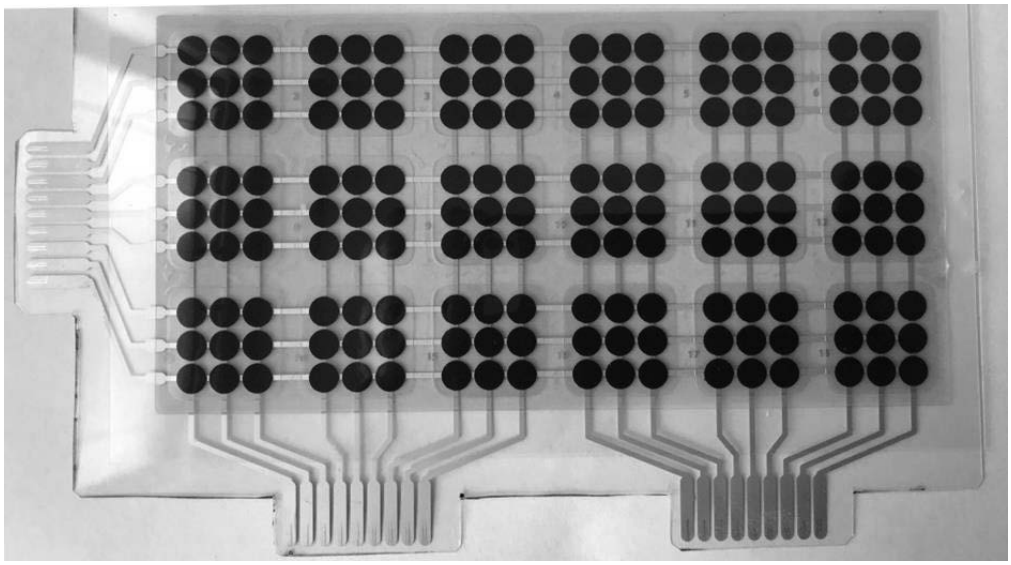

Fig. 1 Sample plate with circular electrodes.

Due to the proposed extend 162 ink – electrode combinations, we decided to perform the measurement as automatically as possible. This included four key parts, namely using a robotized arm to extend selected force on the electrode, a control program to set the exerted force automatically, an electric circuit to determinate the electrical resistance as the output variable and a LabView program to collect the data and calculate the quantities. More detail about the used methodology can be found in (*Volf et al., 2019*). Measurements of the dependency of the output voltage (or else electrical resistance) were performed at a robotized workplace equipped with a Turbo Scara SR60 robot. The basic step of the vertical motion of the robot's arm is 0.01 mm. Pressure was applied by the measuring tip with 3 mm in diameter by means of the vertical motion of the robot's arm. The arm was moved in 0.02 mm increments for a general overview of the behaviour of an electrode and further in 0.01 mm step for a more detailed analysis; this more detailed course was measured only on selected (the most convenient) electrodes and will be presented separately. The loading force was exerted from 0,37 N up to cca. 17,6 N. The pressure applied on the electrodes was calculated from the known area of the surface of the measuring tip and the exerted force. This resulted in the measured range of pressure values approximately from 30 kPa up to 1 400 kPa for the particular measuring tip. A photograph of the robotized measuring workspace is depicted in Fig. 2.

Fig. 2 Robotized measuring workspace.

The electrical resistance of a particular electrode depends on several variables, namely on the dimension of the used electrode, on the used ink or ink mixture and on the thickness of the applied ink layer. We expect a significant impact of the thickness of the ink layer on the electrical resistance; within a thinner ink layer, there are created less conductive paths and the resistance should theoretically increase. The impact of the dimensions of an electrode on the electrical resistance is more complex and will be evaluated statistically in the next chapter. Theoretically, the electrical resistance should increase with the area size, as there are created more conductive paths within the ink, and it should also decrease with smaller gap between the inner and outer electrode as the conductive path shortens.

RESULTS AND DISCUSSION

The aim of this evaluation is to determine the dependency of the electrical resistance on the dimension of the electrodes and to make a mathematical model of this dependency. As the variables area of the electrode and the gap between the inner and outer electrode are not independent on each other, a direct statistical evaluation of the impact of the gap size and of the electrode area itself on the electric conductivity is not possible. Therefore, we introduce a new variable called Active Electrode Area P_A, that includes both parameters (1), where the others (ink thickness, mixture) are kept constant. The values of R_1 – R_4 are graphically explained in Fig. 2; the calculated values of P_A (%) for individual electrodes are stated in Tab. 1.

$$P_a = \frac{\pi R_4^2 - \pi R_3^2 + \pi R_2^2 - \pi R_1^2}{\pi R_4^2} = \frac{R_4^2 - R_3^2 + R_2^2 - R_1^2}{R_4^2} \quad (1)$$

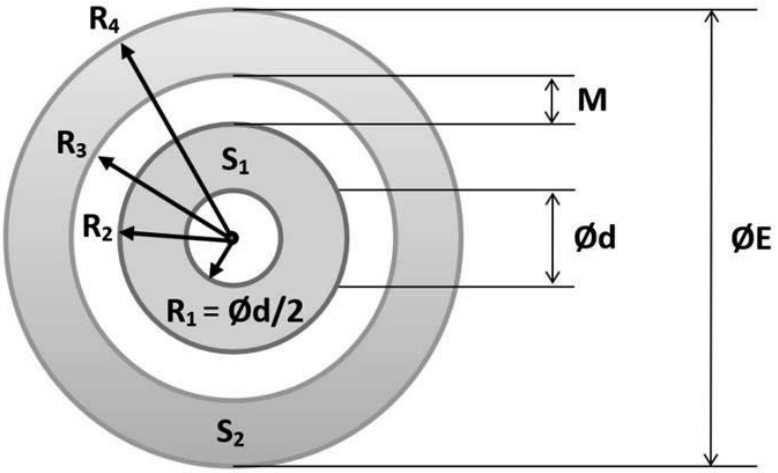

Fig. 2 Dimensions of the electrodes.

Tab. 1 Active electrode area P_A for individual electrodes

Electrode	E1	E2	E3	E4	E5	E6	E7	E8	E9
P_A (%)	86	89,75	77,44	79,84	94,20	91,35	88,49	85,63	82,78
Electrode	E10	E11	E12	E13	E14	E15	E16	E17	E18
P_A (%)	79,92	77,06	93,65	90,53	87,40	84,28	81,15	78,03	74,90

An arithmetic mean of measured electrical resistances of individual electrodes has been calculated and depicted by a scatter graph. Subsequently we used regression analysis to find a model, that describes the dependency of the electrical resistance on the Active Electrode Area. In following graphs in Figs. 3 and 4, there are depicted two models with the regression function and with the coefficient of determination R^2.

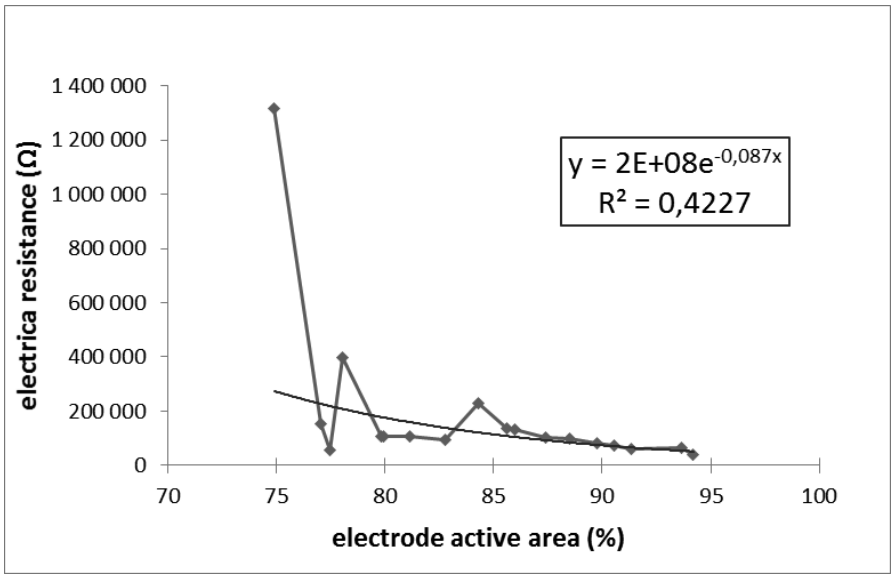

Fig. 3 Regression analysis – exponential.

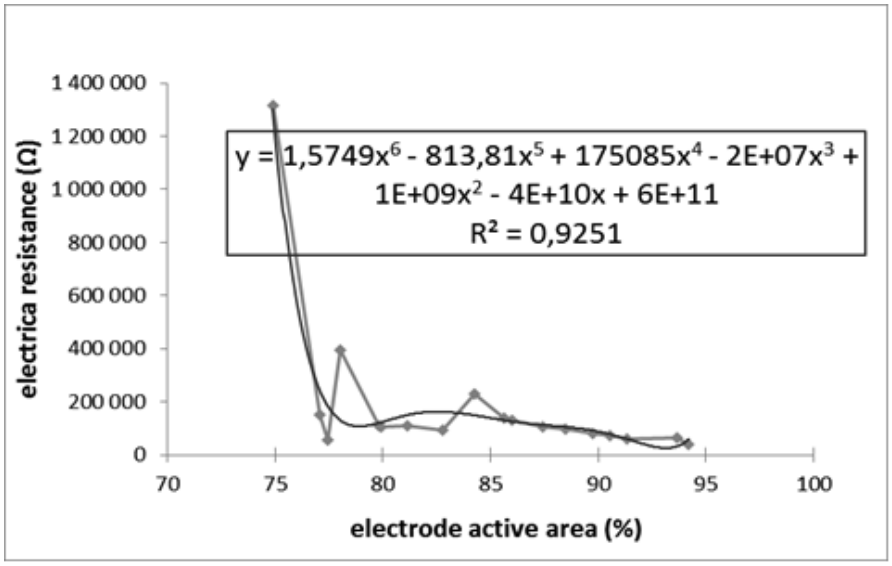

Fig. 4 Regression analysis – polynomial.

The dependency is better captured by a 6th degree polynomial (Fig. 4 above). With increasing Active Electrode Area P_A the electrical resistance decreases significantly, up to values under 100 kΩ. This is a very important finding for the design and selection of the electrodes for the transducer. According to the requirements on the designed transducer (expected pressure range, control electronics), electrodes with higher or lower active electrode area should be selected. This is in accordance with our introductory measurements with conductive inks and circular electrodes, where the PD electrode exhibited slightly higher electrical resistance by constant outer dimensions (*Volf et al., 2019*). More discussion about the impact of the electrode shape and dimensions on their resistivity can be found in (*Yang et al., 2021*). It is also important to keep the variable Active Electrode Area P_A constant when designing same sensitive transducers with different resolution (i.e. with bigger or smaller electrodes), as the dimensions of the electrode are not independent.

CONCLUSIONS

Within our research, we evaluated the impact of the dimensions of the electrodes and of the ink layer thickness on the measured electrical resistance. The results will be applicable in the design of the new transducer SITSCAN CS, that converts the applied pressure into electric signal. Furthermore, the results can be used in design of any tactile transducer basing on an ink-based piezorezistive layer. We performed an extensive set of measurements of 162 individual combinations of ink layer thickness – electrode size – ink mixture ratio. The results should simplify the design of tactile pressure transducers in the future, as there will be no need for the time-demanding preparatory measurements and evaluations of the electrodes.

Within the first part of our work, we concentrated on the test sample plates Nr. 3 to Nr. 5, with constant ratio of ink mixture and with 3 different ink thickness layers. The impact of the dimensions of the electrodes on the electrical resistance has been investigated and modelled. Due to the dependency of the individual dimensions of an electrode on each other, a new variable called Active Electrode Area has been introduced. This variable determinates the ratio between the area of the gap and the area of the electrode. Using a regression analysis, the course is better captured using a 6th degree polynomial. With the increasing the Active Electrode Area the electrical resistance decreases up to values below 100 kΩ. This properties of the electrodes have to be taken into account by designing a new tactile transducer, too. The first set of electrodes proved them to be suitable for use in the new developed tactile sensor SITSCAN CS. The main limitation is now the partially limited pressure range, i.e. big uncertainties for low pressure ranges and zero sensitivity for high pressure ranges. The thinnest ink layer can be preliminary excluded for the use in the tactile sensor. We will continue on the measurements with different ink mixtures to obtain the full set of 162 electrode – ink mixture – ink ratio combinations.

ACKNOWLEDGMENT
This study was supported by TECHNOLOGY AGENCY OF THE CZECH REPUBLIC, grant number FW01010217.

REFERENCES

1. Volf, J.; Svatos, J.; Koder, P.; Novak, V.; Papezova, S.; Ryzhenko, V. & Hurtecak, J. (2015). Pressure Distribution Measurement System PLANTOGRAF V12 and its Electrodes Configuration. *Agronomy Research* 13(3), 732–738.
2. Koder, P.; Novak, V.; Ryzhenko, V.; Hruby, D.; Volf, J. & Novak, D. (2018). Plantograf V18 - New construction and properties. *Agronomy Research* 16(Special issue 1), 1085–1094.
3. Volf, J.; Novak, D.; Novak, V. & Papezova, S. (2019). Evaluation of foil transducers and their use in tactile sensors. *Measurement* 136, 573–578.
4. Barman, S. & Guha, S.K. (2006). Analysis of a new combined stretch and pressure sensor for internal nodule palpation. *Sensors and Actuators A-Physical*, 125 (2), 210-216.
5. Giovanelli, D. & Farella, E. (2016). Force Sensing Resistor and Evaluation of Technology for Wearable Body Pressure Sensing. *Journal of Sensors*, Article number 9391850.
6. Dimitriou E. & Michailidis, N. (2021). Printable conductive inks used for the fabrication of electronics: An overview. *Nanotechnology*, 32(50), Article number 502009.
7. Yang, E.-C., Chen, Y.-W., Wu, J.-Y., Chen, R. & Lo, C.-Y. (2021). Enhancing the Detection Sensitivity in Capacitive Tactile Sensors with Optimized Electrode Shapes. *IEEE Sensors Journal*, 21(23), 26294-26303.
8. LOCLITE NCI 7002. Available online: https://www.henkel-adhesives.com/cz/cs/produkt/industrial-inks-and-coatings/loctite_nci_7002ec.html (accessed on 11.4.2022).
9. LOCLITE NCI 7004. Available online: https://www.henkel-adhesives.com/cz/cs/produkt/industrial-inks-and-coatings/loctite_nci_7004hr.html (accessed on 11.4.2022).

Corresponding author:
Ing. Viktor Novák, Department of Electrical Engineering and Automation, Faculty of Engineering, Czech University of Life Sciences Prague, Kamýcká 129, Praha 6, Prague, 16521, Czech Republic, e-mail: novakviktor@tf.czu.cz

THE BRAKE DECELERATION OF THE FORKLIFT TRUCKS AND THE WAREHOUSE SAFETY

Eva OLMROVÁ[1], Martin PEXA[1], Jan PALÁTKA[1]

[1]*Department of Quality and Dependability of Machines, Czech University of Life Sciences Prague, Kamýcká 129, 165 21 Prague, The Czech Republic*

Abstract
The article is comparing the braking deceleration of two front forklifts, a new and a slightly used forklift truck, with technically identical specifications. The focus of the article is on the braking effect of the new and slightly used trucks and the operational safety. The results were compared with the required braking deceleration according to the standards for granting a technical control. Later, the safety aspects in normal warehouse operation were evaluated 32% more control force was applied to the brake pedal on the forklift with the new brakes in comparison with the slightly used forklift, where about 18% less braking deceleration was achieved. Although both forklifts meet the standard norms, the difference in braking effect can create a collision situation. Such instance can be avoided if the forklift is slightly used before its normal operation.

Key words: *brake deceleration; forklift; warehouse safety.*

INTRODUCTION

Large proportion of the handling trucks' final braking deceleration is influenced by the brakes' construction, the types of materials and the condition of the individual structural elements *(Swiderski, et al., 2019)*. Generally, with the change of the brake linings and other friction elements, precaution and anticipation of a lower braking effect is recommended *(Arman, et al., 2018)*. This is rather common, if the brake components on an older forklift wear out and are replaced by new ones *(Liu, et al., 2014).*

In the same way with a new handling truck, as with the road vehicles, it's often automatically expected that everything in the new handling truck functions impeccably. It is strongly recommended not to load the new vehicle with 100% weight at the beginning of its use, but to run it down slightly before *(Tretsiak, 2012)*. But what about the braking effect? Usually, no recommendations and restrictions are given. At the same time, when taking into an example the case of forklift trucks, this is a very important aspect from the warehouse safety operation point of view. Especially when considering, that multi-ton forklifts often operate with loads of similar weight to the forklifts *(Horberry et al., 2004)*. The warehouse spaces are very limited and even though the forklifts move at slower speeds, a contact with the pedestrians could be dangerous *(Lehtonen, et al., 2021)*. Therefore, the magnitude of the braking effect is an important safety parameter.

Safety in the warehouses can be improved by using slightly used forklifts.

The aim of the study is to evaluate the safety of using new forklifts in the warehouse in relations to its braking efficiency values.

MATERIALS AND METHODS

A decelerometer was used to measure braking deceleration on the forklift, which was placed next to the driver in a horizontal position. It was secured against movement with a locking screw. A CT 3010 type decelerometer with production number 16107 was used during the measurement, the current calibration was valid. The pedometer was placed on the brake pedal.

Fig. 1 Tested forklifts

Fig. 2 Pedometr location

The measurements of the forklifts braking deceleration were carried out at the premises of Toyota Material Handling CZ in Rudná u Prahy. The measurements took place in outdoor areas and then in the warehouse of the Toyota MHCZ company. During the experiment, the outside temperature was 29 °C and 24 °C in the warehouse. Both surfaces' tops were dry. In the outdoor conditions, the braking deceleration was measured on an asphalt surface, in the indoor spaces the braking deceleration was measured on a concrete surface. The measurements were carried out only on the front forklifts with a seated operator, where the presence of the decelerometer is permitted. A front four-wheel forklift with a Toyota type 02-8 FDF20 combustion engine was used for the measurements. Each measurement was performed repeatedly, at least five times. Table number 1 lists the parameters of the front carriages, which can be found from the identification labels and which must be on each handling technique. For the clarity of the differences between the forklift trucks used, the cells of the table are divided by the shades of grey colour. The forklift marked in light grey and with the letter N is a completely new forklift that was only used to test the technical condition for the under carried measurements. The data marked in dark grey are the parameters of the used forklift that was already in operation at the Toyota MHCZ rental company. The data marked in white are completely identical.

Tab. 1 Technical parameters of the forklifts

Toyota – front forklift	N	
Model	02 -8FDF20	
Series number	66719	60197
Total weight	3790 kg	
Front tire size	7.00-12/5.00	
Tire pressure	SOLID	
Back tire size	6.00 -9/ 4.00	
Year of manufacture	2018	2015
Working hours	2 mth	3640 mth

The functionality of the braking system is evaluated by using the average deceleration and the maximum force applied to the brake pedal. The applied force on the brake pedal must be checked and must not exceed the prescribed control force on the service brake table below the text. To grant a technical inspection, the braking deceleration value must correspond to the values specified in the methodology for carrying out technical inspections: NV No. 176/2008 sb., ČSN EN ISO 3691-1, and ČSN ISO 6292. The standards are given by the Engineering Testing Institute in Jablonec nad Nisou. Super elastic tires, marked SE, were used. The brands Solodeal Magnum grey colour 7.00-12/5.00 for the rear wheels and Solodeal Magnum grey colour 6.00-9/4.00 for the front wheels. The dimensions were chosen accordingly to the identification plate of the machine.

The distance was calculated from the measured deceleration according to relation number 1

$$s = \frac{1}{2}at \qquad (1)$$

where s is distance[m], a is deceleration [m/s^2], t *is* time [s]

The speed *v* [m/s] was calculated according to the relationship number 2:

$$v = \sqrt{2 \cdot a \cdot s} \quad (2)$$

where *a* is deceleration [m/s^2], *s* is distance [m]

The calculation of the braking force *B* [kN] is given in relation 3

$$B = m \cdot a \quad (3)$$

where, *m* is weight [kg], *a* is deceleration [m/s^2]

Used relationship number 4 to detect braking C_b [%]:

$$C_b = \frac{a}{g} \cdot 100 \text{ [\%]} \quad (4)$$

where *a* is deceleration [m/s^2], *g* is gravitational deceleration [m/s^2],

Braking power P_B is calculated according to the relationship number 5

$$P_B = B \cdot v \quad (5)$$

where *B* is braking force [kN], *v* is speed [m/s],

RESULTS AND DISCUSSION

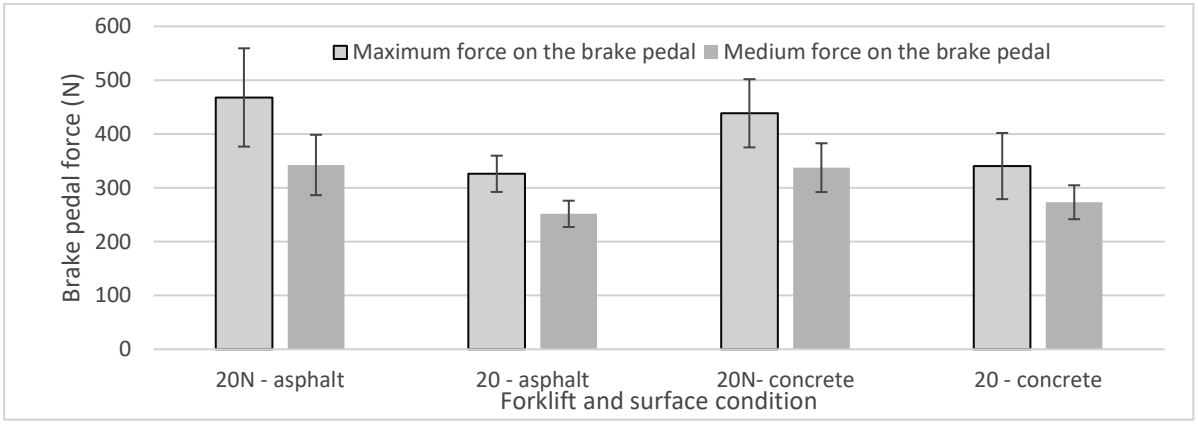

Fig. 1 Brake pedal force applied

Fig. 3 shows the amount of the brake pedal force on asphalt and concrete surfaces for a forklift with new (20N) and used brakes (20). The maximum values that were recorded during the measurements and the average values are listed. From Fig. 3, it is apparent that the truck with the new brakes used approximately 32% more control force on the pedal than the truck with the used brakes. According to ANOVA, the result is significant.

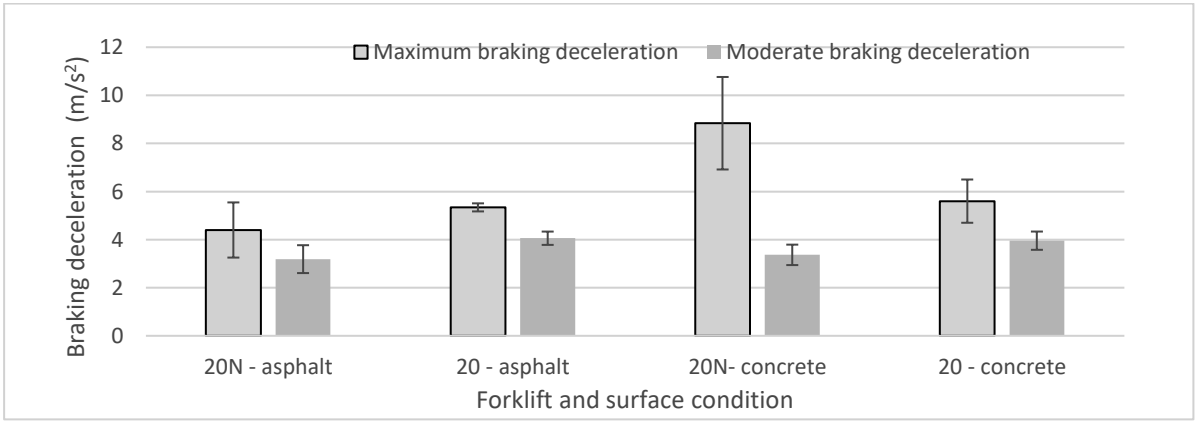

Fig. 2 Braking deceleration on different surfaces

Fig. 4 shows the achieved deceleration on asphalt and concrete surfaces for the forklift with new (20N) and used brakes (20). The maximum values that were recorded during the measurement and the average values are listed. From the Fig. 4 it is clear, that the forklift with new brakes achieved approx. 18% lower braking deceleration than the forklift with the used brakes. According to ANOVA, the result is not significant.

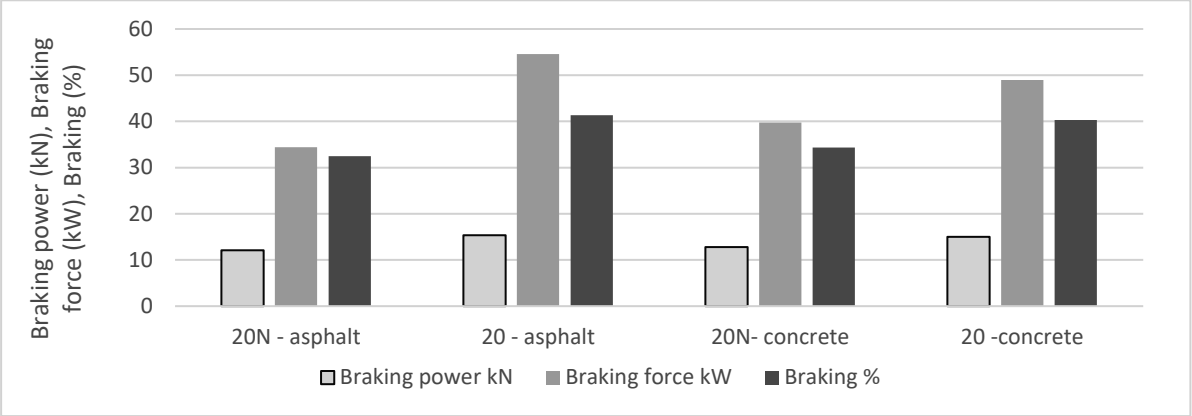

Fig. 3 Comparison of braking force, braking performance and braking

Fig. 5 shows a comparison of the achieved braking power, braking performance and braking on asphalt and concrete surfaces by a forklift with new (20N) and used brakes (20). From the Fig. 5, it is evident, that the forklift with the new brakes achieved approx. 18% lower braking force, approx. 28% lower braking power and approx. 7.5% lower braking than the truck with the used brakes *(Halawa, et al., 2020).* According to ANOVA, the result is significant.

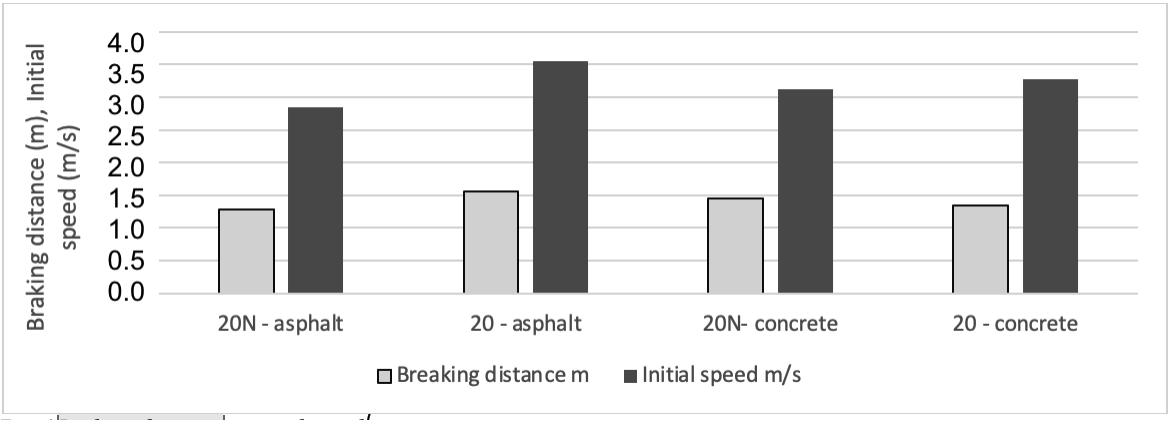

Fig. 4 Braking distance at initial speed

On basis of the collected measurements for medium power deceleration and the time of decelerating, the braking distance and the entry speed were calculated. The values are shown in the Fig. 6. The objective was to achieve a similar entry approach speed; the achieved value was 3.20 ± 0.29 m/s for all recorded measurements. The braking distance values are put into the context of the approach speed with the values of achieved deceleration (*Stein, et al.*, 2018). According to ANOVA, the result is not significant.

a) b)

Fig. 7 The ratio of braking power between the new and used brakes expressed in percentage: a) asphalt, b) concrete

A comparison of the braking force values is shown in Fig. 7 on asphalt and concrete surfaces by a forklift with the new (20N) and the used brakes (20). The values of the braking force are shown on the pie chart proportionally and are presented in the percentage values. It is clear that in both cases, of asphalt and concrete surfaces, a higher braking force (by approx. 10%) is achieved by the forklift with worn brakes, despite the fact that the new forklift achieves approx. 13% higher control force on the brake pedal (Fig. 8).

a) b)

Fig. 8 Brake pedal force ratio between new and used brakes expressed as a percentage: a) asphalt, b) concrete

Braking distance and safety in warehouses also depends on many factors especially on human (*Horberry, et al., 2004*).

CONCLUSIONS

From the point of view of the forklift safety operation with new and used brakes, the following can be stated.

- From the point of the regulations view, it can be stated that the maximum developed force on the brake pedal (max. 600 N) was observed and both front forklifts met the requirements of the standard for handling technology with a maximum nominal load capacity of up to 16,000 kg and a speed in the range of 5 to 13 .4 km/h (1.39 to 3.72 m/s).
- On the forklift with new brakes, approx. 32% more control force was applied to the brake pedal than in the case of the forklift with used brakes, and yet approx. 18% lower braking deceleration was achieved.

The forklift with new brakes also achieved lower braking force (approx. 18%), lower braking power (approx. 28%) and lower braking than the truck with used brakes (approx. 7.5%).

In the case of asphalt and concrete surfaces, a higher braking force (about 10%) is achieved by the forklift with used brakes, even though the new forklift achieved about 13% higher control force on the brake pedal.

In general, it is therefore necessary to consider that during the first few hours of operation, the efficiency of the brakes will be higher with the used brakes than the new brakes. This can have a negative effect,

especially in a situation where a truck driver operating on a slightly used forklift, unexpectedly receives a forklift with the new brakes and is not advised about the situation accordingly. Although the forklift meets the standards, the difference in the braking effect can create a collision situation. The reaction of the driver and his experience is an important factor for safety in the warehouse, as has already been found *(Halawa, et al., 2020)*.
Such instance can be avoided by test-driving loaded truck intentionally before its normal operation. When a forklift is driven, there is a slight wear on the tires, which increases adhesion, whilst a slight wear on the brake lining, increases the braking power.

ACKNOWLEDGMENT
This study was supported by grant from the IGA 2022 (No. 2022:31190/1312/3109) of the Czech University of Life Sciences Prague.

REFERENCES

1. Borucka A., Jacyna-Golda I., Swiderski A.,& Szczepanki E. Wear of brake system components in different operating states of the vehicle in the transport company. exploitation and reliability – Maintenance and reliability (2019); 21 (1): 1–9, http://dx.doi.org/10.17531/ein.2019.1.1.
2. Arman M., Chopra P., Sarkar M. & Singhal S.,2018.A review on material and wear analyses of automotive break Pad-Materials Today: Processing, (2018). 5 (14), https://doi.org/10.1016/j.matpr.2018.10.114
3. Huang, G.J., Liu, Y.M. & Wang, X.H., (2014). Typical Faults Analysis and Treatment Measures for Forklifts. AMM. https://doi.org/10.4028/www.scientific.net/amm.494-495.899
4. Tretsiak D. Experimental investigation of the brake system's efficiency for commercial vehicles equipped with disc brakes. Proceedings of the Institution of Mechanical Engineers, Part D: Journal of Automobile Engineering. (2012);226(6):725-739. Doi:10.1177/0954407011427640
5. Horberry T, Johnston I, Larsson T J, et al. Forklift safety, traffic engineering and intelligent transport systems: A case study[J]. Applied Ergonomics. (2004), 35(6): 575-581. DOI: 10.1016/j.apergo.2004.05.004
6. Lehtonen, Maasalo, I.,E., Perttula, P., et al. Learning game for improving forklift drivers' safety awareness. Cogn Tech Work 23, 743–753 (2021). https://doi.org/10.1007/s10111-020-00648-7
7. H. Dauod, S.H. Chung, F. Halawa, , I. G. Lee, Y. Li, & S. W.Yoon. Introduction of a real time location system to enhance the warehouse safety and operational efficiency, International Journal of Production Economics, Volume 224,(2020), https://doi.org/10.1016/j.ijpe.2019.107541
8. A. Dorofeev, J. Fottner & A. M. v. Stein, "Visual collision warning displays in industrial trucks," (2018) IEEE International Conference on Vehicular Electronics and Safety (ICVES), pp. 1-7, doi: 10.1109/ICVES.2018.8519519

Corresponding author:
Ing. Eva Olmrová, MBA, Department of Quality and Dependability of Machines, Czech University of Life Sciences Prague, Kamýcká 129, 165 21 Prague, The Czech Republic, email: Olmrova@tf.czu.cz

MULTI-CROP BIOMASS UTILIZATION FOR BIOENERGY PURPOSSES AND EVALUATION OF PRESSED BIOFUEL PROPERTIES

Rita PETLICKAITĖ[1], Algirdas JASINSKAS[2], Rolandas DOMEIKA[2], Kęstutis ROMANECKAS[3], Jiri MAŠEK[4]

[1]*Laboratory of Heat Equipment Research and Testing, Lithuanian Energy Institute*
[2]*Department of Agricultural Engineering and Safety, Faculty of Engineering, Agriculture Academy, Vytautas Magnus University*
[3]*Department of Agroecosystems and Soil Sciences, Agronomy Faculty, Agriculture Academy, Vytautas Magnus University*
[4]*Faculty of Engineering, Czech University of Life Sciences Prague*

Abstract
The article focuses on the evaluation of the suitability of multi-crop biomass to produce solid biofuels. For this purpose, three species of plants were investigated and studied: field bean, maize, and fibrous hemp, grown as a binary (3 samples) and trinomial (1 sample) crops. The object of this research was the biomass of three grown and harvested multi-crop plants (a total of 4 different options), which was processed and utilized for pressed biofuel production. At the beginning, the harvested plant biomass was chopped and milled, and later pressed biofuel (cylindrical 6 mm diameter granules) was produced. The granules were produced using a granulator with a horizontal matrix. Determined fractional composition of the flour in all four samples was optimal to produce biofuel pellets: 65-78% of flour particle size was 2.0 mm, 1.0 mm or 0.63 mm. Determined length of the produced granules ranged from 23.4 to 26.4 mm and the diameter was sufficiently stable and varied from 6.1 to 6.2 mm. The density of the granules produced in all investigated samples reached more than 1100 kg m^{-3} (DM). The moisture content of pellets ranged from 4.4% to 8.8%, and ash content ranged from 4.5 to 6.8%. Determined lower calorific value of pellets varied from 16.8 to 17.0 MJ kg^{-1}. Harmful emissions from the combustion of all binary and trinomial crop pellets were sufficiently low and did not exceed the legal allowed values.

Key words: *multi-crop plants; biofuel pellets; physical-mechanical properties; harmful emissions.*

INTRODUCTION

Ensuring energy independence and use of renewable energy sources for biofuels is becoming increasingly important on a daily basis. Scientists have conducted numerous studies to substantiate the suitability of herbaceous plants for solid biofuels. Sustainable produced biofuel can be seen as a renewable energy source and burning them can help combat the negative effects on climate change (*Pierrehumbert, 2022*). However, to date there are no comprehensive studies to support the use of multi-crop biomass for the production of solid biofuels pellets.

The cultivation of multicultural crops is a good practice that meets the requirements of the European Green Course; so it is important to increase knowledge about their suitability for solid biofuels. Studies have shown multi-cropping stabilized gas concentrations and emissions from the soil. The share of microstructures in the upper soil layers was also found to decrease (*Romaneckas et al., 2022*). When several different crops are grown on the same area of land, not only are resources used more efficiently, but higher yields can be obtained (*Wu et al., 2021; Tumuluru et al., 2020*). Co-cultivation of legumes with non-legumes ensures better nitrogen accumulation and facilitates disease and pest control (*Jensen et al., 2020*). Cannabis is worth growing in multi-crops. Fibber hemp is suitable for multi-crop plants growing. It grows large amounts of biomass, is resistant to diseases and pests, and its biomass is suitable for biofuels, among other uses (*Ahmed et al., 2022*). *Li et al., (2021)* experiment showed that growing maize together with field beans produced more biomass compared to monoculture. Maize also has a high yield. In 2017, they were cultivated on 7.246 million hectares worldwide (*Supasri et al., 2020*).

The use of biomass to produce densified solid biofuels is projected to increase by 56% in 2040 compared to 2010 (*Bajwa, et al., 2018*). The production of pellets from plant biomass ensures their higher density and better energy properties (*Artemio, et al., 2018*). Granulation of biomass ensures uniform shape, size, easy transport, storage and use (*Mock, et al., 2021*). Due to the great diversity of biomass feedstocks,

granular biofuels are produced in very different qualities (*Cui, et al., 2021a*). Research by *Cui et al., (2021b)* shows that the quality of pellet fuel can be improved by pelletizing different biomass feedstocks. The aim of this study is to evaluate the suitability of multi-crop (binary and ternary) biomass for the production of solid biofuel pellets.

MATERIALS AND METHODS

Plants grown in the test fields of Experimental station of Vytautas Magnus University Agriculture Academy as binary and ternary crops were used for the research. Plants grown in four different fields were studied:

- field 1 – maize and hemp (binary crop, abbreviated below – Sample 1);
- field 2 – hemp and field beans (binary crop, Sample 2);
- field 3 – maize and field beans (binary crop, Sample 3);
- field 4 – maize, hemp and field beans (trinomial crop, Sample 4).

Samples were taken from each field and the plants were naturally dried to 12% moisture. The plants were then crushed and ground. Pellets were made from the obtained flour and their main properties were studied.

The grinding quality is determined using a Retsch AS 200 sieve shaker (Germany). Sieves with holes of different 0.1, 0.25, 0.5, 0.63, 1.0 and 2.0 mm holes in diameter were used.

A low power granulator (200–300 kg h^{-1}) with horizontal matrix with 6 mm holes (Poland) was used for production of pellets.

The main parameters of the pellets were determined according to the standards:

- moisture content – according to the standard LST EN 14774-1: 2010;
- ash content – according to the standard LST EN 14775: 2010;
- lower calorific value – according to the standard LST EN 14918: 2010.

The pellets were burned in a 5 Kw furnace, and harmful emissions were found.

Arithmetic means of the measurement data and their confidence intervals were calculated at the 95% confidence level.

RESULTS AND DISCUSSION

An important parameter for the production of biomass pellets is the fractional composition of the flour. The results of the research show that the largest flour fractional composition was obtained in the ground biomass of Sample 2 and Sample 1. 67%, and 42% of the flour accumulated on the 2 mm sieve, respectively (Fig. 1).

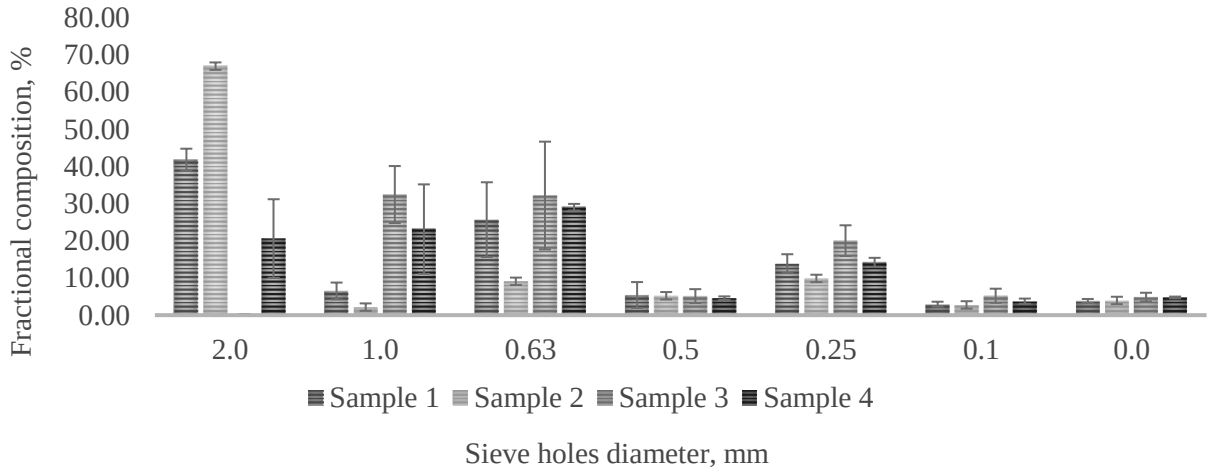

Fig. 1 The mill fraction of multi-crop biomass

In all samples, 65-78% of the flour was distributed on a 2.0 mm, 1.0 mm, or 0.63 mm sieve. It can be stated that the fractional composition of the obtained flour is optimal to produce pellets.

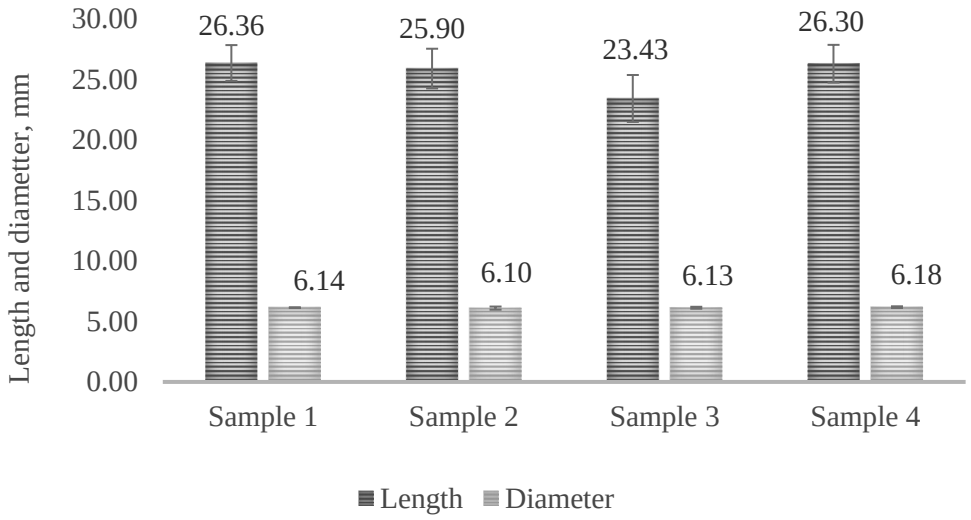

Fig. 2 Biometric properties of multi-crop pellets

The length of the pellets produced in all samples ranged from 23.4 to 26.4 mm and the diameter from 6.1 to 6.2 mm (Fig. 2). The length and diameter of the pellets comply with the standards of ISO17225-6 for solid non-wood biofuels.

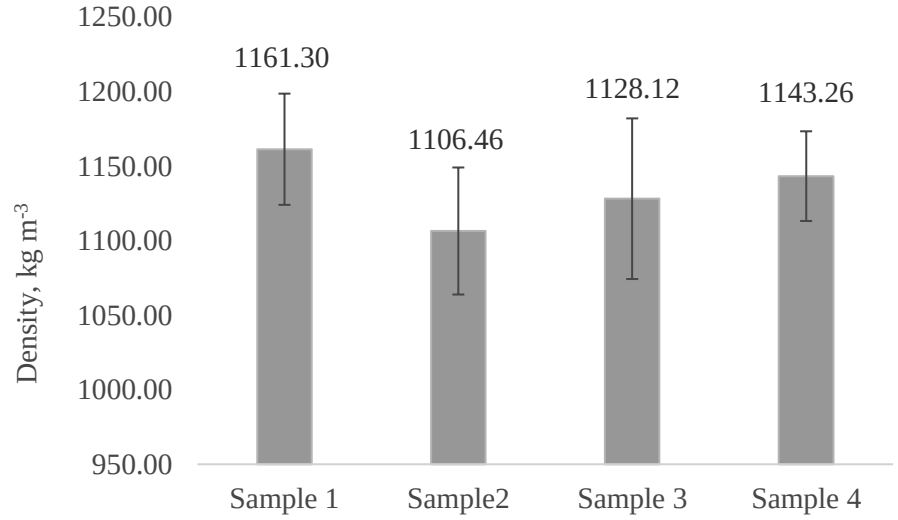

Fig. 3 The density of pellets

The density of the granules produced in all the samples was very similar and amounted to 1100 kg m^{-3} dry mass (Fig. 3). The highest density was of Sample 1 pellets – 1161 kg m^{-3} dry mass. According to this parameter, the granules of these samples meet the requirements of the ISO17225-6 standard for class A pellets (≥ 600 kg m^{-3}).
The elemental composition of the granules was also determined. The three main elements, C, O and H, were found to predominate, accounting for 92.5% to 94.9%.

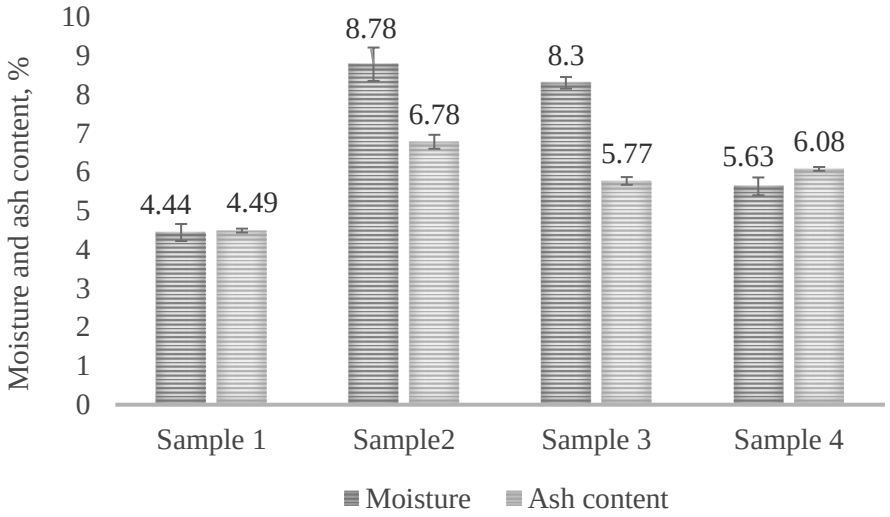

Fig. 4 Pellets moisture and ash content

One of the most important parameters affecting the quality of granulation is the moisture content (*Cui, et al., 2021b*). The other important parameter that defines the quality characteristics of biofuel pellets is ash content. The lowest was the moisture content of Sample 1 granules – 4.4%, and the highest – the moisture content of Sample 2 granules – 8.8% (Fig. 4). (According to the standard, the permissible moisture content of the pellets is ≤ 12% for Class A pellets and ≤ 15% for Class B pellets). The ash content of all 4 samples of pellets ranged from 4.5 to 6.8% and also did not exceed the requirements of the standard (≤ 6% for Class A pellets and ≤ 10% for Class B pellets).

A lower calorific value of produced pellets was also determined. The lower calorific value of all the samples was very similar, and it was about 17 MJ kg^{-1}. The highest calorific value was Sample 3 pellets - 17.02 MJ kg^{-1}, and the lowest – Sample 2 pellets, 16.80 MJ kg^{-1}.

For comparison, *Suleiman et al., (2019)* found that moisture content of corn cob pellets was 3.05%, and ash content was 2.7%. For corn stalk pellets, these parameters were 3.75 and 0.7% respectively.

For comparison according to *Carrillo & Parra et al., (2021)* research data the moisture content of the pellets made from perennial grass, patula pine sawdust and apple firewood was 5.84, 5.62 and 5.58% respectively, and ash content was 9.71, 0.47 and 2.12% respectively.

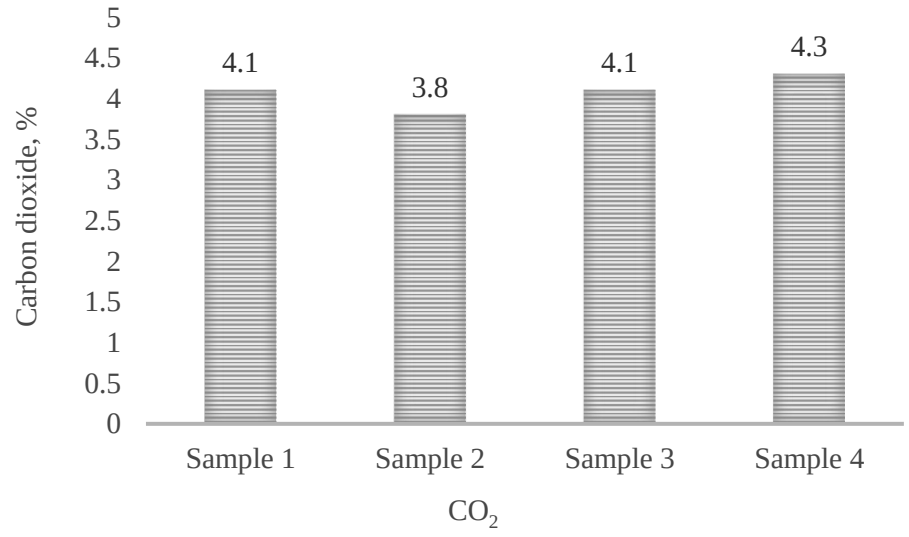

Fig. 5 CO_2 emissions by burning pellets

The quality of a fuel is also determined by the emissions that result from burning fuel. When burning pellets of multi-crop plants, the highest CO_2 concentrations were found when burning Sample 3 pellets – 4.3%, and the lowest – burning Sample 2 pellets – 3.8% (Fig. 5). For comparison, *Jasinskas et al., (2020)* found that CO2 emissions from burning biofuel pellets produced from faba bean waste ranged from 4.1 to 5.0%.

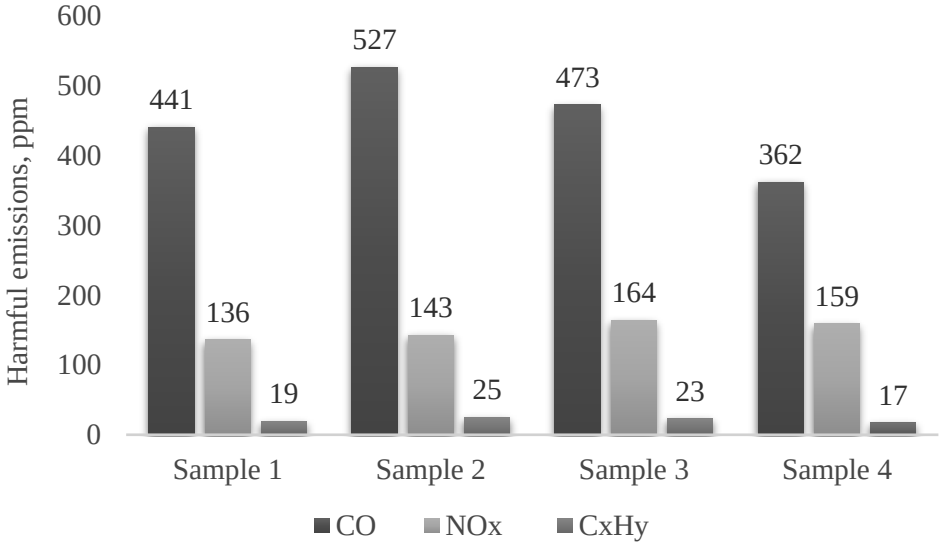

Fig. 6 CO, NO_x and C_xH_y emissions

The highest concentrations of CO and C_xH_y were in the combustion of Sample 4 pellets (527 and 25 ppm, respectively), and the highest concentrations in the incineration of Sample 2 pellets (362 and 17 ppm, respectively). Meanwhile, the lowest NO_x emissions were recorded by burning Sample 1 pellets (136 ppm), and the highest – by burning Sample 3 pellets (164 ppm) (Fig. 6). For comparison, the aforementioned study by *Jasinskas et al., (2020)* showed that burning pellets made from faba bean waste resulted in significantly higher CO emissions and ranged from 1072 to 2785 ppm. The nitrogen oxide emissions was very similar – 133-266 ppm.
The results of the pellet burning and emission studies presented in this article show that harmful emissions do not exceed the legal emission limit values for combustion of biomass pellets in low-power boilers.

CONCLUSIONS

The length of the pellets produced from 4 different biomass blends was 23.4-26.4 mm, and the diameter was 6.1-6.2 mm. The maximum moisture content of the granules did not exceed 8.8%, and the ash content did not exceed 6.8%. Lower calorific values from all four samples were higher than 16.8 MJ kg^{-1}. Biomass pellets made from binary and trinomial crops (maize, hemp and beans) meet the quality requirements for solid biofuels set out in the standard ISO17225-6. Burning of all 4 types of pellets has resulted in harmful emissions that do not exceed the legal limit values. Biomass pellets made from multi-crop plants (maize, beans and hemp grown for fiber) can be used as pressed solid biofuels of high quality.

REFERENCES

1. Ahmed, F., Islam Z., Mahmud, S., Sarker, E. & Islam, R. (2022). Hemp as a potential raw material toward a sustainable world: A review. Heliyon, 8, 1-15.
2. Artemio, C., P., Maginot, N.H. Serafín, C.U., Rahim, F.P, Guadalupe, R.Q.J., & Fermín C.M. (2018). Physical, mechanical and energy characterization of wood pellets obtained from three common tropical species, PeerJ, 1-16.
3. Bajwa, D.S., Peterson, T., Sharma, N., Shojaeiarani, J. & Bajwa, S.G. (2018). A review of densified solid biomass for energy

production. Renewable and Sustainable Energy Reviews, 96, 296–305.
4. Carrillo-Parra, A., Rutiaga-Quiñones, J.G., Ríos-Saucedo,·J.C., Ruiz-García, V.M., Ngangyo-Heya, M., Nava-Berumen, C.A., Núñez-Retana, V. D. (2021). Quality of Pellet Made from Agricultural and Forestry Waste in Mexico, BioEnergy Research, 15, 977–986.
5. Cui, X., Yang, J. & Wang, Z. (2021a). A multi-parameter optimization of the bio-pellet manufacturing process: Effect of different parameters and different feedstocks on pellet characteristics. Biomass and Bioenergy, 155, 106299.
6. Cui, X., Yang, J., Wang, Z. & Shi, X. (2021b). Better use of bioenergy: A critical review of co-pelletizing for biofuel manufacturing. Carbon Capture Science & Technology, 1, 100005.
7. INTERNATIONAL STANDARD ISO 17225-6 Solid biofuels — Fuel specifications and classes —Part 6: Graded non-woody pellets.
8. Jasinskas, A., Minajeva, A., Šarauskis, E., Romaneckas, K., Kimbirauskienė R., & Pedišius, N. (2020) Recycling and utilisation of faba bean harvesting and threshing waste for bioenergy. Renewable Energy, 162, 257-266.
9. Jensen, E.S., Carlsson, G. & Hauggaard-Nielsen, H. (2020). Intercropping of grain legumes and cereals improves the use of soil N resources and reduces the requirement for synthetic fertilizer N: A global-scale analysis. Agronomy for Sustainable Development, 40, 5.
10. Li, B., Liu, J., Shi, X., Han, X., Chen, X., Wei, Y. & Xiong, F. (2021). Effects of belowground interactions on crop yields and nutrient uptake in maize-faba bean relay intercropping systems. Archives of Agronomy and Soil Science, 1-13.
11. Mock, Ch., Park, H., Ryu, Ch., Manovic, V. & Choi, S.Ch. (2020). Particle temperature and flue gas emission of a burning single pellet in air and oxy-fuel combustion. Combustion and Flame, 156–171.
12. Pierrehumbert, R. (2022). Plant power: Burning biomass instead of coal can help fight climate change—but only if done right. Bulletin of The Atomic Scientists, 78, 3, 125–127.
13. Romaneckas, K., Balandaitė, J., Sinkevičienė, A., Kimbirauskienė, R., Jasinskas, A., Ginelevičius, U., Romaneckas, A. & Petlickaitė, R. (2022). Short-Term Impact of Multi-Cropping on Some Soil Physical Properties and Respiration. Agronomy, 12, 141.
14. Sulaiman, M.A., Adetifa, B.O., Adekomaya, S.O, Lawal, S.N. & Adama, O.O. (2019) Experimental Characterization of Maize Cob and Stalk Based Pellets for Energy Use. Engineering Journal, 23, 6.
15. Supasri, T., Itsubo, N., Gheewala, S.H. & Sampattagul, S. (2020). Life Cycle Assessment of Maize Cultivation and Biomass Utilization in Northern Thailand. Scientific Reports, 10:3516.
16. Tumuluru, J.S., & Fillerup, E. (2020). Briquetting Characteristics of Woody and Herbaceous Biomass Blends: Impact on Physical Properties, Chemical Composition, and Calorific Value. Biofuels Bioproducts and Biorefining, 14:1105–1124.
17. Wu, Y., He, D., Wang, E., Liu, X., Huth, N.I., Zhao, Z., Gong, W., Yang, F., Wang, X., Yong, T., Liu, J., Liu, W., Du, J., Pu, T., Liu, Ch., Yu, L., Wopke, W. & Yang, W. (2021). Modelling soybean and maize growth and grain yield in strip intercropping systems with different row configurations. Field Crops Research, 265, 108122.

Corresponding author:
Rita Petlickaitė, Laboratory of Heat Equipment Research and Testing, Lithuanian Energy Institute, Breslaujos Str. 3, LT-44403 Kaunas, Lithuania, phone: +370 685 286 46, e–mail: rita.petlickaite@lei.lt

DESIGN OF SERVICE UNIFYING INFRASTRUCTURE FOR CHARGING OF ELECTRIC VEHICLES

Štěpán PÍCHA[1], Martin KOTEK[1], Veronika HARTOVÁ[1], Veronika ŠTEKEROVÁ[1], Tomáš PÍCHA[2,3]

[1]Department of Vehicles and Ground Transport, Faculty of Engineering, Czech University of Life Sciences Prague, Kamýcká 129, Praha 6, Prague 16521, Prague, Czech Republic
[2]Department of Electrical Engineering and Automation, Faculty of Engineering, Czech University of Life Sciences Prague, Kamýcká 129, Praha 6, Prague 16521, Prague, Czech Republic
[3]Department of Agricultural Machines, Faculty of Engineering, Czech University of Life Sciences Prague, Kamýcká 129, Praha 6, Prague 16521, Prague, Czech Republic

Abstract
The article focuses on the future growth of electric vehicles on our roads. As the number of electric vehicles gradually increases, it is necessary to ensure sufficient charging infrastructure. The topic elaborates the design of a service unifying the charging infrastructure for electric vehicles in individual passenger transport, develops the design of the service embedded in a real environment and describes its functioning. The charging infrastructure needs in the capital city of Prague were identified.

Key words: *electromobility, charging station, digital services.*

INTRODUCTION

More than half of the world's population lives in cities. They are, and have historically been, the sites of significant cultural, political and technological change. Cities are at the heart of the world's economy, accounting for more than 80% of total gross domestic product. By 2030, up to one billion more people are expected to live in cities (*Bouton et al., 2017*). This growth will place increased demands on the provision of logistics in cities. The transport of goods and food-in will place greater demands on the efficiency of freight transport. Further development of public transport will be important for passenger transport. Equally important will be individual passenger transport. Leaving aside walking as the most widespread mode of individual transport, the most widespread mode of transport today is the car. The trend today is to use other modes of individual transport. It is not only in countries like the Netherlands that people are starting to use bicycles more for transport (*Walking and cycling as transport modes, 2020*). The use of bicycles, both private and shared, is on the rise. Other means of micro-mobility, such as electric scooters or electric scooters, especially in the form of shared facilities, are also growing in popularity (*Heineke et al., 2019*). Passenger cars are also moving from internal combustion engines to hybrid and pure electric drives. Currently, the share of electric passenger cars in the total fleet in the European Union is around 2%. By 2030, the share of electric passenger cars in the total fleet is projected to increase to 23%. Western countries such as Germany, the Netherlands and France will be the main contributors to this increase. In other countries, the increase in the number of EVs will not be as steep and fleet renewal will be slower (*Niestadt a Bjørnåvold 2019*). The aim of this study is to design charging infrastructure for electric vehicles.

MATERIALS AND METHODS

Service design to unify the infrastructure

In order to meet the demand for charging, additional charging stations will need to be built in the future. This study develops a proposal for the operation of a mobility centre service and station that will provide a unified experience for EV owners, car share users and public transport passengers. The biggest benefit for users from all groups is the possibility to find all the services they need in one place and to choose the most appropriate mode of transport for the moment.

Design of the charging station - Mobility hub distribution

The basic criterion for the location of mobility nodes is the demand for charging infrastructure or the demand for modal shift. Other criteria for station location are technical requirements for construction. If the charging stations are for electric and hybrid vehicles, the location of the stations will be most

appropriate near or within existing parking lots. Suitable P+R car parks are those located on the outskirts of the city with good public transport accessibility. Vehicles usually spend several hours in these types of car parks, so that a large number of fast charging stations are not needed for charging. The opposite situation occurs in car parks located close to the city centre. Due to higher parking prices and lower capacity, people leave their vehicles in these types of car parks for shorter periods of time, so the need for fast charging stations will be higher. For charging micro-mobility vehicles, a location is defined by the number of people moving around the location and transferring to another means of transport. Within the periphery, the demand for micromobility is different than in the city centre.
According to the different demands, the stations were divided into the following types: central, urban, peripheral, suburban (Table 1).

Tab. 1 Types of stations

Central	vehicle charging, shared micro-mobility facilities, transfer to public transport, additional services
Urban	shared micro-mobility facilities, transfer to public transport, limited vehicle charging
Peripheral	vehicle charging, transfer to public transport, P+R parking, limited shared micromobility facilities
Suburban	vehicle charging, transfer to public transport, P+R parking

The Figure 1 shows the possible location of stations within Prague and the distribution by type.

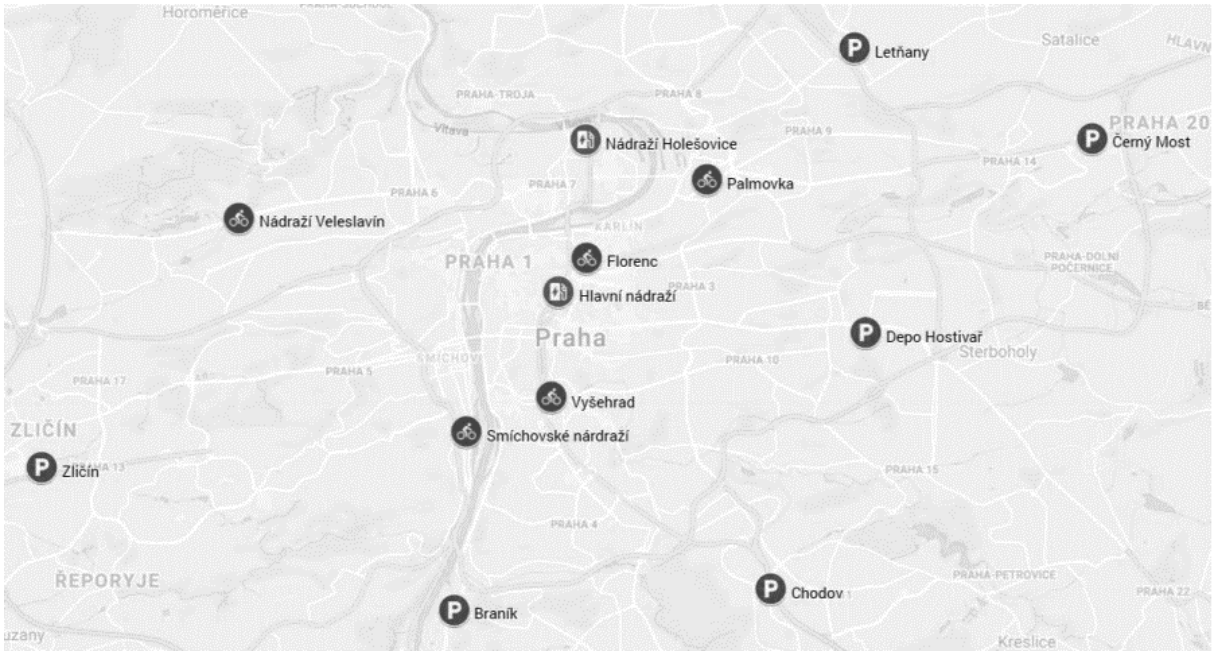

Fig. 1 Map of station locations in Prague

A central type of station, located for example at the Main Railway Station or Nádraží Holešovice. Location with high turnover of people, central location in the city and good accessibility by car. The development of the station is possible due to good electrical infrastructure (proximity to the station) and sufficient number of parking spaces for cars. Suitable for building a large number of DC fast charging stations and standard AC charging stations. Central location advantageous for the use of micro-mobility. Possibility to transfer to public transport.

Urban-type stations (Florenc, Palmovka, Vyšehrad, Smíchovské nádraží, Nádraží Veleslavín) are characterised by a high turnover of people transferring between means of transport. Suitable prerequisite for

micromobility and other shared services. Due to the lack of parking space for a large number of vehicles, only a few fast charging stations should be built.

Peripheral type stations (Letňany, Černý Most, Depo Hostivař, Chodov, Braník, Zličín) located within P+R car parks. The car parks are directly connected to public transport, in most cases to the metro. Due to the distance from the city centre, it is not entirely advantageous to build for micro-mobiles or only for electric scooters, which are able to travel at lower speeds.

The suburban type of station (Neratovice, Brandýs nad Labem, Říčany, Beroun, Kladno), which is located in the cities adjacent to Prague. It is most often located near the train station, where people park their cars and change to public transport. AC charging stations are suitable in this solution. If there is a shared transport system in the city, it is advisable to have a station directly at the station.

RESULTS AND DISCUSSION

Nowadays, each type of vehicle has its own specifics, different uses and different vehicle care needs. Therefore, for an inexperienced user, it is not entirely straightforward how to charge or use a given type of vehicle. Hence the myths surrounding electric vehicles and the emergence of die-hard fans or opponents of electric vehicles. In future, it would be very useful to establish standards that would ensure carefree operation for users and operators of these vehicles.
The biggest obstacle to the development of charging infrastructure is the financing of its construction. This is also the case for the proposed mobility hubs. The purchase costs of individual hardware elements of the stations are in the hundreds of thousands of crowns. The cost of one 50 kW DC station is approximately CZK 500 000, while the previously proposed mobility hub at the Main Station would accommodate ten such stations. AC charging stations are cheaper, but the cost is still around CZK 100 000 per station. Other necessary equipment and building modifications, such as bringing in sufficient power, battery stations, transformers, solar panels, software or identification and communication equipment, are also expensive. Building a single mobility center can cost tens to hundreds of millions of crowns (*Nelder a Rogers, 2019*).
In terms of charging station requirements, it is advisable to locate them close to or preferably directly in larger P+R parking areas. Here, vehicles are usually parked all day and can therefore be recharged throughout this time. The second type is vehicles that arrive directly in the city center, where they usually do not spend long hours but only minutes. According to this logic, it is possible to use different types of chargers with different values of charging currents and thus different time required to charge the vehicles, as described by (*Bräunl et al., 2020*). In this comparison, it is necessary to include the possibilities and methods of charging public transport vehicles, which are directly linked to the individual transport segment. Whether by car, bicycle or other modes. Buses often have to be operated for hours a day and therefore different ways of charging them arise. Such as, recharging at certain stops or changing individual batteries, which on average takes 8-10 minutes (*Li, 2016*).

For specific use, the city was divided into 4 areas. Namely, centre, urban area, periphery and extra-urban area (Table 1). In the centre, it is advisable to build a large number of fast-charging DC stations, as well as standard AC stations with less power. Here the use of micro-mobility and a large possibility of transfer to public transport is appropriate. A similar mode of transport is in the urban type, where there is a greater possibility of using shared transport services. In the peripheral type of transport there is a high concentration of vehicles that remain parked in so-called P+R car parks, where each car park is connected to the public transport network. Here there is a need for charging stations, but it is possible to use slower AC types. The last type is suburban, where people travel mostly for work and the commuting distance is greater. These problems are addressed in the study (*Sheppard et al., 2016*), where they are tackling the issue of electric vehicles in Delhi. Delhi, which has a population of just under 19 million, is considering setting up 2,764 charging stations for the expected number of hybrid and electric vehicles in operation. The infrastructure of charging stations in such a large city is complex, not just in terms of installation but in terms of its quality of deployment. India projects that over 6 million electric vehicles should be on its roads in the coming years.

CONCLUSIONS

The size and technical level of the charging infrastructure depends on the number of electric vehicles. In general, charging infrastructure should be as user-friendly and accessible as possible. However, the design of the infrastructure may be quite different if the actual number of vehicles differs significantly from the values assumed in this document and exceeds the number of PHEVs. In addition, regulations that would, for example, prohibit vehicles from entering city centers may also have an impact.
The solutions for a large-scale EV charging system are divided into 4 types. These are the center, the urban area, the periphery and the non-urban area. In relation to the charging points, it is necessary to solve the problem of the continuity of individual transport and public transport. This issue is strongly linked to the high input costs and electricity connection.

ACKNOWLEDGMENT

This study was supported by Department of Vehicles and Ground transport at Czech University of Life Sciences, Faculty of Engineering. IGA 2021:31150/1312/3111 „Analýza pozornosti řidiče za různých světelných podmínek pomocí systému pro sledování oční aktivity“

REFERENCES

1. Bouton, S., Hannon, E., Haydamous, L., Heid, B., Knupfer, S., Naucler, T., Neuhaus, F., Nijssen, J., Ramanathan, S. (2017). An integrated perspective on the future of mobility, part 2: Transforming urban deliverynt. : 48. www.mckinsey.com/client_service/
2. Bräunl, T., Harries, D., Mchenry, M,. Wager, G. (2020). Determining the optimal electric vehicle DC-charging infrastructure for Western Australia. https://doi.org/10.1016/j.trd.2020.102250
3. Heineke, K., Kloss, B., Scurtu, D., Weig, F. (2019). Micromobility’s 15,000-mile checkup. https://www.mckinsey.com/industries/automotive-and-assembly/our-insights/micromobilitys-15000-mile-checkup
4. Li, Y. (2016). Infrastructure to facilitate usage of electric vehicles and its impact. *Transportation Research Procedia* 14: 2537–43.
5. Nelder, Ch., Rogers, E. (2019). Reducing EV Charging Infrastructure Costs - RMI. https://rmi.org/insight/reducing-ev-charging-infrastructure-costs/
6. Niestadt, M., Bjørnåvold, A.(2019). BRIEFING EPRS | European Parliamentary Research Service.
7. Sheppard, C., Gopal, A., Harris, A., Jacobson, A. (2016). Cost-effective electric vehicle charging infrastructure siting for Delhi. *Environmental Research Letters* 11(6): 064010. https://iopscience.iop.org/article/10.1088/1748-9326/11/6/064010.
8. European Commission, (2020), Walking and cycling as transport modes. https://road-safety.transport.ec.europa.eu/eu-road-safety-policy/priorities/safe-road-use/cyclists/walking-and-cycling-transport-modes_en.

Corresponding author:
Ing. Štěpán Pícha, Department of Vehicles and Ground Transport, Faculty of Engineering, Czech University of Life Sciences Prague, Kamýcká 129, Praha 6, Prague, 16521, Czech Republic, e-mail: pichas@tf.czu.cz

THE IMPORTANCE OF THE INFORMATION PROVIDED BY THE VEHICLE FROM THE DRIVER'S POINT OF VIEW

Jakub POVÝŠIL[1], Sudeep Sangamesh BABU[1], Michal HRUŠKA[1], Stanislav JELEN[1], Petr VACULÍK[1], Petr BENDA[2], Anna Maria ZIFIA[3]

[1]Czech University of Life Sciences, Faculty of Engineering, Department of Technological Equipment of Building, Kamýcká 129, 165 21 Prague 6, Czech Republic
[2]Czech University of Life Sciences, Faculty of Economics and Management, Department of Information Technologies, Kamýcká 129, 165 21 Prague 6, Czech Republic
[3]Tilburg University, Department of Psychology, Warandelaan 2, 5037 AB Tilburg, Netherlands

Abstract
The article is aimed at evaluating the subjective opinions of drivers on the information provided to them by the vehicle through the communication interface. A quantitative methodology using an online questionnaire was chosen to obtain data. For this research, only the information provided to the driver by the vehicle systems was used that can be described as unnecessary and that is not essential for the operation of the vehicle or traffic safety. The aim is to find out whether drivers are willing and can do without some information when driving vehicles. The results of this study could provide an expert opinion for manufacturers, who could achieve a reduction in the driver's information burden by appropriate modification of dashboards. This could in the long term, contribute to reducing driver physical and mental fatigue and as a result increase traffic safety.

Key words: *cockpit; dashboard; displays; driver; vehicle; ergonomics.*

INTRODUCTION

The automotive industry has undergone significant changes in the exterior and interior areas since its inception. Engines have become more efficient and reliable, cockpit structures are more stable, and additional features have been added to the vehicle to ensure driver safety. At the same time speed; power of vehicle engines and the density of traffic have increased significantly (*Regan et al., 2017*). In the last decade, more emphasis has been placed on the comfort and safety of drivers. Audio-visual technologies, newly used in vehicles provide the driver with a wide range of information, which on the other hand, represents an ever-increasing cognitive load to which the driver is exposed (*Häne et al., 2017*).

Just as the number of information inputs and outputs in the process of driving a passenger vehicle continues to increase, the demands on the drivers' cognitive functions logically also increases (*Hruška, 2016*). Along with the increasing psychological demands on the driver, the influence of the human factor in accidents caused by the inability to control the car, misinterpretation of the provided information or overloading of the driver's cognitive functions is becoming increasingly common (*Edwards et al., 2011*). Today, these situations increasingly lead to considerations of replacing the human factor with completely autonomous driving of vehicles. However, this technology still has a long way to go and therefore it is necessary to choose other solutions (*Huhtamo, 2020*). One such solution could be the creation of a minimalist cockpit, through which the driver would receive only the necessary information, thereby significantly reducing the cognitive load on drivers while driving.

The aim of this article is to find out the meaning of individual information available in the cockpit of a passenger car from the driver's subjective point of view, and further to find out which of the selected information provided by the vehicle could be omitted in the process of controlling the vehicle. Another goal is to confirm or refute the existence of statistically significant dependencies, how drivers of diverse groups divided by gender, age or experience approach this issue. In the case of this study, the research hypothesis is defined in such a way that it can be assumed that some of the commonly found information in passenger vehicles will be considered unnecessary from the point of view of the respondents.

MATERIALS AND METHODS

A quantitative research strategy using a questionnaire was chosen to obtain data for this study. Two entry conditions were set for the research, firstly that the volunteer must be over 18 years old and secondly to have a group B driver's license. A total of 386 respondents filled out the entire questionnaire. The questionnaire contained a total of 33 questions, which were divided into two basic sets. The created questionnaire was available online and the questions in the questionnaire were supplemented with a description or a picture so that each respondent knew exactly what the question was about. Due to the planned scope of this work, only ten significant questions were selected regarding the information commonly found in most of today's passenger vehicles.

In the first part of the questionnaire, socio-demographic information was obtained about the respondents such as age, gender, as well as information on kilometers driven, type of car they currently drive and in which large cities they drive most often. For the purposes of this study, the selection was again narrowed down to three basic data, namely age, gender and the number of kilometers driven, which represented the respondent's driving experience.

The second part of the questionnaire was focused on the several types of information that the vehicle provides to the driver. The participants were asked to rate the importance and necessity of the audio-visual information based on their opinion and experience.

RESULTS AND DISCUSSION

A homogeneous group of 386 participants from the Czech Republic took part in the survey. Selected basic socio-demographic parameters were, as independent input data, collected from the participants for further statistical analysis. A total of 194 men and 192 women successfully completed the questionnaire. The participants primarily consisted of university and secondary school students and their employees together with a small group of anonymous people who were interested in the survey. In addition to gender and age, parameters related to personal driving experience and the total number of kilometers driven are shown in Tab. 1.

The statistical software platform SPSS was used for the analysis of the obtained data, which is used to extract information. Thanks to the advanced procedures and feature set, it was possible to ensure high accuracy. The data from the questionnaire survey were exported to the SPSS program, where descriptive statistics were subsequently performed, from which it was possible to secure socio-demographic or other data about the respondents. Subsequently, Chi-square was chosen for the treatment of variable relationships due to the nature of nominal and ordinal data. The data was further processed in the MS Excel program.

Tab. 1 Primary information on the participants concerning the measurements

Gender		Age			Number of km driven		
Man	Woman	18-30	31-50	51+	0-50.000 km	50.000-200.000 km	200.000 km+
194	192	240	104	42	144	138	104

The questionnaire was divided into 2 main categories. The first category consisted of questions related to socio-demographic data while in the second, participants answered specific questions that related to the information that a modern passenger vehicle provides to the driver. A total of 7 questions (marked as A – G) were used for the purposes of this work, the exact wording and percentage results are shown in Tab. 2. All the questions below were about the commonly found audio-visual information in many passenger vehicles. The participant also had the option to indicate as an answer that he had no experience with the given technology, in which case this participant was not used for statistical evaluation.

Tab. 2 Questions used for clinical data collection

#	Questions	Answers	
		I can do without it	I cannot live without it
A	Is it important for you to have the rev. indicator displayed?	272 (70.5%)	114 (29.5%)
B	Is it important for you to have the continuous coolant temperature displayed?	194 (50.3%)	192 (49.7%)
C	Is it important for you to have information displayed in your car about the total kilometres driven, on the given day, etc.?	284 (73.6%)	102 (26.4%)
D	Is it important for you to have the currently engaged gear visible?	356 (92.2%)	30 (7.8%)
E	Is it important for you to be warned about speeding if you have active driving assistants?	314 (81.3%)	72 (18.4%)
F	Is it important for you to be warned about exceeding the recommended driving time?	348 (90.2%)	38 (9.8 %)
G	Is it important for you to be alerted to a low fuel level?	74 (19.2%)	312 (80.8%)

Data collection and statistical processing were achieved with high quality, most of the data were verified as valid and the results can be used for further research or development of production solutions. Thanks to the participation of mostly technically educated experts in the field of automotive, the results can be given immense importance. Furthermore, the adjusted residuals method was used for further refinement and better interpretation of the found dependencies. The results with statistical parameters and with an evaluation of whether there was a statistical dependence on specific input data are shown in Tab. 3. Based on the results presented in Tab. 3, there are several significant statistical dependences between the questions from the questionnaire and the data collected in Tab. 1 and Tab. 2.

Tab. 3 Dependency of questions from the questionnaire (questions A to G from Tab. 2) on driver parameters as specified in Tab. 1 evaluated using Pearson's chi-squared test

#		Gender	Age	Number of km driven
	Critical value	3.841	5.991	5.991
A	χ^2	0.024	4.083	1.126
	P-value	0.875	0.130	0.569
	Cramer V	0.008	0.103	0.054
	Dependence	None	None	None
B	χ^2	3.43	1.300	19.364
	P-value	0.053	0.522	0.0000623
	Cramer V	0.098	0.058	0.223
	Dependence	None	None	Confirmed
C	χ^2	6.143	1.295	14.692
	P-value	0.013	0.523	0.00064
	Cramer V	0.126	0.058	0.195
	Dependence	Confirmed	None	Confirmed
D	χ^2	0.167	3.093	7.305
	P-value	0.681	0.213	0.025
	Cramer V	0.020	0.090	0.137
	Dependence	None	None	Confirmed
E	χ^2	0.326	6.713	9.100
	P-value	0.567	0.035	0.010
	Cramer V	0.020	0.132	0.153
	Dependence	None	Confirmed	Confirmed
F	χ^2	0.094	1.064	3.539
	P-value	0.758	0.587	0.170
	Cramer V	0.015	0.052	0.095
	Dependence	None	None	None

G	χ^2	0.527	4.551	11.189
	P-value	0.467	0.103	0.003
	Cramer V	0.036	0.109	0.170
	Dependence	None	None	Confirmed

The results obtained during the measurements were statistically processed and evaluated using Pivot tables and Pearson's chi-squared test at a significance level of 0.05.

In general, it is very remarkable how large a percentage of people do not want to let the car talk into their own decisions. People do not want the car to check how tired they are, what speed they are driving and, paradoxically, they are not even interested in, for example, a warning about potential ice on the road. They also have the opinion that by knowing the coolant temperature they can have better control of the car, which is not logical considering that the most of cars today cannot be repaired without the assistance of a technician.

From the obtained data, it can be concluded that the respondents do not consider the speed indicator (Question A) to be relevant, given that more than 70 percent of them would do without this information as shown in Tab. 2. No dependence was also demonstrated for this question, which can be seen as a certain surprise.

The data for the information on the coolant temperature (Question B) was remarkably interesting, where a high dependence on the level of the respondent's driving experience was also confirmed. Based on the statistical dependence found, it can be concluded that less experienced drivers significantly want to have this information available (statistically 92 wanted, while 52 did not want to display the information), while medium and highly experienced drivers would not miss this information (64/72 and 38/ 66). This shift in opinion can be precisely explained by higher experience of the second and third groups of drivers, who are more aware that they would not use this information in practice anyway.

The answers to the question regarding the distance traveled (Question C) were also surprising, when most respondents are not interested in this information as shown in Tab. 2. In this case, no simple explanation for this result can be found. There is a possibility that people in the Czech Republic draw this information from external navigation applications and therefore do not consider the data provided by the vehicle to be essential. The observed statistical dependencies show that the demand for this information is in the group of women and subsequently in the group of less experienced drivers. For women it is 152/42, which is a ratio of about 15/4, and for men it is 132/62, which is a ratio of about 13/6. So, overall, drivers can get by without it, but women will miss that information less than men.

According to the results obtained, information about the currently engaged gear (Question D) is clearly indispensable, as over 92 percent of respondents could do without it. Based on the statistical evaluation, it can also be stated that no statistical dependence was confirmed for this question and the results can be perceived as evenly distributed.

The attitude towards information warning about exceeding the maximum allowed or set speed is also noticeably clear (Question E). Over 81 percent of respondents would easily omit this information in the cockpit. The weak statistical dependence that was confirmed for this question concerns older and less experienced drivers, who would like to see this information in the vehicle, even though they are a minority in the total numbers.

A significant percentage difference was shown between the answers to the question whether it is important to be warned about exceeding the recommended driving time (Question F). Over 90% of respondents do not want to be warned by the vehicle about exceeding the recommended time behind the wheel. In this case too, no statistical dependencies were confirmed, and the distribution can be described as equal. In addition, the two questions (Questions E and F) can be interpreted so that drivers do not want to let the car interfere with the way they drive and thus want to have everything under their own control.

The answers regarding the information about the low fuel level turned out to be completely in line with the assumption. Based on the survey, it can be said that most drivers want to be alerted to a low fuel level (Question G). In this case, a statistical dependence on the experience of the driver was confirmed, where it can be said that less experienced drivers required this information more often than more experienced ones.

CONCLUSIONS

This study looked at the essential information on the dashboard of a passenger car from the driver's point of view. The aim of the work was to find out the meaning of the individual information that is available in the cockpit of a passenger car from the driver's point of view. The evaluation took place depending on gender, age and kilometers driven. Based on the results that have been evaluated, it can be noticed that the tachometer is no longer the necessary information that the driver needs to see on his dashboard or virtual cockpit. Indicators such as a fuel gauge and associated signaling when the fuel level is low are desirable for all groups and for both genders.

According to the answers of the respondents, it was possible to find out the meaning of individual information available in the cockpit of a passenger car from the subjective point of view of the driver, and to find out which of the selected information provided by the vehicle can be omitted in the cockpit development process. Through omitting this unnecessary information, as described by the participants, the cognitive load of the driver was reduced, which has a direct impact on traffic safety and the ability to perform primary tasks, which in the case of a vehicle is driving, decreases with the amount of secondary information that the driver is forced to process as discussed in the study of *Hamish and Merat (2005)*. At the same time, it can be argued that with a higher load on cognitive functions, the probability of a bad assessment of the situation increases, which can lead to a decrease in traffic safety and, in extreme cases, to an accident, which supports with its results, in research of *O'Hare (2006)*.

If we start from the premise that too much received information leads to reduced performance of cognitive functions, it is clear, that the reduction of this information load will lead to an improvement in the driver's performance. Increased performance of cognitive functions affects the driver's attention while driving and this leads to an increase in traffic safety.

In conclusion, it can be said that younger drivers are more open to innovations in the cockpit of the car, as mentioned in a similar study (*Muslim, 2021*), but not every change in the driver assistance system is accepted. The aim of the research was verified, and the results showed that drivers are willing and can do without certain information while driving. Another goal was to confirm or refute the existence of statistically significant dependencies, how drivers of diverse groups divided by gender, age and experience approach this issue. The statistical analysis in this study clearly confirms the dependence of gender, age and driving experience on preferences in the display of individual indicators in the vehicle, like the study published by *Wechsler (2018)*. The research hypothesis, which assumes that some commonly found information in passenger vehicles will be considered useless from the point of view of the respondents, was confirmed.

The presented results can serve as a basis for further research that would help clarify the above or serve for further research that addresses the issue of cockpit technology and infotainment in vehicles or machines. Findings presented in this work could help to design a minimalist cockpit or a cockpit with less information load and thereby help reduce the information load on the driver's cognitive functions and, as a result, increase traffic safety. Cockpit design is a core area of human factors and ergonomics. Ideally, good design compensates for human capacity limitations by distributing task requirements over human and interface to improve safety and performance (*Sabatino, 2002*). The data and hypotheses presented in this thesis can serve as auxiliary factors in the car design process focused on optimizing human-machine interfaces to improve traffic safety and regarding potential target customer groups.

ACKNOWLEDGMENT

This study was supported by “University Grant Competition - UGC” as a part of the project “Improvement in Quality of the Internal Grant Scheme” at the Czech University of Life Sciences, under project number 62/2021 (CZ.02.2.69/0.0/0.0/19_073/0016944).

REFERENCES

1. Edwards, C., Hankey, J., Kiefer, R., Grimm, D., and & Leask, N. (2011). Understanding Driver Perceptions of a Vehicle to Vehicle (V2V) Communication System Using a Test Track Demonstration. SAE International Journal of Passenger Cars – Mechanical Systems, 4(1), 444-461.

2. Häne, C., Heng, L., Lee, G. H., Fraundorfer, F., Furgale, P., Sattler, T. &, Pollefeys, M. (2017). 3D visual perception for self-driving cars using a multi-camera system: Calibration, mapping, localization, and obstacle detection. Image and Vision Computing, vol. 68, pp. 14–27.
3. Hamish J., A., & Merat, N. (2005). Surrogate in-vehicle information systems and driver behaviour: Effects of visual and cognitive load in simulated rural driving. Transportation Research Part F: Traffic Psychology and Behaviour, 8(2), 79–96.
4. Hruška M. &, Jindra P (2016). Presentation title: Ability to handle unfamiliar systems in passenger cars according to driver skills. Agronomy Research 14(5), 1601–1608.
5. Huhtamo, E. (2020). The Self-Driving Car: A Media Machine for Posthumans?. Andrés Burbano; Ruth West (coord.) AI, Arts & Design: Questioning Learning Machines. Artnodes, no. 26,: 1-14.
6. Muslim, H., Itoh, M., Liang, C. K., Antona-Makoshi, J., & Uchida, N. (2021). Effects of gender, age, experience, and practice on driver reaction and acceptance of traffic jam chauffeur systems. Scientific reports, 11(1), 17874.
7. Regan, M. A., Horberry, T., Stevens, A. (2017). Driver acceptance of new technology: Theory, measurement and optimisation. Farnham Surrey, Burlington, Vt : Ashgate Publishing Company, 384 pp. ISBN 9781138077034.
8. Sabatino, A. E., & Flegal, T. (2002). Virtual cockpits (D. G. Hopper, Ed.). SPIE.Sabatino, A. E., Flegal, T., "Virtual cockpits", Proc. SPIE 4712, Cockpit Displays IX: Displays for Defense Applications, (28 August 2002)
9. Wechsler, K., Drescher, U., Janouch, C., Haeger, M., Voelcker-Rehage, C., & Bock, O. (2018). Multitasking During Simulated Car Driving: A Comparison of Young and Older Persons. Frontiers in Psychology, 9.
10. O'Hare D. (2006) Cognitive Functions and Performance Shaping Factors in Aviation Accidents and Incidents, The International Journal of Aviation Psychology, 16:2, 145-156

Corresponding author:
Ing. Jakub Povýšil, Department of Technological Equipment of Building, Faculty of Engineering, Czech University of Life Sciences, Faculty of Engineering, Kamýcká 129, 165 21 Prague 6, Czech Republic, phone: +420 739 063 760, e-mail: povysil@tf.czu.cz

MOISTURE CONDITIONING OF BULK RAPESEEDS AND DETERMINATION OF MECHANICAL PROPERTIES AND PERCENTAGE OIL YIELD UNDER UNIAXIAL COMPRESSION LOADING

Nor Hafiy Adli RAZALI[1,2], Emir Asyraff AGUS[1,2], Je Zen CHEONG[1,3], Abraham KABUTEY[1], David HERÁK[1], Čestmír MIZERA[1]

[1]Czech University of Life Sciences Prague, Faculty of Engineering, Department of Mechanical Engineering, Czech Republic
[2]Universiti Teknologi PETRONAS, Faculty of Engineering, Department of Electrical & Electronic Engineering, Malaysia
[3]Universiti Teknologi PETRONAS, Faculty of Engineering, Department of Chemical Engineering, Malaysia

Abstract
This study described the mechanical properties and estimation of the percentage oil yield of bulk rapeseeds samples at different moisture content under compression loading. The initial moisture content was determined to be 4.879 % w.b. The moisture content levels of 6.615, 7.144, 8.325 and 9.375 % w.b. were determined using the moisture conditioning oven at different relative humidity levels from 60 to 75 % with 5% interval. The mass of the samples was kept constant at 111.69 g repressing an initial pressing height of 60 mm using the vessel diameter of 60 mm. The samples were compressed at a the maximum force of 100 kN and a speed of 5 mm/min. The observed parameters were deformation, oil yield, oil expression efficiency, hardness and deformation energy. Based on the correlation analysis, it was found that all the observed parameters negatively correlated significantly ($P < 0.05$) with moisture content. The correlation values were between -0.933 and -0.983. The model parameter estimates were also described from the simple linear regression analysis. The moisture content of 4.875 % w.b. was established to be optimum for a higher oil yield of 14.849 ± 2.475 %, oil expression efficiency of 46.593 ± 7.767 %, deformation energy of 447.375 ± 22.710 J, deformation of 30.7 ± 0.410 mm and hardness of 3257.62 ± 43.519 N/mm.

Key words: *moisture content, percentage oil yield, strength properties, deformation energy, regression models.*

INTRODUCTION

Moisture content is one of the most important factors to consider in the processing and handling of agricultural products (*Mamman & Umar, 2005; Burubai, Akor, Igoni & Puyate, 2007*). In the literature, considerable studies have been conducted on the effect of moisture content on the mechanical properties and loading orientations of seeds/kernels/nuts which are not limited to the following authors (*Baumler, Cuniberti, Nolasco & Riccobene, 2006; Burubai, Akor, Igoni & Puyate, 2007; Lzli, Unal & Sincik, 2009; Carcel et al., 2012; Adejumo, Inaede & Adamu, 2013*). Under the uniaxial compression loading, the mechanical/strength properties of agricultural products include the rupture force, deformation to rupture point, failure stress and strain, Young's modulus, toughness, hardness and strain energy (*Sirisomboon, Kitchaiya, Pholpho & Mahuttanyavanitch, 2007; Chakespari, Rajabipour & Mobli, 2010; Carcel et al., 2012*). In particular, *Burubai, Akor, Igoni & Puyate (2007)* reported the mechanical properties namely compressive force, deformation, failure stress, strain energy and Young's modulus of African nutmeg (Monodora myristica) in the moisture content range of 8.0 to 28.7 % d.b. The authors indicated that compressive force, failure stress and Young's modulus decreased with an increase in moisture content whiles deformation and strain energy increased with an increase in moisture content. *Lzli, Unal & Sincik (2009)* also studied the physical and mechanical properties of rapeseed at different moisture levels in the range of 7.3 to 27.4 % d.b. for three varieties of rapeseeds. Regarding the mechanical properties, the authors reported only the rupture force for the mechanical properties which decreased as a function of moisture content. Most importantly, for oil yield, *Adejumo, Inaede & Adamu (2013)* studied the effect of moisture content on the yield and characteristics of oil from *Moringa oleifera* seeds. The authors found a decrease in oil yield with the increase in moisture

content from 7.28 to 20 % d.b. *Orhevba, Chukwu, Osunde & Ogwuagwu (2013)* also reported a decrease in oil yield of neem seed kernel in the moisture content values from 6.3 to 16.6 % w.b. In our previously published studies on bulk rapeseeds under compression loading, single moisture content was considered to examine the mechanical properties, force-deformation characteristic curves, oil yield and optimum operating factors (*Divišova et al., 2014; Demirel et al., 2021; Demirel et al., 2022*). Moisture dependence on mechanical properties and percentage oil yield of bulk rapeseeds is not adequate in the literature. Therefore, this present study aims to add to the literature the information on the compressive force, deformation, energy, hardness, oil yield and oil expression efficiency of bulk rapeseeds at different moisture content under compression loading.

MATERIALS AND METHODS

A bag of 25 kg of rapeseeds was obtained from Česká Skalice, Czech Republic and kept in the laboratory. The initial moisture content of the sample of 4.879 (% w.b.) was determined using the standard oven method at 105 °C and drying time of 17 h (*ISI, 1996*). The oil content of the sample of 31.87±0.01% by the Soxhlet extraction procedure as reported in our previously published study (*Demirel et al., 2021*) was used in the calculation of the oil expression efficiency. The moisture conditioning of the samples was done using the hot oven (MEMMERT GmbH+Co.KG, Schwabach, Germany) equipped with a distilled water container placed atop. The relative humidity was set in the range between 60 and 75% with a 5% interval. For each sample, the minimum and maximum temperatures were set at 48 °C and 52 °C respectively and the actual temperature was set at 50 °C where the moisture conditioning for each sample was run for 24 h. The electronic balance (Kern 440-35, Kern & Sohn GmbH, Balingen, Germany) was used to measure the mass of the samples. To determine the moisture content at each relative humidity, the samples after 24 h conditioning were further put into the standard oven method. The moisture content of the sample was calculated using equation (1) (*Blahovec, 2008*).

$$MC\ (\%) = \left[\left(\frac{m_b - m_a}{m_b}\right) \cdot 100\right] \quad (1)$$

where m_b and m_a represent the masses of rapeseed samples before and after oven drying (g).

Tab. 1 Calculated moisture content at different relative humidity

Relative humidity (%)	Moisture content (% w.b.)
47*	4.879
60**	6.615
65**	7.144
70**	8.325
75**	9.375

* Laboratory condition ** Moisture conditioning

The universal compression machine (ZDM 50, Czech Republic) and the pressing vessel diameter of 60 mm with a plunger were used to describe the force-deformation curves of the samples at a maximum force of 100 kN and speed of 5 mm/min. The initial pressing height of the sample was measured at 60 mm corresponding to a mass of 111.69 g. The compression tests with the moisture levels are shown in Fig. 1. The tests were repeated twice, and averaged values were used in further analyses.

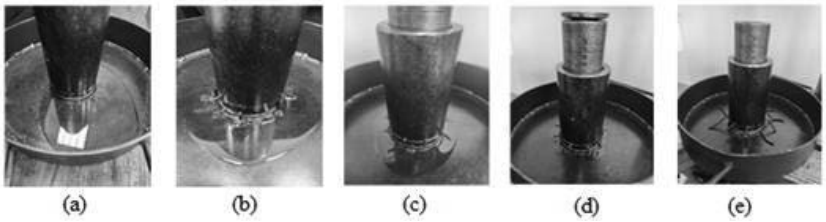

Fig. 1 Compression test of rapeseed samples at different moisture levels (a) 4.879 % w.b. (b) 6.615 % w.b. (c) 7.144 % w.b. (d) 8.325 % w.b. and (e) 9.375 % w.b showing the output oil and seedcake ejection.

Deformation values were obtained directly from the compression test for each sample. Oil yield and oil expression efficiency were determined according to equations (2) and (3) (*Deli et al., 2011; Demirel et al., 2021*).

$$OY = \left(\frac{M_O}{M_S}\right) \cdot 100 \quad (2)$$

$$OEE = \left(\frac{OY}{O_C}\right) \cdot 100 \quad (3)$$

where *OY* is the oil yield (%), M_O is the mass of oil (g), M_S is the mass of sample seeds (g), *OEE* is the oil expression efficiency (%) and O_C is the oil content (%) by the Soxhlet extraction the Soxhlet extraction procedure (*Niu, Li, Chen & Xu 2014*). The energy is the area under the force-deformation curve which was calculated using equation (4) (*Gupta and Das, 2000; Lysiak, 2007; Karaj and Muller, 2010*).

$$EN = \sum_{n=0}^{n=i=1} \left[\frac{F_{n+1} + F_N}{2} . X_{n+1} - X_n\right] \quad (4)$$

where EN is the energy (J), *F* is the compressive force (N), and *X* is the deformation (mm), which was converted to meters during the calculation. The hardness was calculated using equation (5) (*Chakespari, Rajabipour & Mobli, 2010*).

$$HD = \frac{F}{X} \quad (5)$$

where HD is the hardness (N/mm), *F* is the compressive force (N) and *X* is the deformation (mm). The data were analyzed using Statistica software (*Statsoft, 2013*) by employing correlation and simple regression techniques.

RESULTS AND DISCUSSION

The obtained data are given in Tabs. 1 to 3 and Fig. 2. It can be seen Tab. 1 that the increment in moisture content linearly decreased the amounts of oil yield, oil expression efficiency, deformation energy, deformation and hardness. For the moisture content range of 4.879 to 9.375 (% w.b.); the oil yield ranged from 14.849±2.475 to 3.446±0.998 %; oil expression efficiency ranged from 46.593±7.767 to 10.811±3.130 %; deformation energy ranged from 447.375±22.710 to 180.041±14.271 J; deformation ranged from 30.7±0.410 to 25.48±0.156 mm and the hardness ranged from 3257.62±43.519 to 2188.074±27.234 N/mm. All the parameters negatively correlated significantly ($P < 0.05$) with moisture content increment with high correlation values between -0.936 and -0.983 (Tab. 2). The simple regression analysis (Tab. 2) also proved significant (F value > F critical or P value < 0.05) where the values of the coefficient of determination (R^2) were high within the range of 0.876 to 0.966. The simple regression models for all the parameters are given in Tab.3. The intercept and moisture content coefficient were significant ($P < 0.05$) indicating the adequacy of the determined models. The force-deformation curves for each moisture content value are shown in Fig. 2. The area under the curve is the deformation energy (*Gupta and Das, 2000; Lysiak, 2007; Karaj and Muller, 2010*). The control moisture content of 4.879 % w.b. showed a smooth curve compared to the moisture content value of 6.615% w.b. which indicated a serration effect being characterized by the ejection of the seedcake through the holes of the pressing vessel (*Divišova et al., 2014*). Based on this observation, the compression test for the other moisture content values was stopped at the limit force without the serration effect. The serration effect was also observed in our published study on jatropha seeds at moisture levels of 32 % w.b. and 37 % w.b. (*Kabutey, Herak & Sedlacek, 2011*). It is relevant to indicate that the serration effect is not only attributed to the high moisture content but also to the combination of high pressure and speed and diameter of the pressing vessel (*Divišova et al., 2014; Kabutey, Herak, Mizera & Wasserbauer, 2018*). The limit or rupture force values for the above-mentioned moisture content values were 100 kN, 86 kN, 79 kN, 66 kN and 57 kN respectively. It was found that the limit force decreased linearly with moisture content. Similar results were indicated by *Lzli, Unal & Sincik (2009)* for rapeseed varieties as a function of moisture content, and then *Gupta and Das (2000)* on sunflower seed and kernel. The results also confirm the study by *Burubai, Akor, Igoni & Puyate, (2007)* on African nutmeg. In this present study, oil yield decreased with the increase in moisture content. The optimum moisture content was observed at 4.879 % w.b. *Adejumo, Inaede & Adamu (2013)* reported a decrease

in oil yield for Moringa oleifera seeds in the moisture content range of 7.28 to 20 % d.b. The authors further indicated that the oil yield of moringa seeds decreased with moisture content above 10 % d.b. *Orhevba, Chukwu, Osunde & Ogwuagwu (2013)* also found a decrease in neem kernel oil yield from 24.86 to 15.62 % in the moisture content range of 6.3 to 16.6 % w.b. The authors mentioned that the optimum moisture content was between 6.3 and 8.1 % d.b.

Tab. 1 Calculated parameters at different moisture levels of bulk rapeseed samples

Moisture content (% w.b.)	Oil Yield *OY* (%)	Oil Expression Efficiency *OEE* (%)	Deformation Energy *EN* (J)	Deformation *X* (mm)	Hardness *HD* (N/mm)
4.879	14.849±2.475	46.593±7.767	447.375±22.710	30.7±0.410	3257.62±43.519
6.615	9.813±1.151	30.790±3.611	364.214±6.771	28.28±0.198	3182.619±22.244
7.144	8.361±1.686	26.235±5.289	313.112±22.766	26.52±0.665	2979.152±21.341
8.325	4.075±0.964	12.788±3.023	217.7412±13.200	25.235±0.064	2536.169±6.396
9.375	3.446±0.998	10.811±3.130	180.041±14.271	25.48±0.156	2188.074±27.234

Tab. 2 Results of correlation and simple regression with the effect of moisture content

Correlation			Simple regression		
Calculated parameters	R	R^2	F-value	F-critical	P-value
OY (%)	-0.952	0.907	77.667	5.318	< 0.05
OEE (%)	-0.952	0.907	77.667	5.318	< 0.05
EN (J)	-0.983	0.966	229.845	5.318	< 0.05
X (mm)	-0.936	0.876	56.464	5.318	< 0.05
HD (N/mm)	-0.941	0.886	62.209	5.318	< 0.05

R: Correlation; R^2: Coefficient of determination; F-value > F-critical or P-value < 0.05 is significant.

Tab. 3 Model estimates under the effect of moisture content

	Model	Standard		
Effect	*OY* (%)	Error	t-value	P-value
Intercept	27.563	2.256	12.218	< 0.05
Moisture content (% w.b.)	-2.677	0.304	-8.813	< 0.05
	Model	Standard		
Effect	*OEE* (%)	Error	t-value	P-value
Intercept	86.487	7.078	12.218	< 0.05
Moisture content (% w.b.)	-8.399	0.953	-8.813	< 0.05
	Model	Standard		
Effect	*EN* (J)	Error	t-value	P-value
Intercept	761.029	30.773	24.731	< 0.05
Moisture content (% w.b.)	-62.818	4.143	-15.161	< 0.05
	Model	Standard		
Effect	*X* (mm)	Error	t-value	P-value
Intercept	36.35924	1.239785	36.35924	< 0.05
Moisture content (% w.b.)	-1.25437	0.166931	-1.25437	< 0.05
	Model	Standard		
Effect	*HD* (N/mm)	Error	t-value	P-value
Intercept	4649.978	235.9717	19.70566	< 0.05
Moisture content (% w.b.)	-250.599	31.7725	-7.88729	< 0.05

OY: Oil Yield (%); *OEE*: Oil Expression Efficiency (%); *EN*: Deformation Energy (J); *X*: Deformation (mm) and *HD*: Hardness (N/mm).

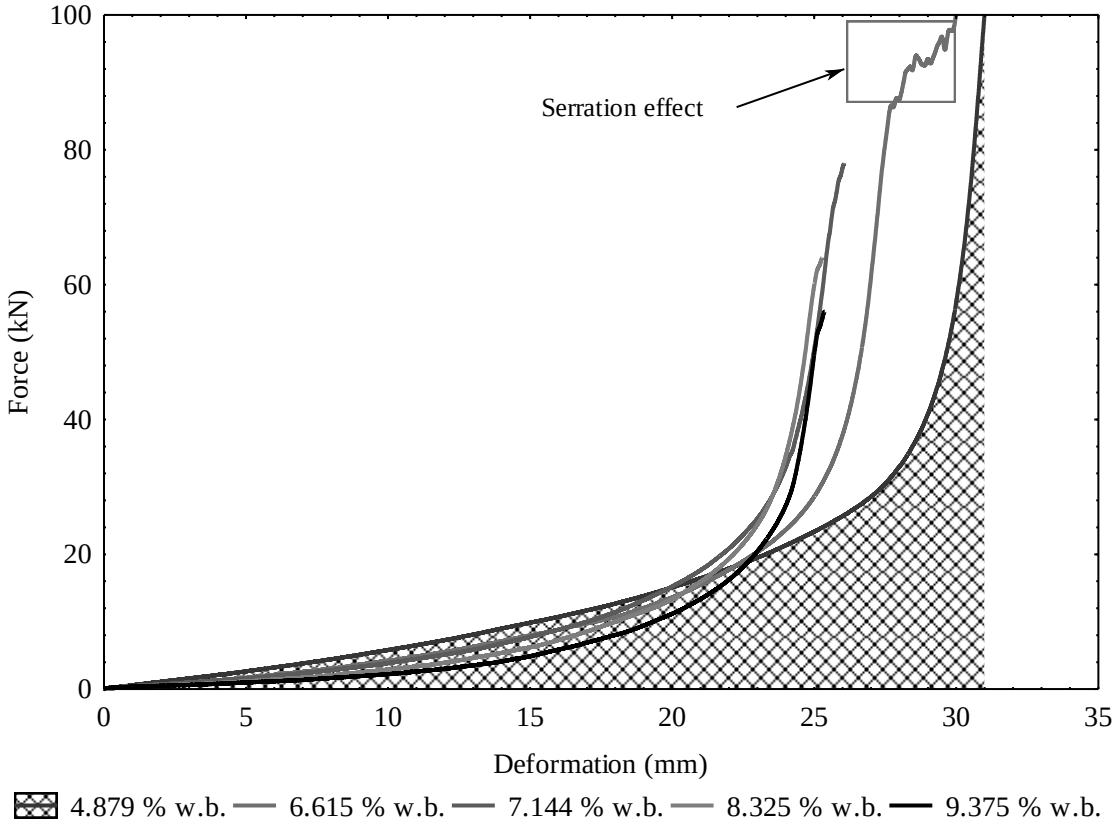

Fig. 2 Force-deformation curves of bulk rapeseed samples at different moisture levels with the serration effect.

CONCLUSIONS

The moisture content value of 4.879 % w.b. obtained the highest oil yield of 14.849±2.475 % and oil expression efficiency of 46.593±7.767. The corresponding deformation energy was 447.375±22.710 J. The increase in moisture content decreased the oil yield, oil expression efficiency, deformation energy, deformation and hardness of the rapeseed samples. Under the uniaxial compression loading, the moisture content of 4.879 % w.b. of the rapeseeds sample was found to be optimum for a higher percentage oil yield. In a future study, the mechanical screw press Farmet Duo would be used to validate the observed optimum moisture content for oil recovery efficiency, throughput, energy input, specific energy, temperature and oil residue in press cake.

ACKNOWLEDGMENT

The study was supported by the Internal Grant Agency of Czech University of Life Sciences Prague, Grant Number: IGA 2020: 31130/1312/2114.

REFERENCES

1. Mamman, E. & Umar, B. (2005). Effects of moisture content and loading orientation on the mechanical properties of *Balanites aegyptialia* nuts. *Agricultural Engineering International: The CIGR Ejournal*, *7*, 1-16.
2. Burubai, W., Akor, A.J., Igoni, A.H. & Puyate, Y.T. (2007). Effects of temperature and moisture content on the strength properties of African nutmeg (Monodora myristica). *International Agrophysics*, *21*, 217-223.
3. Baümler. E.. Cuniberti. A.. Nolasco. S. M.. & Riccobene. I. C. (2006). Moisture dependent physical and compression properties of safflower seed. *Journal of Food Engineering*. *72*(2), 134-140.
4. Izli, N., Unal, H. & Sincik, M. (2009). Physical and mechanical properties of

rapeseed at different moisture content. *International Agrophysics*. *23*, 137-145.
5. Carcel, L. M., Bon, J., Acuña, L., Nevares, I., del Alamo, M., & Crespo, R. (2012). Moisture dependence on mechanical properties of pine nuts from *Pinus pinea* L. *Journal of Food Engineering*. *110*(2), 294-297.
6. Adejumo, B. A., Inaede, S. G. & Adamu. T. S. (2013). Effect of moisture content on the yield and characteristics of oil from *Moringa oleifera* seeds. *Academic Research International*, *4*(4), 1-11.
7. Sirisomboon, P., Kitchaiya, P., Pholpho, T. & Mahuttanyavanitch, W. (2007). Physical and mechanical properties of *Jatropha curcas* L. fruits, nuts and kernels. *Biosystems Engineering*, *97*, 201-207.
8. Chakespari, A.G., Rajabipour, A. & Mobli, H. (2010). Strength behaviour of study of apples (cv. *Shaft Abadi & Golab Kohanz*) under compression loading. *Modern Applied Science*, *4*(7), 173-182.
9. Orhevba, B.A., Chukwu, Z.D. & Ogwuagwu, V. (2013). Influence of moisture content on the yield of mechanically expressed neem seed kernel oil. *Academic Research International*, *4*(5), 1-6.
10. Divisova, M., Herak, D., Kabutey, A., Sleger, V., Sigalingging, R. & Svatonova, T. (2014). Deformation curve characteristics of rapeseeds and sunflower seeds under compression loading. *Scientia Agriculturae Bohemica*, *45*(3), 180-186.
11. Demirel, C., Kabutey, A., Herák, D., Hrabě, P., Mizera, Č. & Dajbych, O. (2021). Optimizing uniaxial oil extraction of bulk rapeseeds: spectrophotometric and chemical analyses of the extracted oil under pretreatment temperatures and heating intervals. *Processes*, *9*(10), 1-26.
12. Demirel C, Kabutey A, Herák D, Sedlaček A, Mizera Č, Dajbych O. (2022). Using Box–Behnken Design coupled with response surface methodology for optimizing rapeseed oil expression parameters under heating and freezing conditions. *Processes*, *10*(3), 1-18.
13. ISI. *Indian Standard Methods for Analysis of Oilseeds*; IS:3579; Indian Standard Institute (ISI): New Delhi, India, 1966.
14. Blahovec, J. Agromatereials Study Guide; Czech University of Life Sciences Prague, Czech Republic, 2008, p.7.
15. Deli, S., Masturah, F., Aris, T.Y., Nadiah, W.W.A. (2011). The effects of physical parameters of the screw press oil expeller on oil yield from *Nigella sativa* L. Seeds. *International Food Research Journal*, 18, 1367–1373.
16. Niu, L., Li, J., Chen, M.S. & Xu, Z.F. (2014). Determination of oil contents in Sachia inchi (*Plukentia volubilis*) seeds at different developmental stages by two methods: Soxhlet extraction and time-domain nuclear magnetic resonance. *Industrial Crops and Products*, *56*:187-190.
17. Gupta, R.K. & Das, S.K. (2000). Fracture resistance of sunflower seed and kernel to compressive loading. *Journal of Food Engineering*, *46*, 1-8.
18. Lysiak, G. (2007). Fracture toughness of pea: Weibull analysis. *Journal of Food Engineering*, *83*, 436-443.
19. Karaj, S. & Muller, J. (2010). Determination of physical, mechanical and chemical properties of seeds and kernels of *Jatropha curcas* L. *Industrial Crops and Products*, *32*, 129-138.
20. Statsoft Inc. STATISTICA for Windows; Statsoft Inc: Tulsa, OK, USA, 2013.
21. Kabutey, A., Herák, D. & Sedláček, A. (2011). Behaviour of different moisture contents of Jatropha curcas L. seeds under compression loading. *Research in Agricultural Engineering*, *57*(2), 72-77.
22. Kabutey, A., Herak, D., Mizera, C. & Wasserbauer, M. (2018). Assessment of undulation behaviour of rape and sunflower bulk oilseeds under compression loading. In: *IOP Conference Series: Materials Science and Engineering*, 2nd Nommensen International Conference on Technology and Engineering, NICTE, (pp: 1-7).

Corresponding author:
doc. Ing. Abraham Kabutey, Ph.D., Department of Mechanical Engineering, Faculty of Engineering, Czech University of Life Sciences Prague, Kamýcká 129, Praha 6, Prague, 165 20, Czech Republic, phone: +420 22438 3180, e-mail: kabutey@tf.czu.cz

MODELLING OF SHAFT TRAJECTORY IN SLIDING BEARING LUBRICATED WITH DIFFERENT LUBRICANTS

Jozef RÉDL[1], František TÓTH[1], Davood KALANTARI[2], Jozef BANGO[1]

[1]*Institute of Design and Engineering Technologies, Slovak University of Agriculture in Nitra, Slovak Republic*
[2]*Sari Agricultural Sciences and Natural Resources University, Iran*

Abstract
In this paper, we are dealing with design of a mathematical model for prediction of the moving trajectory of a shaft supported in the sliding bearing. The mathematical model describes the real tribologic couple lubricated with two types of lubricants. The first lubricant we used, was the bio lubricant Texaco Hydra 46 and the second one was Madit PP80. The tribologic couple consists of a shaft with a diameter $\phi 29.960 mm$*, with fit* $H8/f7$ *and bush* $B60$ *type with dimensions* $\phi 35r7 \times \phi 30H8 \times 20$*. The shaft is manufactured from steel EU E355 and the bush is manufactured from copper-tin alloy CuSn12. In mathematical procedures the stiffness and damping properties was substituted with dimensionless parameters. The general properties of the tribological couple were defined in moving equations with Sommerfeld number. By solving of moving equations, we get the trajectory of shaft center, mounted in the sliding bearing. We also get the critical angular velocity where the tribological couple became unstable range.*

Key words: *bearings, tribological couple, Sommerfeld number, bio lubricant.*

INTRODUCTION

Rotors represent a very important part in many machines, devices, and plants, and give rise to engineering and design challenges. While some problems in rotor dynamics nowadays can be considered as solved, new problems have emerged from the broad utilization, but also from the frequent need to increase the operating range, the rotational speed, the load, or the power of rotating machinery. New solutions for increasing demands are necessary and this emphasizes the importance of rotor dynamics and its status as an innovative field of research (*Gupta, 2011*). The hydrodynamic forces in bearing bushing lifted the rotating shaft, which reduces the loss of transmitted power. Result of application of different types of lubricants is the different degree of material degradation and different lifetime of tribological couple (*Gasch et al., 2006*). For case of accident possibly, there arevery often chosen the natural safe lubricants called bio lubricants. In many cases, the operating environment or various special performance requirements, other than load capacity, may be of overriding the importance of the selection of an appropriate type of bearing (*Neale, 2011*). Many researchers have analyzed the different operating conditions, used lubricants and materials for stability of rotating shaft mounted in sliding bearings. The existing definitions of the linearized stiffness and damping coefficients in polar coordinates are derived from the Taylor series expansions of the radial component and tangential component of the fluid force and neglecting higher than first order terms (*Wang et al., 2006*). The physical and mechanical properties of used bio lubricants for simulating temperature were defined by the value of its Sommerfeld number. The differences in stiffness and damping are obvious in case the temperature of the oil was 100°C and the values of Sommerfeld numbers corresponded to this temperature. The viscosity of the oil is changing with increased temperature. The material and lubricants within the contact region usually define the friction characteristics of bearing systems. Sliding bearings have good damping and stiffness properties but suffer from high stiction and nonlinear friction characteristics. Evaluation of friction coefficient of different types of lubricants by experimental way is at nowadays very often-used methodology. The experimental stage of the test in terms of given methodology was characterized by increasing the load with a load intensity of defined force every certain time point, regardless the stabilization of measured parameters, and at a constant shaft speed (*Engel et al., 2016*). The mathematical modeling of sliding couples is very effective way to get the information about the couple behavior under different conditions. The journal stability in sliding bearing by solving of dynamical motion equations was done by many researchers at all (*Krämer 1993; Šesták et al., 2001; Muszyńska 2005*). Both, the appropriate selection of the lubricant type as well as material of bearing housing have radical influence on the degradation of

bearing housing liner and lifetime of bearing itself. For this reason, the clearance between shaft and housing liner is filled with oil layer with appropriate lubrication. The degradation of shaft and bushing liner depend on applied lubricant's properties, types, and values of applied interaction dynamic forces (*Šesták et al., 2001; Neale 2001*). The tribological processes in lubricated journal bearing are described well by Reynolds equation. If the numerical solution is considered as not general enough, some simplifications must be introduced to allow the pressure to be computed in closed form. If the bearing is assumed very long, it is possible to neglect the fluid flow and pressure gradient in axial direction, obtaining the so-called long-bearing approximation (*Mahrenholtz, 1984; Genta, 2005; Kudish, et al., 2010; Stachowiak, 2013*).
The aim of this article was to provide the research about the influence of applied lubricants in sliding bearing on the stability of rotating journal. The properties of applied lubricants were substituted by Sommerfeld number.

MATERIALS AND METHODS

Tribological system properties

The components of tribological system are shown in figure 1. The tribological system contains the fixing head (A), sliding bushing (B) and shaft (C). The shaft is manufactured from steel 11 600 (EU – E355). The contact surface of the shaft is grinded to dimension $\phi 29.60mm$ with tolerance on fit $H8/f7$. For the fit of hole with deviation H and degree of sharpness refers the tolerance range $^{+39\mu m}_{0}$ and for shaft with deviation f and degree of sharpness refers the tolerance range $^{-20\mu m}_{-40\mu m}$.

The bushing with commercial signature $B60$ with dimension $\phi 35r7 \times \phi 30H8 \times 20$ is shown in figure 3. All dimensions and tolerances were calculated according to the ISO 286-2 standard. The bushing is manufactured from full bronze with centrifugal casting technology from material $CuSn12$. The material $CuSn12$ is tin bronze used for manufacturing of sliding bearings and is available for the working environment with hydrodynamic lubrication and with limited lubrication. The $CuSn12$ bushing is available for transmitting the rotational and translational moving. Technical drawing of bushing is shown in figure 2.

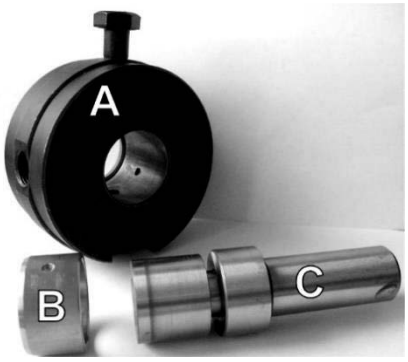

Fig. 1 Tribological components

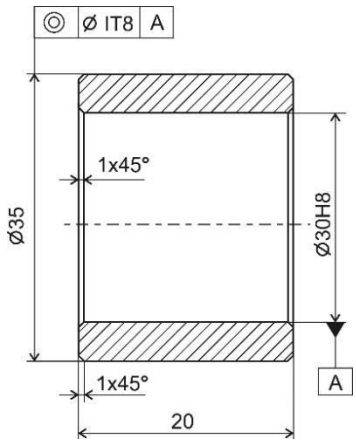

Fig. 2 Technical drawing of bushing

Fig. 3 Bushing

For the experimental process was used the experimental device called Tribotestor M10. The roughness of tribological components was measured before the test and after the test, with application of different lubricants defined in tables 2 and 3. The real test running time was 60 seconds, with constant axial loading with force F_S . Lubricant flow pressure was 101.325 kPa. Kinematic parameters of sliding couple are shown in table 1.

Tab. 1 Kinematic parameters of sliding couple

Parameter	Label	Unit	Value
Rotational speed	n	min^{-1}	180
Axial force	F_S	N	1000
Bearing length	B, L	m	0.02
Radial clearance	C	m	$38.75 \cdot 10^{-6}$
Bushing inner diameter	D	m	$30.038 \cdot 10^{-3}$
Shaft diameter	d	m	$29.960 \cdot 10^{-3}$
Shaft roughness before test	R_{AS1}	μm	0.32
Bushing roughness before test	R_{AB1}	μm	1.14
Shaft roughness after test with Texaco Hydra	R_{ASX2}	μm	0.336
Bushing roughness after test with Texaco Hydra	R_{ABX2}	μm	0.46
Shaft roughness after test with Madit PP80	R_{ASP2}	μm	0.331
Bushing roughness after test with Madit PP80	R_{ABP2}	μm	0.64

Used Lubricants specifications

For lubrication of sliding bearing, we used two types of liquid lubricants. The parameters of lubricants are shown in table 2. TEXACO Hydra 46 is the biodegradable hydraulic fluid (87.5%) based on synthetic ester, usable in systems with higher operating temperatures. It has no negative effects on sealing materials, and it does not contain zinc (*Chevron products UK LTD, 2014).* The oil Madit PP80 is suitable for using in manual and mechanical gearboxes for commercial vehicles, manual transmissions for passenger cars and light commercial vehicles, oil lubricated roller bearings, manual transmissions, agricultural and construction transmissions, manual and mechanical transmissions of commercial vehicles, manual transmissions for passenger cars and light commercial vehicles (*Technicko-informačný list-MADIT PP 80, 2020*). The technical parameters of oil Texaco Hydra 46 are shown in table 2, and Madit PP80 are shown in table 3.

Tab. 2 Basic properties of TEXACO Hydra lubricant *(Chevron Products UK LTD, 2014*)

TEXACO Hydra 46	ν	ρ
	$mm^2 \cdot s^{-1}$	$kg \cdot m^{-3}$
Kinematic viscosity at 100°C	9.3	
Density at 15°C		922

Tab. 3 Basic properties of Madit PP80 lubricant (*Madit PP80, 2022*)

Madit PP80	η	ρ
	$mm^2 \cdot s^{-1}$	$kg \cdot m^{-3}$
Kinematic viscosity at 100°C	8.6	
Density at 15°C		885

Mathematical model and its assumptions

For creating a mathematical model of sliding bearing we defined the assumptions published by *Lee (1993)* as follows:

- gyroscopic or rotary inertia effects are neglected,
- the disk is located at the shaft mid span, only allowing its translational motion,
- the mass of the shaft is neglected compared with that of the disk,
- the flexibility of the (rigid) hearings is neglected compared with that of the shaft.

- it is assumed that the external damping force, which can be air friction against the shaft whirl, is proportional to the linear velocity of the geometrical center of the disc,
- neglecting the influence of difference between oil density at 15°C and 100°C.

The rotor sliding bearings were substituted with spring-dumper combinations, what is shown in figure 4. The limits of stability of the shaft in sliding bearings are determined with its stiffness and damping coefficients. In the figure 4 we are defining the stiffness coefficients k with respect to the y,z coordinate axes and damping coefficients c with respect to the y,z coordinate axes.

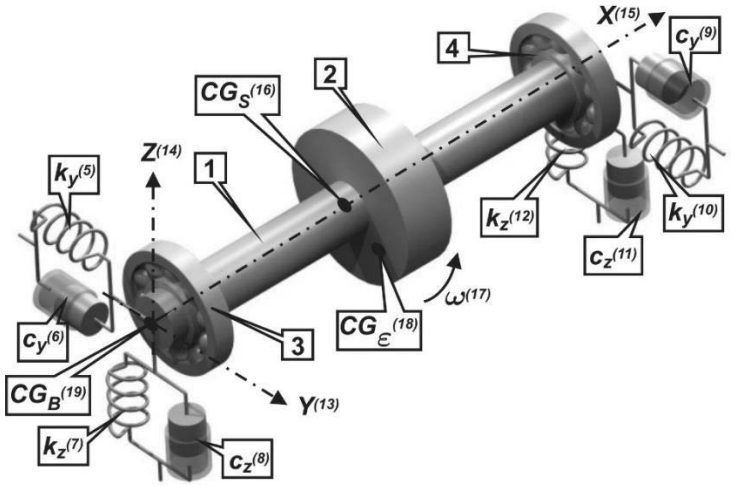

Fig. 4 Rotor-bearings model
1-shaft, 2- mass, 3-4- bearings, 5-7-10-12-stiffnes coefficients, 6-8-9-11- damping coefficients,13-14-15 coordinate system, 16-shaft's center of gravity, 17- angular velocity, 18- mass yaw, 19 – bearing's center of gravity.

Fig. 5; ω – angular velocity, M – torsional moment; ε – eccentricity; φ – angle

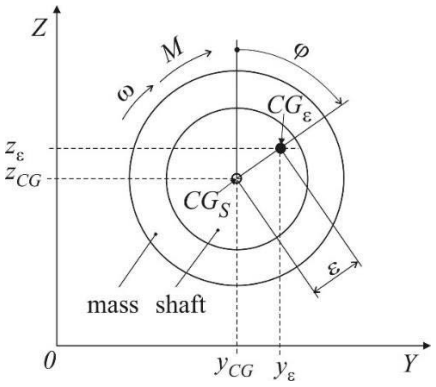

Fig. 5 Rotor displacement
CG_S – center of gravity of shaft; Y,Z – coordinate systems; y_{CG},z_{CG} – coordinate of the center of gravity of shaft; $y_\varepsilon,z_\varepsilon$ - coordinate of the CG_S displacement with refer to CG_M

By the redrawing the figure 4 to the two-dimensional view with the rotor displacement we get the figure 5. Relationship between the stiffness coefficients of the oil film and the shaft loading will be in the matrix form:

$$\begin{bmatrix} y_{CG_S} \\ z_{CG_S} \end{bmatrix} = \begin{bmatrix} k_{yy} & k_{yz} \\ k_{zy} & k_{zz} \end{bmatrix} \cdot \begin{bmatrix} F_y \\ F_z \end{bmatrix}_k . \tag{1}$$

The stiffness forces should be rewritten from equation (1) as follows:

$$\begin{bmatrix} F_y \\ F_z \end{bmatrix}_k = \begin{bmatrix} k_{yy} & k_{yz} \\ k_{zy} & k_{zz} \end{bmatrix} \cdot \begin{bmatrix} y_{CG_S} \\ z_{CG_S} \end{bmatrix} . \tag{2}$$

The damping coefficients of the oil film will be in matrix form:

$$\begin{bmatrix} \dot{y}_{CG_S} \\ \dot{z}_{CG_S} \end{bmatrix} = \begin{bmatrix} c_{yy} & c_{yz} \\ c_{zy} & c_{zz} \end{bmatrix} \cdot \begin{bmatrix} F_y \\ F_z \end{bmatrix}_c . \tag{3}$$

The damping forces form equations (3) can be rewritten as follows:

$$\begin{bmatrix} F_y \\ F_z \end{bmatrix}_c = \begin{bmatrix} c_{yy} & c_{yz} \\ c_{zy} & c_{zz} \end{bmatrix} \cdot \begin{bmatrix} \dot{y}_{CG_S} \\ \dot{z}_{CG_S} \end{bmatrix} . \tag{4}$$

The rotor should be in unstable state when the damping mechanism of bearing is non-conservative and must by satisfied that $k_{yz} \neq k_{zy}$. If we combine the equations 2, 4 and rewriting to its components, with respect to the dynamical moving equations, we got:

$$\begin{aligned} m \cdot \ddot{y}_\varepsilon &= -c_{yy} \cdot \dot{y}_{CG_S} - k_{yy} \cdot y_{CG_S} , \\ m \cdot \ddot{z}_\varepsilon &= -c_{zz} \cdot \dot{z}_{CG_S} - k_{zz} \cdot z_{CG_S} , \end{aligned} \tag{5}$$

$$I \cdot \ddot{\varphi} = M + \varepsilon \cdot \left(y_{CG_S} \cdot k_{yy} \cdot \cos\varphi + \dot{y}_{CG_S} \cdot c_{yy} \cdot \cos\varphi - z_{CG_S} \cdot k_{zz} \cdot \cos\varphi - \dot{z}_{CG_S} \cdot c_{zz} . \cos\varphi \right). \quad (6)$$

We assume the stationary system and the mass is rotating with constant angular velocity $\omega = const.$ and $\alpha = 0$. If we will respect the shaft center of gravity coordinates transformation, we got:

$$\begin{aligned} y_\varepsilon &= z_{CG_S} + \varepsilon \cdot sin\varphi \\ z_\varepsilon &= z_{CG_S} + \varepsilon \cdot cos\varphi \end{aligned} \quad (7)$$

We respect that the rotating shaft is lifted in bushing by hydrodynamic forces which raised by acting the oil film. The moving equations has the next form in matrix notation:

$$\frac{m}{2} \cdot \begin{bmatrix} \ddot{z}_{CG_S} \\ \ddot{y}_{CG_S} \end{bmatrix} + \begin{bmatrix} b_{zz} & b_{zy} \\ b_{yz} & b_{yy} \end{bmatrix} \cdot \begin{bmatrix} \dot{z}_{CG_S} \\ \dot{y}_{CG_S} \end{bmatrix} + \begin{bmatrix} k_{zz} & k_{zy} \\ k_{yz} & k_{yy} \end{bmatrix} \cdot \begin{bmatrix} z_{CG_S} \\ y_{CG_S} \end{bmatrix} = \varepsilon . \omega^2 . \frac{m}{2} \cdot \begin{bmatrix} cos\,\omega t \\ sin\,\omega t \end{bmatrix} \quad (8)$$

We set up the equation rearrangement for better mathematical solving as follows. The eqn. 8 was multiplied by $\frac{1}{K} = \frac{S_o \cdot \Delta R}{g}$, $C_\Omega = \frac{1}{\Omega}$, where S_o is a Sommerfeld number, $\Delta R\,(m)$ is a bearing clearance, $g\,(m \cdot s^{-2})$ is gravitation acceleration, $\Omega\,(rad \cdot s^{-1})$ is self-angular velocity where $\Omega = \frac{\omega}{sin(45)}$. Each stiffness and damping coefficients of bearing that are dependent on the dynamic viscosity are solved with equations 9, 10, published by *Wang and Khonsari (2006).*

$$\begin{aligned} k_{yy} &= \frac{\varepsilon\omega\eta\bar{R}L^3}{C^3(1-\varepsilon^2)^2}, \; k_{yz} = -\frac{\pi\omega\eta\bar{R}L^3(1+2\varepsilon^2)}{4C^3\sqrt{(1-\varepsilon^2)^5}}, \\ k_{zy} &= \frac{\pi\omega\eta\bar{R}L^3}{4C^3\sqrt{(1-\varepsilon^2)^3}}, \; k_{zz} = \frac{2\omega\eta\bar{R}L^3\varepsilon(1+\varepsilon^2)}{C^3(1-\varepsilon^2)^3}, \end{aligned} \quad (9)$$

$$\begin{aligned} c_{yy} &= \frac{\pi\eta\bar{R}L^3}{2C^3\sqrt{(1-\varepsilon^2)^3}}, \; c_{yz} = -\frac{2\varepsilon\eta\bar{R}L^3}{C^3(1-\varepsilon^2)^2}, \\ c_{zy} &= -\frac{2\varepsilon\eta\bar{R}L^3}{C^3(1-\varepsilon^2)^2}, \; c_{zz} = \frac{\pi\eta\bar{R}L^3(1+2\varepsilon^2)}{2C^3\sqrt{(1-\varepsilon^2)^5}}, \end{aligned} \quad (10)$$

The stiffness and damping coefficients we substituted with dimensionless parameters as published by *Gasch and Pfutzner (1980)* as follows:

$$\gamma_{ik} = k_{ik} . \frac{S_o . \Delta R}{F_S}, \; \beta_{ik} = b_{ik} . \frac{S_o . \Delta R . \omega}{F_S}. \quad (11)$$

and finally, we got:

$$\begin{bmatrix} \ddot{z}_{CG_S} \\ \ddot{y}_{CG_S} \end{bmatrix} = \varepsilon . \omega^2 \begin{bmatrix} cos\,\omega t \\ sin\,\omega t \end{bmatrix} - \frac{1}{C_\Omega \cdot K} \begin{bmatrix} \beta_{zz} & \beta_{zy} \\ \beta_{yz} & \beta_{yy} \end{bmatrix} \cdot \begin{bmatrix} \dot{z}_{CG_S} \\ \dot{y}_{CG_S} \end{bmatrix} - \frac{1}{K} \begin{bmatrix} \gamma_{zz} & \gamma_{zy} \\ \gamma_{yz} & \gamma_{yy} \end{bmatrix} \cdot \begin{bmatrix} z_{CG_S} \\ y_{CG_S} \end{bmatrix} \quad (12)$$

We set up the Sommerfeld number in the form:

$$S_o = \frac{F_S . \Psi^2}{B.D.\eta_{ol}.\omega}, \quad (13)$$

where F_S is statical loading (N) the bearing, B is bearing height (m), D is bearing diameter (m), r is shaft radius (m), $\Delta R = R - r$ is a bearing clearance (m), $\Psi = 0.8 \cdot 10^{-3} . \sqrt[4]{v_H} = 0.97936 \cdot 10^{-3}$ is a bearing hydrodynamic effective clearance, η is dynamic viscosity $(Pa \cdot s)$ of the oil, ω is an angular velocity $(rad \cdot s^{-1})$. The stability of journal movement in the bearing should be considered by solving the system of homogenous differential equations (12). We will search the solution of this system in the form:

$$\begin{bmatrix} z_{Jo} \\ y_{Jo} \end{bmatrix} = \begin{bmatrix} \hat{z}_{Jo} \\ \hat{y}_{Jo} \end{bmatrix} . e^{\lambda . t}. \quad (14)$$

If we will respect an assumption:

$$\dot{z}_{Jo} = \lambda.\hat{z}_{Jo}.e^{\lambda t},\ \ddot{z}_{Jo} = \lambda^2.\hat{z}_{Jo}.e^{\lambda t},$$
$$\dot{y}_{Jo} = \lambda.\hat{y}_{Jo}.e^{\lambda t},\ \ddot{y}_{Jo} = \lambda^2.\hat{y}_{Jo}.e^{\lambda t}, \tag{15}$$

and put the equations (14) into the equations (12), then, after some modifications we get the system of algebraic equations in the following form:

$$\left(\frac{S_O.C}{g}.\lambda^2 + \frac{\lambda}{\omega}.\beta_{zz} + \gamma_{zz}\right).\hat{z}_{Jo} + \left(\frac{\lambda}{\omega}.\beta_{zy} + \gamma_{zy}\right).\hat{y}_{Jo} = 0$$
$$\left(\frac{S_O.C}{g}.\lambda^2 + \frac{\lambda}{\omega}.\beta_{yy} + \gamma_{yy}\right).\hat{y}_{Jo} + \left(\frac{\lambda}{\omega}.\beta_{yz} + \gamma_{yz}\right).\hat{z}_{Jo} = 0 \tag{17}$$

The characteristic equation is a polynomial of fourth degree:

$$\alpha^2\left(\frac{\lambda}{\omega}\right)^4 + \alpha^2.A_3\left(\frac{\lambda}{\omega}\right)^3 + \left(\alpha.A_4 + A_2\right).\left(\frac{\lambda}{\omega}\right)^2 + A_1\left(\frac{\lambda}{\omega}\right) + A_0 = 0. \tag{18}$$

The parameter α in equation 18 is not an angular acceleration.

The dimensionless parameters $A_i, i = 0..4$ are the influence factors and they have following form:

$$A_0 = \gamma_{zz}.\gamma_{yy} - \gamma_{yz}.\gamma_{zy},\ \ A_1 = \beta_{zz}.\gamma_{yy} + \beta_{yy}.\gamma_{zz} - \left(\beta_{zy}.\gamma_{yz} + \beta_{yz}.\gamma_{zy}\right),$$
$$A_2 = \beta_{zz}.\beta_{yy} - \beta_{yz}.\beta_{zy},\ A_3 = \beta_{zz} + \beta_{yy},\ A_4 = \gamma_{zz} + \gamma_{yy}. \tag{19}$$

The parameter α has the form: $\alpha = \frac{S_o.C}{g}.\omega^2$. The stability condition for the equation (18) is:

$$\alpha^2.A_1^2 - A_1\left(\alpha.A_4 + A_2\right).\alpha.A_3 + \alpha^2.A_3^2.A_0 \le 0. \tag{20}$$

We obtain the limit stability if we put the parameter α into the equation (18), modifying it and put this equal to zero, we get:

$$\left(\frac{S_O.C}{g}.\omega^2\right)^2.A_1^2 - A_1\left[\left(\frac{S_O.C}{g}.\omega^2\right).A_4 + A_2\right].\left(\frac{S_O.C}{g}.\omega^2\right).A_3 + \left(\frac{S_O.C}{g}.\omega^2\right)^2.A_3^2.A_0 = 0 \tag{21}$$

and finally, we get the critical angular velocity of the journal:

$$\omega_{Cr} = \sqrt{\frac{g}{S_0.C}.\frac{A_1.A_2.A_3}{A_1^2 - A_1A_3A_4 + A_0A_3^2}}. \tag{22}$$

Exceeding this critical angular velocity, the rotation of shaft will become unstable. Equation (21) is depending on the Sommerfeld number because the values from A_0 to A_4 are also depending on the Sommerfeld number.

RESULTS AND DISCUSSION

To solve the system of differential equation (12) we have been setting up the calculation of few parameters before. All calculations were performed by PTC Mathcad Prime 5.0.0.0 software.

The circumferential speed v_H:

$$v_H = \pi \cdot d \cdot n = 1.774\, m \cdot s^{-1}, \tag{23}$$

-bearing hydrodynamic effective clearance Ψ,

$$\Psi = 0.8 \cdot 10^{-3}.\sqrt[4]{v_H} = 923.29 \cdot 10^{-6}. \tag{24}$$

minimum film thickness h_0

$h_0 = 3.4 \cdot \left(R_{AS} + R_{AB}\right) + \alpha$, where $\alpha = 14\mu m$ is the maximal value of dimension of microparticles in oil, for all configurations separately. (25)

-relative eccentricity ε,

$\varepsilon = 1 - \left(\frac{2 \cdot h_0}{D - d} \right)$, for all configurations separately. (26)

Oil dynamic viscosity:

$\eta = \nu \cdot \rho$. (27)

Tab. 4 Dynamic viscosities

Material	η $Pa \cdot s$
Dynamic viscosity Madit PP80	0.00727
Dynamic viscosity Texaco Hydra	0.00923

The damping and stiffness coefficient we have solved by equations 9 and 10 and values are listed in the table 5 and table 6.

Tab. 5 Damping and stiffness coefficient for oil TEXACO Hydra

Parameter	Unit	Value before experiment	Value after experiment
k_{yy}	$N \cdot m^{-1}$	$1.039 \cdot 10^6$	$6.963 \cdot 10^5$
k_{yz}	$N \cdot m^{-1}$	$-2.331 \cdot 10^6$	$-1.326 \cdot 10^6$
k_{zy}	$N \cdot m^{-1}$	$8.078 \cdot 10^5$	$6.401 \cdot 10^5$
k_{zz}	$N \cdot m^{-1}$	$6.318 \cdot 10^6$	$3.426 \cdot 10^6$
c_{yy}	$N \cdot s \cdot m^{-1}$	$8.571 \cdot 10^4$	$6.792 \cdot 10^4$
c_{yz}	$N \cdot s \cdot m^{-1}$	$-1.102 \cdot 10^5$	$-7.388 \cdot 10^4$
c_{zy}	$N \cdot s \cdot m^{-1}$	$-1.102 \cdot 10^5$	$-7.388 \cdot 10^4$
c_{zz}	$N \cdot s \cdot m^{-1}$	$3.481 \cdot 10^5$	$2.167 \cdot 10^5$

Tab. 6 Damping and stiffness coefficient for oil Madit PP80

Parameter	Unit	Values before experiment	Values after experiment
k_{yy}	$N \cdot m^{-1}$	$8.184 \cdot 10^5$	$6.062 \cdot 10^5$
k_{yz}	$N \cdot m^{-1}$	$-1.837 \cdot 10^6$	$-1.204 \cdot 10^6$
k_{zy}	$N \cdot m^{-1}$	$6.364 \cdot 10^5$	$5.335 \cdot 10^5$
k_{zz}	$N \cdot m^{-1}$	$4.977 \cdot 10^6$	$3.426 \cdot 10^6$
c_{yy}	$N \cdot s \cdot m^{-1}$	$6.752 \cdot 10^4$	$5.661 \cdot 10^4$
c_{yz}	$N \cdot s \cdot m^{-1}$	$-8.684 \cdot 10^4$	$-6.432 \cdot 10^4$
c_{zy}	$N \cdot s \cdot m^{-1}$	$-8.684 \cdot 10^4$	$-6.432 \cdot 10^4$
c_{zz}	$N \cdot s \cdot m^{-1}$	$2.742 \cdot 10^5$	$1.919 \cdot 10^5$

We have performed a set of simulations based on the shaft and bushing roughness. The roughness has been measured before the experimental test and after the experimental test. From simulation we got the results of trajectory of shaft in bushing of bearing and critical angular accelerations as well as the values of stability conditions. The trajectories of shaft center are shown in figures 5, 6, 7, 8. For a better visualisation of the process, we set the joint trajectories before and after the test what is shown in figures 9, 10.

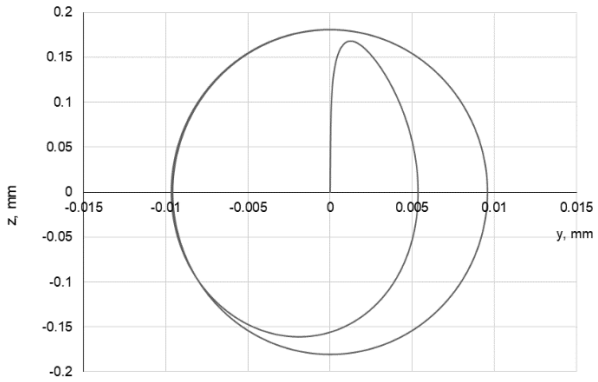

Fig. 5 Trajectory with Madit PP80 before the test

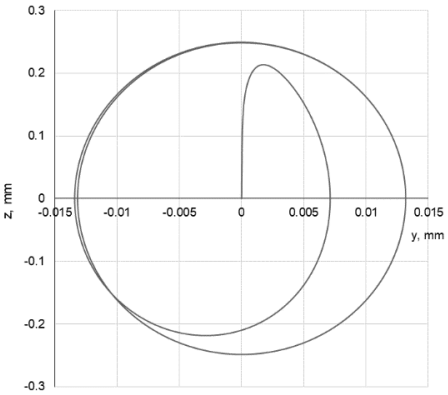

Fig. 6 Trajectory with Madit PP80 after the test

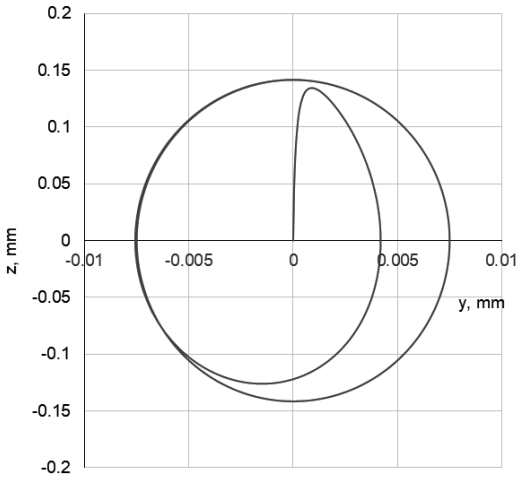

Fig. 7 Trajectory with Texaco before the test

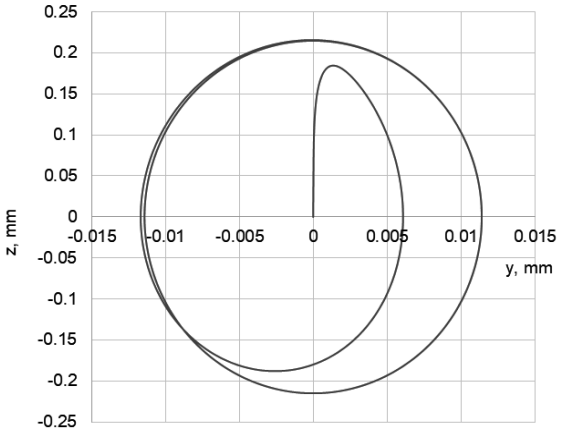

Fig. 8 Trajectory with Texaco after the test

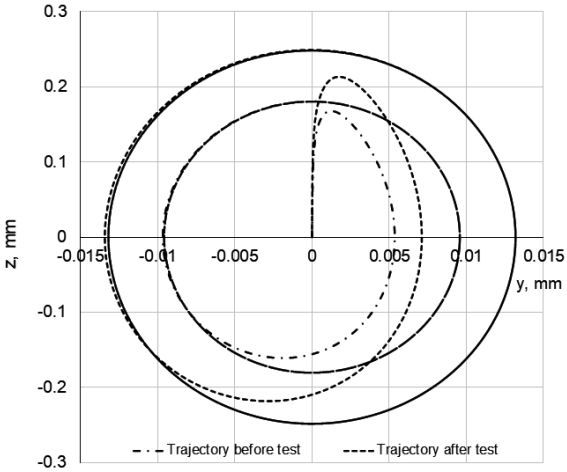

Fig. 9 Joint trajectories Madit PP80

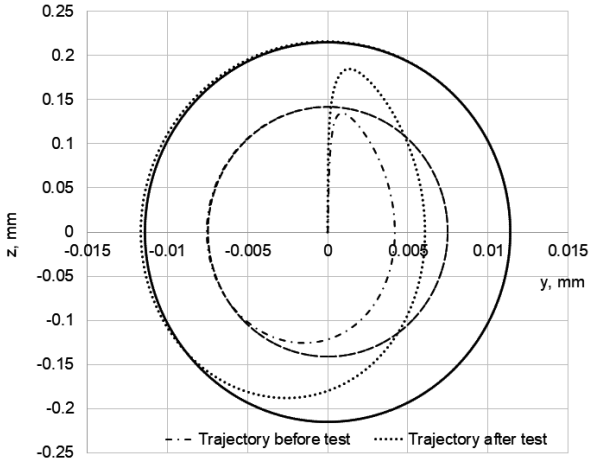

Fig. 10 Joint trajectories Texaco

The stability state of moving shaft in sliding bearing depends on few key factors. The influence of surface roughness has been proved. The other key factor is the Sommerfeld number. The solved results are in table 7. We also determined the maximal and minimal value of the shaft centre position during the simulation. These coordinates are important in relation with the bearing clearance. In the first column of the table 7 the listed coordinates y, z are the aliases in relation of sign convention mentioned in the

figure 5. The similar analysis was performed by *Šesták et al. (2001)*, but in their simulation many parameters were chosen by guess. For this reason, their results are only demonstrative. The mathematical model was defined almost identical to the presented model. Our mathematical model is based on the model published by *Gasch et al. (2006).* The vibrations of journal bearing have been investigated by *Chen et al. (2022)*. They performed the semi-analytical prediction of sliding bearing-rotor system in nonlinear rotor system. In our case we performed the linear rotor system. The difference between our model and model of *Chen et al. (2022)* was that the oil film thickness was constant in our case.

Tab. 7 Results from simulations

Parameter	Unit	Values before experiment		Values after experiment	
		Madit PP80	Texaco Hydra	Madit PP80	Texaco Hydra
S_o		10.358	8.16	10.358	8.16
ω_{Cr}	$rad \cdot s^{-1}$	267.522	301.415	327.746	415.147
Stability		0.532	0.599	0.651	0.825
$y_{\min}$ (y_ε)	*mm*	-0.00966	-0.00758	-0.01342	-0.01166
$y_{\max}$ (y_ε)	*mm*	0.00958	0.00751	0.01318	0.01144
$z_{\min}$ (z_ε)	*mm*	-0.1805	-0.1415	-0.24848	-0.21488
$z_{\max}$ (z_ε)	*mm*	0.18069	0.1416	0.24921	0.21577

Mathematical model of sliding bearing based on Reynolds equation was published by *Badescu (2020)*. He has proved, that the slider bearings operation under variable load is stable. A sensitivity analysis identified the design parameters which have the highest impact on bearing performance. The optimal slider bearing shapes obtained for Newtonian lubricants do not change if the most common couple stress fluids are used. Our simulation results are showing the similar conclusions, i.e., the movement of the shaft under the constant loading was stable (See the table 6 of the stability parameters). As published by *Gasch et al. (2006)*, the ratio of z coordinate of the rotating shaft regarding to rotational speed n always lay inside the stable region. With tribological performance optimization of sliding bearing is dealt with by *Zhang et al. (2022)*. Surface of the bearing slider was divided into a rectangular mesh, in which each rectangular grid was assumed to be local slip region or no-slip region. The influence of the surface of slip region on the tribological performance was confirmed. In our simulation we have confirmed that the roughness of the bushing liner and the shaft surface have the significant influence on the stability of the shaft movement.

CONCLUSIONS

Mathematical model of sliding bearing has been developed. The initial condition of simulation has been defined according to the recommendations of many nowadays researchers. The mathematical procedures were performed by PTC Mathcad Prime 5.0.0.0 software. Some relevant input parameters, like roughness, were acquired from the real experimental measurement. The roughness was measured before the test and after the test. The sliding bearing was loaded with axial force where the carrier of force was parallel with *z* axis. The sliding bearing was lubricated with two different lubricants. The first one was the mineral oil Madit PP80 and the second one was the bio-oil Texaco Hydra. The obtained trajectories of shaft center are depicted on the figures 5 to 10. We calculated the Sommerfeld parameter for each simulation. We calculated the stiffness and damping coefficient and finally we substituted them with dimensionless parameters in the system of differential equation. The investigated parameters are listed in the table 7. From table 7, we can conclude that the performance and stability of shaft movement were stable in all cases. The important fact which follows from the values in *x* axis directions, is that the direction of loading has the significant influence on the wearing of bushing liner. The *z* axis coordinates have higher values than *x* axis. This is caused by influence of the acting force. The higher values of roughness before the test in comparison with values of roughness after the test, were caused by filling the micro-particles as a product of wearing. The better lubrication abilities were proved by the bio-oil Texaco Hydra because the wearing of the bushing liner was lower and subsequently the production of

the micro-particles was lower. This fact caused better distribution of the oil film inside the bushing. The significant influence of performance has the value of the dynamic viscosity at last.

ACKNOWLEDGMENT
This study was supported by EU project Erasmus+ KA2 Capacity Building in the field of higher education, No. 585596-EPP-1-2017-1-DE-EPPKA2-CBHE-JP : "Fostering Internationalization in Agricultural Engineering in Iran and Russia" as a joint publication.

REFERENCES

1. Badescu, V. (2020). Two classes of sub-optimal shapes for one dimensional slider bearings with couple stress lubricants. In *Applied Mathematical Modelling* 81, 887–909.
2. Chen, B.- Wang, D.- Liu, K.- Zhang,Q. - He , T.- Chen, Z. (2022). Semi-analytical prediction of the periodic vibration in a sliding bearing–rotor system. In *International Journal of Non-Linear Mechanics*, 145.
3. Chevron Products UK LTD. (2014). Hydra® Premium performance biodegradable hydraulic fluid. [Available at: https://cglapps.chevron.com/msdspds/PDSDetailPage.aspx?docDataId=281458&docFormat=PDF] 01.07.2022
4. Engel,T. - Lechler,A.- Verl. A. (2016). Sliding bearing with adjustable friction properties. In *CIRP Annals - Manufacturing Technology*, 65, 353–356.
5. Gasch, R. - Nordmann, R. - Pfützner. H. (2006). Rotordynamik. Die Bewegungsgleichungen (pp. 253-260). *Springer International Publishing.*
6. Genta, G. (2005). Dynamics of Rotating Systems. *Springer International Publishing*.
7. Gupta, K. (2011). IUTAM Symposium on Emerging Trends in Rotor Dynamics. Proceedings of the IUTAM Symposium on Emerging Trends in Rotor Dynamics. *Springer Science+Business Media*.
8. ISO 286-2:2010 Geometrical Product Specifications (GPS). ISO code system for tolerances on linear sizes. Part 2: Tables of standard tolerance classes and limit deviations for holes and shafts. www.iso.org.
9. Krämer, E. (1993) Dynamics of Rotors and Foundations (pp.377). *Springer-Verlag Berlin Heidelberg*.
10. Kudish, I.I. - Covitch, M. J. (2010). Modeling and Analytical Methods in Tribology. *Chapman and Hall/CRC.*
11. Lee, CH. (1993). Vibration Analysis of Rotors, 1993 *Springer Science+Business Media*.
12. Madit PP80. [Available at: https://slovnaft.sk/sk/maziva/preprava/produkty/prevodove-oleje/madit-pp-80/] 30.07.2022.
13. Mahrenholtz, O. (1984). Dynamics of rotors stability and system identification. *Springer-Verlag Wien.*
14. Muszyńska, A. (2005). Rotordynamics. *Taylor & Francis Group.*
15. Neale,M.J. (2001). The Tribology Handbook, Butterworth-Heinemann 2001,
16. Stachowiak, G. W. - Batchelor. A.W. (2013). Engineering tribology. *Butterworth-Heinemann*.
17. Šesták, J. - Ryban, G. - Rédl, J. - Pršan, J. (2001). Stabilita pohybu hriadeľa v klznom ložisku. In *Nové trendy v konštruovaní a v tvorbe technickej dokumentácie.* (pp. 115-119). Slovenská poľnohospodárska univerzita v Nitre.
18. Wang, J. K. – Khonsari, M.M. (2006). A new derivation for journal bearing stiffness and damping coefficients in polar coordinates. In *Journal of Sound and Vibration* (290), , s. pp.500–507.
19. Zhang, H.- Liu, Y.- Dai, S - Li, F.- Dong, G. (2022). Optimization of boundary slip region on bearing sliders to improve tribological performance. In *Tribology International* 168.

Corresponding author:
doc. Ing. Jozef Rédl, Ph.D., Institute of Design and Engineering Technologies, Faculty of Engineering, Slovak University of Agriculture in Nitra, Tr. A. Hlinku 2, Nitra, Nitra, 94976, Slovak Republic, phone: +421 37 641 5670, e-mail: jozef.redl@uniag.sk

MULTI-CROP BIOMASS PRODUCTION FOR ENERGY PURPOSES

Kęstutis ROMANECKAS[1], Jovita BALANDAITĖ[1], Austėja ŠVEREIKAITĖ[1], Algirdas JASINSKAS[2], Saira KALIJEVA[3]

[1]Department of Agroecosystems and Soil Sciences, Agronomy Faculty, Agriculture Academy, Vytautas Magnus University
[2]Department of Agricultural Engineering and Safety, Faculty of Engineering, Agriculture Academy, Vytautas Magnus University
[3]Department of Soil Science and Agrochemistry, Faculty of Agrobiology, Kazakh National Agrarian Research University

Abstract
The research was conducted in 2020–2021 at Vytautas Magnus University, Academy of Agriculture, Research Station. The soil of the experimental field is light loam Planosol. The aim of the study was to determine the impact of multi-crops grown for energy purposes on the development and productivity of crops. Crops with different biodiversity were studied:
1. Single maize crop (MA);
2. Single hemp crop (HE);
3. Single faba bean crop (FB);
4. Binary maize and hemp crop (MA + HE);
5. Binary maize and faba bean crop (MA + FB);
6. Binary hemp and faba bean crop (HE + FB);
7. Ternary crop of maize, hemp and faba beans (MA + HE + FB).
The highest total fresh biomass of crops was established in single and multi-cropped maize; however, as expected, the highest total dry biomass was found in the ternary crop. The highest dried biomass of individual species (maize, hemp or beans) was observed of singly grown species, except faba bean in ternary crop. In this crop, the dried biomass of faba bean was the highest, and it replace ternary crop to the first place according to the dried biomass.

Key words: *Cannabis sativa; Zea mays; Vicia faba; multi-crops; productivity.*

INTRODUCTION

The faba bean (Vicia faba L.) is an important legume crop of the Fabaceae family; it is widely grown in the world for its economic and ecological value in sustainable agriculture (*Zong et al., 2019*). Faba bean are well able to adapt to different climatic conditions, as evidenced by their worldwide distribution (*Duc et al., 2015*). Technical hemp belongs to the family of magnolias (Cannabaceae) and has been used for medicine, fibre and food for more than six thousand years (*Pain, 2015*). Hemp is most commonly grown for seed or fibre. Its seeds are rich in starch, protein, and oil (*Galasso et al., 2016*). Hemp is also a promising crop for biofuel production. The amount of biomass obtained per unit area does not lag behind other energy crops (*Hodsonetal, 2011*). Maize (Zea mays L.) is an annual crop belonging to the mistletoe family (*Jakienė et al., 2013*). It is one of the most widely grown cereals in the world and is a major food source in many developing countries (*Kumawat et al., 2020*). Maize is also widely grown for animal feed, in the form of fresh biomass, grain or fermented and preserved in the form of silage, which could be used during colder periods of the year. In addition, one of the important targets for maize cultivation, mainly associated with developed countries, is ethanol production (*Barnes et al., 2016*).
Crop functionality is enhanced by sowing fast-growing other species of crops into the main crop. With increasing biodiversity, hemp and maize protect each other from the spread of pests, weeds and diseases, as well as increase productivity of total biomass per unit area. The nutritional and energetic value of the main products is also improving. However, the physical, biological and chemical properties of the soil are rapidly deteriorating, with a reduction in nutrients and humus, an increase in soil hardness and a deterioration of the soil structure (*Brussaard et al., 2007*).

Until now, the cultivation technologies of multifunctional multi–crops of hemp, faba bean or maize have been little studied abroad and in Lithuania. Future research results are a perspective for developing productive energy agrocenoses rotations and producing high quality biofuels. Hypothesis of investigation states that diversification of crops is likely to improve productivity per unit area. The aim of investigations was to evaluate the productivity of single and multi-cropped agrocenoses.

MATERIALS AND METHODS

A stationary field experiment was started in 2020 at the Research Station (54°52′ N, 23°49′ E) of Vytautas Magnus University, Agriculture Academy. Research data from 2021 is presented in this study. Soil of experimental field is light loam Planosol (Endohypogleyic-Eutric Planosol – Ple-gln-w). Soil pH_{HCl} is from 7.0 to 7.5, total nitrogen content – from 0.103 to 0.153%, available phosphorus – from 179 to 310 mg kg^{-1}, available potassium – from 95 to 172 mg kg^{-1}, available sulphur – from 1.5 to 2.5 mg kg^{-1}, magnesium – 488 to 820 mg kg^{-1}. The water regime is regulated by closed drainage, the micro relief is levelled. The arable layer of the soil is 23–27 cm thick.

Three crops are grown in the experiment: maize (Zea mays L.) (Pioneer breeding hybrid P8105), technical hemp (Cannabis sativa L.) (variety Austa SK) and field bean (Vicia faba L.) (variety Vertigo).

A total of seven treatments were tested (Tab. 1) (*Romaneckas et al., 2022*).

Tab. 1 Crop biodiversity

Level of crop biodiversity	Cultivation	Abbreviation
single crop	maize	MA
	hemp	HE
	faba bean	FB
binary crop	maize + hemp	MA+HE
	maize + faba bean	MA+FB
	hemp + faba bean	HE+FB
ternary crop	maize + hemp + faba bean	MA+HE+FB

The experimental plots were distributed in a random order. The initial size of each plot is 8 m^2. The experiment was performed in 3 replications. The buffer strip of the experiment field is 1 m wide, and between the repetitions and treatments– 2 m wide.

In autumn, the soil was ploughed up to 22–25 cm depth. In spring, the soil was cultivated twice with a complex cultivator. Depth of the last cultivation was 3–4 cm. The experimental plots were measured and the complex fertilizer NPK 5:15:30 was scattered on the soil before sowing. Fertilizer rate – 200 kg ha^{-1} (170 g per plot). The experimental plots were then seeded according to the intended sowing schemes (Fig. 1). They were sown by hands. When the weeds germinated abundantly, the crop spacing was loosened 2 times.

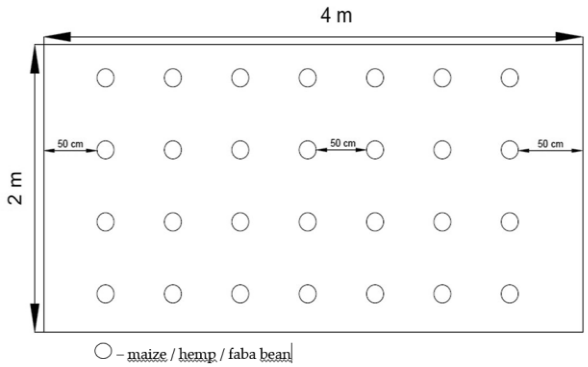

Single crops (MA, HE, FB)

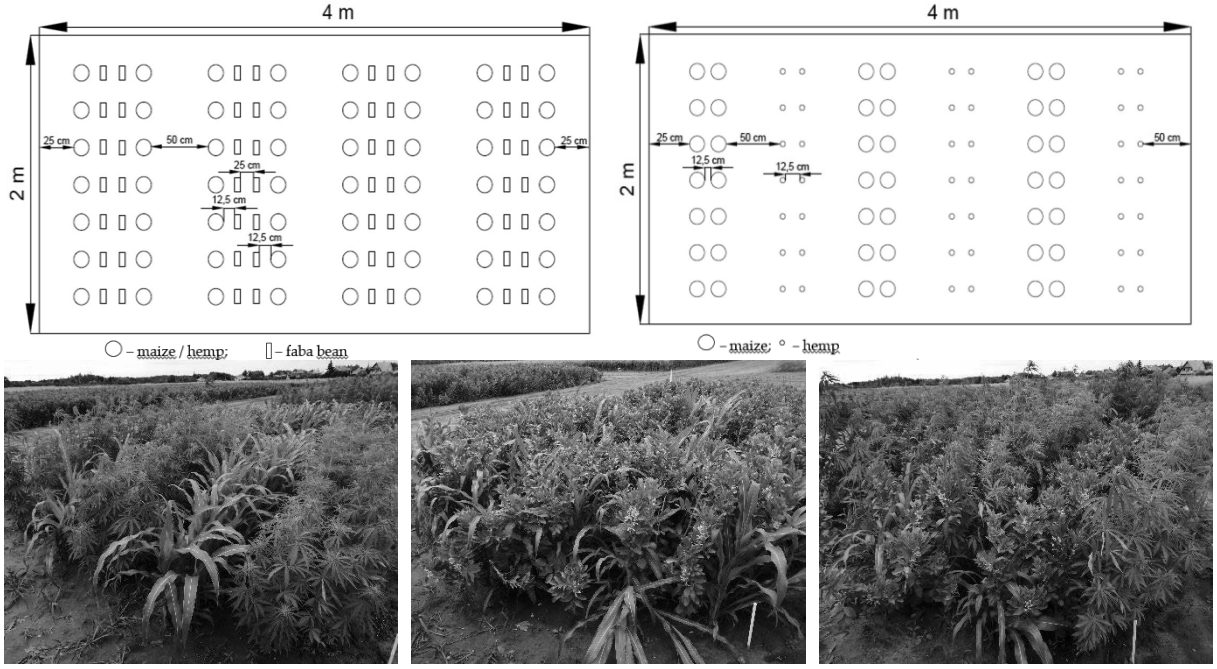

Binary crops (MA+HE, MA+FB, HE+FB)

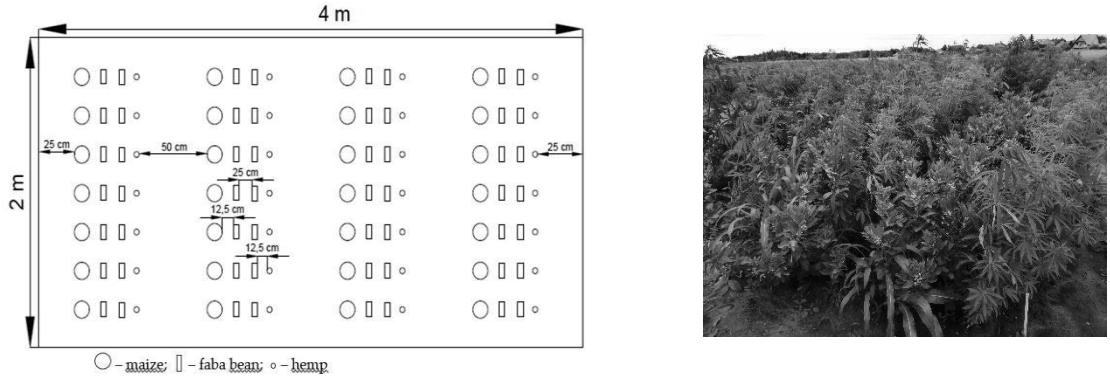

Ternary crop (MA+HE+FB)

Fig. 1 The sowing scheme (*Romaneckas et al., 2022*)

According to the amount of precipitation, the territory of Lithuania is in the zone of surplus moisture. The climate is maritime shifting to continental; so, meteorological conditions vary. The average annual rainfall is 600–650 mm and evaporates about 500 mm. The vegetation of agricultural plants lasts 150–170 days. In our experiment, in 2021, faba bean vegetation was lacking for only 103 days (period from germination to BBCH 09–10 to maturity at BBCH 83–86) because June and July were dry and hot. At the beginning of the vegetative season in 2021, the average air temperature was 6.2° C or 0.7° C lower than the long-term average. Precipitation was relatively low, only 33.7 mm or 7.6 mm less than the long-term average. Such conditions for the growth of crops were favourable. There was a lot of rainfall in May, about 121.6 mm; the temperature was only 11.4° C. The month of June was warm; the average temperature was 19.5° C. This month was dry – 40.3 mm of precipitation. July was extremely warm and received on average 2 times less precipitation than the long-term norm (96.6 mm). August was 0.8° C colder than usual. Precipitation was 33.3 mm higher than the usual norm. Such conditions were favourable for faba bean maturation. The crops were harvested at the end of the month.

Crop productivity parameters were carried out at harvest. Samples have been taken in a longitudinal row of 1 m (2 rows of beans) from at least 5 spots per plot. An average sample was formed. A total of 36 samples were prepared for more detailed studies. Biomass of crops were dried in the oven in 105° C

temperature. The experimental data were analysed by programme ANOVA for EXCEL (vers. 4.0, author Pavelas Tarakanovas, PhD. Lithuanian Institute of Agriculture, Akademija, Kedainiu distr., Lithuanija), for SELEKCIJA software was employed.

RESULTS AND DISCUSSION

Crop fresh biomass. Crop biomass is one of the most important indicators of crop development and productivity. Testing of crop fresh biomass at the end of vegetative season revealed that the significantly lowest fresh biomass was by the single faba bean crop (822.2 g m^{-2}), and insignificantly the highest – in the single maize crop (4163.3 g m^{-2}), or about 5 times higher (Fig. 2).

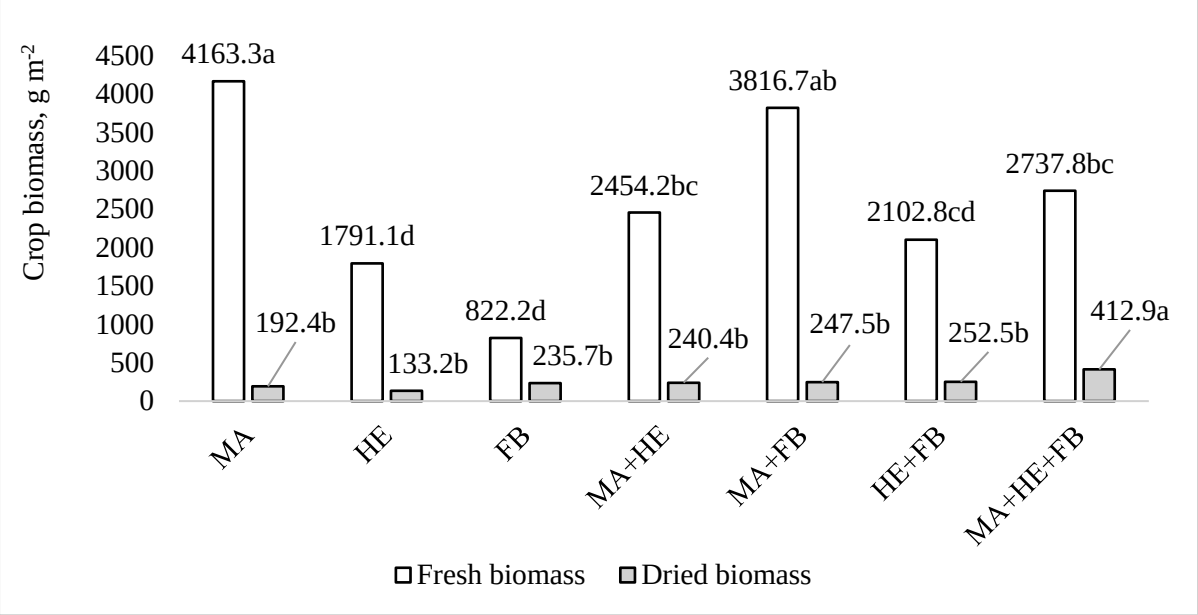

Fig. 2 Effect of diversification on crop biomass
Note: values marked with different letters differ significantly at P<0.05. Treatments: MA – single maize crop, HE – single hemp crop, FB – single faba bean crop, MA + HE – binary maize and hemp crop, MA + FB – binary maize and faba bean crop, HE + FB – binary hemp and faba bean crop, MA + HE + FB – ternary crop of maize, hemp and faba bean.

Out of binary crops, the highest amount of fresh biomass was grown by MA + FB crop, or 8.3% less than in single MA crop. The ternary crop (MA + HE + FB) produced 2737.8 g m^{-2} of fresh biomass, or about 3.3 times more than the single faba bean crop. The results differed significantly. According to *Streit et al. (2019)*, faba bean grows on average of 5% more fresh biomass in mixtures than in single crops. *Li et al. (2014)* reported a positive effect of maize fresh biomass yield when maize and bean roots in the mixture were freely mixed, and interspecies interactions were affected. *Streit (2018)* found that faba bean produces more fresh biomass than spring wheat, but did not show higher amounts of fresh biomass in binary crops (beans with spring wheat) than in single faba bean crop. *Shtaya et al. (2021)* also confirms that beans grown in combination with other plants increase the total fresh biomass. Growing faba bean together with triticale produced the highest fresh biomass of beans. Although a decrease in fresh biomass of beans was observed when growing binary crop with barley.
The highest fresh biomass mainly was observed of singly grown species; however significance of differences varied (Fig. 3).
Crop dried biomass. This indicator is perhaps the most important for determining a crop's productivity and energy potential. At the end of the vegetative season, significantly highest dried biomass was found in the ternary (MA + HE + FB) crop, although the maximum amount of fresh biomass was not found in this treatment (Fig. 2).

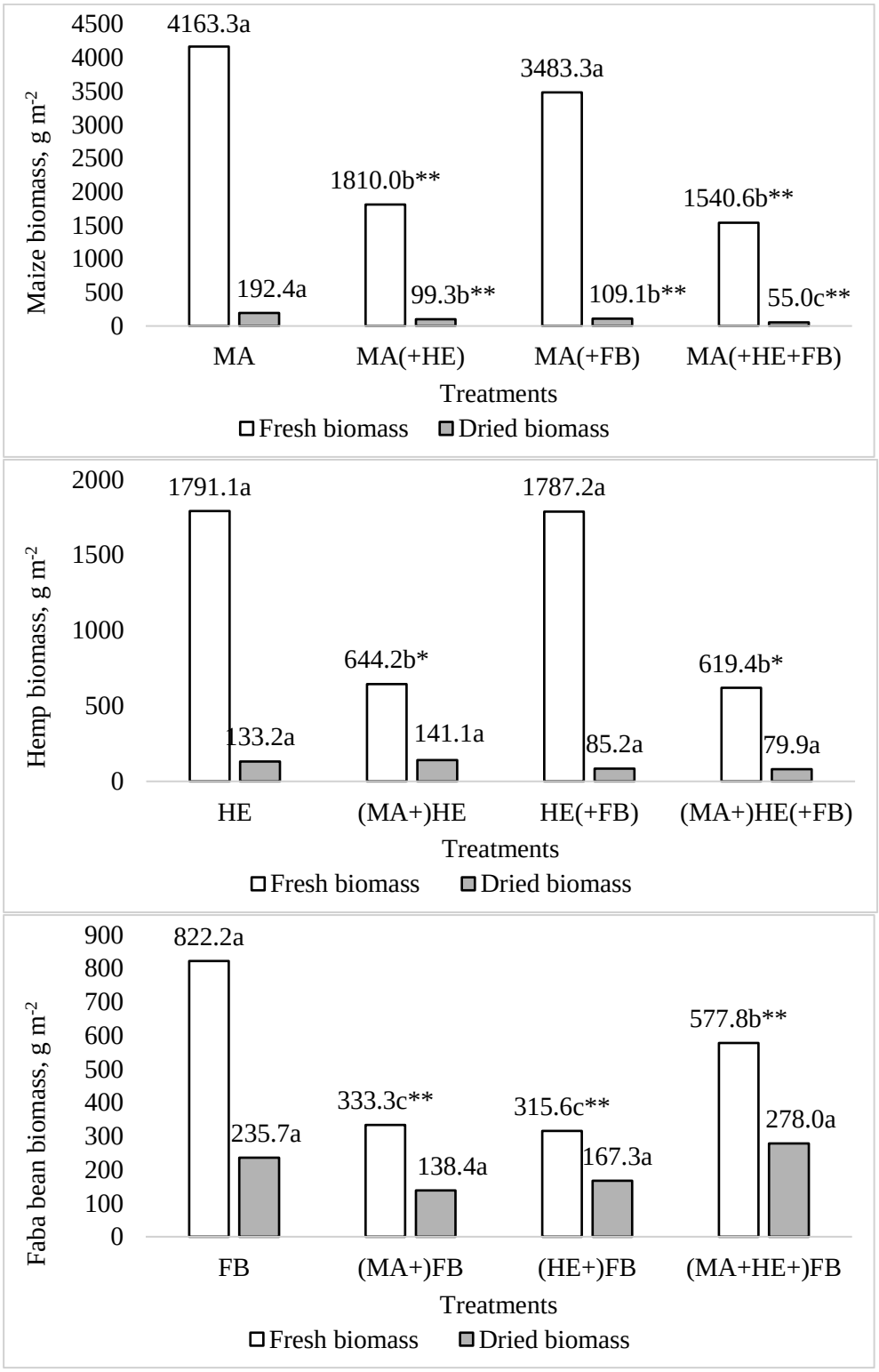

Fig. 3 Effect of crop diversification on species individual biomass
Note: values marked with different letters differ significantly at P<0.05. * – significant difference from control treatment (single crop) at 95% probability level, ** – at 99% probability level. Treatments: MA – single maize crop, HE – single hemp crop, FB – single faba bean crop, MA + HE – binary maize and hemp crop, MA + FB – binary maize and faba bean crop, HE + FB – binary hemp and faba bean crop, MA + HE + FB – ternary crop of maize, hemp and faba bean.

Meanwhile, during the period under review, the insignificant lowest dry biomass was found in the single hemp crop (133.2 g m^{-2}). The content of dry biomass in binary crops was similar, ranging from 240.4 to 252.5 g m^{-2}. Only the MA + FB crop was distinguished; it had a negligible maximum dry biomass content compared to other binary crops.
The highest dried biomass was observed of singly grown species, except faba bean in ternary crop (Fig. 3). In this crop, the dried biomass of faba bean was the highest, but not significantly.

CONCLUSIONS

The highest total fresh biomass of crops was established in single and multi-cropped maize. However, as expected, the highest total dry biomass was found in the ternary crop. The highest dried biomass of individual species (maize, hemp or beans) was observed of singly grown species, except faba bean in ternary crop. In this crop, the dried biomass of faba bean was the highest, and that replace ternary crop to the first place according to the dried biomass.

REFERENCES

1. Barnes, L. (2016). *Zea Mays* L.: Molecular Genetics, Potential Environmental Effects and Impact on Agricultural Practices. Hauppauge, New York: Nova Science Publishers.
2. Brussaard, P.C., De Ruiter. & Brown, G.G. (2007). Soil biodiversity for agricultural sustainability. Agriculture Ecosystems and Environment, 121, 233–244.
3. Galasso, I., Russo, R., Mapalli, S., Ponzoni, E., Brambilla, I. M., Battelli, G. & Reggiani, R. (2016). Variability in seed traits in a collection of *Cannabis sativa* L. genotypes. Frontiers in Plant Science, 7, 688.
4. Hodson, E.M., Nowakowski, D.J., Shield, I., Riche A., Bridgwater, A.V. & Donnison, I. S. (2011). Variation in *Miscanthus* chemical composition and implications for conversion by pyrolysis and thermo-chemical biorefining for fuels and chemicals. Bioresource Technology, 102, 3411–3418.
5. Jakienė, E., Liakas, V., Klimas, E. & Bačkaitis, J. (2013). Growing Technologies for energy herbaceous and woody plants. Akademija, Kaunas distr: press of Aleksandras Stulginskis University. (in Lithuanian)
6. Kumawat, G., Shahi, J.P. & Kumar, M. (2020). Electronic Journal of Plant Breeding. Assessment of genetic diversity of maize (*Zea mays* L.) hybrids under water logging condition. Electronic Journal of Plant Breeding, 11(1), 252–258.
7. Li, C., Dong, Y., Li, H., Shen, J. & Zhang, F. (2014). The dynamic process of interspecific interactions of competitive nitrogen capture between intercropped wheat (*Triticum aestivum* L.) and faba bean (*Vicia faba* L.). Plos One, 9(12), 115804.
8. Pain, S. (2015). A potted history. Nature. doi: 10.1038/525S10a. PMID: 26398731.
9. Romaneckas, K., Balandaitė, J., Sinkevičienė, A., Kimbirauskienė, R., Jasinskas, A., Gineleviˇius, U., Romaneckas, A. & Petlickaitė, R. (2022). Short-Term Impact of Multi-Cropping on Some Soil Physical Properties and Respiration. Agronomy, 12, 141.
10. Shtaya, M.J.Y., Ameran, A.A., Fernandez-Aparicio, M., Qaoud, H.A, Abdallah, J. & Rubiales, D. (2021). Effects of crop mixtures on rust development on faba bean grown in Mediterranean climates. Crop protection, 146, 105686.
11. Streit, J. (2018). Biomass, root distribution and overyielding potential of faba bean/wheat and white clover/ryegrass mixtures: Dissertation. Göttingen: University of Göttingen.
12. Streit, J., Meinen, C., Nelson, W.C.D. Rauber R. (2019). Above- and belowground biomass in a mixed cropping system with eight novel winter faba bean genotypes and winter wheat using FTIR spectroscopy for root species discrimination. Plant and Soil, 36, 141–158.

Corresponding author:
Agr. Kęstutis Romaneckas, Ph.D., Department of Agroecosystems and Soil Sciences, Faculty of Agronomy, Agriculture Academy, Vytautas Magnus University, Studentu str. 11, Akademija, 53361, Kaunas distr., Lithuania, phone: +370 656 300 44, e–mail: kestutis.romaneckas@vdu.lt

INCREASE IN THE HOP BELT DRYER DRYING INTENSITY

Adolf RYBKA, Petr HEŘMÁNEK, Ivo HONZÍK

Department of Agricultural Machines, Faculty of Engineering, Czech University of Life Sciences Prague, Czech Republic

Abstract
The aim of the experiments was to improve the permeability of the flattened hop layer to the drying air on the first belt of the dryer and intensified drying and fuel saving. For this purpose, one rotor was installed above the first belt and the rotor peripheral speed would be higher than the belt speed. By means of data loggers, three measurements with the rotor switched off and with the rotor switched on were carried out and repeated three times. The average moisture content of hops with the rotor being switched off was 53.03 %, and 48.63 % with the rotor being switched on. The drying process will intensify by 8.30 % with the rotor switched on. Without the rotor installed, the average consumption ELFO (Extra light fuel oil) was 486.5 $l.t^{-1}$ of dried hops, compared to 415.5 $l.t^{-1}$ when the rotor had been installed, resulting in significant fuel savings of 14.59 % when the rotor was used.

Key words: *hops; double-arm rotor; quality of hops; belt dryer; drying air.*

INTRODUCTION

Hops need to be preserved immediately after picking to prevent any loss of their quality. Picked cones have a moisture content of 72-82 %, they breath intensively, increasing the temperature and there is a risk of damage by spontaneous heating that might lead to a gloss loss, change in the basic colour and to a negative impact on the overall cone quality. Therefore, the drying process needs to be initiated rapidly. In the Czech Republic, majority of hop growers use continuous belt dryers for drying, where hops are dried on a set of three successive drying belts, followed by conditioning. Hop cones are dried at a temperature of 55-60°C for 6-9 h which is a very long time that is not beneficial at all for the final product quality, leaving aside the high energy requirements for drying. Dying on the first belt has a significant role as the moisture content is reduced here minimum by a third of total value of the input hop moisture content (*Rybka et al., 2016*).

The experience of the growers brings the knowledge that upon entering the first belt the hop layer flattens and hop cone bracts stick together due to their surface moisture. That causes lower layer permeability (surface crust is created) for the passing air, thus the drying speed decreases (*Rybka et al., 2018*). After this problem had been eliminated, a double-arm rotor located above the first belt of the dryer was designed, installed and verified in operation (Fig. 1).

The rotor was mounted between the first and second inspection window. This double-arm rotor has its arms fitted with reinforcement at their ends and rotates about its horizontal axis perpendicular to the belt motion. The rotor arms reach into the lower level of the hop layer moving on the dryer belt (Fig. 2). The shaft is fitted to the vertical walls of the dryer in bearing housings. It is driven by an electric motor with transmission gearbox. The rotational frequency of the rotor is selected in a way so that its peripheral speed was greater than the belt speed, however, in order to ensure that the rotor would not push the hops off the belt, thus forming vacant spots without hops above the belt through which the drying air would freely penetrate. This, in turn, would lower the intensity of hop drying. The rotor arms in their actual operation break up and rearrange the flattened layer of hops stuck together, thus enable better penetration of the drying air and faster removal of the hop moisture (*Heřmánek et al., 2018; Rybáček et al., 1980*).

The aim of the measurement and the article resulting from them was to improve the permeability of the dried layer of hops through the drying air on the first belt of the belt dryer, to reduce the relative humidity of the drying air more quickly, to intensify drying and to save fuel.

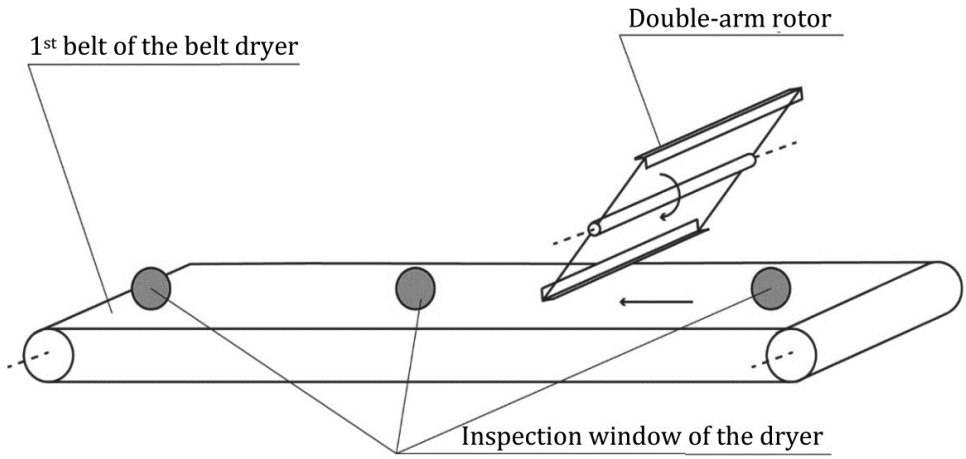

Fig. 1 Scheme showing the location of the double-arm rotor above the first belt of the belt dryer

Fig. 2 Rotor between the first and second inspection window above the first belt of the belt dryer

MATERIALS AND METHODS

Measurement by inserted data loggers

To measure the temperature and relative humidity inside the hop layer continuously we used VOLTCRAFT DL-121-TH data loggers (Fig. 3) which enable to programme the frequency of data storage. In our case this frequency was set to 5 minutes. The data logger internal memory has its storage capacity of 32,000 measured data. The data logger was integrated together with a sensor in a plastic casing and supplied by an inserted battery. The plastic casing had been fitted with a USB connector at one end via which the stored data were imported to a computer (*Jech et al., 2011*).

Fig. 3 VOLTCRAFT DL-121-TH data logger

To protect the data loggers against mechanical damage while carried throughout the dryer as well as against pollution caused by lupulin, the data loggers were fixed rigidly in polyurethane foam and inserted into two stainless sieves half-spherical in form. This was the best guarantee of protection and at the same time the sieves did not impede the air permeability, hence no measurement error occurred (Fig. 4).

Fig. 4 Insertion of a data logger into a protective sieve

The measurements were carried out from 27 to 29 August 2018 with the Saaz variety, which is the most widespread and is grown on 85.19 % of the Czech hop acreage. Three data loggers were placed through the first inspection window onto the first (upper) belt of the PCHB 750 belt dryer in Rakochmel, Co., Ltd. in Kolešovice. Two of them were inserted into a hop layer approx. 0.5 m far from both left and right dryer wall, and one in the middle. Three measurements with the rotor switched off and three measurements with the rotor switched on were carried out and repeated three times, the rotor being located between the first and second inspection window. The average values of the hop moisture content were determined based on these results, the dispersion of the values obtained from three measurements around the mean did not exceed 6 %. The specific values of the drying air temperature and relative humidity are taken as the average data from the three data loggers in passing through the third inspection window at the same time as the samples taken for laboratory determination of the hop moisture content. The advantage of data loggers, compared to rigidly fixed sensors in a dryer, is that they pass through the dryer together with the hops, continuously sensing the whole drying process (*Krofta, 2008; Mitter & Cocuzza, 2013*).

Laboratory analysis of the samples

The laboratory analyses monitored the moisture content of all hop samples, which was subsequently compared to the drying medium relative humidity measured by means of data loggers. The samples had been taken at the end of the first dryer belt. The moisture content in the hops was determined by the Mettler-Toledo HE53 moisture analyser (Fig. 5). The measurements were carried out 3 times repeatedly and the resulting values were averaged (*Forster & Gahr, 2013; Henderson & Miller, 1972*).

Fig. 5 Mettler-Toledo HE43 moisture analyser

RESULTS AND DISCUSSION

Tab. 1 shows the parameters of the drying process determined this way. The values from individual data loggers placed in the middle and on the edges of the belt differed minimally, thus confirming a presumption about drying process being even over the whole width of the dryer. The measurement results are further shown below in the graphs of Fig. 6 and Fig. 7.

Tab. 1 Parameters of the drying process

Date of measurement: 27. - 29. 8. 2018	Site: Rakochmel, Co., Ltd. in Kolešovice PCHB 750 belt dryer							Variety: Saaz
Sampling point	1st belt							
Rotor	Switched off				Switched on			
Measurement number	1	2	3	Mean	1	2	3	Mean
Sampling time [h:min]	13:20	12:45	13:01		16:20	16:00	16:01	
Drying air temperature [°C]	40.6	41.0	41.5	41.03	40.8	41.0	40.7	40.83
Drying air relative humidity [%]	40.2	41.6	42.8	41.53	33.2	34.8	33.2	33.73
Hop moisture content [%]	48.4	53.7	57.0	53.03	46.9	50.4	48.6	48.63

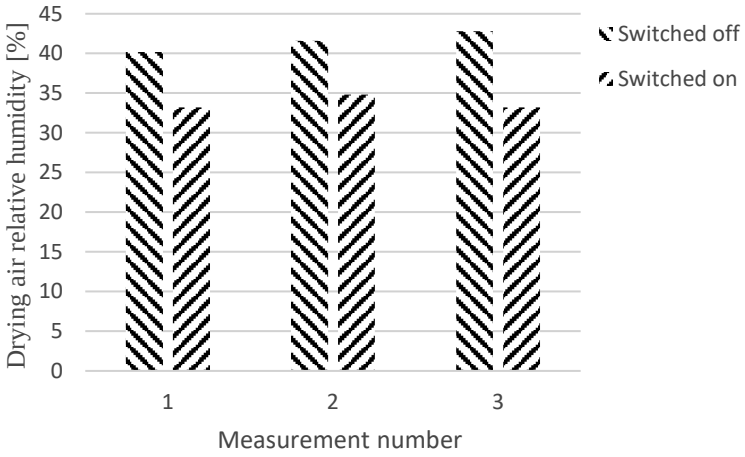

Fig. 6 Drying air relative humidity measured by data loggers on the first belt with the rotor switched on and off

In his comprehensive study, *J. Münsterer (2020)*, who deals with a detailed study of hop drying in chamber and belt dryers, points out the prevention of hop failure in the first third of the first belt. It summarizes the results of many experiments showing that the intensity of drying in the first third of the first belt has the greatest effect on performance and quality retention. However, it does not mention the installation of such a device.

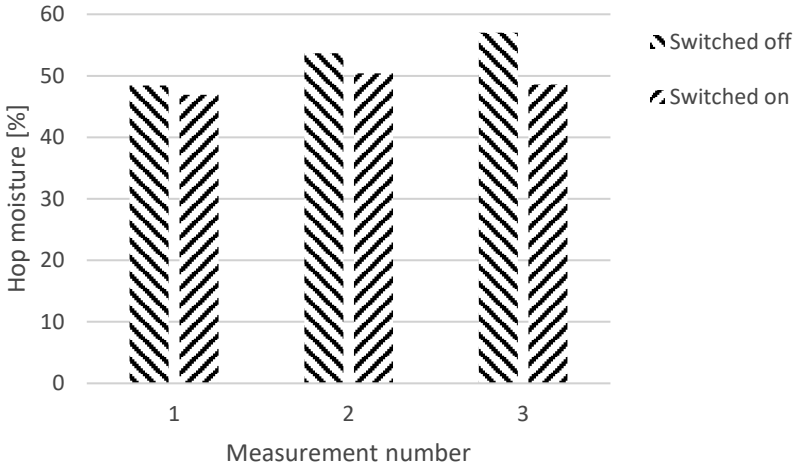

Fig. 7 Hop moisture at the end of the first belt with the rotor switched on and off

The average moisture content of hops with the rotor being switched off was 53.03 % at the end of the first belt, and 48.63 % with the rotor being switched on. If we consider the value of 53.03 to be 100 %, then the drying process will intensify by 8.30 % with the rotor switched on.
Further observations of the rotor switched on or off emerged from the company's four-year monitoring of the ELFO (Extra light fuel oil) consumption for heating the drying air (Tab. 2). The average consumption between 2011 and 2014 related to the harvest season was 486.5 $l.t^{-1}$ of dried hops without the rotor installed, and 415.5 $l.t^{-1}$ of dried hops with the rotor installed between 2015 and 2018 related to the harvest season, which implies significant fuel savings of 14.59 % when using a rotor.

Tab. 2 ELFO consumption for each year of the measurement

	Year of measurement	ELFO consumption [l]	Dried hops [t]	Average consumption [$l.t^{-1}$]
Without rotor installed	2011	21949	42.48	517
	2012	12300	30.90	398
	2013	22200	43.87	506
	2014	24100	45.90	525
With rotor installed	2015	13600	32.94	413
	2016	29369	69.47	423
	2017	28444	63.30	449
	2018	22756	60.30	377

CONCLUSIONS

The experiments carried out in the PCHB 750 hop belt dryer of Rakochmel, Co., Ltd. in Kolešovice comparing the drying process with its rotor switched on and off above the first belt show that by involving the rotor in the technological process a hop layer becomes more air-permeable and it also has a positive impact on reducing the drying air relative humidity at almost identical temperature. Tab. 1 and the graphs in Fig. 6 and Fig. 7 depict the measurement results in the harvest season of 2018. The graph in Fig. 6 shows the average measurement data obtained by means of three data loggers. The graph in

Fig. 7 shows the hop cone moisture content detected by means of Mettler-Toledo HE43 moisture analyser. Both graphs clearly illustrate a decrease in both moisture contents when the rotor was switched on. The hop moisture decreased by 8.30 % with the rotor switched on. The variability of results, however, may be influenced by the variable moisture of the hops entering the dryer. In case of these measurements this moisture content was relatively steadied (75±2 %), but not necessarily always. Therefore, it will be appropriate to carry out repeated measurements in the following harvesting seasons. However, the inclusion of a rotor had a significant positive impact on the long-term monitoring of fuel consumption. Between 2011 and 2014, the total fuel consumption without using the rotor was 80,549 l of ELFO for drying 163.15 t of hops. This implies that the average consumption of ELFO was 493.7 $l.t^{-1}$ of dried hops. Between 2015 and 2018, the total fuel consumption using the rotor was 94,169 l ELFO for drying 226.01 t of hops, giving the average consumption of ELFO 416.7 $l.t^{-1}$ of dried hops. Four years of the rotor operation generate fuel savings of 15.6 %.

ACKNOWLEDGEMENT
This paper was created with the contribution of the Czech Ministry of Agriculture as a part of NAZV n° QJ1510004 research project. In the project solution, besides CULS Prague, are involved: Hop Research Institute Co., Ltd. in Žatec, Chmelařství, cooperative Žatec, Agrospol Velká Bystřice Co., Ltd. and Rakochmel, Co., Ltd. in Kolešovice.

REFERENCES

1. Forster, A., & Gahr, A. (2013). On the fate of Certain Hop Substances during Dry Hopping. *Brewing Science, July/August, 66,* 2-22.
2. Henderson, S. M., & Miller, G. E. (1972). Hop Drying-Unique Problems and Some Solutions. *J. Agric. Engng Res., 17,* 281-287.
3. Heřmánek, P., Rybka, A., & Honzík, I. (2018). Determination of moisture ratio in parts of the hopcone during the drying proces in belt dryer. *Agronomy Research, 16 (3),* 723-727.
4. Jech, J., Artim, J., Angelovičová, M., Angelovič, M., Bernášek, K., Honzík, I., Kvíz, Z., Mareček,J., Krčálová, E., Polák, P., Poničan, J., Rybka, A., Ružbarský, J., Sloboda, A., Sosnowski, S.,Sypula, M., & Žitňák, M. (2011). Machines for Crop Production 3 (Stroje pre rastlinnú výrobu 3).*Profi Press s.r.o., Prague,* pp. 368.
5. Krofta, K. (2008). Evaluation of hop quality (Hodnocení kvality chmele). *Hop Research Institute Co. Ltd., Žatec,* pp. 50.
6. Mitter, W., & Cocuzza, S. (2013). Dry hopping - a study of various parameters. *Brewing and Beverage Industry International, 4,* 70-74.
7. Münsterer, J. (2020). Trockung und Konditionierung von Hopfen. *LFL Information. Wolnzach.* (in German).
8. Rybáček, V., Fric, V., Havel, J., Libich, V., Kříž, J., Makovec, K., Petrlík, Z., Sachl, J., Srp, A., Šnobl, J., & Vančura, M. (1980). Hop production. (Chmelařství). *SZN Prague,* pp. 426.
9. Rybka, A., Heřmánek, P., Honzík, I., Hoffmann, D., & Krofta, K. (2016). Analysis of the technological process of hop drying in belt dryers. *6th International Conference on Trends in Agricultural Engineering 2016, II,* Prague, Czech Republic, 557-563.
10. Rybka, A., Krofta, K., Heřmánek, P., Honzík, I., & Pokorný, J. (2018). Effect of drying temperature on the content and composition of hop oils. *Plant, Soil and Environment, 64 (10),* 512-516.

Corresponding author:
Asc. Prof. Ing. Adolf Rybka, CSc., Department of Agricultural Machines, Faculty of Engineering, Czech University of Life Sciences Prague, Kamýcká 129, Praha 6, Prague, 16521, Czech Republic, phone: +420 22438 3121, e-mail: rybka@tf.czu.cz

SPECTRAL INDICES AS A TOOL FOR HOP GROWTH EVALUATION

Jana SEIDLOVÁ[1], Pavel PROCHÁZKA[2], Jitka KUMHÁLOVÁ[1]

[1]Department of Vehicles and Ground Transport, Faculty of Engineering, Czech University of Life Sciences Prague, Czech Republic
[2]Department of Agroecology and Crop Production, Faculty of Agrobiology, food and Natural Resources, Czech University of Life Sciences Prague, Czech Republic

Abstract
The use of unmanned aerial vehicles (UAV) to monitor crop growth is nowadays a common non-invasive way how to obtain information on the current state of crops. Spectral indices derived from multispectral images obtained in the right growth stage can then serve as a good data source for agro-technical interventions and yield estimation. Hop belongs among the crops where it is possible to scan the individual growth parameters very exactly. In the year 2021, significant precipitation amounts were recorded during the growing season, when it turned out that UAVs are a very powerful tool for determining the quality of production or quantification of vegetation damage compared to the previous year (2020). It was found that the common spectral indices were possible to use for calculation leaf area, structure, vigor and chlorophyll content of hop gardens.

Key words: *unmanned aerial vehicles; geoinformatics; crop stress; vegetation parameters.*

INTRODUCTION

Monitoring of the growing process, gathering information and collecting data about the plants belongs to one of the main tasks of agronomy (*Yang et al., 2015*). The variability of plants reflects the characteristics of different varieties and abiotic as well as biotic factors occurring annually, e.g. weather conditions, temperature and relative humidity; or seasonally, e.g. diseases, irrigation systems malfunctions or weather events (*Bégue et al., 2008*). The ground-based monitoring can collect data with very high accuracy, but it is limited due to high workload and the time requirements (*Kumhálová & Matějková, 2017*). For this reason, for collecting these data, remote sensing has become a very popular technique (*Comba et al., 2018*). Among benefits of remote sensing use belongs continuous scanning during the whole vegetation season and time series collection to capture the growth phases (*Domínguez et al., 2015*), make current images during short time or in one moment. The data could help to analyse the crops growth process and the growth conditions (*Yang et al., 2015*). The remote sensing became a resource for acquiring agronomical data thanks to its affordability in compare with on-ground platforms of measuring and its sensing efficiency (*Andújar et al., 2019*).
Hop belongs to marginal crops with regards to its growing area, but its cultivation is efficient, in addition, hops play a very important role in the world and especially in the Czech brewing industry. For this reason, Czech hop is an important export crop (*Rybáček, 1991*). Plants observation and counts in early stages of growth are very valuable for the hop growers because they still have time to replant the plants. The camera-based observation is also important for the determination of the plant volume and the yield of hops. The important aspect is how to identify the green object, the usual method is to use the spectral indices (*Guijarro et al., 2011*).
One of them spectral indices Normalised Difference Vegetation Index NDVI (*Rouse et al., 1974*) is often stated as reliable estimator of crop health and structure. This spectral index belongs among according to the scientific literature the most used for crop condition estimation as well (*Khan et al., 2018*). For example, *Pádua et al. (2019)* created a vitality map based on NDVI values with the aim to analyse vineyards vegetation during the whole growing season.
Another is Green Normalized Difference Vegetation Index GNDVI (*Gitelson & Merzlyak, 1996*). This spectral index is an indicator of the photosynthetic activity of the vegetation and is most used for multispectral data which do not have an extreme red channel. Compared to the NDVI, GNDVI is more sensitive to chlorophyll concentration, it is used in assessing depressed and aged vegetation (*Candiago et al., 2015*).

Next index of them Chlorophyll Vegetation Index CVI (*Hunt et al., 2011*) has an increased sensitivity to the content of chlorophyll in the deciduous cover. CVI is used from early to mid of the crop growth cycle for a wide range of soils and sowing conditions by analysing a large synthetic data set obtained using a leaf surface reflectance model. This index uses to the concentration of chlorophyll in the leaf an effective normalization of various values obtained with the introduction of red and green colours (*Vincini et al., 2014*).
Pádua et al. (2019) used only RGB images to calculate area of vegetation (in this case vineyards) for crop growth estimation. RGB images works only with the visible part of electromagnetic spectrum, there are several RGB spectral indices for estimating the area.
One of these, Triangular Greenness Index TGI (*Hunt et al., 2013*), appears to be sensitive to the chlorophyll concentration in the green parts of plants and is able to extract green parts well from other vegetation (*Hunt et al., 2013*). This procedure seems to be effective in case of typical hop garden row structure.
The data processing for the calculation of vegetation indices has limits in the choice of threshold for the detection of green object and bare soil. These problems help to eliminate the Otsu´s method, which is based on automatic threshold selection for picture segmentation. This procedure results in a binary image that can improve the final results obtained from vegetation indices (*Otsu, 1979*). *Pádua et al. 2018* used this method for binary image extraction in vineyards, but the use of remote sensing data is challenging in hop gardens due to the row structure and plant canopies. It is the challenge to use similar methods to vineyard monitoring to derive the green vegetation of hop gardens and calculate its volume. That is why the main aims of this study were to compare the hop gardens in two following years with other meteorological condition in terms of calculating the green area of canopy and structure, vigor and chlorophyll content with the help of selected spectral indices.

MATERIALS AND METHODS

The 1.72 ha study field is located near to Kněževes village (50.1491481N, 13.6205150E), in the Czech Republic, where Premiant hop variety was grown. The monthly precipitation and temperature during the main vegetation season was measured with Agrometeorological station located near to the study site (see Table 1).

Tab. 1 Monthly precipitation and temperature measured during the main vegetation season 2020 and 2021 at study site

Year	2020				2021			
Months	May	June	July	August	May	June	July	August
Temperature (°C)	11.3	16.8	18.4	19.6	10.8	19.4	18.8	16.6
Precipitations (mm)	43.4	85.0	40.4	68.4	70.0	131.0	68.8	70.6

Premiant is a hybrid semi-late variety with a growing season of 128 to 134 days. This variety is characterized by increased demands on nitrogen fertilization as well as tolerance to lack of water during vegetation. The yield is in the range of 1.8 to 2.5 t/ha.
The hop garden was scanned in two terms – 1st July 2020 and 7th July 2021 using eBeeX fixed wing drone with built-in RTK-PPK functionality (senseFly SA, Cheseaux-Lausanne, Switzerland) equipped with MicaSense Red Edge MX camera (MicaSense, Inc. Seattle, WA, USA) consists of five spectral bands: Blue band (with central wavelength of 475 nm and 20 nm bandwidth), Green (560 nm, 20 nm), Red (668 nm, 10 nm), Red Edge (717 nm, 10 nm), NIR (840 nm, 40 nm). The flights were performed at 75 m above ground with resulting 0.06 m spatial resolution of images, and 75% longitudinal and lateral overlaps. The obtained images were pre-processed in eMotion SW with the help of postflight tool in order to refine the georeferenced. Orthophotos and spectral indices were derived in Pix4D SW during the photogrammetric procedure. Normalised Difference Vegetation Index (NDVI), Green Normalised difference Vegetation Index (GNDVI), Chlorophyll Vegetation Index (CVI), Triangular Greenness Index (TGI) (details in Table 2) were then analysed in ENVI (version 5.6.1), ArcGIS Pro (version 2.9.2) and QGIS (version 3.16.8) SWs. The data extracted from images were then analysed in Statistica (version 13.5.0.17) SW.

Tab. 2 Vegetation indices derived for hop growth evaluation

Spectral Index	Algorithm	Used for:	References
Normalized Difference Vegetation Index	$NDVI = \frac{NIR - R}{NIR + R}$	Biomass, structure, vigor	*Rouse et al. (1974)*
Green Normalized Difference Vegetation Index	$GNDVI = \frac{NIR - G}{NIR + G}$	Chlorophyll	*Gitelson et al. (1996)*
Chlorophyll Vegetation Index	$CVI = \frac{NIR}{Red\ Edge} - 1$	Chlorophyll	*Gitelson et al. (2005)*
Triangular Greenness Index	$TGI = G - 0.39 \times R - 0.61 \times B$	Chlorophyll, nitrogen, green leaves detection	*Hunt et al. (2013)*

R = red reflectance, G = green reflectance, NIR = near-infrared reflectance, Red Edge = red edge reflectance.

TGI spectral index was used for deriving binary model with the help of Otsu threshold method (*Otsu, 1979*). The resulting vector layer exactly delimited the green area of the crop, where a value of 0 meant green crop parts and a value of 1 meant bare soil or another surface. The layer of green vegetation was then smoothed in order to delete errors. The individual selected rows were bounded, and zonal statistics were calculated with the help of raster analysis and geoprocessing tools. The area and vigor of green crops in individual rows were calculated and evaluated.
In 2020 were analyzed the first ten rows from the eastern edge of the hop garden. Because in 2021 it was not possible to do in-situ analyzes of the same crop rows as in 2020 due to high precipitation totals and the subsequent flooding of part of the hop garden with water, the rows 14, 15, 20 and 21 were selected for a more detailed in-situ analysis in 2021. The UAV campaign covered the entire hop garden, regardless of the flooded parts of the hop garden (Fig. 1).

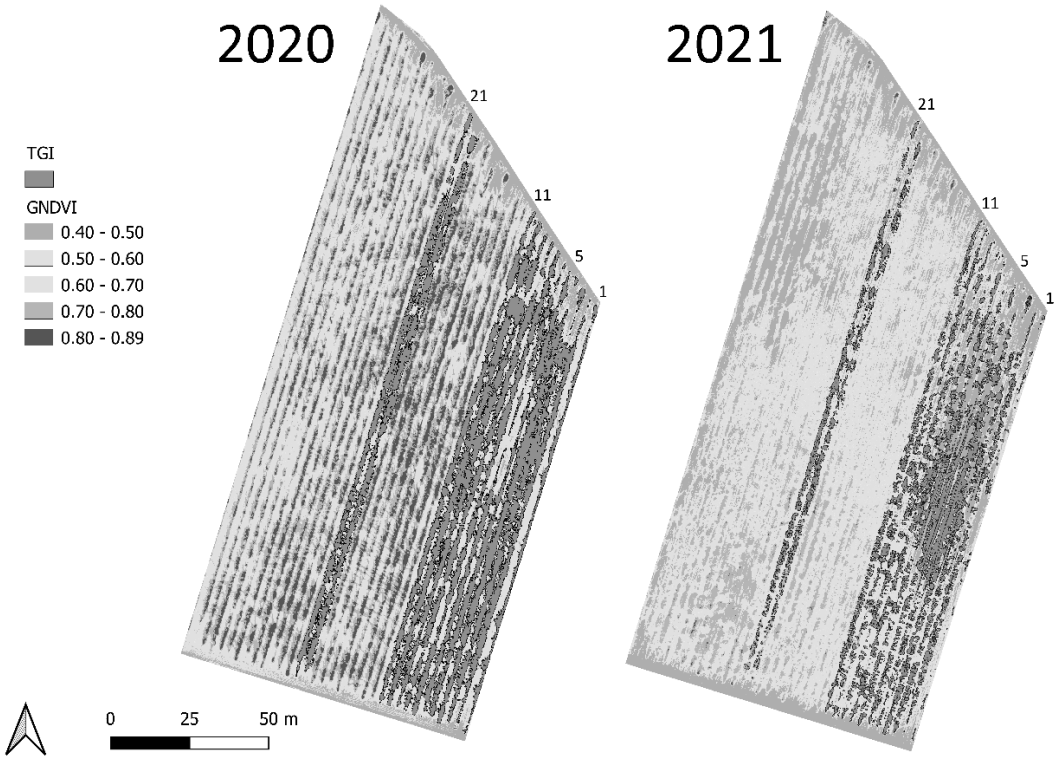

Fig.1 The difference between of the hop garden for 2020 and 2021 (GNDVI = Green Normalized Difference Vegetation Index and TGI = Triangular Greenness Index)

RESULTS AND DISCUSSION

Calculated area of green crops and selected variables (mean, standard deviation (StDev) and range) of zonal statistics for NDVI, GNDVI and CVI vegetation indices in individual rows are given in Table 3 for 2020 and in Table 4 for 2021.

Tab. 3 Calculated area and spectral indices values (NDVI = Normalized Difference Vegetation Index, GNDVI = Green NDVI and CVI = Chlorophyll Vegetation Index) for selected hop rows and in average (Avg) in 2020.

Row	Area	NDVI			GNDVI			CVI		
	(m^2)	Mean	StDev	Range	Mean	StDev	Range	Mean	StDev	Range
1	113.2	0.75	0.11	0.51	0.73	0.06	0.31	1.30	0.37	2.44
2	202.8	0.79	0.10	0.52	0.76	0.05	0.32	1.57	0.40	2.55
3	238.0	0.77	0.11	0.56	0.75	0.06	0.40	1.49	0.44	2.61
4	282.6	0.79	0.11	0.52	0.77	0.06	0.32	1.63	0.47	2.63
5	208.0	0.78	0.11	0.55	0.76	0.06	0.34	1.56	0.45	2.82
6	156.4	0.76	0.12	0.52	0.75	0.06	0.33	1.51	0.46	2.43
7	220.5	0.78	0.11	0.51	0.76	0.06	0.34	1.56	0.43	2.83
8	223.9	0.78	0.11	0.51	0.76	0.06	0.33	1.59	0.45	2.55
9	249.3	0.78	0.11	0.56	0.76	0.06	0.35	1.59	0.46	3.00
10	310.4	0.80	0.11	0.53	0.77	0.06	0.35	1.69	0.48	3.15
11	243.8	0.79	0.11	0.57	0.77	0.06	0.36	1.65	0.48	3.05
20	304.9	0.79	0.10	0.55	0.76	0.06	0.36	1.61	0.46	3.18
21	293.7	0.78	0.11	0.54	0.76	0.06	0.38	1.58	0.48	3.17
Avg	435.4	0.78	0.11	0.53	0.76	0.06	0.35	1.56	0.45	2.80

Tab. 4 Calculated area (absolute values in m^2 and comparison to 2021 in %) and spectral indices values (NDVI = Normalized Difference Vegetation Index, GNDVI = Green NDVI and CVI = Chlorophyll Vegetation Index) for selected hop rows and in average (Avg) in 2021.

Row	Area	Area to 2021	NDVI			GNDVI			CVI		
	(m^2)	(%)	Mean	StDev	Range	Mean	StDev	Range	Mean	StDev	Range
1	18.5	16.3	0.76	0.12	0.51	0.63	0.10	0.46	1.05	0.47	2.32
2	113.8	56.1	0.80	0.07	0.55	0.65	0.06	0.51	1.00	0.30	2.26
3	119.1	50.0	0.76	0.10	0.59	0.60	0.09	0.57	0.82	0.36	3.35
4	198.6	70.3	0.73	0.13	0.67	0.58	0.11	0.55	0.73	0.37	2.66
5	146.6	70.5	0.65	0.15	0.68	0.49	0.12	0.54	0.47	0.35	2.19
6	131.4	84.0	0.69	0.14	0.62	0.52	0.12	0.56	0.56	0.34	1.99
7	153.1	69.4	0.74	0.11	0.61	0.58	0.10	0.56	0.73	0.32	2.27
8	137.3	61.3	0.76	0.09	0.56	0.60	0.08	0.51	0.77	0.25	2.05
9	118.5	47.5	0.77	0.08	0.54	0.62	0.06	0.45	0.83	0.26	2.28
10	125.0	40.3	0.80	0.07	0.49	0.65	0.05	0.41	0.97	0.30	2.46
11	147.3	60.4	0.78	0.08	0.57	0.63	0.05	0.42	0.86	0.25	1.99
20	140.1	45.9	0.78	0.10	0.54	0.65	0.07	0.45	1.00	0.37	2.68
21	157.2	53.5	0.79	0.09	0.51	0.66	0.07	0.48	1.04	0.38	2.56
Avg	131.3	55.8	0.75	0.10	0.57	0.60	0.08	0.50	0.83	0.33	2.39

The results showed that the area of the selected rows in 2021 was in average 55.8% (from 16% to 84%) smaller than in the previous year 2020 due to higher precipitation totals in 2021, which caused the subsequent flooding of the hop garden with water (details in Table 4). The green area extraction method used proved to be useful in terms of the possibility of calculating for a larger area and in case it is not possible to evaluate the vegetation in-situ. For example, *Andújar et al. (2019)* found that the use of aerial imagery techniques resulted in positive net returns, whereas the on-ground technologies needed a faster time of acquisition in order of them to be profitable.
NDVI as an indicator of vigor and structure of the canopy (*Rouse et al., 1974*) showed lower values in the year 2021 when the crop hops were damaged. On the other hand, the standard deviation was lower, and the range was higher in 2021 than in 2020.
The results of GNDVI and CVI values were contradictory in standard deviation and data range, although both indices are often used as indicators of chlorophyll content in leaves (*Meng et al., 2015*). This could be probably caused due to the use of other spectral bands in the calculation (*Lorencs et al., 2014*). While GNDVI worked with reflectance values of GREEN and NIR bands, the CVI index used the NIR and RED EDGE spectral bands. This agrees with the findings of *Segarra et al. (2022)* that Greenness sensitive indices such as CVI had different results in contrast with the biomass sensitive indices (GNDVI). Mean GNDVI value was much higher in 2020 with lower standard deviation and data range than in the year 2021. A very high difference between the mean CVI values in 2020 and 2021 confirmed the lack of chlorophyll in leaves and poorer crop vigor in 2021. On the other hand, the canopy had higher variability in 2020, when the crops were in better condition.

CONCLUSIONS

This study addressed the hop gardens in two following years with other meteorological condition. The results showed that the area of the selected rows in 2021 was in average 55.8% smaller than in the previous year 2020 due to higher precipitation totals in 2021. NDVI as an indicator of vigor and structure of the canopy showed lower values in the year 2021 when the crop hops were damaged. On the other hand, the standard deviation was lower, and the range was higher in 2021 than in 2020. The results of GNDVI and CVI values were contradictory in standard deviation and data range. Mean GNDVI value was much higher in 2020 with lower standard deviation and data range than in the year 2021. A very high difference between the mean CVI values in 2020 and 2021 confirmed the lack of chlorophyll in leaves and poorer crop vigor in 2021. On the other hand, the canopy had higher variability in 2020, when the crops were in better condition. The selected common spectral indices were possible to use for calculation leaf area, structure, vigor and chlorophyll content of hop gardens.

ACKNOWLEDGMENT

This study was supported by IGA – Geoinformatics as a tool for optimization and efficiency of production and operational processes in Agriculture 4.0.

REFERENCES

1. Andújar, D., Moreno, H., Bengochea-Guevara, J., de Castro, A., & Ribeiro, A. (2019). Aerial imagery or on-ground detection? An economic analysis for vineyard crops. *Computers and Electronics in Agriculture*, 157, 351-358.
2. Bégue, A., Todoroff, P., & Pater, J. (2008). Multi-time scale analysis of sugarcane within-field variability: improved crop diagnosis using satellite time series? *Precision Agriculture*, 9(3), 161-171.
3. Candiago, S., Remondino, F., De Giglio, M., Dubbini, M., & Gattelli, M. (2015). Evaluating multispectral images and vegetation indices for precision farming applications from UAV images. *Remote sensing*, 7(4), 4026-4047.
4. Comba, L., Biglia, A., Aimonino, D. R., & Gay, P. (2018). Unsupervised detection of vineyards by 3D point-cloud UAV photogrammetry for precision agriculture. *Computers and Electronics in Agriculture*, 155, 84-95.
5. Domínguez, J. A., Kumhálová, J., & Novák, P. (2015). Winter oilseed rape and winter wheat growth prediction using remote sensing

methods. *Plant, Soil and Environment*, 61(9), 410-416.
6. Gitelson, A. A., Vin˜a, A., Ciganda, V., Rundquist, D. C., Arkebauer, T. J. (2005). Remote estimation of canopy chlorophyll content in crops. *Geophysical Research Letters 32*, L08403.
7. Gitelson, A. A., Kaufman, Y, J., & Merzlyak, M. N. (1996). Use of a green channel in remote sensing of global vegetation from EOS-MODIS. *Remote Sensing of Environment*, *58*(3), 289-298.
8. Guijarro, M., Pajares, G., Riomoros, I., Herrera, P. J., Burgos-Artizzu, X. P., & Ribeiro, A. (2011). Automatic segmentation of relevant textures in agricultural images. *Computers and Electronics in Agriculture*, 75(1), 75-83.
9. Hunt, E. R., Doraiswamy, P. C., McMurtrey, J. E., Daughtry, C. S. T., Perry, E. M., & Akhmedov, B. (2013). A Visible Band Index for Remote Sensing Leaf Chlorophyll Content at the Canopy Scale. *International Journal of Applied Earth Observation and Geoinformation*, 21, 103-112.
10. Hunt, E. R., Daughtry, C. S. T., Eitel, J. U., & Long, D. S. (2011). Remote sensing leaf chlorophyll content using a visible band index. *Soil Fertility & Crop Nutrition*, 103(4), 1090-1099.
11. Khan, Z., Rahimi-Eichi, V., Haefele, S., Garnett, T., & Miklavcic, S. J. (2018). Estimation of vegetation indices for high-throughput phenotyping of wheat using aerial imaging. *Plant methods*, 14(1), 1-11.
12. Kumhálová, J. & Matějková, Š. (2017). Yield variability prediction by remote sensing sensors with different spatial resolution. *International Agrophysics*, 31, 195-202.
13. Lorencs, A., Mednieks, I., & Sinica-Sinavskis, J. (2014). Simplified classification of multispectral image fragments. *Elektronika ir Elektrotechnika*, 20(6), 136-139.
14. Meng, J., Xu, J., & You, X. (2015). Optimizing soybean harvest date using HJ-1 satellite imagery. *Precision Agriculture*, 16(2), 164-179.
15. Otsu, N. (1979). A Threshold Selection Method from Gray-Level Histograms. *IEEE Transactions on Systems, Man, and Cybernetics*, 9(1), 62-66.
16. Pádua, L., Marques, P., Adão, T., Guimarães, N., Sousa, A., Peres, E., & Sousa, J. J. (2019). Vineyard variability analysis through UAV-based vigour maps to assess climate change impacts. *Agronomy*, 9(10), 581.
17. Rouse, J. W., Haas, R. H., Schell, J. A., & Deering, D. W. (1974). Monitoring vegetation systems in the Great Plains with ERTS. In: Freden, S. C., Mercanti, E. P., Becker, M. (Eds.), Third Earth Resources Technology Satellite-1 Symposium, Vol. 1: Technical Presentations, NASA SP-351. National Aeronautics and Space Administration, Washington, DC, pp. 309-317.
18. Rybáček, V. (1991). Hop production. Elsevier.
19. Segarra, J., Araus, J. L., & Kefauver, S. C. (2022). Farming and Earth Observation: Sentinel-2 data to estimate within-field wheat grain yield. *International Journal of Applied Earth Observation and Geoinformation*, 107, 102697.
20. Vincini, M., Amaducci, S., & Frazzi, E. (2014). Empirical Estimation of Leaf Chlorophyll Density in Winter Wheat Canopies Using Sentinel-2 Spectral Resolution. *IEEE Transactions on Geoscience and Remote Sensing*, 52, 6, 3220-3235.
21. Yang, W., Wang, S., Zhao, X., Zhang, J., & Feng, J. (2015). Greenness identification based on HSV decision tree. *Information Processing in Agriculture*, 2(3-4), 149-160.
22. Zhang, J., Tian, H., Wang, D., Li, H., & Mouazen, A. M. (2021). A novel spectral index for estimation of relative chlorophyll content of sugar beet. *Computers and Electronics in Agriculture*, 184, 106088.

Corresponding author:
Ing. Jana SEIDLOVÁ, Department of Vehicles and Ground Transport, Faculty of Engineering, Czech University of Life Sciences Prague, Kamýcká 129, Praha 6, Prague, 16521, Czech Republic, phone: +420 733 360 060, e-mail: seidlova@tf.czu.cz

APPLICATION OF ARTIFICIAL NEURAL NETWORK IN PREDICTING THE DRYING KINETICS AND CHEMICAL ATTRIBUTES OF LINDEN (TILIA PLATYPHYLLOS SCOP.) DURING THE INFRA-RED DRYING PROCESS

Kemal Çağatay SELVI[1], Alfadhl Yahya KHALED[2], Taner YILDIZ[1]

[1]*Department of Agricultural Machinery and Technologies Engineering, Faculty of Agriculture, University of Ondokuz Mayıs-Samsun/Turkey*
[2]*Department of Horticulture, College of Agricultural & Life Sciences, University of Wisconsin – Madison, Madison, WI, USA*

Abstract
This study investigates the potential of applying artificial neural networks (ANNs) to describe the drying kinetics of linden leave samples during infra-red drying (IRD) under different drying temperatures of 50˚C, 60˚C and 70˚C and samples thickness (0.210, 0.220, and 0.230). Kinetic models were developed using selected thin layer models, and ANN methods. The statistical indicators of the coefficient of determination (R^2), and root mean square error (RMSE) were used to evaluate the suitability of the models. The effective moisture diffusivity varied between 4.13 x 10^{-12} m^2/s and 5.89 x 10^{-12} m^2/s and the activation energy was 16.339 kJ/mol. The thin-layer models illustrated that all used models (Page, Midilli et al., Henderson and Pabis, Logarithmic, and Newton models) can adequately describe the drying kinetics of linden leave samples with R^2 values (> 0.9900) and lowest RMSE (<0.0200). The ANN model showed R^2 and RMSE values of 0.9986, and 0.0210, respectively. Also, the ANN model shows the significant prediction for the linden chemical attributes for Total phenolics content (TPC), Total flavonoids assay (TFA), DPPH, and FRAP of R^2 and RMSE values of 0.9975, 2.6100, 0.9891, 0.1346, 0.9980, 2.9317, 0.9845, and 0.9808, respectively.

Key words: *linden leaves, infrared drying, artificial neural network model; total phenolic content; total flavonoid, DPPH, FRAP content.*

INTRODUCTION

Linden (Tilia platyphyllos Scop.) is a medicinal plant with a pleasant taste in its tea which has several dozen different species and varieties *(Chmielewska & Sadowska, 2010).* It is rich in polyphenols and presents high antioxidant activity against DPPH radicals *(Wissam, Nour, Bushra, Zein &Saleh, 2017; Siger, Antkowiak, Dwiecki, Rokosik & Rudzińska, 2021).* The high agricultural value of linden in terms of many valuable elements it contains is emphasized in many articles *(Yıldırım, Mavi, Oktay, Kara, Algur & Bilaloğlu, 2000; Buřičová & Reblova 2008; Kowalski 2017; Kelmendi, Mustafa, Zahiri, Nebija & Hajdari, 2020).*

The drying of agricultural products causes the enzymatic reactions to be inactivated as a result of heat and mass transfer leading to a reduction of the moisture content inside the product *(Rodríguez, Clemente, Sanjuan & Bon, 2013).* Drying methods such as hot-air drying (HAD), infrared drying (IRD), vacuum drying (VD), and microwave drying (MWD) have been used in drying agricultural crops *(Onwude, Hashim, Abdan, Janius & Chen, 2018; Si, Wu, Yi, Li, Chen, Bi & Zhou, 2015; Tekin & Baslar, 2018).* Amongst these drying methods, the IRD is the most common commercially used drying method as they provide a more uniform dried product, naturally harmless and nontoxic *(Onwude, Hashim, Janius, Nawi & Abdan, 2016).*

IRD radiation had been implemented in food processing, reducing energy consumption and time spent in the process, securing and ensuring the quality of foodstuffs processed**.** There are some studies, related to the IRD process, reported in the literature on mint *(Ertekin & Heybeli, 2014)*, pepper *(Soysal, Keskin, Arslan & Sekerli, 2018)*, and kiwifruit slices *(Doymaz, 2018).* Computational intelligence tools such as artificial neural networks (ANN) are considered complex tools for complex systems and dynamic modeling *(Khaled, Aziz, Bejo, Nawi & Abu Seman, 2018).* The application of ANN offers many advantages compared to conventional modeling techniques due to the learning ability, improved flexibility, online non-destructive measurements, reduced assumptions, suitability to the non-linear process, and tolerance

of incomplete data (*Bai et al., 2018*). For instance, ANN is inspired by the biological neural system as a useful statistical tool for nonparametric regression *(Khaled, Aziz, Bejo, Nawi & Abu Seman, 2018).* The objectives of this study are to investigate the drying characteristics of linden leave samples at different temperatures (50˚C, 60˚C, and 70˚C) using IRD, to evaluate the likelihood of applying ANN modeling as a non-destructive technique in describing the drying behavior of linden leave samples under different drying conditions and to compare the results with mathematical thin-layer models.

MATERIALS AND METHODS

Samples preparation

Linden leaves (T. platyphyllos Scop.) were collected from the campus area of Ondokuz Mayıs University under open-air conditions located in the Samsun city coastline, Black Sea region, Turkey.

Drying experiments

The IRD technique was carried out using a laboratory-scale drying unit (Radwag balances and scales, Warsaw, Poland). This device has transmitting electromagnetic radiation in the range of medium to shortwave IR (radiator). The linden leave samples were dried at three temperatures (50˚C, 60˚C, and 70˚C). During drying, the amount of evaporating water was designated in about 3-min intervals at each drying temperature. Trials were replicated three times and average weight loss was reported.

Drying kinetics

The variation in moisture content during the IRD technique was expressed in the form of moisture ratio (dimensionless) as described in Equation 1.

$$MR = \frac{(M_t - M_e)}{(M_o - M_e)} \quad (1)$$

where M_t, M_e and M_o are the moisture content of the samples at time t, equilibrium moisture content and initial moisture content, respectively. According to *Aghbashlo et al. (2009)* M_e values did not change because they were relatively low compared to M_t and M_o values, resulting in negligible error during simplification, thus in this study, the moisture ratio was expressed as shown in Equation 2:

$$MR = \frac{M_t}{M_o} \quad (2)$$

Effective moisture diffusivity and activation energy

Fick's diffusion equation as a dimensional approach was applied due to its simplicity to describe the mass transfer of drying samples. The effective moisture diffusivity of samples for IRD was estimated using Crank's solution of Fick's diffusion equation as described in Equation 3 (*Erbay and Icier, 2010*).

$$\frac{\partial M_t}{\partial t} = \nabla . \ (D_{eff} \nabla M_t) \quad (3)$$

Assuming constant diffusion and uniform initial moisture distribution, the Crank's solution for cylindrical shaped sample is shown in Equation 4.

$$MR = \frac{8}{\pi^2} \sum_{n=1}^{\infty} \frac{1}{(2n+1)^2} \exp\left(-\frac{(2n+1)^2 D_{eff}\, t}{r^2}\right) \quad (4)$$

where D_{eff} is the effective moisture diffusivity (m^2/s), *r* is the radius of the sample (m), *n* is the positive integer, and *t* is the drying time (s). For the sake of mathematical simplicity, Equation 4 was restricted to the first term, resulting in Equation 5:

$$MR = \frac{8}{\pi^2} \exp\left(-\frac{\pi^2 D_{eff}\, t}{r^2}\right) \quad (5)$$

The activation energies for IRD were calculated from the relationship between effective moisture diffusivity and the average temperature of the samples based on the Arrhenius equation as shown in equation (6).

$$D_{eff} = D_o \exp\left(-\frac{E_a}{R(T + 273.15)}\right) \quad 6)$$

where, D_o is the pre-exponential factor, E_a is the activation energy (kJ/mol), *R* is the universal gas constant (8.3143 × 10-3 kJ/mol) and *T* is the average temperature of the sample (K). The values of E_a for

IRD method for different linden leave thickness levels were measured from the resulting slope values by plotting the fitting curve between *lnD* and *1/(T + 273.15)* (Equation 7).

$$\text{Slope} = -\frac{E_a}{R} \quad (7)$$

Mathematical thin-layer modelling

The selected mathematical models namely: Page, Midilli et al., Henderson and Pabis, Logarithmic, and Newton model as listed in Table 1. The mathematical models applied based on non-linear least squares regression analysis using Sigma plot software (Version12.0, Systat Software Inc., California, USA). The application of these models gives better prediction with fewer assumptions (*Khaled, Kabutey, Selvi, Mizera, Hrabe & Herak, 2020*).

Tab. 1 Mathematical thin-layer drying models.

Model no.	Model name	Model expression
1.	Page model	MR = exp(-ktn)
2.	Midilli et al. model	MR=aexp(-kt)+bt
3.	Henderson and Pabis model	MR = *a* exp (-*k*t)
4.	Logarithmic model	MR = *a* exp (−*k*t) +*c*
5.	Newton model	MR = exp (−*k*t)

Artificial neural network

The structure of a neural network is in the form of interconnected layers. *Haykin (1999)* divided an ANN into 3 clusters of structures based on their connection called: (1) single layer feed-forward network, (2) the multi-layer feed-forward network, and (3) the recurrent network. A back-propagation algorithm was applied in the training of the model and sigmoid function was used in all cases as illustrated in Equation 8.

$$f(x) = \frac{1}{1 + e^{-x}} \quad (8)$$

The datasets were prepared by randomly dividing the data into training and testing datasets of 70%, 30%, respectively. The chosen hidden layer architectures were [3], [6], [9], [3, 3], [6, 6], [9, 9], [3, 3, 3], [6, 6, 6] and [9, 9, 9] matrix, where for example, [3, 3] and [3, 3, 3], represents the 2 and 3 hidden layers with 6 and 9 neurons each (Figure 1). The software (Weka 3.6, Hamilton, New Zealand) was used to analyze the ANN model.

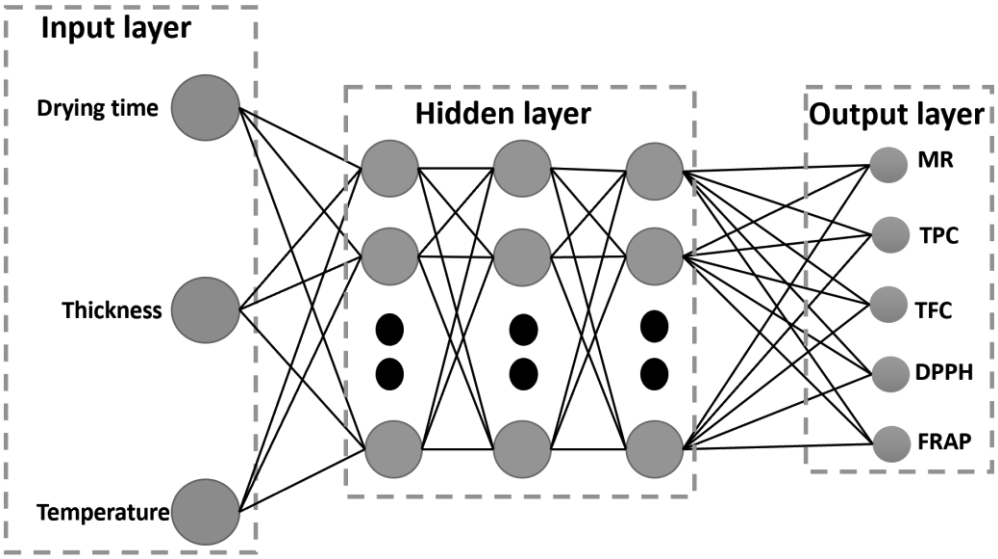

Fig. 1 Artificial Neural networks topology applied for this study

Extract preparation of the chemical characteristics

The powdered sample was extracted with methanol/distilled water (80:20, v/v) for 12 hours at room temperature by the maceration method, and centrifuged for 20 min. The supernatant was used for the estimation of antioxidants and antioxidant activity. The total phenolic content (TPC) was determined by applying the Folin-Ciocalteu method (*Singleton and Rossi, 1965*). For the total flavonoids content (TFC) was measured using an $AlCl_3$ colorimetric assay according to *Gao et al. (2014)*.

Free radical scavenging activity was measured using the stable DPPH free radical, according to the method described by *Brand-Williams et al. (1995)*. The scavenging activity on the DPPH free radical was compared with that of the Trolox, a water-soluble vitamin E analog. Results were expressed in mmol Trolox equivalents (TE)/g of powder. The ferric reducing/antioxidant power (FRAP) assay was conducted according to *Benzie and Strain (1996)*.

Statistical analysis for mean comparison

Statistical analysis was performed using the Statistical Analysis System software (SAS version 9.2, Institute, Inc., Cary, N.C.). ANOVA at 5% level of significance and 95% confidence interval was performed using the Duncan test to compare the mean significant differences between different drying time intervals at the IRD technique. These statistical indicators are the coefficient of determination (R^2) and root mean square error (RMSE). They are computed mathematically as highlighted in Equations 9 and 10:

$$R^2 = 1 - \frac{\sum_{i=1}^{N}(V_{pred} - V_{exp})^2}{\sum_{i=1}^{N}(V_{pred} - V_m)^2} \quad (9)$$

$$RMSE = \sqrt{\frac{\sum_{i=1}^{N}(V_{pred} - V_{exp})^2}{N}} \quad (10)$$

where V_{pred} is the predicted value, V_{exp} is the actual observation from experimental data, V_m is the mean of the actual observation, and N is number of observations.

RESULTS AND DISCUSSION

Drying process behavior

The variations of moisture ratio with time for the IRD technique at different temperatures (50˚C, 60˚C, and 70˚C) is presented in Figure 2. According to Figure 2, the moisture ratio values of 0.20 and 0.42 were determined at a drying time of 10 min and at temperatures of 60˚C and 70˚C. At a drying time of 37 min was found the moisture ratio of 0.20 at 50˚C. Also, results showed that higher drying temperature resulted in a greater slope and the drying time is reduced by about 250%. The results are in agreement with other researchers on the drying behavior of various varieties of materials (*Ayadi, Ben Mabrouk, Zouari, Bellagi, 2014; Khaled, Kabutey, Selvi, Mizera, Hrabe & Herak, 2020*).

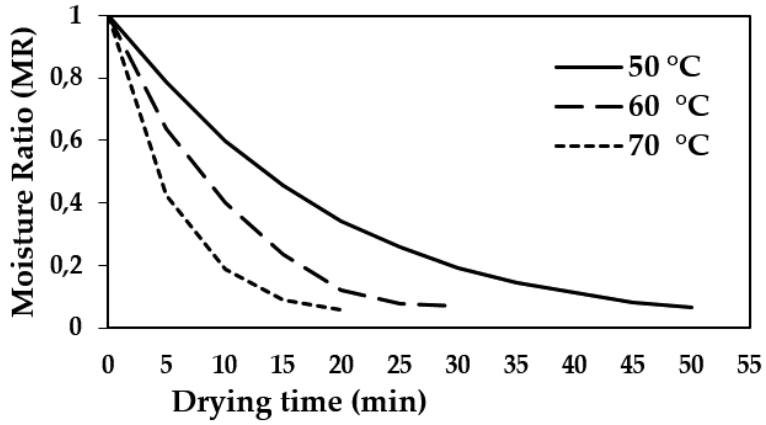

Fig. 2 Drying characteristics of linden leave samples

Effective moisture diffusivity and activation energy

The values of the D_{eff} are presented in Table 2. The D_{eff} values were varied between the range of 4.13 x 10^{-12} m^2/s and 5.89 x 10^{-12} m^2/s. The values of D_{eff} obtained in this study were within the general range of 10^{-6} to10^{-12} m^2/s for drying of food materials. The values of D_{eff} are comparable with previous works for strawberry drying (2.40-12.1 x 10^{-9} m^2/s), apple drying (2.27-4.97 x 10^{-10} m^2/s), persimmon slices (1.330-9.221 x 10^{-9} m^2/s) and pumpkin drying (1.19-4.27 x 10^{-9} m^2/s) (*Xiao, Pang, Wang, Bai, Yang & Gao, 2010; Abbaspour-Gilandeh, Jahanbakhshi & Kaveh, 2020; Sacilik & Elicin, 2006*).

On the other hand, the diffusivity constant in other words "pre-exponential factor" of the Arrhenius equation (D_0) was predicted as 1.746×10^{-9} m^2/s for linden leaves. The activation energy (E_a) of linden leave samples was calculated from the values of effective moisture diffusivity. The relationship between E_a and D_{eff} was described by an Arrhenius-type equation (Equation 6). The values of activation energy were obtained by plotting *ln(Deff)* versus 1/(T+273.15) for the IRD method (Figure 3).

Tab. 2 Values for *Deff* and E_a of linden leave samples during IRD technique.

Drying Temperature (˚C)	D_{eff} (m^2/s)	D_0 (m^2/s)	E_a (kJ/mol)
50	4.13 x 10^{-12}		
60	4.47 x 10^{-12}	1.746 x 10^{-9}	16.339
70	5.89 x 10^{-12}		

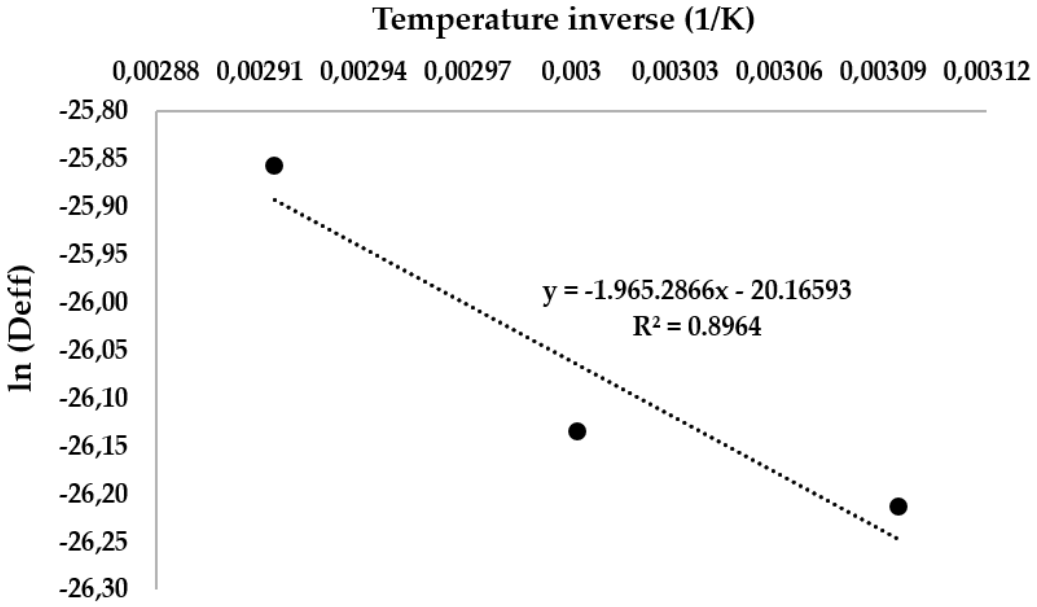

Fig. 3 Arrhenius-type relationship of E_a versus temperature for IRD method

A Comparison between mathematical thin-layer models

The mathematical thin-layer models were applied to describe the drying kinetics of linden leave samples during the IRD method. Table 3 shows the selected mathematical models that fitted the experimental moisture content data in relation to the sample.

Tab. 3 Statistical evaluation of the mathematical drying models for linden leaves samples of IRD

Drying Temperature (˚C)	Model no	Model parameters	R^2	RMSE
50	1	k= 0.0472, n= 1.0381,	0.9992	0.0090
	2	k= 0.0413, n= 1.0933, a= 0.9998, b= 0.0003	0.9999	0.0025
	3	a= 1.0128, k= 0.0538	0.9990	0.0098

	4	a= 1.0096, k= 0.0547, c= 0.0053	0.9991	0.0099
	5	k= 0.0532	0.9988	0.0104
60	1	k= 0.0955, n= 0.9915	0.9935	0.0257
	2	k= 0.0716, n= 1.1305, a= 0.9984, b= 0.0009	0.9992	0.0102
	3	a= 1.0032, k= 0.0937	0.9935	0.0256
	4	a= 0.9844, k= 0.1028, c= 0.0286	0.9969	0.0188
	5	k= 0.0934	0.9935	0.0245
70	1	k= 0.2584, n= 0.7815	0.9931	0.0269
	2	k= 0.1300, n= 1.1340, a= 0.9914, b= 0.0013	0.9984	0.0152
	3	a= 0.9935, k= 0.1625	0.9896	0.0330
	4	a= 0.9611, k= 0.1866, c= 0.0405	0.9998	0.0055
	5	k= 0.1635	0.9896	0.0312

Results of artificial neural network

Time, temperature, and linden leave thickness levels were used to predict moisture ratio using the ANN model at IRD technique. Tables 4 show the statistical results related to training and validation of the multilayer feed-forward network structure of samples drying experimental data for the IRD method.

Tab. 4 Statistical results of drying kinetics of linden leaves samp. for the ANN model using IRD

No. hidden layer	No. Neurons	Training		Testing	
		R^2	RMSE	R^2	RMSE
1	3	0.9620	0.0654	0.9978	0.0152
1	6	0.9602	0.0666	0.9943	0.0194
1	9	0.9717	0.0566	0.9866	0.0302
2	3,3	0.9549	0.0706	0.9974	0.0132
2	6,6	0.9769	0.0546	0.9986	0.0210
2	9,9	0.9743	0.0568	0.9974	0.0327
3	3,3,3	0.9424	0.0795	0.9962	0.0215
3	6,6,6	0.9672	0.0616	0.9971	0.0163
3	9,9,9	0.9704	0.0587	0.9961	0.0412

Comparison between artifitial neuron networks and mathematical thin-layer models

The highest results obtained from the computational intelligence (ANN) and the top two mathematical thin-layer (page, Midilli et al, and Logarithmic) models of prediction moisture ratio is summarized in Table 5. The best results found by applying ANN in the case of IRD method were R^2 of 0.9986 and RMSE of 0.0210 at 2 hidden layers with 12 neurons.

Tab. 5 Statistical results of drying kinetics of linden leave samples for artificial neural networks and mathematical thin-layer models using IRD

Model		R^2	RMSE
Computational intelligence	ANN	0.9986	0.0210
Mathematical model	Logarithmic	0.9998	0.0055
	differences	0.9992	0.0090
	Midilli et al.	0.9999	0.0025

Total Phenolic Content (TPC) and Flavonoids (TFC)

The results are given by calculating dry matter values to prevent errors arising from dry matter difference. The total phenolic content (TPC) of fresh leaves material was significantly ($p < 0.05$) higher than dried leaves. Table 6 presents the TPC and TFC content of the linden leaves under different temperatures process.

Tab. 6 Total phenolic and flavonoid content of the fresh and dried linden leaves.

Temperature (˚C)	TPC (mg/g, DW)	TFC (mg/g, DW)
Fresh	12.773 ± 0.76 b	0.567 ± 0.015 b
50	95.184 ± 0.47 a	2.790 ± 0.150 a
60	99.756 ± 0.63 a	2.631 ± 0.084 a
70	99.756 ± 0.63 a	2.583 ± 0.145 a
Significance	<0.001	<0.001

The total phenolic content (TPC), total flavonoid content (TFC), a, b: Different letters within same column shows the statistical difference ($p < 0.01$).

To analyze the data, a non-parametric permutation test was used because of heteroscedasticity. TPC and TFC values were corrected and evaluated based on dry matter values to prevent errors arising from dry matter differences. Table 6 shows that the TPC of linden leaves was significantly different between fresh and dried samples and the values ranged from 99.756 ± 0.63 mg/g to 127.73 ± 0.76 mg/g. The TPC in the dried leaves (for 50 ◦C, 60 ◦C, 70 ◦C) was significantly ($p<0.001$) lower than that in the fresh.
On the other hand, as can be seen in Table 6, the Duncan test indicates no statistical difference among temperatures (50 ◦C, 60 ◦C, and 70 ◦C). This means that linden leaves seem to be thermostable in the studied temperature range.
The TFC in linden leaves is shown in Table 5; it varied significantly between fresh and dried samples and ranged from 0.567 ± 0.015 mg/g to 2.790 ± 0.150 mg/g. The reason for this may be the decrease of the solution viscosity due to the increase in temperature as the lime leaves change from a wet state to a dry state, and the increase of solubility, accordingly. In this study, depending on the type of flavonoids and the number of substituents, there could be no change in the flavonoid contents. In addition, the TFC results obtained in the present study correlated with Olsson et al.
This finding suggests that besides the Midilli drying model, a simpler Page model can also be preferred for linden leaves under an IR thin layer drying process. In addition, 50 ◦C will be sufficient in terms of phenol content and flavonoid content in a thin layer lime leaf drying process with IR.

Results of artificial neuron networks to predict chemical properties of linden leave samples

Temperature and linden leave thickness levels were used to predict total phenolics (mg/g, DW), Total flavonoids (mg/g, DW), DPPH (mmol/g, DW), and FRAP (mmol/g, DW) using ANN model. Tables 7 illustrate the statistical results from the four chemical properties of the multilayer feed-forward network structure of samples drying experimental data. The ANN data set were used to assess the optimum number of neurons and hidden layers for multilayer neural network modelling for determining the best predictive power. In the case of total phenolics, total flavonoids, and FRAP, the results found that architecture with 2 hidden layers with 6 (3, 3 neurons), obtained the best results of R^2 (0.9975, 0.9891, and 0.9845) and the lowest RMSR of (2.6100, 0.1346, and 0.9808) as compared to those of 1 hidden layer (3, 6 and 9 neurons), 2 hidden layers (12, 18 neurons) and 3 hidden layers (9, 18 and 27 neurons), respectively (Table 6). While, DPPH, the highest results were found that architecture with 3 hidden layers with 18 (6, 6, 6 neurons), obtained the best results of R2 (0.9980) and the lowest RMSR of (2.9317) as compared to those of 1 hidden layer (3, 6 and 9 neurons), 2 hidden layers (6, 12, 18 neurons) and 3 hidden layers (9 and 27 neurons), respectively (Table 7).

Tab. 7 Statistical results of chemical characteristics of linden leave for the ANN model using IRD.

No. Hidden Layer	No. Neurons	Total phenolics (mg/g, DW)		Total flavonoids (mg/g, DW)		DPPH, mmol/g, DW		FRAP, mmol/g, DW	
		R^2	RMSE	R^2	RMSE	R^2	RMSE	R^2	RMSE
1	3	0.9969	2.8914	0.9884	0.1393	0.9977	3.1420	0.9816	1.0760
1	6	0.9965	3.1026	0.9882	0.1404	0.9977	3.1396	0.9824	1.0485
1	9	0.9965	3.0855	0.9877	0.1439	0.9975	3.3549	0.9839	1.0017
2	3,3	**0.9975**	2.6100	**0.9891**	0.1346	0.9978	3.0660	**0.9845**	0.9808
2	6,6	0.9974	2.6835	0.9890	0.1356	0.9978	3.0664	0.9840	0.9986
2	9,9	0.9972	2.7533	0.9888	0.1370	0.9978	3.0894	0.9833	1.0197
3	3,3,3	0.9970	2.8433	0.9881	0.1401	0.9979	3.0421	0.9826	1.0402
3	6,6,6	0.9968	2.9741	0.9876	0.1439	**0.9980**	2.9317	0.9818	1.0690
3	9,9,9	0.9965	3.0873	0.9873	0.1460	0.9979	3.0024	0.9812	1.0906

CONCLUSIONS

This study investigated the potential of using the ANN as a modeling tool for predicting the drying process and the chemical characteristics of linden leave samples. The results showed that IRD had a significant effect on the drying kinetics, moisture diffusivity, and activation energy of linden leave samples. An increase in drying temperature and sample thickness influenced the drying kinetics and moisture diffusivity of samples. The effective moisture diffusivity varied between 4.13 x 10^{-12} m^2/s and 5.89 x 10^{-12} m^2/s and the activation energy was 16.339 kJ/mol. The mathematical thin-layer modeling results showed that page, Midilli et al., and Logarithmic models can adequately ($R^2 > 0.9900$) describe the drying kinetics of linden leave samples. The highest R^2 value of 0.9986 was observed for ANN (2 hidden layers with (6, 6) neurons) model. ANN tool as a computational intelligence method produced closer results compared to mathematical thin-layer. Also, the ANN model shows the significant prediction for the linden chemical attributes for Total phenolics content (TPC), Total flavonoids assay (TFA), DPPH, and FRAP of R^2 and RMSE values of 0.9975, 2.6100, 0.9891, 0.1346, 0.9980, 2.9317, 0.9845, and 0.9808, respectively. Therefore, the ANN model can describe a wider range of experimental data whereas the application of theoretical models is limited to specific experimental conditions in most cases. Thus, ANN may be considered a suitable alternative modeling method for describing the drying behavior of linden leave samples.

A universal method for appropriate estimation of wire diameter of helical compression spring was determined. The estimation can be based only on the amount and type of load and selected wire material. This procedure can be useful when only force and deflection of spring are specified.

REFERENCES

1. Abbaspour-Gilandeh, Y., Jahanbakhshi, A., & Kaveh, M. (2020). Prediction kinetic, energy and exergy of quince under hot air dryer using ANNs and ANFIS. *J. Sci. Food Agric.*, *8*, 594–611.
2. Aghbashlo, M., Kianmehr, M.H., Khani, S., & Ghasemi, M. (2009). Mathematical modelling of thin-layer drying of carrot. *Int. Agrophys., 23,* 313–317.
3. Ayadi., M. Ben Mabrouk, S., Zouari, I., & Bellagi, A. (2014). Kinetic study of the convective drying of spearmint. *J. Saudi Soc. Agric. Sci., 13,* 1–7.
4. Bai, J., Xiao, H., Ma, H. & Zhou, C. (2018). Artificial neural network modeling of drying kinetics and color changes of ginkgo biloba seeds during microwave drying process. *J. Food Qual.*, 1–8.
5. Benzie, IFF. & Strain, JJ. (1996). The Ferric Reducing ability of plasma (FRAP) as a measure of Antioxidant power: The FRAP assay. *Analytical Biochemistry, 239 (1),*70-76.
6. Brand-Williams, W., Cuvelier., M.E. & Berset, C. (1995). Use of a free radical method to evaluate antioxidant activity. *LWT, 28*:25-30.
7. Buřičová, L. & Reblova, Z. (2008). Czech medicinal plants as possible sources of antioxidants. *Czech J. Food Sci, 26(2),* 132-138.

8. Doymaz, I. (2018). Infrared drying of kiwifruit slices. *Int. J. Green Energy, 15,* 622–628.
9. Erbay, Z. & İcier, F. (2010). A Review of Thin Layer Drying of Foods: Theory, Modeling, and Experimental Results. *Crit Rev Food Sci Nutr.* 50 (5). 441-464.
10. Ertekin, C. & Heybeli, N. (2014). Thin-layer infrared drying of mint leaves. *J. Food Process. Preserv. 38,* 1480–1490.
11. Gao, H., Cheng, N., Zhou, J., Wang, B.N., Deng, J.J. & Cao, W. (2014). Antioxidant activities and phenolic compounds of date plum persimmon (Diospyros lotus L.) fruits. *J Food Sci Technol., 51(5):*950-956.
12. Haykin, S. (1999). Neural Networks a Comprehensive Introduction; *Prentice Hall: Upper Saddle River*, NJ, USA,
13. Kelmendi, N., Mustafa, B., Zahiri, F., Nebija, D., & Hajdari, A. (2020). Essential Oil Composition of Tilia platyphyllos Scop. Collected from Different Regions of Kosovo. *Records of Natural Products, 14(5),* 371.
14. Khaled, A.Y., Aziz, S.A., Bejo, S.K., Nawi, N.M., & Abu Seman, I.A. (2018). Spectral features selection and classification of oil palm leaves infected by Basal stem rot (BSR) disease using dielectric spectroscopy. *Comput. Electron. Agric., 144,* 297–309.
15. Khaled, A.Y.; Kabutey, A.; Selvi, K.Ç.; Mizera, C.; Hrabe, P. & Herak, D. (2020). Application of computational intelligence in describing the drying kinetics of persimmon fruit (Diospyros kaki) during vacuum and hot air drying process. *Processes, 8(5),* 544.
16. Kowalski, R., Baj, T., Kalwa, K., Kowalska, G., & Sujka, M. (2017). Essential oil composition of Tilia cordata flowers. *Journal of Essential Oil Bearing Plants, 20(4),* 1137-1142.
17. Olsson, M.E., Gustavsson, K.E. & Vågen, I.M. (2010). Quercetin and isorhamnetin in sweet and red cultivars of onion (allium cepa l.) At harvest, after field curing, heat treatment, and storage. *J. Agric. Food Chem.* 58(4), 2323–2330.
18. Onwude, D., Hashim, N., Abdan, K., Janius, R. & Chen, G. (2018). The potential of computer vision, optical backscattering parameters and artificial neural network modelling in monitoring the shrinkage of sweet potato (Ipomoea batatas L.) during drying. *J. Sci. Food Agric., 98,* 1310–1324.
19. Onwude, D.I., Hashim, N., Janius, R.B., Nawi, N. & Abdan, K. (2016). Evaluation of a suitable thin layer model for drying of pumpkin under forced air convection. *Int. Food Res. J., 23,* 1173
20. Rodríguez, J., Clemente, G., Sanjuan, N. & Bon, J. (2013). Modelling drying kinetics of thyme (Thymus vulgaris L.): Theoretical and empirical models, and neural networks. *Food Sci. Technol. Int., 20,* 13–22.
21. Sacilik, K. & Elicin, A.K. (2006). The thin layer drying characteristics of organic apple slices. *J. Food Eng., 73,* 281–289.
22. Si, X., Wu, X., Yi, J.Y., Li, Z., Chen, Q., Bi, J. & Zhou, L. (2015). Comparison of different drying methods on the physical properties, bioactive compounds and antioxidant activity of raspberry powders. *J. Sci. Food Agric., 96,* 2055–2062.
23. Siger, A., Antkowiak, W., Dwiecki, K., Rokosik, E., & Rudzińska, M. (2021). Nutlets of Tilia cordata Mill. and Tilia platyphyllos Scop.–Source of bioactive compounds. *Food Chemistry, 346,* 128888.
24. Singleton, V.L. & Rossi J.A. (1965). Colorimetry of total phenolics with phosphomolybdic-phosphotungstic acid reagents. *Am J Enol Viticult 16:*144–153.
25. Soysal, Y., Keskin, M., Arslan, A. & Sekerli, Y.E. (2018). Infrared drying characteristics of pepper at different maturity stages. *In Proceedings of the International Conference on Energy Research,* Alanya, Turkey, 1–2 November; pp. 293–304.
26. Tekin, Z.H. & Baslar, M. (2018). The effect of ultrasound-assisted vacuum drying on the drying rate and quality of red peppers. *J. Therm. Anal. Calorim., 132,* 1131–1143.
27. Weryszko-Chmielewska, E. & Sadowska, D. A. (2010). The phenology of flowering and pollen release in four species of linden (Tilia L.). *Journal of Apicultural Science, 54(2),* 99-108.
28. Wissam, Z., Nour, A.A., Bushra, J., Zein, N. & Saleh, D. (2017). Extracting and studying the antioxidant capacity of polyphenols in dry linden leaves (Tilia cordata). *J. Pharmacogn. Phytochem., 6,* 258–262.
29. Xiao, H., Pang, C., Wang, L., Bai, J., Yang, W. & Gao, Z. (2010). Drying kinetics and quality of Monukka seedless grapes dried in

an air-impingement jet dryer. *Biosyst. Eng.*, *105*, 233–240.
30. Yıldırım, A., Mavi, A., Oktay, M., Kara, A. A., Algur, Ö. F., & Bilaloğlu, V. (2000). Comparison of antioxidant and antimicrobial activities of Tilia (Tilia argentea Desf ex DC), sage (Salvia triloba L.), and Black tea (Camellia sinensis) extracts. *Journal of Agricultural and Food Chemistry, 48(10),* 5030-5034.

Corresponding author:
Ing. Kemal Çağatay Selvi, Ph.D., Department of Agricultural Machines and Technologies Engineering, Faculty of Agriculture, Ondokuz Mayıs University, Atakum 55139, Samsun, Turkey, phone: +90 507 9262829, e-mail: kcselvi74@gmail.com

THE PROBLEMATIC OF PRECISION SOWING

Ladislav ŠEVČÍK[1], Michal PETRŮ[2]

[1]*Department of Machine Design, Mechanical Faculty, Technical University of Liberec*
[2]*Department of Machine Design, Mechanical Faculty, Technical University of Liberec*

Abstract
The paper deals with the principle of precise seed dosing using a high - frequency pneumatic nozzle. Design of equipment for testing and measurement in order to achieve the highest possible accuracy of seed frequency. Transport the seeds to the places of their germination in the soil. The seed hopper, the conveyor to the high-frequency sorting mechanism, the sorting nozzle and the output from the seed conveyor to the row were tested. The measurement results are given in this publication. The tests were performed on the seeds of black lentils and red lentils.

Key words: *precision sowing, two-segment sowing device, high-frequency pneumatic nozzle.*

INTRODUCTION

The seed for sowing contains not only the seed, but also protective pickling and growth-promoting substances. In order to reduce the cost of buying seeds for sowing and increase yields with regard to soil quality, controlled sowing is necessary (*Ram, Lohan, Singh, 2014*). The sowing frequency depends on the seed type and ranges from 30 to 400Hz. This frequency also depends on the travel speed of the seed drill or the towing device. The device can be imagined as a two-segment device. The segments are relatively independent. The first segment sets the number of seeds to the length, or otherwise the frequency with which the seeds are to be placed in a row. The second segment ensures the seed output speed, such that the relative travel speed of the seed drill and the seed output speed are equal. The impact velocity of the seed relative to the soil should be equal to 0 so that the name does not jump in the row (*Parrish, 2014*). The aim of the study was design of high frequency precision seeding mechanism.

Tab. 1 Sowing frequency depending on the travel velocity of the seeder

Type of seed	Sowing speed 10 km/h	Sowing speed 15 km/h	Sowing speed 20 km/h
Sugar beet	11-17 Hz	17-26 Hz	22-35 Hz
Soybeans	75-100 Hz	112-150 Hz	150-200 Hz
Peas dry	78-106 Hz	116-160 Hz	155-213 Hz
Rye	173-312 Hz	260-468 Hz	347-625 Hz

The highest values of the required sowing frequency are for flax, even over 2600 Hz and a seeder speed of 20 km/h. The principle of the proposed device is based on a high-frequency pneumatic nozzle reaching a frequency of up to 600 Hz. The valve must be lubricated with oil contained in the compressed air.

MATERIALS AND METHODS

The seed is added to the 5-liter hopper 3, Fig. 1. The inlet opening of the screw conveyor 2 is immersed below the seed level in order not to distort the tests by reducing the amount of seed transported. The inclination of the two-pass screw conveyor was adjusted to suit the required transported quantity as much as possible. The transported seed at the end of the conveyor descends along a sheet metal chute to its edge, which is hit by a pulse of air flow from the nozzle 1. Several types of chutes 4 have been designed, manufactured and tested with regard to sowing different crops. It is important that the seed has the lowest possible forward speed at the end of the slide, ie low kinetic energy. This changes the direction of the seed by rotating over the breaking edge of the chute. At the end of the rotation, some of the seeds should be struck by an air pulse. The other seeds (about 70%) fall back into the hopper after the slide 6.

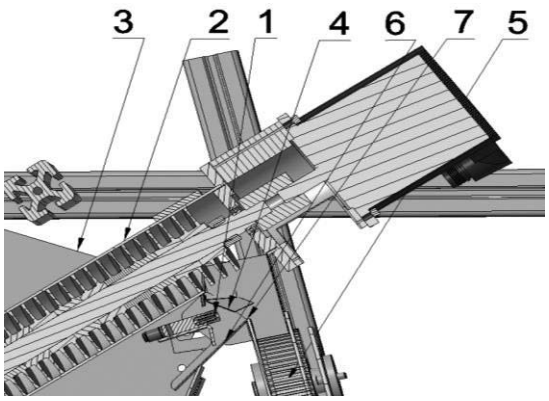

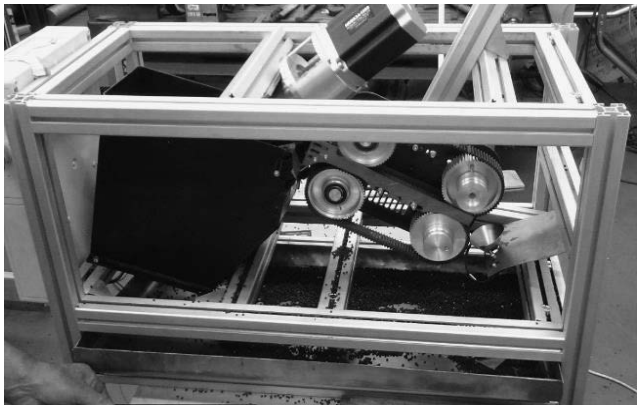

Fig. 1 Principle of model operation

Fig. 2 Stationary device for parameter verification

The position, distance and inclination of the nozzle from the chute edge have been optimized. The optimal diameter of the nozzle orifice and the shape of its edge were also sought. The nozzle was redesigned several times during the tests. It was necessary that the air flow was not constant even for higher nozzle frequencies. If the seed is hit, it flies over the edge 7 to the seed transport system 5. If it is not hit by the air stream, it slides back into the seed hopper after the slide 6. Tests with lentil, rape, radish and pea seeds were performed on the device of Fig. 2.

The control system of the unifying device must allow the setting of the following parameters:

1. Nozzle valve frequency from 0 - 600Hz.
2. Air pressure in the nozzle 0.01 - 0.8 MPa.
3. Screw feeder speed 0.2-10 rpm.
4. Nozzle opening percentage in the cycle - air pulse length. It is a parameter that sets the percentage of nozzle valve opening during one cycle.
5. Single seed conveyor speed in the line 2-50 rpm.
6. Counts the pulses sent to the air nozzle valve
7. Lists the number of seeds passed through the sensor.

Fig. 3 is a copy of the control system settings screen. It was taken with the following parameters: Nozzle valve frequency 70 Hz, air pressure in the nozzle 0.6 MPa, screw feeder speed 6 rpm, nozzle opening percentage 50% in one cycle.

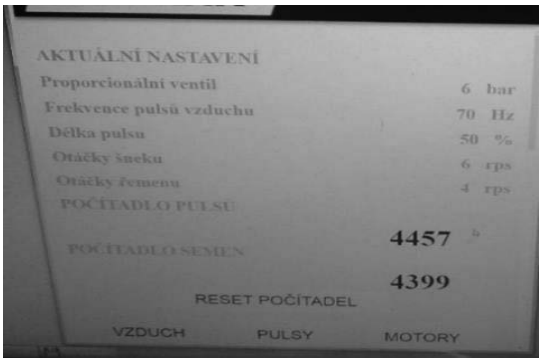

.

Fig. 3 Screenshot of the control system

Fig. 4 Used seed count sensor

The data in Fig. 3 are at a frequency of 70 seeds per second. Sensor of number of seeds is in Fig. 4, It is possible to obtain a match between the number of pulses on the nozzle and the number of seeds passed through the sensor by setting the parameters. The picture shows 4457 pulses and 4399 seeds registered by the sensor. In case the data would differ, the parameters would have to be changed so that they could be balanced. Tests have shown that the error can be kept at 5%. Fig. 4 shows a seed count sensor in a row.

RESULTS AND DISCUSSION

The results of measuring the number of seeds over time are shown in Fig. 5. The horizontal axis shows the time in seconds, the vertical axis the number of seeds sensed by the sensor every tenth of a second. At the beginning of the graph is the start-up of the machine and the setting of the quantities so that the required seed frequency of 50 Hz is achieved. Due to the possible error of the sensor, which must round the seed numbers at the time limits, a moving average of three measurements (solid line in the graph) was made. The polynomial trend line (dotted line in the graph) corresponds to the setpoint.

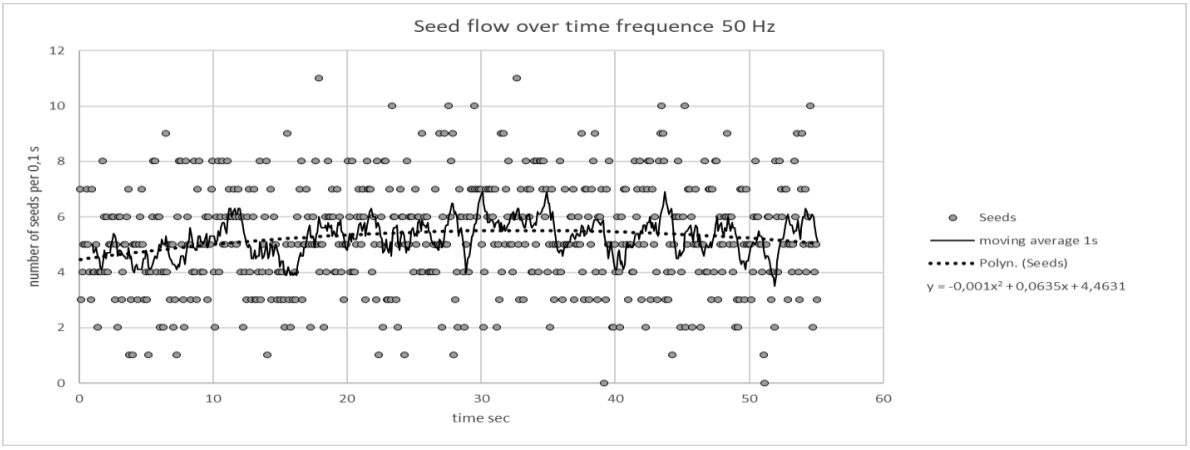

Fig. 5 Time distribution of the number of seeds at a sowing frequency of 50 Hz

The results of measuring the number of seeds over time at a frequency of 90 Hz are shown in Fig. 6. The time in seconds is plotted on the horizontal axis and the number of seeds scanned every hundredth of a second on the vertical axis. The control of the air pressure in the nozzle, the speed of the feeder, and the percentage of the nozzle opening was switched on so that the required frequency of 90 seeds per second was achieved. Due to the possible error of the sensor, which must round the seed numbers at the time limits, a moving average of three measurements was made (solid line in the graph). The polynomial trend line (dotted line in the graph) corresponds to the setpoint.

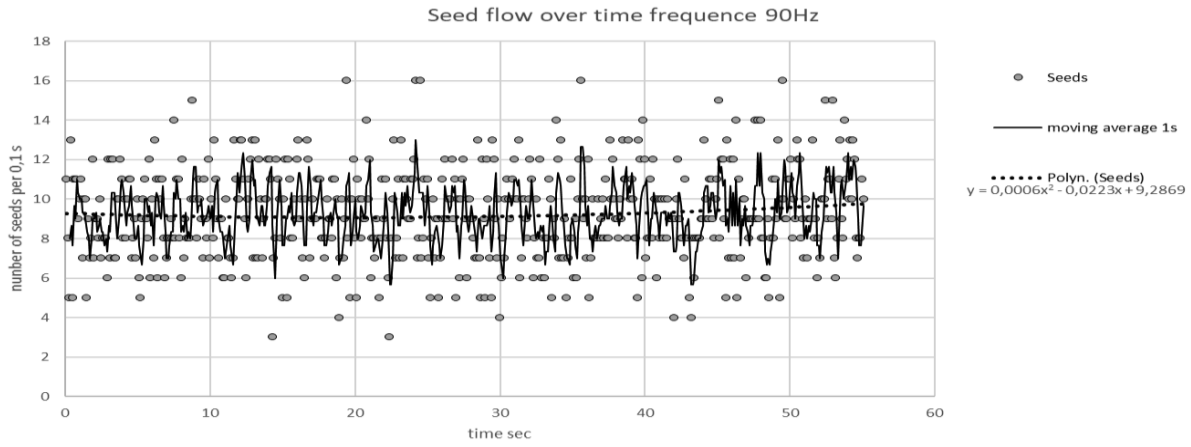

Fig. 6 Time distribution of the number of seeds at the sowing frequency of 90 Hz - onset of regulation

The results of measuring the number of seeds over time at a frequency of 90 Hz are shown in Fig. 7. The time in seconds is plotted on the horizontal axis and the number of seeds scanned every hundredth of a second on the vertical axis. The control of the air pressure in the nozzle, the speed of the feeder, and the percentage of the nozzle opening was switched off so that the value of the required frequency of 90 seeds per second could be seen. The graph shows how stable the process of steady state regulation is. Due to the possible error of the sensor, which must round the seed numbers at the time limits, a

moving average of three measurements was made (solid line in the graph). The polynomial trend line (dotted line in the graph) corresponds to the setpoint.

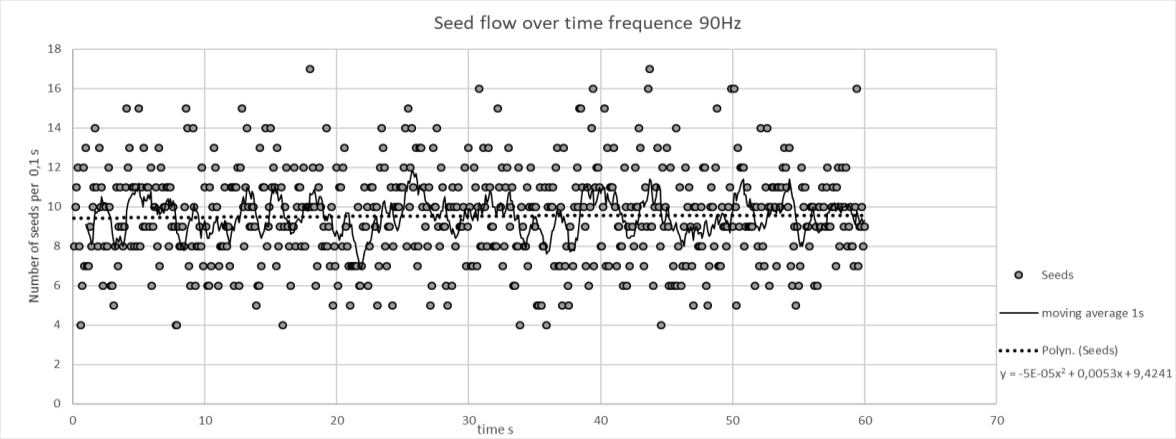

Fig. 7 Time distribution of the number of seeds at the sowing frequency of 90 Hz - end of regulation

CONCLUSIONS

The seeds from the unifying device fall between the belts of the transport device. The straight-line speed of the conveyor belts is 5.5 m/s at 20 km/h when the seed drill travels (*Shannon, Clay, Kitchen, 2020*). The speed of the sorted seed from the energy of the compressed air of the nozzle is approximately 0.1 m/s. If the seed hits the fast-moving belt at low speed, it will gain a large acceleration, which will cause its uncontrolled rebound. (*Virk, Fulton, Porter, et al., 2020*). This had to be managed structurally. Many tests and adjustments have been made to reduce the difference between seed and conveyor speeds. Mechanical rebound barriers of various shapes were also made. However, the desired result was not achieved. (*Akhalaya, Shogenov, & Starovoitov, 2021*).

ACKNOWLEDGMENT

The result was obtained through the financial support of the TA ČR, Program TREND 1, number of project FW01010577.

REFERENCES

1. Ram, T., Lohan, S., Singh R. (2014) Precision Farming a New Approach, , Astral International Pvt Ltd., ISBN: 935130258X
2. Parrish, A. (2014) Mechanical Engineer's Reference Book, 11th Edition, Elsevier.
3. Shannon, D., Clay, D., Kitchen, N. (2020) Precision Agriculture Basics, American Society of Agronomy, ISBN: 0891183663
4. Virk, S.S., Fulton, J.P., Porter, W.M. *et al.* (2020) Row-crop planter performance to support variable-rate seeding of maize. Precision Agriculture 21, 603–619. https://doi.org/10.1007/s11119-019-09685-3
5. Akhalaya, B.K., Shogenov, Y.K. & Starovoitov, S.I. (2021) Effect of Design Changes in Pneumatic Seeding Devices on Quality Indicators of Seeding. Russ. Agricult. Sci. 47, 93–98. https://doi.org/10.3103/S106836742101002X

Corresponding author:
Prof. Ing. Ladislav Ševčík., Department of Mechanical Design, Mechanical Faculty, Technical University of Liberec, Studentská 2, Liberec 1, Liberec, 46117, Czech Republic, phone: +420 485353316, e-mail: ladislav.sevcik@tul.cz

COMBINING SIMULATION AND MTM TO IMPROVE GLASS EYES PRODUCTION

Vladimír SOJKA[1], Petr LEPŠÍK[1]

[1]*Faculty of Mechanical Engineering, Technical University of Liberec, Czech Republic.*

Abstract
The article focuses on the use of computer process simulation and MTM-1 analysis to improve the production process of handmade black glass eyes. The eyes are produced for taxidermy or toys. The production process was analyzed, and based on observation and measurement, the simulation model was created to search for improvement in material flow, identify bottlenecks, and find the optimal batch size. The MTM-1 was used to analyze movements in production and change the order or optimize the micro-layout of the workplace to reduce production time and improve the ergonomics of the operation. By combining improvement opportunities from simulation and MTM-1, the proposed processing time has been shortened by more than 3%.

Key words: *process improvement; MTM; simulation; micro-layout; glass production.*

INTRODUCTION

Using different and new approaches can be beneficial in improving the production system or just one of the production processes. If only one approach (tool or method) is used, some aspects of the production process can be missed. Only specific parameters of the process would be improved. That is why the used tools should be changed or used in combination.
The benefits of the use of different methods in combination are discussed and described by many authors. For instance reducing the lead time in chemical manufacturing by combining TOC (Theory of Constraints) and Lean by (*Lopez-Osorio et al., 2022*). The combination of Lean with agile principles is described by (*Ding et al., 2021*), Lean and green principles for sustainable improvement are combined in (*Teixeira et al., 2022*). Authors in (*Gupta et al., 2022*) combine TOC, Lean, and Six sigma. Other examples such as the combination of SMED (Single Minute Exchange of Dies) with Production Scheduling (*Parwani & Hu, 2021*), or with FMEA (Failure Mode and Effects Analysis) (*Yazıcı et al., 2021*). A combination of FMEA with computer simulation is shown in (*Leeftink et al., 2021*). More examples of tools and methods combined can be found in *(Apornak et al., 2021; Lizarelli et al., 2021; Purushothaman & Ahmad, 2022; Rihar & Kušar, 2021*).
One of the new approaches to combining two tools for process improvement could be the use of computer simulation together with movement measurement tools. The idea is that simulation can provide a broader point of view on the system. Simulation can focus on improving material flow, identifying bottlenecks, searching for the optimal batch size, and others (*Al-zqebah et al., 2022; Kormin et al., 2021; Murugesan et al., 2021; Pekarcikova et al., 2021*). The movement measurement method such as MTM or MOST can provide a more focused point of view on the detail of each activity. These methods are based on the research and measurement of many movements in industrial processes. The movements are categorized into types, and by the lengths, the time needed to execute the movement is found. From tables of movement codes, opportunities for improvement can be found. The result of using these methods can be an improvement of ergonomics, reducing unnecessary movements, redefining the order of movements, and others (*Gorobets et al., 2021; Hernandez Moreno et al., 2022; Riedel et al., 2022*).
This paper aims at the description of the use of the computer process simulation together with the MTM-1 method for improvement of the manual process of black glass eyes production.

MATERIALS AND METHODS

The process of the manual production of black glass eyes can be divided into several main steps. Firstly the wired loop is attached to the glass tube. Then a body of the eye is formed in the flame using several actions such as melting the glass, rotating it, and forming it in the metal mold. The diameter is also checked. Then the eye must be slowly cooled down to avoid tension in glass that can lead to breaks. After the eye is cooled down, it is broken off from the glass tube. Residual glass from the tube is attached

to the loop, so the loop is then cleaned up by the use of pliers. Just one person makes all operations in the process. Changes of material between process steps are shown in the figure (Fig. 1) below.

Fig. 1 Material change during the process

In a real production, activities were measured, and from the measured data, probability distribution was set using a goodness of fit testing in the software Statgraphic 18. The Kolmogorov-Smirnov test of the equality of probability distributions described by equation (1) below was used.

$$D_n = \sup_{-\infty<x<\infty} \left|F_n(x) - \Phi(x)\right| \tag{1}$$

Where F_n is the distribution function of the sample, and Φ is the reference distribution. The Probability distribution fitting for the whole production process is described in (*Sojka & Lepsik, 2021*). The figure (Fig. 2) shows plots of fitted probability distributions.

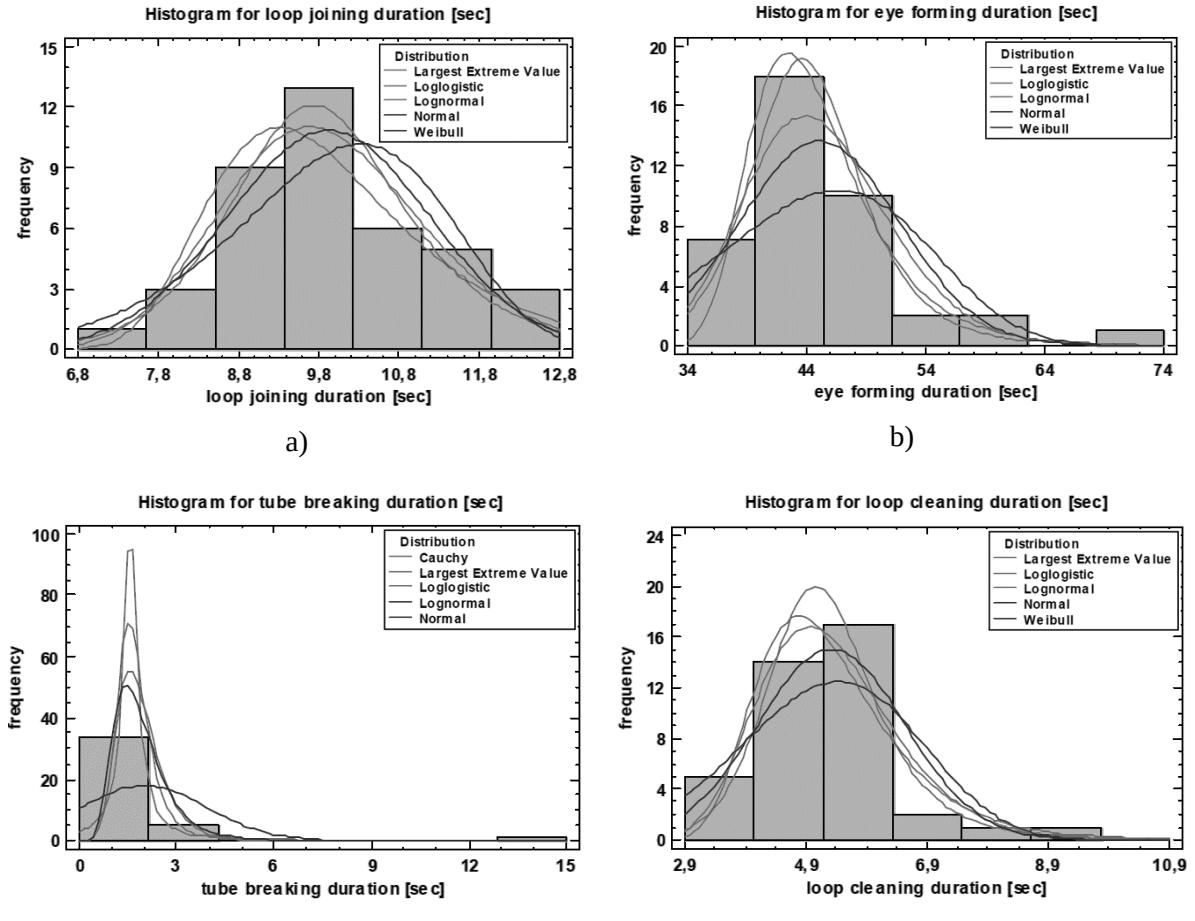

Fig. 2 Distribution fit from Statgraphic 18: a) loop joining; b) eye forming; c) tube breaking; d) loop cleaning

Using simulation software Siemens Tecnomatix Plant Simulation 14, the production process model was created. The probability distribution chosen from Statgraphic software was used for the times in the model steps. The process model can be seen in the figure (Fig. 3) below.

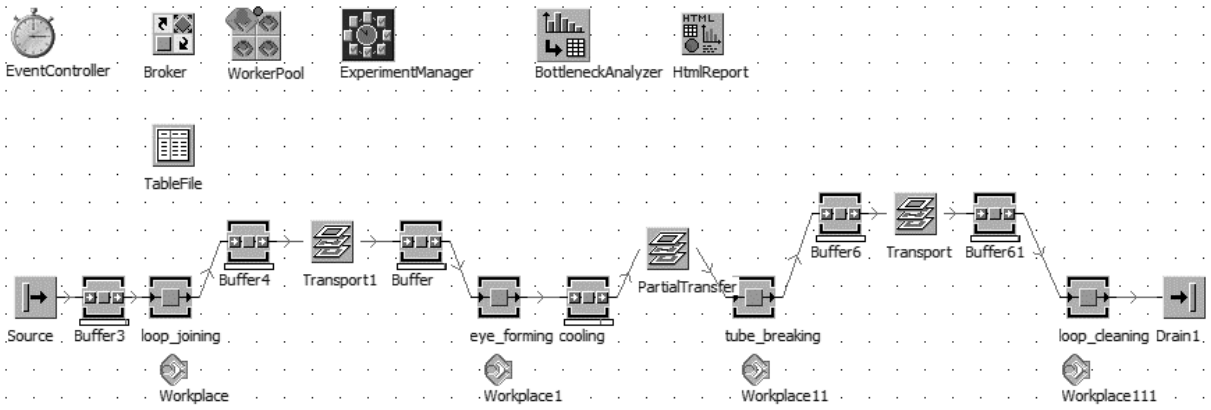

Fig. 3 Process model in Siemens Tecnomatix Plant Simulation

Several ideas and improvement opportunities were found from the simulation model and experiments that were run on it.
The workplace was measured, and a digital micro-layout was created. Based on observations and captured video records of processing, the MTM-1 analysis for each process step was made. The lengths of movements were measured from a digital model of the micro-layout of the work table. See figure (Fig. 4).

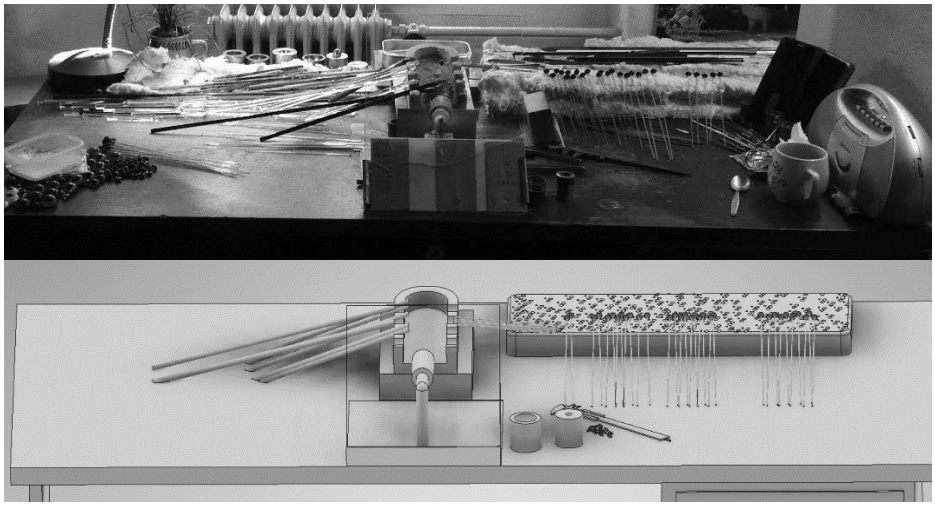

Fig. 4 Real work table and model of the micro-layout for measurement

From the MTM-1 analysis, several more improvement ideas and opportunities were found. Also, VA (Value added) analysis of the process activities was done to see what process activities should be focused on improving efforts.
Based on the findings from the simulation and MTM-1 analysis, improving changes to the process were proposed.
Another MTM-1 analysis was applied to the newly proposed process state. From these times, relatively to the analysis of MTM-1 of original state and real determined probability distributions of the process times. A shift of distribution means was determined. These shifted distributions were used in de new simulation model for overall comparison.

RESULTS AND DISCUSSION

As the main result, a new process proposal was developed. Findings in the MTM-1 analysis lead to the re-design of the micro-layout of the work table. Positions of materials were slightly changed to shorten the length of movements. The steps of breaking off the tube and cleaning the loop were integrated together. Using a special tool in a proposed method worker can break the tube with one hand, and directly after the break, the loop can be cleaned by pliers in a second hand. A comparison of micro-layouts is shown in the figure (Fig. 5).

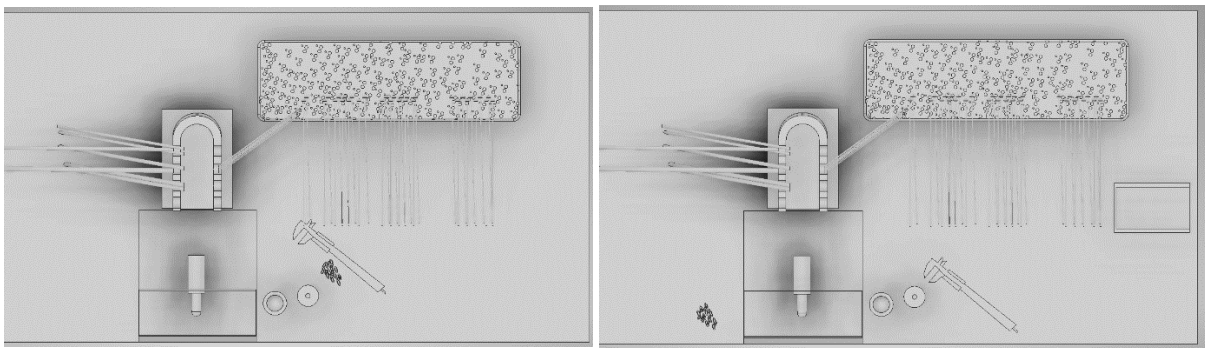

Fig. 5 Comparison of micro-layouts original state (left), and proposed state (right)

From the simulation, findings about the process were learned. The bottleneck of the process is cooling. Unfortunately, there is impossible to speed up the cooling process because more defects would occur by speeding up the cooling time. Due to this cooling procedure, the bigger the batch size, the faster the production. Because when a new batch starts, no eyes are cooled, and overall time is longer. Based on that, there is a recommended to make all the requested eyes as one batch, to reduce stops in the cooling. A comparison of the original state and the proposed one is summarized in the table (Tab. 1) below.

Tab. 1 Comparison of production time by simulation and MTM-1, comparison of VA-index

Process state	Simulation	MTM-1		VA-index
	50 pcs.	min/pcs.	min/50 pcs.	-
Original process	1:19:31.2310	1.04130	52.065	0.10558
Improved process	1:16:52.6474	0.98082	49.041	0.10810

From the table (Tab. 1), there can be seen that the time of manual processing was improved. Measured by computer simulation, the production time reduction is 3.33%. Time reduction by MTM-1 analysis is by 5.81%. VA-index of the process was increased by 2.39%. The real improvement rate should be measured after the realization of the improvement proposal. These values are just approximations.

The benefits of using the simulation and MTM together are clear; if only simulation would be used, a bottleneck of the process would be found, and the information about the relation between batch size and production time. See simulation case studies (*Kutin et al., 2018; Rosova et al., 2022*). On the other hand, if only MTM would be used, there would be found and improved lengths of movements and handling, but there would be no information about the batch size or bottleneck step. See case studies using MTM or MOST (*Bedny et al., 2019; Bures & Pivodova, 2013*).

These particular improvements also positively affect other production processes since all types of eyes are made at one workstation. Improved micro-layout reduces time and improves handling in other similar eye production processes. The findings of the beneficial use of MTM-1 with computer simulation can be used in any production process with manual operations. By using both methods, we focus on the process details and worker comfort, but we also see a broader point of view on the production system and material flow. There are studies where the MTM or MOST principles are used together with simulation software. However, the software is focused on the ergonomic aspects of the production (*Kim et al., 2021; Santos et al., 2007*).

CONCLUSIONS

The production process of the glass eyes was described, and improvement opportunities were identified based on experimenting with computer process simulation and the use of MTM-1 analysis, improvement opportunities were identified. Based on that findings new process state was proposed and again analyzed by computer simulation and MTM-1 analysis. The main change in the process is re-layout of the micro-layout to change the order of some activities and improve movement lengths. Also, two process steps were integrated to eliminate several handling activities. Overall improvement rate of production time was bigger than 3%, but it should be verified on the final improved process after implementation of changes. The improvement in the VA-index is by 2.39%.

The use of simulation with MTM can be beneficial because, by this combination, the improvement focus is both on the overall process and on process details. Results of the use can bring improvements in material flow, bottleneck step improvement, batch size optimization, re-layout of the workshop, movement improvement, better ergonomics, movement elimination or integration, and others.

ACKNOWLEDGMENT

This work was supported by the Student Grant Competition of the Technical University of Liberec under the project No. SGS-2020-5027 - Research of new approaches to process improvement.

REFERENCES

1. Al-zqebah, R., Hoffmann, F., Bennett, N., Deuse, J., & Clemon, L. (2022). Layout optimisation for production systems in the wool industry using discrete event simulation. *Journal of Industrial Engineering and Management*, *15*(2), 296. DOI: 10.3926/jiem.3721
2. Apornak, A., Raissi, S., & Pourhassan, M. R. (2021). Solving flexible flow-shop problem using hybrid multi criteria Taguchi based computer simulation model and DEA approach. *Journal of Industrial and Systems Engineering*, *13*(2), 264–276.
3. Bedny, G., Bedny, I., & Karwowski, W. (2019). Time Study in Ergonomics and Psychology. In H. Ayaz & L. Mazur (Eds.), *Advances in Neuroergonomics and Cognitive Engineering* (Vol. 775, pp. 217–224). Springer International Publishing. DOI: 10.1007/978-3-319-94866-9_22
4. Bures, M., & Pivodova, P. (2013). Comparison of the predetermined time systems MTM-1 and BasicMOST in assembly production. *2013 IEEE International Conference on Industrial Engineering and Engineering Management*, 546–550. DOI: 10.1109/IEEM.2013.6962471
5. Ding, B., Ferràs Hernández, X., & Agell Jané, N. (2021). Combining lean and agile manufacturing competitive advantages through Industry 4.0 technologies: An integrative approach. *Production Planning & Control*, 1–17. DOI: 10.1080/09537287.2021.1934587
6. Gorobets, V., Holzwarth, V., Hirt, C., Jufer, N., & Kunz, A. (2021). A VR-based approach in conducting MTM for manual workplaces. *The International Journal of Advanced Manufacturing Technology*, *117*(7–8), 2501–2510. DOI: 10.1007/s00170-021-07260-7
7. Gupta, M., Digalwar, A., Gupta, A., & Goyal, A. (2022). Integrating Theory of Constraints, Lean and Six Sigma: A framework development and its application. *Production Planning & Control*, 1–24. DOI: 10.1080/09537287.2022.2071351
8. Hernandez Moreno, V., Carmichael, M. G., & Deuse, J. (2022). *Towards Learning by Demonstration for Industrial Assembly Tasks* [Preprint]. DOI: 10.36227/techrxiv.19975829.v1
9. Kim, J., Golabchi, A., Han, S., & Lee, D.-E. (2021). Manual operation simulation using motion-time analysis toward labor productivity estimation: A case study of concrete pouring operations. *Automation in Construction*, *126*, 103669. DOI: 10.1016/j.autcon.2021.103669
10. Kormin, T. G., Ovchinnikova, V. A., & Tsumbu, J.-D. B. (2021). Simulation modeling of manufacturing. *IOP Conference Series: Materials Science and Engineering*, *1047*(1), 012090. DOI: 10.1088/1757-899X/1047/1/012090
11. Kutin, A., Dolgov, V., Podkidyshev, A., & Kabanov, A. (2018). Simulation Modeling of

Assembly Processes in Digital Manufacturing. *Procedia CIRP*, *67*, 470–475. DOI: 10.1016/j.procir.2017.12.246
12. Leeftink, A. G., Visser, J., de Laat, J. M., van der Meij, N. T. M., Vos, J. B. H., & Valk, G. D. (2021). Reducing failures in daily medical practice: Healthcare failure mode and effect analysis combined with computer simulation. *Ergonomics*, *64*(10), 1322–1332. DOI: 10.1080/00140139.2021.1910734
13. Lizarelli, F. L., Osiro, L., Ganga, G. M. D., Mendes, G. H. S., & Paz, G. R. (2021). Integration of SERVQUAL, Analytical Kano, and QFD using fuzzy approaches to support improvement decisions in an entrepreneurial education service. *Applied Soft Computing*, *112*, 107786. DOI: 10.1016/j.asoc.2021.107786
14. Lopez-Osorio, A. T., Vila-Moretti, N. F., Flores-Perez, A., Quiroz-Flores, J., & Collao-Diaz, M. (2022). Production Model Integrating TOC and Lean for Lead Time Reduction in Chemical Manufacturing: An Empirical Research in Peru. *2022 The 9th International Conference on Industrial Engineering and Applications (Europe)*, 44–49. DOI: 10.1145/3523132.3523140
15. Murugesan, V. S., Jauhar, S. K., & Sequeira, A. H. (2021). Applying simulation in lean service to enhance the operational system in Indian postal service industry. *Annals of Operations Research*. DOI: 10.1007/s10479-020-03920-1
16. Parwani, V., & Hu, G. (2021). Improving Manufacturing Supply Chain by Integrating SMED and Production Scheduling. *Logistics*, *5*(1), 4. DOI: 10.3390/logistics5010004
17. Pekarcikova, M., Trebuna, P., Kliment, M., & Dic, M. (2021). Solution of Bottlenecks in the Logistics Flow by Applying the Kanban Module in the Tecnomatix Plant Simulation Software. *Sustainability*, *13*(14), 7989. DOI: 10.3390/su13147989
18. Purushothaman, K., & Ahmad, R. (2022). Integration of Six Sigma methodology of DMADV steps with QFD, DFMEA and TRIZ applications for image-based automated inspection system development: A case study. *International Journal of Lean Six Sigma*. DOI: 10.1108/IJLSS-05-2021-0088
19. Riedel, A., Brehm, N., & Pfeifroth, T. (2022). Hand Gesture Recognition of Methods-Time Measurement-1 Motions in Manual Assembly Tasks Using Graph Convolutional Networks. *Applied Artificial Intelligence*, *36*(1), 2014191. DOI: 10.1080/08839514.2021.2014191
20. Rihar, L., & Kušar, J. (2021). Implementing Concurrent Engineering and QFD Method to Achieve Realization of Sustainable Project. *Sustainability*, *13*(3), 1091. DOI: 10.3390/su13031091
21. Rosova, A., Behun, M., Khouri, S., Cehlar, M., Ferencz, V., & Sofranko, M. (2022). Case study: The simulation modeling to improve the efficiency and performance of production process. *Wireless Networks*, *28*(2), 863–872. DOI: 10.1007/s11276-020-02341-z
22. Santos, J., Sarriegi, J. M., Serrano, N., & Torres, J. M. (2007). Using ergonomic software in non-repetitive manufacturing processes: A case study. *International Journal of Industrial Ergonomics*, *37*(3), 267–275. DOI: 10.1016/j.ergon.2006.10.022
23. Sojka, V., & Lepsik, P. (2021). Probability Distribution of Time Duration of Manual Operation in the Production of Glass Eyes. *AD ALTA: Journal of Interdisciplinary Research*, *11*(2), 340–342. DOI: 10.33543/1102340342
24. Teixeira, P., Coelho, A., Fontoura, P., Sá, J. C., Silva, F. J. G., Santos, G., & Ferreira, L. P. (2022). Combining lean and green practices to achieve a superior performance: The contribution for a sustainable development and competitiveness—An empirical study on the Portuguese context. *Corporate Social Responsibility and Environmental Management*, csr.2242. DOI: 10.1002/csr.2242
25. Yazıcı, K., Gökler, S. H., & Boran, S. (2021). An integrated SMED-fuzzy FMEA model for reducing setup time. *Journal of Intelligent Manufacturing*, *32*(6), 1547–1561. DOI: 10.1007/s10845-020-01675-x

Corresponding author:
Ing. Vladimír Sojka, Department of Design of Machine Elements and Mechanisms, Faculty of Mechanical Engineering, Technical University of Liberec, Studentská 1402/2, Liberec, 461 17, Czech Republic, e-mail: vladimir.sojka@tul.cz

LANDFILLING OF BIODEGRADABLE WASTE AND GENERATION OF LANDFILL GAS

Jan ŠONSKÝ[1], Shuran ZHAO[2], Petr VACULÍK[1], Vlastimil ALTMANN[2]

[1]Department of Technological Equipment of Buildings, Faculty of Engineering, Czech University of Life Sciences Prague, Kamýcká 129, 165 21 Prague, Czech Republic
[2]Department of Machinery Utilization, Faculty of Engineering, Czech University of Life Sciences Prague, Kamýcká 129, Prague 6, 165 21, Czech Republic

Abstract
Landfilling of organic waste generates landfill gas. Landfill gas is primarily made up of greenhouse gases and its release into the atmosphere is undesirable. Despite the obligation to capture landfill gas from the landfill, emissions to air may occur. With this in mind, since 2015, legislation has restricted which organic waste can be landfilled. Therefore, instead of landfilling, organic waste is diverted to facilities for its further use, such as composting facilities. Despite this pressure to reduce landfilling, the organic component is increasing. This is mainly due to the increasing amount of mixed municipal waste being landfilled, which, according to regular analyses by EKOKOM, a.s., contains up to 25 % organic content. Despite the increasing share of the organic component within the landfill body, the amount of landfill gas has been decreasing year by year. It appears that the amount and production of landfill gas is therefore dependent on more than just the quantity of waste, but mainly on the moisture content and composition of the organic material.

Key words: *waste, waste management, landfill, landfill gas, emissions.*

INTRODUCTION

Landfill gas is produced by the decomposition of organic materials inside the landfill body. Its formation is conditioned by a sufficient content of organic material. Important factors are the moisture content of the waste, the volume of the landfill body, the degree of compaction, and most importantly, the overall composition of the disposed waste (*Kumar & Sharma, 2014*). Landfill gas must be extracted from the landfill body and its utilization must be ensured, e.g., in cogeneration units. With respect to environmental protection, there is a gradual pressure to reduce landfilling of biodegradable wastes and hence less generation of landfill gas, which has an impact on global warming (*Sanjuan-Delmas et al. 2021*).

Landfill gas is mainly composed of methane (CH_4) and carbon dioxide (CO_2). Other gases are minor (*Cáb and Šeděnková, 2019*). Landfill gas is produced in 2 phases - aerobic and anaerobic. During the aerobic phase, which lasts only a few days, growth of organisms and exothermic reactions occur. During the aerobic phase, mainly O_2 is consumed, and CO_2 is the main product of this phase and anaerobic environment is gradually formed. The anaerobic phase occurs in 3 successive phases (*Williams, 2005*). In the first phase, acetogenesis, there is a complete transition between the aerobic and anaerobic environment. Gradual hydrolysis results in microbial conversion of biodegradable matter to produce volatile organic acids, hydrogen, ammonia nitrogen and carbon dioxide. The electron acceptor oxygen is displaced by carbon dioxide and the electron acceptors become nitrates and sulphates. The second anaerobic phase is the methanogenic unsterilized phase. The acids formed from the acetogenesis phase are consumed by methanogenic bacteria to form methane and carbon dioxide (*Obersky et al., 2018*). The electron acceptors nitrate and sulfate are reduced to sulfide and ammonia. The third anaerobic phase is the methanogenic stabilized phase. The final phase of landfill stabilization. Gradually, the remaining substrate and nutrients are utilized causing a dampening of biological activity (*Sel et al., 2016*).

Landfill gas is extracted from the landfill body using a degasification system. This is composed of 2 parts - a collection and a conveyance network. The collection network collects the gas from the landfill body. The intake network diverts the gas from the collection network inside the landfill body to the landfill gas recovery facility (*Zheng et al., 2018*). The degasification system is either active or passive. The active method involves the collection of gas by means of a vacuum created by an external device. The passive method uses the pressurized gas inside the landfill body. The landfill gas is used as a fuel

due to its energy properties. It is most often burned in cogeneration units where electricity and heat are produced (*Friesenhan et al., 2017*).
According to the above information, it is evident that the abundance of organic material in the landfill has a great influence on the generation of landfill gas. Due to the pressure to reduce the landfilling of biodegradable waste according to Decree No. 273/2021 on the details of waste management, it can be assumed that the amount of organic material in the landfill and the amount of landfill gas should decrease. The Decree allows the disposal of biodegradable waste only if it is a component of mixed municipal waste (MSW). The organic component in MSW accounts for 17 to 26% of the total amount of MSW (*Najfus, 2021*). Considering the composition of MSW, it can be concluded that the amount of organic component in landfill will increase if more MSW is landfilled (*Sel et al., 2016*). The main objective of this work is to analyze the amount of organic material in MSW landfill and its effect on landfill gas generation.

MATERIALS AND METHODS

The analysis of the amount of landfilled organic material and its impact on the amount of landfill gas was carried out at a landfill in the Central Bohemia Region, where 93 000 tons of municipal waste have been landfilled on average since 2014. The landfill has separate sections from industrial and municipal waste. Data on the amount of municipal waste disposed between 2014 and 2021, by individual catalogue numbers according to the internal records of the company operating the landfill, were used. Data from cogeneration units that burn landfill gas were also used. The cogeneration units measure continuously the amount of electricity produced and the consumption of landfill gas. The data were processed using MS Excel.
The amount of landfilled organic material and its percentage in the total amount of landfilled waste is evaluated. This quantity is then related to the consumption of landfill gas in the cogeneration unit.

RESULTS AND DISCUSSION

Ríos and Picazo-Tadeo (2021) state that landfilling is an undesirable method of waste disposal compared to waste utilization. Despite this fact, and legislative pressure, the amount of landfilled waste in the country is increasing. The amount of municipal waste landfilled between 2014 and 2021 is shown in Table 1.

Tab. 1 Quantity and composition of landfilled waste

Type of waste / Year / Weight	2014	2015	2016	2017	2018	2019	2020	2021
					kt			
Organic component	0.101	0.397	0.025	0.034	0.025	0.032	0.021	0.013
Packaging (plastic, tetra-pak, metals, glass)	0.325	0.237	0.265	0.333	0.392	0.356	0.243	0.281
Hazardous waste	0.037	0.028	0.002	0.003	0.002	0.008	0.019	0.223
Other materials	0.169	0.120	0.109	0.186	0.221	0.257	0.230	0.202
Inert waste	18.876	24.425	24.888	26.615	30.659	27.462	31.170	31.759
MSW	52.640	54.458	61.552	68.159	69.622	73.969	72.220	77.182
Total	72.148	79.664	86.841	95.330	100.921	102.084	103.903	109.660

Table 1 and Figs. 1 and 2 show the total production of the monitored waste components disposed in landfill. The total amount of waste disposed to landfill showed an increasing trend between 2014 and 2021. Fig. 2 shows that the amount of directly landfilled biodegradable waste that must be reduced according to the waste ordinance is decreasing. These are mainly catalogue numbers (according to Decree No. 8/2021, on the Waste Catalogue and the Assessment of Waste Properties (Waste Catalogue)):

- 20 02 03 – other non-biodegradable waste,
- 20 02 01 – biodegradable waste.

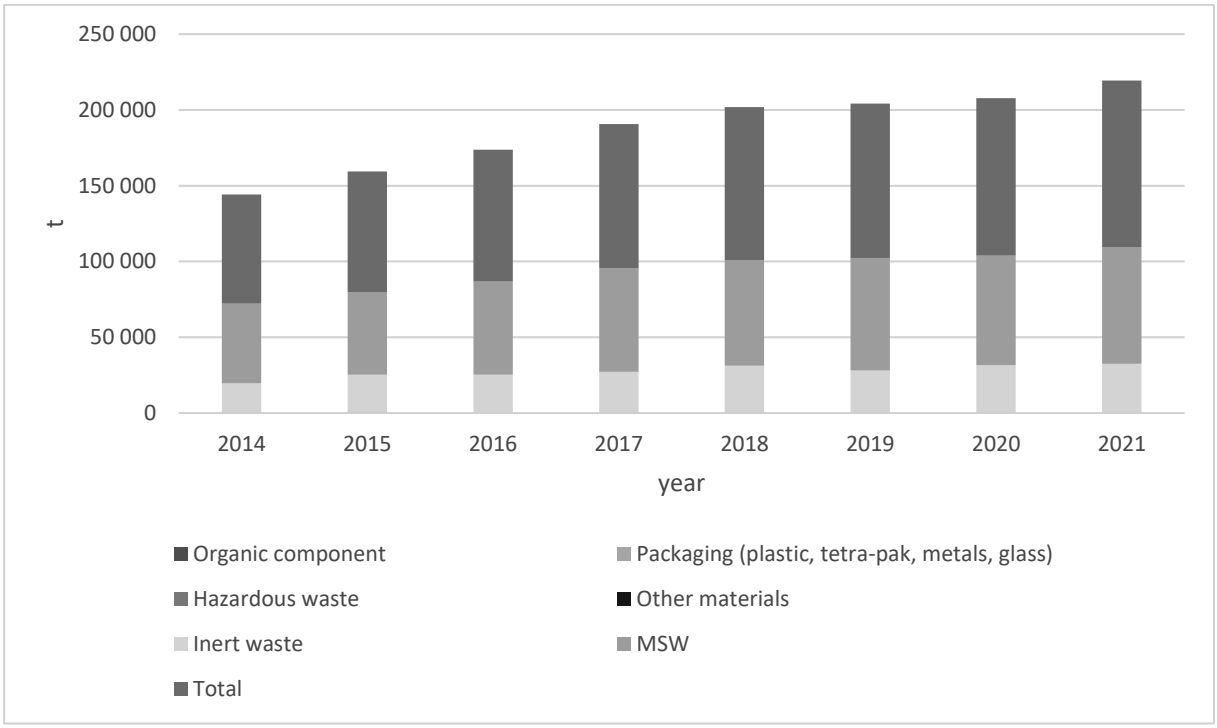

Fig. 1 Quantity and composition of landfilled municipal waste between 2014 and 2021

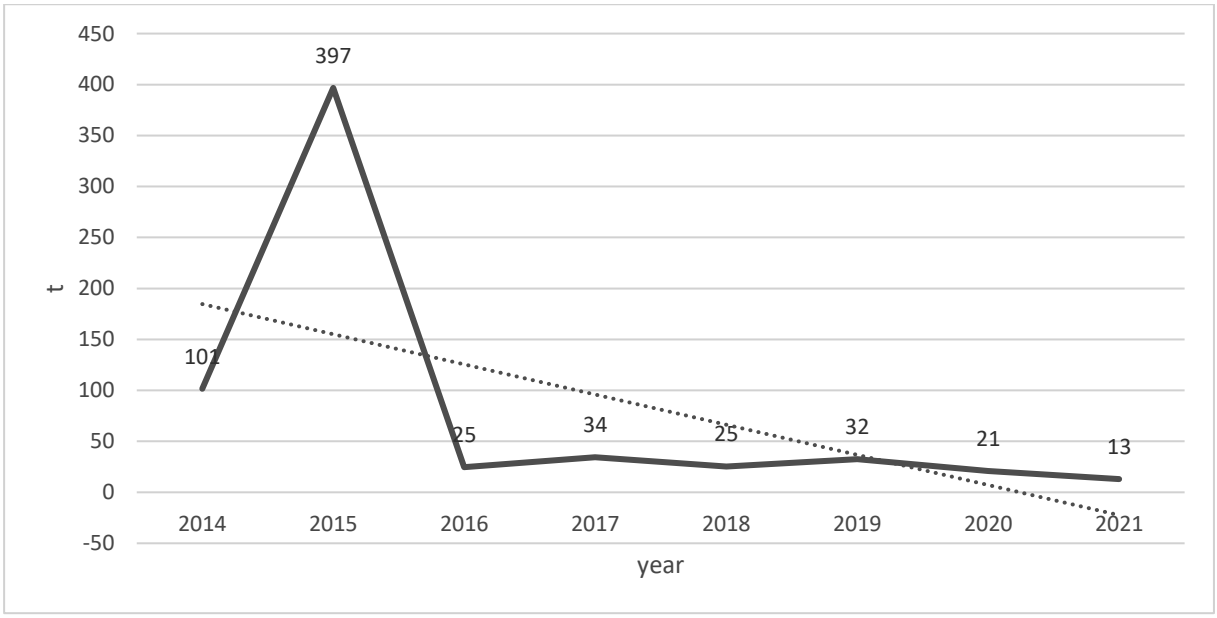

Fig. 2 Amount of directly landfilled organic waste, cat. no. 20 02 03 and 20 02 01

The organic component of mixed municipal waste also contributes to a large extent to the development of landfill gas. The amount of landfilled MSW increased by 46.62% between 2014 and 2021 from 52 640 tons to 77 182 tons per year. The analyses of MSW show that the share of the organic component is between 17 and 26% (*Najfus, 2021*). Considering the composition of MSW, it can be concluded that MSW contributes largely to the generation of landfill gas.

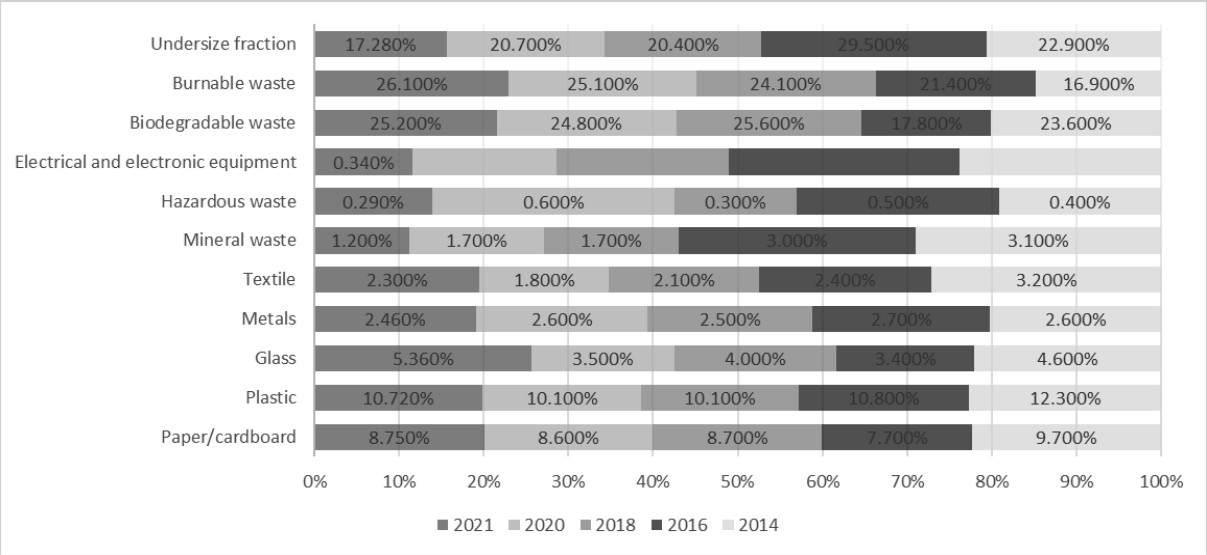

Fig. 3 Average composition of MSW

Fig. 3 shows that the amount of the organic component in the MSW varies between 17 and 26 %. For the years not shown, the composition of the MSW is not provided and the same composition as in the previous year is considered. Table 2 shows the recalculation of the organic component in the MSW.

Tab. 2 Conversion of the organic component in MSW

Compo-nent Year / Amount	2014	2015	2016	2017	2018	2019	2020	2021
					t			
Organic compo-nent in MSW	12 424	12852	10 956	12 132	17 823	18 936	17 911	19 450
Organic compo-nent directly land-filled	101	396	23	34	25	31	21	13
Total organic com-ponent	12 524	13 248	10 980	12 167	17 849	18 967	17 932	19 463

From Table 2 is notable, when the organic component in the MSW is included, the amount of organic material in the landfill is increasing, both as a unit and as a percentage of the total amount. Paper and cardboard have not been included in the organic component due to its unclear chemical composition. Despite the overall increase in the amount of organic material in the landfill, Fig. 4 shows that the amount of landfill gas that is used in the cogeneration unit is decreasing despite the larger amount of organic material. *Sauve and van Acker (2020)* also conclude that the amount of landfill gas decreases with time.

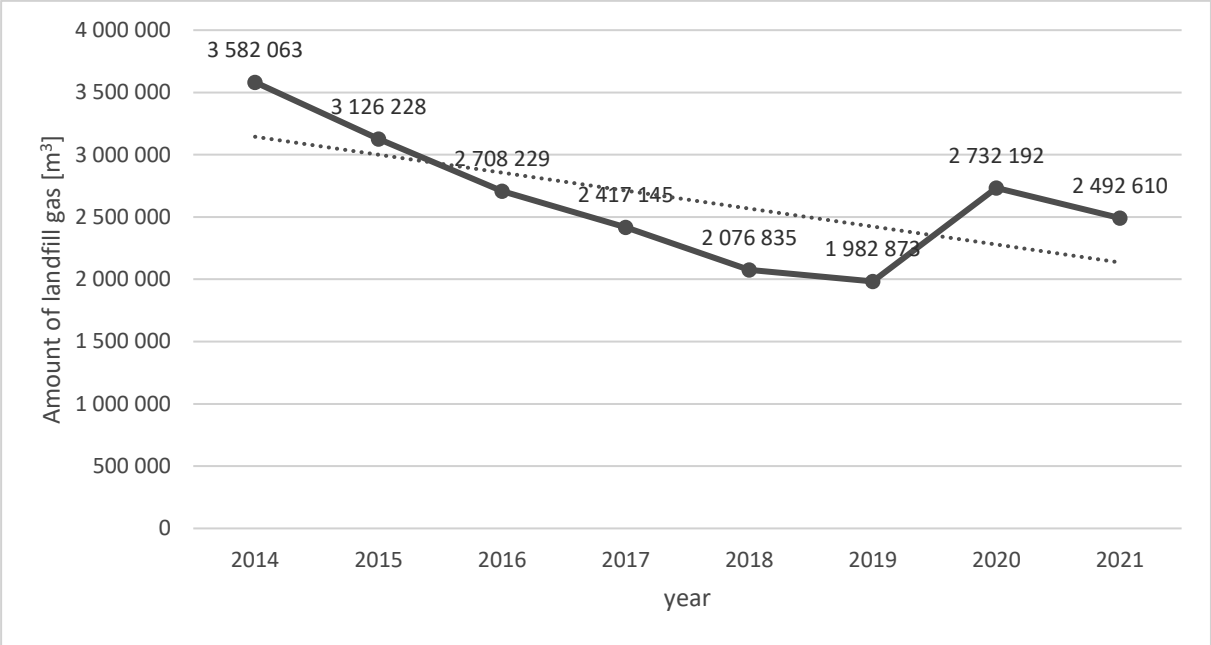

Fig. 4 Gas consumption in the cogeneration unit

CONCLUSIONS

Legislative restrictions on landfilling of organic material, excluding the organic component in MSW, can be seen in Fig. 2. The restriction is mainly due to the development of the collection network for organic waste and the diversion of previously landfilled waste to composting plants. Despite this legislative pressure, the amount of organic material in landfill is increasing, mainly due to increased landfilling of MSW. At the same time, the amount of gas consumption in the cogeneration unit has been decreasing gradually since 2014. The decreasing trend in gas consumption is probably due to the quality of the landfilled organic component. Directly landfilled municipal waste, i.e. waste catalogue numbers 20 02 03 and 20 02 01, consists primarily of an organic component derived from plant production, i.e. grass, leaves, fruit and vegetables. Diversion of these materials from landfill may affect the amount of landfill gas. The organic component contained in the MSW is mainly made up of the living animal component, e.g., food residues, meat, etc. Considering the potential energy and environmental benefits, the use of organic waste in a biogas plant is better than landfilling (*Mavridis & Voudrias, 2021*).
Furthermore, it can be concluded from the results that the amount of landfill gas depends not only on the amount of organic material but also on other parameters such as waste moisture, waste composition, waste age, quality of collection network and compliance with the landfilling procedure (*Duan et al., 2022*). The results show that there is still a large amount of organic component in MSW. Therefore, in the future, it is necessary to develop a collection network for collecting organic waste, food residues such as meat, to reduce the amount of organic waste in MSW.

REFERENCES

1. Cáb, I. S., & ŠEděnková, I. M. (2019, September 3). Rizika vzniku a kumulace hořlavých plynů při skládkovaní odpadů. TZB-info. https://www.tzb-info.cz/pozarni-bezpecnost-staveb/18395-rizika-vzniku-a-kumulace-horlavych-plynu-pri-skladkovani-odpadu
2. Duan, Z., Kjeldsen, P., & Scheutz, C. (2022). Efficiency of gas collection systems at Danish landfills and implications for regulations. Waste Management, 139, 269–278. https://doi.org/10.1016/j.wasman.2021.12.023
3. Friesenhan, C., Agirre, I., Eltrop, L., & Arias, P. L. (2017). Streamlined life cycle analysis for assessing energy and exergy performance as well as impact on the climate for landfill gas utilization technologies. Applied Energy, 185, 805–813. https://doi.org/10.1016/j.apenergy.2016.10.097

4. Jiří Najfus, EKO-KOM a.s. (2021). Rozbory skladby směsného komunálního odpadu z obcí v roce 2020 – EKO-KOM. EKO-KOM a.s. https://www.ekokom.cz/rozbory-skladby-smesneho-komunalniho-odpadu-z-obci-v-roce-2020/
5. Kumar, A., & Sharma, M. (2014). Estimation of GHG emission and energy recovery potential from MSW landfill sites. Sustainable Energy Technologies and Assessments, 5, 50–61. https://doi.org/10.1016/j.seta.2013.11.004
6. Mavridis, S., & Voudrias, E. A. (2021). Using biogas from municipal solid waste for energy production: Comparison between anaerobic digestion and sanitary landfilling. Energy Conversion and Management, 247, 114613. https://doi.org/10.1016/j.enconman.2021.114613
7. Obersky, L., Rafiee, R., Cabral, A. R., Golding, S. D., & Clarke, W. P. (2018). Methodology to determine the extent of anaerobic digestion, composting and CH4 oxidation in a landfill environment. Waste Management, 76, 364–373. https://doi.org/10.1016/j.wasman.2018.02.029
8. Ríos, A. M., & Picazo-Tadeo, A. J. (2021). Measuring environmental performance in the treatment of municipal solid waste: The case of the European Union-28. Ecological Indicators, 123, 107328. https://doi.org/10.1016/j.ecolind.2020.107328
9. Sanjuan-Delmás, D., Taelman, S. E., Arlati, A., Obersteg, A., Vér, C., Óvári, G., Tonini, D., & Dewulf, J. (2021). Sustainability assessment of organic waste management in three EU Cities: Analysing stakeholder-based solutions. Waste Management, 132, 44–55. https://doi.org/10.1016/j.wasman.2021.07.013
10. Sauve, G., & van Acker, K. (2020). The environmental impacts of municipal solid waste landfills in Europe: A life cycle assessment of proper reference cases to support decision making. Journal of Environmental Management, 261, 110216. https://doi.org/10.1016/j.jenvman.2020.110216
11. Sel, L., Çakmakcı, M., Özkaya, B., & Suphi Altan, H. (2016). Case study on prediction of remaining methane potential of landfilled municipal solid waste by statistical analysis of waste composition data. Waste Management, 56, 310–317. https://doi.org/10.1016/j.wasman.2016.07.023
12. Wang, Y. N., Xu, R., Wang, H., Shi, H., Kai, Y., Sun, Y., Li, W., Bian, R., & Zhan, M. (2021). Insights into the stabilization of landfill by assessing the diversity and dynamic succession of bacterial community and its associated bio-metabolic process. Science of The Total Environment, 768, 145466. https://doi.org/10.1016/j.scitotenv.2021.145466
13. Williams, P. T. (2005). Waste Treatment and Disposal. Wiley.
14. Zheng, Q. T., Rowe, R. K., & Feng, S. J. (2018). Design of vertical landfill gas collection wells considering non-homogeneity with depth. Waste Management, 82, 26–36. https://doi.org/10.1016/j.wasman.2018.10.012

Corresponding author:
Ing. Jan Sonsky, Department of Technological Equipment of Buildings, Faculty of Engineering, Czech University of Life Sciences Prague, Kamýcká 129, Praha 6, Prague, 16521, Czech Republic, e-mail: sonskyj@tf.czu.cz

PARAMETERS OF HEMP OIL FILTRATION USING A PLATE FILTER

Jiří SOUČEK[1], Petr JEVIČ[1], Martin DĚDINA[1], Veronika TOMÁNKOVÁ[1], Kornél SZALAY[2], Vladimír MAŠÁN[3], Algirdas JASINSKAS[3]

[1]Research Institute of Agriculture Engineering, 161 01 Prague 6 , Czech Republic; jiri.soucek@vuzt.cz
[2]Hungarian University of Agriculture and Life Sciences , Institute of Technology, Páter Károly utca 1, 2100, Gödöllő, Hungary, Szalay.Kornel@uni-mate.hu[3]Department of Horticultural Machinery,
[3]Faculty of Horticulture, Mendel University in Brno, Valtická 337, 691 44 Lednice, Czech Republic; vladimir.masan@mendelu.cz
[4]Department of Agricultural Engineering and Safety, Faculty of Engineering, Agriculture Academy, Vytautas Magnus University

Abstract
The article is focused on determining the effect of pressure on the filtration parameters of vegetable oils. The experiments were carried out with hemp oil on an experimental filter device. The main part of the filter equipment is the Farmet plate filter. The monitored parameters were measured online using sensors and the COMET MS6D measuring center. The filtration rate was mainly influenced by oil pressure and filter pressure loss. It changed due to clogging of the filter membrane. A temperature change in the range of 15 - 25 °C had no effect on the filtration rate.

Key words: *vegetable oil; oilseeds; oil processing; filtration.*

INTRODUCTION

The fibrous plants, which include seeded hemp, are traditional crops grown in Central Europe. Their importance historically consisted in the use of fibers suitable for further processing. By the experience (*Mendel et al, 2020*) hemp can be well used as part of phytoremediation procedures or as an energy raw material (*Souček & Jasinskas, 2020; Malaťáková, J., et al., 2021*). Currently, hemp seed is an important raw material. In practice, it is most often used as part of human nutrition, or feed. It is most often used in peeled form, or pressed in the form of hemp oil and crumbs. The high dietary value of hemp seeds and oil, which contains a significant amount of unsaturated fatty acids, is appreciated. Unfortunately, this advantage results in low oxidation stability (*Kyselka et al., 2017*). To obtain quality oil, the main operations are storage, pressing and filtration. The parameters of these operations have a fundamental influence on the composition and quality of the oil.

According to the literature (*Tura et al., 2022; Vitorovič et al., 2021*), hemp oil is valued primarily for its nutritional properties, which are associated with beneficial health effects. Hemp seeds contain up to 35% fatty acids, a high proportion of protein (25%), carbohydrates (30%) and fiber (10%). Hemp oil is rich mainly in linoleic and linolenic acid in a suitable ratio for nutrition. Linolenic acid gives hemp oil a higher nutritional value. The main production of hemp oil is concentrated in Canada, where, thanks to more modern procedures, the unwanted content of the psychoactive substance THC (Tetrahydrocannabinol) is reduced.

The hemp seed can be stored relatively well if the right conditions are maintained. It is important to ensure the correct temperature and humidity of the storage atmosphere. It is advisable to aerate the stored seed layer regularly and prevent damage during handling. The next step in processing is pressing, usually on screw presses. The temperature of the oil at the outlet of the press should not be higher than 50 °C. Oxidative stability is most often defined in the literature (*Bárta et al., 2021*) by the value of the peroxide number and the acidity number.

Virgin hemp oil has a high content of unsaturated fatty acids. If technological discipline is observed during its processing, it retains all nutritionally important substances and does not contain the psychoactive substance THC. On the sensory side, hemp oil has a slightly nutty smell and a light green color.

Aim of this research was to verify the effect of filtration conditions on the operating parameters and properties of the filtered oil and thus contribute to the improvement of the processing quality of vegetable oils.

MATERIALS AND METHODS

Unfiltered hemp oil of the Bialobrzeskie variety grown in the village of Částrov (Vysočina region, Czech Republic) was used for the implementation of the experiment. The harvested seed was subjected to post-harvest treatment and stored for 30 days. It was subsequently pressed on a low-tonnage screw press Farmet Duo (Farmet, s.r.o., Czech Republic) at an outlet oil temperature of 43 ± 3.5 °C. The pressed oil was stored for four days at a temperature of 8 ± 1.2 °C. During storage, the solid part (sludge) naturally separated from the liquid part by gravity. As part of the analytical analysis (elemental composition), these parts were analyzed separately and subsequently subjected to experimental filtration.
For the experimental determination of the filtration curves of the investigated samples, the VÚZT experimental equipment was used (fig. 1). The basis of the device is the FARMET plate filter (Farmet, s.r.o., Czech Republic).

Fig. 1 Experimental device for measuring filtration

For the measured samples, the agrochemical laboratory of VÚZT determined their properties important from the point of view of further use.
- Analytical composition (about EN 15297:2011, ISO 16948:2015) [38,39].
Microbiological analyzes of the total number of microorganisms, mold and yeast content (ČSN EN ISO 4833, ČSN ISO 21527-1,2, ČSN ISO 16649-2 and ČSN EN ISO 7899-2).
- Oxidative stability of the oil expressed by the value of the peroxide number (ČSN EN ISO 3960). The peroxide number value was determined in the stored oil before starting the experiments. In the tested oil before entering the filter and at the exit from the filter.
- Determining the content of impurities microscopically.
- Measurement uncertainties are determined according to documents ČIA European cooperation for accreditation EA 4/02. Measuring devices meet the requirements of ČSN EN ISO/IEC 17 025.

The experimental device enables the setting of operating parameters and online sensing of monitored physical quantities at nodal points. For uniform flow, the device is equipped with a system of adjustable static oil pressure in the range of 0-300 kPa (limited by the filter design).
During the experiment, the oil is pushed through the membrane by static pressure into the plate filter. The pressure is set to the desired level before the start of the experiment.
The flow rate is determined by mass using a KERN FTC 60K2 tensometric balance with a measuring range of 60 ± 0.002 kg with a digital on-line output.
The oil pressure before the filter is measured using a Greisinger DMP 331 110 pressure transducer with a measuring range of 0...1600 ± 40 kPa.

The oil temperature is measured by jacketed thermocouples type K*0.25 mm with a time constant*1 s. The oil temperature is measured in the inlet reservoir, at the filter inlet, at the filter outlet and in the outlet reservoir. The relative humidity and temperature of the surrounding air is measured by the Testo 6651 temperature and humidity converter (accuracy ± 0.5°C, ± 2.5% RH) during the experiments. All the listed gauges are connected to the COMET MS6D measuring and recording center as well as the weight measurement.
All data were recorded using the COMET MS6D control unit with a set interval during online connection with a PC or in recording mode with subsequent data export to a PC.
As part of the experiments, oil filtration curves at constant pressure were determined. A sample of 15 kg of oil was prepared when measuring the filter curves. The sample was released from the storage container by gravity into the inlet reservoir and after stabilization was released into the storage pressure vessel. After setting the desired pressure value, the filter inlet pipe was filled with the sample. If necessary, excess air was removed with the help of a venting valve, and then the recording of values was started. The measured values could be monitored online on a PC connected to the measuring station. A sample of material was considered filtered if the measured oil flow was zero for 30 seconds.
The measured data were processed in the MS Excel program and statistically evaluated in the STATISTICA program.

RESULTS AND DISCUSSION

Table 1 shows the results of elemental analysis of oil and sludge.

Tab. 1 Composition of hemp oil and sludge according to analytical analysis

Parameters	Value, %	
	oil	sludge
amount of carbon, %	68.07 ± 1.12	77.86 ± 1.14
amount of hydrogen, %	10.15 ± 0.45	11.31± 0.42
amount of sulphur, %	0.26 ± 0.001	0.08± 0.001
amount of nitrogen, %	1.82 ± 0.1	0.05± 0.001
amount of chlorine, %	0.069 ± 0.004	26± 0.004
amount of silicon %	0.80 ± 0.003	0.24± 0.004
amount of calcium, %	0.253 ± 0.025	<0.07
amount of magnesium, %	<0.05	<0.04
amount of potassium, %	0.814 ± 0.016	0.07± 0.020
amount of phosphorus, %	0.650 ± 0.004	0.005± 0.002
amount of zinc, mg/kg	0.002 ± 0.75	0.002 ± 0.75
amount of cadmium, mg/kg	<0.2	<0.2
amount of lead, mg/kg	<0.002	<0.002
amount of chromium, mg/kg	<0.002	<0.002
amount of copper, mg/kg	<0.001	<0.001

The oil was subsequently subjected to microbiological analyses. These were carried out for the content of the total number of microorganisms, the number of yeasts and molds, Escherichia coli and intestinal enterococci. The results according to the analysis of the VÚZT microbiology laboratory are shown in Table 2.

Tab. 2 Results of the microbiological analysis of the oil

Parameters	Value
total number of microorganisms, CFU/ml	< 10
yeast and mold count, CFU/ml	< 10
Escherichia coli, CFU/ml	0
intestinal enterococci, CFU/ml	0

The figures 2 and 3 graphically show examples of the filter curves at set pressure values of 200 and 250 kPa. The pressure in the system was maintained at the set value using a pressure reducing valve with an accuracy of ± 10 kPa. The temperature of the sample increased slightly during filtration due to the increased pressure.

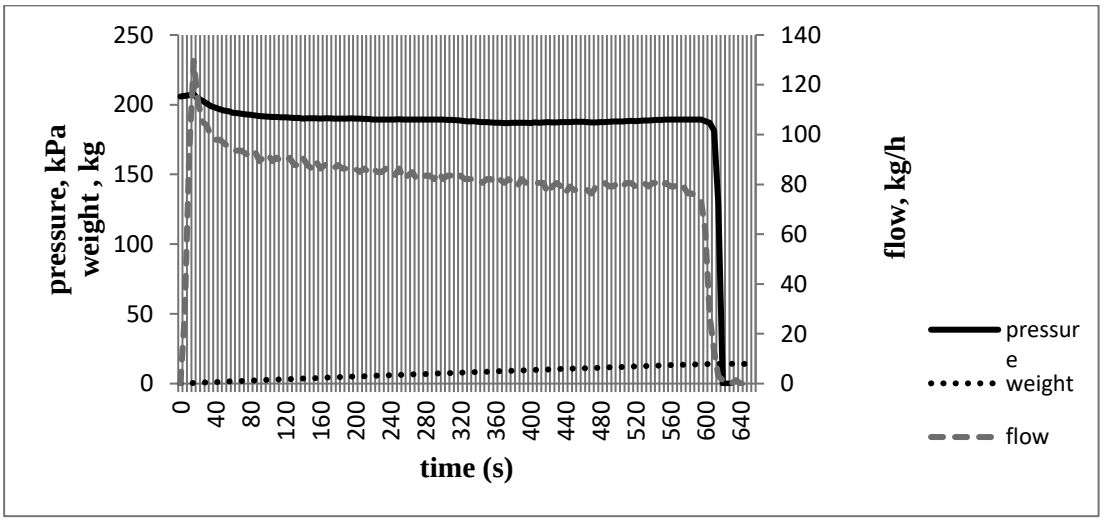

Fig. 2 Graphic representation of the course of oil pressure, flow through the plate filter and the weight of filtered oil within the experiment – 200 kPa

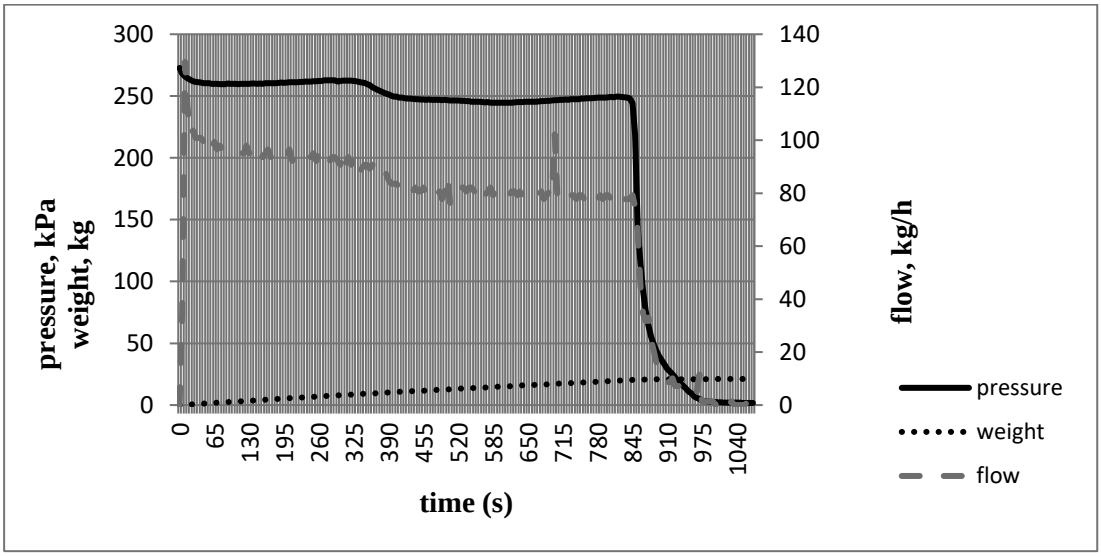

Fig. 3 Graphic representation of the course of oil pressure, flow through the plate filter and the weight of filtered oil within the experiment – 250 kPa

It is clear from the graphs in Figures 2 and 3 that the greatest flow through the filter was recorded at the beginning of the measurement. During the experiment, it gradually decreased due to the sludge clogging of the filter plates.
The filtration parameters for other pressure values in the range of 0-250 kPa were determined in the same way as in the given examples. The dependence of oil flow through the filter on its pressure is shown in Figure 4.

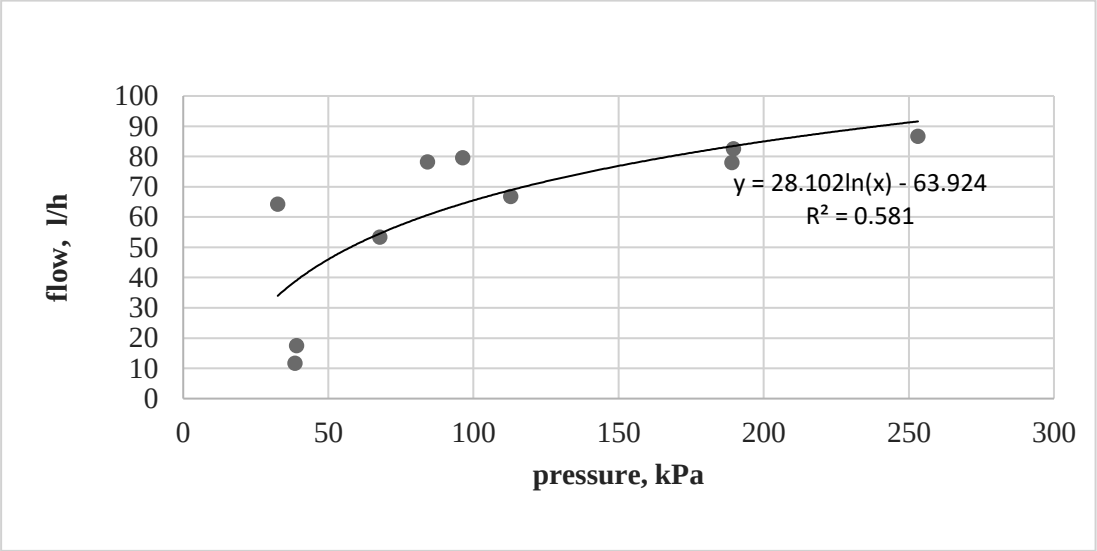

Fig. 4 Dependence of filtered oil flow on pressure - filter N 15-25

From the results in Figure 4, it is clear that the pressure change at a lower level (up to approx. 100 kPa) has a greater influence on the flow value. When the pressure changes above approx. 150 kPa, the change in the flow is no longer evident - it is so significant, as well as in literature (*Guerrini et al., 2020*). Minor discrepancies are caused by differences in the temperature of the filtered oil and the level of filter clogging (pressure losses). This finding is consistent with (*Yamamoto and, Toda, 2018*).
Another monitored parameter was the oil temperature, while in the monitored range of 15-25 °C, the temperature had no significant effect on the filtration rate. The stated temperature range was within the range also stated by According to the literature (*Vitorovič et al., 2021*). According to the literature (*Kyselka et al., 2017*), the temperature in the specified range has no effect on the quality parameters of the oil. Logically, however, it can be assumed that with larger temperature differences, the viscosity of the oil will change more significantly and the effect on the flow value will also be more pronounced. Verification will be the subject of further research.

CONCLUSIONS

The measurement results show that when filtering vegetable oils on plate filters, the oil pressure is a decisive factor for the filtration speed. Higher pressure is supposed to result in faster oil flow. In the area of lower pressures (up to 100 kPa), the effect of pressure on flow is more significant than at higher pressures. The upper limit of the applied pressure is given by the constriction solution of the filter.
Another important aspect that affects the material flow is the gradual clogging of the membranes during the formation of the filter cake. With a higher layer, the pressure drop increases and the flow decreases. In the monitored temperature range of 15 – 25 °C, no statistically significant effect on the oil flow through the filter was recorded.
The achieved results confirmed the predicted expectations. At this moment, the knowledge can be used and the conclusions can be drawn for operations processing plant sludge for technical purposes. In order for recommendations to be formulated also for the areas of food industry, pharmacy, etc., the experimental activity will continue with the fact that the research will be focused on questions of the effect of the filtration process on the composition and oxidative stability of oils.

ACKNOWLEDGMENT
This study was supported by the project of the Ministry of Agriculture of the Czech Republic No. QK21010151 Obtaining vegetable oils using modern methods and the project of long time development of Research Institute of Agricultural Engineering p.r.i. no. RO0618.

REFERENCES

1. P. Mendel , T. Vyhnánek , E. Braidot , A. Filippi , V. Trojan , M. Bjelková , M.D. Vaverková , D. Adamcová , J. Zloch , M. Brtnický & B. Đorđević (2020): Fiber Quality of Hemp(Cannabissativa L.) Grown in Soil Irrigated by Landfill Leachate Water., *Journal of Natural Fibers*,DOI: 10.1080/15440478.2020.1843101
2. Bárta, J.; Bártová, V.;Jarošová, M.; Švajner, J.; Smetana, P.;Kadlec, J.; Filip, V.; Kyselka, J.;Berčíková, M.; Zdráhal, Z.; et al. (2021). Oilseed Cake Flour Composition,Functional Properties and Antioxidant Potential as Effects ofSieving and Species Differences. *Foods*, 10, 2766.
3. Souček, J., Jasinskas, A. (2020). Assessment of the Use of Potatoes as a Binder in Flax Heating Pellets. *Sustainability*, 12, 10481
4. Kyselka et al. (2017). Antioxidant and antimicrobial activity of linseed lignansand phenolic acids. *Eur Food Res Technol*. 243:1633–1644
5. Tura, M, et al. (2022). Evaluation of Hemp Seed Oils Stability under Accelerated Storage Test. *Antioxidants.* 11(3), 490.
6. Vitorovič et al. (2021). Antioxidant Activity of Hemp (Cannabis sativa L.) Seed Oil in Drosophila melanogaster Larvae under Non-Stress and H2O2-Induced Oxidative Stress Conditions. *Antioxidants.* 10(6), 830.
7. Malaťáková, J., et al (2021). Evaluation of Small-Scale Gasification for CHP for Wood from Salvage Logging in the Czech Republic. *Forests.* 12(11), 1448
8. Yamamoto, K., Toda, Y. (2018). Numerical Simulation on Flow Dynamics and Pressure Variation in Porous Ceramic Filter. *Computation*. 52(2), 1-14.
9. Guerrini L, Zanoni B, Breschi C, Angeloni G, Masella P, Calamai L, Parenti A. (2020). Understanding Olive Oil Stability Using Filtration and High Hydrostatic Pressure. *Molecules*. 25(2). 420

Corresponding author:
Ing. Jiří Souček, Ph.D., Research Institute of Agriculture Engineering, 161 01 Prague 6 , Czech Republic; phone: +420 233022214, e-mail: jiri.soucek@vuzt.cz

DEVELOPING OF CONTROL SYSTEM FOR INDOOR HYDROPONIC VERTICAL FARMING

Miroslav STROB[1], Jiří ZHOŘ[1], Pavel OLŠAN[1], Martin FILIP[1]

[1]Department of Technology and Cybernetics, Faculty of Agriculture and Technology, University of South Bohemia in České Budějovice, Studentská 1668, 370 05 České Budějovice

Abstract
Vertical farming systems are engineering solutions aiming to increase agricultural productivity per unit area of cultivated land, on account of growing in multiple layers. This research focuses on developing of new control system, which is controlling individual factors, that have an effect on growth process and quality and yield of crops. To be able to monitor hydroponic solution, the electronic analyzer and conductometer were assembled. The methods for proposed quantities verification and calibration were proposed. To measure quantities such as concentration, and other ions, the ion selective probes (ISE) were chosen. To measure pH, DO and EC special measuring electrodes were used. The pH, EC and K+ probes were calibrated.

Key words: *vertical farm, hydroponics, control system, leafy vegetables.*

INTRODUCTION

Vertical farming systems were designed as an engineering solution that aimed to increase agricultural productivity per unit area of cultivated land. Production in vertical farming systems takes place in vertical dimension, which enhances crop production capacity, using less area. *(Eigenbrod and Gruda 2014; Hochmuth and Hochmuth 2001; Resh 2012)*. Vertical farming system has shown potential for producing high-quality crops and high yields. Hydroponic cultivation is the most common method in vertical farms, as the system consumes 90% less water compared to conventional agriculture. This is considered as one of the biggest advantages, as it resolves one of the biggest challenges of agriculture in the drought-affected areas *(Farhangi et al., 2021)*.

Leafy vegetables account for over half of the indoor farming operations worldwide *(Wong et al., 2020)*, especially lettuce which is commonly used as a model plant *(Safaei et al. 2015)*. Lettuce (*Lactuca sativa* L.) has short production cycle and is suitable for hydroponic growing. Moreover, lettuce is popular for tender taste, sweet and refreshing flavor, and nutritional and antioxidant compounds *(Riga et al.; 2019)*. Environmental factors can be fully controlled in a vertical farm *(Jin et al., 2022)*. However, there is a lack of precise data of the influence of different factors such as the concentration of the nutrient solution, light conditions, humidity, and temperature on the growth of different kind of plants in vertical farms *(Sihombing et al., 2018)*.

Concentration of dissolved nutrients that are absorbed by plant roots vary with temperature, light and growth stage. During the period of growth, plant roots are secreting several substances, whereas they are continuously absorbing specific nutrients. Therefore, some nutrients in the nutrient solution appear to be insufficient or excessive. Among the most commonly monitored parameters in the nutrient solution belong pH, electrical conductivity, dissolved oxygen and temperature. In the case the parameters exceed a threshold, relevant amount of nutrients should be supplied, in order to maintain the electrical conductivity and pH in the nutrient solution. Such system increases the workload *(Chang et al., 2018)*. Most of hydroponic regulating systems are focused on changes in pH, EC, and DO of nutrient solution, whereas only a few studies considered adding ion concentrations and flow rate control methods *(Genuncio et al., 2012; Neto et al., 2014; Ban et al., 2021).*

Different light conditions (light quality, light intensity and photoperiod) induce various morphogenetic and photosynthetic responses in plants *(Lin et al., 2013; Bian et al., 2018; Yan et al., 2019)*. Unfortunately, electricity use for lighting in vertical farms causes high energy consumption, which is in the end substantially higher in comparison with conventional production *(Kozai, 2013)*. Light conditions, especially light intensity, seem to have a strong effect on nutrient accumulation in plant tissues *(Chen et al., 2021)*. It has been proposed, that the light environment needs to be optimized in order to provide optimal conditions for growth and to reduce electricity consumption *(Fan et al., 2013; O'Carrigan et al., 2014)*.

In indoor farms with controlled environment, CO_2 is often supplemented, as research reports have shown that CO_2 enhanced growth at CO_2 enrichment concentrations *(Kozai, 2018; Zheng et al., 2019)*.
Many researches have focused on the advantages of individual factors (such as light conditions, hydroponic solution, CO_2 etc.) but fewer studies have focused on interaction and on separate controlling of those factors. The aim of this research is to propose various methods to automatically regulate and replenish the nutrient solution, to measure and optimize light conditions and to supply the environment with higher CO_2 concentration. This system will measure the concentration of individual ions (N, P, K, Ca, Mg, S) in a nutrient solution, with the aim of maintaining the appropriate nutrient composition by supplying relevant amounts of only insufficient ions. Systems will also measure light intensity and spectra, same as CO_2 level in all layers of vertical farm.

MATERIALS AND METHODS

Fundamental concept of the control system

The control system of the indoor farm is designed to be modular, low-power consumption, easy to expand and reliable. The control system has to be able to serve also big farming areas, up to several thousands of meters of farming technology. The proposed solution is based on custom made electronic which allows fulfil the specific requirement of concrete farm or experiment. For example, number of channels, type of power supply and variability of actuators, sensors required by the user etc. The basic concept of control system is shown in Fig. 1.
Main parts of control system in developing progress are:

- chemical analyzer with conductometer and pH measuring
- CO_2 probes
- ambient conditions measuring (relative humidity, temperature, atmospheric pressure)
- light switches
- pump and valve switches
- fan control
- light spectrum meter

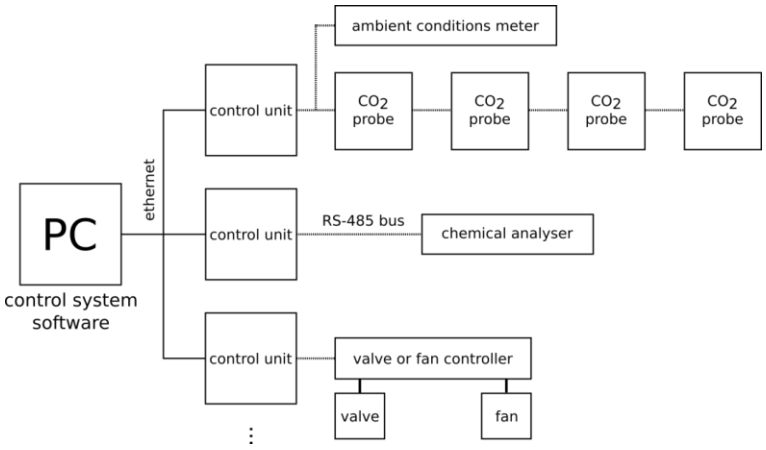

Fig.1 Block schematics of proposed control system

Electrical parameters of whole control system match the standard industrial properties, such as supply voltage 24 VDC, standard bus wiring etc. The communication is based on the RS-485 single twisted pair (100 Ω impedance) bus with proprietary protocol BeeCOM Hyperion, max. speed up to 1Mbaud.

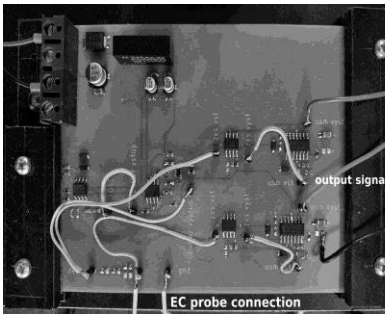

Fig. 2 Prototype of conductometer

Manufactured control system parts

The fundamental part of the control system is central unit, Fig. 4. Central unit could be connected to the standard LAN network. Present network infrastructure could be used. Central unit communicates with all others parts of control system.

The mail goal of the first stage of developing of the farm system is hydroponic solution monitoring. It means in-line measuring of these selected parameters:

- pH
- DO – dissolved oxygen
- EC – electrical conductivity
- NO_3^- – concentration of nitrate ions
- NH_4^+ – concentration of ammonium ions
- K^+ – concentration of potassium ions
- P – phosphorus

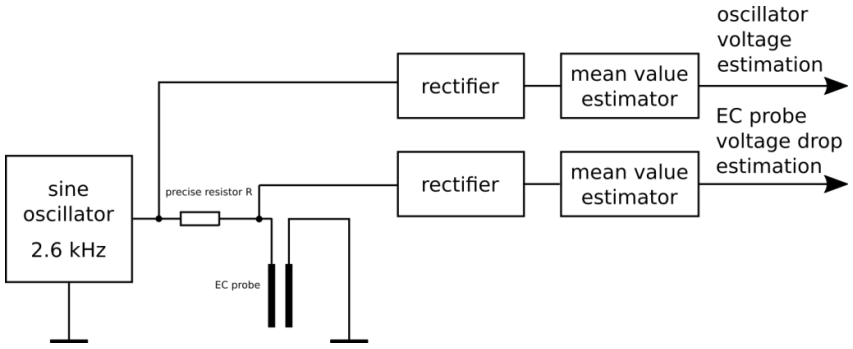

Fig. 3 Block schematics of conductometer

To achieve it, the electronic analyzer and conductometer were produced, Fig. 2 and Fig. 5. It is possible to connect to the analyzer up to 4 analogue outputs from ion selective electrodes (ISE), pH probe or dissolved oxygen (DO) probe and conductometer. Because of temperature dependency of the most quantities, one Pt100 temperature sensor could be also connected.

The principle of conductometer is shown in the Fig. 3. An electric conductivity probe with sink electrodes is used. Principle of measuring is based on the voltage drop on the EC probe and known sensing resistor compared to oscillator voltage. When the oscillator voltage is used as reference voltage of AD converter, we can estimate the conductivity (admittance) of the measured solution between electrodes of EC probe as:

$$Y = \frac{ADC_{range} - 1 - ADC_{code}}{R_{sense} \cdot ADC_{code}} \; [S]$$

RESULTS AND DISCUSSION

Fig. 4 Central unit

To verify the analyzer and the conductometer, the measuring chain was connected (PC, central unit and analyzer with conductometer). All quantities are converted to electric voltage. The verification was made on the level of electrical measuring without real chemical solution measurement. The result of verification is to determine the calibration polynom, it is assumed the 1st or 2nd order, end error fit estimation.

In the case of Pt100 temperature probe and conductometer, the calibrational resistance decade was applied to the input. Resistance of decade was measured with laboratory ohmmeter with verified accuracy 10 mΩ. ISE analogue

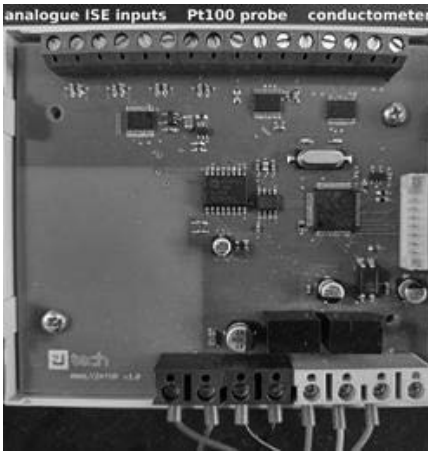

Fig. 5 Chemical analyzer DPS with 4 channels ISE connections, Pt100 temperature probe connection and conductometer input

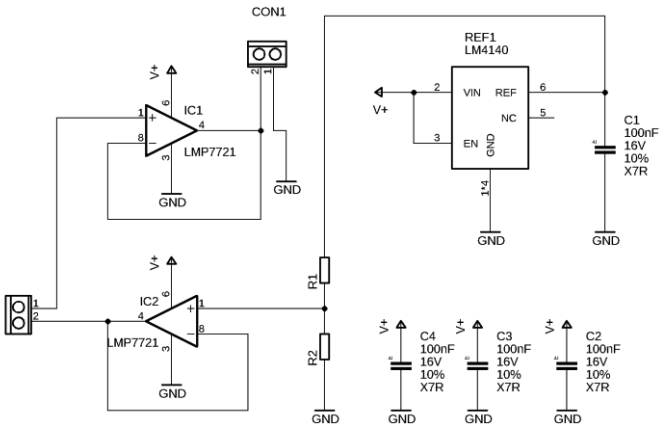

Fig. 6 Analogue buffer

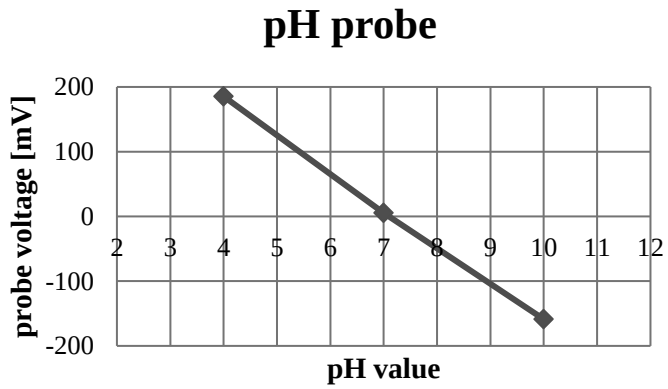

Fig. 7 pH calibration graph

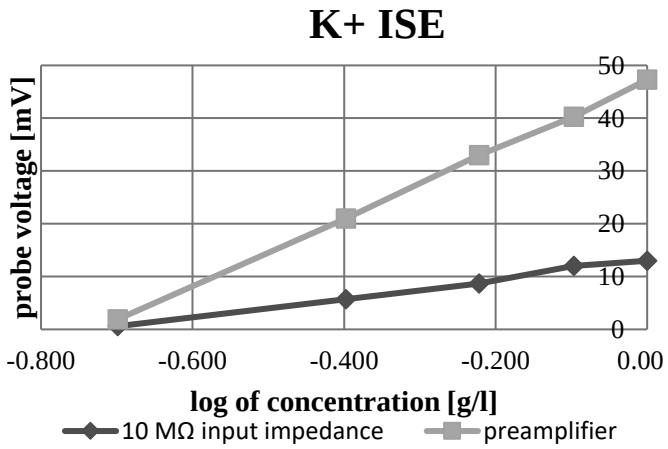

Fig. 8 K+ calibration graph

input channel was verified by appliing DC voltage and, used voltmeter had verified precision 0.2 mV.

Maximal absolute error of Pt100 temp probe after polynomial fitting, using minimalisation of root mean square error, is $|\Delta_{Rm}| = 18\,\text{m}\Omega$, this value corresponds to the used ohmmeter accuracy.

Maximal absolute error of conductivity measurement after polynomial fitting is $|\Delta_{Gm}| = 0.763\,\mu\text{S}$, this value corresponds, in resistance, to 275 mΩ. This corresponds also with accuracy of resistance decade 0.5 % and ohmmeter accuracy.

Maximal absolute error of voltage (ISE) measurement after polynomial fitting is $|\Delta_{Um}| = 0.347\,\text{mV}$. The verification prooved, that accuray of analyzer (Pt100 and ISE measuring) and conductometer is appropriate, comparable to laboratory multimeter measurement.

Ion-selective electrodes (ISEs) are promising technology as they can directly measure the analyte with a wide sensitivity range. Above that, they are are small and portable *(Kim et al., 2013)*. Therefore, to measure quantities such as concentration K^+, NH_4^+ and other ions, the ion selective probes (ISE) were chosen. To measure pH, DO and EC also special measuring electrodes were used. To this time, the calibration of pH, EC, and K^+ is done, other quantities will follow.

Because of high internal resistance of pH probe (approx. 150 MΩ), the special analogue buffer with precise operational amplifier with low input current (pA) LMP7721 was designed. Also offset voltage was added to be able to measure negative probe voltage. See Fig. 6. The calibration of pH probe was based on the known pH of solution (pH puffers 4, 7 and 10). In Fig. 7 we can see the linear dependency of probe voltage on the pH of solution. The determined slope of electrode is 57 mV/pH.

Electrical conductivity determines the amount of mineral salts dissolved in the hydroponic solution *(Ashley, 2015)*.

During the electrical conductivity measurement, the solutions with defined conductivity were prepared – 1491, 745, 497 and 372 µS/cm. These conductivities match with conductometer range 0.2 – 5 mS.

In the case of ISE calibration of K^+ and also for the other ions measuring, the calibration graph was drawn, see Fig. 8. The slope of ISE could be determined from the graph in accordance with the equation:

$$S = \frac{U_{con1} - U_{con2}}{\log\left(\frac{c_{con2}}{c_{con1}}\right)} \; [mV \cdot g^{-1} \cdot l]$$

Where S is slope, c is ion concentration and U is according ISE voltage. Two measurements were done, direct voltmeter measurement with 10 MΩ input resistance and with analogue buffer with analyzer. The internal resistance of ISE is also high, the measurement should be done with the high input resistance voltmeter (more than 10 MΩ) or with analogue buffer, e.g. from Fig. 6. The determined slope using analogue buffer is 57.5 $\mathrm{mV \cdot g^{-1} \cdot l}$.
The methods for proposed quantities verification and calibration were proposed. The uncertainty of measurement should be also determined in the next steps.

CONCLUSIONS

We carried out a comprehensive proposal of control system for indoor hydroponic vertical farming. Part of the chemical analyzer and conductometer were implemented. We verified the function of presented system and performed the basic calibration procedures. Currently, we are working on the testing part, that takes place in the phytotron at University of South Bohemia. Simultaneously, we adjust nutrient solution pumping control, in-line chemical analysis, lighting control, taking into account the qualitative analysis of plant biomass. Future studies with growing plants would provide the evidence of utility and applicability of control system for indoor hydroponic vertical farming. This would give us an overview on the whole process of vertical farming, so we will be able to implement technologies to a various farms, including different modifications.

ACKNOWLEDGMENT

This study was supported by the Technology Agency of the Czech Republic, grant number: TM03000063. In collaboration with companies 4Jtech s.r.o. and 2050farm s.r.o.

REFERENCES

1. Kozai, T. (2018). Smart Plant Factory: Next-Generation Indoor Vertical Farms. Singapore: Springer. doi: 10.1007/978-981-13-1065-2.
2. Zheng, Y., Li, F., Hao, L., Yu, J., Guo, L., Zhou, H., et al. (2019). Elevated CO2 concentration induces photosynthetic down-regulation with changes in leaf structure, non-structural carbohydrates and nitrogen content of soybean. BMC Plant Biol. 19:255. doi: 10.1186/s12870-019-1788-9.
3. Genuncio, G. C., Gomes, M., Ferrari, A. C., Majerowicz, N., & Zonta, E. (2012). Hydroponic lettuce production in different concentrations and flow rates of nutrient solution. Hort. Brasileira, 30(3), 526-530. https://doi.org/10.1590/S0102-05362012000300028.
4. Neto, A. J. S., Zolnier, S., & de Carvalho Lopes, D. (2014). Development and evaluation of an automated system for fertigation control in soilless tomato production. Comput. Electron. Agric., 103, 17-25.
5. Safaei, M., J. Panahandeh, S. J. Tabatabaei, and A. R. M. Azar. 2015. Effects of different nutrients solutions on nutrients concentration and some qualitative traits of lettuce in hydroponics system. J. Sci. Technol. Greenh. Cult. 6:Pe1–Pe7, En8.
6. CHANG, Chung-Liang, Guo-Fong HONG a Wei-Lun FU. Design and Implementation of a Knowledge-Based Nutrient Solution Irrigation System for Hydroponic Applications. Transactions of the ASABE. 2018, 61(2), 369-379. ISSN 2151-0040. Dostupné z: doi:10.13031/trans.11564.
7. BAN, Byunghyun, Janghun LEE, Donghun RYU, Minwoo LEE a Tae Dong EOM. Nutrient Solution Management System for Smart Farms and Plant Factory. In: 2020 International Conference on Information and Communication Technology Convergence (ICTC). IEEE, 2020, 2020-10-21, s. 1537-1542. ISBN 978-1-7281-6758-9. Available at: doi:10.1109/ICTC49870.2020.9289192.
8. Riga, P.; Benedicto, L.; Gil-Izquierdo, Á.; Collado-González, J.; Ferreres, F.; Medina, S. Diffuse light affects the contents of vitamin C, phenolic compounds and free amino acids in

lettuce plants. Food Chem. 2019, 272, 227–234.
9. WONG, Chui Eng, Zhi Wei Norman TEO, Lisha SHEN a Hao YU. Seeing the lights for leafy greens in indoor vertical farming. Trends in Food Science & Technology [online]. 2020, 106, 48-63, ISSN 09242244. Available at: doi:10.1016/j.tifs.2020.09.031.
10. Hochmuth, R., and G. J. Hochmuth. 2001. A decade of change in Florida's greenhouse vegetable industry: 1991–2001 Pp. 280–283 in Proc. Fla. State Hort. Soc.
11. Resh, H. M. 2012. Hydroponic food production: a definitive guidebook for the advanced home gardener and the commercial hydroponic grower. CRC Press.
12. Eigenbrod, C., and N. Gruda. 2014. Urban vegetable for food security in cities. A review. Agron. Sustain. Dev. 35:483–498.
13. Farhangi, M.; Farhangi, S.; van de Vlasakker, P.C.H.; Carsjens, G.J. The Role of Urban Agriculture Technologies in Transformation toward Participatory Local Urban Planning in Rafsanjan. Land 2021, 10, 830.
14. Sihombing, P.; Karina, N.; Tarigan, J.; Syarif, M. Automated hydroponics nutrition plants systems using arduino uno microcontroller based on android. J. Phys. Conf. Ser. 2018, 978, 012014.
15. Jin, W., Formiga Lopez, D., Heuvelink, E., & Marcelis, L. F. M. (2022). Light use efficiency of lettuce cultivation in vertical farms compared with greenhouse and field. Food and Energy Security, 00, e391. https://doi.org/10.1002/fes3.391.
16. Kozai, T. (2013). Resource use efficiency of closed plant production system with artificial light: Concept, estimation and application to plant factory. Proceedings of the Japan Academy. Series B, Physical and Biological Sciences, 89, 447–461. https://doi.org/10.2183/pjab.89.447.
17. Lin, K.H.; Huang, M.Y.; Huang, W.D.; Hsu, M.H.; Yang, Z.W.; Yang, C.M. The effects of red, blue, and white light-emitting diodes on the growth, development, and edible quality of hydroponically grown lettuce (*Lactuca sativa* L. varcapitata). Sci. Hortic. 2013, 150, 86–91.
18. Bian, Z.; Cheng, R.; Wang, Y.; Yang, Q.; Lu, C. Effect of green light on nitrate reduction and edible quality of hydroponically grown lettuce (*Lactuca sativa* L.) under short-term continuous light from red and blue light-emitting diodes. Environ. Exp. Bot. 2018, 153, 63–71.
19. Yan, Z.; He, D.; Niu, G.; Zhai, H. Evaluation of growth and quality of hydroponic lettuce at harvest as affected by the light intensity, photoperiod and light quality at seedling stage. Sci. Hortic. 2019, 248, 138–144.
20. Chen, Z.; Shah Jahan, M.; Mao, P.; Wang, M.; Liu, X.; Guo, S. Functional growth, photosynthesis and nutritional property analyses of lettuce grown under different temperature and light intensity. J. Hortic. Sci. Biotechnol. 2021, 96, 53–61.
21. Fan, X., Xu, Z., Liu, X., Tang, C., Wang, L., and Han, X. (2013). Effects of light intensity on the growth and leaf development of young tomato plants grown under a combination of red and blue light. Sci. Horticult. 153, 50–55. doi: 10.1016/j.scienta.2013.01.017.
22. O'Carrigan, A., Hinde, E., Lu, N., Xu, X. Q., Duan, H. L., Huang, G. M., et al. (2014). Effects of light irradiance on stomatal regulation and growth of tomato. Environ. Exp. Bot. 98, 65–73. doi: 10.1016/j.envexpbot.2013.10.007.
23. Ashley, "Electrical Conductivity and hydroponic gardening," FifthSeasonGardening, 2015. [Online]. Available: https://fifthseasongardening.com/electrical- conductivity-and-hydroponic-gardening
24. KIM, Hak-Jin, Won-Kyung KIM, Mi-Young ROH, Chang-Ik KANG, Jong-Min PARK a Kenneth A. SUDDUTH. Automated sensing of hydroponic macronutrients using a computer-controlled system with an array of ion-selective electrodes. Computers and Electronics in Ag-riculture [online]. 2013, 93, 46-54 [cit. 2022-08-25]. ISSN 01681699. Available at: doi:10.1016/j.compag.2013.01.011

Corresponding author:
Ing. Jiří Zhoř, Department of Technology and Cybernetics, Faculty of Agriculture and Technology, University of South Bohemia in České Budějovice, Studentská 1668, 370 05 České Budějovice, phone: +420 775 258 880, e-mail: jiri.zhor@2050farm.cz, zhorji00@fzt.jcu.cz.

MECHANICAL PROPERTIES OF BIOMASS PELLETS

Maroš SZENTESI[1], Viera KAŽIMÍROVÁ[1], Ľubomír KUBÍK[2]

[1]*Department of Building Equipment and Technology Safety, Faculty of Engineering, Slovak University of Agriculture in Nitra*
[2]*Department of Physics, Faculty of Engineering, Slovak University of Agriculture in Nitra*

Abstract
The presented paper deals with the assessment of mechanical properties of pellets. Waste biomass in a form of wooden parts of vine prunings, spruce sawdust, and ground sunflower straw were utilized for the pellet production. Mechanical properties were observed by an experimental device Andilog Stentor 1000, using a quasi-static test – compressive loading test between two pistons in the pellets' axial direction. Based on the measured values, loading curves between compress force F(ε) and compressive strain σ(ε) were plotted, and moduli of elasticity were calculated for each of the materials. The maximum compressive force was 180.76 N for vine prunings pellets; 315.98 N for spruce sawdust pellets; 239.89 N for sunflower straw pellets. The modulus of elasticity showed mean values of 70.83 MPa for vine prunings pellets, 47.37 MPa for spruce sawdust pellets, and 7.48 MPa for sunflower straw pellets.

Key words: *biomass; force; pellet; stress; modulus of elasticity.*

INTRODUCTION

The change in climate conditions and the exhaustion of fossil fuels represent the basic arguments for changing the approach to heat production and biomass processing for energy purposes, whether it is the biomass from fast-growing trees or waste biomass. For its thermal properties, popularity of biomass is growing (*Božiková et al., 2021*); furthermore, the energy sector considers it an extremely important element in terms of reducing CO_2 emissions and it can be seen as an ecological fuel (*Mohanti et al., 2014*). Investigating the properties of fuels is the basis for their efficient utilization. In terms of solid biofuels, compacted biomass represents an alternative for reducing emissions and eliminating landfills (*Malaťák et al., 2020*). Biomass in a form of pellets and briquettes eliminates the disadvantages of so-called raw biomass, which has an irregular shape, low bulk density, high moisture content, which results in issues during handling and storage (*Puig-Arnavat et al., 2014; Zhou et al, 2016*). The pellet quality is influenced by the basic properties of input biomass – particle size, moisture content and chemical composition – and operating conditions under which they are produced, such as die temperature, application pressure, pressing time and mold geometry (*Lestander et al. 2012*). Leftovers from forestry and agricultural production sectors are considered an input biomass for the purposes of solid biofuel formation process (*Križan et. al., 2015; Liu et al., 2016; Nizamuddin et al., 2016*). As a part of the policy for reducing emissions in energetics, significant efforts are made to produce high-quality pellets with utilization of different types of materials – the pellets can be produced from a single material or from a mixture of various types of biomass (*Liu et al., 2013*), by combining mineral raw materials with biomass (*Tsuchia et al., 2017*). Pelleting and briquetting are the most frequently utilized methods for solid biofuel production; mechanical properties represent the essential data on the quality of produced biofuel regardless of whether it is a pellet or a briquette (*Stasiak et al., 2017*). The goal of this paper was to determine the mechanical properties of pellets produced from waste biomass, which can serve as a substitute for fossil fuels.

MATERIALS AND METHODS

The pellet samples were produced from waste biomass including vine prunings, spruce wood and sunflower straw. All materials were obtained locally. All materials were compressed to a pellet form using a MGL 200 pellet press (Kovo Novak, Czech Republic) without adding a binder. Pressing die hole size was 8mm. For the purposes of stabilization, the pellets produced were left on the mat for 48 hours at a constant environmental temperature and humidity. The length and weight of pellets did not change after this time. In order to subject the pellets produced to the experimental loading test to determine their

mechanical properties, the pellet contact surfaces were adjusted for the purposes of test requirements. Ten pellets made of each material were subjected to loading test.

The mechanical properties of biomass pellets were assessed using a static loading test on an Andilog Stentor 1000 experimental device. A pellet was placed on the piston of the experimental device and compressed by the second piston at a speed of 10 mm.min^{-1} in the axial direction until the pellet strength limit was reached, destroying the pellet tested. The upper piston of experimental device automatically returned to its initial position after breaking the pellet.

The test output is a compression diagram expressing the dependence of $F(\varepsilon)$, where F represents the loading force and ε represents the pellet strain following the equation (1):

$$\varepsilon = \frac{\Delta L_0}{L_0} \quad (1)$$

where ε stands for strain (-), L_0 stands for original pellet length (mm), ΔL_0 movement of the upper experimental device piston.

The maximum loading force F_m and maximum strain ε_m were determined based on the compression diagram.

Subsequently, the dependence was established, in which σ represents the compressive stress calculated according to the equation (2):

$$\sigma = \frac{F}{S} \quad (2)$$

where σ stands for compressive stress (MPa), F stands for force (N), S stands for cross-sectional area of the pellet (mm^2).

The pellet cross-sectional area was calculated based on the following equation (3):

$$S = \frac{\pi d^2}{4} \quad (3)$$

where S stands for cross-sectional area of the pellet (mm^2), d stands for pellet diameter (mm).

The maximum compressive stress σ_m was determined based on the compression diagram $\sigma(\varepsilon)$. The modulus of elasticity was determined based on the startup part of the compression diagram. The linear regression method was used to calculate the modulus of elasticity, which is expressed by equation (4):

$$\sigma = E\varepsilon + b \quad (4)$$

where σ stands for compressive stress (MPa), E stands for modulus of elasticity (MPa), ε stands for strain (-), b stands for σ-intercept (MPa).

RESULTS AND DISCUSSION

Tab. 1 shows the statistical evaluation of observed parameters of pellets made of all investigated types of biomass.

Considering the results of observed pellets from all materials, it was found that the mechanical properties of pellets produced utilizing an industrial press are quite variable, which is mainly due to the fact that the material is not pressed in a closed mold with a fixed bottom, but continuously pushed through the machine die.

The highest loading force, and consequently pressure, was showed by pellets made of spruce sawdust. *Gorzelány et al. (2020)* achieved an average value of F_m = 222.85 N when testing spruce pellets, which is a value lower than the value observed in the experiment presented. On the contrary, the authors also achieved an average value of σ_m = 7.88 MPa that is higher than the value found in the experiment presented, which is most likely due to the different diameters of tested pellets. The strength of pellets made of spruce sawdust was also investigated by *Huang et al. (2017)* who monitored the compressive strength of spruce pellets. The authors achieved significantly higher values of strength and modulus of elasticity, which was caused by application of higher pressure and temperature values during compaction process.

Lower mean force and pressure values were recorded for sunflower straw pellets. The median values of F_m did not differ significantly for spruce and sunflower pellets.

The lowest values of F_m and σ_m were showed by vine prunings pellets. *Gallego et al. (2020)* also dealt with the topic of determining the modulus of elasticity, observing the mean modulus of elasticity value of spruce pellets of 73.33 MPa, which might have been affected by the increasing moisture content in the samples. Very similar value was observed for the vine prunings pellets.

Tab. 1 Descriptive statistics of pellet compression tests

	F_m N	E MPa	ε_m -	σ_m MPa
Vine prunings pellets				
Mean	180.76	70.83	0.12	3.17
Standard Error	34.84	8.63	0.06	0.61
Median	174.31	63.24	0.05	3.07
Standard Deviation	104.53	25.88	0.19	1.84
Minimum	86.86	37.23	0.02	1.53
Maximum	437.49	123.80	0.63	7.71
Spruce sawdust pellets				
Mean	315.98	47.37	0.18	5.58
Standard Error	48.21	10.06	0.02	1.51
Median	275.98	46.43	0.17	8.86
Standard Deviation	144.64	30.17	0.07	4.52
Minimum	117.78	17.00	0.07	2.09
Maximum	548.72	111.60	0.34	9.67
Sunflower pellets				
Mean	239.89	7.48	0.35	4.06
Standard Error	37.27	1.61	0.04	0.66
Median	208.65	6.09	0.33	3.43
Standard Deviation	111.79	4.83	0.11	1.98
Minimum	100.84	3.43	0.23	1.59
Maximum	436.85	19.54	0.56	7.70

Values of modulus of elasticity similar to the values presented were obtained by *Matkowski et al. (2020)* when investigating pellets produced from wheat straw with addition of calcium carbonate. The mean value of the modulus of elasticity of the mixture pellets examined was E = 7.42 MPa, which is approximately the same value as in pellets made of pure sunflower biomass observed in this research.
The mean maximum strain values ε_m were approximately the same for vine and spruce pellets. A higher value was recorded for sunflower pellets, which is due to the fact that the ground straw is culm plant material.

CONCLUSIONS

The work presented was aimed at determining the mechanical properties of pellets made of three types of wood and plant biomass. Based on the results obtained utilizing compression tests, it can be concluded that the mechanical properties of pellets produced by employing industrial technology are quite variable, yet it is possible that the plant waste biomass can be used for the production of pellets in the same way as wood biomass. Improving the mechanical properties of pellets produced from plant biomass will be the subject of future research.

ACKNOWLEDGMENT

This publication was supported by the Operational Program Integrated Infrastructure within the project: Demand-driven research for the sustainable and innovative food, Drive4SIFood 313011V336, co-financed by the European Regional Development Fund.

REFERENCES

1. Božiková, M., Kotoulek, P., Bilčík, M., Kubík, Ľ., Hlaváčová, Z., & Hlaváč, P. (2021). Thermal properties of wood and wood composites made from wood waste. *International Agrophysics, 35*(3), 251-256.

2. Gallego, E., Fuentes, H. M., Ruiz, A., Hernandez-Rodrigo, G., Aguado, P., & Ayuga, F. (2020). Determination of mechanical preperties for wood pellets used in DEM simulation. *International Agrophysics, 34*(4), 485-494.
3. Gorzelany, J., Zardzewiałyb, M., Murawskic, P., & Matłok, N. (2020). Analysis of selected quality features of wood pellets. *Agricultural Engineering, 24*(1), 25-34.
4. Huang, Y., Finell. S., Larson, S., Wang, Y., Zhang, J., Ewi, R., & Liu, L. (2017). Biofuel pellets made at low moisture content – Influence of water in the binding mechanism of densified biomass. *Biomass and Bioenergy, 98*, 8-14.
5. Kažimírová, V., Kubík, Ľ., & Mihina, Š. (2020). Evaluation of properties of pellets made of swine manure. *Acta technologica agriculturae, 23*(3), 137-143.
6. Križan, P., Matúš, M., Šooš, Ľ., & Beniak, J. (2015). Behavior of Beech Sawdust during Densification into a Solid Biofuel. *Energies,8*(7), 6382-6398.
7. Lestander, A. T., Finell, M., Samuelsson, R., Arshadi, M., & Thyrel, M. (2012). Industrial scale biofuel pellet production from blends of unbarked softwood and hardwood stem – the effect of raw material composition and moisture content on pellet quality. *Fuel Processing Technology, 95*, 73-77.
8. Malaťák, J., Gendek, A., Aniszevska, M., & Velebil, J. (2020). Emision form combusion of renewable solid biofuels from coniferous tree cones. *Fuel, 276*, 118001.
9. Malaťák, J., Velebil, J., Bradna, J., Gendek, A., & Tamelová, B. (2020). Evaluation of CO and NOx emission in real- life operatingconditions of herbacerous biomass briquettes combustion. *Acta Technologica Agriculturae, 23*(2), 53-59.
10. Matkowski, P., Lisowski, A., & Swietochowski, A. (2020). Characterisation of wheat straw pellets individually and in combination with cassava starch or calcium carbonate inder various compaction conditions: Determination of pellet strength and water absorption capacity. *Materials, 13*(19), 4375.
11. Mohanty, P., Pant, K. K., Naik, S. N., Parikh, J., Hornung, A., & Sahu, J. N. (2014). Synthesis of green fuels from biogenic waste through thermochemical route – The role of heterogeneous catalyst: A review. *Renewable and Sustainable Energy Reviews, 38*, 131-153.
12. Nizamuddin, S., Mubarak, N. M., Tiripathi, M., Jayakumar, N. S., Sahu, J. N., & Ganesan, P. (2016). Chemical, dielectric, and structural chracterization of optimized hydrochar produces from hydrotermal carbomization of palm shell. *Fuel, 163*, 88-97.
13. Puig-Arnavat, M., Shang, L., Sárossy, Z., Ahrenfeldt, J., & Henriksen, U. B. (2016). From a single pellet press to a bench scale pellet mill - Pelletizing six different biomass feedstocks. *Fuel Processing Technology, 142*, 27-33.
14. Stasiak, M., Molenda, M., Bánda, M., Wiacek, J., Parafiniuk, P., & Gondek, E. (2017). Mechanical and combustion preperties of sawdust-Straw pellets blended in different proportions. *Fuel Processing Technology, 156*, 366-375.
15. Tsuchiya, Y., Yoshida, T. (2017). Pelletization of brown coal and rice bran in Indonesia: Characteristic of the mixture pellets including safety during transportation. *Fuel Processing Technology*. *156*, 68-71.
16. Zhou, Y., Zhang, Z., Zhang, Y., Wang, Y., Yu, Y., Ji, F., Ahmad, R., & Dong, R. (2015). A comprehensive review on densified solid biofuel industry in China. *Renewable and Sustainable Energy Reviews, 54*, 1412-1428.

Corresponding author:
Ing. Mgr. Maroš Szentesi, Department of Building Equipment and Technology Safety, Faculty of Engineering, Slovak University of Agriculture in Nitra, tr. A. Hlinku 2, 949 76 Nitra, Slovak Republic, phone: +421 37 641 5678, e-mail: xszentesi@uniag.sk

SUSTAINABLE IRRIGATION USING INTERNET OF THINGS

Zisis TSIROPOULOS[1,2], Vasilios LIAKOS[1], Athanasios MAKRIS[1], Georgios PROIAS[1], Ioannis RAPTIS[1], Eleni WOGIATZI[1], Ioannis GRAVALOS[1]

[1]Agricultural and Environmental Solutions (AGENSO), Markou Mpotsari 47, 11742 Athens, Greece
[2]Department of Agrotechnology, School of Agricultural Sciences, University of Thessaly, Gaiopolis, 41500 Larissa, Greece

Abstract
Water is one of the most essential natural resources, which plays an important role in agriculture. The ever-increasing shortage of water and the continuous deterioration of its quality are evident in many countries of the world. The rational use of water in irrigation can be achieved by adopting scientific irrigation scheduling. Today, the traditional irrigation systems should be transformed to smart-irrigation systems for sustainable water management. This highlights the importance of adopting a set of emerging technologies that promise minimising implications of water scarcity. An Internet of Things (IoT) system uses various enabling technologies, such as wireless sensor networks, cloud computing, big data, embedded systems, security protocols and architectures, communication protocols, and web services. In this paper is presented an IoT-based precision irrigation technology using wireless sensor network (WSN). The system was installed in hemp plots to monitor soil moisture and satellite images were analyzed to understand the impact of soil moisture on hemp canopy. The results showed that the soil moisture variability remained the same at each plot during the one-year experiment while canopy properties depended on other factors that will be studied next year. This emerging technology is promising to improve irrigation water use efficiency.

Key words: *irrigation scheduling; capacitance sensor; wireless technology.*

INTRODUCTION

Water is one of the most essential diminishing natural resources. Farming is the dominant water consumer because it uses the 70% of the available fresh water. The ever-increasing shortage of water and the continuous deterioration of its quality are evident in many countries of the world. Especially in Greece, where the largest consumer of available water resources is irrigated agriculture (70%), water demand is significant in the summer, when water availability decreases to meet irrigation needs. In Greece, the quantities of water per irrigated area of 1000 m^2 amount to an average of 376 m^3. The higher quantity is used by southern Greece, where the number reaches 576 m^3. In contrast, northern Greece uses smaller amounts of water per 1000 m^2, such as 248 m^3. Irrigation in Greece is still applied by farmers after soil and plant observation without using scientific documentation and guidance resulting in the waste of water resources. Over-irrigation usually does not have a direct effect on the crops, thus farmers tend to "feel safe" by increasing irrigation above the real plant needs, especially when the price of irrigation water is too low. It is estimated that of the irrigation water applied, only 65% is used from crops, while 8% is lost during transport, 7% during its application in the field and 20% is lost due to over-irrigation (*Chartzoulakis & Bertaki, 2015*).

The rational use of water in irrigation can be achieved by adopting scientific irrigation scheduling (also known as irrigation water management). For this reason, it is necessary to calculate the irrigation needs as accurate as possible, using data from agro-meteorological station located in the near area. In addition, it is necessary to utilize sensors to monitor soil moisture in fields. Therefore, irrigation management is considered a vital component in agriculture, both for the environmental protection and for the stability of agricultural income.

Nowadays, the traditional irrigation systems transforms to smart-irrigation systems for sustainable water management. This highlights the importance of adopting a set of emerging technologies - such as Internet of Things (IoT) and precision irrigation models and controls - that promise minimizing implications of water scarcity. IoT refers to a system in which applications and services are driven by data collected from spatially planned and distributed remote sensing devices that sense and interface with the physical world. A typical IoT system architecture is based on three layers: a) device layer, b) gateway layer, and

c) platform layer. The device layer of IoT comprises of sensors and actuators for sensing and actuating the physical environmental conditions. The gateway layer is considered as the various communication protocols or computing devices that bridge the connection between the things layer and IoT platform layer. The IoT platform layer is a suite of cloud-based and/or on premise software components which facilitates data communication, flow, device management, and application support and management (*Sheng et al., 2017; Boursianis et al., 2020*).
An IoT system uses various enabling technologies, such as wireless sensor networks, cloud computing, big data, embedded systems, security protocols and architectures, communication protocols, and web services (*Sheng et al., 2017; Boursianis et al., 2020*). A wireless sensor network (WSN) is a group of spatially distributed smart sensors for monitoring, and recording the environmental conditions (such as soil water content; swc), storing the collected data, and transmitting the gathered information at a central station (*Liakos et al., 2017*). The main building block of the wireless sensor network is the sensor node. The main components of a sensor node are a microcontroller, transceiver, external memory, and power source. WSN is an important tool that is used in numerous applications such as to perform precision irrigation, providing farmers with a detailed knowledge of the amount of water exists in the soil at relatively low cost (*Delin, 2002; Liakos et al., 2017*).
The objectives of this study are a) to present an IoT-based precision irrigation technology using wireless sensor network (WSN), b) to show how this technology can help farmers to improve irrigation water use efficiency and c) to study if soil moisture plays an important role on canopy properties.

MATERIALS AND METHODS

The study was conducted in six experimental plots located in the Department of Agrotechnology - University of Thessaly, Larissa, Greece (39°37′34.0″ N, 22°22′52.8″ E, elevation of 80 m above sea level). The size of each plot was 7m x 8m.
Before the establishment of the crop, a soil sampling took place in the experimental site. Soil samples were taken from each plot at a depth of 0.3 m. The soil samples were then mixed to form a single composite soil sample, as representative as possible. The modified Bouyoucos method was used to determine the soil mechanical composition (*Gee and Bauder, 1986*), while the field capacity (FC) and permanent wilting point (PWP) of the soil were determined according to *Klute (1986)*. According to the above method, the soil texture of the plots is categorized as sandy clay loam (SCL). Further information for the particles size distribution and soil physical characteristics of the plots are presented in Table 1.

Tab. 1 Particles size distribution and soil physical characteristics of the plots

Properties		Depth 0 – 0.3 m
Particles size distribution	Sand	65 %
	Silt	10 %
	Clay	25 %
Soil physical characteristics	Dry bulk density	1.3 g/cm^3
	Field capacity	28 %
	Permanent wilting point	14 %

To develop a desirable soil structure suitable for seedbed, plowing with a depth of 25 cm was carried out, followed by secondary tillage with a rotary tiller at depth of 15 cm. A hemp crop (Cannabis sativa L.) was established on May 5, 2020 at the plots. The variety used for the experiment was Futura 75 and it was selected based on climate adaptation requirements and on seed and fiber yields potentials. Hemp plants were established in a row distance of 30 cm and plant distance of 3 cm.
Irrigation of hemp is one of the most important factors in crop yield and quality (*Tang et al., 2017a*). A drip irrigation system was installed in the experimental site. It consisted of hardware (electrovalves, filters, pressure gauges etc.) and the driplines with connection fittings. The PE lateral lines were placed between the sowing rows, at a distance of 1.2 m. Each lateral line had in-line emitters which the discharge rate was 3.6 L/h. The spacing between emitters was chosen as 1 m. During the growing season, irrigation was applied in total 487 mm.

The implementation of the Internet of Things (IoT) and wireless sensors (WS) in the proposed remote soil moisture monitoring and logging system consists of several parts as shown in Fig. 1. Wireless sensors which are distributed on the experimental site collect field sensing data, process and communicate over wireless channel with the Internet. End user (farmer) can monitor soil moisture and weather station data by browsing the cloud web server. In addition, the IoT based soil moisture monitoring and logging system includes databases, information files and a friendly graphical user interfaces (GUI) for computers and mobile devices.

The WS are an ecosystem of soil moisture sensors and a weather station placed in the experimental site. Air temperature, relative humidity, barometric pressure, rainfall, wind speed, wind direction, and solar radiation are standard measurements taken by the nearest weather station. Sensor nodes were developed by the Agricultural and Environmental Solutions (AGENSO), Athens, Greece. Each sensor node plays the role of a base station that transmitting its information through the Internet to cloud server. A node can support one soil moisture sensor, a weather station, and an external power unit (solar cell). The architecture for such node comprises of analog sensor channels, onboard digital signal processor (DSP), RAM and flash memory, GSM modem, global navigation satellite system (GNSS) receiver, LCD display, and power source. The hardware components are enclosed in an IP68 box, to protect them from damages and environmental conditions. These sensor nodes were developed to be power efficient and run by one rechargeable battery for a long period of time, since the whole system enters in deep sleep mode after collecting and transmitting the sensor information to save energy (*Tsiropoulos et al., 2022*).

The measurements of volumetric water content (VWC) are essential for assessing the status of hemp crop available moisture in soil. Thus, six low-cost sensors (ECH_2O probe model EC-5) were utilized to measure the volumetric swc under natural conditions in each plot. One sensor was installed in each plot horizontally in a depth of 25 cm from the surface. The EC-5 was selected because it is much less sensitive to variation in texture and electrical conductivity as it runs at a frequency of 70 MHz. The EC-5 sensor had dimensions 8.9 x 1.8 x 0.7 cm. It determines VWC by measuring the dielectric constant of the soil using capacitance/frequency domain method.

Several researchers (*Iwata et al., 2017; Dong et al., 2020*) reported that the performance of the factory-based calibrated EC5 sensors have shown overestimate or underestimate the soil moisture, depending on the characteristics of the soil. Thus, sensors should be calibrated for specific types of soil in order to improve their accuracy. The manufacturer has provided different calibration equations to describe the relationships between the output and VWC for the EC-5 sensor. This relationship (for non-METER data logger) is often linear as shown below:

$$\theta = (11.9\text{x}10^{-4})(mV) - 0.401 \quad (1)$$

where θ is the volumetric water content, mV is the output of the EC-5 sensor when excited at 2.5 V. According to manufacturer this equation reaches a maximum at ~60% VWC in pure water. To display data on a scale from 0% to 100%, VWC should be modeled with a quadratic equation (which would result in a 100% VWC in water), but a linear equation fits the mineral soil VWC range as well as the quadratic, and linear equations are easier to deal with, especially since mineral soil typically saturates at ~40% to 50% VWC.

Ardeusi.gr web interface is graphical user interface (GUI) for farmers use. The user component includes a task/query management component that collaborates with task management on sensor node, forming a channel for information and control flow between the sensor node and the GUI. By this way the GUI provides the ability to send tasks or queries to a sensor node and to display the following results: soil moisture data, weather data (e.g. air temperature, relative humidity, barometric pressure, rainfall, wind speed, wind direction, etc.), soil water reservoir thresholds (field capacity - FC, permanent wilting point - PWP, maximum allowable depletion- MAD) and charge battery. Soil moisture and weather data updates displayed as soon as they become available at the workstation and in the time sequence in which the measurements occurred.

Fig. 1 The wireless sensors (WS) placed in the experimental site

Sentinel 2 satellite images were analyzed for the 2020 growing season as far as the Normalized Difference Vegetation Index (NDVI) and the Normalized Difference Water Index (NDWI). Additionally, swc maps created based on the data collected from sensors and descriptive statistics for swc were estimated utilizing the SPSS 16.

RESULTS AND DISCUSSION

The descriptive statistics of swc are presented at table 2. It is worth mentioning that data follows normal distribution because skewness is higher than -1 and less than 1. Additionally, the mean swc is almost equal to median, which means that the bell curve of the dataset is symmetrical. The fact that the kurtosis is less than three means that there are no extreme high or low values (outliers). Moreover, the soil moisture values did not varied too much thus the coefficient of variation is low (0.14).

Tab 2. Descriptive statistics of swc during the 2020 growing season

Property	Value
Min	42.4
Max	74.4
Mean	59.6
Median	59.9
Standard deviation	8.5
Variance	72.3
Skewness	-0.4
Kurtosis	-0.2
Coefficient of variation	0.14

Figure 2 presents the average values of NDVI and NDWI for each plot during the 2020 growing season. According to it, the NDVI was lower at the northwest plot and higher at the south west plot while the NDVI values at the rest plots was almost the same. On the other hand the NDWI was higher at the northwest and southeast plots and lower at southern central plot. At the rest plots the NDWI value was the same. Variability between NDVI and NDWI map has already mentioned at the literature (*Hussain et al. 2019*).

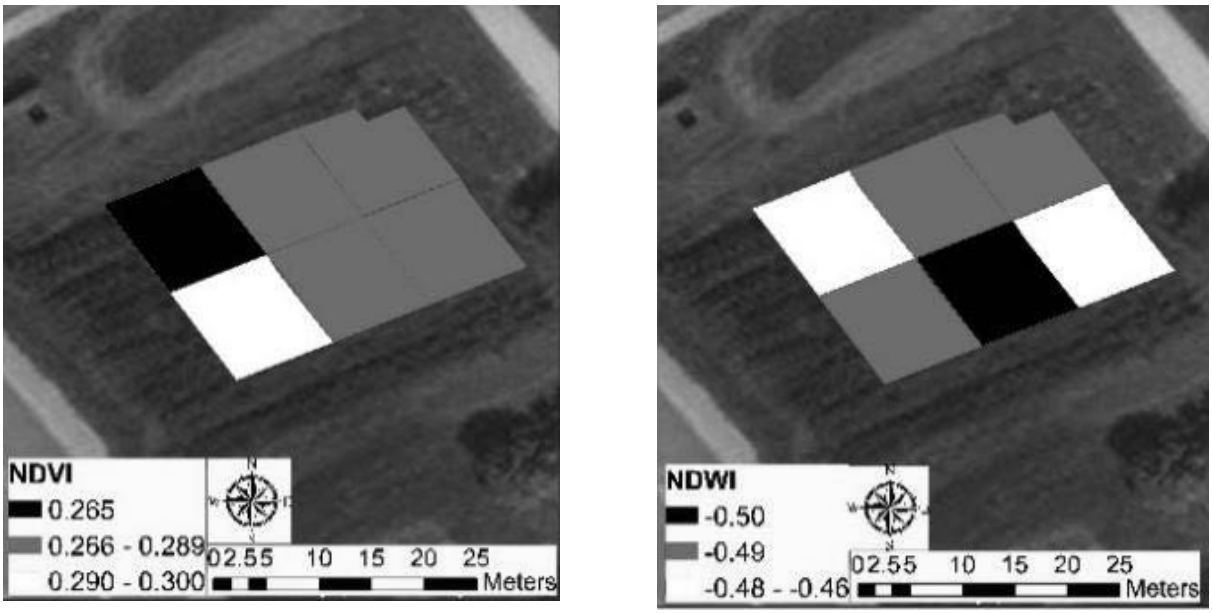

Fig. 2 Right: Normalized Difference Vegetation Index (NDVI) map, Left: Normalized Difference Water Index (NDWI) map. Both maps uses all the data from the 2020 growing season. The darker the colour the lower the value and the opposite

Figure 3 shows the monthly spatial variability of the swc as it was recorded by the installed soil moisture sensors. The color of each plot is given based on the average swc during the 2020 growing season. Surprisingly, the swc variability was the same every month and the only noticeable changes are the values of swc. In overal, the plots at the east side of the site had higher average swc than the plots at the western side. Thus, it is clear that the spatial variability of the soil water content is high even if the plots are close to each other and the total area is small (*Liang et al. 2016*). This explains why yield variation is high even in small fields (*Gemtos et al., 2005*).

The comparison of the swc maps with the NDVI and NDWI maps does not reveal specific patterns or any correlation among them. This means that there are other factors than irrigation that affect the vigour of the plants (NDVI) and the leaf moisture (NDWI). On the other hand, the fact that the average monthly swc variability was the same every month demonstrates that soil variability is high even in small areas and promotes the importance of utilizing a system to monitor soil moisture and the necessity of using Variable Rate Irrigation systems to manage this variability increasing the farmers' profit.

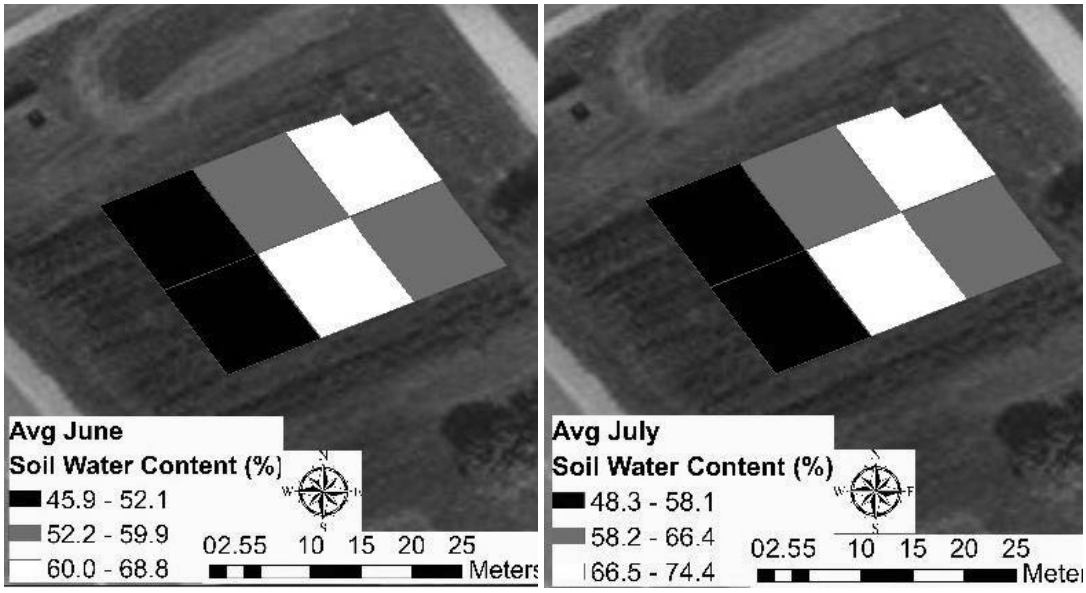

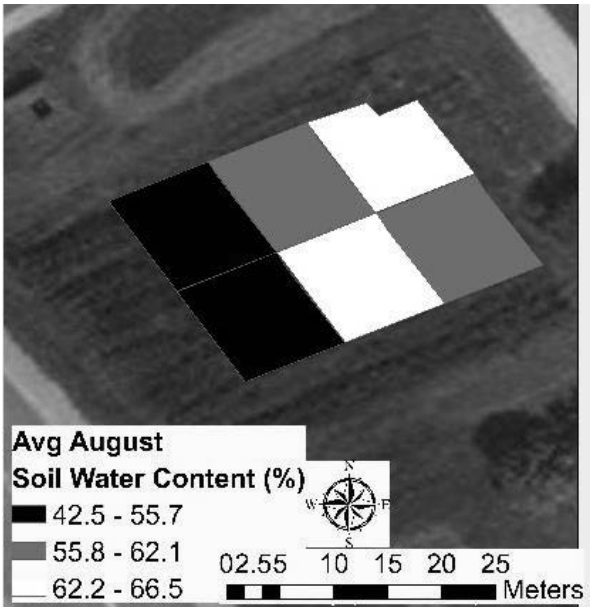

Fig. 3 Six experimental plots. One node was installed at each plot. Left: average swc in June, Center: average swc in July, Right: average swc in August. The grey scale color represents the average monthly swc in each plot. The darker the color the lower the swc and the opposite.

CONCLUSIONS

This study deals with sustainable irrigation and soil moisture monitoring systems. Thus, commercial soil moisture monitoring systems installed in six plots. The crop at the plots was hemp. The results demonstrated that swc variability remained the same in every growth stage of hemp. For this reason, it is very important to understand the soil moisture variability in every field using soil moisture monitoring systems. On the other hand, the vigor of the plants and the leaf moisture during the growing season did not depend on irrigation but on other factors that will be studied the following years. Finally, long-term soil moisture monitoring is needed to sufficiently clarify the results and conclusions of this study.

ACKNOWLEDGMENT

This research was supported by the European Union and Greek national funds through the Operational Program Competitiveness, Entrepreneurship and Innovation, under the call RESEARCH - CREATE-INNOVATE research and innovation program "Development of an energy-independent system for precision irrigation and application of Regulated Deficit Irrigation by using Rain Water - ReDIrri" (project code: T2EΔK-03987).

REFERENCES

1. Boursianis, A. D., Papadopoulou, M. S., Diamantoulakis, P., Liopa-Tsakalidi, A., Barouchas, P., Salahas, G., Karagiannidis, G., Wan, S., & Goudos, S. K. (2020). Internet of Things (IoT) and Agricultural Unmanned Aerial Vehicles (UAVs) in Smart Farming: A Comprehensive Review. *Internet of Things*, 100187.
2. Dong, Y., Miller, S., & Kelley, L. (2020). Performance Evaluation of Soil Moisture Sensors in Coarse-and Fine-Textured Michigan Agricultural Soils. *Agriculture*, *10*(12), 598.
3. Chartzoulakis, K., & Bertaki, M. (2015). Sustainable water management in agriculture under climate change. *Agriculture and Agricultural Science Procedia*, *4*, 88-98.
4. Delin, K. A. (2002). The sensor web: A maro-instrument for coordinated sensing. *Sensors*, *2*(7), 270-285.
5. Gee, G. W., & Bauder, J. W. (1986). Particle-size Analysis. In: Klute, A., (editor). Methods of soil analysis. Physical and mineralogical methods. *Agronomy Monograph 9. (2ed). American Society of Agronomy* (pp. 383-411). Madison, WI.
6. Gemtos, T. A., Markinos, A., Nassiou, T. (2005). Cotton lint quality spatial variability and correlation with soil properties and yield. In J. V. Stafford (Ed.) *Precision Agriculture '05: Proceedings of the 5th European conference on precision agriculture* (pp. 361-368). Wageniggen: Wageniggen Academic Publishers.
7. Hussain, S., Mubeen A., Ahmed A., Akram W., Hammad M. A. (2019). Using GIS tools to detect the land use/land cover changes during forty years in Lodhran district of Pakistan. *Environmental Science*, 1-17.
8. Iwata, Y., Miyamoto, T., Kameyama, K., & Nishiya, M. (2017). Effect of sensor installation on the accurate measurement of soil water content. *European Journal of Soil Science*, *68*(6), 817-828.
9. Klute, A. (1986). Water retention: Laboratory methods. In: Klute, A., (editor). Methods of soil analysis. Physical and mineralogical methods. *Agronomy Monograph 9. (2ed). American Society of Agronomy* (pp. 635-662). Madison, WI.
10. Liakos V., Porter W., Liang, X., Tucker, M. A., Mc Lendon, A., Vellidis G. (2017). Dynamic variable rate irrigation – A tool for greatly improving water use efficiency. *Advances in Animal Biosciences: Precision Agriculture (ECPA) 2017*, 8:2 pp 557 – 563.
11. Liang X., Liakos V., Wendroth O., Vellidis G. (2016). Scheduling irrigation using anapproach based on the van Genuchten model. *Agricaltural Water Management, 176,* 170 – 179.
12. Sheng, M., Qin, Y., Yao, L., & Benatallah, B. (2017). Managing the web of things: linking the real world to the web. Morgan Kaufmann.
13. Tang, K., Struik, P. C., Yin, X., Calzolari, D., Musio, S., Thouminot, C., Bjelková, M., Stramkale, V., Magagnini, G., & Amaducci, S. (2017a). A comprehensive study of planting density and nitrogen fertilization effect on dual-purpose hemp (*Cannabis sativa* L.) cultivation. *Ind. Crops Prod., 107*, 427-438.
14. Tsiropoulos, Z., Gravalos, I., Skoubris, E., Poulek, V., Petrík, T., & Libra, M. (2022). A Comparative Analysis between Battery-and Solar-Powered Wireless Sensors for Soil Water Monitoring. *Applied Sciences*, *12*(3), 1130.

Corresponding author:
Prof. Ing. Ioannis Gravalos, CSc., Department of Agrotechnology, School of Agricultural Sciences, University of Thessaly, Gaiopolis, 41500 Larisa, Greece, phone: +030 2410 684216, e-mail: iogravaos@uth.grl

MEASUREMENT OF THE PROCESS OF MAKING WINE WITH THE HELP OF IOT

Jakub VOŠAHLÍK[1], Jan HART[2]

[1]Faculty of Engineering, Department of Technological Equipment of Buildings, Kamýcká 129, Prague, Czech University of Life Sciences Prague, Czech Republic
[2]Faculty of Engineering, Department of Vehicles and Ground Transport, Kamýcká 129, 165 00 Prague, Czech University of Life Sciences Prague, Czech Republic

Abstract
The article deals with the fermentation process of rice wine and obtaining data during fermentation with the help of IoT. The process of converting D-glucose into ethanol together with the oxidation of reduced coenzymes is called fermentation. Ethanol fermentation takes place anaerobically, i.e. without access to air with the help of yeast. The fermentation process is gradually being improved with the help of acquired sensor data and the gradual possibility of automation. The main objective of this paper is to develop an experimental environment for measuring rice wine fermentation processes with the help of IoT. During the fermentation of rice wine, there are measurable attributes that can be measured with the help of sensors. These attributes affecting the final product quality, positively but also negatively (pH, temperature, humidity, etc.). It is therefore necessary to select a given sensor that can monitor the attributes and then devices that can then manage and evaluate it. the correct selection and use of sensors and computing equipment, the acquisition and processing of data and the application of the resulting values to fermentation procedures, the resulting product quality increases.

Key words: *automation, IoT, fermentation, rice wine, senzors, ethanol*

INTRODUCTION

The development of industrial technologies nowadays is moving forward relatively quickly, and that is why sensorics can be applied to a wider extent in the food-agricultural complex. The Internet of Things includes technologies that present themselves as a network of physical objects that are connected using the Internet and acquire data, then send them via the Internet to compute units that process them. It is a relatively demanding architecture, which must be properly designed, connected, and equipped with suitable sensors and devices for communicating with each other *(Gilchrist, 2016).*
Today, thanks to industrial technologies, the fermentation process can be monitored and tracked via programmed internet interfaces with the help of IoT. These measured data can then be processed and used in the food-agricultural complex for the subsequent improvement of processes and output products. In this case, to improve the resulting properties of fermented rice wine and thus minimize the resulting negative properties of the product *(Lokman et al., 2020).*
One of the main units in systems designed for IoT are the sensors themselves, external devices designed to measure and collect the required data. Subsequently, these measured data are stored on computing units that are connected to the internet, and then these data are sent to storage, such as the Linux server. The measured data are in the fermentation processes about temperature, humidity, acidity etc. Complete information about the fermentation process is obtained and processed continuously in the fermentation process. Subsequently, they can be processed for various applications that can run locally or be presented to the world of the internet with the help of web interfaces *(Tomtsis et al., 2016).*
Fermentation is the process in which D-glucose C6H12O6 is converted into C2H5OH ethanol along with the oxidation of reduced coenzymes (NADH, FADH) - called fermentation *(Keot et al., 2020).*
Overall, fermentation processes are very demanding regarding the technological process, especially to ensure the inaccessibility of air, as there is a risk of mold attack. To improve the fermentation process, the process of automation, i.e. the IoT industry, is also suitable. The design of an autonomous stainless-steel mixer can also be applied here. To better mix the released substances into the solution during the fermentation process, it is also advisable to use a stirrer, which mixes the so-called dead spots during the fermentation process. The aim of this arcite was measure and compare data during fermentation process using a stirrer and without stirrer *(Uehara et al., 2018; Cai et al., 2019).*

MATERIALS AND METHODS

To realize the fermentation process of rice wine, an experimental environment was designed and assembled in which the specified fermentation process took place under constant conditions for all fermented products in Fig. 1. The fermentation process was fitted in two vessels with a designed and constructed stirrer and two vessels were not fitted with an experimental stirrer and here the fermentation process took place naturally.

Fig. 1 Experimental fermentation environment

The applied autonomous stirrer in the fermentation process was made of stainless food grade steel ČSN 17240. AISI 304 in the Czech Republic in Fig. 2. Subsequently constructed, it was installed in two fermentation vessels.

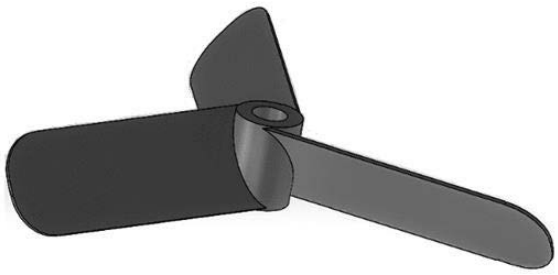

Fig. 2 Part of autonomic food stainless-steel stirrer

Before the actual implementation of the fermentation process and production of the autonomous mixer, information was obtained about the individual types of sensors that can be used in the fermentation process. Subsequently, they were acquired and applied to the fermentation process. A Raspberry Pi 4 model B 4GB RAM microcomputer was chosen as the main computing unit for the task of data collection and subsequent processing. This sensors had to be properly programmed in Python or C++.
The first measurable attribute in rice wine fermentation was moisture, and this attribute was measured by the BMP-280. The program for this sensor was programmed using the Python language. Another well-measurable attribute is the temperature inside the container and the external temperature outside the container. For this purpose, the experimental environment was fitted with a DS18S20 sensor. The temperature sensor placed inside the container was made in a waterproof version and was placed directly in the solution. Another sensor that was also immersed in the solution was the E-201C-Bue solution pH probe, which was properly calibrated and programmed in C++.

RESULTS AND DISCUSSION

The best measurable quantity in the rice wine fermentation process is clearly the temperature of the solution in which the fermentation takes place. Heat is generated by the process of converting D-Glucose into the desired ethanol. The measured temperature before starting the fermentation process was, as in the previous project, 21 °C to obtain the most accurate results. During vigorous fermentation, i.e. when the highest amount of conversion of D-glucose by the yeast into ethanol occurs, lower temperature values were measured in vessels with a stirrer compared to fermentation vessels without a stirrer in the order of 2 °C. Later, after vigorous fermentation, the fermented solution began to gradually cool down

due to the gradually decreasing activity of the yeast. Here, the temperatures of 11.6 and 13.6 differed by 1.85 °C, and on the other remaining days the temperature difference was in the order of tenths of a degree Celsius (up to 0.20 °C). Following the completion of the yeast fermentation process, consumption of D-glucose, the fermented solution was subsequently cooled to a constant temperature of 12 °C, corresponding to the previous project. The temperature was subsequently maintained by cooling boxes (with thermoregulation) at the mentioned temperature. The highest temperature reached during the fermentation process was reached on 10.6 at a temperature of 29.9 °C in the vessel without a stirrer and 29.7 °C in the vessel with an experimental stirrer on the sixth day in Fig. 3. The rise in temperature in containers without a stirrer is higher in vigorous fermentation than in containers with a stirrer, but after vigorous fermentation, the solution cools down faster in containers without a stirrer than in containers with a stirrer.

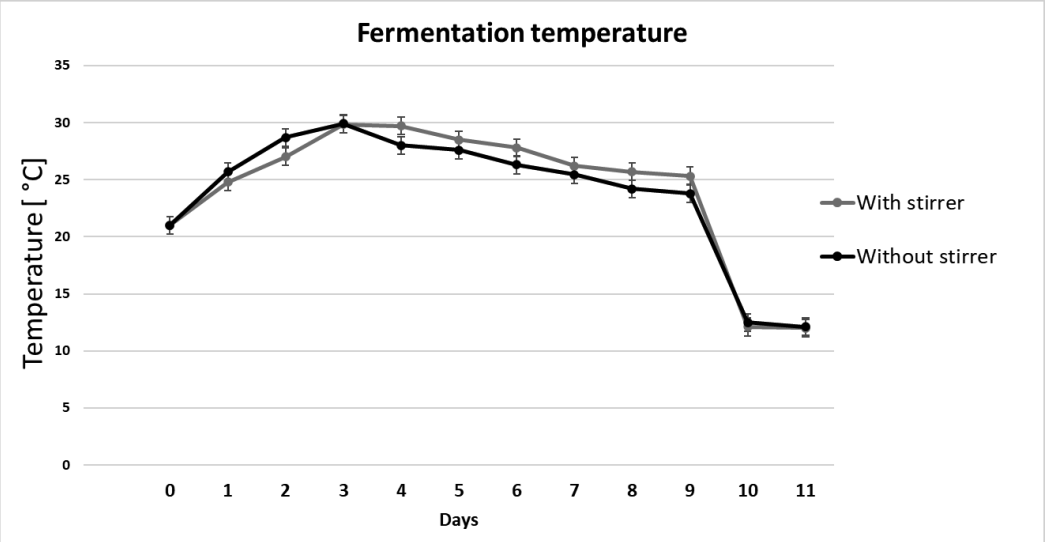

Fig. 3 The course of fermentation temperature

The next well-measurable quantity during the fermentation process is the humidity in the fermentation vessels. The measured values in the same conditions as in the previous project were an average of 85% with a 5% deviation in all vessels measured by sensors. The percentage moisture during vigorous fermentation was 4.7 °C higher in the container with the fermented solution without a stirrer on the first day than in the container with the experimental 3D printed stirrer in Fig. 4.

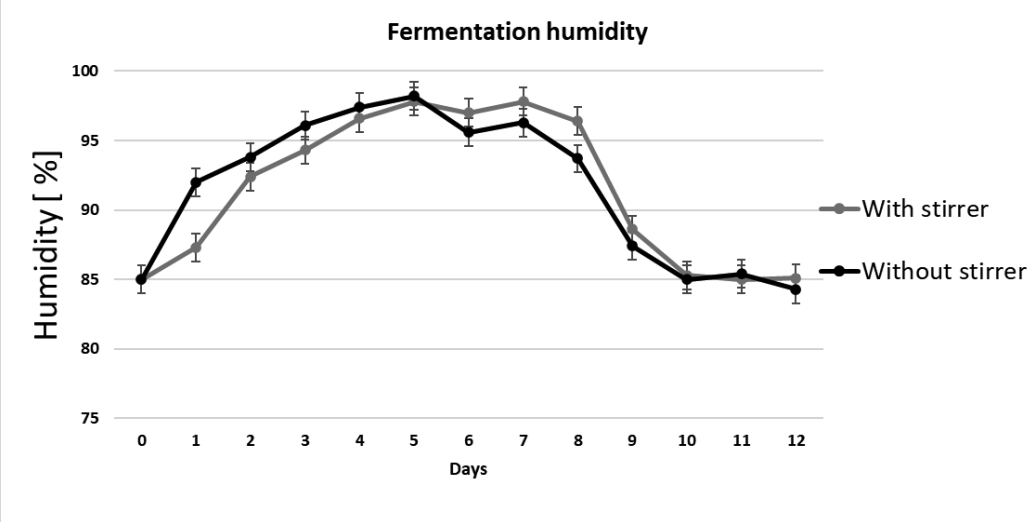

Fig. 4 The course of fermentation humidity

A well-measurable aspect is the pH value, or the acidity of the fermented solution, which is indicated by the hydrogen exponent. The initial pH was measured to be 7.28 before fermentation started. As a

result of the gradual conversion of D-Glucose into the desired ethanol by yeast, the pH value in the fermented solution decreases. the acidity of the solution increases in Fig. 5. Throughout the fermentation of the solution, as in the previous measurement, the solution with the experimental self-sustaining stirrer showed lower pH values compared to the containers with solution, in which the experimental spontaneous stirrer was not applied. However, there was now a lower dispersion of values between these fitted and unfitted vessels with an experimental stirrer compared to the previous measurement, in the order of hundreds to tenths of units of the hydrogen exponent pH.

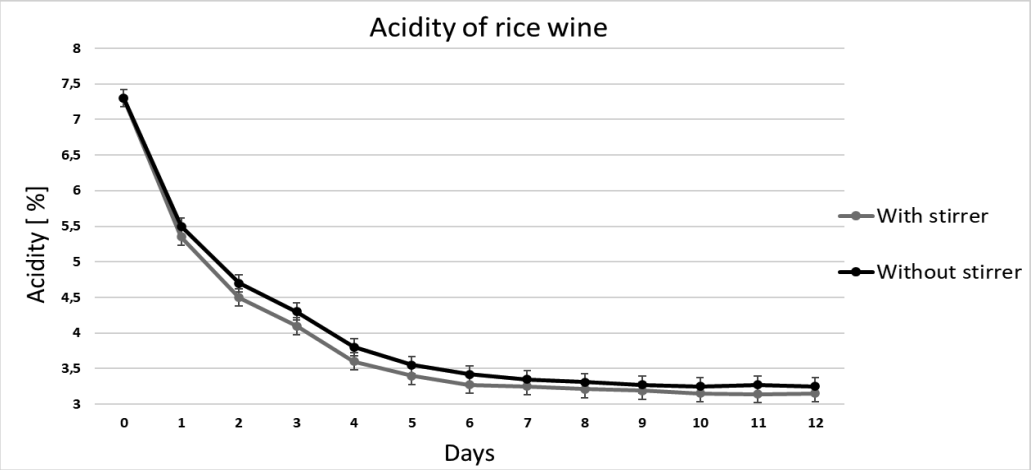

Fig. 5 The course of fermentation acidity

The value of the percentage content of sugar content with the applied additives was fine-tuned to a value of 23.5% sugar content with a minimal deviation (up to 0.66%). When the fermentation process starts, the sugar content in the solution is gradually consumed by the yeast up to 0 %. This means that all the sugar has been converted to alcohol.
The alcohol value reached a value of 13.9% and in a container with an applied experimental stirrer, the value was 13.6%. The fermented rice wine reached low values for the typical alcohol range of rice wines.

CONCLUSIONS

The application of experimental stirrers affects, albeit in some cases minimally, the ongoing and final properties of fermented rice wine.
The moisture percentages are higher in the vessels without the applied experimental stirrer in the vessels during the rampant fermentation process. After the vigorous fermentation process, the opposite effect occurs, with the vessels with the experimental stirrer reaching higher continuous values.
In both cases, however, the percentage of alcohol met the criteria for the percentage of alcohol content in rice wine (lower limits). With a higher amount of initial sugar content in the solution, the resulting alcohol value would be higher.
In vessels without an experimental stirrer, the value of both the continuous and the final pH was higher than in the vessels with an experimental stirrer printed on a 3D printer. The resulting pH value is desirable at lower values, as it indicates a better mixing of the individual ingredients into the solution.

ACKNOWLEDGEMENT

This study was supported by the CULS IGA TF “The University Internal Grant Agency” (2020: 31170/1312/3116).

REFERENCES

1. Cai, H., Zhang, Q., Shen, L., Luo, J., Zhu, R., Mao, J., Zhao, M., Cai, C. 2019. "Phenolic profile and antioxidant activity of Chinese rice wine fermented with different rice materials and starters". *LWT* 111: 226-234
2. GILCHRIST, Alasdair, 2016. *Industry 4.0: the industrial internet of things*. 2016. New York, NY: Apress.
3. Keot, J., Bora, S., Das Kangabam, R., Barooah, M. 2020. "Assessment of microbial quality and health risks associated with traditional rice wine starter Xaj-pitha of Assam, India: a step towards defined and controlled fermentation". *3 Biotech* 10 (2)
4. Lokman, T., Islam, M., Apple, M. 2020. "Design & Implementation Of IoT Based Industrial Automation Syste". Pp. 1-6in *2020 11th International Conference on Computing, Communication and Networking Technologies*
5. Slapkauskaite, J., Kabasinskiene, A., Sekmokiene, D., 2019. "Application of fermented soya as a bacterial starter for production of fermented milk". *Czech Journal of Food Sciences* 37 (6) 403-408
6. Tomtsis, D., Kontogiannis, S., Kokkonis, G., Zinas, N. 2016. "IoT Architecture for MonitoringWine Fermentation Process of Debina Variety Semi-Sparkling Wine". Pp. 42-47in *Proceedings of the SouthEast European Design Automation, Computer Engineering, Computer Networks and Social Media Conference on*
7. Uehara, Y., Ohtake, S., Fukura, T. 2018. "A Mash Temperature Monitoring System for Sake Brewing". Pp. 1-2in *2018 IEEE International Conference on Consumer Electronics-Taiwan*
8. Yang, Y., Hu, W., Xia, Y. 2020. Flavor Formation in Chinese Rice Wine (Huangjiu): Impacts of the Flavor-Active Microorganisms, Raw Materials, and Fermentation Technology. *Frontiers in Microbiology* [online]. 2020, 11 [cit. 2021-01-31].

Corresponding author:
Ing. Jakub Vošahlík, Department of Technological Equipment of Buildings, Faculty of Engineering, Czech University of Life Sciences Prague, Kamýcká 129, Praha 6, Prague, 16521, Czech Republic, phone: +420 775 907 621, e-mail: blackzerocz @gmail.com

NEW DESIGN SOLUTIONS FOR WORKING UNITS OF MACHINES IN TERMS OF EFFICIENCY OF THEIR OPERATION

Marcin ZASTEMPOWSKI[1], Andrzej BOCHAT[1], Jerzy KASZKOWIAK[1], Lubomir HUJO[2], Maciej JANIEC[1]

[1]*Faculty of Mechanical Engineering, Bydgoszcz University of Science and Technology*
[2]*Technical Faculty, Slovak University of Agriculture in Nitra*

Abstract
In this paper new design solutions of a drum cutting unit are presented, which can be applied in agricultural forage harvesters. The influence of the design features of the drum cutting unit on the performance characteristics in the biomass cutting process, which is one of the most important stages in the harvesting of plant material for energy, feed and food purposes, was determined. The tests described in the paper were carried out on a test stand developed by the authors of the paper. This test stand ensures the realisation of the process under the conditions reflecting the real cutting process. The tests were carried out for cross cutting, traditionally used in forage harvesters, but the tests were also extended to diagonal cutting, carried out for three different angles of plant material feeding. At the stage of experimental tests the influence of selected features and design parameters of the cutting drum on unit cutting resistance, cutting work, efficiency of the cutting unit and the degree of unevenness of the length of cut pieces was determined. It was found that the greatest influence on the energy consumption of the process of cutting stem plants has the cutting method, i.e. the material feeding angle, the cutting speed and the thickness of the blade.

Key words: *cutting of the material, biomass, drum cutting unit of the forage harvester, layer of plant material, cutting resistance, energy consumption, efficiency of the cutting process, degree of unevenness of the chopped material.*

INTRODUCTION

The cutting units are the basic working units of machines for harvesting biomass for consumption, feed or energy purposes. Among these machines we can distinguish choppers, where the basic working unit, cutting a layer of material into pieces of a specified length (chopped material), is a drum cutting unit. Due to the selectivity of the tests carried out so far, it is not possible to unambiguously determine which features and design parameters of the cutting unit in question have a decisive impact on the cutting efficiency, and the balance of power (Sankey) consumed by the forage harvester with a drum cutting unit shows that the power consumed by the cutting unit clearly dominates over the power consumed by the other working units and amounts to 75-80% (*Zastempowski & Bochat, 2020*). Currently operating versions of cutting units in forage harvesters are characterised by a high energy-consumption of the cutting process, and as a result, their drive systems are equipped with high-power engines. This indicates that the known design solutions have been developed largely on the basis of the designer's intuition. The problem of cutting plant material is a current topic and has been dealt with by many authors. However, publications often deal only with the mechanics of cutting selected plants without considering the design of cutting units (*Zhang et al., 2003; Zastempowski, Borowski & Kaszkowiak, 2013; Persson, 1987; Igathinathane et al., 2008, 2010*) or the researchers in their publications provide test results with respect to cutting different materials or layers of materials (*Igathinathane et al., 2009; Du &Wang, 2016; Abilzhanov et al.,2017*). However, these results are often not comparable due to differences in the testing programmes. At the same time, very often there is also a lack of precise information on the material tested in laboratory tests. Therefore, the aim of this study was to determine the influence of the selected features and design parameters of the drum cutting unit on its performance characteristics.

MATERIALS AND METHODS

The drum cutting unit is the basic working unit of a forage harvester. Its task is to cut plant material into pieces of a specific length (chopped material).

The use of this type of unit in forage harvesters makes it possible to achieve the required degree of material fragmentation. An exemplary design of a drum cutting unit is presented on fig. 1a.

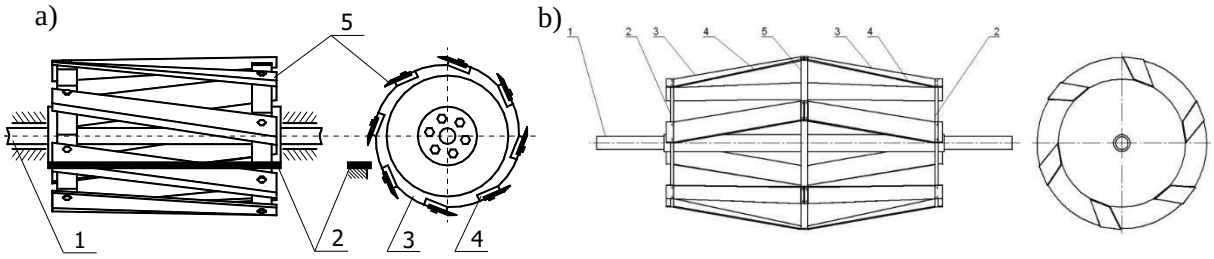

Fig. 1a Cutting drum of a forage harvester [Bochat, 2010]: 1- cutting drum shaft, 2 - counter cutting edge, called nib, 3 - cutting drum disc, 4 - knife vice, 5 - cutting knife
Fig. 1b New design of the cutting drum [own elaboration]: 1 - shaft, 2 - external discs, 3 - knives, 4 - knife cutting edges, 5 - central disc

Searching for more energy-efficient solutions for the construction of a drum cutting unit designed to cut plant material into chopped straw at the Department of Machinery and Technical Systems at the Faculty of Mechanical Engineering of Bydgoszcz University of Science and Technology, a new design of the cutting unit was developed, patented and manufactured. The essence of the new design of the cutting drum is that it consists of a driving shaft and three discs, of which the central one has a larger diameter than the side ones. Knives in V-shape with straight or curved blades along a helical line are bolted directly to the discs (Fig. 1b). Such a construction of the drum enables cutting the material in a slanting manner, which results in reduction of energy consumption of the cutting unit operation.
For the purposes of conducting experimental research, a test stand was designed and constructed to study the process of cutting a layer of plant material, including rye straw (Dańkowskie Złote winter rye). The test stand allows the process to be carried out with the use of interchangeable cutting drums, such as cylindrical or double conical drums with the possibility of changing the cutting angle.

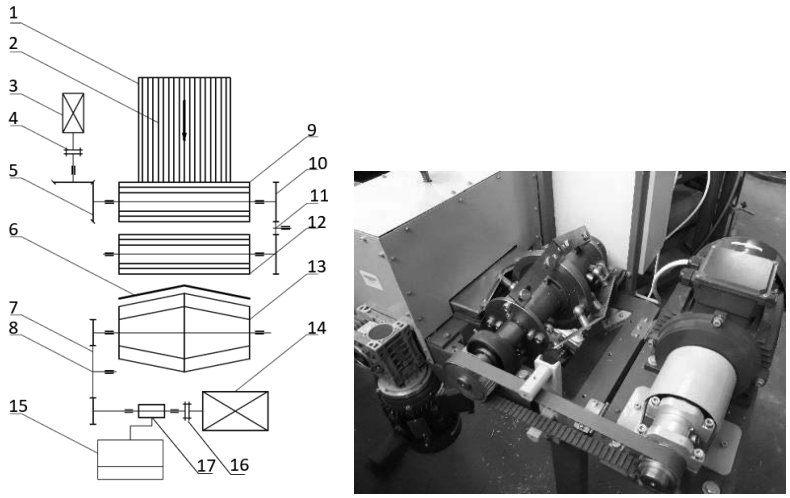

Fig. 2 Test stand: 1-trough of the forage harvester, 2-material to be cut, 3-electric motor, 4-coupling, 5-angle gear, 6-crosscutting edge, 7-gear belt transmission, 8-tension roller, 9-retracting-compacting roller upper, 10-gear belt transmission, 11-pinch roller, 12-retracting-compacting roller lower, 13-cutting drum, 14-electric motor, 15-computer (recorder of measuring system), 16-clutch, 17-torque and rotational speed measuring system on the drum shaft

In order to determine the influence of the selected features and design parameters of the drum cutting unit on its performance characteristics and to assess the possibility of applying an alternative design of the drum cutting unit for diagonal cutting, an experiment was planned according to the test scheme in Figure 3.

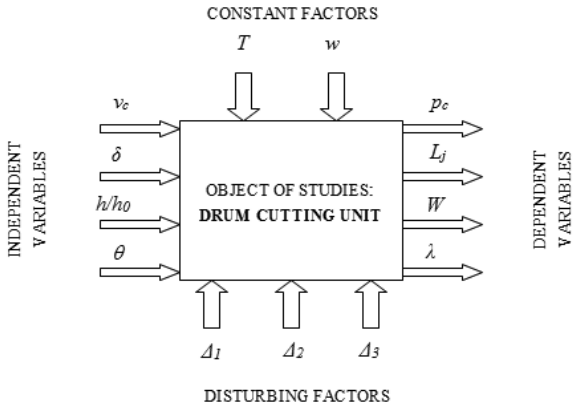

Fig. 3 Scheme of the experimental tests of the drum cutting unit (Błaszczyk, 2010): v_c - cutting speed, δ - thickness of knife blade, h/h_o - degree of plant material compaction, θ - angle of plant material feeding, pc - unit cutting resistance, L_j - unit cutting work, λ - degree of chaff length irregularity, W - efficiency of the cutting unit, Δ_1 - instrument setting error, Δ_2 - instrument inaccuracy, Δ_3 - reading error, T- air temperature, w - moisture content of the cut material.

RESULTS AND DISCUSSION

The selected results from the conducted tests are summarised in the table 1 and presented graphically in the form of a diagram of the impact of material feeding angle on the unit cutting resistance (fig. 4.)

Tab. 1 The selected experimental results for all the independent variables adopted in the research programme

Measurement no	θ [...°]	v_c [m·s^{-1}]	h/ho	δ [μm]	p_c [N·m^{-1}]	L_S [J·m^{-2}]	W [kg·s^{-1}]	L_m [J·kg^{-1}]	λ [%]
1	2	3	4	5	6	7	8	9	10
1	90	3,85	0,65	40	4590	5354	0,078	6588	6,85
…	…	…	…	…	…	…	…	…	…
30	75	3,85	0,65	300	7013	8179	0,077	10609	7,39
…	…	…	…	…	…	…	…	…	…
60	60	3,85	0,54	300	7252	8458	0,077	10198	8,38
…	…	…	…	…	…	…	…	…	…
90	45	3,85	0,47	300	8317	9700	0,075	12838	9,26

In order to analyse the experimental results for all the independent variables included in the research programme, equations of a multivariate regression function were developed.
The general form of the regression function applicable in the presented analysis is presented in the following equation (1):

$$Y_E = a_1 + a_2\theta + a_3 v_c + a_4 \frac{h}{h_o} + a_5\delta + a_6\theta^2 + a_7 v_c^2 + a_8 \left(\frac{h}{h_o}\right)^2 + a_9\delta^2 \quad (1)$$

where Y_E is the generalised dependent variable obtained as a result of the experimental tests, v_c is the cutting speed (m·s^{-1}), δ is the blade thickness (μm), h/h_o is the degree of compaction of the cut material, θ is defined as the angle of the cut material feed (…°),and a_n are the regression coefficients.

Initially, for all the dependent variables, 9 regression coefficients were determined by solving a matrix equation. The significance of the regression coefficients was thus analysed at the significance level α_{pi} =0,05, for which t_{kr} =1,98. The value of t_{kr} was determined on the basis of Student's t-distribution for 108-9-1 degrees of freedom. The analysis of significance of regression coefficients was conducted in stages. In each stage, the least significant component, i.e. the one which met the inequality $t < t_{kr}$ was rejected from the overall regression function. If, in a given stage of the regression function study, the

significance test showed that the regression coefficients were significant, they were accepted for determining the function for a given variable.
In this way, the final formulas for:
- unit cutting resistance p_c,

$$p_c = 21128 - 65{,}898\theta - 209{,}3v_c - 45135\frac{h}{h_o} + 0{,}7399\theta^2 + 32684\left(\frac{h}{h_o}\right)^2 + 0{,}03692\delta^2 \quad (2)$$

- unit cutting work related to the surface area of the cut L_S,

$$L_S = 24321 - 75\theta - 244v_c - 51795\frac{h}{h_o} + 0{,}849\theta^2 + 37409\left(\frac{h}{h_o}\right)^2 + 0{,}0429\delta^2 \quad (3)$$

- unit cutting work related to the weight of the material to be cut L_m,

$$L_m = 27539 - 325{,}4\theta - 303{,}2v_c - 33512\frac{h}{h_o} + 2{,}3\theta^2 + 30583\left(\frac{h}{h_o}\right)^2 + 0{,}05135\delta^2 \quad (4)$$

- capacity of the cutting unit W,

$$W = -0{,}0186 + 0{,}0217\theta + 0{,}0399v_c + 2{,}55\cdot 10^{-6}\frac{h}{h_o} + 2{,}16\cdot 10^{-7}\delta - 0{,}00011\theta^2 - 0{,}0293v_c^2 + 12{,}97\left(\frac{h}{h_o}\right) \quad (5)$$

- the degree of unevenness of the length of the cut material pieces λ,

$$\lambda = 18{,}61 - 0{,}05838\theta - 1{,}132v_c - 15{,}077\frac{h}{h_o} + 1{,}333\cdot 10^{-3}\delta + 2{,}181\cdot 10^{-4}\theta^2 + +0{,}06978\left(\frac{h}{h_o}\right)^2 + 12{,}97\delta^2 \quad (6)$$

Fig. 4 shows graphically the influence of the selected independent variables on the value of the unit cutting resistance p_c based on the equation (2).

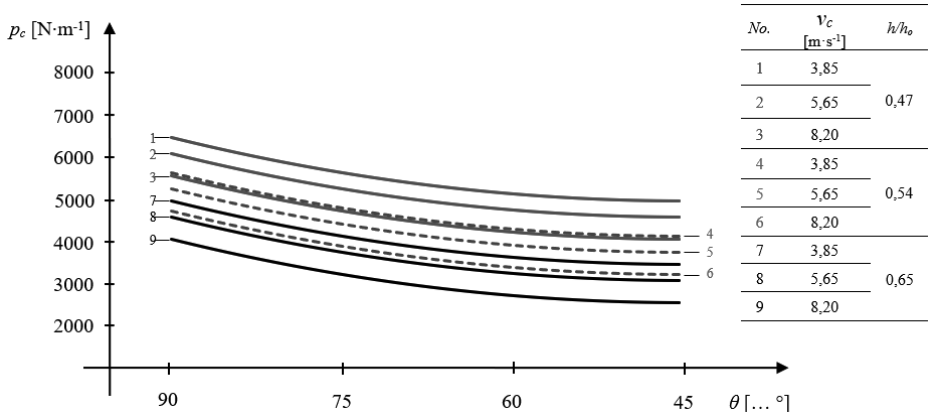

No.	v_c [m·s⁻¹]	h/h_o
1	3,85	
2	5,65	0,47
3	8,20	
4	3,85	
5	5,65	0,54
6	8,20	
7	3,85	
8	5,65	0,65
9	8,20	

Fig. 4 The effect of material feed angle θ on the unit cutting resistance of rye straw p_c for the values of cutting speed v_c and the degree of material compaction h/h_o contained in the table attached to the graph and a blade thickness $\delta=40\mu m$

From the diagram presented in fig. 4 it can be seen that as the material feed angle θ decreases, the unit cutting resistance p_c, decreases, assuming the highest value for a transverse cut (θ=90°), and the lowest value for a diagonal cut at an angle θ=45°.
From the tests carried out on the unit cutting resistance p_c it can be concluded that:

- for all the tested values of the angle θ the effect of the cutting speed v_c on the specific cutting resistance p_c is a linear function and the specific resistance decreases with the increase of the cutting speed.
- with increasing the degree of material compaction h/h_o the unit cutting resistance p_c, increases, and the dependence is a quadratic function and has the same course for all tested values of the angle θ.
- increasing the thickness of the knife blade δ also results in the increase of the unit cutting resistance p_c. The dependence is a quadratic function and takes a similar course for all the tested values of the angle θ.

On the basis of the conducted experimental tests and statistically elaborated mathematical models, a system of independent variables was established for the tested drum cutting unit, which corresponds to the minimum and maximum values of the dependent variables adopted in the testing programme, as shown in the table 2.

Tab. 2 An arrangement of independent variables for the highest and lowest values of the dependent variables

		Independent variable			
Dependent variable	The highest/lowest value of the dependent variable obtained from the experimental tests	Material feeding angle θ […°]	Cutting speed v_c [m·s^{-1}]	Degree of compaction of the material $h \cdot h_o^{-1}$	Thickness of blade δ [μm]
p_c	11535 N·m^{-1} / 3212 N·m^{-1}	90 / 45	3,85 / 8,20	0,47 / 0,65	300 / 40
L_S	13454 N·m^{-2} / 3746 N·m^{-2}	90 / 45	3,85 / 8,20	0,47 / 0,65	300 / 40
L_m	12838 J·kg^{-1} / 4971 J·kg^{-1}	45 / 90	3,85 / 8,20	0,65 / 0,55	300 / 40
W	0,167 kg·s^{-1} / 0,075 kg·s^{-1}	90 / 45	8,20 / 3,85	0,65 / 0,55	40 / 300
λ	9,26 % / 6,04 %	45 / 90	3,85 / 8,20	0,47 / 0,58	300 / 40

The authors did not have the opportunity to directly compare their research results with those reported in the literature by other researchers. This is caused by the fact that the research results presented in this article mainly concern a new design of the drum cutting unit, which is covered by legal protection. In the specialist literature there is a lack of data describing the process of cutting rye straw into pieces of a specified length using a cutting drum of a forage harvester with a double-cut cone shape. The first proposal for the design of a cutting drum of this shape, which can realise a diagonal cut in two directions, was presented by Bochat (*Bochat, 2010*). Other authors in their works provide only data related to commonly functioning design solutions of cutting drums realizing transverse cutting. The results presented above by the authors, concerning the classical design of the cutting drum, are comparable with the data presented in the literature in this field (*Abilzhanov, 2017; Persson, 1987, Bochat & Zastempowski 2020*).

CONCLUSIONS

This work resulted in the following conclusions:

1. From the conducted experimental tests it results that the following factors have a significant influence on the unit cutting resistance p_c, unit cutting work L_j, efficiency of the cutting unit W efficiency of the cutting unit λ there have the following: the method of cutting (transverse or diagonal), the cutting speed, the thickness of the blade of the knife, the degree of density of the cut material;
2. In the design works on the drum cutting units it is necessary to take into account the possibility of performing a diagonal cut, which is a very important alternative to the traditional - transverse - way of cutting;
3. In order to assess the quality of cutting plant material by the drum cutting unit, the degree of unevenness of the length of the cut material was assumed. As a result of the experimental tests, the values of independent variables were determined for which this quantity takes the lowest values (θ=90°, v_c=8,20 m·s^{-1}, h/h_o=0,58, δ=40 μm);
4. On the basis of the results obtained for the diagonal cutting of the material layer, it can be concluded that it seems advisable to conduct works on the development of new designs of drum cutting units, implementing other than traditional ways of cutting;

ACKNOWLEDGMENT

This article was supported by funding from the Research Budget of the Technical University.

REFERENCES

1. Abilzhanov D, Abilzhanuly T, Golikov V, Adilsheyev A, Alshurina A. Development of universal pick-up chopper for harvesting of chopped hay and haylage. Journal of Engineering and Applied Sciences. 2017;12(13):3309-14.
2. Bochat A. Theory and construction of cutting units of agricultural machines. In: UTP, editor. UTP University of Science and Technology. Bydgoszcz 2010.
3. Błaszczyk M. The impact of constructional features of the drum cutting unit on the utility characteristics of cutting plant materials. In: UTP, editor. UTP University of Science and Technology. Bydgoszcz 2010.
4. Du DD, Wang J. Research on mechanics properties of crop stalks: A review. Int J Agr Biol Eng. 2016; 9(6):10-9.
5. Igathinathane C, Pordesimo LO, Schilling MW, Columbus EP. Fast and simple measurement of cutting energy requirement of plant stalk and prediction model development. Industrial Crops and Products. 2011; 33(2):518-23.
6. Igathinathane C, Womac AR, Sokhansanj S, editors. Effect of angle of cut on corn stalks mechanical cutting strength and energy. American Society of Agricultural and Biological Engineers Annual International Meeting 2010, ASABE 2010; 2010.
7. Igathinathane C, Womac AR, Sokhansanj S, Narayan S. Size reduction of high- and low-moisture corn stalks by linear knife grid system. Biomass and Bioenergy. 2009;33(4):547-57.
8. Igathinathane C, Pordesimo LO, Schilling MW, Columbus EP, editors. Fast and simple measurement of energy requirements for plant stalk cutting. American Society of Agricultural and Biological Engineers Annual International Meeting 2008, ASABE 2008; 2008.
9. Persson S, Engineers ASoA. Mechanics of Cutting Plant Material: American Society of Agricultural Engineers; 1987.
10. Zastempowski M, Bochat A. Innovative Constructions of Cutting and Grinding Assemblies of Agricultural Machinery. Proceeding of 6th International Conference on Trends in Agricultural Engineering 2016. 2016:726-35.
11. Zastempowski M, Borowski S, Kaszkowiak J. New Solutions in Harvesting Plants for Power Purposes. Trends in Agricultural Engineering 2013. 2013:673-6.
12. Zastempowski, M., Bochat, A. Research issues in the process of cutting straw into pieces. Sustainability (Switzerland), 2020, 12(15), 6167
13. Bochat, A., Zastempowski, M. Comparative study of rape straw cutting with two drum cutting assemblies. Transactions of the ASABE, 2020; 63(2):345-350.
14. Zhang M, Sword ML, Buckmaster DR, Cauffman GR. Design and evaluation of a corn silage harvester using shredding and flail cutting. Transactions of the American Society of Agricultural Engineers. 2003; 46(6):1503-11.

Corresponding author:
Assoc. Prof. Marcin Zastempowski, Ph.D., Faculty of Mechanical Engineering, Bydgoszcz University of Science and Technology, Al. prof. S. Kaliskiego 7, 85-796 Bydgoszcz, Poland, e-mail: zastemp@pbs.edu.pl

AN EVALUATION OF THE GRAPE VINE GROWTH AFTER DEEP COMPOST INCORPORATION

Patrik ZATLOUKAL[1], Vladimír MAŠÁN[1], Patrik BURG[1], Alice ČÍŽKOVÁ[1]

[1]Department of Horticultural Machinery, Faculty of Horticulture, Mendel University in Brno, Valtická 337, 691 44 Lednice, Czech Republic

Abstract
Experiments were set up in vineyards in two different locations, Lednice and Velké Bílovice, in order to verify the effect of compost and compost enriched with Lignohumax applied to the areas around trunks on vine growth. The compost rates applied in autumn 2017 were 30 $t \cdot ha^{-1}$. The purpose of the initial measurements was to compare the length of new shoots, indicating a predominantly positive effect in relation to the application of compost. At the Lednice site, the length of shoots was 8-16% longer in the fertilised variant, while at the Velké Bílovice site it was 4-10% longer compared to the unfertilised control variant. The applied compost also had a positive effect on soil moisture.

Key words: *Lignohumax; soil moisture; shoot length; viticulture; Vitis vinifera.*

INTRODUCTION

Most wine-growing areas in Europe are currently facing a lack of rainfall and only 10% of vineyards are equipped with supplementary irrigation (*Costa et al., 2016*). The increasing scarcity of water is becoming an ever-growing problem for vines, even in relatively cooler and wetter European countries such as Austria, Germany, Luxembourg, Czech Republic etc. (*Santos et al., 2020*). This is probably caused by the increase in daily temperatures over recent years, which has been accompanied by more extreme weather events such as heat waves, long periods of drought, etc. (*Fraga et al., 2020*). The lack of water, combined with high temperatures during the growing season, may be the main limiting factor for the growth of shoots on vines and the production of grapes (*Chacón-Vozmediano et al., 2020*). In the long term, this condition leads to a general weakening of the growth of vines, which may result in their drying out. Another problem is the limited production of above-ground biomass, especially of shoots. Once they have matured, they are used to shape the vines and form canes in the following year (*Gambetta et al., 2020*). Therefore, in practice, it is very important to focus on ways of increasing water availability and limiting potential water stress in vines during the growing season without the use of supplementary irrigation (*Ramos & Martínez de Toda, 2020*). In this respect, innovative agrotechnical interventions that provide the desired effect, are easy to implement and economically viable can be considered promising solutions (*Yang et al., 2021*).

One such promising solution in this context is the application of organic fertilisers to the soil profile in the spacing between vineyard rows. It is generally known that organic matter plays an indisputable role in improving the physical and chemical properties of soil, including improving its retention capacity (*Nardi et al., 2002*). Especially in older plantings (typically over 25 years old), we see a significant deficit of organic matter in soil. This is a consequence of the cultivation itself, which depletes the soil of organic matter, as well as the more difficult application and incorporation of organic fertilisers, and their unavailability due to the decline in livestock farming (*Hudetzová, 2021*).

For that reason, viticulture is addressing issues related to the replacement of traditional organic fertilisers, such as manure, new types of fertilisers (compost), digestates, green manure (*Chou & Vanden Heuvel, 2019*), etc. The advantage of quality compost is its favourable composition and relatively wide availability in terms of quantity and price (*Pessina et al., 2019*).

In vineyards, traditional fertilisers as well as new types of fertilisers face the same problems associated with their application. Existing systems apply compost to the surface of the fertilised spacing between rows, followed by incorporating it shallowly below the soil surface (*Burg et al., 2021*). Other application methods are also being tested, e.g. application in a furrow pre-ploughed in parallel with the treated rows where the applied compost reaches a deeper depth where roots with the capacity to actively take up water and nutrients are distributed (*Gaiotti et al., 2017*). Another positive effect of this method of application is related to the acidification of the soil, the creation of a drain groove for water and air exchange,

the partial removal of soil compaction in trackways, and the disruption of the root system with subsequent regeneration and renewal (*Burg et al., 2021*).
The aim of this paper is to evaluate the effect of deep compost application in the areas around trunks of fertile vines on soil moisture and the growth of vines expressed by the length of shoots.

MATERIALS AND METHODS

The characteristics of the experimental site
Experimental measurements were carried out in between 2018 and 2020 in two locations in the Moravia viticulture region that differ in paedological and micro-climate properties, under the wine-growing conditions of the Czech Republic.

Lednice Experimental Site (Mikulov´s subregion)
With coordinates of 48° 47’ 30’’ north latitude and 16° 47’ 56’’ east longitude, the area of interest is located in a vineyard southwest of the Lednice village (Na Valtické vineyard track). For the needs of measuring meteorological data (monthly precipitation and temperature) a meteorological station with remote data transmission (AMET, Velké Bílovice, Czech Republic) was installed at the experimental sites. The measured values of precipitation and temperature during the monitored years at the Lednice site are shown in Fig. 1.
The predominant soil types are modal chernozem and carbonate chernozem; the parent substrate is loess. The Sauvignon Blanc variety is planted in the vineyard, grafted on the rootstock Kober 5BB, and shrubs are cultivated using high-culture training with a cut to a single cane. The support structure formed of steel columns reaches a height of 1.8 m. The plantation was established in 2012; shrubs are planted in a clutch of 2.5x1.0 m.

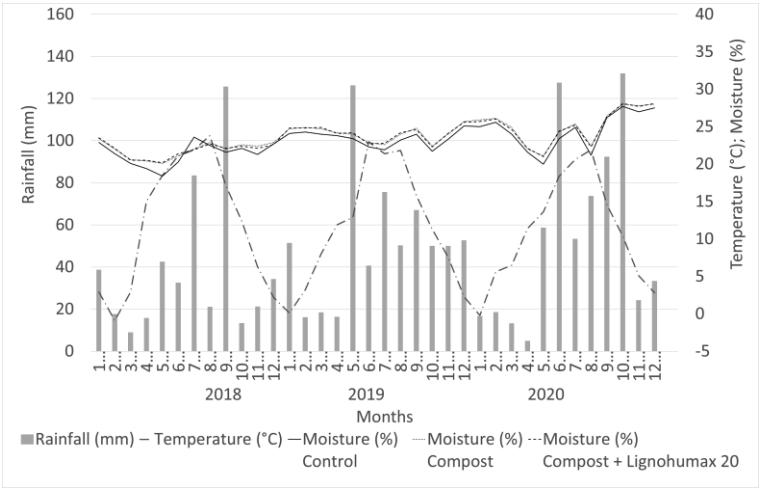

Fig. 1 Average month temperature rainfall and soil moisture under variant in Lednice

Velké Bílovice Experimental Site (Velkopavlovic´s subregion)
With coordinates of 48° 52’ 59” north latitude and 16° 53’ 5’’ east longitude, the area of interest is located northwest from the Velké Bílovice village (Úlehle vineyard track). The measured values of precipitation and temperature during the monitored years at the Velké Bílovice site are shown in Fig. 2.
The predominant types of soil are chernozem and pelic chernozem; the parent substrate is loess. The soil is slitty; this is moderately heavy skeletonless soil, a very deep soil with a mainly favourable water regime. The vineyard is planted with a variety of Pinot Gris, grafted on the rootstock SO4, and shrubs are cultivated using high-culture training with a cut to a single cane. The plantation was established in 2007; shrubs are planted in a clutch of 2.7×1.0 m.

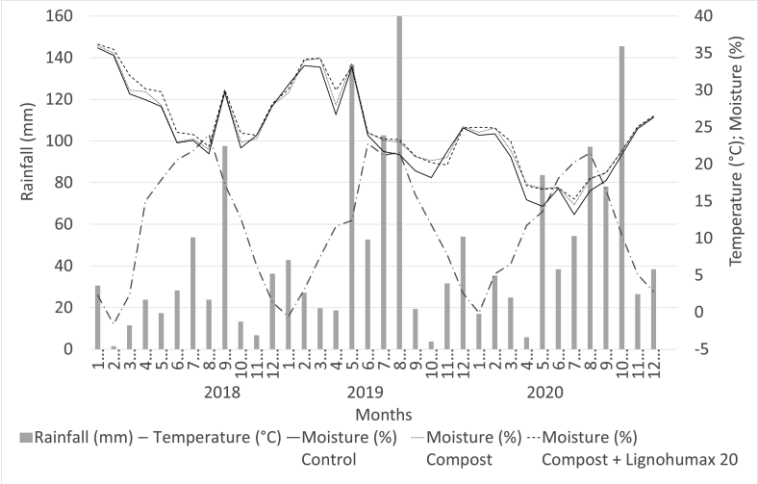

Fig. 2 Average month temperature rainfall and soil moisture under variant in Velké Bílovice

Compost characteristics and experimental variants
The applied compost was made from biologically degradable garden waste. The main components were grass cuttings, vegetable and fruit waste, wood chips and grain straw. The input raw materials were composted in strip bases triangular profiles and a base widths of 1.5 m. In terms of composition, the applied compost met the requirements of the CSN 46 5735 – Composting standard. In Tab. 1 are the average values of selected parameters of the compost applied in the vineyards in year 2017. The compost was applied to the cultivated in-rows using a specially designed prototype of a device for deep placement of compost in the spacing between vineyard rows. The embedment depth varied between 0.25–0.30 m.

Tab. 1 Selected physical and chemical parameters of the applied compost

Parameter	K	Mg	P	Ca	Dry matter	N_C	C_{OX}	pH_{KCL}
	$mg \cdot kg^{-1}$	$mg \cdot kg^{-1}$	$mg \cdot kg^{-1}$	$mg \cdot kg^{-1}$	(%)	(%)	(%)	
Value	4256±240	1190±57	608±64	7605±282	67.85±1.63	0.87±0.08	4.01±1.13	7.05±0.07

The experiment was based on the following variants:
Variant I – control without compost
Variant II – compost (dose of 30 $t \cdot ha^{-1}$)
Variant III – compost (30 $t \cdot ha^{-1}$) + Lignohumax 20 (0,4 $l \cdot ha^{-1}$)

Each variant was based on the method of random blocks of 100 m length in three repetitions. The applied dose of compost was 30 $t \cdot ha^{-1}$. Lignohumax 20 (Agrostim Biotechnologieprodukte, Saxony, Germany) was added to Variant III. This is a concentrated water solution produced by the hydrolytic-oxidation degradation of technical lignosulphonates made up of a mixture of humic and fulvic acids, including their salts. The application of Lignohumax increases the usage of nutrients contained in the soil, supports the development of the root system.

Evaluation of the soil moisture
Soil moisture was measured using "VIRRIB" (AMET, Velké Bílovice, Czech Republic) volumetric soil moisture sensors. These are mechanical sensors with a circular design, with a diameter of 280 mm, which were located at a depth of 0.1 m. Soil humidity was recorded to Datalogger, every day at regular fifteen-minute intervals.

Evaluation of the length of shoots
The length of shoots was assessed at regular weekly intervals, using a non-destructive method, from the beginning of the growing season until the first pollination. For taking the measurements, 3 vines were randomly selected for each of the treatments, leaving 8 annual shoots. The length of each shoot was then

measured using a caliper from the base towards the growing point. The measurements were then averaged.

Statistical analysis
Results were reported as averages and standard deviations at a significance level of α= 0.05. The software package Statistica 12.0 (StatSoft Inc., Tulsa, OK, USA) were used.

RESULTS AND DISCUSSION

Fig. 1 and 2 show the evolution of the volume of moisture in the soil during the monitored period. The results show a positive effect of applied compost on soil moisture values compared to the unfertilised control variant. Moisture values at the Lednice site were higher each year by 1–3%, while at the Velké Bílovice site they were 2–4%. *Perez-Alvarez, Garcia-Escudero, & Peregrina (2015)* states that soil moisture conditions can impact subsequent plant growth and nutrition by effecting soil nutrient availability. Also, *Cavagnaro (2016)* and *Burger et al., (2005)* states that soil moisture impact on nutrient availability and cycle may be particularly important for systems where organic matter is the dominant nutrient source. This is caused by the nutrient cycle and release from organic matter sources being largely a microbially mediated process and the activity of soil microbes is strongly dependent on soil moisture. When compost is incorporated into the soil, it is mineralised, which ensures a sustained release of available nutrients that can be more readily available to plants (*D'Hose et al., 2004*). *Meissner et al., (2019)* also states that a sufficient supply of soil organic matter can significantly reduce competition for water and nutrients between vines under hot and dry conditions, especially when it occurs at sensitive stages (e.g. when flowering and building berries), which has a positive effect on vine growth and grape yield.
Fig. 3 show the lengths of the shoots at the Lednice site and Fig. 4 at the Velké Bílovice site. The growth rate of vine shoots is mainly influenced by temperature and soil moisture (*Pavloušek, 2011*).
Overall, the graphs generated at both sites show a shorter length of shoots in the unfertilised control variant. For the variant using compost and compost in combination with lignohumate, the lengths of shoots were greater. *Pavloušek (2011)* states that high temperatures cause the mobilisation of substances stored in the root system, the production of auxins, and an intense and rapid growth of annuals. The problem of evaluating the growth of shoots in relation to the application of composts of different origin, applied on the surface and at depth, was addressed, for example, by *Gaiotti et al., (2017)*. The results of his experiments performed between 2009 and 2013 on the Cabernet Sauvignon varietal show that compost has a conclusive effect on the vegetative growth of vines compared to a control unfertilised variant. The length of shoots in the experiment variant with a fertiliser exceeded the control variant by more than 50%. *Nardi et al., (2002)* state that in order to optimise production, it is necessary to find a balanced relationship between vegetative growth and vine fertility and the yield of grapes produced. Measurements in this context were taken by *Arrobas et al., (2022)*, who applied compost from municipal waste at a quantity of 20 tonnes per hectare in the vineyard. The cumulative grape yield increased by 28% over the three-year period in the experimental plot.

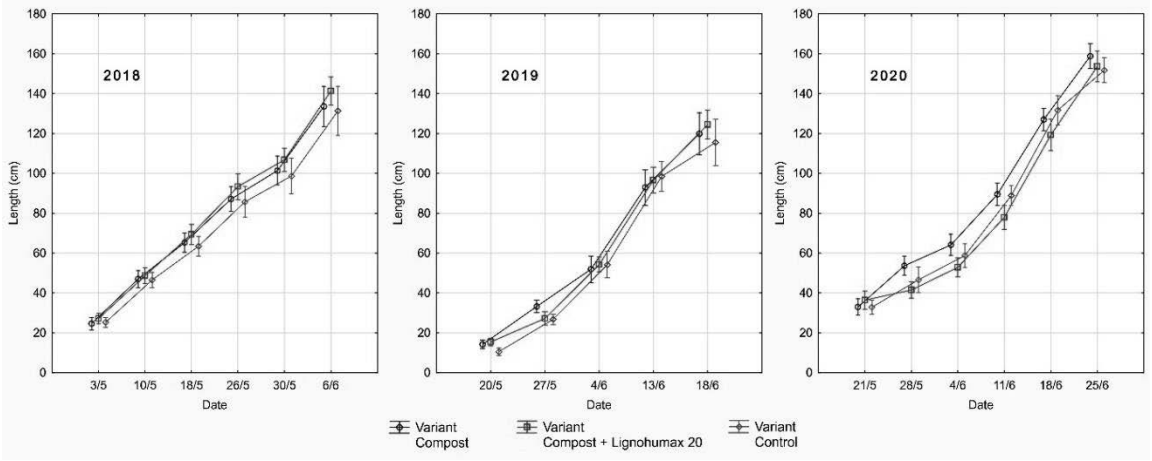

Fig. 3 Average lengths of the shoots at the Lednice site (2018-2020)

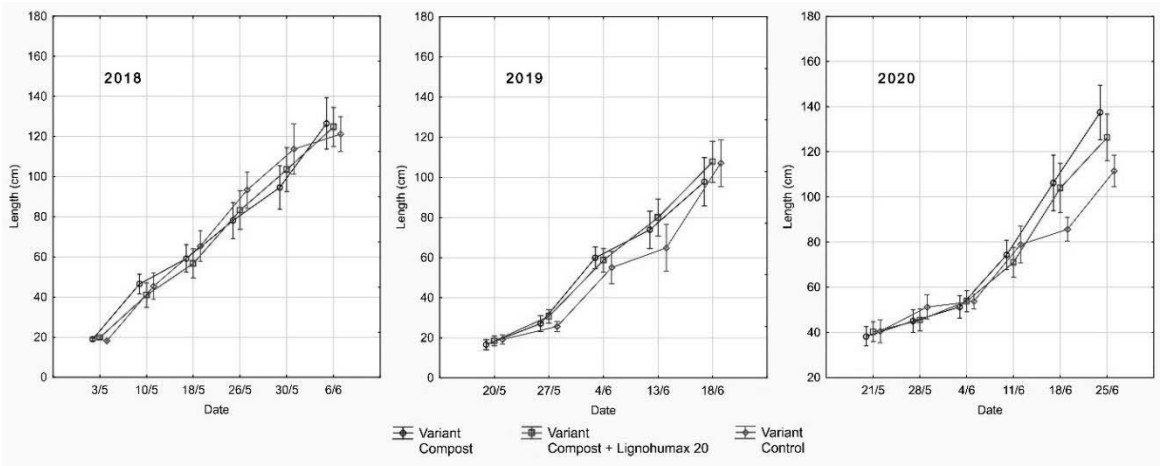

Fig. 4 Average lengths of the shoots at the Velké Bílovice site (2018-2020)

CONCLUSIONS

The results of the measurements taken over a three-year period indicate a positive effect of the deep application of compost to the area around trunks, which is reflected in increased soil moisture and more substantial growth of vine shoots. The wider implications and effects of this method of applying fertiliser will need to be verified over a longer term. Based on the results to date, the deep application of compost in vineyards can be recommended as an important agronomic intervention associated with the enhancement of sustainable viticulture aspects. In terms of future research activities, it would be advisable to focus more attention on variant verification of applied compost rates, verification of the possibility of adding soil improvers, expansion of the evaluation with emphasis on the assessment of vine nutrition, and yield and grape quality parameters in a wider range of grape varietals.

ACKNOWLEDGMENT

This article originated within the project by Operational Programme Research, Develop-ment and Education—Research Infrastructure for Young Scientists, project number CZ.02.1.01/0.0/0.0/16_017/0002334.

REFERENCES

1. Arrobas, M., Thais Nepomuceno Carvalho, J., Raimundo, S., Poggere, G., & Rodrigues, M.A. (2022). The safe use of compost derived from municipal solid waste depends on its composition and conditions of application. *Soil Use and Management, 38*(1), 917-928. DOI:10.1111/sum.12737.
2. Burg, P., Zemánek, P., Badalíková, B., Mašán, V., Zatloukal, P., Čížková, A., & Vašinka, M. (2021). Hloubková aplikace organické hmoty u vinic a ověření jejího vlivu na půdní a růstové podmínky (Depth application of organic matter in vineyards and a verification of effect on soil and growth conditions). Brno: Mendelova univerzita v Brně, Folia Universitatis Agriculturae et Silviculturae Mendelianae Brunensis. ISBN 978-80-7509-793-4. (In Czech).
3. Burger, M., Jackson, L.E., Lundquist, E.J., Louie, D.T., Miller, R.L., Rolston, D.E., & Scow, K.M. (2005). Microbial responses and nitrous oxide emissions during wetting and drying of organically and conventionally managed soil under tomatoes. *BIol. Fert. Soil., 42*, 109-118. DOI: 10.1007/s00374-005-0007-z.
4. Cavagnaro, T. R. (2016). Soil moisture legacy effects: Impacts on soil nutrients, plants and mycorrhizal responsiveness. Soil Biol. Biochem., 95, 173-179. DOI:10.1016/j.soilbio.2015.12.016.
5. Costa, J.M., Vaz, M., Escalona, J., Egipto, R., Lopes, C., Medrano, H., & Chaves, M.M. (2016). Modern viticulture in southern Europe: vulnerabilities and strategies for adaptation to water scarcity. Agric. Water Manag, 164, 5-18. DOI:10.1016/j.agwat.2015.08.021.
6. D'hose, T., Cougnon, M., De Vliegher, A., Vandecasteele, B., Viaene, N., Cornelis, W., Van Bockstaele, E., & Reheul, D. (2014). The positive relationship between soil quality and crop production: A case study on the effect of

farm compost application. Appl. Soil Ecol. 75, 189-198. DOI:10.1016/j.apsoil.2013.11.013.
7. Fraga, H., Molitor, D., Leolini, L., & Santos, J.A. (2020). What Is the Impact of Heatwaves on European Viticulture? A Modelling Assessment. Appl. Sci., 10, Article 3030. DOI:10.3390/app10093030.
8. Gaiotti, F., Marcuzzo, P., Belfiore, N., Lovat, L., Fornasier, F., & Tomasi, D. (2017). Influence of Compost Addition on Soil Properties, Root Growth and Vine Performances of Vitis vinifera cv Cabernet sauvignon. *Scientia Horticulturae, 225*: 88-95. DOI: 10.1016/j.scienta.2017.06.052.
9. Gambetta, G.A., Herrera, J.C., Dayer, S., Feng, Q., Hochberg, U., & Castellarin, S.D. (2020). The physiology of drought stress in grapevine: towards an integrative definition of drought tolerance. *J. Exp. Bot., 71*, 4658-4676. DOI:10.1093/jxb/eraa245.
10. Hudetzová, K. (2021). Situační a výhledová zpráva: Skot - hovězí maso (Situation and Outlook Report: Cattle - beef). Praha: Ministerstvo zemědělství České republiky, 66 p. (In Czech).
11. Chacón-Vozmediano, J.L., Martínez-Gascueña, J., García-Navarro, F.J., & Jiménez-Ballesta, R. (2020). Effects of Water Stress on Vegetative Growth and 'Merlot' Grapevine Yield in a Semi-Arid Mediterranean Climate. *Hortic, 6*, Article 95. DOI:10.3390/horticulturae6040095.
12. Chou, M.Y., & Vanden Heuvel, J.E. (2019). Annual Under-Vine Cover Crops Mitigate Vine Vigor in a Mature and Vigorous Cabernet franc Vineyard. *American Journal of Enology and Viticulture, 70*(1), 98-108. DOI:10.5344/ajev.2018.18037.
13. Meissner, G., Athmann, M.E., Fritz, J., Kauer, R., Stoll, M., & Schultz, H.S. (2019). Conversion to organic and biodynamic viticultural practices: impact on soil, grapevine development and grape quality. *OENO One, 53*(4). DOI:10.20870/oeno-one.2019.53.4.2470.
14. Nardi, S., Pizzeghello, D., Muscolo, A., & Vianello, A. (2002). Physiological effects of humic substances on higher plants. *Soil Biology and Biochemistry, 34*(11), 1527-1536. DOI: 10.1016/S0038-0717(02)00174-8.
15. Pavloušek, P. (2011). Pěstování révy vinné: moderní vinohradnictví (Growing the vine: modern viticulture). Praha: Grada. ISBN 978-80-247-3314-2. (In Czech).
16. Perez-Alvarez, E.P., Garcia-Escudero, E., & Peregrina, F. (2015). Soil Nutrient Availability under Cover Crops: Effects on Vines, Must, and Wine in a Tempranillo Vineyard. *American Journal of Enology and Viticulture, 66*(3), 311-320. DOI:10.5344/ajev.2015.14092.
17. Pessina, D., Facchinetti, D., Tardaguila, J., Ghiglieno, I., & Valenti, L. (2019). Mechanical behaviour of three organic fertilisers to optimise spreading methods in the vineyard. *Rivista Di Studi Sulla Sostenibilita, 2*, 375-390. DOI:10.3280/RISS2019-002-S1024.
18. Ramos, M.C., & Martínez de Toda, F. (2020). Variability in the potential effects of climate change on phenology and on grape composition of Tempranillo in three zones of the Rioja DOCa (Spain). *Eur. J. Agron., 115*, Article 126014. DOI:10.1016/j.eja.2020.126014.
19. Santos, J.A., Fraga, H., Malheiro, A.C., Moutinho-Pereira, J., Dinis, L.T., Correia, C., Moriondo, M., Leolini, L., Dibari, C., Costafreda-Aumedes, S., Kartschall, T., Menz, C., Molitor, D., Junk, J., Beyer, M., & Schultz, H.R. (2020). A review of the potential climate change impacts and adaptation options for European viticulture. *Appl. Sci., 10*, Article 3092. DOI:10.3390/app10093092.
20. Yang, C., Menz, C., Fraga, H., Reis, S., Machado, N., Malheiro, A.C., & Santos, J.A. (2021). Simultaneous Calibration of Grapevine Phenology and Yield with a Soil–Plant–Atmosphere System Model Using the Frequentist Method. *Agron, 11*, Article 1659. DOI:10.3390/agronomy11081659.

Corresponding author:
Ing. Vladimír Mašán, Ph.D., Department of Horticultural Machinery, Faculty of Horticulture, Mendel University in Brno, Valtická 337, 691 44 Lednice, Czech Republic, phone: +420 519367370, e-mail: vladimir.masan@mendelu.cz

QUANTIFICATION AND DETERMINATION OF MUNICIPAL WASTE AND ITS RELATION TO HOUSEHOLD SIZE IN THE CZECH REPUBLIC

Shuran ZHAO[1], Vlastimil ALTMANN[1], Jan ŠONSKÝ[2], Petr VACULÍK[2]

[1]Department of Machinery Utilization, Faculty of Engineering, Czech University of Life Sciences Prague (CZU), Kamýcká 129, 165 00 Praha – Suchdol, Czech Republic
[2]Department of Technological Equipment of Buildings, Czech University of Life Sciences Prague (CZU), Kamýcká 129, 165 00 Praha – Suchdol, Czech Republic

Abstract
Municipal waste with more than 14 % share on total waste production in the Czech Republic plays important role. Understanding household waste sorting behaviour allows more effective design of municipal waste system in accordance with the waste hierarchy. This article focuses on determination and quantification of municipal waste generated at household in the Czech Republic and studies its relation to the family size. Waste generation and separation at source was measured on a 14day basis in households. Results of this study proved a significant relation between waste production and household size. One-member family produce more waste (plastics, mixed and biodegradable waste) than families with more members. This knowledge in combination with population structure will help municipality to better set up its waste collection system and develop a system that is suitable for the inhabitants based on the demographic segmentation.

Key words: *waste composition; waste generation; family size; source-separation.*

INTRODUCTION

Municipal solid waste is a long-term challenge for municipal authorities to face, especially due to the increasing pressure of the European Union on diversion of waste from landfill. In the Czech Republic, just 39 % of municipal solid waste (MSW) was reused or recycled in 2020, 13 % was recovered for energy consumption and 48 percent ended up in landfills. However, the priority of the Czech Republic are in the reverse order: waste prevention comes first, followed by reuse and recycling. Then follows energy recovery, and finally the landfill itself. The described situation was supported by the fact that the landfill ban was postponed from 2024 to 2030 and that the landfill fee remained unchanged for 12 years at CZK 500 per tonne of waste (*NKU, 2022)*. Municipal waste with more than 14 % share on total waste production in the Czech Republic plays important role and households themselves can also make a significant contribution to waste reduction (*Suthar & Singh, 2015)*. Understanding household waste separating behaviour is increasingly essential in waste collection planning and treatment strategies, and establishing policies toward a sustainable waste management system *(Abbasi et al., 2013; Chen & Chang, 2000)*. The aim of this study was to describe the household wastes (HW) generated by families of different sizes in order to identify the potential of the wastes for recycling.

MATERIALS AND METHOD

Data of household waste production were collected during 2021. Over 100 families were included in this experiment to measure their waste production at home. The experiment was designed on assessing of household waste production including recyclable waste based on 14-day period with repetition. Families in this experiment sorted municipal waste into 7 groups: paper, plastics, glass, TetraPak, metal, organic waste (BIO), municipal solid waste (MSW).

Produced waste was weighted using kitchen scale by each family and recorded by the end of day. After all repetitions, data were collected from households and entered in Excel form. Raw data were converted to unit ‘kilogram per capita per year (kg/pc/yr)’ in order to analyse the difference in waste production among different family size. Selected families were divided into 4 groups according to their size: one-member, two-member, three-member and four-member family. Data from these families were converted and compared based on production in kilograms per capita per year.

During the statistical analysis, the data were tested with the normal distribution by Shapiros *test (Shapiro & Wilk, 1965)*. The result has shown that variables of interest did not have normal distribution, therefore the non-parametric Kruskal-Wallis test for differences between those families was applied in our experiment *(Kruskal & Wallis, 1952)*.

RESULTS AND DISCUSSION

The total of 115 families were involved in this experiment to measure their 2-week period waste production at home. Data from these families were converted and compared based on production in kilograms per capita per year to study the differences between them. Table 1 demonstrates the composition of household solid waste generated by different groups. One-member family produced in average 157 kg of municipal waste (MS) in total per capita per year according to this study. As compared with it, other sized families produced less MS in total. The same trend can be observed at level of particular waste types. All monitored waste types (plastics, glass, organic waste and MSW) except paper waste demonstrated a declining tendency in production with increasing number in family (**Chyba! Nenalezen zdroj odkazů.**). It suggests that multi-person family may generate less waste per person than family with single member (Fig. ***3***). This suggestion did not apply on paper waste, which's average production did not indicate a clear trend among families. The statistical results of Kruskal-Wallis test have shown similar signs. Waste types i.e. plastics, glass, organic waste and MSW demonstrated that multi-person families (2-4 members) had different waste production than one-person families ($p<0.05$). Again, paper waste did not prove significant difference between variously sized families ($p=0.5062$).

This connection between the waste generation and family size as one of the socioeconomic parameters is supported by other studies. For example, *Rawat & Daverey (2018)* have showed in their study that the amount of household waste produced per person declines as family size rises. *Monavari et al. (2012)* have proved that family size as one of the socioeconomic parameters beside income and education level has direct effect on household waste generation.

Due to their insufficient quantity and extreme values, Tetrapak and metals have been excluded from the overall statistical analysis and are depicted in a special chart (**Chyba! Nenalezen zdroj odkazů.**). The data so far demonstrate a similar trend as MSW in total or others, but Tetrapak and metals will need more data collection and evaluation to prove the significance.

Tab. 1 Average waste production of municipal waste in families of different sizes

Household Members	PAPER	PLASTICS	GLASS	BIO	MSW	TOTAL (kg/capita/yr)
One	9.54	11.97	28.02	47.67	60.10	157.29
Two	11.18	13.22	32.04	40.80	35.71	132.95
Three	13.30	10.92	18.01	37.16	39.37	118.76
Four	8.53	8.44	16.01	22.33	26.71	82.02

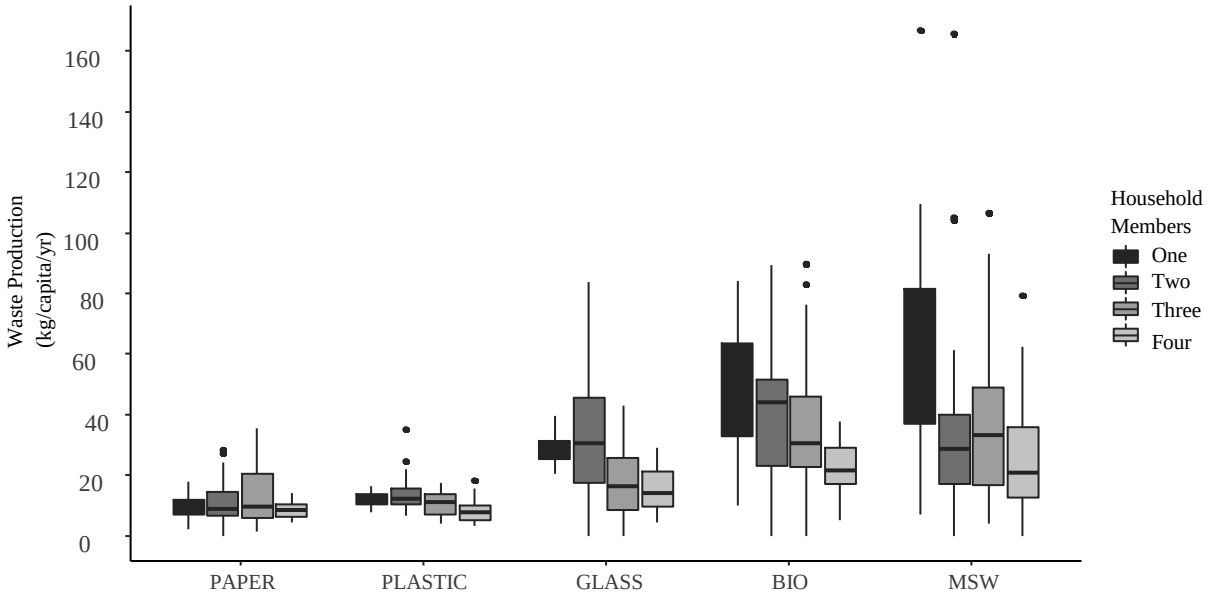

Fig. 1 Various type of municipal waste produced within differently sized families

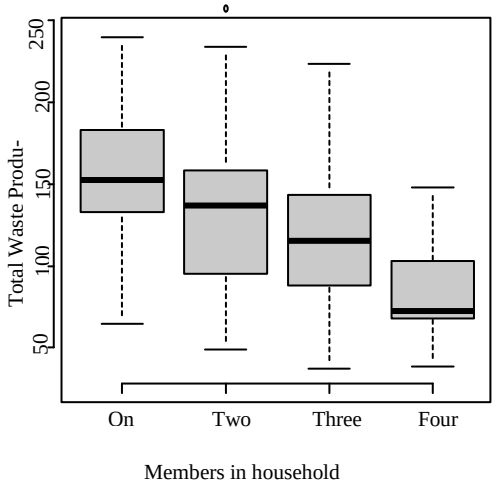

Fig. 3 Total waste production compared within families with different number of members.

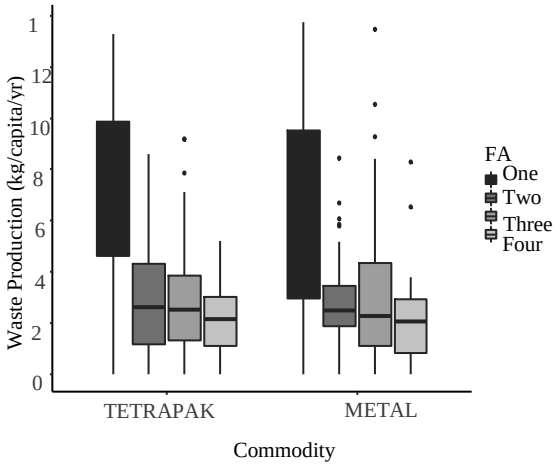

Fig. 2 Production of Tetrapak and metal waste in household.

CONCLUSIONS

Results of this study proved relation between waste production and household size. It is a fundamental indicator for decision-making process to set up the waste system in the municipalities of the Czech Republic. Knowledge of population structure will help the municipality to better set up its waste system including logistics and the financial aspects. The authorities will have a better understanding of the waste situation and may implement a suitable system for the citizens according to the population structure. For the future studies, it is highly recommended to design a longer measuring time and include social – economic aspects into study.

ACKNOWLEDGMENT

This study was supported by Intern grant agency of Faculty of Engineering, Czech University of Life Sciences Prague with no. 2021:31180/1312/3104.

REFERENCES

1. Abbasi, M., Abduli, M. A., Omidvar, B., & Baghvand, A. (2013). Forecasting Municipal Solid waste Generation by Hybrid Support Vector Machine and Partial Least Square Model. *International Journal of Environmental Research*, *7*(1), 27–38.
2. Chen, H. W., & Chang, N.-B. (2000). Prediction analysis of solid waste generation based on grey fuzzy dynamic modeling. *Resources, Conservation and Recycling*, *29*(1), 1–18.
3. Kruskal, W. H., & Wallis, W. A. (1952). Use of Ranks in One-Criterion Variance Analysis. *Journal of the American Statistical Association*, *47*(260), 583–621.
4. Monavari, S. M., Omrani, G. A., Karbassi, A., & Raof, F. F. (2012). The effects of socioeconomic parameters on household solid-waste generation and composition in developing countries (a case study: Ahvaz, Iran). *Environmental Monitoring and Assessment*, *184*(4), 1841–1846.
5. NKU. (2022). *Waste management in the Czech Republic: Billions in subsidies have not brought change, landfilling still plays a major role*. Czech Republic Supreme Audit Office. https://www.nku.cz/en/
6. Rawat, S., & Daverey, A. (2018). Characterization of household solid waste and current status of municipal waste management in Rishikesh, Uttarakhand. *Environmental Engineering Research*, *23*(3), 323–329.
7. Shapiro, S., & Wilk, M. (1965). An analysis of variance test for normality (complete samples). *Biometrika*, *52*(3–4), 591–611.
8. Suthar, S., & Singh, P. (2015). Household solid waste generation and composition in different family size and socio-economic groups: A case study. *Sustainable Cities and Society*, *14*, 56–63.

Corresponding author:
Ing. Shuran Zhao, Department of Machinery Utilisation, Faculty of Engineering, Czech University of Life Sciences Prague, Kamýcká 129, Praha 6, Prague, 16521, Czech Republic, phone: +420 720364856, e-mail: zhao@tf.czu.cz

Proceeding of the 8th International Conference on Trends in Agricultural Engineering 2022

September 20th 2022 – September 23rd 2022

Publisher: Czech University of Life Sciences Prague Kamýcká 129, Prague Czech Republic
Editor in chief: David Herák
Printing house: Powerprint s.r.o.
Number of copies: 100
Number of pages: 431
Issue: First
Year: 2022
All manuscripts in conference proceedings have been reviewed by a peer review process

ISBN 978-80-213-3207-2

The authors shall be solely responsible for the technical and linguistic accuracy of the manuscripts